Geology and Geochemistry of the Laird Lake Property and Associated Gold Mineralization, Red Lake Greenstone Belt, Northwestern Ontario

Brigitte Rachel Gélinas

Submitted in partial fulfillment of

the requirements for the degree of

Master of Science in Geology

Department of Geology

Lakehead University

Thunder Bay, Ontario

April 2018

Abstract

The Laird Lake property encompasses the tectonic contact between the Balmer (2.99 to 2.96 Ga) and the Confederation (2.74 to 2.73 Ga) assemblages on the south-western end of the Red Lake greenstone belt, Northwestern Ontario. The purpose of this study was to determine the tectonic setting in which the assemblages formed, and to characterize the controls on and nature of the gold mineralization associated with the tectonic contact between the Balmer and Confederation assemblages.

Detailed mapping of the area highlighted major differences between the two assemblages. The Balmer assemblage is typically composed of fine-grained, aphyric, locally pillowed mafic volcanic rocks, ultramafic intrusive and volcanic rocks with flow-breccia textures and local spinifex-bearing clasts, and banded-iron formations. In contrast, the Confederation assemblage consists of porphyritic (feldspar) or poikiloblastic (amphibole) mafic volcanic rocks intercalated with intermediate to felsic volcanic rocks that include crystal lapilli tuffs, crystal tuffs and tuffs. Syn-volcanic and syn- to post-D_2 intrusions commonly cross-cut the volcanic packages. A regional foliation (~E-trending) is present throughout the volcanic rocks and increases in intensity at the tectonic contact between the two assemblages where a shear zone no thicker than 100 m is present within the Balmer assemblage.

Whole-rock geochemical analyses were undertaken on 161 samples from the Laird Lake area. The Balmer assemblage is composed of tholeiitic mafic volcanic rocks with minor Al-undepleted komatiites, whereas the Confederation assemblage is composed of calc-alkalic mafic and intermediate to felsic volcanic rocks, which display FI, FII, and FIIIb rhyolite trends. Neodymium isotope analyses, in conjunction with trace element geochemistry, suggests that parts of the Balmer assemblage were weakly contaminated by an older intermediate basement. The data suggests both arc and back arc volcanism within the Confederation assemblage, with the arc rocks showing stronger a crustal component than the back arc rocks. U-Pb geochronology of volcanic and intrusive Confederation units yielded ages of 2741 ± 19 Ma (FI quartz-feldspar porphyritic crystal tuff) and 2737.68 ± 0.79 Ma (diorite). The geochemistry and age of the tuff correlates within error to the Heyson sequence of the Confederation, whereas the diorite is likely a syn-volcanic intrusion.

The Balmer assemblage is interpreted to represent an oceanic plateau formed by plume magmatism on the margins of the North Caribou Terrane whereas the Confederation assemblage was likely built in an oceanic arc setting where both arc and back arc volcanism were occuring simultaneously. The presence of xenocrystic zircons within the 2741 Ma quartz-feldspar porphyritic crystal tuff suggest that melts within the main arc incorporated xenocrystic zircons during ascent through a thin Mesoarchean crustal fragment. Juxtaposition of the Confederation assemblage onto the Mesoarchean assemblages likely occurred between 2739-2733 Ma.

Gold mineralization at the Laird Lake property is controlled by a D_2 shear zone within the Balmer assemblage at the tectonic contact between the Balmer and Confederation assemblages. The mineralization is commonly found associated with a mineral banded texture, accompanied by disseminated arsenopyrite, pyrrhotite, pyrite ± chalcopyrite, similar to the features observed at the nearby Madsen gold mine. Oxygen isotope data from early- to syn-D_2 gold-mineralized and barren quartz veins suggest both vein types originated from a similar source and overlap with $\delta^{18}O_{H2O}$ values of metamorphic, magmatic and meteoric waters, over crystallizing temperatures ranging from 300 to 500°C. Evidence for a second gold event (post-2702 ± 1 Ma) is characterized by the presence of gold-rich shears and lamprophyres cross-cutting the regional foliation, and the lack of overprinting amphibolite

facies mineralogy. The Laird Lake property likely represents the continuation of the same mineralized structure found at both the Madsen and Starrat-Olsen mines and was later displaced as far as 10 km west by the dextral Laird Lake fault post-2704 Ma.

Acknowledgements

First I would like to thank Dr. Pete Hollings for his guidance, insight and support throughout my Masters project. His patience when reviewing my work and discussing complex ideas was much appreciated. This project wouldn't have been possible without the financial and logistical support of Bounty Gold Corp. – thank you Jason and Chris Leblanc. A big thanks goes out to my field assistants, Carli Nap and Matt Greco who shared my excitement in the field and got up each day knowing what bugs, swamps and uphill traverses lied ahead. In addition, I would like to thank the geologists at the Red Lake MNDM office for giving us a tour of the greenstone belt, maps to conduct field work and visiting the project area: Andreas Lichtblau, Carmen Storey and Greg Paju. Further thanks go to Mark Epp of Premier Gold Mines Ltd. for providing me with all of the literature on the Red Lake greenstone belt, geology tours around the RLGM and insightful discussions; and Phil Smerchanski of Pure Gold Mining Inc. for the tour of the Madsen Mine property.

Thanks to the Geoscience Laboratories, Ontario Geological Survey (OGS) in Sudbury for in-kind support for the analysis of rock samples. Financial support was also provided by the Mitacs–Accelerate Internship program, a Society of Economic Geologists (SEG) Graduate Student Fellowship and the Ontario Graduate Scholarship program.

Many thanks go to Anne Hammond and Kristi Tavener for producing terrific thin sections for this project. In addition, I would like to thank Richard Friedman (University of British Columbia – U-Pb isotopes), Ryan Sharp (University of Manitoba – O isotopes) and Sherri Strong (Memorial University – Nd isotopes) for their help in collecting, interpreting and understanding all isotope data.

Finally, many thanks go to Dennis and Debbie Leblanc for treating me like family during my time in Red Lake. Most of all, I would like to thank my friends and family for their continuous support and encouragement throughout this project.

Table of Contents

List of Figures

List of Tables

Chapter 1 – Introduction

1.1 Background

Greenstone belts in Archean provinces have long been established as prospective environments for gold mineralization and represent a significant mineral resource in the Superior Province of Canada (Robert et al., 2005; Dubé and Gosselin, 2007). More specifically, the Red Lake greenstone belt (Fig. 1.2) is one of the most well-endowed gold camps in northern Ontario with a number of recent new discoveries even after 86 years of mining (Sanborn-Barrie et al., 2001; Lichtblau et al., 2016a). Initial prospecting of the area began in the late 1800s and the first discovery of gold was made in 1897 (Horwood, 1940a). In 1926, the first gold rush in Red Lake started and since then a total of 19 mines have operated and roughly 28,944,937 oz of gold have been extracted as of December 2016 (Blais et al., 2015; Lichtblau et al., 2017). Recent exploration by Bounty Gold Corp. has identified gold mineralization within the 2.98 Ga Balmer and 2.75 Ga Confederation assemblages on the Laird Lake property roughly 25-30 km from the world-class Red Lake Gold Mines and 10 km from the past-producing Madsen mine. Due to the presence of similar features observed at the Laird Lake property as seen at the Madsen mine, exploration by junior mining companies on the property has been ongoing since 1936 (Willoughby, 1988), but no academic research has been carried out on the property in order to fully characterize and understand the geology and associated mineralization.

1.2 Objective

The purpose of this thesis was to achieve a better understanding of the nature and genesis of gold mineralization at the Laird Lake property, in the south-west portion of the Red Lake greenstone belt. Mapping of the property has helped develop an integrated model for the geology and gold mineralization of the area. The model has been compared to existing lode gold deposit data sets in order to assess the likelihood of significant gold mineralization and to help enhance current gold

exploration models. The project has characterized the nature and tectonic setting of the host rocks of the mineralization and provides a framework for subsequent studies of the gold-bearing fluids. The mineralization and the petrogenesis of the host rocks have been investigated using a combination of mapping, petrology, geochemistry and isotope studies. Specific objectives included: (a) producing a map of the Laird Lake Property and of the Gold-Bearing Zone trench; (b) characterizing the host rocks, alteration and gold mineralization; (c) determining the paragenetic sequence of events; and (d) characterizing the mineralizing fluid.

1.3 Lode Gold Overview

Lode gold deposits have formed throughout most of Earth's history and share multiple diagnostic characteristics (Groves et al., 1998; Poulsen et al., 2000; Goldfarb et al., 2001). These deposits have been referred to as lode gold, mesothermal, orogenic, shear-zone-related, quartz-carbonate, gold-only and metamorphic gold (Dubé and Gosselin, 2007). Many attempts have been made to unify and classify gold deposits to lessen the confusion created by the inconsistent terminology and the number of names inferring a specific ore genesis (Robert et al., 1997; Groves et al., 1998; Poulsen et al., 2000; and references therein).

Lode gold deposits form in regionally metamorphosed terranes in which the ore is structurally controlled and associated with hydrothermal alteration (Groves et al., 1998; Goldfarb et al., 2001). These deposits occur in greenschist to amphibolite grade rocks but the majority form in greenschist facies rocks or at the transition between the two, as seen at the Red Lake Gold Mines (Kerrich and Cassidy, 1994; Thompson, 2003; Goldfarb et al., 2005). Lode gold deposits are thought to have formed during compressional to transpressional deformation events in accretionary and collisional orogens where the mineralization is structurally controlled by 2nd to 3rd order faults as splays from the main translithospheric structures, such as the Destor-Porcupine and Larder Lake-Cadillac fault zones in the

Abitibi greenstone belt, or from terrane boundaries (Fig. 1.1; Kerrich and Cassidy, 1994; Groves et al., 1998; Kerrich et al., 2000; Groves et al., 2003; Goldfarb et al., 2005). The mineralization associated with these deposits is epigenetic, meaning it formed post-orogen with respect to the tectonism of the host rocks, but the ore itself is usually syn- to post-peak metamorphism (Goldfarb et al., 2005). Commonly, mineralization is concentrated at the brittle-ductile transition zone which can coincide with, or lie just above, the greenschist-amphibolite facies transition zone (Kerrich and Cassidy, 1994; Robert et al., 2005).

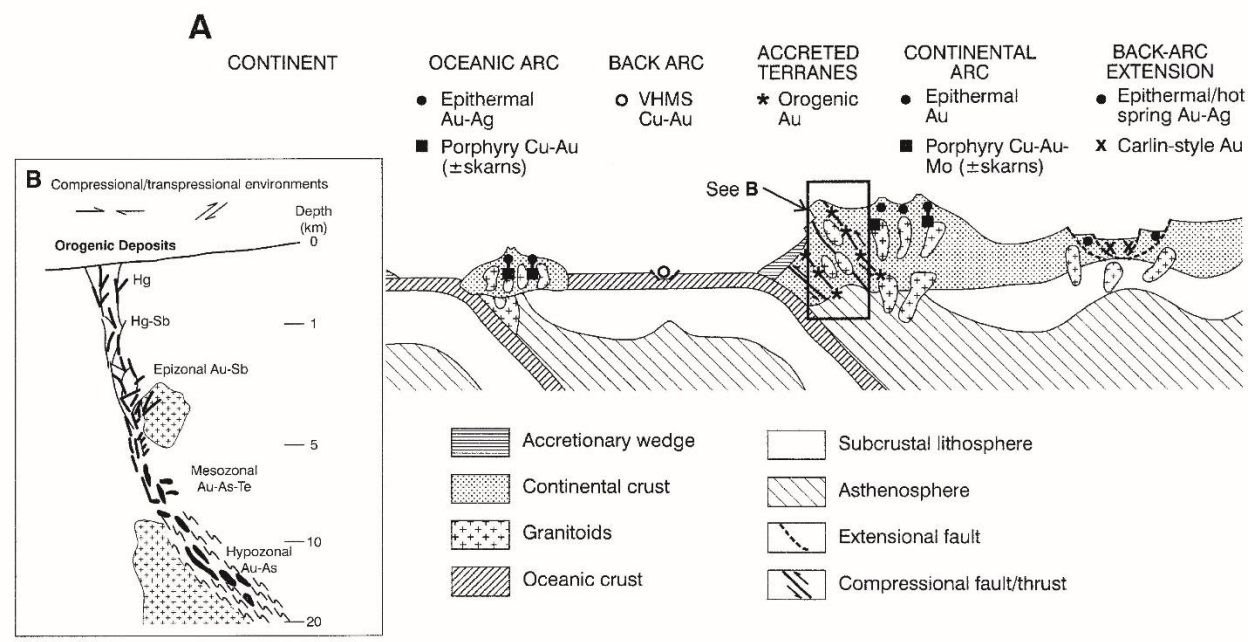

Figure 1.1 Schematic diagram displaying the setting and nature of orogenic gold deposits. (A) Plate tectonic environments of gold-rich deposits. (B) Depth profile of orogenic gold deposits. Modified from Goldfarb et al. (2001).

In orogenic settings, the change in metamorphic conditions results in devolatization of the hydrated minerals and in turn, releases H_2O, CO_2, S, and Au into solution and creates large fluid volumes (Goldfarb et al., 2005; Phillips and Powell, 2010). Gold is complexed with sulphur and hydrogen to form $\mathrm{Au(HS)_2^-}$ (250-400°C) and the complex is carried upwards by the metamorphic fluid through a series of shear zones and fractures until it reaches ideal conditions for gold precipitation. At higher temperatures (~500°C), gold-chlorine ($\mathrm{AuCl_2^-}$) and gold-hydroxide (AuOH(aq)) complexes can become increasingly

important (Stefánsson and Seward, 2004). Most commonly, a combination of chemical and structural traps determine if gold will precipitate in an economic form. Good chemical traps include, but are not limited to, banded iron formations (Musselwhite Mine; Oswald et al., 2015), tholeiitic basalts (Red Lake Gold Mines; Dubé et al., 2004), black slate (Meguma Gold deposit; Sangster and Smith, 2007), and magnetite-bearing diorite (Victorian gold province; Phillips and Powell, 2010). Structural traps that favor gold deposition include fold hinges, dilational jogs along faults or shear zones and zones of competency contrast (Groves et al., 2003; Dubé and Gosselin, 2007). Robert et al. (2005) argued that three reoccurring conditions appear in all major lode gold deposits: shear zones and faults produced at the contact between rocks with a large contrast in competency, competent rocks hosted in less component, and fold hinges and anticlines. Other factors such as the fluid:rock ratio, pH, pressure, gold solubility and mixing of external fluids will additionally influence gold deposition on a more local scale (Groves et al., 2003). Multiple styles of mineralization exist within lode gold deposits and are the cause of a combination of various lithologic and structural settings. These include: (a) quartz-carbonate veins; (b) sulfidic replacement in banded iron formation (BIF); (c) sulfidic replacements and crustiform veins; (d) disseminated-stockwork zones; (e) sulfide-rich veins and veinlet zones; (f) semi-massive to massive sulfide lenses (Robert et al., 2005). The major characteristics of lode gold deposits are summarized in Table 1.1. Most small deposits will display one style of mineralization, whereas larger deposits display overprinting styles of mineralization and associated hydrothermal alteration patterns. For example, the Dome mine in the Timmins gold camp has deformed low-grade colloform-crustiform ankerite veins which are cut by auriferous quartz veins that in turn, both cut Timiskaming age conglomerates that are carbonatized and host clasts of the ankerite veins (Dubé and Gosselin, 2007). The complexities between mineralization, alteration and deformation events can only be explained through a series of multiple episodes of mineralization and remobilization, and require more than one method of concentrating the ore (Robert et al., 2005).

Style of mineralization	Characteristics	Associated alteration assemblage	Metal association	Selected examples where mineralization type is dominant or important
Quartz-carbonate veins	Quartz veins with <25% carbonate, <10% sulfide, ±albite, tourmaline, scheelite. Vein types include laminated fault-fill and extensional veins. Sulfides are mainly pyrite, with arsenopyrite and pyrrhotite	Carbonate-sericite-(albite)-pyrite-(arsenopyrite), at greenschist grade. Biotite-actinolite-pyrite ±carbonate, at lower amphibolite grade. Biotite-calc-silicate-pyrrhotite ±pyrite at mid amphibolite grade	Au > Ag As, W ± Te, Mo, B	**Hollinger-McIntyre, Kirkland Lake, Sigma-Lamaque,** San Antonio
Sulfidic replacements in BIF	Strata-bound replacements of Fe-rich layers by mainly pyrite, arsenopyrite, or pyrrhotite. Associated with quartz veins or zones of veinlets or silica flooding	Pyrite (arsenopyrite)-sericite-chlorite-carbonate at greenschist grade Pyrrhotite (loellingite) grunerite-garnet at amphibolite grade	Au > Ag As ± Cu	Musselwhite, Cockshutt-McLeod, Pickle Crow
Sulfidic replacements and crustiform veins	Crustiform-colloform carbonate-quartz veins and breccias, with various proportions of sulfidic replacements of wall rocks or vein carbonates Sulfides are pyrite or arsenopyrite; stibnite and tellurides abundant in some deposits	Sericite-carbonate-(alvite)-pyrite at greenschist grade Biotite-carbonate-silica ± alumino-silicate at amphibolite grade	Au > Ag As, Te, ± Sb, Hg, W, Zn	**Red Lake Gold Mines**, Cochenour
Disseminated-stockwork zones	Zones of 5 to 20% sulfides, as uniform disseminations or along foliation-parallel bands, with variably developed stockworks of sulfidic fractures of quartz veinlets, and crackle-type breccias Sulfides are pyrite or arsenopyrite, with molybdenite abundant at Hemlo	Albite-carbonate-sericite-pyrite at greenschist grade Biotite-calc-silicate-pyrrhotite ± pyrite at amphibolite grade K-feldspar-muscovite ± calc-silicates at Hemlo	Au > Ag As, Te, ± W, Hg, Cu, Mo, Sb	**Malartic, Hemlo, Kerr Addison** (Flow ore), Ross, Beattie, Madsen
Sulfide-rich veins and veinlet zones	Sulfide-rich (25-100% sulfide) veins and veinlet zones with interveining disseminated sulfides Sulfides include pyrite, sphalerite, chalcopyrite, and galena	Sericite-chlorite ± chloritoid at greenschist grade Biotite-garnet-cordierite at amphibolite grade	Ag > Au Cu, Zn, Pb ± As, Te	**Doyon**, Mouska, Copper Rand, Sleeping Giant
Semimassive to massive sulfide lenses	Semi-massive to massive sulfide lenses or pyrite, chalcopyrite, sphalerite, and galena, with pyrrhotite and magnetite in some cases	Sericite-quartz ± chlorite or garnet-biotite Quartz-andalusite-kyanite-pyrophyllite	Ag > Au Cu, Zn, Pb, As ± Te, Sb	**Horne, LaRonde-Penna**, Bousquet 2-Dumagami, Bousquet 1

Table 1.1 Summary of characteristics of various styles of mineralization with examples from the Superior Province. Bolded examples have produced > 5 Moz Au. Modified from Robert et al. (2005).

Using diverse isotopic and fluid inclusion studies, the gold mineralizing fluid in lode gold deposits has been characterized as an aqueous-carbonic fluid with low salinity (<6 wt.% NaCl equiv) also containing CH_4, N, K and S (Kerrich et al., 2000). The fluid is generated at 1.5 ± 0.5 kbar (5-10 km) and at temperatures of 350 ± 50°C (Dubé and Gosselin, 2007). The source of the mineralizing fluid is still debated, with authors suggesting fluid origins such as magmatic (Burrows et al., 1986), metamorphic-derived (Kerrich and Fyfe, 1981), and deeply circulating meteoric water (Nesbitt et al., 1986). Fluids derived from metamorphic devolatilization are now more widely accepted due to the results obtained from fluid inclusion investigations (Bodnar et al., 2014). Oxygen isotope data on lode gold deposits are often ambiguous since the fluid typically has a $\delta^{18}O$ of 6 to 11 ‰ and δD of -30 to -80‰ and therefore overlaps between the magmatic or metamorphic fields (McCuaig and Kerrich, 1998). Alteration and distinct elemental associations can be used as vectors towards the main ore zone with lode gold deposits. The alteration typically consists of quartz, iron-carbonate, mica (±albite), chlorite and pyrite (± scheelite and tourmaline) in greenschist facies, and biotite, amphibole, pyrite, pyrrhotite, aresenopyrite, diopside and garnets in amphibolite facies (Kerrich et al., 2000; Groves et al., 2003; Dubé and Gosselin, 2007). Parker (2000) used alteration minerals as vectors towards ore in the Red Lake gold camp where it was shown that Fe-carbonate was always more proximal to the major gold deposits whereas Ca-carbonate was found more distally to the deposits. Enrichment in Au, Ag (± As, Sb, Te, W, Mo, Bi, B, Cu, Zn) found as native phases or within minerals (arsenopyrite, pyrite, sheelite, molybdenite, chalcopyrite, sphalerite, etc.) can also be used as vectors towards ore (Groves, 1993; Kerrich et al., 2000; Fig. 1.1; Table 1.1)

With the accumulation of evidence in favour of a metamorphic origin for the gold mineralizing fluid, it is still important to consider other proposed models for lode gold deposits. The main models are: (1) Tonalite-Trondhjemite-Granodiorite (TTG) model: due to the close association of gold deposits and TTG plutons in the Superior Province, it has been suggested that the gold mineralizing fluid originated as

magmatic fluids exsolved from TTG intrusions (Burrows and Spooner, 1987); (2) Granulitization model: granulitization of the mid- to lower-crust caused by a large fluid flux of mantle CO_2 into the lower crust. This model was used to explain the gold found in the Kapuskasing Structural Zone in the Superior Province (Cameron, 1988); (3) Gold-shoshonite association 1, the spacial association between gold, shoshonites (lamprophyres), and structures is interpreted to signify a common geodynamic setting (Kerrich and Wyman, 1990); (4) Gold-shoshonite association 2, shoshonites (lamprophyres) are gold-rich as they are derived from the core-mantle boundary (Rock et al., 1989); (5) Crustal continuum model: recognition that epigenetic lode gold deposits occurring in greenschist facies have their counterparts in amphibolite to granulite facies. All are broadly coeval with peak metamorphism (Groves, 1993); (6) Delayed dehydration: dehydration of thickened greenstones during thermal rebound post-collision, with dehydration and mineralization occurring roughly 100 m.y. after collision (Hodgson et al., 1989); (7) Late deep metamorphic activity: late gold mineralization in the supercrustal sequences of greenstone belts is related to deep fluid and metamorphic activity (Jemielita et al., 1990). Kerrich and Cassidy (1994) provided a summary with the strengths and weaknesses of the previously mentioned models.

Despite the large amount of research conducted on lode gold deposits there are still many unknowns regarding the specifics of the genesis of these deposits. These include: (a) constraining the tectonic environment and accurately dating mineralization; (b) understanding the source of the fluids and metals; (c) architecture of hydrothermal system; (d) the depositional mechanism for gold (Groves et al., 2003).

1.4 Location and Access

The Laird Lake property, currently held by Bounty Gold Corp; is in the Red Lake area of north-western Ontario, roughly 565 km by road (430 km direct) northwest of Thunder Bay (Fig. 1.2). The property is located at the intersection of the Killala and Mulcahy Townships, and Medicine Stone Lake

area. It lies approximately 22 km south-west of the town of Red Lake and can be accessed by taking Highway 618 to Flat Lake-Suffel Lake Road (gravel) roughly 2 km past the town of Madsen. Thirteen km past the exit on Flat Lake-Suffel Lake Road is the turn-off onto Draco Medicine Stone Road (gravel/dirt) which leads to the Laird Lake property. Once on the property, the road extends to Molar Lake south of Laird Lake and additional ATV roads from the main road can be used to access the eastern half of the property. The western portion is accessed by boat with a portage between Laird and Lee lakes.

Figure 1.2 Simplified map of the geology of Ontario. Modified from Ontario Geological Survey (1995).

Chapter 2 – Regional Geology

2.1 Superior Province

The Superior Province is the world's largest Archean craton with a total surface area covering ~1,572,000 km^2 (Fig. 2.1; Thurston et al., 1991; Stott, 1997). It is the core component of Laurentia; a larger assembly of Archean provinces amalgamated during Proterozoic orogenic events (Hoffman, 1988). The Superior Province is bounded by Proterozoic orogens that include of the Trans-Hudson Orogen (2.07-1.92 Ga) to the north-west, the New Quebec Orogen (2.17-1.79 Ga) to the north-east, the Grenville Province (1190-980 Ma) to the south-east and the Penokean Orogen (1.88-1.85 Ga) to the south (Rivers, 1997; Schulz and William, 2007; Houle and Perreault, 2008; Corrigan et al., 2009).

The Superior Province is mainly composed of granite-greenstone terranes separated by metasedimentary belts, plutonic zones and high-grade gneiss terranes located in the northern and southern portions of the craton (Card, 1990). Major crust-forming events occurred at 3.1-2.8 Ga and again at 2.75-2.65 Ga where volcanic, sedimentary and plutonic domains were formed (Card and King, 1992). The province was previously subdivided into subprovinces but more recent mapping and improved age determinations now allows for more precise subdivisions of the craton into superterranes, terranes, domains and lithotectonic assemblages, however, the presence of superterranes in the Superior Province is still debated (Stott et al., 2007, 2010). For more detailed information on the most current subdivision terminology (superterranes, terranes, domains and lithotectonic assemblages), refer to Stott et al. (2010) and Percival et al. (2012).

Major subdivisions in the province are recognised by fault boundaries, contrasting lithological assemblages, isotopic character, geochemistry, metamorphic grade, structural styles, geophysical properties and ages (Card, 1990; Stott, 1997; Stott et al., 2010). Card and Ciesielski (1986) identified four

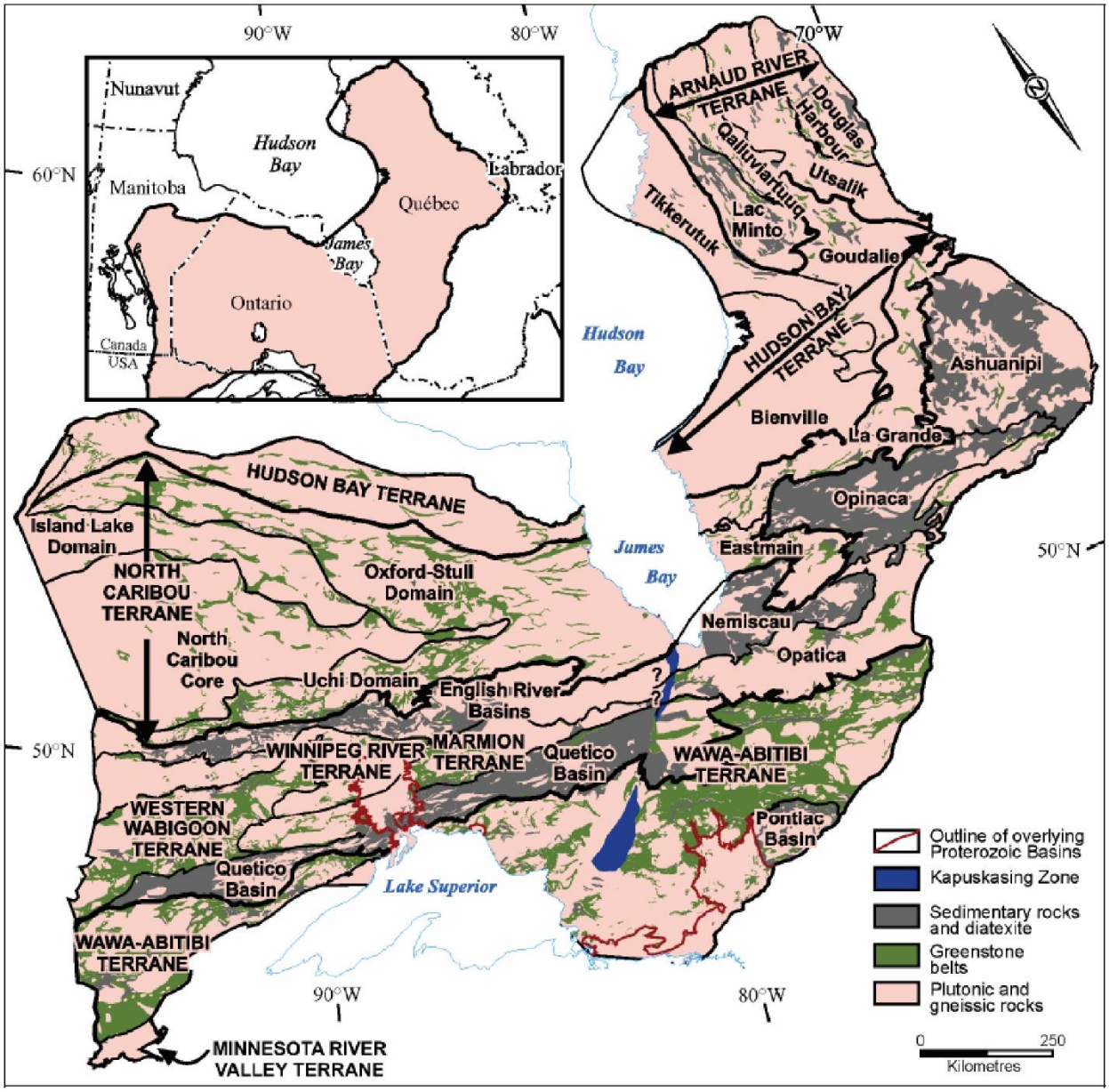

Figure 2.1 Divisions of the Superior Province (From Stott et al., 2010)

different types of subprovinces; volcano-plutonic, metasedimentary, plutonic and high-grade gneiss. Volcano-plutonic domains such as the Wawa-Abitibi, Wabigoon and Uchi (Fig. 2.1) are dominated by metavolcanic-rich supracrustal rocks that comprise greenstone belts, bordered and intruded by syn- to post-orogenic granitoid plutons (Stott, 1997). Greenstone belts themselves are composed of various lithotectonic assemblages that record complex Archean geodynamic environments such as ocean floor, plateaux, island arc and back-arc settings (Card, 1990; Percival, 2007). Thurston and Chivers (1990) and

more recently, Thurston (2015) has demonstrated the presence of lithostratigraphic associations in greenstone belts: (1) quartzite-carbonate platforms; (2) shallow- to deep-water komatiite-tholeiite sequences; (3) deep-water komatiite-tholeiite sequences; (4) deep-water bimodal volcanic sequences; (5) shallow-water to emergent bimodal successions; and (6) "Timiskaming-type" sequences of fluvial sedimentary rocks and calc-alkaline to alkaline volcanic rocks. Greenstone belts display complex multi-deformational histories with metamorphic grades ranging from greenschist to lower-amphibolite facies (Card and Ciesielski, 1986; Easton, 2000). The volcano-plutonic domains host most of the major Au, Cu, Zn and Fe deposits found in greenstone belts within the Superior Province (Card and Ciesielski, 1986). Metasedimentary domains such as the Quetico, Pontiac and English River (Fig. 2.1) mostly consist of long linear belts of turbiditic greywacke and pelites, which have been metamorphosed to schists, paragneiss and migmatites, and are later cut by large S-type granites (Thurston et al., 1991). Plutonic domains such as the Berens River and Winnipeg River (Fig. 2.1) are characterized by the scarcity of supracrustal rocks and abundance of plutonic rocks consisting of tonalitic gneiss with common mafic enclaves and massive older sodic plutons and younger potassic plutons (Beakhouse, 1983). Last, high-grade gneiss domains such as the Pikwitonei (combined with the Hudson Bay Terrane by Stott et al. (2010)) and Kapuskasing Structural Zone (Fig. 2.1) display metamorphic grades from amphibolite to granulite facies with domal structural patterns and well-developed gneisses showing evidence of multiple phases of deformation (Card and Ciesielski, 1986).

Percival et al. (2006) proposed a five step accretionary model for the accretion of landmasses to produce the Superior Province by 2.6 Ga. The North Caribou Core or possibly the Hudson Bay Terrane have been interpreted as the nucleus that terranes amalgamated to during the assembly of the Superior Province (Goodwin, 1986; Thurston et al., 1991; Percival et al., 2006; Percival et al., 2012). Two periods of major accretional events occurred, one between 2.9-2.8 Ga (pre-Kenoran Orogeny) and another at 2.7 Ga (Kenoran Orogeny). The pre-Kenoran Orogeny events occurred mostly in the northern

domains with the exception of the complex deformational history of the Minnesota River Valley terrane. With more recent age constraints on deformational events, the ~2.7 Ga Kenoran Orogeny is now subdivided into five discrete accretional events. Percival et al. (2006) recognized the following orogenies: Northern Superior (2.71 Ga), Uchian (~2.72-2.70 Ga), Central Superior (2.71-2.70 Ga), Shebandowanian (2.69 Ga), and Minnesotan (2.68 Ga). The southwards subducting Northern Superior orogeny amalgamated the Northern Superior superterrane (renamed by Stott et al. (2010) as the Hudson Bay Terrane) to the northern margin of the North Caribou Superterrane (renamed by Stott et al. (2010) as North Caribou terrane), trapping the Oxford-Stull domain between the two (Fig. 2.1). On the southern margin of the North Caribou terrane, the Uchian orogeny drove the northbound subduction of the Winnipeg River terrane, trapping the Uchi domain and producing the English River basin (Fig. 2.1). The Central Superior orogeny includes the amalgamation of the western Wabigoon Terrane to the Winnipeg River Terrane prior to incorporation in the Superior Province (Fig. 2.1). The northward Shebandowanian orogeny juxtaposed the Abitibi-Wawa Terranes to the Superior Province and formed an accretionary wedge to foreland basin to the north known as the Quetico Terrane (renamed by Stott et al. (2010) as Quetico basin; Fig. 2.1). The northward subducting Minnesotan orogeny represents the amalgamation of the ancient Minnesota River Valley Terrane to the Superior Province, also creating the Pontiac metasedimentary belt (renamed by Stott et al. (2010) as the Pontiac Basin) in the eastern Superior Province (Fig. 2.1). Additional models of the assembly of the Superior Province are noted in Percival et al. (2006).

2.2 North Caribou Terrane

The North Caribou Terrane (NCT; Fig. 2.2) is the largest Mesoarchean terrane in the Superior Province and is located on the northwestern margin of the craton (Fig. 2.1; Percival, 2007). The NCT has been interpreted to have been amalgamated by 2.87 Ga with evidence for ca. 3.0 Ga basement crust (Percival et al., 2006). It mainly consists of Mesoarchean batholiths with Meso- to Neoarchean

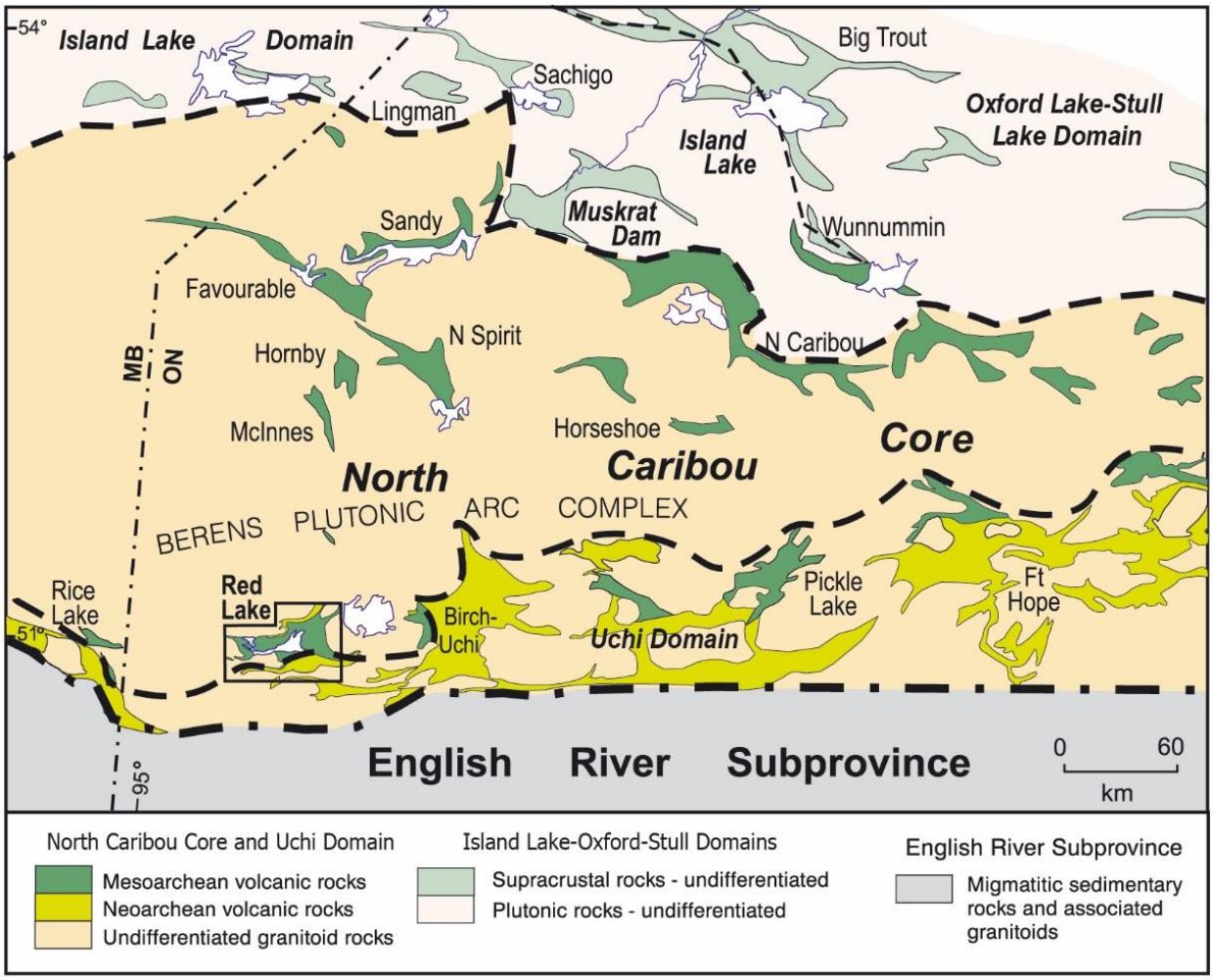

Figure 2.2 Map of the North Caribou Terrane, including the Oxford Lake-Stull, Island Lake and Uchi domains, and the North Caribou Core, more specifically, showing the location of the Red Lake greenstone belt. (Modified from Sanborn-Barrie et al., 2004 and Stott et al., 2010)

greenstone belts representing early rift-related and younger arc volcanism (Percival, 2007; Stott et al., 2010). Located in greenstone belts of the central NCT, sequences of ~2.9 Ga quartz-arenite carbonate-komatiite have been interpreted as platformal cover by Thurston et al. (1991) and plume-related rift sequences by Hollings and Kerrich (1999). Two main episodes of plutonism and metamorphism are recorded in the NCT at 2.89-2.895 and 2.85-2.89 Ga (Stott et al., 2010). Neoarchean arc assemblage crust has been added to the southern and northern margins of the NCT and have plutonic equivalents within the Berens River plutonic complex (Percival et al., 2006; Stott et al., 2010). Douglas (1973) previously subdivided the area into the Sachigo Volcanic Belt, Berens Plutonic Belt and Uchi Volcanic

Belt, but more recent work by Stott et al. (2010) now has the area consisting of three domains and a central core.

2.2.1 North Caribou Core

The North Caribou Core (NCC) is located in the west-central portion of the NCT and has been interpreted as the nucleus to which the Island-Lake, the Oxford-Stull and Uchi domains were added to post-2.87 Ga (Fig. 2.1; Percival et al., 2006; Stott et al., 2010). It consists of 3.0-2.7 Ga plutons with several greenstone belts that range in age from 2.9-3.0 Ga and rarely as young as 2.73 Ga (Fig. 2.2; Thurston et al., 1991; Stott, 1997; Biczok et al., 2012). These include the North Caribou, Horseshoe Lake, North Spirit Lake, Sandy Lake and Favourable Lake greenstone belts. The Berens River plutonic complex (BRPC) dominates the central and south-western side of the NCT and extends as far east as the North Spirit Lake and Lang Lake greenstone belts to the south, covering an area of roughly 35,000 km^2 (Corfu and Stone, 1998). The BRPC records continuous magmatism from 2.75-2.69 Ga and intrudes 3.0-2.8 Ga tonalitic basement (Corfu and Stone, 1998; Percival et al., 2006; Percival, 2007). The oldest intrusions in the BRMC record interaction with mafic magmas, interpreted as the result of basaltic underplating, whereas younger intrusions may have been partial melts of this basalt (Corfu and Stone, 1998). Corfu and Stone (1998) and Percival et al. (2006) suggested that the intrusive suites of the Berens River complex have extrusive equivalents within the Confederation, Graves and St. Joseph assemblages of the Uchi domain.

2.2.2 Island Lake Domain

The Island Lake domain (ILD) is located in the north central part of the NCT and south of the Oxford-Stull domain (Fig. 2.2). It consists of plutonic rocks with several small greenstone belts with volcanism at 2.89, 2.85 and 2.74 Ga (Parks et al., 2006; Percival et al., 2006). The greenstone belts include the Island Lake, Muskrat Dam Lake and Pierce-Ponask-Sachigo greenstone belts (Thurston et al.,

1991). The ILD has a similar magmatic history to the Oxford-Stull domain, however, Nd isotope data suggests that the ILD has been locally contaminated by older crust whereas the Oxford-Stull domain has a more juvenile signature (Stott et al., 2010). Thurston et al. (1991) determined that the ILD was younger than the North Caribou Core based on geochronology and the continuity of shear zones. Later work concluded that the previously known Munro and Island Lake terranes were built on ca. 3.0 Ga pre-Kenoran crust that has been suggested to be the northern extent of the North Caribou Core (Stevenson and Turek, 1992; Corfu and Lin, 2000; Parks et al., 2006).

2.2.3 Oxford-Stull Domain

The Oxford-Stull domain (OSD) is located in the northeast portion of the NCT where it merges with the Uchi domain (Fig. 2.2; Stott et al., 2010). It consists of multiple 2.83-2.71 Ga greenstone belts and intrusions that show juvenile signatures and have been interpreted to represent material accreted to the northern border of the NCT (Lin et al., 2006; Percival et al., 2006; Percival, 2007). Neo- to Mesoarchean Nd model ages, and positive ε_{Nd} values indicate that the domain evolved in an oceanic setting, until it was juxtaposed alongside the Hudson Bay Terrane (Percival, 2007; Stott et al., 2010). The domain has faulted contacts to the north and south that formed during docking of adjacent domains (Skulski et al., 2000; Stott et al., 2010).

2.2.4 Uchi Domain

The Uchi domain (Fig. 2.2) is a linear belt located on the southern margin of the NCT that extends the entire length of the northwestern Superior Province (Fig. 2.1). Magmatic U-Pb zircon ages and Nd model ages are comparable with those of the Island Lake domain (Stott et al., 2010), yet, high-resolution aeromagnetic images support the suggestion that the eastern Uchi domain merges with the Oxford-Stull domain on the eastern edge of the NCT (Stott, 2008). The Uchi domain consists of magmatic

and sedimentary packages that record roughly 300 m.y. of tectonostratigraphic evolution (Stott and Corfu, 1991; Hollings and Kerrich, 2000; Sanborn-Barrie et al., 2001; Percival, 2007).

Two main packages are recognised in the Uchi; a dominantly tholeiitic basalt package with minor komatiite units, and a dominantly calc-alkaline andesite, dacite and rhyolite package with tholeiitic basalts (Stott and Corfu, 1991). Stratigraphic correlation between the Rice Lake, Wallace Lake, Red Lake, Confederation Lake, Meen-Dempster Lake, Pickle Lake and Fort Hope greenstone belts show the oldest package reflecting a rift-related sequence beginning ca. 2.99 Ga, followed by extensive intervals of continental or oceanic arc magmatism at 2.94-2.91, 2.90-2.89, 2.85 and 2.75-2.72 Ga (Sanborn-Barrie et al., 2004; Percival, 2007 and references therein). Batholiths within the Uchi domain are mostly felsic in composition and range from syn-volcanic intrusions intruded into older volcanic sequences to late -to post-tectonic intrusions (Williams suite; Stott and Corfu, 1991).

An unconformity or tectonic contact between the Mesoarchean and Neoarchean assemblages represents a ~200-100 m.y. gap in geologic time and is associated with later gold mineralization in the Red Lake and Pickle Lake greenstone belts (Stott, 1997; Sanborn-Barrie et al., 2001; Percival et al., 2006; Young et al., 2006). Gold mineralization within the Uchi domain is often related to D_2 structures which correspond to the Uchian phase of the assembly of the Superior Province (Penczak and Mason, 1997; Menard and Pattison, 1998; Sanborn-Barrie et al., 2004). Stott and Corfu (1991) described a southward younging in the Uchi domain which would reflect addition of crustal units to the growing southern margin of the NCT. Regional-scale deformation and metamorphic zonations that overprint assemblages and plutons within greenstone belts indicate that the tectonic forces to create such patterns are at a much larger scale than the individual greenstone belts, and can be attributed to the Uchian orogeny (Percival et al., 2006).

2.3 Red Lake Greenstone Belt

The Red Lake greenstone belt (RLGB; Fig. 2.3) is located at the boundary between the Uchi domain and the North Caribou Core according to recent modifications to the domain boundary map of Stott et al. (2010). Previously, the belt was situated completely within the Uchi subprovince (Thurston et al., 1991). The RLGB preserves approximately 300 m.y. of geologic activity including multiple episodes of volcanism, sedimentation, plutonism and deformation that range from Meso- to Neoarchean in age, with gold mineralization constrained to the Neoarchean (Corfu and Andrews, 1987; Sanborn-Barrie et al., 2001). The Red Lake gold camp is known to host some of the highest grade gold deposits found in Archean greenstone belts and therefore multiple studies have been carried out to investigate the primary volcano-stratigraphy of the belt along with the controls on gold mineralization (Horwood, 1940a; Ferguson, 1965; Pirie, 1981; Andrews and Wallace, 1983; Andrews et al., 1986; Corfu and Andrews, 1987; Gulson et al., 1993; Parker, 2000a; Sanborn-Barrie et al., 2000; Sanborn-Barrie et al., 2001; Parker, 2002; Dubé et al., 2003).

2.3.1 Tectonic Assemblages

The RLGB includes a total of seven supracrustal assemblages that have been subdivided according to rock type, U-Pb geochronology and geochemistry (Fig. 2.3; Sanborn-Barrie et al., 2001).

2.3.1.1 Balmer Assemblage

The Balmer assemblage is the oldest and most extensive unit, covering roughly 50% of the belt (Fig. 2.3). It dominates the eastern and central parts of the belt with a small sliver of it cropping out south of the Killala-Baird batholith. The nature of this mafic-ultramafic dominated package is favorable for gold deposition due to its high Fe content with additional Fe-rich alteration and, as a result, the Balmer assemblage is host to all major gold camps in the RLGB (Dubé et al., 2001). The Balmer assemblage consists of Fe-tholeiitic basalts, komatiitic basalts and komatiites with minor felsic volcanic

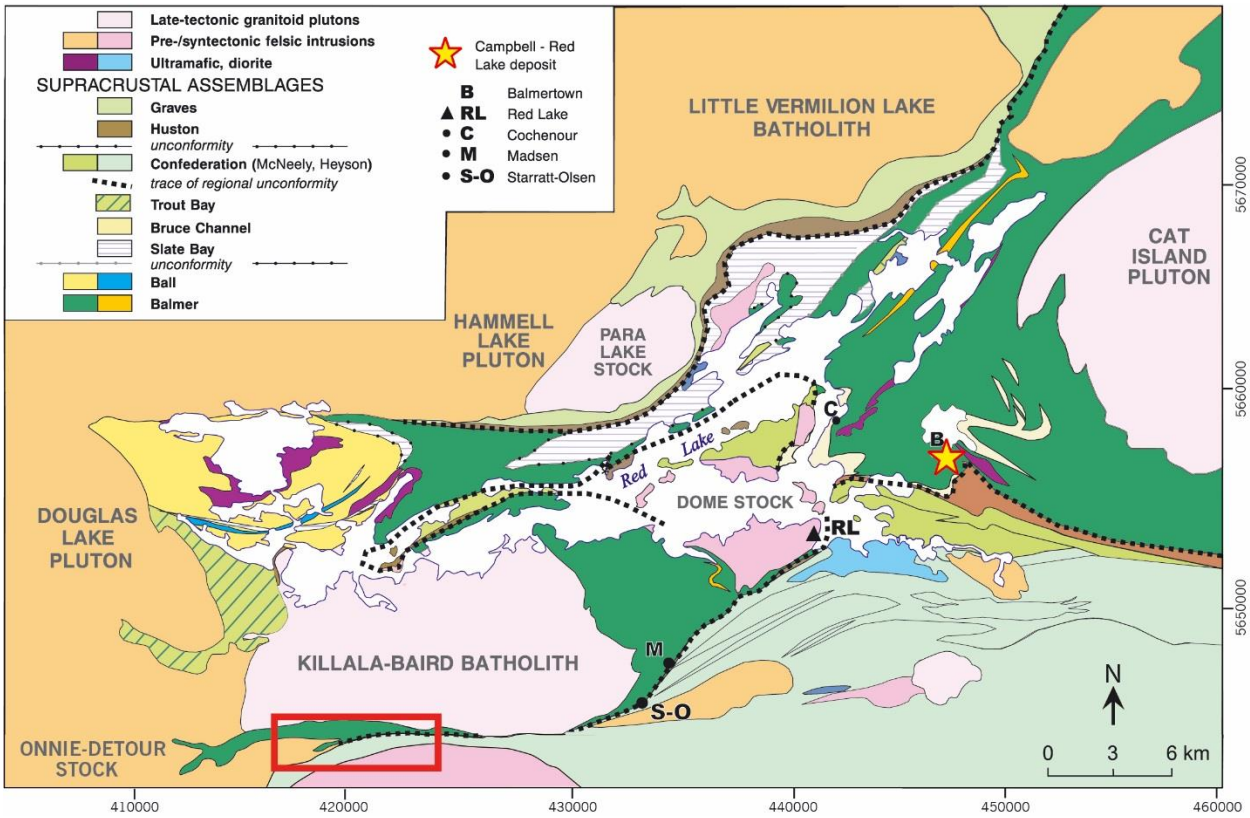

Figure 2.3 Geological map of the Red Lake greenstone belt showing assemblages, intrusive bodies, regional breaks, major gold deposits and the Laird Lake property highlighted in red. Modified from Sanborn-Barrie et al., 2004.

rocks, chert-magnetite iron formations, fine-grained clastic rocks and mafic to ultramafic intrusions (Sanborn-Barrie et al., 2000, 2001, 2004). A compilation of ages obtained from various felsic volcanic units (flows and tuffs) by Corfu and Wallace (1986) and Corfu and Andrews (1987) determined an age of 2.99-2.96 Ga for the assemblage. The basalts are commonly pillowed and have relatively high Ti contents up to 2 wt.%. The komatiites to komatiitic basalts are pillowed or display spinifex textures. Sanborn-Barrie et al. (2004) separated the assemblage in to lower, middle, and upper sequences. The lower sequence is characterized by TiO_2 >1.5 wt.% and light rare-earth element (LREE) enrichment, with an abrupt change to the middle sequence marked by the appearance of andesitic flows and basaltic units with TiO_2 <1.5 wt.% and flat to depleted LREE trends, whereas the upper sequence contains rocks with the lowest TiO_2 (<1.3 wt.%) and depleted LREE profiles. The komatiites to komatiitic basalts are of the Al-undepleted variety and typically have depleted LREE trends with negative Nb anomalies

(Tomlinson et al., 1998; Hollings et al., 1999). Epsilon Nd values of the basalts range from +3.3 (indicating depleted mantle at 3 Ga) to 0.3 (indicating a longer lived history of LREE enrichment) whereas the komatiites range from -2.2 to -1.5 (Tomlinson et al., 1998; Sanborn-Barrie et al., 2001). Tomlinson et al. (1998) interpreted the ε_{Nd} komatiite data together with REE geochemistry to represent the evolution of an enriched source at ca. 3.4 Ga, which underwent melting at ~3.1 Ga to leave behind a LREE depleted residue that was source to the komatiites generated at ~3.0 Ga, whereas Hollings and Kerrich (1999) interpreted the data to be the result of crustal contamination.

The widespread occurrence of pillow basalts, and the minor amount of sedimentary rocks (mainly chemical), indicates the Balmer assemblage was erupted in a sediment-starved subaqueous environment. The presence of widespread komatiites infers plume magmatism (Tomlinson et al., 1998; Sanborn-Barrie et al., 2000, 2001, 2004). The associated intercalated felsic volcanic rocks within the assemblage have been interpreted to be the result of a plateau-arc interaction (Hollings et al., 1999). A regional study by Hollings et al. (1999) determined that crustal contamination within the Balmer assemblage can account for the geochemical anomalies. Together with negative Nb anomalies, negative epsilon Nd values in the ultramafic rocks could indicate the existence of older continental crust in the RLGB. However, such sialic basement has not yet been identified (Sanborn-Barrie et al., 2004).

2.3.1.2 Ball Assemblage

The Ball assemblage is situated in the northwestern portion of the RLGB (Fig. 2.3) and comprises a wide range of rock types interpreted to be in tectonic contact with the Balmer as the two assemblages young toward one another (Sanborn-Barrie et al., 2001). Corfu and Wallace (1986) identified two major periods of volcanism; the lower unit has a U-Pb age of 2940.1 +2.4/-1.7 Ma and the upper at 2925.4 +3.4/-2.9 Ma. The oldest package is dominated by felsic flows and pyroclastic rocks, calc-alkaline basalt with lesser basaltic komatiites and a variety of sedimentary rocks including stromatolite-bearing

marbles, conglomerate, quartzite and chert-magnetite ironstones (Sanborn-Barrie et al., 2000, 2001, 2004). The sedimentary units deposited during the ~15 m.y. volcanic quiescence have been interpreted to reflect shallow water conditions (Sanborn-Barrie et al., 2004). A younger package comprised of felsic to intermediate flows intercalated with tholeiitic basalts to andesites and pillowed komatiites directly overlies the stromatilitic carbonate rocks (Sanborn-Barrie et al., 2004).

Volcanic rocks of the Ball assemblage typically have lower TiO_2 (<0.5 wt.%) compared to Balmer assemblage rocks and show a wide range in silica content (Sanborn-Barrie et al., 2001). The komatiites are of the Al-undepleted variety (Hollings et al., 1999) and show an ε_{Nd} value of +2.2, consistent with a depleted mantle source at 2.9 Ga (Sanborn-Barrie et al., 2001). Sanborn-Barrie et al. (2004) interpret these data as reflecting intra-arc extension which would have permitted the magmas to ascend. Felsic rocks of the Ball assemblage have ε_{Nd} values ranging from +0.8 to +1.1 indicating magmas derived from a LREE-enriched mantle source (Sanborn-Barrie et al., 2001). The trace element geochemistry suggests contamination of the magmas by differentiated crust, on the basis of negative Nb anomalies and enrichment in LREE and LILE (Hollings, 1998; Sanborn-Barrie et al., 2001). Earlier studies conducted by Henry et al. (2000) indicated that rocks from 2.92-3.02 Ga in the western Superior Province formed during a period of crustal growth, with ε_{Nd} values between 0 and +3 interpreted to record mixtures of juvenile and older crustal end-members. Two felsic rock samples of the Ball assemblage yielding an ε_{Nd} value of +1 and T_{2DM} (Nd model ages by two-stage calculation) of 3.05 Ga were used to suggest the recycling of ca. 3 Ga or older crust to form the volcanic unit, however, Henry et al. (2000) also states that since the T_{2DM} ages is slightly older than the age of crystallization, the ε_{Nd} value can still represent a mixture of 2.92-3.02 Ga depleted mantle material and crust from the older terranes.

2.3.1.3 Slate Bay Assemblage

The clastic metasedimentary rocks of the Slate Bay assemblage encompass the north portion of the RLGB (Fig. 2.3). Rock types include feldspathic wacke interbedded with lithic wacke, argillite, conglomerate and quartzose arenite. The quartz-rich units that contain clasts of vein quartz, felsic volcanic rocks, and fuchsite-bearing material have been interpreted to have been derived from felsic and ultramafic protoliths (Sanborn-Barrie et al., 2000, 2001, 2004). Corfu et al. (1998) dated a detrital zircon at 2916 ± 4 Ma, providing the maximum age of deposition for the Slate Bay assemblage whereas the minimum deposition age of 2850 Ma was acquired by dating the overlying intermediate tuff and lapilli tuff of the Trout Bay assemblage (Sanborn-Barrie et al., 2004). The sedimentary sequences seen in the Slate Bay assemblage suggest fluvial deposition of material derived from the erosion of the Ball, and to a lesser extent, the Balmer assemblages. Locally, the contact between the Balmer and Ball assemblages is covered by Slate Bay clastic rocks, possibly indicating re-deposition of Ball material onto Balmer basement (Sanborn-Barrie et al., 2004).

2.3.1.4 Bruce Channel Assemblage

The Bruce Channel assemblage is observed in the eastern portion of the belt, in close proximity to the mineralized Balmer mafic volcanic rocks (Fig. 2.3). Initial explosive volcanism recorded by intermediate volcaniclastic fragmental rocks has been dated at $2893.5\ ^{+1.4}_{-1.2}$ Ma by Corfu and Wallace (1986) and confirmed by Corfu and Andrews (1987). This unit is locally overlain by chert-pebble conglomerate, crossbedded wacke, siltstone and quartz-magnetite iron formation, interpreted to have been deposited in a marine setting (Sanborn-Barrie et al., 2001).

The calc-alkalic volcanic rocks are dacites to rhyodacites and are enriched in LREE and LILE, typically with negative Nb anomalies. Initial ε_{Nd} of a dacite sample yielded a value of +2.0 indicating new crustal growth from a depleted mantle source (Henry et al., 2000; Sanborn-Barrie et al., 2001). A

systematic change is observed in the isotopic data; from the Balmer to the Bruce Channel assemblage, with volcanic rocks showing more isotopically depleted mantle signatures in the Bruce Channel which has been interpreted to reflect crustal growth at a juvenile continental margin (Sanborn-Barrie et al., 2004).

2.3.1.5 Trout Bay Assemblage

The Trout Bay assemblage is mostly situated in the south-western portion of the RLGB (Fig. 2.3) and was considered part of the Balmer assemblage until Sanborn-Barrie et al. (2001) determined it was a separate volcano-sedimentary package based on new field, geochronological and geochemical data. The assemblage consists of a lower and upper sequence, separated by a middle fragmental unit composed of mafic volcanic and chemical sedimentary fragments appearing to be pyroclastic in origin (Sanborn-Barrie et al., 2001). The lower sequence consists of LREE-depleted basalts facing towards the northeast, clastic rocks, intermediate tuffs dated at 2853 ± 1 Ma (Skulski (unpublished) referenced in Sanborn-Barrie et al., 2004) and chert-magnetite iron formation. The upper sequence is composed of pillowed basalts capped by oxide-facies iron-formation and interbedded siltstone. The mafic volcanic rocks have very low overall trace-element concentrations and are depleted in LREE and LILE, display negative Nb anomalies and show ε_{Nd} values of +2 and +1.8, interpreted to represent a depleted mantle source with negligible crustal contamination (Sanborn-Barrie et al., 2001; 2004).

2.3.1.6 Confederation Assemblage

The Confederation assemblage is widespread throughout greenstone belts of the eastern to central Uchi domain and in the RLGB it is situated at the southern margin of the belt (Fig. 2.3; Sanborn-Barrie et al., 2004; Percival et al., 2006). The assemblage is separated into two distinct volcanic packages; the McNeely and Heyson sequences. The calc-alkalic McNeely package, dated at 2745-2742 Ma, is situated in the center of the RLGB and is composed of intermediate to felsic volcanic rocks

including intermediate tuff breccia, lapilli tuff, and feldspar-phyric amygdaloidal pillowed basalts (Corfu et al., 1998; Sanborn-Barrie et al., 2001). This sequence typically has less than 1 wt.% TiO_2, is LREE and LILE-enriched, has negative Nb anomalies, and is depleted in HREE and HFSE. Sanborn-Barrie et al. (2004) described the felsic metavolcanic rocks of this sequence as the FI-type of Lesher et al. (1986) with steep chondrite-normalized REE patterns, weakly negative to moderately positive Eu anomalies, high Zr/Y, low abundances of HFSE and high abundances of Sr.

The mainly tholeiitic Heyson sequence, dated at ca. 2739 Ma (rhyolitic crystal tuff; Corfu and Wallace, 1986), includes massive to pillowed basaltic andesites with feldspar phenocrysts, quartz-feldspar crystal tuff, FIII type rhyolite (defined by Lesher et al. (1986) as having relatively flat REE patterns, negative Eu anomalies, low Zr/Y, and variable abundances of HFSE and Sr) and basalt (Sanborn-Barrie et al., 2001, 2004). The tholeiitic basalts and andesites are locally intercalated with calc-alkalic volcanic rocks in the southeastern to central part of the belt near the Madsen and Keg Lake areas (Fig. 2.3). The felsic volcanic rocks of the Heyson sequence are spherulitic and appear as lobe-hyaloclastic flows indicating their proximity to a subaqueous fissure vent system and sea floor spreading (Parker, 1999). The geochemistry of the Heyson sequence is very similar to the McNeely sequence; LREE and LILE enrichment, negative Nb anomalies but with flat HREE and HFSE on an extended REE diagram.

Initial ε_{Nd} of a dacitic tuff from the McNeely sequence yielded values of +1 to +0.8 whereas a basalt from the Heyson sequence yielded an initial ε_{Nd} value of +0.77 and a rhyolitic tuff has an initial ε_{Nd} of +2.9. Sanborn-Barrie et al. (2004) suggested that the Confederation assemblage started off as a shallow marine to subaerial arc (McNeely) on a Mesoarchean continental margin, with later intra-arc extension and eruption of high temperature, tholeiitic, FIII rhyolite and tholeiitic basalt (Heyson). Henry et al. (2000) suggested that a period of crustal growth between 2.67 to 2.76 Ga in the western Superior Province formed rocks with ε_{Nd} values between -8 and +4, where the range in values is caused by mixing of depleted mantle-like sources and crustal end-members. The majority of the Confederation

assemblage ε_{Nd} values range from +3 (depleted mantle) and -1 (ca. 3.0 Ga crustal values) and representing a time of new crustal growth from the depleted mantle, as well as recycling of older crust (Henry et al., 2000)

Elsewhere in the Uchi domain (Meen-Dempster greenstone belt), the Confederation assemblage is interpreted to represent a back-arc environment which allows for the wide variety of geochemically distinct volcanic rocks (Hollings et al., 2000). The contact relationship between the Confederation assemblage and the Mesoarchean assemblages is locally covered by the Huston assemblage, however, Sanborn-Barrie et al. (2004) interpreted the angular unconformity as erosional and/or structural. The unconformity is marked by the presence of a polymictic conglomerate (Austin tuff) at the Madsen mine, which yielded Balmer- and Ball-age detrital zircons (Sanborn-Barrie et al., 2001). Additionally, Sanborn-Barrie et al. (2004) proposed that as the Balmer is cut by 2.75-2.74 Ga felsic intrusions, combined with the Mesoarchean inheritance in Confederation volcanic rocks, there is likely a stratigraphic relationship between the two. Other authors such as Stott (1997) and Kerrich et al. (1999) imply an allochtonous model where the Mesoarchean assemblages and Confederation assemblage have been tectonically juxtaposed.

2.3.1.7 Huston Assemblage

The Huston assemblage consists of a regionally extensive polymictic conglomerate that separates the Meso- to Neoarchean assemblages (Fig. 2.3). The unit overlies the McNeely sequence but underlies the Graves assemblage in a sequence of thin veneers of coarse and fine clastic detritus to thick sections of well bedded argillite and turbiditic wacke (Sanborn-Barrie et al., 2001, 2004). Detrital zircons from two basal conglomerate units show a peak in age at ca. 2.74 Ga indicating a Confederation origin. The sedimentary package has been interpreted to have been deposited in a marine environment during a hiatus in Neoarchean volcanism (Sanborn-Barrie et al., 2004).

2.3.1.8 Graves Assemblage

The Graves assemblage is located at the northern margin of the RLGB and represents the youngest volcanism in the belt with an age of at 2733 Ma (rhyodacite tuff; Corfu and Wallace, 1986; Fig. 2.3). The calc-alkaline assemblage consists of andesitic to dacitic pyroclastic tuff, and synvolcanic diorite to tonalite, interpreted to represent a shallow-water to subaerial arc complex (Sanborn-Barrie et al., 2001, 2004). The rocks are LREE and LILE-enriched, have a negative Nb anomaly and depletion in HREE and HFSE on a primitive mantle normalize trace element diagram.

2.3.1.9 Plutonism

There are three main episodes of felsic plutonism in the Red Lake greenstone belt. The first episode, at ca. 2730 Ma, is represented by the Graves plutonic suite (Sanborn-Barrie et al., 2004). The Little Vermillion Lake batholith (2731 ± 3 Ma; Corfu and Andrews, 1987) and Douglas Lake pluton (2734 ± 2 Ma; Corfu and Stone, 1998) are synchronous with Graves volcanism and appear to the north and southwest of the belt. These represent the first major felsic to intermediate plutonic event in the RLGB. The Douglas Lake pluton is dominated by biotite tonalite that is LREE-enriched, HREE-depleted and has been interpreted to have formed by partial melting of mafic crust. The Little Vermillion Lake batholith shares many geochemical characteristics with the Douglas Lake pluton, and has been interpreted to have assimilated older sialic crust (Corfu and Stone, 1998). More recent data collected by Sanborn-Barrie et al. (2001; 2004) showed that initial ε_{Nd} values of zero for the Douglas Lake pluton could indicate significant assimilation of older continental crust. The second episode of plutonism, at ca. 2720 Ma, is represented by the Hammell Lake pluton (2717 ± 2 Ma; McMaster, 1987) and multiple additional plutons internal to the belt, some of which are host to gold mineralization, including the 2718 ± 1 Ma Dome Stock (Corfu and Wallace, 1986), the 2720 ± 2 Ma McKenzie Lake stock (Corfu and Andrews, 1987) and the 2720 +7/-5 Ma Abino granodiorite (Corfu and Andrews, 1987). The third plutonic event, at ca.

2700 Ma, is typified by the granodioritic 2704 ± 1.5 Ma Killala–Baird batholith (Corfu and Andrews, 1987), the 2699 Ma Cat Island pluton (Noble, 1989) and the 2699 ± 4 Ma post-ore dikes at the Madsen Mine (Corfu and Andrews, 1987; Sanborn-Barrie et al., 2004).

2.3.2 Deformation and Metamorphism

Multiple deformation events are recorded in the Red Lake greenstone belt. The D_0 event (pre-2.75 Ga) represents a non-penetrative event that is characterized by the overturning of the Balmer assemblage, and is indicated by the opposing facing pillow directions on either side of the angular unconformity seen near the Madsen Mine (Sanborn-Barrie et al., 2001). A stage of penetrative deformation defines the D_1 event (2.744 to 2.733 Ga), which is characterized by north trending, south-plunging F_1 folds and S_1/L_1 fabrics. Sanborn-Barrie et al. (2004) suggested that D_1 deformation may have been a result of a change in plate dynamics between the deposition of the Graves and Confederation assemblages. The D_2 event is defined by east- to northeast-trending structures that are associated with folding (F_2), foliation (S_2) and lineation (L_2); however, southeast-trending folds and fabrics are also associated with this deformation event. D_2 is interpreted to be associated with the Uchian phase of the Kenoran orogeny (Penczak and Mason, 1997; Menard and Pattison, 1998; Sanborn-Barrie et al., 2004). The D_3 event (post-2.7 Ga) is post-collisional and is interpreted to be the result of northeast regional shortening during a late stage within the Uchian phase and occurs as a penetrative fabric coplanar to D_2 fabrics (Dubé et al., 2004; Sanborn-Barrie et al., 2004). Last, the D_4 event is defined by “black line faults”, which are tourmaline-filled hairline faults that are observed to displace ore zones and multiple other rock types (Roger, 1992; Penczak and Mason, 1997; Tarnocai, 2000; Dubé et al., 2004).

Metamorphic grades within the supracrustal rocks of the RLGB are typical of greenstone belt regional metamorphism. The metamorphic pattern outlines a concentric zonation of grades starting with lower greenschist facies (metabasites: actinolite-epidote-chlorite-albite) in the core, to the

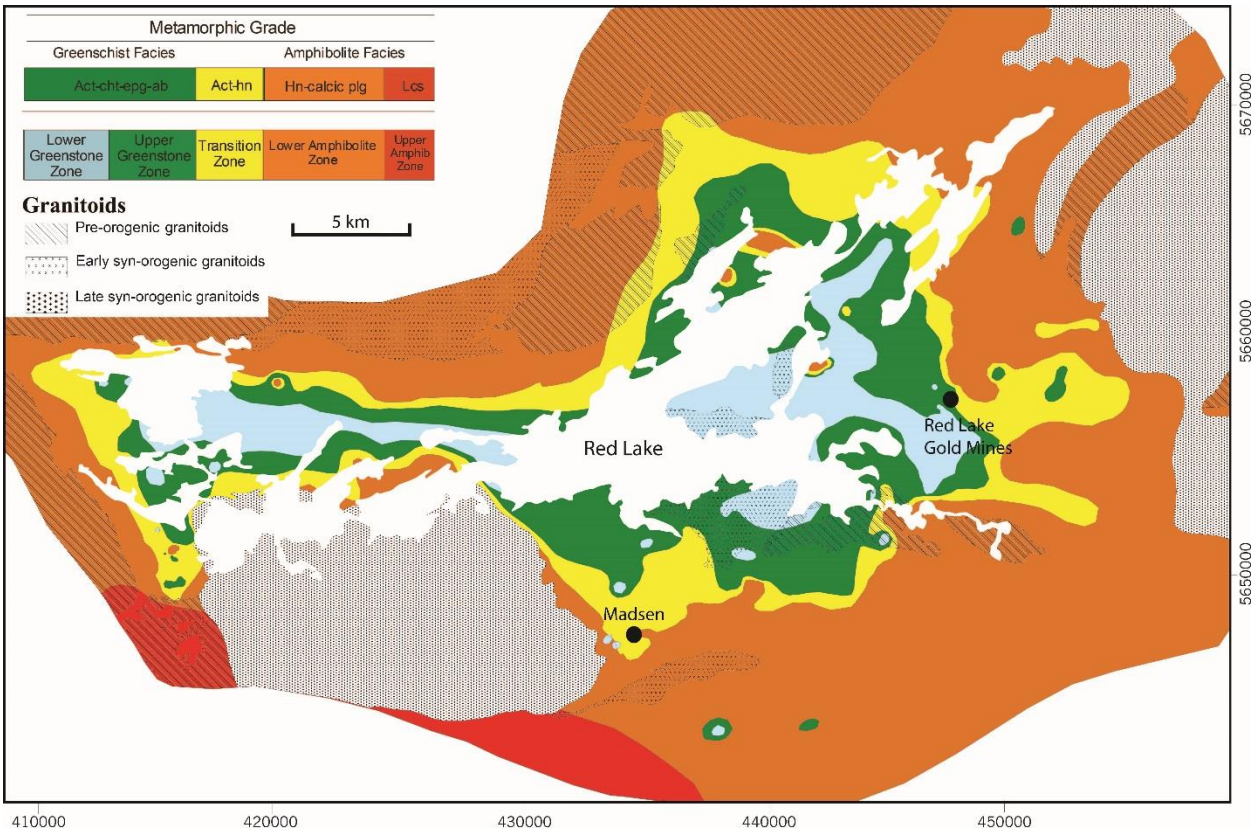

Figure 2.4 Simplified map of the regional metamorphic grades of the Red Lake greenstone belt (modified from Thompson, 2003)

transition zone between greenschist and amphibolite facies and last, upgrading to upper amphibolite facies (metabasites: hornblende-calcic plagioclase) on the outer margins of the greenstone belt (Fig. 2.4; Thompson, 2003). The higher metamorphic grades at the margins have been interpreted to be the result of contact metamorphism by the surrounding plutons (Andrews et al., 1986; Menard and Pattison, 1998; Tarnocai, 2000), however, other interpretations describe the zonations as the result of polyphase tectonometamorphism occurring in close relationship to the main deformation events (Thompson, 2003; Sanborn-Barrie et al., 2004). Relative timing of metamorphic events is constrained by regional syn- and post-tectonic textures in aluminous biotite alteration zones. Sanborn-Barrie et al. (2004) have narrowed down the timing of metamorphic events with cross-cutting relationships, indicating that metamorphic events likely occurred at 2735 Ma (pre-collisional D_1), 2720-2715 Ma (syn-collisional D_2) and ca. 2690 Ma (post-collisional D_3). Major gold camps such as the Red Lake Gold Mines (previously

known as the Campbell-Red Lake deposit) and the past-producing Madsen Mine (Fig. 2.4) lie near the transition zone between greenschist and amphibolite facies, suggesting a link between metamorphic grade and gold mineralization (Thompson, 2003).

2.3.3 Alteration

Hydrothermal alteration in the RLGB is regionally distributed in zoned envelopes that are spatially associated with gold deposits (Fig. 2.5; Parker, 2000a; Sanborn-Barrie et al., 2004). Carbonitization is the most widespread type of alteration, and depending on the type of carbonate present, it can be divided into distal and proximal zones around the gold deposits. Distal alteration is belt-scale and mainly affects the Balmer, Ball, Trout Bay, Bruce Channel and Confederation assemblages (Sanborn-Barrie et al., 2004). It consists of calcite, chlorite, quartz, epidote, seritization of chlorite and plagioclase, and weak potassic alteration and is more prominent within mafic to ultramafic rocks relative to intermediate to felsic metavolcanic rocks, metasedimentary rocks and granitoids (Sanborn-Barrie et al., 2004). The proximal alteration zones are more localized and mostly affect the Balmer, Ball, and Confederation assemblages. These tend to surround areas of abundant gold occurrences and consist of ferroan-dolomite (iron carbonate), potassic alteration seen as sericite/ muscovite, and local fuschite in ultramafic rocks. This type of alteration affects mostly mafic and ultramafic rocks but is still manifested within pyroclastic rocks of the Confederation assemblage and granitoids (Parker, 2000a).

Aluminosilicate alteration including andalusite, staurolite, cordierite, garnet, chloritoid, cummingtonite and anthophyllite is well developed in the Balmer assemblage where the metamorphic grade is up to amphibolite facies. This type of alteration within mafic to ultramafic rocks is typically characterized by depletion in Na_2O, MgO and CaO, enrichment in K_2O and apparent enrichment in Al_2O_3 (Sanborn-Barrie et al., 2004). Dubé et al. (2000) suggested that it was possible that the aluminous assemblage in the basalts could be the metamorphosed product of strong hydrothermal leaching.

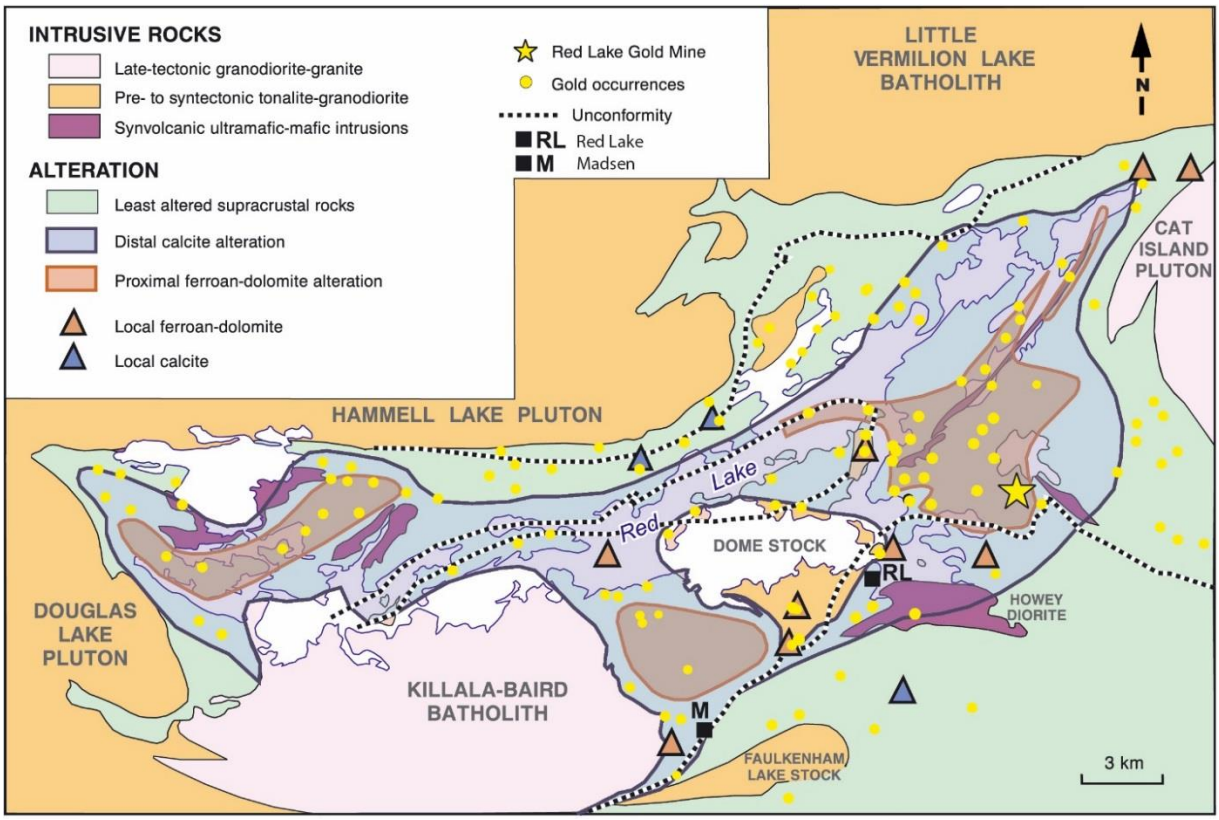

Figure 2.5 Alteration zones of the Red Lake greenstone belt (modified from Sanborn-Barrie et al., 2004)

Silicification is a key alteration type for gold mineralization since most alteration zones are barren unless silicified (Parker, 2000a). This type of alteration is typically accompanied by sulphides such as arsenopyrite, pyrite, and pyrrhotite. Silicification is observed as extension and fault-fill quartz veins, jigsaw-puzzle breccia veins, open-space filling of primary features or as pervasive replacement of ferroan-dolomite (Sanborn-Barrie et al., 2004).

2.3.4 Mineralization

The Red Lake gold camp consists of multiple styles of gold mineralization, the most common being hosted within mafic metavolcanic rocks of the Balmer assemblage in proximity to the regional angular unconformity with the Confederation assemblage; these include the Red Lake Gold Mines, Cochenour Mine and the past-producing Madsen Mine (Dubé et al., 2004; Sanborn-Barrie et al., 2004; Robert et al., 2005). Gold mineralization elsewhere in the belt can be hosted within felsic plutons

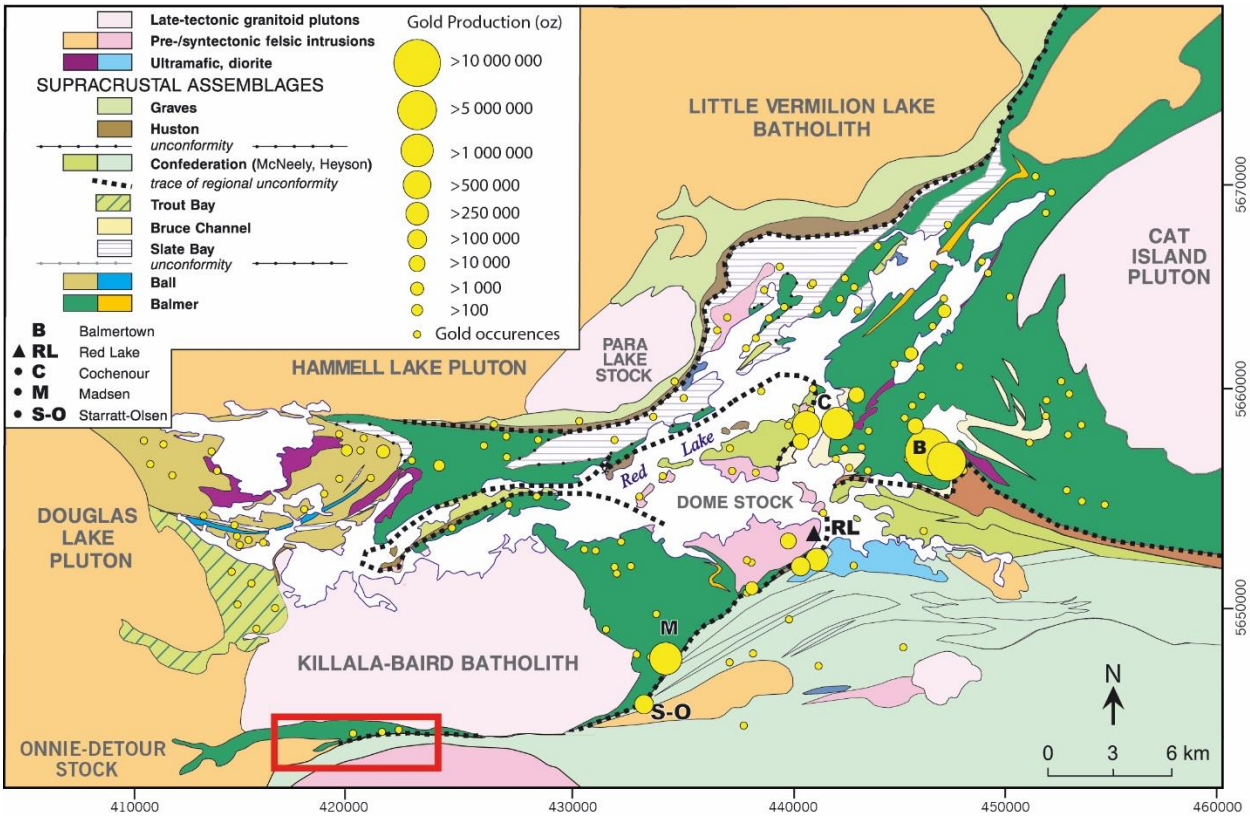

Figure 2.6 Geological map of the Red Lake greenstone belt showing the historical gold production between 1930-present and known gold occurrences. Laird Lake property highlighted in red (modified from Sanborn-Barrie et al., 2004). Gold values from Lichtblau et al. (2016b).

(McKenzie, Gold Eagle, Howey/Hasaga and Buffalo mines) or be stratabound (Bonanza deposit; Blais et al., 2015). The gold within the Red Lake Gold Mines is typically associated with crustiform carbonate veins that have been overprinted by auriferous sulfidic replacement (Robert et al., 2005). The presence of the large crustiform carbonate veins has lead geologists to propose that the deposit had an epithermal origin (Penczak and Mason, 1997) whereas later interpretations suggested multistage alteration and veining event(s) that included pre- and early-D_2 iron-carbonate and aluminous alteration, followed by arsenopyrite-rich silicification and gold precipitation (Dubé et al., 2004; Robert et al., 2005). Dubé et al. (2000) has suggested a different origin for the Madsen deposit, similar to a high-temperature gold deposit or gold skarns hosted in mafic metavolcanic rocks. Gold mineralizing events at the Campbell–Red Lake deposit are estimated to have occurred between 2723 and 2712 Ma, based on

timing constraints related to the intrusion of the Dome and McKenzie Island stocks, Abino granodiorite and the Hammel Lake batholith, as well as with the timing of D_2 deformation, whereas mineralization at the Madsen Mine is estimated to be earlier than 2698 Ma (Dubé et al., 2004). A second stage of mineralization throughout the belt, smaller than the first, is thought to have occurred later than 2702 Ma and is associated with syn- to post-tectonic plutons and remobilization of gold (Dubé et al., 2004).

2.3.5 Madsen Deposit

The Madsen mine is the closest major deposit to the study area (Fig. 2.3). The mine operated between 1938-1976 and 1997-1999, and produced roughly 2.45 million oz. of gold (Lichtblau et al., 2016b). Madsen is located at the angular unconformity between the Balmer and Confederation assemblages just southeast of the Killala-Baird batholith (2704 Ma) within amphibolite facies rocks (Fig. 2.3, 2.4; Dubé et al., 2000). The ore is located within the Austin and McVeigh ore horizons (Fig. 2.6) which are hosted by hydrothermally altered mafic volcaniclastic rocks, epiclastic rocks (wackes and conglomerates) and basalt flows of the Balmer assemblage. Previous interpretations suggest that the Austin and McVeign ore zones are hosted in altered dacitic pyroclastic rocks (Horwood, 1940a), heterogeneous sequences of strongly altered and deformed mafic flows and intermediate to felsic pyroclastic rocks (Durocher, 1983), mylonites (Hugon and Schwerdtner, 1984), and altered and deformed mafic flows (Andrews et al., 1986). The epiclastic component of the Austin ore zone has been suggested by Dubé et al. (2000) to represent fragmental rocks that mark an unconformity between the Balmer and Confederation assemblages. The deposit has been described by Dubé et al. (2000) as an Archean disseminated, stratabound, replacement-style gold deposit which shares similarities to higher temperature (400-600 °C) gold deposits and gold skarns hosted by mafic rocks.

The intensity of deformation at Madsen is heterogeneous, with local high-strain zones (cm to m scale), but is generally within a low- to medium-strain regime. Two deformational events are recorded,

D_1 and D_2. D_1 is defined by foliations (S_1) parallel to bedding (S_0) striking north-northeast while D_2 is the dominant fabric and is characterized by east-northeast trending foliations (S_2) and folds (F_2) that deform both S_0 and S_1. Previous studies conducted by Hugon and Schwerdtner (1984) and Andrews et al. (1986) suggest that the Madsen deposit is located on a 100 m wide sinistral shear zone that coincides with the Flat Lake-Howey Bay Deformation Zone. However, Dubé et al. (2000) proposed that the preservation of primary bedding and the angle at which S_0-S_1 and S_2 cleavage intersect suggest that there is no large scale shear zone or mylonite associated with the Austin and McVeigh ore zones.

Dubé et al. (2000) described two types of hydrothermal alteration mineral assemblages; an aluminous outer alteration zone and an inner alteration zone with gradational boundaries. The aluminous outer alteration zone is barren to anomalous in gold, metres- to tens of metres-wide, is strongly depleted in Na and is characterized by the presence of andalusite, garnet, biotite, staurolite and amphibole that alternate with zones of stockwork veining (amphibole). The strain is generally low in this zone and the foliation is typically defined by biotite and muscovite. The inner alteration zone is metres to a few tens of metres wide and hosts very discrete ore zones. Banded-laminated textures produced by metasomatic layering were formed by the replacement, and fracture filling of the host rock. The bands typically consists of alternating amphibole-rich (including actinolite, hornblende, microcline, calcite and tourmaline) and biotite-rich (including biotite, quartz, calcite, muscovite and local diopside) bands. Trace to a few percentages of garnet and clinozoisite are locally present. Disseminated sulphides including pyrite, pyrrhotite, arsenopyrite, chalcopyrite and sphalerite, plus magnetite typically occur in trace amounts to 30% in the high-grade zones. When arsenopyrite is abundant (up to 15%), the grades can be up to 120 g/t Au over tens of centimetres (Dubé et al., 2000). Typically, the ore at the Madsen deposit is associated with elevated values of Au, Ag, As ± Zn, Sb, Cu, and Hg (Durocher, 1983).

The mineralization event at the Madsen deposit occurred between 2744 ± 1 Ma (age of the overlying Confederation assemblage; Corfu and Andrews, 1987) and 2698 ± 1 Ma (age of a crosscutting

post-ore dyke; Dubé et al., 2004). The gold is closely associated with D_2 fabrics, however, the mineralization and alteration are affected by D_2 indicating that the gold event is early or pre-D_2. Folds associated with D_2 typically have hinges with higher gold values suggesting a potential remobilization of gold caused by D_2 (Dubé et al., 2000). Additional structural controls include the boundary between the Balmer and Confederation assemblage which has a strong competency contrast and thereby acted as a permeable channel for the mineralizing fluid (Dubé et al., 2000). Chemical traps caused by the Fe-Mg-Ca-rich nature of the Austin and McVeigh ore zones allowed for the precipitation of gold (Dubé et al., 2000).

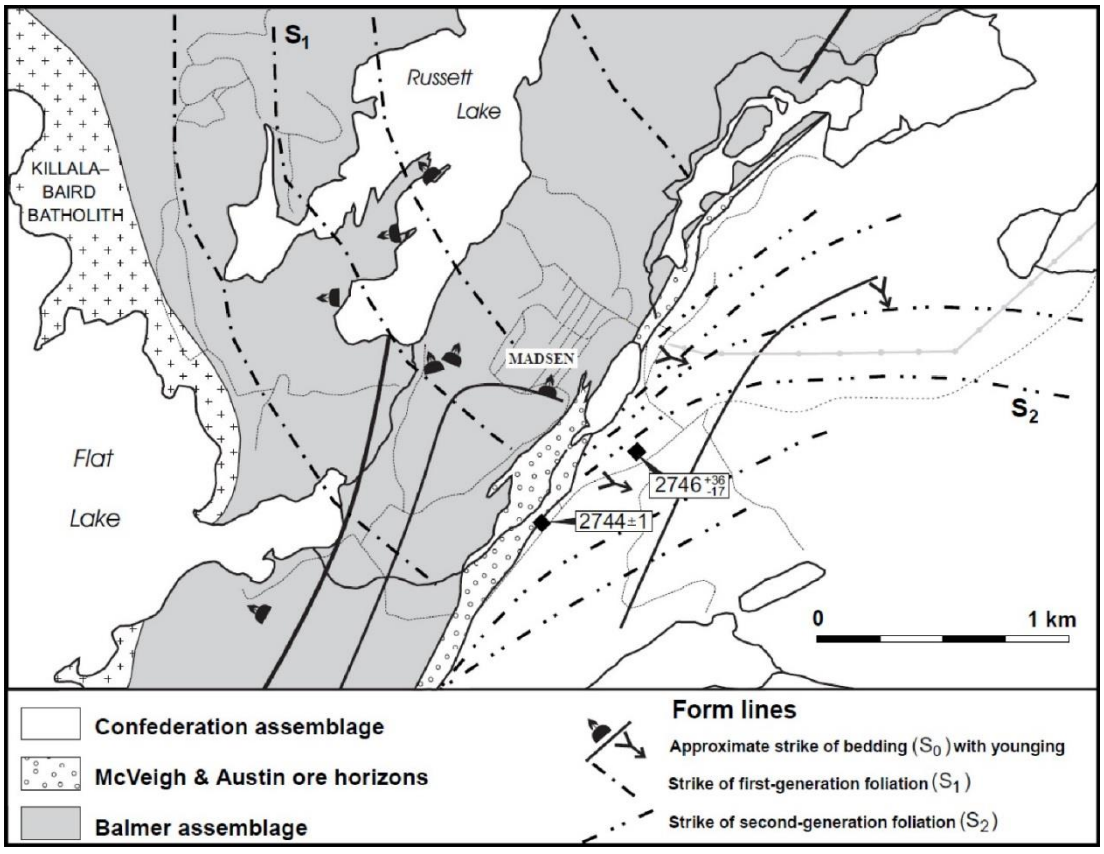

Figure 2.7 Simplified map of the geology of the Madsen Mine area (Sanborn-Barrie et al., 2000).

2.4 Previous Work

The first recorded exploration activity in the area around Laird, Medicine Stone and Lee lakes area was in 1936 when T. Christianson and E. Fredericton staked 45 claims. During the summer of 1937, Tom Johnson secured an option on the claim and carried out an exploration and development campaign. The next year, J. E. Hammell optioned the property and drilled 19 holes for a total of 2,000 feet on the known gold showings (Horwood, 1940a). Two gold showings were outlined; No. 1 Showing (now referred to as Pit Zone trench), situated southeast of the Laird Lake peninsula. No. 1 showing was described as a narrow quartz vein (4") hosted by a shear zone within altered greenstone. Visible gold was reported and the vein was stripped for 35 m along strike. Gold grades ranged from trace to 3.06 oz. per ton (Willoughby, 1988). No. 2 Showing is located on the south-east shore of Laird Lake where several foot wide pyritic shears with quartz are hosted by greenstones. The grade ranged from 0.10 to 0.20 oz. gold per ton (Willoughby, 1988). In 1940, the Laird Lake property was incorporated into the west Red Lake area geologic map by Horwood (1940b) but no detailed mapping of the Laird Lake area is recorded. From 1950-1964, 50 drill holes were completed totalling up to 1,888 m of diamond drilling near the Laird Lake area. Drill logs and drill collar locations were filed yet there was no indication as to who completed the work and assay values were not recorded (Willoughby, 1988). In 1965, the Geological Survey of Canada completed an airborne magnetic survey around the Trout Lake area which identified the magnetic high under Laird Lake (Willoughby, 1988). The presence of this magnetic anomaly was later confirmed in 1978 by the Ontario Geological Survey who completed an airborne electromagnetic survey covering the entire Red Lake area (Ontario Geological Survey, 1978).

Around 1980, Sherritt Gordon Mines Ltd. conducted detailed sampling of 23 trenches and sunk one shaft on the property (Hannigan, 1980). They reported pyrite and chalcopyrite mineralization within fractured and sheared mafic metavolcanic rocks and iron formations, with an increase in sulphides at the contacts of quartz veins. Gold mineralization was noted in several trenches with assays reaching up

to 0.02 oz. gold per ton over a width of 60 cm within rusty andesite (Willoughby, 1988). In 1987, Tasu Resources Ltd. carried out geological mapping and sampling of the property and obtained assays up to 5.97 g/t Au from a cherty rock in a shear zone with 10% pyrite and 1-3% chalcopyrite (Willoughby, 1988). In 1988, Black Cliff Mines Limited completed geological mapping, sampling, very-low-frequency electromagnetic (VLF EM), ground magnetometer and IP (induced polarization) surveys (Belanger, 1988; Farkas, 1988). In 1989, Cyprus Gold (Canada) Limited drilled 19 holes totaling 3092 m. They targeted known gold occurrences and geophysical anomalies, which graded up to 0.205 oz. Au/ton over 1.5 m (Guy, 2008).

In 1994, the Killala Township was mapped by B.T. Atkinson in order to complete township-scale mapping of the Red Lake greenstone belt. Atkinson's preliminary map showed for the first time the subdivision between assemblages (Balmer and Confederation; Atkinson, 1994). The assemblages in the Laird Lake area were subdivided by rock type associations alone. A set of medium-grained syenodiorite and intrusive breccias were observed at the contact between the Balmer and Confederation assemblages (Atkinson, 1994).

In 2004, the Laird Lake area was incorporated into the regional map of the Red Lake greenstone belt (Sanborn-Barrie et al., 2004). The only points marked as "visited outcrops" by the mappers were on the north shore of lower Medicine Stone Lake which is the contact between the Confederation assemblage and the Medicine Stone Lake pluton. From 2008 to 2010, Laird Lake Resources Inc. undertook a surface prospecting program on the property and submitted samples for whole-rock geochemistry and Au assay (Guy, 2008, 2009). From 2010 to 2012, Champlain Resources conducted a lake sediment sampling survey where 126 samples were analysed for whole-rock and precious metals. They also flew induced polarization/magnetometer geophysical surveys with lines with 200 m spacing (Fraser, 2011; Mochoruk, 2011).

Bounty Gold Corp. has owned the Laird Lake Claim Group since 2012 and has been surface prospecting since that time. The company has been successful in identifying a number of gold showings and occurrences (Leblanc, 2016). Prior to the 2015 field season, exploration was focused on re-examining previously marked gold occurrences and trenches. Three trenches in particular (Sheared Pit Zone (SPZ) East Gold Bearing Zone-Hill Side Zone (EGBZ-HSZ), and Gold Bearing Zone (GBZ)), were extensively sampled, and GBZ was mechanically stripped in order to better expose the occurrence and prepare it for subsequent mapping. In 2015, they exposed a narrow (80 cm) auriferous quartz vein in what seems to be sheared intermediate dike and called the showing Shear Hosted Gold Zone (SHGZ). During the 2016 field season, Bounty Gold Corp. continued to mechanically strip at HSZ and uncovered the unconformity between the Balmer and Confederation assemblages. As a result of the work completed by the author over the two field seasons, the company found and established a new gold occurrence on the south side of Lee Lake and called it the Lee Lake Shear Zone (now referred to as the Lee Lake Au showing). A more detailed description of the trench follows in Chapter 4.

During 2017, Premier Gold Mines Limited conducted additional prospecting on Bounty Gold Corp.'s Laird Lake property. An airborne magnetic and EM survey was flown at 50 m line spacing (oriented north-south) and 500 m line spacing (oriented east-west). Following their initial prospecting efforts, a diamond drill program was undertaken to test for potential gold mineralization within the mafic and ultramafic rocks of the Balmer assemblage below Laird Lake. A total of 3660.1 m were drilled over six drill holes in which all but one drill hole was collared in the Balmer assemblage and trended north. The best intersection was from a drill hole collared near the Pit Zone trench and reached up to 2.92 g/t over 1 m.

Chapter 3 – Methods

3.1 Field Work

Mapping of the Laird Lake property for this project took place over two separate seasons; summers of 2015 (July-August) and 2016 (June), for a total of 11 weeks in the field. The project area measured a total of 7.6 x 2.4 km and was mapped at a scale of 1:5,000 using old geological maps, aerial photographs, GPS, and a Brunton compass. The old geologic maps were utilized for locating previously documented outcrops and comparisons with field observations. Maps that included the Laird Lake area or maps specifically of the Laird Lake area were produced by the Ontario Department of Mines (Horwood, 1940b), Sherritt Gordon Mines Limited (Hannigan, 1980), Tasu Resources Ltd. (Willoughby, 1988), Black Cliff Mines Limited (Farkas, 1988), Ontario Geological Survey (Atkinson, 1994, 1995, 1999), and the Geological Survey of Canada (Sanborn-Barrie et al., 2004). Limited mapping in the area by junior companies and government geologists resulted in maps that were either ambiguous when comparing observations or at a scale that was too large to see any important structural or lithological features that would promote mineral exploration in the area.

Mapping of the Laird Lake property entailed a total of 35 traverses completed over the 11 weeks spent on the project area, with remaining days used doing road work with either truck or ATV, shoreline work with a 13 foot aluminum boat and/or work on trenches. Additionally, four drill cores from the 1989 Cyprus Gold (Canada) Limited drill program were re-logged and sampled in order to investigate the unconformity between the Balmer and Confederation assemblages. A week was spent mapping the Gold Bearing Zone trench at a scale of 1:20. A 2 x 2 metre grid was set on the 65 metre long trench to add precision and accuracy to the final product. Overall, 540 stations were marked, including roughly 670 rock type descriptions and over 8,000 photographs taken. In total, 435 hand samples and 48 drill core samples were taken for petrological examination, geochemical analysis, U-Pb geochronology, O and Nd

isotope analysis. Field observations and geochemical analysis were used to produce a detailed geologic map of the Laird Lake property and Gold Bearing Zone trench. Field descriptions are presented in Appendix A.

3.2 Petrography

Eighty-six polished thin sections were produced at Lakehead University. An Olympus Bx51 microscope with an attached Olympus DP-70 camera was used for transmitted and reflected light petrographic analysis.

3.3 Whole-Rock and Trace Element Geochemistry

Whole-rock geochemistry of 161 samples was undertaken at the Geoscience Laboratory (GeoLabs) of the Ministry of Northern Development and Mines in Sudbury, Ontario. The samples were pulverized in a 99.8% pure alumina planetary ball mill. Loss on ignition (LOI) was determined gravimetrically by heating at 100°C under a nitrogen atmosphere and then at 1000°C under an oxygen atmosphere until a constant weight loss was measured. Major and selected trace elements concentrations were determined by wavelength-dispersive X-ray fluorescence spectrometry with a XRF-PANalytical instrument on borate fused glass discs (major elements) and pressed powder pellets (trace elements). Trace elements were analysed by XRF to allow comparison with data generated by inductively coupled-mass spectrometry (ICP-MS). Totals for major element oxide data were generally 100% ±2% and have been recalculated to a 100% volatile-free basis. Detection limits for major elements are 0.01 weight % and relative standard deviations of duplicate analyses are within 5%. Trace elements, including the REE and HFSE were completed on a PerkinElmer Elan 9000 ICP-MS following a variation on the protocol described by Burnham (2008). The samples underwent a closed vessel multi-acid digestion by a solution composed of HCl, HF and HNO_3. A total of 45 trace elements were analysed with an average detection limit of 0.56 ppm. Major elements were analysed by ICP-atomic emission

spectrometry (ICP-AES) with an average detection limit of 45 ppm. Precious metals including Au, Ir, Pd, Pt, Rh and Ru are analysed by ICP-MS after the nickel sulphide fire-assay procedure. Detection limits averaged 0.13 ppb. All analyses performed during the course of this study utilized standards, duplicates of samples, and blanks, as part of the normal procedures of the GeoLabs. Results are presented in Appendix B.

3.4 Back-Scattered Electron Petrography

Back-scatter electron petrography was performed on three thin sections (two from the Gold Bearing Zone trench and one from Lee Lake Au showing) at Lakehead University using an SEM-EDS JEOL 5900 scanning electron microscope equipped with an Oxford energy dispersion system with a resolution of 139eV. These data were used to characterize gold mineralization at a 25 µm scale, as gold was only observed in one hand sample and once in thin section from the samples collected.

3.5 Neodymium Isotopes

Thirteen samples were analysed for Nd isotopes (Appendix C). The samples were chosen on the basis of rare-earth element primitive mantle normalized profiles which outlined discrete trends within various lithologies. The samples were analysed at the Earth Resources Research and Analysis Facility at Memorial University, St. John's, Newfoundland. Whole rock powders were dissolved in Savilex© Teflon capsules using a mixture of HF and HNO_3. Prior to acid digestion, a mixed $^{150}Nd/^{149}Sm$ spike was added to each sample. After digestion, the samples were dried and taken back up in various mixtures of HCl. Samples were then loaded into a column containing cation exchange resin where Sr fractionation can be isolated followed by collection of bulk rare earth elements (REES). This bulk sample was then dried, taken up in HCl and loaded on a second column containing Eichrom© Ln resin to isolate Sm and Nd separately from the other REES. Sm and Nd concentrations were determined using a multi-collector Finnigan Mat 262 mass spectrometer (TIMS) in dynamic mode for isotopic composition determination.

Instrumental mass fractionation of Sm and Nd were corrected using a Raleigh law relative to $^{146}Nd/^{144}Nd$ = 0.7219 and $^{152}Sm/^{147}Sm$ = 1.783. The reported $^{143}Nd/^{144}Nd$ ratios were corrected for the deviation from repeated duplicates of the standard JNdi-1 ($^{143}Nd/^{144}Nd$ = 0.512115; Tanaka et al., 2000). Replicates of the standards give a 6-month mean value of $^{143}Nd/^{144}Nd$ = 0.512102 ± 14 (2SD, n=18) for JNdi-1. Analyses of the USGS standard BCR-2 was included in each batch using a separate dissolution and thus provides the best estimate of the reproducibility of an individual whole rock analysis.

3.6 Uranium-Lead Isotopes

Three samples were analysed for U-Pb geochronology and results are presented in Appendix D. The samples chosen were based on field observations, cross-cutting relationships and the likelihood of having sufficient zircon in the samples. The samples were analysed at the Pacific Centre for Isotopic and Geochemical Research at the University of British Columbia, Vancouver. First, the rocks underwent a series of mineral separation procedures that included conventional crushing, grinding, a Wilfley table and Frantz magnetic separator. Zircons were then handpicked in alcohol under a binocular microscope where the clearest, crack- and inclusion-free grains were selected. Prior to dissolution, the grains were annealed and chemically abraded. The zircon grains were placed in a series of acid solutions and underwent heating on hot plates until the single grains were transferred into crucibles and spiked with a $^{233\text{-}235}U\text{-}^{205}Pb$ tracer solution (EARTHTIME ET535). The grains were then placed in another series of acid solutions and heated on hot plates after which they were loaded onto degassed, zone-refined Re filaments in a silicic acid emitter (Gerstenberger and Haase, 1997).

Isotopic ratios were measured using a modified single collector VG-54R or 354S (with Sector 54 electronics) thermal ionization mass spectrometer (TIMS) equipped with analogue Daly photomultipliers. All major Pb and U isotopic data were collected in an analogue Daly detector. U fractionation was determined directly on individual runs using the EARTHTIME ET535 $^{233\text{-}235}U\text{-}^{205}Pb$ tracer

solution and Pb was corrected for a fractionation of 0.25%/amu ± 0.02% (2s) based on replicate analyses of the NBS-982 Pb reference material and the values recommended by Thirlwall (2000). Data reduction was completed using the Excel-based program of Schmitz and Schoene (2007). Standard concordia diagrams were constructed and regression intercepts and weighted averages were calculated with Isoplot (Ludwig, 2003). All errors were quoted at the 2 sigma or 95% level of confidence. Isotopic dates were calculated with the decay constants λ_{238}=1.55125E-10 and λ_{235}=9.8485E-10 (Jaffey et al., 1971).

3.7 Oxygen Isotopes

Oxygen isotope compositions of quartz were measured on four quartz vein samples at the Department of Geological Sciences at the University of Manitoba, Winnipeg. Eight polished thin sections were produced at Lakehead University to cover the width of the four quartz veins (two thin sections per vein). A cathodoluminescence map was produced for each thin section to view the possible zonations within the quartz veins, however, no zonations were observed. The thin sections were then cut into 1 inch diameter circular thin sections and gold coated.

Oxygen isotope ratios ($^{18}O/^{16}O$) of quartz were measured in situ using a CAMECA IMS 7f secondary ion mass spectrometer with a primary ion beam of Cs^+ accelerated to 10kV. A normal-incidence flood gun was employed to neutralize potential sample charging. The primary ion beam was focused to a 15x30 μm spot using a 100 μm aperture in the primary column. Secondary ions were detected by switching the magnetic field. The detection system using an electron multiplier was coupled with an ion counting system with an overall dead time of 10.5 ns. A typical analysis comprised 70 cycles and lasted roughly 10 minutes.

During measurement, a mass-dependent bias is introduced. The observed fractionation is the result of several processes including secondary atom ionization (sputtering) and extraction, secondary ion transmission, and detection. The mass bias is most influenced by sputtering and ionization, which

depend strongly on the chemistry of the sample. The variability in the mass bias is often referred to as the “matrix effect”. A reference material compositionally similar to the samples being analysed, was used to calibrate the SIMS in order to receive accurate isotopic data. After comparing the data produced by the SIMS for the reference material, a correction factor was attained and used to recalculate the true isotopic ratios of the samples. The standard used for oxygen isotopes in quartz is Brazil quartz (20.5 ‰ SMOW). The precision and accuracy of the analyses included errors arising from counting statistics, calibration to a known standard, and uncertainty in dead-time corrections owing to variable count rates. The analytical precision for quartz was ± 1.2‰. Values are reported in standard notation relative to Vienna standard mean ocean water (V-SMOW). Results are presented in Appendix E. For a detailed description of operating conditions and strategy for correction of instrumental mass fractionation and matrix effects, see Fayek et al. (2002).

Chapter 4 – Field and Petrographic Results

4.1 Field and Petrographic Observations

The geology of the study area can be divided into two main assemblages; the Balmer (2.99-2.96 Ga) and Confederation (2.75-2.73 Ga) assemblages with later cross-cutting plutons bordering the northern and southern portions of the field area, and a series of smaller intrusions scattered throughout the volcanic-dominated packages (Fig. 4.1). During field mapping, protolith rock names were given (if possible) in order to subdivide the original volcanic, plutonic, and sedimentary packages. The volcanic rocks of the Laird Lake area have been subjected to amphibolite grade metamorphism associated with a general east trending foliation and therefore metamorphic names were provided for each sample once petrography was completed. Since every rock has been metamorphosed to some degree (plutons to a lesser extent than the volcanic and sedimentary rocks), the prefix “meta-“ has been omitted from the following descriptions for brevity.

4.1.1 Balmer Assemblage

The Balmer assemblage on the Laird Lake property is found south of the Killala-Baird batholith and north of the Confederation assemblage (Fig. 4.1). The assemblage reaches a maximum thickness of 1.5 km in the western portion of the field area, and thins towards the east where an inferred contact between the Killala-Baird batholith and Confederation assemblage is interpreted. The Balmer assemblage mainly consists of amphibolite grade mafic volcanic rocks, with rare occurrences of ultramafic volcanic rocks and banded iron formations. Gold mineralization on the property is mostly found within the Balmer assemblage mafic volcanic rocks and banded iron formation.

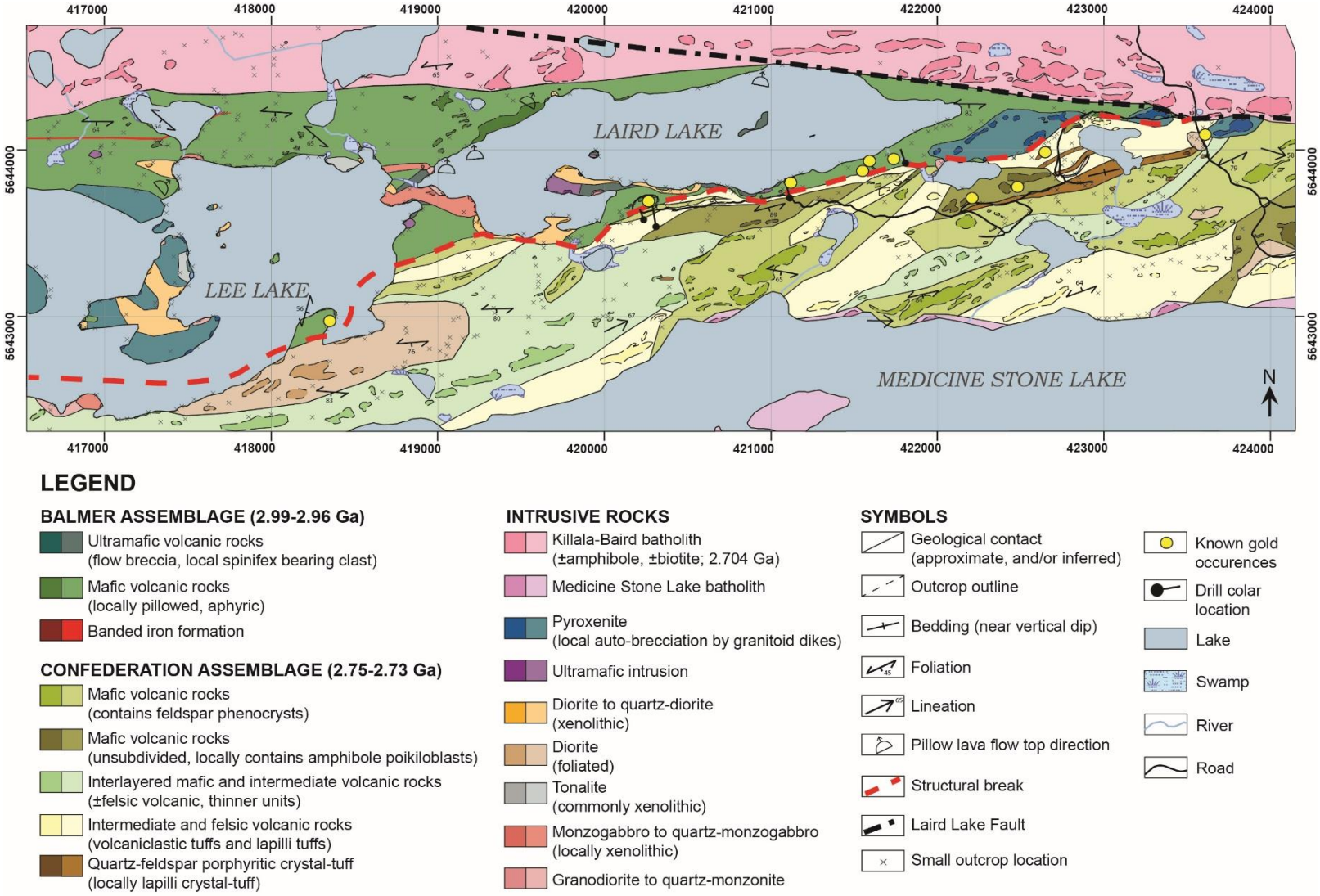

Figure 4.1 Geological map of the Laird Lake property, showing the location of the known gold occurrences and the drill hole collars of the examined drill core. Darker colours indicate observed outcrops or exposed areas; lighter colours indicate interpreted geology. The UTM co-ordinates are provided in Zone 15 using NAD83.

4.1.1.1 Ultramafic Volcanic Rocks

Ultramafic volcanic rocks were only found at a few localities on the Laird Lake property. These are concentrated in the center of the field area with most showings being on the water's edge (Fig. 4.1). The unit is commonly fine-grained, light grayish green or rarely light brown on the weathered surface and dark bluish gray on the fresh surface and yields high magnetic susceptibility readings compared to all other metavolcanic rocks on the property. Well explosed ultramafic volcanic flows, reveal complex relationships between flow breccias and massive flows/feeder dikes (Fig. 4.2A). The massive flows/feeder dikes measure between 20 cm to 15 m (possibly thicker), display potential lava tubes and are parallel to sub-parallel to the roughly east-west alignment of the elongated clasts within the flow breccia. The contact between the breccias and massive portions of the unit are sharp to irregular (Fig. 4.2A), and in thin section the contact zone is define by fibrous patches (potentially anthophyllite) that are aligned parallel to the contact with no chill margins observed. The flow breccias are clast supported with up to 90% rounded clasts from 20 to 1 cm in diameter (Fig. 4.2A). The flows locally host vesicles or eroded pits at the surface of both clasts and volcanic matrix (Fig. 4.2B). Foliation is locally defined by flattened clasts and pits within the flows. One breccia layer (3 m thick) within the flow sequence observed on an island in western Laird Lake, displays spinifex texture within all clasts (Fig. 4.2C). The spinifex needles are unoriented and measure up to 6 cm long and 1 cm wide.

Petrographic observations indicate that the ultramafic volcanic rocks are magnetite-bearing serpentine-amphibole-talc amphibolite. The spinifex needles have been replaced by serpentine with magnetite-rich cores (Fig. 4.2D). The groundmass is composed of locally radiating amphibole and talc, and rare disseminated magnetite. Commonly, these rocks are undeformed. Serpentine veinlets up to 0.3 mm in thickness cross-cut the sample.

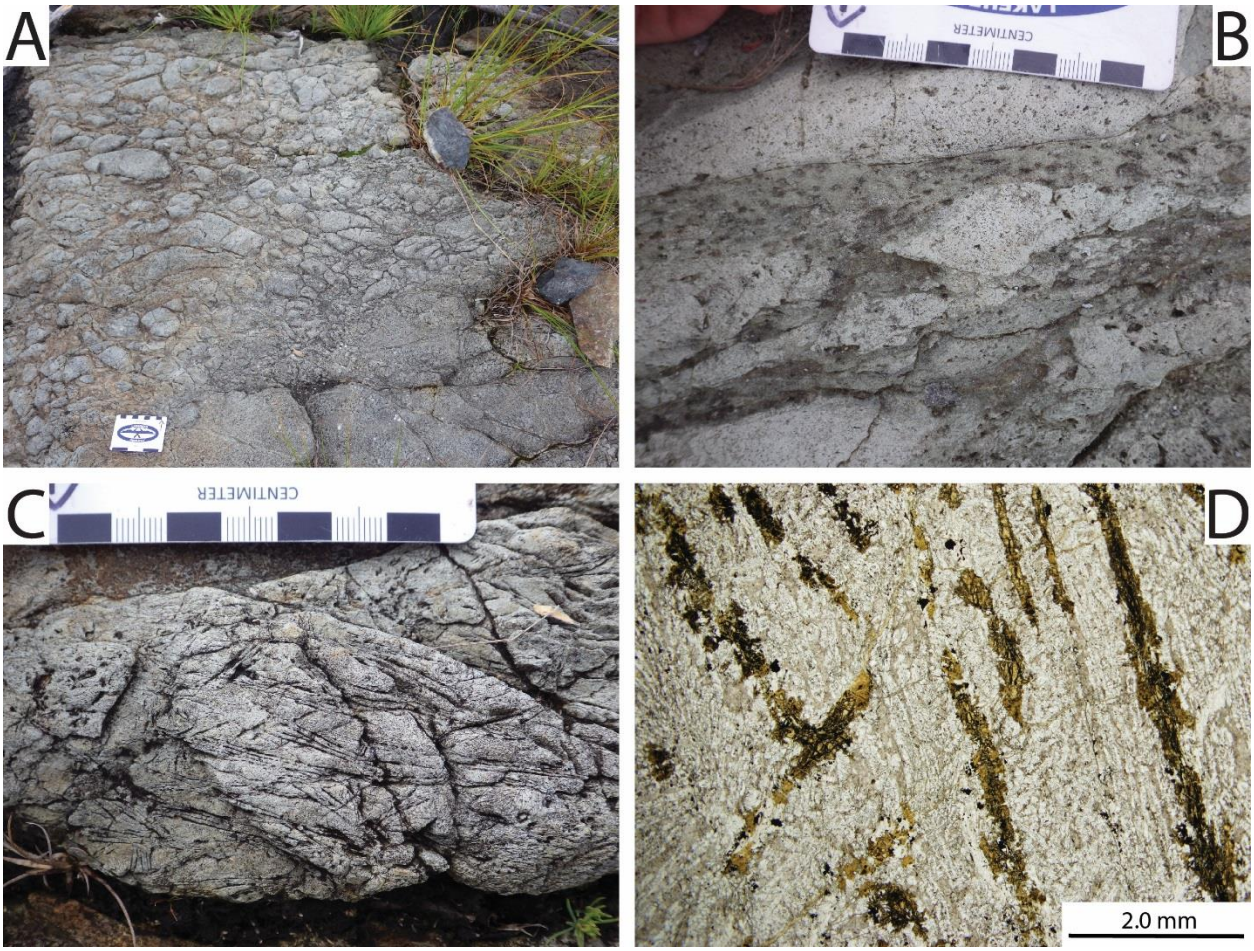

Figure 4.2 Field and petrographic photographs of Balmer assemblage ultramafic volcanic rocks at the Laird Lake property. A) Flow breccia in fairly sharp contact with massive feeder dike or flow (UTM 419956E 5643998N; station 15BG177). B) Vesicles in volcanic matrix of flow breccia (UTM 418836E 5643608N; station 15BG288). C) Spinifex-bearing clasts within a flow breccia horizon (UTM 419957E 5643995N; station 15BG177). D) Spinifex needles retrograded to serpentine with magnetite rich cores within an amphibole-rich matrix (UTM 419957E 5643995N; station 15BG177).

4.1.1.2 Mafic Volcanic Rocks

The mafic volcanic rocks are the most abundant rock type of the Balmer assemblage on the Laird Lake property, comprising roughly 95 vol.% of the assemblage (Fig. 4.1). The mafic volcanic rocks are typically dark grayish blue on the weathered surface and dark gray on the fresh surface. This unit is typically composed of fine-grained, aphyric massive flows, although primary features such as pillows, amygdules and varioles are commonly well preserved on the northern shores of Laird and Lee lakes. Pillows commonly young towards the north to north-east, defined by the orientation of the pillow keel (Fig. 4.3A). They measure up to 70 cm in length but have been deformed and flattened within the east-

west trending foliation. Quartz-filled amygdules, up to 10 vol.% and up to 5mm in length are found either on the outermost edges of the pillows (Fig. 4.3B), or throughout the pillows. The pillow selvages are up to 3 cm thick, and are brown (biotite-rich), dark grayish blue (amphibole-rich) or white (quartz-rich). The cores of the pillows can vary in colour from dark grayish blue to a light brown (Fig. 4.3B). Varioles were only observed at one locality. The light grayish green varioles measure up to 1cm in diameter, are slightly flattened by the foliation and are most abundant on the outermost rinds of the pillow where they grade into homogeneous pale patches between the pillows (Fig. 4.3C).

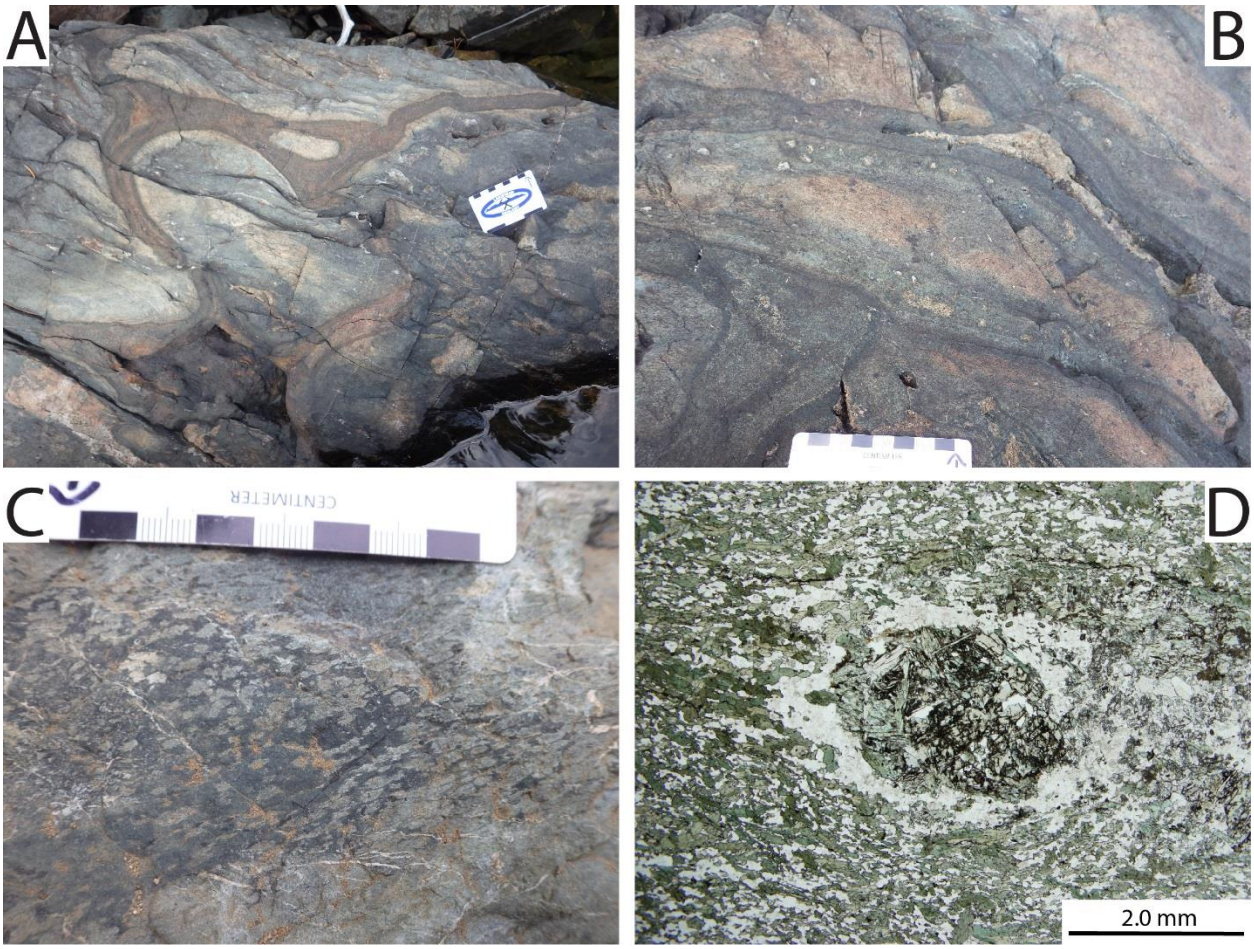

Figure 4.3 Field and petrographic photographs of Balmer assemblage mafic volcanic rocks at the Laird Lake property. A) Pillowed rock with biotite-altered selvages and way up direction to the northeast (UTM 419452E 5644143N; station 15BG145). B) Pillowed rock with biotite-rich cores, amphibole-rich selvages, and quartz-rich amygdules on the outermost edge of the pillow (UTM 419168E 5644021N; station 15BG147). C) Varioles (light grayish green ovals) in potentially pillowed rock (UTM 421627E 5643874N; station 16BG484). D) Amphibole and clinopyroxene rich amygdule with quartz rim within a typical mafic volcanic flow (UTM 419011E 5643936N; station 15BG148).

Petrographic analyses of least-altered mafic metavolcanic rocks indicate that they are plagioclase-quartz-biotite-hornblende amphibolites. The foliation is defined by up to 60% aligned hornblende and biotite grains. Quartz and plagioclase comprise the remaining mass of the rock. Plagioclase shows rare polysynthetic twinning and/or albite twinning. Amygdules can share the same mineralogy as the host rocks with an increase in grain size and with local additional pyrite and clinopyroxene (Fig. 4.3D).

4.1.1.3 Chemical Sedimentary Horizons

Two chemical sedimentary horizons were found within the Balmer assemblage of the Laird Lake property (Fig. 4.1). The horizon to the south of Laird Lake occurs in two trenches just south of the eastern half of Laird Lake, whereas the second horizon is found in the north of Lee Lake and defines a strong linear magnetic anomaly. These sedimentary horizons are typically banded-iron formations (BIF) defined by packages of magnetite-rich bands, ±pyrite interlayered with chert which can locally alternate with packages of interlayered carbonate and fine-grained mafic material with pyrrhotite. The chemical horizons typically trend east-west, parallel to the general foliation of the area, but when slightly subparallel to the foliation, a crenulation fabric between the primary bedding and the foliation is present. Only the horizon in the north-western part of the field area can be displayed on the map due to the multiple sightings and known continuity with the magnetic data (Fig. 4.1).

The chert-magnetite iron formation (Fig. 4.4A) is more than 1.5 m thick, as the lower contact is partly covered. The individual layers show a lot of variation in thickness with chert layers ranging from 1-5 cm thick and magnetite-rich layers ranging from 0.4-7 cm thick. The iron formation is either dominated by chert- or magnetite-rich bands which are in sharp contact with each other. The chert layers are typically white to gray whereas the magnetite-rich layers host magnetite up to 500µm long and can be associated with hematite, pyrite, hornblende, garnet and diopside (Fig. 4.4B). Magnetite also occurs

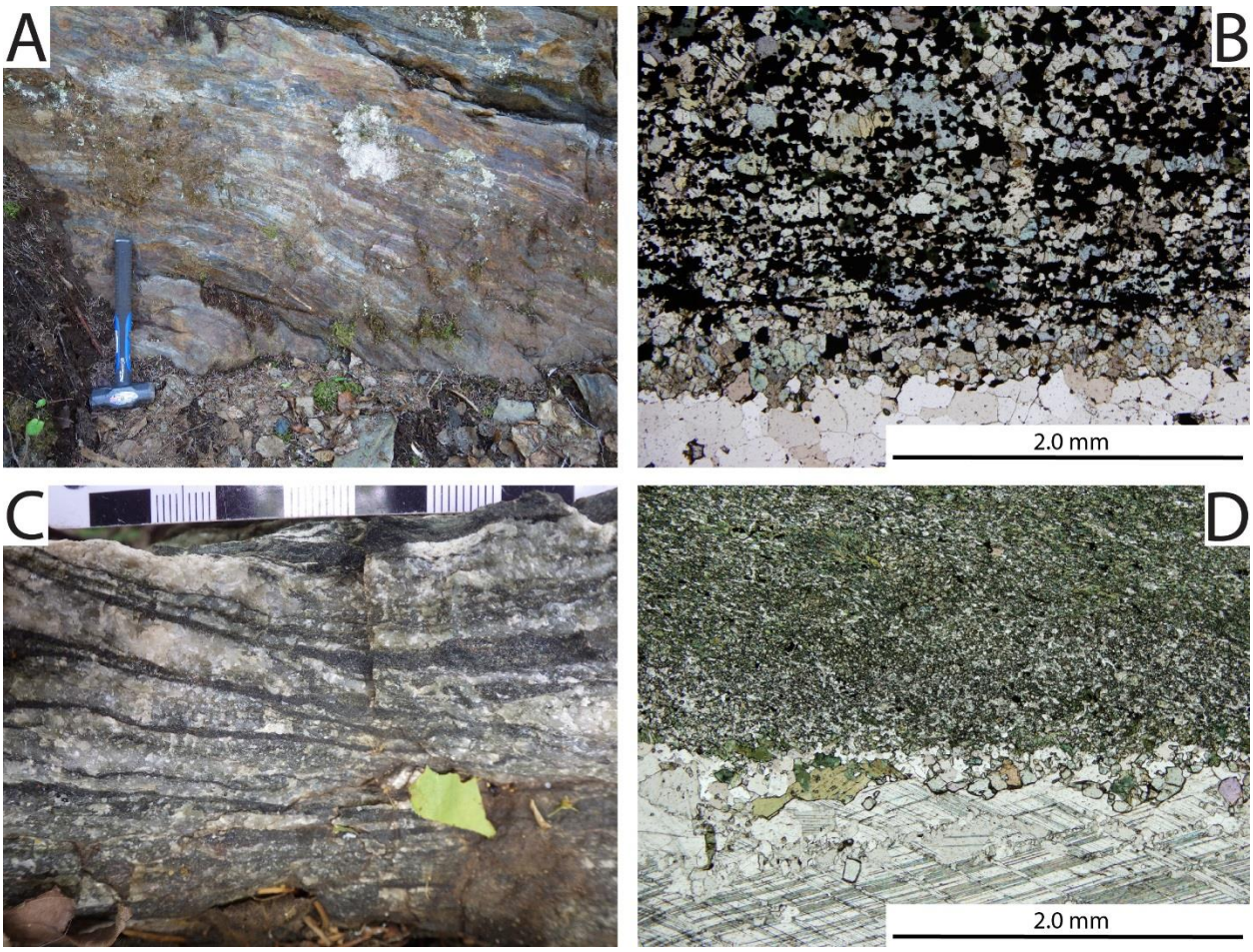

Figure 4.4 Field and petrographic photographs of Balmer assemblage sedimentary horizons at the Laird Lake property. A) Banded iron formation north of Lee Lake showing interlayered chert and magnetite-rich bands (UTM 417703E 5644219N; station 15BG418). B) Sharp contact between quartz-rich chert layer and magnetite-rich layer associated with diopside (UTM 421130E 5643828N; Gold Bearing Zone Trench). C) Fresh surface of the carbonate-rich formation showing calcite bands interlayered with bands composed of mafic material and pyrrhotite (UTM 421566E 5643898N; station 15BG236). D) Irregular contact between calcite and mafic layer showing the appearance of diopside at the contact (UTM 421566E 5643898N; station 15BG236).

as 100µm long interstitial grains within the quartz-rich chert layers. The chert layers are typically composed of 95% quartz grains up to 750µm long but averaging 200µm long. In gold-mineralized iron formations, up to 20% pyrite is present in non-chert layers with rare magnetite inclusions. Hematite is locally seen riming pyrite grains.

The second sedimentary horizon found south of Laird Lake comprises a chert-magnetite iron formation in close relationship with a carbonate-rich formation. The contact between the two is fairly sharp with no gradation between the chert and carbonate layers. The chert-magnetite iron formation

extends to 1.5 m outside of the trench where 10 cm horizons of the carbonate-rich facies lie above and below it. Garnets were locally observed within the magnetite-rich bands of the chert-magnetite formation. A larger exposure of the carbonate-rich unit is observed roughly 15m, west where the unit is 2m thick and bounded by mafic volcanic rocks to the south and an ultramafic intrusion to the north. This unit consists of white calcite bands up to 1.5 cm thick that effervesce strongly when a 10% HCL solution was applied to the surface. The calcite bands are interlayered with dark green, very fine-grained, slightly magnetic mafic bands that measure up to 2.5 cm thick (Fig. 4.4C). Locally, the calcite bands cross-cut stratigraphy at a 45 degree angle, parallel to the foliation. The carbonate bands are composed mostly of calcite grains up to 2 mm long with trace amounts of quartz and pyrrhotite. The dark green bands are composed of very fine-grained hornblende (65%), quartz/feldspar (23%), diopside (10%) and disseminated pyrrhotite (2%). The mineralogy of these mafic layers is very similar to the mineralogy of the mafic volcanic rocks of the Balmer assemblage. Reaction rims bordering the mafic layers are composed of diopside and lesser quartz (Fig. 4.4D). The foliation is only displayed by aligned amphiboles whereas the calcite layers are massive.

4.1.2 Confederation Assemblage

The Confederation assemblage on the Laird Lake property is found south of the Balmer assemblage and north of the Medicine Stone pluton (Fig. 4.1). The assemblage is roughly 1 km wide throughout the property and thins down to less than 100 m on the western end of the map area. Sets of ridges up to 600 m long are inferred to be parallel to the primary volcanic layering. The volcanic stratigraphy within the Confederation assemblage varies in strike from 045° to 080° with local volcanic packages parallel to the contact with the Balmer assemblage and others at a 35° angle. Features such as trachytic alignment of phenocrysts within flows, primary bedding in tuffs, and lithological contacts viewed at the outcrop scale also reflect the primary volcanic stratigraphy observed at the map scale. The Confederation assemblage is observed at a few localities to be in close to direct contact with the rocks

of the Balmer assemblage and is inferred to be in contact with the Killala-Baird batholith on the eastern end of the map area and the Medicine Stone Lake batholith to the south. The assemblage has been subject to amphibolite grade metamorphism and is mainly composed of thick mafic volcanic flows, separated by equally thick intermediate to felsic volcanic rocks, and zones of thin interlayered mafic to felsic volcanic rocks.

4.1.2.1 Mafic Volcanic Rocks

Mafic volcanic rocks are the dominant component of the Confederation assemblage and show great variability in mineralogy and textures between each flow type. There are three types of mafic flows; aphyric flows, feldspar (plagioclase) porphyritic flows, and amphibole poikiloblastic flows. The flows hosting amphibole poikiloblasts tend to be closer and parallel to the contact with the Balmer, whereas the thick flows with feldspar phenocrysts trend NE. All flow types including the aphyric flows are found throughout the field area, in particular within the interlayered package of mafic to intermediate volcanic rocks (± felsic volcanic rocks; Fig. 4.1). Petrographically, all mafic volcanic rocks are amphibolites.

The mafic flows with amphibole poikiloblasts are dark gray rocks with a fine-grained matrix and rounded dark greenish blue amphibole grains up to 5mm in diameter. These typically comprise 30% of the rock with local zones hosting up to 45%. These flows are always foliated, defined by the alignment of amphibole grains. Petrographically, the amphiboles are hornblende porphyroblasts with a poikilitic texture containing inclusions of quartz, feldspar, and subhedral amphibole grains up to 400µm long (Fig. 4.5D). The matrix is composed of fine-grained hornblende, feldspar showing rare polysynthetic and lesser Carlsbad twinning, quartz, sericite, magnetite, biotite and rare pyrite.

Figure 4.5 Field and petrographic photographs of Confederation assemblage mafic volcanic rocks at the Laird Lake property. A) Mafic flow with feldspar phenocrysts showing trachytic alignment (UTM 422205E 5643577N; station 16BG538). B) Feldspar phenocrysts showing polysynthetic twinning with an amphibole, feldspar, quartz and sericite groundmass (UTM 420955E 5643281N; station 15BG199). C) Mafic flow with aligned feldspar phenocrysts and amphibole poikiloblasts defining foliation (UTM 420340E 5643235N; station 15BG219). D) Amphibole poikiloblasts hosting inclusions of feldspar and quartz within an amphibole, feldspar and quartz groundmass (UTM 418068E 5642381N; station 15BG433).

The aphyric mafic volcanic flows are fine-grained, dark grayish green, aphyric units that are not continuous at a large scale. These occur with the mafic flows with amphibole poikiloblasts and show no defining textures. Petrographically, the rock is mostly composed of hornblende, biotite, feldspar, quartz and magnetite, with rare occurrences of chlorite, epidote and calcite.

The feldspar porphyritic flows are equally fine-grained, dark gray rocks, but host anhedral to euhedral white feldspar crystals that range from 0.2-3 cm long and 1-7 mm thick (Fig. 4.5A). Feldspars can comprise up to 40% of the rock but 5-10% is more typical. Locally, the feldspars define a trachytic

alignment. The trachytic texture is typically parallel to the map scale orientation of the volcanic packages. Typically, the foliation is defined by aligned feldspar crystals, where the phenocrysts are stretched and enveloped by the matrix. Locally, the feldspar-rich flows can also host amphibole porphyroblasts interstitially to the feldspar grains (Fig. 4.5C). Petrographically, the feldspars are plagioclase, displaying polysynthetic twinning (Fig. 4.5B) and are locally replaced by sericite and lesser quartz. The matrix is composed of fine-grained amphibole, biotite, quartz, feldspar, magnetite and rare pyrite.

4.1.2.2 Intermediate to Felsic Volcanic Rocks

Individual outcrops of intermediate to felsic volcanic rocks at the Laird Lake property were not extensive enough to map as consistent units (Fig. 4.1). The unit trends NE, similar to the mafic volcanic flows hosting feldspar phenocrysts. The intermediate to felsic volcanic rocks are beige to gray on the weathered surface and gray to light gray on fresh surfaces, and have textures consistent with a volcaniclastic or pyroclastic origin. No flow features such as flow lobes/domes or flow banding were observed.

Outcrops that lack obvious volcaniclastic textures typically display a characteristic joint-like pattern parallel to foliation (Fig. 4.6A). This pattern could represent primary bedding of volcaniclastic or pyroclastic formations, especially when the weathering profile is negative for local laminated layers. The absence of flow features and consistent joint-like patterns seem to point towards a volcaniclastic or pyroclastic origin for the felsic to intermediate volcanic rocks with no obvious distinguishing textures. Petrographically, this unit is a magnetite-bearing, biotite-muscovite-quartz/feldspar schist. The grains within the feldspar and quartz groundmass are equant to elongated and average 200 µm in length. Sericite dustings on feldspar grains distinguish them from quartz grains where twinning is absent.

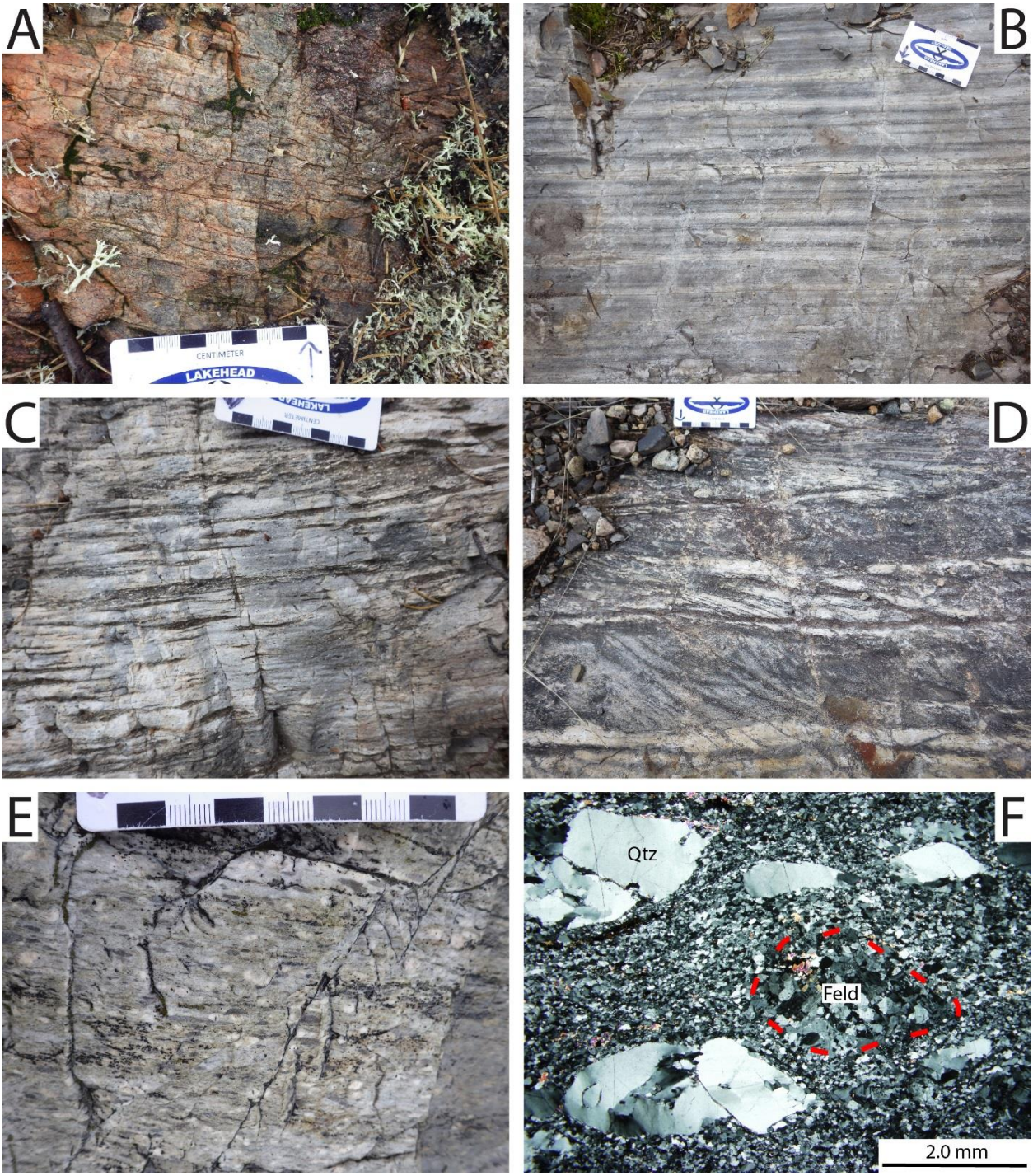

Figure 4.6 Field and petrographic photographs of Confederation assemblage intermediate to felsic volcanic rocks at the Laird Lake property. A) Typical joint-like pattern observed in the outcrops displaying no obvious volcaniclastic textures (UTM 420162E 5642789N; station 15BG225). B) Finely bedded to laminated tuff showing colour variation between layers (UTM 420659E 5643679N; station 15BG442). C) Lapilli tuff hosting feldspar porphyritic-rich clasts flatted by deformation (UTM 420644E 5643695N; station 15BG442). D) Volcaniclastic unit showing cross-bedding at 37 degrees to the original bedding surface (UTM 422936E 5643794N; station 16BG453). E) Quartz-feldspar porphyritic crystal tuff showing aligned porphyritic grains defining the foliation (UTM 422650E 5644000N; station 15BG070). F) Porphyritic grains showing grain size reduction; porphyritic quartz grains showing undulose extinction and porphyritic feldspar grains circled due to their ambiguous margins (UTM 422904E 5643962N; station 15BG032). ***Qtz****: quartz,* ***Feld****: feldspar.*

Biotite (3%) and rare tourmaline are locally present within the groundmass. Muscovite (up to 1.5 mm long) and biotite define the foliation.

Intermediate to felsic lapilli tuffs are more easily identified in roadside exposures close to the contact between the Balmer and Confederation assemblages. This unit generally consists of bedded to laminated layers ranging from 15 cm to 1 mm in thickness (Fig. 4.6B). On the weathered surface, the layers alternate from beige to gray bands with layers locally hosting up to 35% rounded to sub-angular quartz grains up to 1 mm in diameter. In a 50 cm thick layer, flattened lapilli size clasts averaging 4-6 cm long contain anhedral feldspar grains up to 2 mm long (Fig. 4.6C). A local section within one tuff hosted apparent cross-bedding in a 70 cm thick section where layers are 3-15 cm thick (Fig. 4.6D). The material in the cross-bedded section looks very similar to the tuffs displaying planar bedding. The primary bedding strikes 77°, parallel to the stratigraphy of the overall unit, and cross-bedding strikes 100°-110°. Petrographically, this unit is mainly composed of very fine-grained quartz, feldspar, chlorite, and muscovite with the layering being defined by variation in the percentages of muscovite. Coarser-grained layers can have up to 20% muscovite whereas the finer-grained layers typically contain only 2-3% muscovite.

Quartz-feldspar porphyritic crystal tuffs on the Laird Lake property are very distinctive. The unit consists of porphyritic rounded quartz and feldspar grains that comprise up to 20-40% of the rock (Fig. 4.6E). Quartz grains are typically more abundant than feldspar grains and measure up to 1 cm whereas feldspar grains measure up to 7 mm in length. This unit rarely contains lapilli size clasts that range from 2-6.5 cm long and are mostly mafic to intermediate in composition with mm scale feldspar inclusions. The foliation is defined by flattened porphyritic quartz and feldspar grains, whereas primary layering is inferred by the orientation of the elongated lapilli clasts. The quartz and feldspar porphyritic crystals are composed of subgrains (Fig. 4.6E). The quartz subgrains display undulose extinction whereas the

feldspar subgrains locally display polysynthetic twinning. The matrix is composed of very fine-grained quartz, feldspar, muscovite and biotite with traces of chlorite and sericite.

4.1.3 Intrusions

4.1.3.1 Killala-Baird Batholith

The Killala-Baird batholith crops out in the northern part of the map area, as ridges most commonly parallel to the contact with the Balmer assemblage to the south (Fig. 4.1). The batholith varies in composition from mainly granodiorite to monzogranite, is generally medium- to coarse-grained and locally contains centimetre-size anhedral quartz phenocrysts (Fig. 4.7A). The main mafic phases (up to 20%) are biotite and/or amphibole, occurring interstitially to quartz and feldspar. Local faint foliations are observed defined by the aligned mafic phases and/or quartz phenocrysts, but generally, deformation is weak to non-existent. Closer to the contact with the Balmer assemblage, the grain size is reduced to fine-grained and foliation fabrics are locally stronger. Alteration within the granitic body includes local millimetre-scale epidote blebs up to 3% and stringers, parallel or cutting the foliation, along with local pervasive hematite staining (Fig. 4.7B). Rare disseminated pyrite grains are observed. The batholith contains various amounts of quartz, microcline, orthoclase, and plagioclase with lesser amounts of hornblende, chlorite, epidote, titanite, zircon and biotite (Fig. 4.7B). Various degrees of sericite alters the feldspar grains. Petrographically, quartz showed weak undulose extinction and the micas locally define a foliation. Clinozoisite veinlets up to 0.3mm cross-cut the sample.

4.1.3.2 Medicine Stone Batholith

The Medicine Stone batholith is only observed at three locations along the northern shore of Medicine Stone Lake (Fig. 4.1). This intrusion consists of fine- to medium-grained pink granodiorite to granite with up to 5vol.% quartz phenocrysts up to 6 mm long and 10% biotite as the mafic phase. This unit is observed as massive to foliated, defined by aligned biotite grains (Fig. 4.7C). Trace pyrite and red

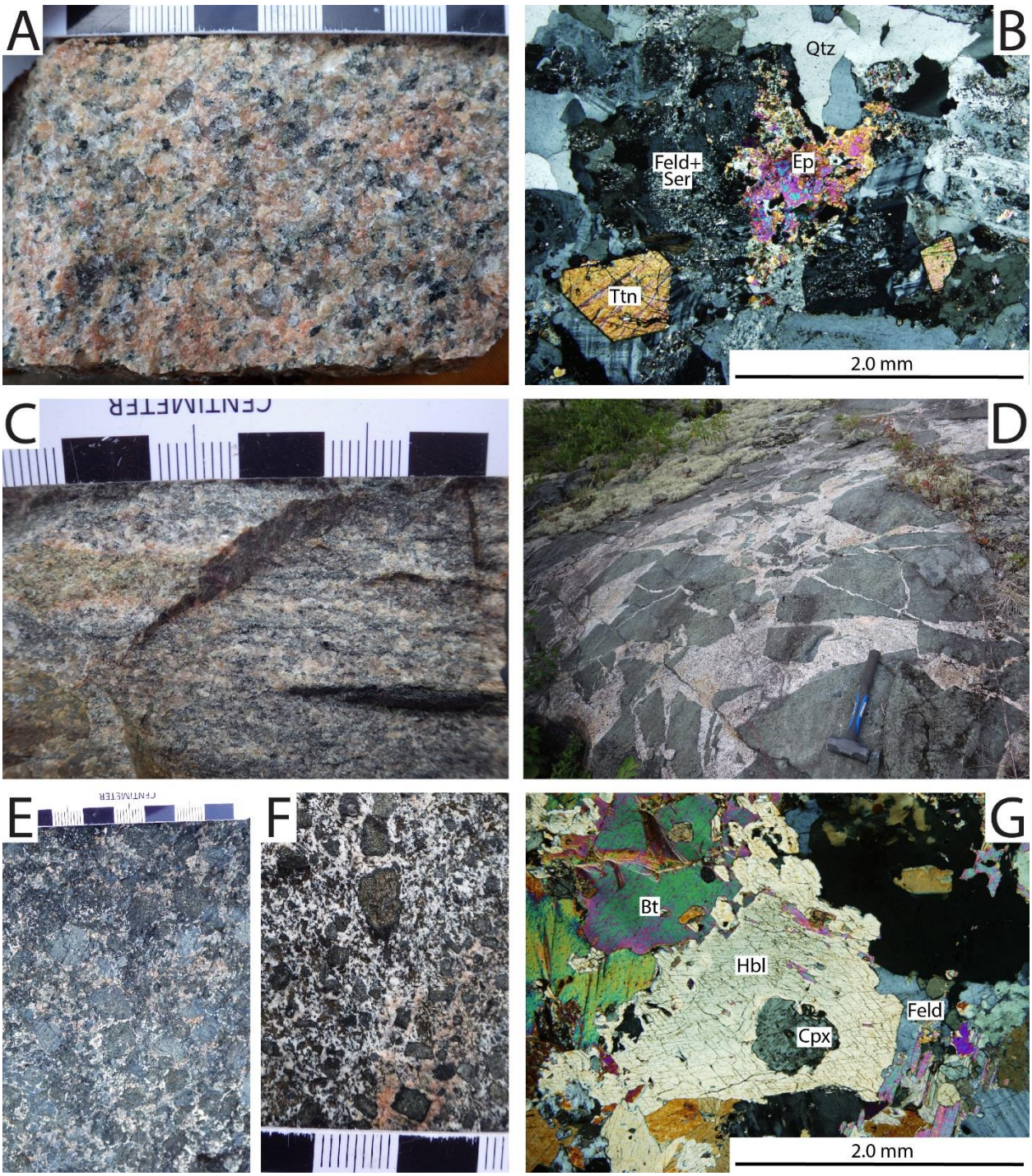

*Figure 4.7 Field and petrographic photographs of intrusive rocks at the Laird Lake property. A) Typical granodiorite of the Killala-Baird batholith (UTM 422123E 5644506N; station 15BG097). B) Epidote alteration surrounded by sericite altered feldspars, quartz, and titanite observed in Killala-Baird batholith sample (UTM 419672E 565644618N; station 15BG268). C) Foliated margin of the Medicine Stone batholith showing faint mineral banding (UTM 423361E 5643014N; station 16BG018). D) Pyroxenite outcrop brecciated by granitic intrusion (UTM 422751E 5644185N; station 15BG028). E) Very coarse-grained pyroxenite showing pyroxene crystals metamorphosed to hornblende up to 2cm within a white to pink feldspar matrix (UTM 416893E 5643070N; station 15BG363). F) Fractionated pyroxenite with pyroxene grains showing 0.5-1mm thick dark reaction rims (UTM 422410E 5644195N; station 15BG058). G) Remnant clinopyroxene grains found as inclusions within metamorphic hornblende (UTM 416656E 5643110N; station 15BG310). **Qtz**: quartz, **Feld**: feldspar, **Ser**: sericite, **Ttn**: titanite, **Ep**: epidote, **Bt**: biotite, **Hbl**: hornblende, **Cpx**: clinopyroxene.*

stringers of hematite or potassic alteration are locally observed. The rock is a monzogranite with accessory minerals such as muscovite, chlorite, carbonate, epidote, zircon, magnetite and pyrite. Sericite often alters the feldspars. Local magnetite grains host pyrite inclusions. The foliation is defined by aligned biotite, chlorite, and muscovite. Quartz grains typically display undulose extinction. Coarser-grained quartz and some feldspar grains are surrounded by quartz and feldspar sub-grains.

4.1.3.3 Pyroxenite

The Laird Lake property hosts two main pyroxenite bodies, along with smaller pyroxenite intrusions associated with the contact between the Balmer and Confederation assemblages (Fig. 4.1). The main pyroxenite bodies are typically restricted to the Balmer assemblage but are also observed in the Confederation assemblage. These are seen as km-scale, dark grayish blue, unfoliated, porphyritic intrusive bodies. This unit is characterized by the presence of up to 90% unoriented, euhedral to subhedral pyroxene crystals that vary from 0.2 to 2 cm in diameter in a fine- to medium-grained matrix (Fig. 4.7E). The pyroxene crystals have been partially or completely metamorphosed to amphibole, but still display blocky pyroxene habit (Fig. 4.7F). Tabular subhedral amphiboles are rarely observed within a dark gray matrix whereas amphibole prism up to 4 cm long occur within a felsic fractionated and pegmatitic portion of the pyroxenite. Typically, the matrix is speckled with interstitial white feldspars, with rare occurrences showing no feldspars at all. Locally, the pyroxene percentage diminishes to 25vol.% and the matrix is almost entirely composed of medium-grained feldspars and amphiboles. The decrease in pyroxene grains and increase in feldspar could represent a more fractionated phase of the true pyroxenite. The pyroxene grains within the more fractionated pyroxenite can locally show 0.5 mm thick black reaction rims (Fig. 4.7F). The pyroxenite intrusion found on Lee Lake (Fig. 4.1) is typically coarser grained with euhedral crystals, whereas the pyroxenite intrusions east of Laird Lake has smaller subhedral pyroxene crystals. The larger pyroxenite bodies are commonly associated with cross-cutting

granitic, and dioritic to syenitic dikes that vary from millimetre to metre scale. These locally, have resulted in brecciation of the pyroxenite with blocks up to 1 m wide (Fig. 4.7D).

Petrographically, this unit is a granofels composed of clinopyroxene, hornblende, biotite, plagioclase, microcline, with trace epidote, actinolite, carbonate, sericite, and pyrite. Remnant clinopyroxene grains up to 2 mm in diameter are found as inclusions within the porphyroblastic hornblende and feldspars (Fig. 4.7G). The groundmass is composed of interstitial feldspar which contains inclusions of epidote. The only signs of deformation are observed in microcline grains showing slightly deformed tartan twinning.

4.1.3.4 Ultramafic Intrusions

The ultramafic intrusions are commonly associated with the ultramafic volcanic flows on the south shore of Laird Lake and east shore of Lee Lake, on the island north of the peninsula on Laird Lake, and at one locality inland (Fig. 4.1). Typically, the intrusions are massive, brown on the weathered surface with rare light grayish green surfaces. These display “elephant skin” texture (Fig. 4.8A) or have a smooth weathered surface. The intrusions have magnetic susceptibility measurements that are indistinguishable from the ultramafic volcanic rocks. They host the same serpentine-rich metamorphic assemblage with additional rare disseminated pyrite. The ultramafic intrusions display a complex pattern with the ultramafic flow breccias as observed on the island on Laird Lake described in section 4.1.1.1. The contact between the two units is often fairly sharp, giving the appearance of cross- cutting feeder dikes/sills. However, the massive unit was observed flowing around breccia clasts (Fig. 4.8B) and has a parallel contact with the flow breccia layers, which could indicate that these ultramafic rocks are thin massive flows. Elsewhere on the property, the contact between the various ultramafic units is covered by overburden.

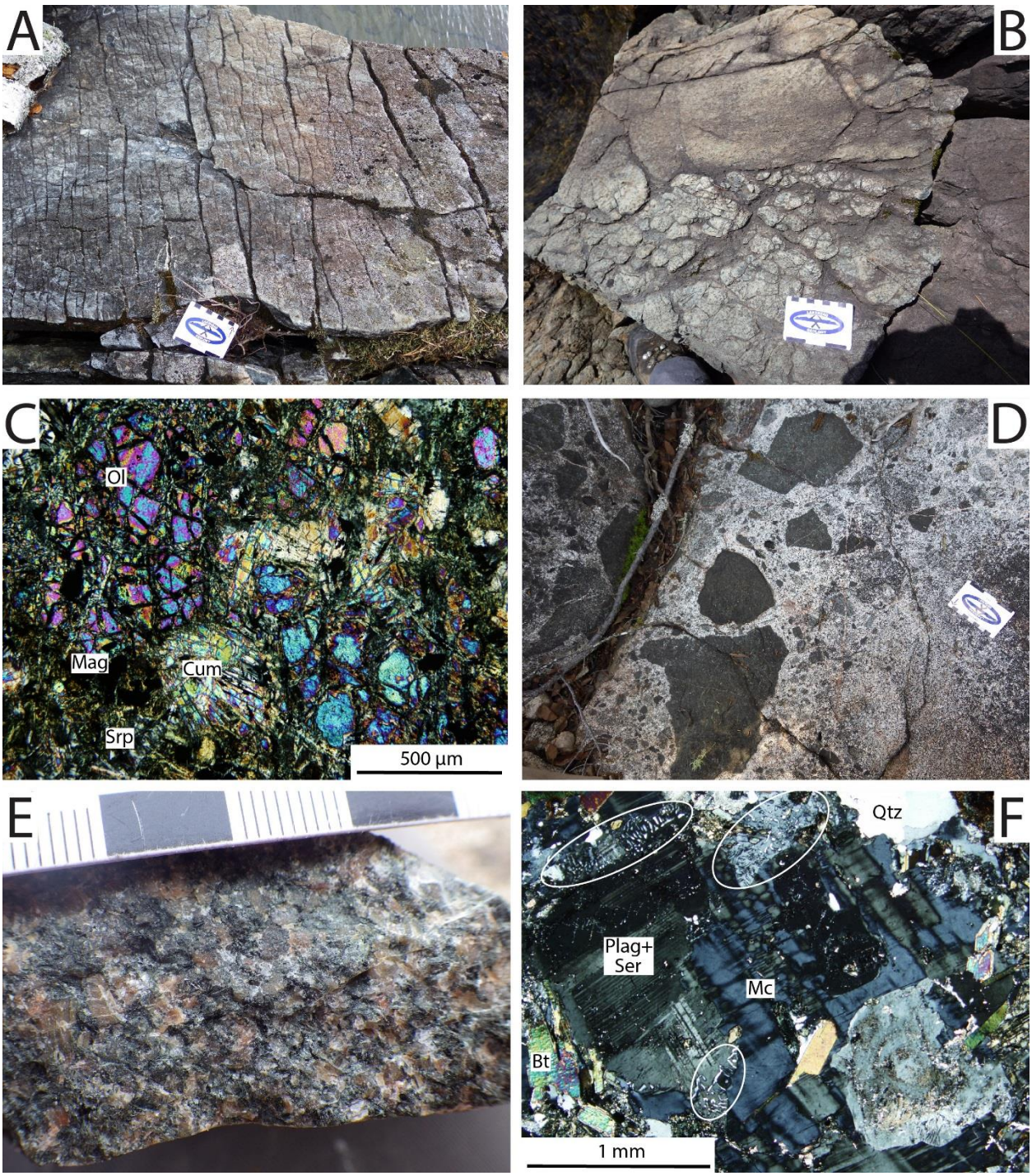

*Figure 4.8 Field and petrographic photographs of intrusive rocks at the Laird Lake property. A) "Elephant skin" texture observed on ultramafic rocks along Laird Lake (UTM 420955E 5643753N; station 15BG188). B) Irregular contact between the ultramafic flow breccia and feeder sill or possible massive flow (UTM 419963E 5643961N; station 15BG176). C) Remnant brecciated olivine grains within a serpentine, cummingtonite, and magnetite groundmass (UTM 419645E 5643764N; station 15BG172). D) Xenolithic diorite hosting clasts of pyroxenite (black), and smaller mafic volcanic and felsic to intermediate plutonic rocks (UTM 417192E 5643146N; station 16BG361). E) Fresh surface of monzogabbro showing amphibole, pink stained feldspars and rare quartz (UTM 418701E 5643790N; station 15BG285). F) K-metasomatism defined by interstitial microcline. Myrmekitic texture (white circles) found at the contact between microcline and sericite altered plagioclase crystals (UTM 418701E 5643790N; station 15BG285). **Qtz**: quartz, **Plag**: plagioclase, **Mc**: microcline, **Ser**: sericite, **Bt**: biotite, **Ol**: olivine, **Cum**: cummingtonite, **Mag**: magnetite, **Srp**: serpentine.*

The ultramafic intrusive rocks are magnetite-bearing olivine, talc, cummingtonite serpentinite. They contains up to 10% remnant sub-rounded brecciated olivine grains (up to 1.5 mm in diameter; Fig. 4.8C). The groundmass is composed of serpentine, talc and cummingtonite. Up to 5% disseminated magnetite is found as inclusions within olivine or patches of serpentine, but is most commonly found as an interstitial phase within the groundmass. Magnetite hosts pyrite and pyrrhotite inclusions and can also be found in veinlets cross-cutting the sample.

4.1.3.5 Diorite to Tonalite and Monzogabbro to Quartz-Monzogabbro

The Laird Lake property host two sets of diorite-like intrusions; one showing rare to local strain and most often hosting xenoliths, whereas the other is located at the contact between the Balmer and Confederation assemblages and displays a strong foliation (Fig. 4.1). The xenolithic intrusions are observed on the south western edge of Laird Lake, on the largest island on Lee Lake, as small outcrops on the edge of Lee Lake and at the contact between the Balmer and Confederation assemblages between the two pyroxenite intrusions on the eastern side of the Laird Lake property. They consist of diorite to quartz-diorite, monzogabbro to quartz-monzogabbro, and less commonly as tonalite. The outcrops range from whitish gray to pinkish gray with black interstitial minerals on the weathered surface and display a characteristic weathering pattern with a sheet like appearance (Fig. 4.8E). The monzogabbros are typically pink and black on the fresh surface due to the presence of K-feldspar alteration (Fig. 4.8F) whereas the diorite to tonalite outcrops are black and white on the fresh surface. The mafic minerals generally consist of biotite and amphibole varying from 5-70%. Roughly 80% of these outcrops are xenolithic with up to 40% xenoliths, varying in composition from ultramafic, mafic volcanic (aphyric and with feldspar phenocrysts), pyroxenite, diorite, and granodiorite (Fig. 4.8D). The latter two are usually larger, measuring up to 15 cm long, whereas the rest range from 1-4 cm. The dioritic intrusion found east of Laird Lake at the contact between the Balmer and Confederation typically hosts larger xenoliths up to 40 cm long, where pyroxenite and mafic volcanic rock xenoliths are the dominant

clast type. The xenoliths are typically rounded to sub-angular and are aligned parallel to the foliation or display a trachytic alignment where a foliation is absent. Monzogabbros are only locally xenolithic and cross-cut the diorites. Generally, these intrusions have a very weak to non-existent deformational strain, but where a fabric is present, it is defined by biotite and amphibole.

The intrusions are mainly composed of various amounts of plagioclase, K-feldspar, quartz, hornblende, and biotite with traces of titanite, epidote, chlorite, carbonate, magnetite, and pyrrhotite. Sericite replaces plagioclase, whereas microcline occurs interstitially and is not altered by sericite. Myrmekitic textures are often seen at the contact between plagioclase and microcline crystals, indicating K-metasomatism (Fig. 4.8F). Tartan twinning is rarely deformed within microcline, quartz shows undulose extinction, and hornblende grains are poikiloblastic with inclusions of quartz.

The diorite intrusion found on the south-eastern shore of Lee Lake lacks xenoliths and is strongly foliated. This intrusion is typically fine-grained, light grayish beige to light grayish pink on the weathered surface, and shows remnant porphyroclasts indicating the grain size prior to deformation (Fig. 4.9A). Although fine-grained, the lack of volcaniclastic textures and intercalated mafic volcanic flows, and the presence of coarser grained sections (Fig. 4.9B) and porphyroclasts suggest an intrusive origin. The porphyroclasts can be up to 15 cm long, and contain up to 80% feldspar grains up to 4mm long. These are aligned parallel to foliation and have sharp to diffuse borders. Coarser sections of the diorite and zones hosting more porphyroclasts are typically found on the southern side of the intrusion, furthest away from the inferred contact between the Balmer and Confederation assemblages. The strong foliation is defined by a banded appearance marked by bands of varying grain size, or by aligned porphyroclasts. Felsic veins within this unit are often boudinaged or folded showing S, M and Z microfolds (Fig. 4.9C).

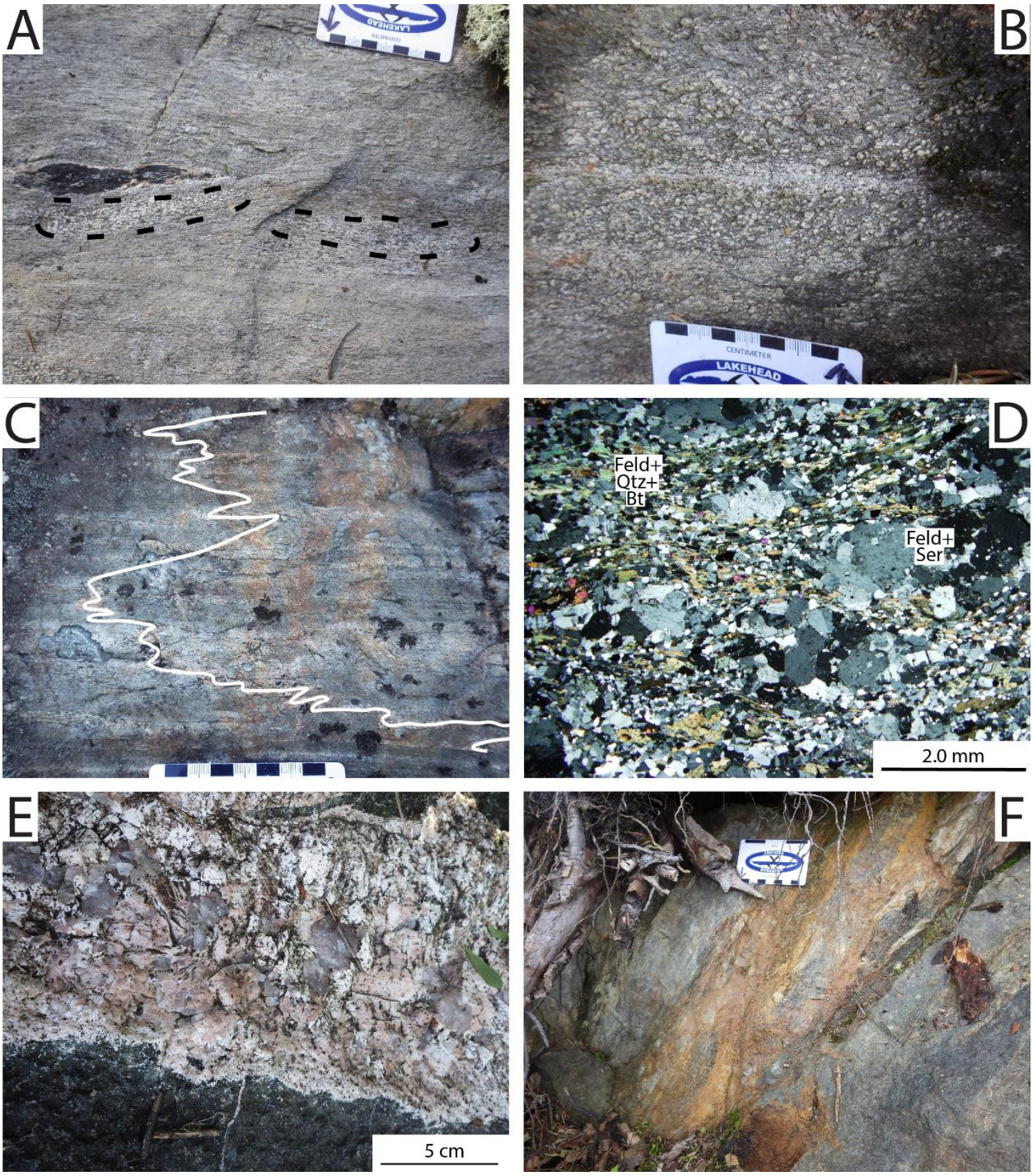

Figure 4.9 Field and petrographic photographs of intrusive rocks at the Laird Lake property. A) Remnant rock porphyroclasts within a fine-grained strongly foliated groundmass, showing the grain size that the plutonic rock could have been pre-deformation (UTM 418798E 5642713N; station 15BG427). B) Coarser grained section within strongly deformed diorite (UTM 418798E 5642713N; station 15BG427). C) Felsic veinlet within strongly deformed diorite, showing Z and M minor folds (UTM 416761E 5644363N; station 15BG349). D) Weakly sericite altered feldspar porphyroclasts within a feldspar, quartz, and biotite foliated groundmass (UTM 417614E 5642455N; station 15BG436). E) Pegmatitic felsic intrusion hosting coarse-grained quartz (clear to gray) and feldspar (white to light pink) crystals, cross-cutting pyroxenite (UTM 416656E 5643110N; station 15BG310). F) Rusty lamprophyre dike cross-cutting ultramafic rocks on the eastern edge of Lee Lake (UTM 4218904E 5643643N; station 16BG287). ***Qtz****: quartz,* ***Feld****: feldspar,* ***Ser****: sericite,* ***Bt****: biotite.*

The diorite consists of hornblende, chlorite, biotite, sericite, quartz and feldspars with trace amounts of clinozoisite, epidote, carbonate, magnetite, pyrite and hematite. The foliation is defined by very fine-grained chlorite, biotite, and hornblende flowing around the porphyroclasts composed mainly of feldspars showing polysynthetic twinning and lesser quartz with undulose extinction (Fig. 4.9D).

4.1.3.6 Granodiorite to Granite

Small granodiorite to granite intrusions occur on the shores of Laird and Lee lakes (Fig. 4.1). These intrusive bodies are typically less than 200 m long and are closely associated with the monzogabbro to diorite intrusions. Granitoid dikes varying from centimetre to metre scale are also seen cross-cutting various lithologies throughout the field area but are most commonly observed intruding and brecciating pyroxenite outcrops. The dikes are locally pegmatitic, hosting coarse-grained quartz and feldspar crystals (Fig. 4.9E). The intrusions are typically pink on the weathered surface, fine- to medium-grained with up to 50% biotite and amphibole and are undeformed. Mineralogically, they are very similar to the Killala-Baird batholith and could represent off-shoots from the main intrusions.

4.1.3.7 Lamprophyre

One lamprophyric dike was observed on the east shore of Lee Lake (Fig. 4.1) where the 20 cm wide dike cross-cuts ultramafic rocks (Fig. 4.9F). The dike is medium-grained, and contains up to 90% biotite which is aligned parallel to the margin of the dike. Petrographically, the intrusion consisted of biotite, amphibole, quartz, feldspar, magnetite and pyrite. The amphibole is bladed and poikiloblastic with inclusions of quartz and feldspar.

4.1.4 Contact Relationships Between the Major Units

4.1.4.1 Balmer and Confederation Assemblages

The contact between the Balmer and Confederation assemblages on the Laird Lake property is defined by multiple features including a lithologic change, increase in deformation and alteration, appearance of mineral banding, and presence of distinct intrusions (Fig. 4.10). At the map scale, the contact between the Balmer and Confederation assemblages is irregular but generally trends 75° (Fig. 4.1). At the two locations where the contact was observed, either a cross-cutting diorite to pyroxenite intruded the contact (Fig. 4.11A), or a 20 cm gap between the outcrops was observed (Fig. 4.11B). The contact appears to be dipping to the south, however, no direct measurements were taken due to lack of exposure and irregular showings.

The lithological contrast between the Balmer (mafic volcanic flows, with minor ultramafic rocks and chemical sedimentary horizons) and the Confederation assemblage (intercalated mafic to felsic volcanic rocks) accentuates the contact between the two assemblages. On the Confederation side of the contact, the combination of light coloured intermediate to felsic volcanic rocks and the well bedded texture of this unit, compared to the dark blueish gray Balmer rocks, makes the contact very evident in well exposed outcrops (Fig. 4.11B). The only common lithology that both assemblages host are mafic volcanic rocks and typically, the mafic volcanic rocks of the Confederation assemblage are porphyritic or poikiloblastic, creating a significant contrast with the aphyric nature of the mafic volcanic rocks of the Balmer assemblage. However, locally, the Confederation mafic volcanic rocks are aphyric, and other methods need to be applied in order to differentiate the assemblages. Of the four drill holes examined, the contact between the Balmer and Confederation should have been intersected in three of the holes (Fig. 4.1). However, no major changes were recorded until strongly magnetic ultramafic rocks of the Balmer assemblage appeared towards the end of some holes.

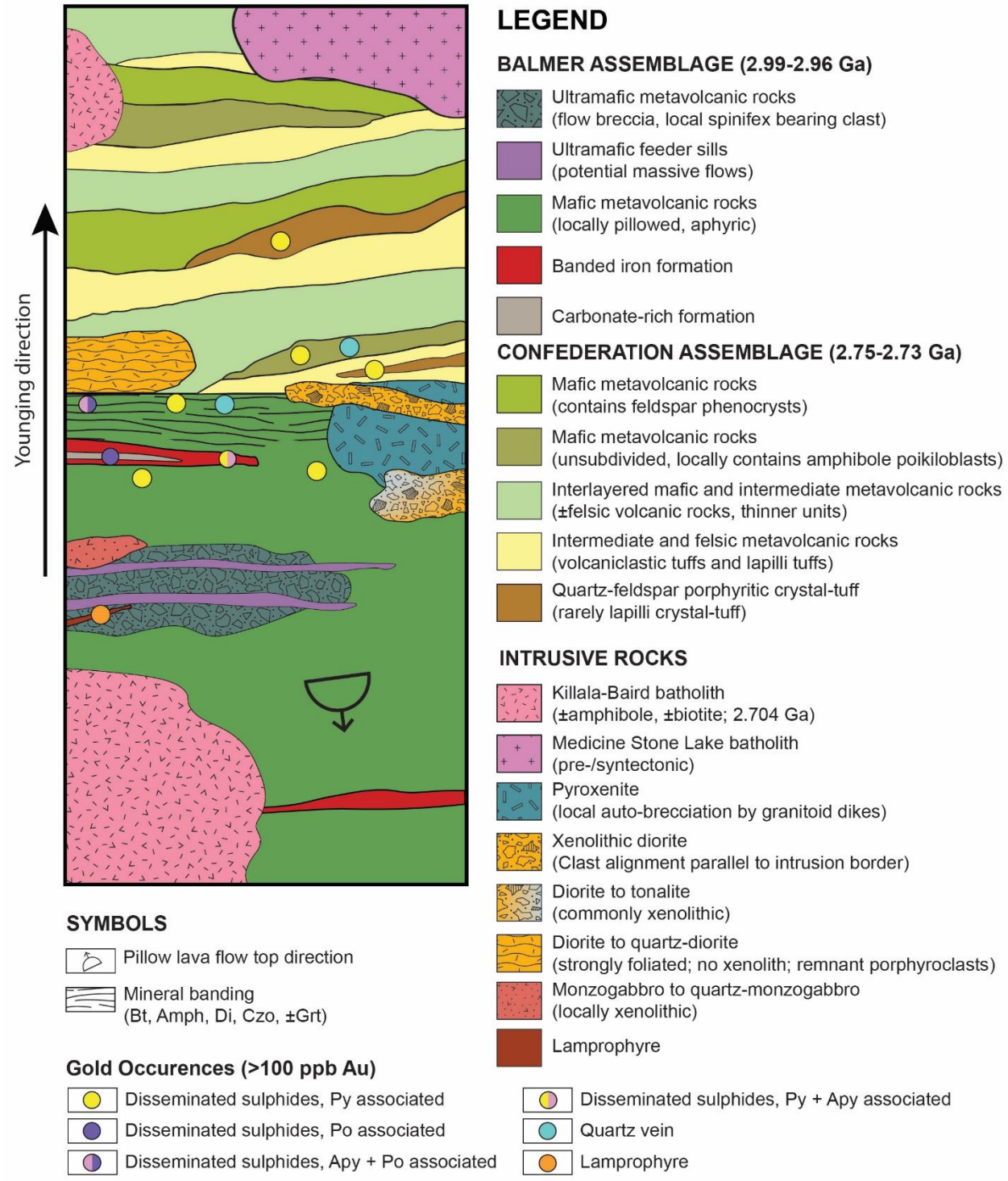

Figure 4.10 Schematic stratigraphic section of the Laird Lake area, showing the relationships between the volcano-sedimentary and intrusive units, and the location of gold occurrences in relation to the geology of the area. The younging direction indicates the order in which the assemblages have been formed. The opposing pillow younging direction is interpreted as being due to the pre-Confederation overturning of the Balmer assemblage. The section is based on a compilation of outcrop observation. Section is not to scale. ***Bt****: biotite,* ***Amph****: amphibole,* ***Di****: diopside,* ***Czo****: clinozoisite,* ***Grt****: garnet,* ***Py****: pyrite,* ***Po****: pyrrhotite,* ***Apy****: arsenopyrite*

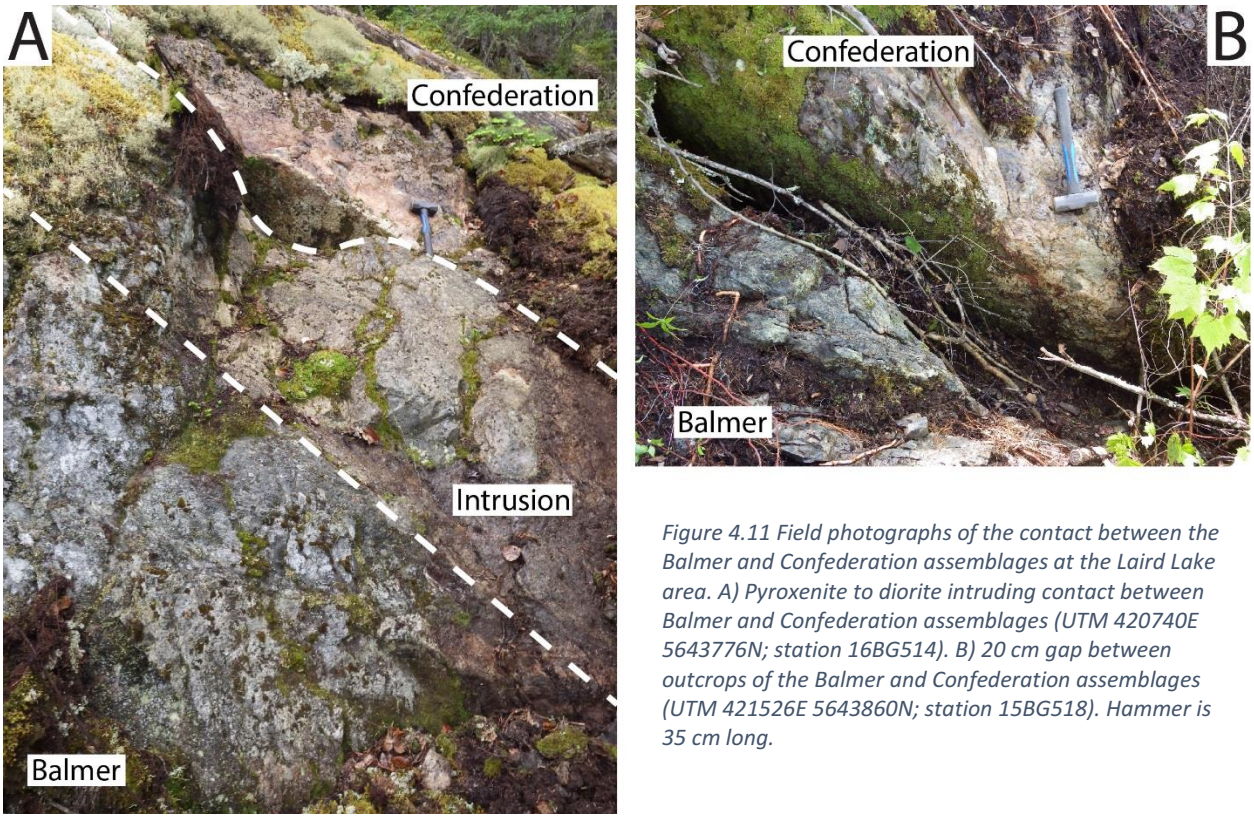

Figure 4.11 Field photographs of the contact between the Balmer and Confederation assemblages at the Laird Lake area. A) Pyroxenite to diorite intruding contact between Balmer and Confederation assemblages (UTM 420740E 5643776N; station 16BG514). B) 20 cm gap between outcrops of the Balmer and Confederation assemblages (UTM 421526E 5643860N; station 15BG518). Hammer is 35 cm long.

Deformation at the Laird Lake property tends to increase when approaching this major contact, especially within the Balmer assemblage where small scale folds and more prominent foliations defined by mineral banding are typically observed. At the Gold Bearing Zone Trench less than 100 m from the contact (Fig. 4.1), quartz-filled sigmoidal tension gashes and possibly strongly flattened pillows were also observed. The banded iron formations at this trench, however, remain mostly unaffected. The Confederation assemblage rocks appear to be less deformed as most of the layering has been interpreted as primary bedding, however, some layering could be caused by deformation. Primary textures include tuffaceous bedding with equant, non-flattened quartz crystals, and easily recognizable lapilli clasts. When no primary features are observed, the rock comprises massive intermediate to felsic volcanic rocks.

One of the most distinguishable features to help establish the proximity to the contact is the presence of alteration mineral banding within the Balmer assemblage. The banded texture is defined by millimetre to 15 centimetre thick alternating biotite-rich (grayish purple to brown), hornblende-rich (dark green), and diopside-rich (light green) layers with local clinozoisite-muscovite-rich (creamy white) layers (Fig. 4.12A). This texture is observed within the first 100 metres from the contact and is absent within the Confederation assemblage. Typically, biotite and hornblende-rich layers are more abundant, whereas diopside and clinozoisite-rich layers are less common. The clinozoisite-rich layers tend to be closely associated with the diopside bands, whereas the hornblende-rich bands tend to border each layer. The bands can locally be associated with up to 50% fine-grained quartz and lesser feldspar, especially within the biotite, hornblende, and clinozoisite-rich layers. The layers are commonly continuous zones, but can locally be very irregular and truncated. The mineral banding defines the foliation within areas where biotite, hornblende, and local quartz grains are parallel to foliation. Local diopside layers are commonly boudinaged (Fig. 4.12B) or occur as porphyroclasts (Fig. 4.12A) indicating prolonged deformation post-alteration. Biotite-rich layers can host up to 30% garnets up to 1 cm across.

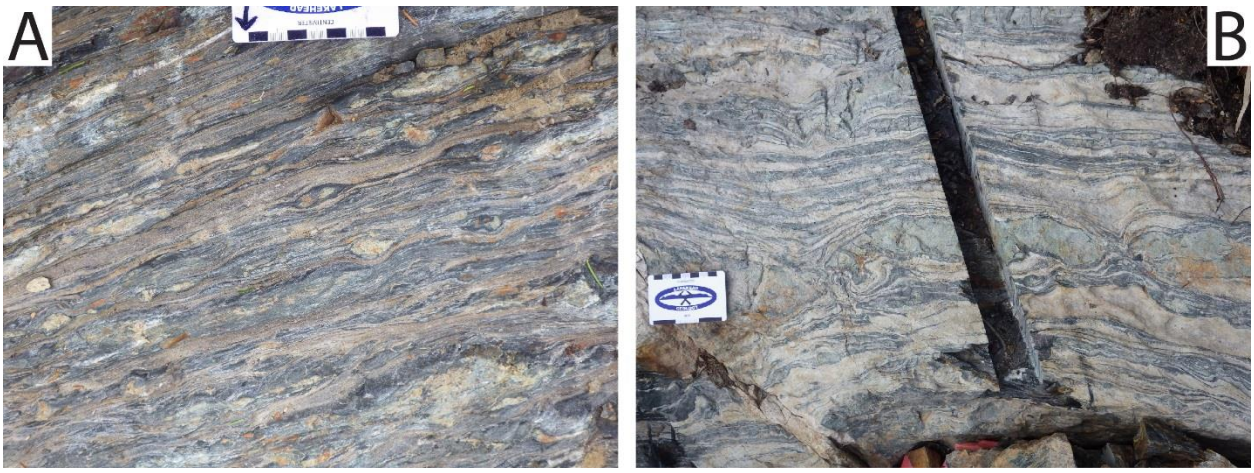

Figure 4.12 Photographs showing the distinctive mineral banding in the Balmer assemblage. A) Interlayered bands that are biotite-, amphibole-, and clinozoisite-rich, with diopside porphyroclasts (UTM 421130E 564828N; Gold Bearing Zone trench). B) Interlayered bands showing boudinaged light green diopside band with less component bands dominated by biotite and amphibole wrapping around the boudins (UTM 418366E 5642963N; station 16BG296 – Lee Lake Au Showing).

Intrusive units such as the pyroxenite and xenolithic diorite also occur close to the contact between the two assemblages (Figs. 4.1, 4.10, 4.11A). The main pyroxenite bodies are found within the Balmer assemblage. However, on the east side of the property, at the contact between the Killala-Baird batholith and the Confederation assemblage, a more fractionated pyroxenite intrusion is present. A 50 cm thick pyroxene-rich intrusion cross-cuts the Confederation parallel to tuffaceous bedding (Fig. 4.13A). At one location south of Laird Lake, a diorite (no xenoliths observed) to pyroxenite measuring 1.2 m thick intrudes along the contact between the Balmer and Confederation assemblages (Fig. 4.11B). On the eastern portion of the property, xenolithic diorite intrusions are common at the contact between the two assemblages and cross-cut the pyroxenite. These intrusions are up to 15m wide but most commonly occurs as smaller 50cm thick intrusions cutting rocks of the Balmer assemblage (Fig. 4.13B).

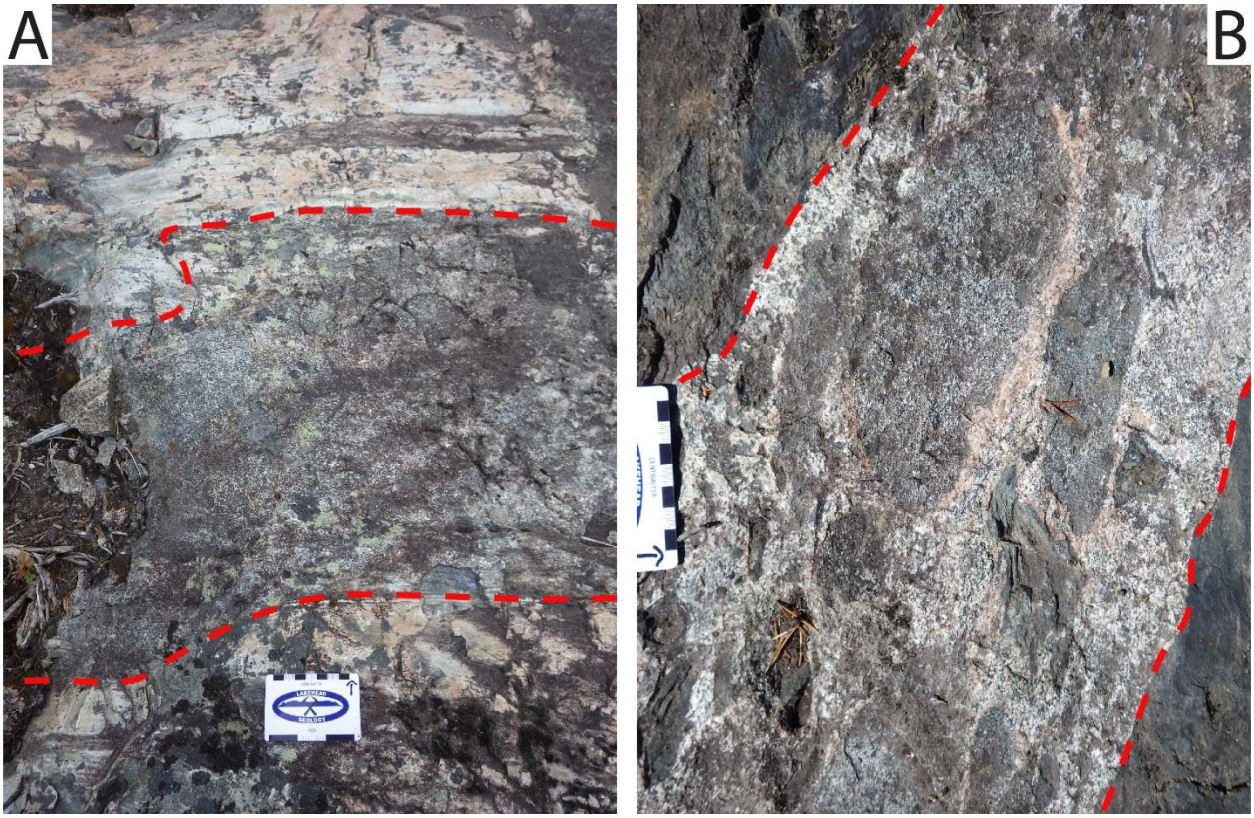

Figure 4.13 Field photographs showing the intrusions which commonly appear near the contact between the Balmer and Confederation assemblages. A) Pyroxenite intruding along bedding planes of intermediate to felsic tuffs (UTM 422485E 5643980N; station 15BG069). B) Xenolithic diorite cutting Balmer assemblage mafic volcanic rocks (UTM 422923E 5644186N; station 16BG025).

A direct contact between the xenolithic diorite and Confederation was not observed. These intrusions commonly occur at the contact between the two assemblages and appear to have used the interface as a conduit to ascend through the crust.

4.1.4.2 Major Batholiths and Volcanic Assemblages

The contacts between the Killala-Baird batholith or Medicine Stone pluton and the volcanic assemblages are not observed due to the presence of overburden. A valley measuring roughly 10-100 m wide is present between the Killala-Baird batholith and the Balmer assemblages. Weak alignment of mafic minerals within the margins of the batholith locally strike parallel to the contact. The transition into the Medicine Stone pluton is less clear due to the fine- to medium-grained minerals within the margin of the pluton and the presence of a moderate to strong foliation.

4.1.4.3 Xenolithic Diorite and Pyroxenite

The relationship between the xenolithic diorites and pyroxenites are complex due to the various cross-cutting relationships observed throughout the Laird Lake area. Three distinct sets of xenolithic diorites were mapped; one on the east side of Laird Lake (too small to display on the Laird Lake property map), another on the south-western shore of Laird Lake, and the last is mostly located on the large island on Lee Lake. The diorite cross-cuts the pyroxenite (Fig. 4.14A) and contains rounded to angular xenoliths of massive pyroxenite up to 25 cm long (Fig. 4.8D) as well as other lithologies (section 4.1.3.5). A sub-rounded xenolith measuring 7 cm long, with a dark coloured matrix, and unoriented feldspar phenocrysts up to 1 cm long (Fig. 4.14B) resembles the Confederation assemblage mafic volcanic flows with feldspar phenocrysts. The diorite was not observed to host xenoliths of intermediate to felsic volcanic lithologies or cross-cut the Confederation assemblage, but it is observed cutting the Balmer assemblage. In summary, the xenolithic diorite hosts pyroxenite xenoliths and possible xenoliths of the Confederation which suggests that the diorite is younger than the pyroxenite and the Confederation.

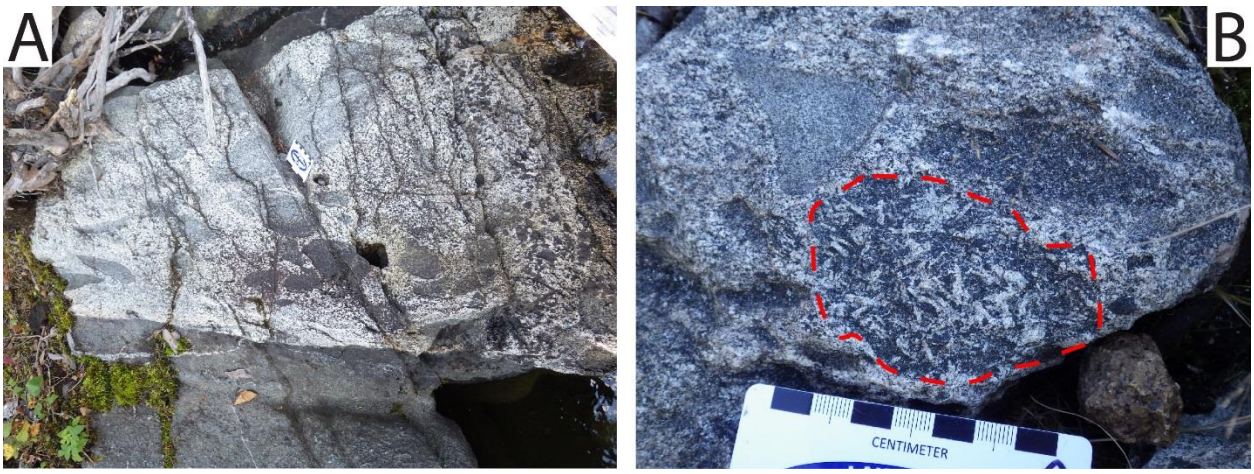

Figure 4.14 Field photographs showing the relationship between the xenolithic diorite and pyroxenite A) Xenolithic diorite with xenoliths oriented parallel to the intrusions border cross-cutting a pyroxenite (UTM 417452E 5643475N; station 15BG377). B) Xenolithic diorite hosting a xenolith (outlined in red), possibly from the Confederation assemblage mafic volcanic flows with feldspar phenocrysts (UTM 419201E 5643714N; station 16BG161).

4.2 Deformation and Metamorphism

The Laird Lake area displays various penetrative, ductile, and brittle deformation fabrics and structures, and lies within the regional amphibolite facies zone of the Red Lake greenstone belt (Fig. 2.4). The metamorphic assemblage throughout the volcanic rocks in the area is consistent with lower amphibolite facies. The mafic volcanic rocks typically have a mineral assemblage dominantly consisting of hornblende, biotite, plagioclase, and quartz with lesser variable amounts of garnet, clinozoisite, sericite, pyrite, magnetite and rare chlorite, epidote, actinolite and calcite. These rocks range from schists to amphibolites and display a foliation defined by the majority of minerals listed above. The ultramafic rocks are typically composed of serpentine, talc and magnetite, with lesser amounts of amphibole and trace amounts of pyrite. The felsic to intermediate rocks are typically composed of quartz, feldspar, muscovite, and sericite with lesser amounts of chlorite, epidote, hornblende, biotite, calcite, pyrite, and magnetite. Undulatory extinction in quartz grains is common, twinning in feldspars is rare, and quartz and feldspar grains within the groundmass only locally display triple junctions. Feldspar

grains rarely show twinning in the volcanic rocks unless they are primary phenocrysts. Banded iron formations locally show the addition of clinopyroxene and typically display triple junctions within the quartz-rich layers. The post-tectonic granitic intrusions (Killala-Baird batholith and associated intrusions) in the area do not show the same intensity of metamorphism and deformation and therefore rarely display any fabrics, whereas the syn-tectonic granitic intrusion (Medicine Stone pluton) does display strong foliations around its margins. The granitic intrusions still have most of their primary mineralogy with greater addition of epidote as stringers and disseminated grains compared to the volcanic rocks in the area. Other intrusions such as the pyroxenite have pyroxenes that have almost all been completely replaced by hornblende, yet only very minor strain is preserved in these rocks.

Metamorphism has largely affected the mineralogy of the volcanic rocks and to a lesser extent the chemical sedimentary rocks, but most primary macroscopic textures such as pillows and bedding have withstood metamorphism and deformation. The mafic pillows in the Balmer assemblage on the north shore of Laird Lake display way-up directions towards the north-east which are facing away from the younger Confederation assemblage to the south (Fig. 4.10). The orientation of the pillows is consistent with observations made elsewhere in the Red Lake camp which were used to previously interpreted an early non-penetrative deformation event (Sanborn-Barrie et al., 2001)

The intensity of ductile deformation in the Laird Lake area is heterogeneous, but overall is low to moderate, with centimeter to meter-scale zones of higher strain. This deformation is defined by a well-developed regional foliation striking on average 077° and dipping 74°SE (Fig. 4.15A; B). In local areas, the dip of the foliation would alternate towards the north, with an average strike of 262° and dip of 78°NW. The foliation is defined by amphibole, biotite, muscovite and chlorite when present, but can also be defined by aligned feldspar phenocrysts (Fig. 4.16A), amphibole poikiloblasts, quartz and feldspar porphyritic crystals in tuffs, quartz phenocrysts in granitic intrusions, flattening direction of pillows (Fig. 4.16B), stretched amygdules, mineral banding in the Balmer assemblage.

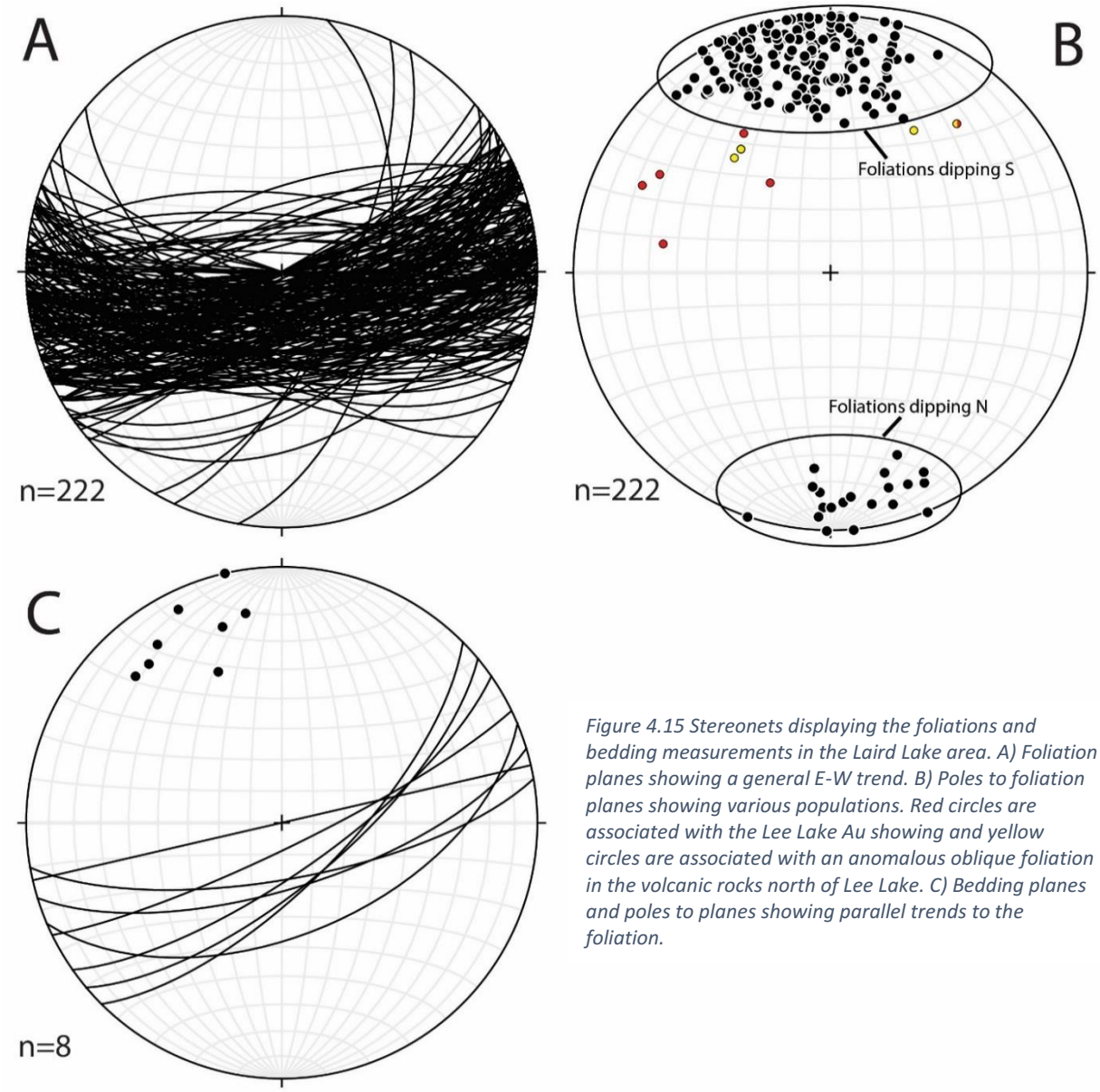

Figure 4.15 Stereonets displaying the foliations and bedding measurements in the Laird Lake area. A) Foliation planes showing a general E-W trend. B) Poles to foliation planes showing various populations. Red circles are associated with the Lee Lake Au showing and yellow circles are associated with an anomalous oblique foliation in the volcanic rocks north of Lee Lake. C) Bedding planes and poles to planes showing parallel trends to the foliation.

Figure 4.16 Field photographs showing the regional foliation in relation to primary features A) Confederation assemblage mafic volcanic flow with a moderate to strong foliation defined by aligned feldspar phenocrysts (UTM 422206E 5643575N; station 16BG538). B) Mafic pillows of the Balmer assemblage flattened parallel to the foliation (UTM 419641E 5644271N; station 15BG143). C) Contact between two units parallel to the regional foliation (S_2). Lower unit is a Confederation assemblage mafic volcanic flow with thin 5mm long feldspar phenocrysts aligned parallel to foliation and upper unit is an intermediate to felsic tuff showing bedding (S_0) equally parallel to foliation (UTM 418884E 5643177N; station 15BG337). D) Balmer assemblage chemical sedimentary rock with primary bedding (S_0) crenulated by the regional foliation (S_2; UTM 421533E 5643875N; station 16BG532).

Chemical sedimentary units and contacts between mafic and intermediate to felsic volcanic units parallel to foliation help identify the overlap between primary and secondary deformation features. Due to the nature of the primary volcanic layering within the Confederation assemblages, the foliation is commonly parallel to bedding (Fig. 4.16C). The bedding varies in strike between 45° and 80° with dips varying from 54°SE to subvertical (Fig.4.15C). When the foliation is not parallel to the bedding, crenulation between S_0 (bedding) and S_2 (S_1 is not observed in the Laird Lake area) are present (Fig. 4.16D). This demonstrates that primary bedding and the foliation are not always parallel.

Near the contact between the Balmer and Confederation assemblages, deformation is characterized by a strong foliation, well-developed folding, boudinage, shearing not parallel to the main foliation, and banding in the rocks. Most of these features were observed in the Balmer assemblage with only locally stronger foliation development observed within the Confederation assemblage. The mineral banding in the rocks (section 4.1.3.1.), defines the foliation macroscopically, but strain in this banded unit is heterogeneous along the assemblage contact. In lower strain areas, the bands are continuous and no folding is observed. Petrographically, only biotite, and local hornblende-rich layers define the foliation whereas other minerals such as diopside, the hornblende-rich rims to the diopside layers, and local clinozoisite patches show no preferred orientation (Fig. 4.17A). The quartz-rich groundmass displays local triple junctions. In higher strain areas, the thicker diopside-rich bands are boudinaged (Fig. 4.12B) or the diopside occurs as patches resembling porphyroclasts enveloped in a hornblende-rich rim (Fig. 4.17B). These could have formed from the boudinage of thinner diopside bands which are no longer present. Quartz grains are foliated and have undulatory extinction whereas diopside grains remain unaffected. Other than the massive diopside, the only unfoliated minerals are the hornblende grains found in the spaces between diopside porphyroclasts. The higher strain areas also tend to display tight to isoclinal folds in which the axial planes are either parallel or sub-perpendicular to foliation (Fig. 4.17C). The observed fold structures measured 2-25 cm in amplitude. Offsets or splays from the main zone of deformation (contact between the two assemblages), are locally found throughout the area and are defined by the presence of a stronger fabric development, the appearance of garnets, an increase in biotite, and mineral lineations (Fig. 4.17D) yet no mineral banding is present.

No major regional fold structures were observed on the Laird Lake property, but a major change in the trend of the foliation is recorded on the south-western shore of Lee Lake. The foliation in this area strikes between 10 and 58°, as opposed to the general NE-E trending foliation more commonly observed in the Laird Lake area. The deviation in foliation indicates the presence of a N-NE trending flexure of the

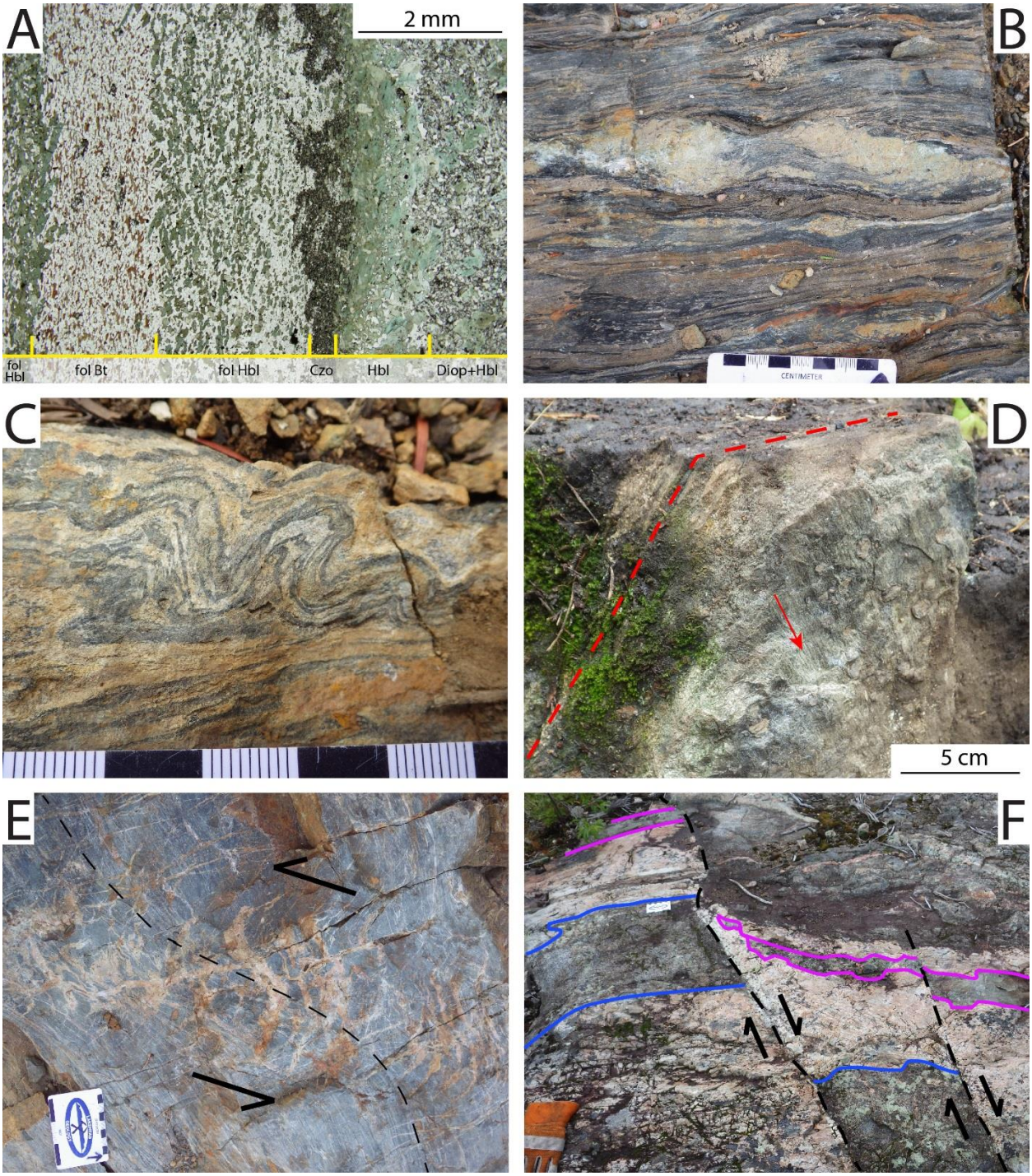

Figure 4.17 Field and petrographic photographs showing ductile and brittle structures A) Mineral banding in the Balmer assemblage with the foliation being defined by aligned biotite and fine-grained hornblende, whereas the diopside and coarser grained hornblende is massive. Foliated layers are marked by "fol" in image (UTM 418356E 5642965N; station 15BG296). B) Strong foliation wrapping around light green diopside porphyroclasts with hornblende-rich rims (UTM 421117E 5643825N; Gold Bearing Zone trench). C) Small folds in mineral banded unit of the Balmer assemblage at the Lee Lake Au showing (UTM 418356E 5642965N; station 15BG296). D) Mafic volcanic rocks of the Confederation assemblage showing a lineation defined by aligned garnets within the plane of the regional foliation (UTM 420040E 5643019N; station 15BG228). E) Small sinistral shear zone trending north-east with associated quartz-filled sigmoidal tension gashes (UTM 421120E 5643823N; Gold Bearing Zone trench). F) Dextral faults trending roughly north. Coloured margins indicate cross-cutting mafic intrusions parallel to stratigraphy within felsic tuffs (UTM 422650E 5643980N; station 15BG069). ***fol****: foliated,* ***Bt****: biotite,* ***Hbl****: hornblende,* ***Czo****: clinozoisite,* ***Diop****: diopside*

contact between the Balmer and Confederation assemblages (Fig. 4.1). The mafic volcanic rocks of the Balmer assemblage display mineral banding, folding, and boudinaged diopside layers. A gradual rotation of the foliation to the regional NE-trending foliation is observed westward along the shoreline. The Lee Lake Au showing sits on this N-striking structure (Fig. 4.15B). The volcanic rocks north of Lee Lake and the Lee Lake Au showing, have an average foliation striking eastward, with no major N-striking features arguing against a N-striking shear zone. However, local outcrops display strong fabrics trending SE and dipping SW (Fig. 4.15b), indicating the potential presence of a large open fold structure north of Lee Lake. The absence of foliations trending north-east and the lack of overprinting foliations by crenulations would argue against the possibility of the presence of large open folds.

Subsequent to the development of the main foliation, ductile and brittle structures developed, displacing the main units on a millimetre- to meter-scale. Best observed on stripped trenches, these structures appear as small ductile shear zones with local appearances of sigmoidal tension gashes (Fig. 4.17E) or clean breaks depending on the rheology of the unit the structures displaced. Petrographically, micro-shears mirroring the larger structures at outcrop scale, are often observed in the higher strain areas. These micro features are often associated with an increase in calcite. At the Gold Bearing Zone trench, the structures are always sinistral and vary in orientation from NNW to NNE (see section 4.3.1.4.). At the Zone 11 trench (UTM 422670E 5644053N), the structures are dominantly sinistral and vary from 022 to 090° (mostly sinistral) and 215 to 325° (mostly dextral; Fig. 4.17F).

Previous work completed in the area by Atkinson (1999) recognised multiple E and NE trending faults on the Laird Lake property. Only the Laird Lake Fault located between the Killala-Baird batholith and the volcanic package on the eastern half of the property shows enough compelling evidence for a fault. A linear, magnetic low anomaly is associated with a depression between the Killala-Baird batholith and the Balmer assemblage and continues NW from the field area into the batholith. No fabrics or displacement were recognised to be associated with the structure.

4.3 Mineralization and Alteration

Alteration in this section refers to hydrothermal metasomatism, which is the change in chemistry and in turn, mineralogy in a rock caused by the reaction between hydrothermal fluids and the host rock (Thompson and Thompson, 1996). The alteration is typically accompanied by an increase in metal abundances (Au, As, Sb, W, Ag, etc). This is distinct from an isochemical reaction caused by regional metamorphism where the chemistry remains the same but mineralogy changes according to metamorphic grade.

The Laird Lake property displays a variety of styles of mineralization and associated alteration, with the highest gold grades often being confined to the zone of highest deformation, which coincides with the contact between the Balmer and Confederation assemblages. There are rare exceptions scattered away from this zone in which deformation has not played a large role in controlling the mineralizing and alteration fluids. The BIF north of Lee Lake (Fig. 4.1) hosts 84.6 ppb Au and is roughly 1.4 km from the zone of strongest deformation. The only lamprophyre occurrence hosts 298 ppb Au, is 250 m away from this zone, and yet is not hosted in strongly deformed rocks. The alteration in the Laird Lake area is not widespread and therefore specific types of alteration will be described with their associated types of mineralization. Three types of gold occurrences (>100 ppb Au) were identified during mapping. The types are (listed in descending order of predominance): disseminated sulphides, ±pyrite, ±arsenopyrite, ±pyrrhotite (type 1), quartz veins (type 2), and lamprophyres (type 3). Figure 4.10 summarizes the types of Au mineralization in relation to the geology of the area.

4.3.1 Type 1 – Disseminated Sulphides

Type 1 gold mineralization forms the bulk of the mineralization and alteration on the Laird Lake property. It is defined by the presence of elevated gold values with associated sulphides such as pyrite, arsenopyrite, pyrrhotite and rarely chalcopyrite. The presence of sulphides however, does not always indicate elevated gold values. The sulphides can be seen in all varieties of volcanic and sedimentary rocks on the property, but an increase in gold mineralization is dominantly, but not always, associated with hydrothermally altered Balmer assemblage mafic volcanic rocks, BIFs, carbonate-rich formations, Confederation assemblage mafic volcanic rocks, and quartz-feldspar porphyritic crystal tuffs. In all these lithologies, the highest gold values are most often found close to the contact between the Balmer and Confederation assemblages.

4.3.1.1 Hydrothermally Altered Balmer Assemblage Mafic Volcanic Rocks

Most of the gold mineralization found on the Laird Lake property is hosted within hydrothermaly altered Balmer assemblage mafic volcanic rocks in the vicinity of the contact between the two assemblages. As previously mentioned, this zone coincides with the area of most intense deformation on the Laird Lake property and has resulted in a banded texture within the mafic volcanic rocks (Figs. 4.12; 4.17A, B, C). The average thickness of the exposed banded unit 2-5 m. The hydrothermally altered mafic volcanic rocks near the major contact consistently yielded higher than background gold values, even when the banded texture was not observed. This type of mineralization is typically associated with variable proportions of biotite, hornblende, diopside, clinozoisite, quartz, feldspar, ±apatite ±garnet ±calcite (Fig. 4.18A). Where the alteration and banded texture is present, but no sulphides are visible, the rock often contains low gold values. The presence of a rusty coating on the outcrops is commonly observed when sulphides are present. The sulphides in the hydrothermally altered mafic volcanic rocks are dominantly pyrite and pyrrhotite, with less common occurrences of

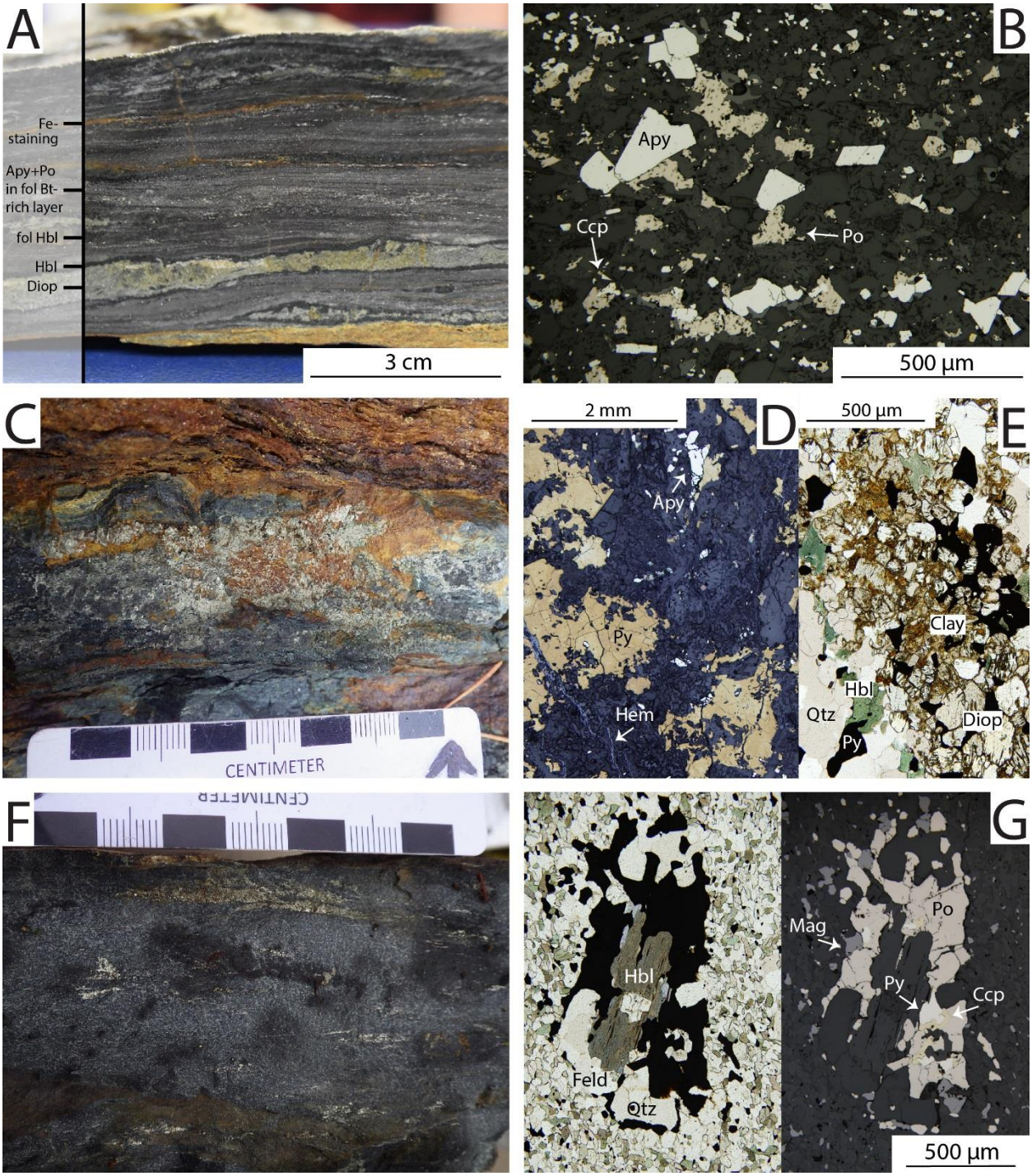

*Figure 4.18 Field, hand sample, and petrographic photographs displaying alteration and mineralization. A) Mineral banding at the Lee Lake Au showing with the alteration and mineralization-rich layers parallel to foliation. The arsenopyrite and pyrrhotite is concentrated in the biotite-rich layers (UTM 418356E 5642965N; station 15BG296). B) Reflected light photograph of the arsenopyrite and pyrrhotite-rich band with fine-grained chalcopyrite, showing a close relationship between the sulphides (UTM 418356E 5642965N; station 15BG296). C) Banded-iron formation showing abundant pyrite (UTM 421110E 5643812N; Gold Bearing Zone trench). D) Reflected light photograph of the semi-massive pyrite (deep yellow due to oxidation) and arsenopyrite within a banded-iron formation, again showing the close association between the two sulfphides. Lake hematite veinlets cross-cut the pyrite (UTM 421110E 5643812N; Gold Bearing Zone trench). E) Clay alteration on the diopside grains within a pyrite-rich layer within a BIF (UTM 421110E 5643812N; Gold Bearing Zone trench). F) Foliated pyrrhotite and pyrite within unaltered Balmer assemblage mafic volcanic rock (UTM 416911E 5643921N; station 15BG340). G) Plain polared (left) and reflected light (right) photographs of pyrrhotite, pyrite, chalcopyrite, and magnetite concentrated in zone with coarser grain silicates (hornblende, quartz, and feldspars; UTM 416911E 5643921N; station 15BG340). **Apy**: arsenopyrite, **Po**: pyrrhotite, **Py**: pyrite, **Hem**: hematite, **Mag**: magnetite, **Ccp**: chalcopyrite, **Bt**: biotite, **Hbl**: hornblende, **Diop**: diopside, **Qtz**: quartz*

arsenopyrite and chalcopyrite. These are typically hosted in the biotite and fine-grained quartz-feldspar layers, and are also aligned parallel to the main foliation. The disseminated sulphides are commonly fine- to very fine-grained, and are rarely in the form of veinlets. Where arsenopyrite has been identified, the gold grades are commonly >100 ppb Au.

At the Lee Lake Au showing, a discrete biotite-rich layer is enriched in arsenopyrite, pyrrhotite, and lesser chalcopyrite and measured roughly 3 cm thick. On a fresh surface, the layer is grayish purple and is closely associated with diopside layers rimmed by coarser-grained massive hornblende. Petrographically, the arsenopyrite grains are euhedral to subhedral, whereas the pyrrhotite and chalcopyrite grains are anhedral (Fig. 4.18B). Arsenopyrite and pyrrhotite can occur as inclusions within each other, whereas chalcopyrite does not host inclusions of other sulphides. The sulphides are commonly seen as interstitial grains to the groundmass, and rarely observed as inclusions within quartz and feldspar grains. Only rarely are the sulphides found within the diopside layers as interstitial grains.

4.3.1.2 Banded-Iron Formations

Banded-iron formations commonly host trace to abundant pyrite mineralization. In areas far from the contact between the two assemblages, disseminated pyrite mineralization will average 2% by volume whereas disseminated magnetite usually ranges from 4-10% (stations 15BG352; UTM 416653E 5644067N; and 15BG418; UTM 417703E 5644219N). Typically, magnetite and pyrite are more closely associated with the diopside-rich layers and to a lesser extent with the hornblende-rich zones, although trace magnetite is common in the quartz layers. Magnetite was not observed as inclusions within pyrite grains, however, pyrite can be seen rimmed by hematite. Hematite stringers are locally observed and cut all minerals. The highest gold grade in BIFs away from the assemblage contact was 84.6 ppb Au.

In a mineralized rusty iron formation (Gold Bearing Zone trench; UTM 421142E 5643838 to 421078E 5643802N), near the contact between the two assemblages, up to 20% pyrite and 1%

arsenopyrite are present in non-chert layers (Fig. 4.18C). Trace amounts of pyrite are found as disseminated interstitial grains within the quartz-rich layers. The BIF is weakly to non-magnetic and only hosts trace amounts of magnetite as rare inclusions within pyrite grains. The layering within the mineralized BIF is irregular and alternates between quartz-rich layers, locally containing fine-grained hornblende, and mica-rich layers containing biotite, muscovite, rare quartz, a very fine-grained deep yellow micaceous phase, and clinozoisite. Anhedral to subhedral pyrite and arsenopyrite are typically hosted within the biotite/muscovite-rich layers, and associated with cross-cutting hematite stringers (Fig. 4.18D) and hematite rimmed pyrite grains. Diopside is not present where gold grades are highest in the BIF. However, along strike in the BIF, very fine-grained diopside, hornblende and pyrite are commonly present as interstitial disseminated phases within the quartz-rich layers, although most of the pyrite mineralization is present within the hornblende and diopside-rich zones. Diopside is weakly to strongly altered by the fine-grained yellow clay, more commonly near the pyrite-rich areas, compared to the quartz-rich zones (Fig. 4.18E). In the pyrite-rich zones, the pyrite is interstitial to the diopside and hornblende crystals. The fine-grained yellow alteration is commonly borders coarser-grained pyrite as veinlets, or cross-cutting pyrite grains and is also locally associated with hematite stringers.

The mineralized BIF was intersected by a pyrite, magnetite and hematite-rich shear zone. The point of intersection between the shear and the BIF is closely associated with the highest gold assay from this study (>3600ppb; BIF; sample GBZ-O15-021). Along strike, further away from the shear, Bounty Gold Corp. reported assays up to 35.34 g/t over 2.1m (LeBlanc, 2016). A second BIF at the Gold Bearing Zone trench is not sulphide-bearing, and contains insignificant gold mineralization. The layering in the unmineralized BIF alternates between quartz-rich layers with less than 5% disseminated diopside, hornblende, and magnetite grains throughout, to diopside, hornblende, and magnetite-rich layers. In these layers, up to 30-50% magnetite is present, with only trace pyrite. The pyrite, magnetite and hematite-rich shear does not intersect this BIF.

4.3.1.3 Carbonate-Rich Formation

The only occurrence of the carbonate-rich formation hosts 1-3% disseminated pyrrhotite with lesser pyrite and chalcopyrite within its hornblende-rich layers (station 16BG532; UTM 421526E 5643860N). Higher than average Au grades (222 ppb) are present within this unit, which are presumably associated with the sulphide mineralization. Diopside-rich zones are found at the contact between the mafic and carbonate layers. No other distinct alteration was observed.

4.3.1.4 Balmer Assemblage Mafic Volcanic Rocks

Sulphide mineralization in Balmer assemblage mafic volcanic rocks outside the zone of hydrothermally altered and deformed rocks (section 4.3.1.1.) is not common. The sporadic occurrences consists of disseminated to stringer pyrite and pyrrhotite with lesser concentrations of chalcopyrite and magnetite (Fig. 4.18F). In the samples analysed under thin section, no major alteration phases were observed. In Figure 4.18G, the sulphides are concentrated in a coarser-grained zone of hornblende, quartz, and feldspar, which also comprise the fine-grained groundmass. The coarser-grained zones could represent filled vesicles caused by metamorphic processes which allowed the growth of coarser-grained phases in voids.

4.3.1.5 Confederation Assemblage Mafic Volcanic Rocks

Within the Confederation assemblage, no significant alteration is associated with the contact. The most significant gold mineralization (>100 ppb Au) within the volcanic rocks of the Confederation assemblage is found roughly 250 m from the contact between the two assemblages within a mafic volcanic unit (RSPZ trench; station 15BG088; UTM 422216E 5643691N). The occurrence is foliated and contains up to 15% fine-grained disseminated pyrite to thin pyrite stringers parallel to foliation. Trace amounts of chalcopyrite are found as inclusions within pyrite, or as individual grains, but always

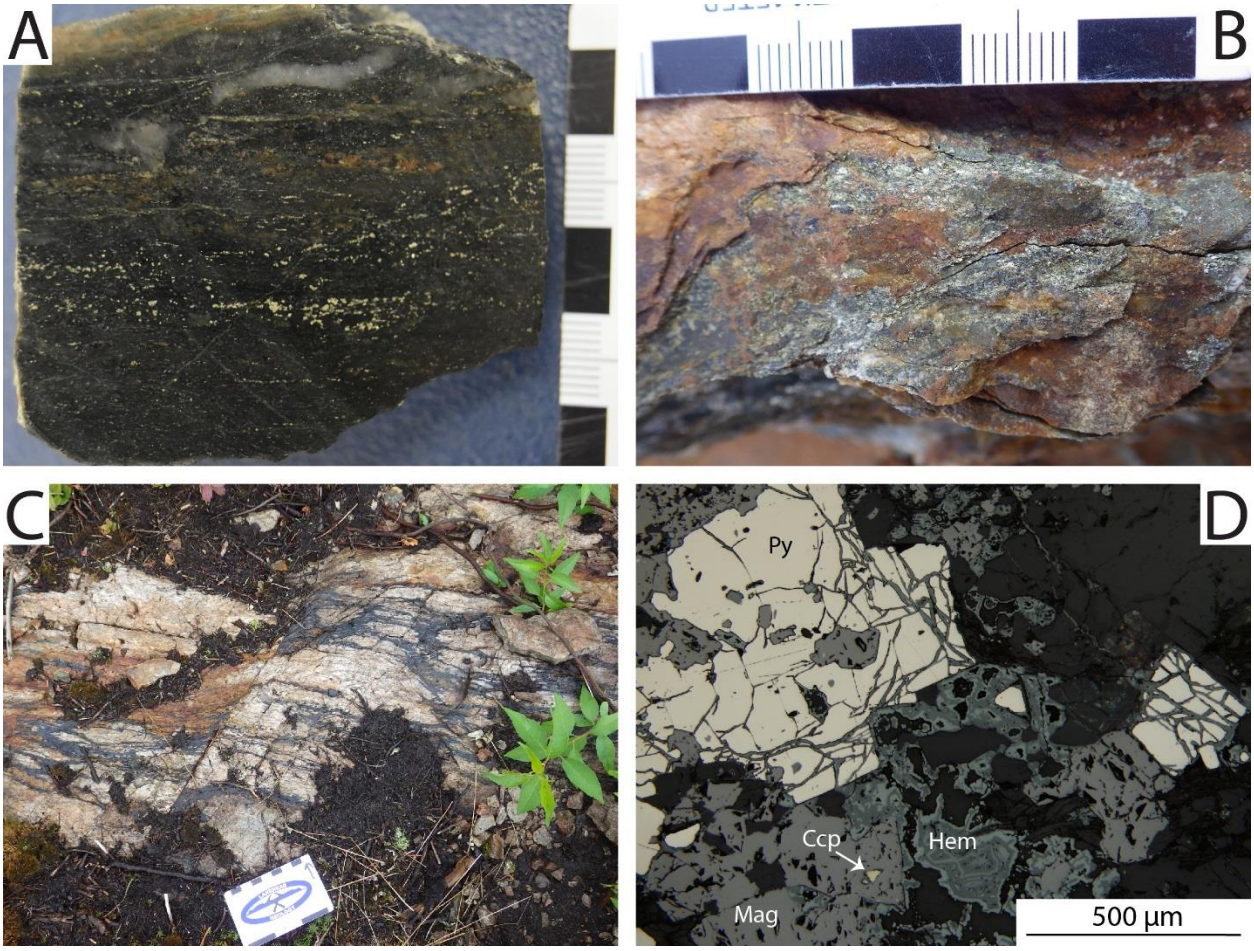

Figure 4.19 Field photographs showing the mineralization within the Confederation assemblage A) Mafic volcanic rock with visible potassic alteration as shown by dark pink microcline patches and disseminated pyrite aligned parallel to foliation (UTM 422216E 5643691N; station 15BG088). B) Pyrite mineralization within a quartz-feldspar porphyritic crystal tuff (UTM 422744E 5644101N to 422668E 5643925N; Zone 11 trench). C) Irregular magnetite veins cutting a quartz-feldspar porphyritic crystal tuff (UTM 422756E 5643969N; station 15BG039). D) Hematite brecciating pyrite and rimming both pyrite and magnetite grains (UTM 422756E 5643969N; station 15BG039). ***Py****: pyrite,* ***Ccp****: chalcopyrite,* ***Mag****: magnetite,* ***Hem****: hematite.*

closely associated with pyrite. Alteration associated with the pyrite mineralization consists of dark pink patches of microcline in Figure 4.19A, but also by an increase in epidote and calcite.

4.3.1.6 Quartz-Feldspar Porphyritic Crystal Tuff

Two sub-types of mineralization are found within the quartz-feldspar porphyritic crystal tuffs of the Confederation assemblages. The first type is associated with 5-20% disseminated to stringer pyrite mineralization and a stronger deformational fabric. This mineralization is observed at the 250 m long Zone 11 trench (UTM 422744E 5644101N to 422668E 5643925N) and station 15BG055 (UTM 422685E 5643763). The outcrop is usually rusty where mineralization is present, however, pyrite was the only

alteration phase present as the sample from Zone 11 simply contained quartz, feldspars, muscovite, and abundant pyrite. The mineralization occurs in zones parallel to the main foliation but itself is not deformed as the pyrite grains occur as euhedral cubes. Coarse-grained quartz zones, possibly veinlets, are associated with pyrite indicating that there could be a component of Type 2 style alteration/mineralization present at the Zone 11 trench. Pyrite mineralization in this trench occurs in a rusty zone parallel to stratigraphy and foliation.

The second mineralization sub-type consist of an irregular type of magnetite mineralization which did not yield more than 100 ppb Au and is observed rarely within the quartz-feldspar porphyritic crystal tuff (station 15BG039; UTM 422756E 5643969N). The mineralization occurs as disseminated magnetite veins measuring up to 2 cm thick, with associated euhedral pyrite borders. Rare chalcopyrite grains are found as inclusions within magnetite. The pyrite is often brecciated and rimmed by hematite (Fig 4.19D).

4.3.2 Type 2 – Quartz Veins

Multiple quartz veins are found on the Laird Lake property, however, only two veins are known to host significant gold mineralization. The mineralized veins are hosted in both the Balmer and Confederation assemblages and are associated with zones of stronger deformation, striking parallel to the main foliation. The quartz vein within the Balmer assemblage is found in the 220 m long Pit Zone trench (station 15BG447; UTM 420313E 4643722N to 420125E 5643651N) and is exposed for roughly 50m along strike. The vein is hosted within locally rusty mafic volcanic rocks having the banded alteration texture (Fig. 4.20A). It is ca. 60 m away from the interpreted contact between the two assemblages. The vein ranges from 5-20cm in thickness and locally branches into several thinner parallel veins before remerging. It is typically smokey gray in colour and can host up to 15% pyrite and lesser chalcopyrite and pyrrhotite, with common occurrences of visible gold flakes along a 2m long section of

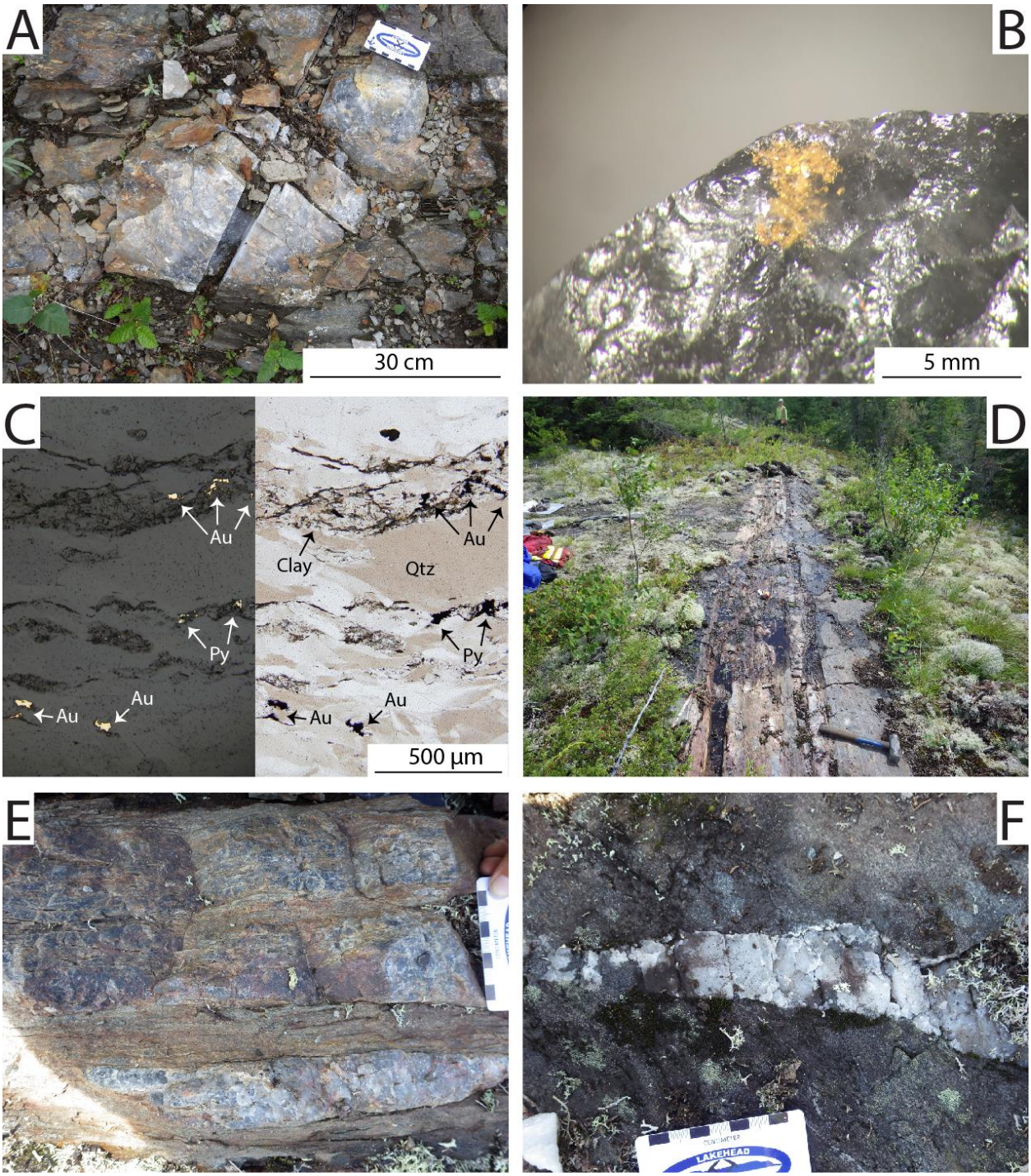

*Figure 4.20 Field and petrographic photographs showing the mineralized quartz veins A) Mineralized smoky quartz vein hosted in Balmer mafic volcanic rocks displaying the banded texture (UTM 420222E 5643701N; station 15BG447; Pit Zone trench). B) Visible gold flake within smoky quartz (UTM 420222E 5643701N; station 15BG447; Pit Zone trench). C) Reflected light (left) and plain polar transmitted light photographs of visible gold and pyrite grains often associated with fine-grained clay minerals within a strongly deformed smoky quartz vein (UTM 420222E 5643701N; station 15BG447; Pit Zone trench). D) High strain zone associated with smoky quartz veins and an intermediate dike (UTM 422491E 5643792N; station 15BG233; SHQZ trench). E) Close up of mineralized smoky quartz veins with dark pink staining, hosted by strongly biotite altered mafic volcanic rocks (UTM 422491E 5643792N; station 15BG233; SHQZ trench). E) Unmineralized milky white quartz vein cutting across foliation just a few metres away from the mineralized veins (UTM 422491E 5643792N; station 15BG233; SQGZ trench). **Py**: pyrite, **Qtz**: quartz.*

the vein (Fig. 4.20B). Higher grade gold values (1.32 to 140.59 g/t Au) were obtained over a 25 m long portion of the vein, but are sporadic outside of that zone (LeBlanc, 2016). A sample of the host mafic volcanic rocks yields only 12 ppb Au. The quartz vein is strongly deformed with the quartz grains being foliated and displaying undulose extinction and grain size reduction along the larger grain boundaries. Visible gold grains up to 150 μm across occur as individual grains, or are closely associated with pyrrhotite and/or pyrite (Fig. 4.20C). The gold commonly occurs in clusters of a few grains, typically on the quartz grain boundaries and rarely as inclusions within quartz. The gold is also locally associated with small clay-rich veinlets that are parallel to the main strain within the sample (Fig. 4.20C).

The second mineralized quartz vein on the Laird Lake property is located within Confederation assemblage mafic volcanic rocks at the SHQZ trench (station 15BG233; UTM 422489E 5643792N). This area is 300 m away from the only significant gold occurrence in the mafic volcanic rocks of the Confederation assemblage at the RSPZ trench (station 15BG088; UTM 422219E 5643691N). The gold is found within a set of 3-4 separate quartz veins that pinch and swell from 2-12 cm and locally merge together. The quartz veins are smokey gray, with local dark pink staining. The veins are hosted in what appears to be a 40 cm thick highly strained zone striking parallel to the regional foliation (Fig. 4.20D). Within this high strain zone, a pinkish-beige intermediate dike is also present. The quartz veins are locally hosted within this dike with the north contact being very sharp and south contact having a gradational to irregular boundary with the host mafic volcanic rocks. The quartz veins on the southern portion of the high strain zone are hosted in rusty, strongly biotite-altered mafic volcanic rocks (Fig. 4.20E). The gold grades in the quartz veins are as high as 7.74 g/t Au (LeBlanc, 2016) whereas the intermediate dike contains at 150 ppb Au. The host mafic rocks outside the high strain zone have low Au grades, with assays of 16.2 ppb Au. Petrographically, the quartz shows undulose extinction, but is not strongly foliated. Local grains show evidence for grain size reduction. No visible gold was observed in this sample but trace disseminated pyrite is present. The high strain zone with the presence of quartz

veins and intermediate dike represents a zone of overprinting ductile and brittle deformation, creating ideal conditions for gold precipitation. A few other quartz veins are observed outside of the high strain zone but are milky white in colour and do not yield any significant gold values (Fig. 4.20F; J. LeBlanc 2016, personal communication, August 20). Folded 1-2 cm thick granitic veins are also seen in Z-fold patterns with the fold limbs being parallel to foliation.

4.3.3 Type 3 – Lamprophyres

Only one lamprophyre dike was observed throughout the Laird Lake property. It cross-cuts ultramafic rocks of the Balmer assemblage on the east side of Lee Lake (Fig. 4.9D; station 15BG287; UTM 418904E 5643643N). It is very rusty in colour, and consists of 85% biotite aligned parallel to the dike margins. Trace amounts of disseminated pyrite are present. The lamprophyre yields an assay of 296 ppb Au. Petrographically, up to 2% magnetite and 1% pyrite are found as anhedral grains in patches parallel to the dikes margins. Biotite, amphibole, magnetite and pyrite define a strong fabric, with unfoliated quartz and feldspar within the groundmass.

4.4 Mineralized Trenches

4.4.1 Gold Bearing Zone Trench

Located on the south side of Laird Lake, the “Gold Bearing Zone” trench (GBZ; Figs. 4.21, 4.22; UTM 421142E 5643838 to 421078E 5643802N) is a 65 m long stripped exposure of Balmer assemblage mafic metavolcanic rocks less than 100 m from the contact between the two assemblages. The trench was mechanically stripped in 2013 by Bounty Gold Corp. after high grade Au zones were outlined by previous companies, and mapped in detail in 2015 for this study. The trench was chosen for detailed mapping due to the elevated presence of gold in various lithologies, the well preserved deformation textures, and because of its proximity to the major contact with the Confederation assemblage. The trench expose mafic volcanic rocks, BIF, and younger cross-cutting intrusive rocks.

Figure 4.21 Photograph of the Gold Bearing Zone trench, displaying the 2x2 m grid (UTM 421110E 5643812N).

4.4.1.1 Mafic Volcanic Rocks

Mafic volcanic rocks are the dominant rock type in the trench. They consist of fine-grained, aphyric rocks which are dark gray on the fresh surface, but can range from light gray, to rusty black on the weathered surface. Deformation and alteration has intensely modified this unit, however, potential pillows and amygdules have been identified in low strain zones.

4.4.1.1.1 Least Deformed Mafic Volcanic Rocks

The least deformed mafic volcanic rocks in the trench are strongly to moderately foliated and are depicted on Figure 4.22 as the unit without any overlaying pattern. The colour, textures, and alteration vary a lot in this unit since the primary features are better preserved, and features were not destroyed by strong deformation. On the far west and central outcrops, the mafic volcanic rocks have an irregular off-white weathered surface which is typically bordered by dark gray zones, which may represent pillow salvages. On the west outcrop, directly north of the intermediate dike, much more convincing pillow salvages are present (Fig. 4.23A). The off-white zones are typically associated with an increase in magnetism, linked to the higher abundance of magnetite. On the middle and east outcrops, a vuggy texture is present where the vugs are outlined by diopside and are commonly associated with a

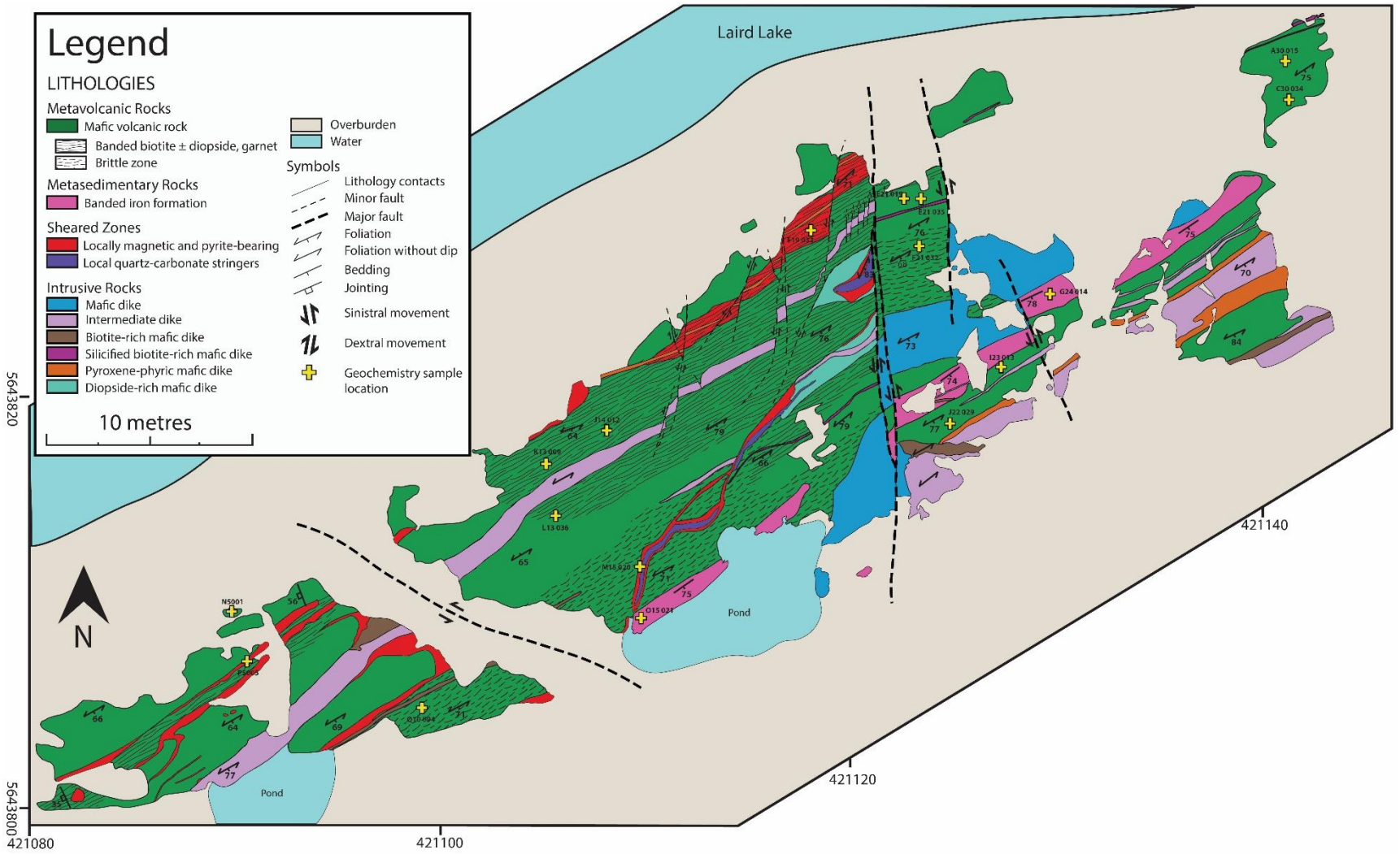

Figure 4.22 Geological map of the Gold Bearing Zone trench, showing the various lithologies, textures, structures, and geochemistry sample location (UTM 421130E 5643828N).

rusty colour. Where the vugs are absent, diopside surrounds quartz-carbonate stringers/pods (Fig. 4.23B). The off-white, amygdaloidal and potentially pillowed zone, and the vuggy/quartz-carbonate zone locally overlap.

4.4.1.1.2 Banded Mafic Volcanic Rocks

The banded mafic volcanic rocks are typically observed near the contact between the Balmer and Confederation assemblages (sections 4.1.3.1; Fig. 4.12A; section 4.2; Fig. 4.17A, B; section 4.3.1.1). In the GBZ trench, these rocks consist of alternating bands of biotite (± garnet; Fig. 4.23B), amphibole, lesser clinozoisite, and diopside as porphyroclasts instead of bands as seen at the Lee Lake Au showing. The texture reflects an increase in deformation, and locally correlates with the red sheared zones depicted on Figure 4.22. The banded texture in the GBZ is more intensely deformed than anywhere else on the Laird Lake property. The grains within the diopside patches are completely undeformed, and could represent the recrystallization of the diopside patches.

4.4.1.1.3 Mafic Volcanic Rocks in the Brittle Zone

The brittle zone is found on the southern portion of the GBZ trench and is locally displaced by late N-trending faults (Fig. 4.22). The brittle and rusty nature of the rock made it challenging to observe textures, however, local biotite-rich bands were observed (Fig. 4.23C). The rock contains intercalated biotite- and amphibole-rich bands (Fig. 4.23D), with trace disseminated fine-grained pyrite and local carbonate stringers. Local clinozoisite-rich veinlets associated with disseminated diopside are present, indicating that this unit shows very similar alteration to the banded unit. The diopside grains are overprinted by a brown alteration.

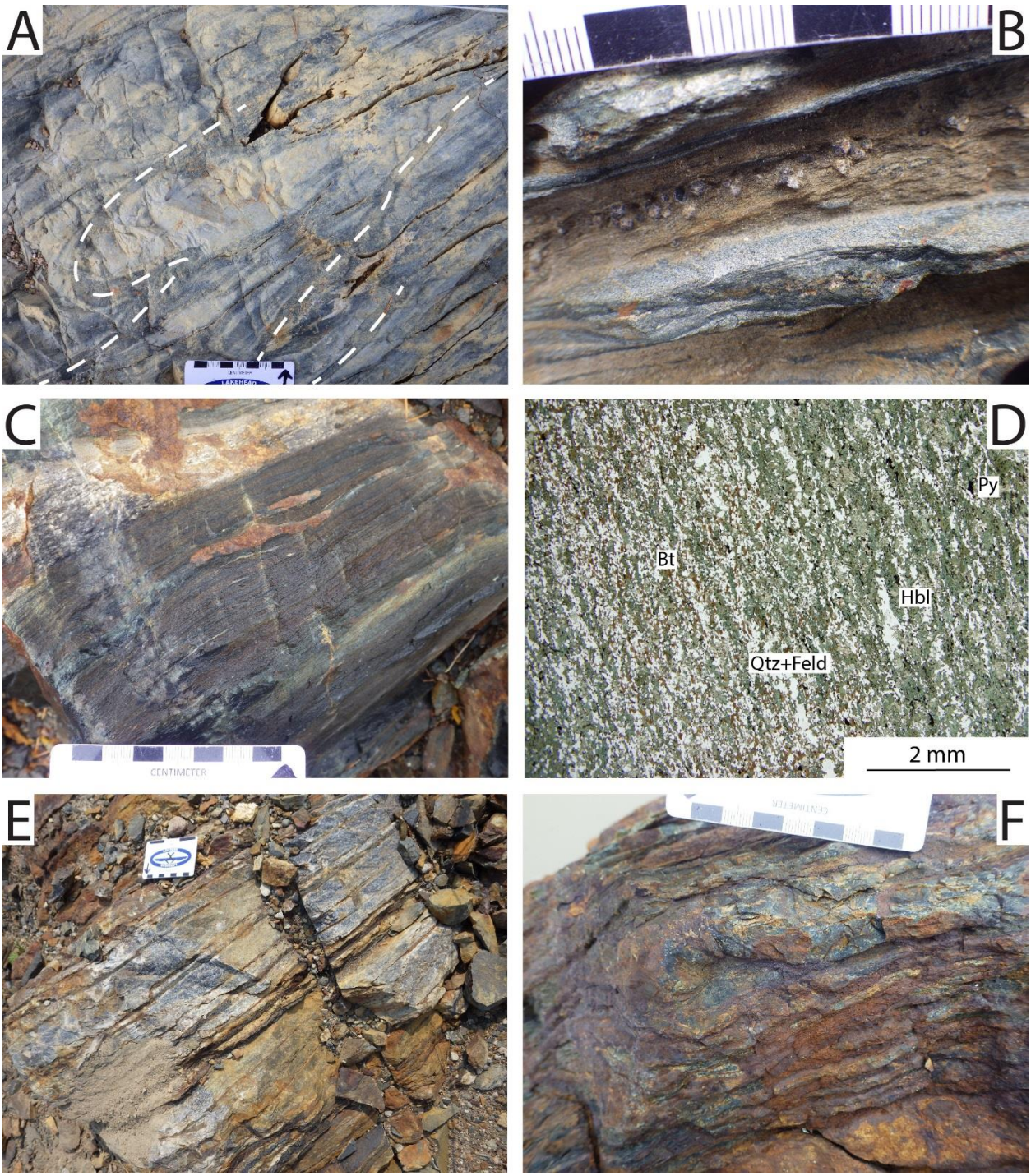

Figure 4.23 Field and petrographic photographs showing the volcanic-sedimentary units at the Gold Bearing Zone trench A) Potential pillow selvages outlined in dashed white lines with off-white bleached cores (UTM 421078E 5643818N). B) Garnet porphyroblasts within a biotite-rich layer in the banded mafic volcanic unit (UTM 421114E 5643822N). C) Biotite-rich bands within the mafic volcanic rocks in the brittle zone (UTM 421112E 5643812N). D) Petrographic photograph of the mafic volcanic rocks within the brittle zone, showing the alternating bands which are biotite-rich and hornblende-rich. The host rock shows similar mineralogy to the mafic volcanic rocks within the banded unit (UTM 421099E 5643804N; sample GBZ-Q10-004). E) Oxide facies banded iron formation showing alternating layers of chert and magnetite (UTM 421126E 5643821N). E) Sulphide facies banded iron formation showing a rusty surface, and alternating layers of chert and rusty sulphide-bearing bands (UTM 421113E 5643811N). ***Qtz****: quartz,* ***Feld****: feldspar,* ***Hbl****: hornblende,* ***Bt****: biotite,* ***Py****: pyrite.*

4.4.1.2 Banded-Iron Formations

There are two BIFs present at the GBZ trench. An oxide facies BIF on the east outcrop, and a sulphide facies BIF on the middle outcrop (Fig. 4.22). The oxide facies BIF contains alternating layers of chert (2-6 cm), and magnetite (0.5-2 cm; Fig. 4.23E). The rock is strongly magnetic and locally contains up to 2% disseminated pyrite associated with the magnetite-rich bands. A 10-15 cm thick pyrite-rich (15% pyrite) unit occurs directly south of the BIF. The magnetite within the oxide facies BIF is hosted within a diopside (Fig. 4.4B) or amphibole-rich matrix with very rare pyrite. The chert layers are composed mainly of quartz displaying undulose extinction, and/or triple junctions.

The sulphide facies BIF has a rusty weathered appearance, ranges from 40-75 cm in thickness and contains regular but less evident layers of chert, and pyrite + arsenopyrite with rare magnetite (Fig. 4.23F). This unit is weakly magnetic, with local magnetic highs where pyrite is absent. The chert layers typically range from 1-2 cm in thickness, whereas the darker sulphide-bearing bands are only 0.5-1 cm thick. Pyrite mineralization comprises up to 20% within the sulphide-bearing layers. Detailed description of the mineralization of the unit is present in section 4.3.1.2. and shown in Figures 4.18C-E.

4.4.1.3 Intrusions

Multiple cross-cutting intermediate to mafic dikes cut the trench parallel to the main NE trending foliation (Fig. 4.22). Most intrusions show very little fabric, but some are intensely foliated. Most of the intrusions predate the displacement on the N-trending faults (section 4.4.1.5.). The intrusions do not host any gold mineralization.

4.4.1.4 Structures

The GBZ trench displays various styles of ductile and brittle deformation. The earliest deformation is recorded by the presence of a NE trending foliation, defined by macroscopic features

such as mineral banding, and microscopic features such as mineral alignment. This deformation is strong and ductile, as seen by the presence of garnet porphyroblasts within the mafic volcanic rocks with the banded texture. Complex fold patterns were only observed at one locality within the banded mafic volcanic rocks (Fig. 4.24A). The folds display S and M folds with limbs trending parallel to sub-parallel to the foliation. Shears trending NE at the north end of the central outcrop, and the western outcrop are parallel to the foliation and most likely formed during this period of ductile deformation. Evidence for the same intensity of deformation is present in the brittle zone, as defined by the presence of biotite banding, trending at the same orientation as the foliation.

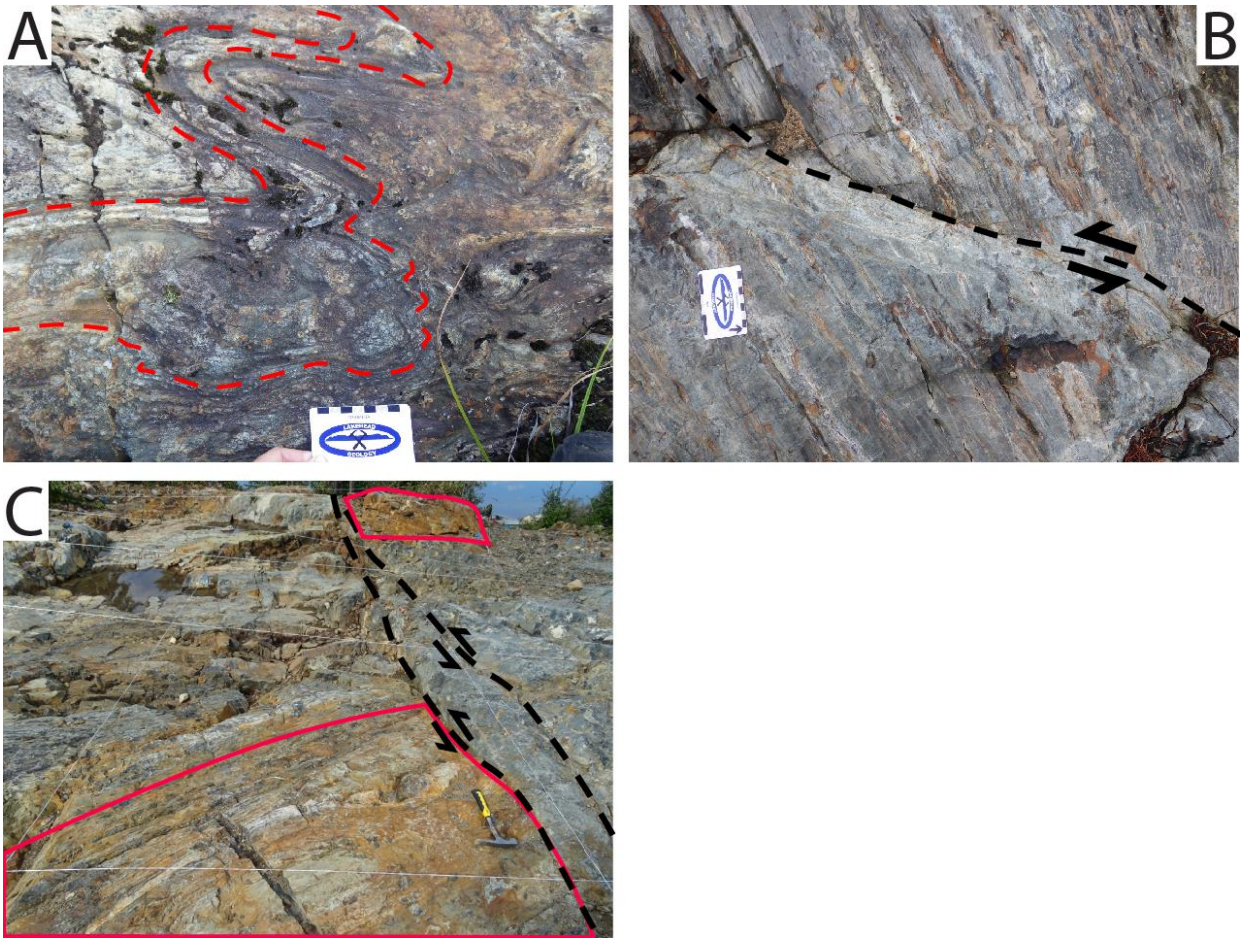

Figure 4.24 Field photographs showing the ductile and brittle structures at the Gold Bearing Zone trench A) Chaotic folding of mafic volcanic rock, showing S and M folds (UTM 421123E 5643835N). B) Banded mafic volcanic rocks cut by a sinistral fault, with localized shearing on the lower block (UTM 421121E 5643820N). C) Major N trending faults cutting all stratigraphy, alteration, and mineralization. Units boxed in red are the same, and suggest roughly 9 metres of displacement (UTM 421099E 5643804N).

Small N to NE trending faults and shear zones displaced the banding and the shear zone on the north-end of the middle outcrop by less than a metre. Most of the displacements are sinistral (Fig. 4.24C) with rare occurrences of dextral movement. A later shear with a highly eroded center and pyrite-rich margins cuts the middle outcrops and intersects the sulphide-facies BIF. The shear is parallel to perpendicular to foliation and formed after the N to NE trending faults, as the faults tend to bend sub-parallel to parallel to the shear, indicating a sinistral movement on the late shear (also confirmed by the displacement of the intermediate dike). The shear post-dates the early ductile deformation, as the pyrite bordering the shear is not foliated. Large N and NW trending sinistral faults displace all units on the centimetre to metre scale and the largest displacement measures 9-10m (Fig. 4.24D).

4.4.1.5 Alteration and Mineralization

The majority of the alteration and mineralization in the GBZ trench fits within the Type 1 style of mineralization: disseminated sulphides and to a lesser extent in Type 2: quartz veins. Since multiple styles of alteration are present in the trench, the alteration is subdivided into further subtypes; type 1: magnetite-rich + bleaching of the weathered surface; type 2: biotite (bands); type 3: diopside bands; type 4: carbonate stringers/pods enveloped by diopside-rich halo; type 5: silicification + diopside (Table 4.1). Figure 4.25 displays the location of each style of alteration. Type 3 (diopside (bands) and diopside replacement) is not shown on the map due to the overlapping occurrences with other alteration types.

Mineralization typically consists of pyrite, pyrrhotite, and arsenopyrite and occurs in three main lithologies: mafic volcanic rocks, BIF, and cross-cutting gold-bearing shears. The gold-bearing shears, depicted as red units on Figures 4.22 and 4.25, are typically rusty shear zones, with the core of the shear ranging from deep purple to black (mostly on the western outcrop), to orange-red (strongly hematized) on the shear zone that cuts the foliation in the middle outcrop. This shear is locally associated with fine-grained dark green rock with quartz-carbonate stringers (Fig. 4.26D), depicted as purple units in Figure

Table 4.1 Summary of the various types of alteration found at the Gold Bearing Zone trench. Gold concentrations were taken from the samples listed in the last column, which best represented that style of alteration. An anomalous increase in the associated metals is defined the geochemistry.

Alteration type	Host units	Field description	Location	Nature of alteration	Associated mineralization	Au grades (ppb)	Metal association	Samples
Type 1 - Magnetite + bleaching	Mafic volcanic	Off-white colour on the weathered surface, high magnetic response on magnetic susceptibility metre	North end of west outcrop, which crosses over to the very north-west end of the middle outcrop. Decrease in bleaching and magnetism towards the south.	Bleaching of the weathered surface. Magnetite and pyrite occur in patches, often associated with coarser grain hornblende grains up to 1 mm long. Figure 4.26A	Magnetite (4%), pyrite (1%)	20.9	Sb, W	N5-001
Type 2 - Biotite (bands)	Mafic volcanic	Continuous biotite-rich bands with local garnets. Always associated with hornblende-rich bands, and local diopside and clinozoisite bands	Consistently present where the banded texture and brittle zones are observed.	Bands of fine-grained biotite within a quartz and feldspar groundmass.	Pyrite (trace-15%)	58.6-10.9	Sb, W, ±Mo, ±As	J14-012, L13-036, Q10-004
Type 3 - Diopside (bands)	Mafic volcanic	Bright green fine-grained diopside porphyroclasts, bands, and patches, often associated with biotite bands, but can equally be seen associated with Type 1	Commonly occurs within the banded zone, and is closely associated with the biotite bands. Is also present within the Type 1 zone.	The diopside grains appear in massive layers in which the grains are never aligned with the foliation, always massive.	Pyrite (trace)	58.6-60.3	Sb, As, W	F21-032, J14-012
Type 4 - Quartz-carbonate + diopside halo	Mafic volcanic	Quartz-carbonate stringers and pods have diopside-rich light green halos up to 2 cm thick	Most commonly observed in the least deformed mafic volcanic rocks.	Quartz-carbonate zones are often rimmed or haloed by very fine-grained disseminated diopside grains within a typical mafic volcanic matrix (hornblende, quartz, feldspar, biotite). The thickness of the quartz-carbonate zone is directly proportional to the thickness of the diopside-rich halo. Figure 4.26B	Pyrite (trace)	19.6	Mo, Sn, Sb, W	J22-029
Type 5 - Silicification + diopside	Mafic volcanic or chert horizon?	Unit is abundant in quartz, very rusty, is more resistant to weathering (caused by the presence of abundant quartz) compared the surrounding mafic volcanic rocks in the brittle zone. Rare showings of banded chert and magnetite (3 cm thick by 25 cm long zones).	Occurs at the contact between the banded and brittle zone.	Quartz appears as a pervasive phase within the strongly foliated sections, and as veinlets within the least foliated section. Up to 45% un-foliated diopside is present, with pyrite and chalcopyrite occuring as disseminated interstitial grains within the diopside zones. Figure 4.26C	Pyrite (4%), Chalcopyrite (1%), Hematite (<1%)	266	Cu, Mo, Pb, Sn, Sb, As, W	E21-019

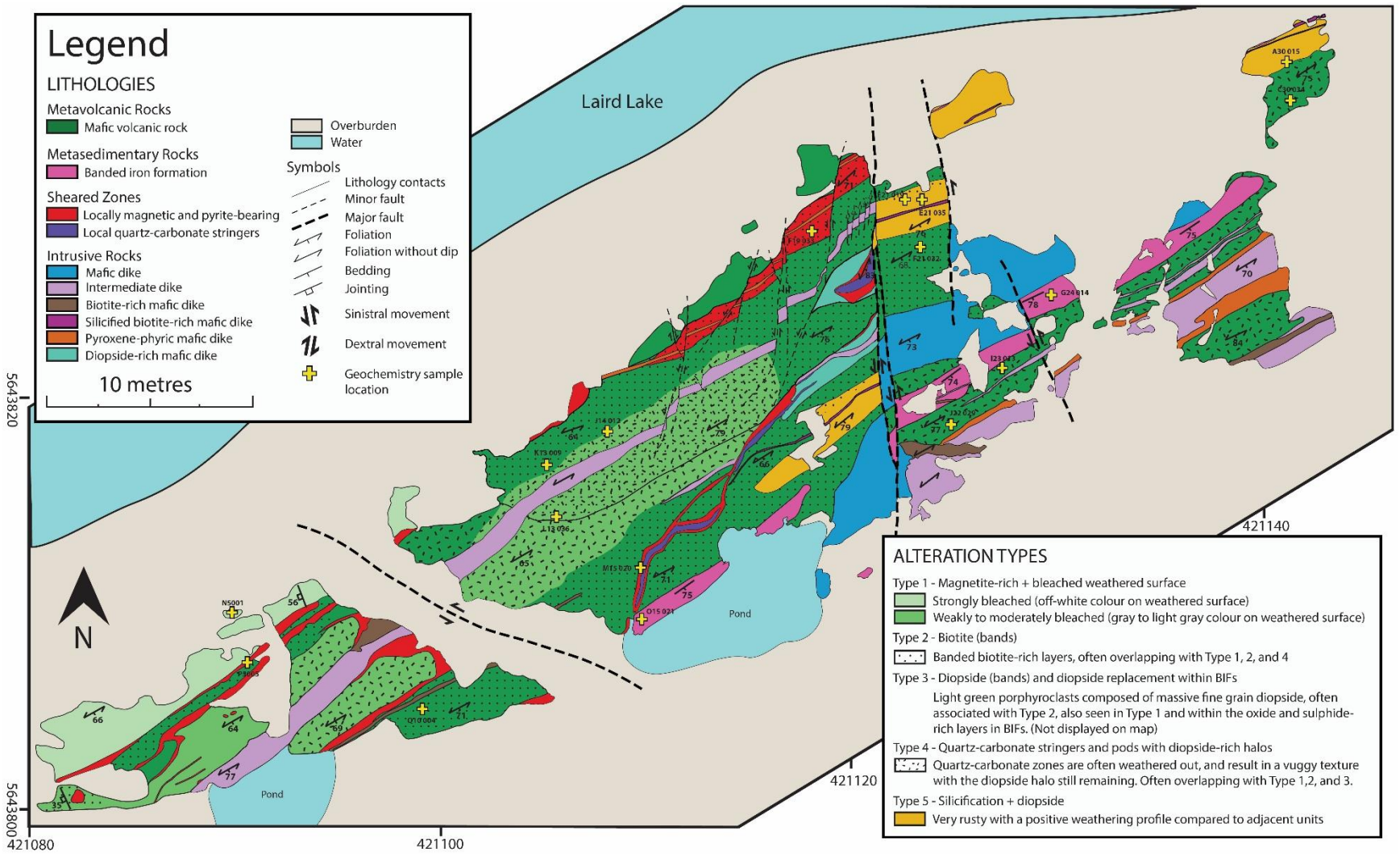

Figure 4.25 Alteration map of the Gold Bearing Zone trench, showing the location of each major alteration phase. Type 3 – Diopside (bands) and diopside replacements within BIFs were not displayed due to the overlapping nature of the alteration.

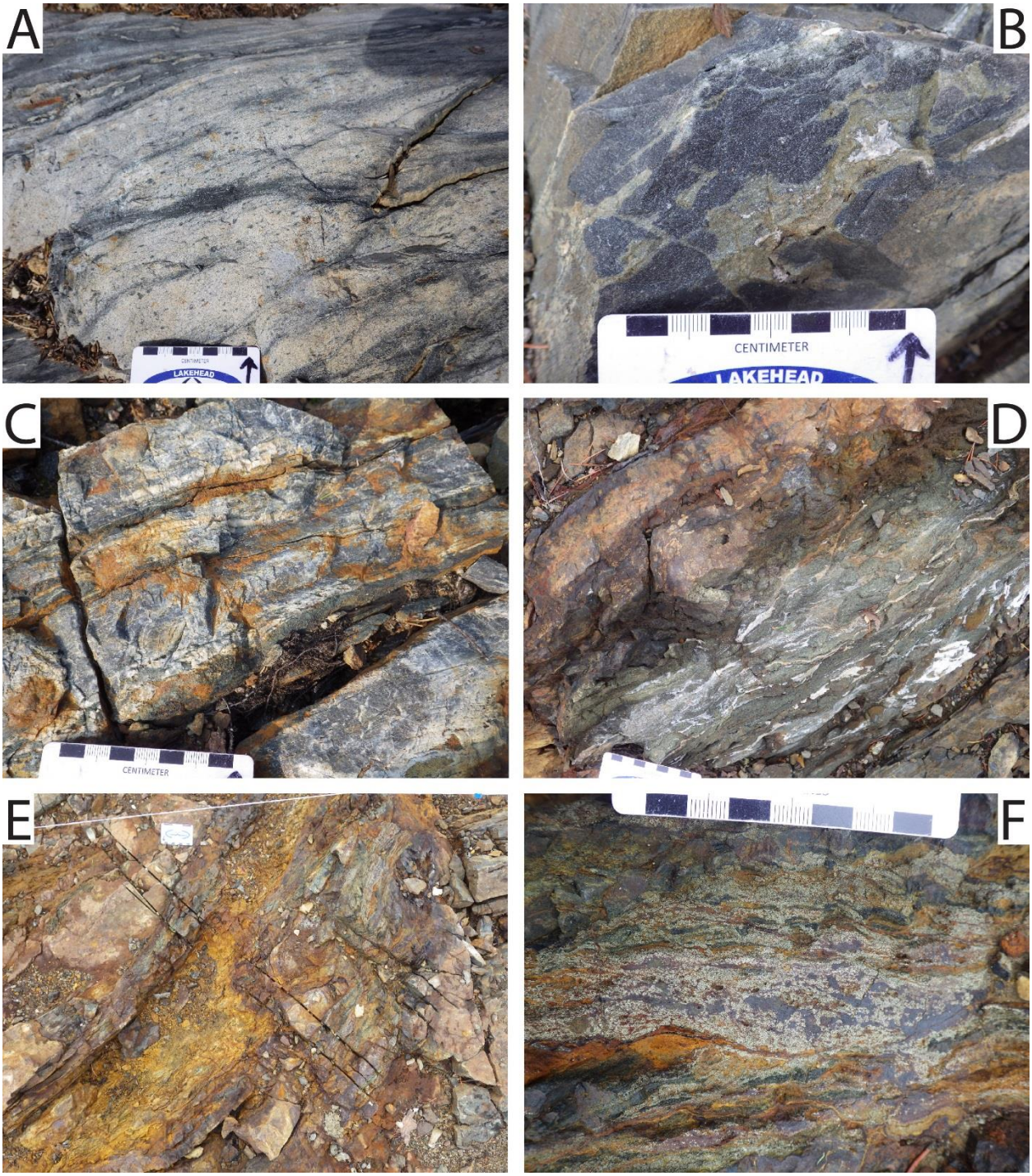

Figure 4.26 Field and petrographic photographs showing the alteration and mineralization at the Gold Bearing Zone trench A) Bleached-white mafic volcanic rocks showing potential filled vesicles (UTM 421092E 5643809N). B) Quartz-carbonate pods to stringers with fine-grained diopside-rich halo with mafic volcanic rock (UTM 421123E 5643820N). C) Silicified banded mafic volcanic rock, defined by the presence of quartz veins and stringers with irregular boundaries (UTM 421124E 5643828N). D) Fine-grained dark green brittle rock with quartz-carbonate stringers associated with gold-bearing shear (top left; UTM 421112E 5643817N). E) Cross-cutting gold-bearing shear with a brittle altered orange-red core, and pyrite, hematite, and magnetite-rich margins (UTM 421110E 5643811N). E) Pyrite and hematite-rich margin on shear (Fig. 4.25E) cutting the sulphide-facies BIF (UTM 421110E 5643811N).

4.22 and 4.25. The host rock is unrecognizable in the core of the shear zone. The shears hosting deep purple cores are typically highly magnetic, due to the presence of 3-5% magnetite. The host rock is strongly foliated, and shows alternating bands of biotite + garnet, separated by layers of quartz + feldspar and hornblende. Up to 5% pyrite is associated with the hornblende whereas magnetite is more commonly associated with garnet. A sample taken from the shear with a deep purple core contains 2042 ppb Au (sample GBZ-P5-005). The shear on the north of the middle outcrop, has a strongly foliated, rusty appearance, with a thickness of ca. 0.5-2 m. An increase in deformation seen by thinner mineral bands in the mafic volcanic rocks is associated with this shear, however, on the north-side of the shear, very little deformation and rusty colouring was observed. The sheared mafic volcanic rocks locally have a quartz-rich component, which is overprinted by rusty weathering. The increase in quartz could be in the form of quartz veins, as seen in the Type 5 alteration (silicification + diopside). Up to 20% pyrite and 3% magnetite is present. A sample from this shear zone yielded 22.4 ppb Au (trace pyrite observed; sample GBZ-F19-033). The shear zone with the orange-red brittle core which cuts across foliation on the middle outcrop has a sulphide and oxide-rich margin with up to 60% pyrite, 5% magnetite, and 20% hematite (Fig. 4.26E and F), and is locally associated with quartz-carbonate veinlets. Up to 5 m movement along this shear zone is recorded by the displacement of an intermediate dike trending parallel to the foliation. The sulphide and oxide-rich margin yielded 423 ppb Au (sample GBZ-M15-020).

Some of the highest gold values are found at the intersection between the shear zone cutting across foliation and the sulphide-facies iron formation. A detailed characterization of the mineralization within the gold-bearing BIF is described in section 4.3.1.2. The highest gold assay from this study (>3600 ppb Au; sample GBZ-O15-021), was from the intersection between the gold-bearing shear zone and BIF. Along the BIF, further away from the shear zone, Bounty Gold Corp. obtained assays up to 35.34 g/t over 2.1m (LeBlanc, 2016).

The mineralization within the mafic volcanic rocks varies from trace to 15% disseminated sulphides to stringers. These zones have a rusty weathering habit and are typically associated with an elevated magnetic susceptibility. A sample from a pyrite-rich zone not hosted within the strongly deformed banded mafic volcanic rocks yielded 356 ppb Au (sample GBZ-K13-009).

The mafic volcanic unit which has undergone Type 5 alteration (silicification + diopside) is typically associated with a strong rusty colour on the weathered surface, with up to 4% pyrite, 1% chalcopyrite and trace hematite. The unit is strongly deformed with the foliation defined by strong banding and the foliation gets locally folded. On fresh exposures, the quartz-rich nature of the unit appears as multiple quartz veins trending parallel to foliation (Fig. 4.26C). The pyrite and chalcopyrite however, are typically linked to the diopside and clinozoisite zones as opposed to the quartz-rich zones. A sample from a zone without pyrite yielded 266 ppb Au (sample GBZ-E21-019).

4.4.2 Lee Lake Au Showing

Field work in 2016 located a new gold zone (Lee Lake Au Showing) on the southeast shore of Lee Lake (UTM 418366E 5642963N). This area is less than 100 metres away from the contact between the Balmer and Confederation assemblages and contains the same mineral banding that is typical of strongly foliated Balmer mafic metavolcanic rocks, with interlayered biotite, hornblende, clinozoisite, and diopside layers with local layers rich in arsenopyrite (Fig. 4.18A). The gold showing lies where the main E to NE foliation changes to more N to NE orientation. Poles of foliation planes plotted on stereonets demonstrate the change in the foliation strike (Fig. 4.15B). Small-scale folds were also observed and demonstrate the intensity of deformation in this area (Fig. 4.17C). Bounty Gold Corp. obtained assay values up to 17 g/t Au over 20 cm and 5.4 g/t Au in hand samples (J. LeBlanc, personal communication, 2016).

4.4.3 East Gold Bearing Zone Trench

The East Gold Bearing Zone trench (EGBZ) is located along strike from the GBZ trench, roughly 470 metres to the east, on the southern edge of Laird Lake (UTM 421585E 5643940N). The trench consists of foliated Balmer assemblage mafic volcanic rocks with a possible thin BIF horizon roughly 10 cm thick striking parallel to foliation. The trench is similar to the GBZ in terms of alteration/mineralization and structures. Biotite-rich zones and quartz-carbonate veinlets locally associated with diopside-rich halos are common. A rusty zone roughly 1-7 m thick, cuts the entire length of the trench (roughly 30 m; Fig. 4.27A), hosts weak to strong silicification (both pervasively and as veins) and up to 10-15% disseminated to layered pyrite with trace pyrrhotite and chalcopyrite. This zone also hosts deep purple to red “shears” which trend parallel to foliation, and have a higher magnetic susceptibility (Fig. 4.27B). Various fold structures are present on the outcrop. An isoclinal fold has folded the rusty unit, with an axial plane trending 240°. Smaller S-folds and asymmetrical micro-folds of quartz veinlets are also present. Bounty Gold Corp. have found the highest gold grades within the 1 m thick portion of the rusty shear with 30 cm long channel lengths averaging 33.9 g/t Au (LeBlanc, 2016). Gold in this rusty zone is erratically distributed as seen by the assay results.

4.4.4 Hill Side Zone Trench

The Hill Side Zone trench (HSZ) is located 65 metres south-west of EGBZ and is within 20 m of the contact with the Confederation assemblage (Fig. 4.11B; UTM 421545E 5643879N). The trench is dominated by Balmer assemblage mafic volcanic rocks and chemical sedimentary rocks. It is in this trench that the transition between the banded iron formation and carbonate-rich formation (Fig. 4.4C) is observed. On the far east side of the trench, varioles on outer pillow margins are present (Fig. 4.3C). The alteration in this trench is often masked by the strong rusty weathering of the mafic volcanic rocks. Local shears trending parallel to foliation are present, and consists of rusty weathering material with slightly

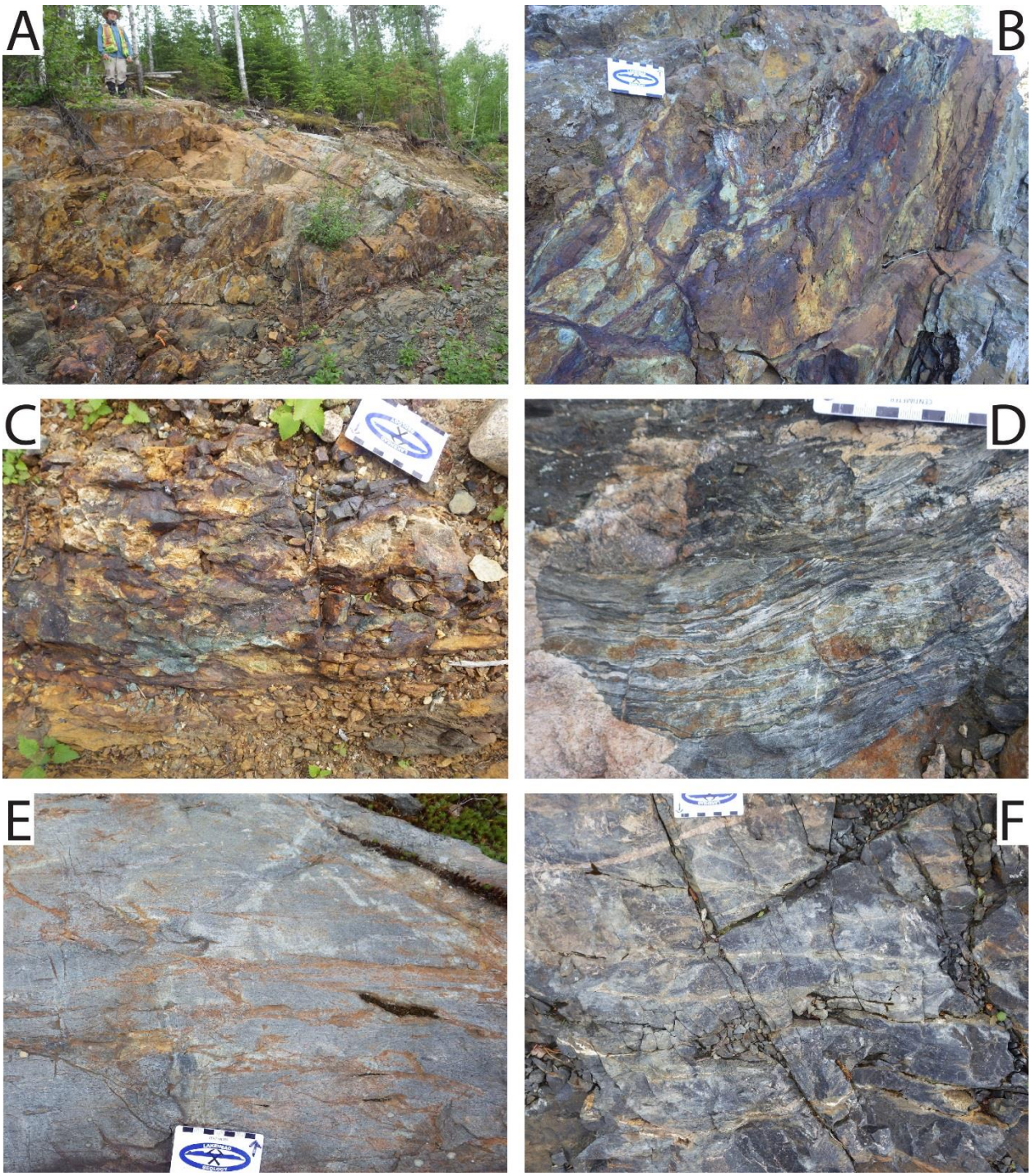

Figure 4.27 Field photographs of the alteration and structures at various gold-bearing trenches at the Laird Lake property A) Outcrop photo of the western portion of the EGBZ displaying the dominantly rusty appearance of the outcrop (UTM 421585E 5643940N). B) Pyrite and magnetite-rich deep purple-red shears cutting the outcrop parallel to foliation, similar to the shears found at GBZ (UTM 421585E 5643940N). C) Rusty shear similar to the ones observed at EGBZ and GBZ (UTM 421545E 5643879N). D) Typical mineral banding displaying alternating biotite, diopside, hornblende, and clinozoisite bands locally observed at SPZ. Local rusty patches indicate the probably occurrence of sulphides within this unit (UTM 420227E 5643705N). E) Potential ankerite veinlets found at the SPZ (UTM 420238E 5643708N). F) Quartz-carbonate stringers with diopside-rich halos cutting mafic volcanic rocks at SPZ (UTM 420227E 5643705N).

magnetic deep purple zones (Fig. 4.27C). Pyrite mineralization is commonly observed associated with the shears.

4.4.5 Pit Zone Trench

The Pit Zone trench (PZ) is located roughly 1 km west along strike from GBZ (UTM 420317E 5643721N to 420173E 5643669N). The trench is hosted entirely within Balmer assemblage mafic volcanic rocks. The Confederation assemblage contact lies 60 m to the south. The banded texture, typical of strongly deformed mafic volcanic rocks is observed in this trench, however, only local occurrences host diopside bands (Fig. 4.27C). Possible ankerite veinlets defined by a rusty weathered surface, and associated vugs (Fig. 4.27E), and quartz-carbonate stringers with diopside-rich halos (Fig. 4.27F) are also observed. The main style of mineralization at PZ is hosted within an auriferous quartz vein. A detailed characterization of the mineralization within the vein is described in section 4.3.2. and shown in Figures 4.20A-C. This vein, and smaller quartz veins parallel to the main vein are rusty on the weathered surface, due to the presence of associated pyrite within the veins.

Chapter 5 – Whole Rock and Isotope Geochemistry Results

5.1 Whole Rock Geochemistry - Introduction

Major and trace elements analyses of 161 field and core samples were undertaken to characterize and subdivide the rocks in order to evaluate the genesis and tectonic environment in which they formed. Additionally, these data were used to classify the alteration types associated with the gold mineralization in the Laird Lake area. In areas of greenstone belts where deformation, metamorphism and hydrothermal metasomatism has affected the rocks, it is important to be careful when interpreting geochemical data, as these processes typically influence the primary geochemical signatures (Pearce, 1996). Mobile elements can be used to establish alteration trends, as these are typically modified by hydrothermal metasomatism, whereas immobile elements better reflect the primary geochemical signature of the rock. In general, Al, Ti, P, the high-field strength elements (HFSE) Th, Zr, Nb, Hf, Y and the rare-earth elements (REE) are typically immobile during metasomatic processes (MacLean and Barrett, 1993; Rollinson, 1993), although the light rare-earth elements (LREE) and Y can be slightly more mobile during alteration (Rollinson, 1993). All samples have been recalculated to a 100% volatile free basis to account for variations in the loss on ignition (LOI) content.

It is important to assess element mobility before using classification diagrams that utilize typically mobile or immobile elements. Bivariate diagrams plotting Al_2O_3, MgO, K_2O, Na_2O, SiO_2 and P_2O_5 versus TiO_2 and plots of Nb versus La, Th, Y, Yb, TiO_2 and Zr are shown in Figure 5.1 A and B. Elements which show a linear trend on the diagrams are deemed immobile whereas the elements which show large scatter are considered mobile (MacLean and Barrett, 1993). The large scatter seen in K_2O and Na_2O, and lesser in SiO_2 and Al_2O_3 suggest these elements were mobile during metamorphism and hydrothermal metasomatism (Fig. 5.1A). Figure 5.1B shows tighter and more linear trends consistent with the relatively immobile nature of La, Th, Y, Yb, Ti and Zr. Consequently, these elements will be used for rock classification and to infer tectonic settings.

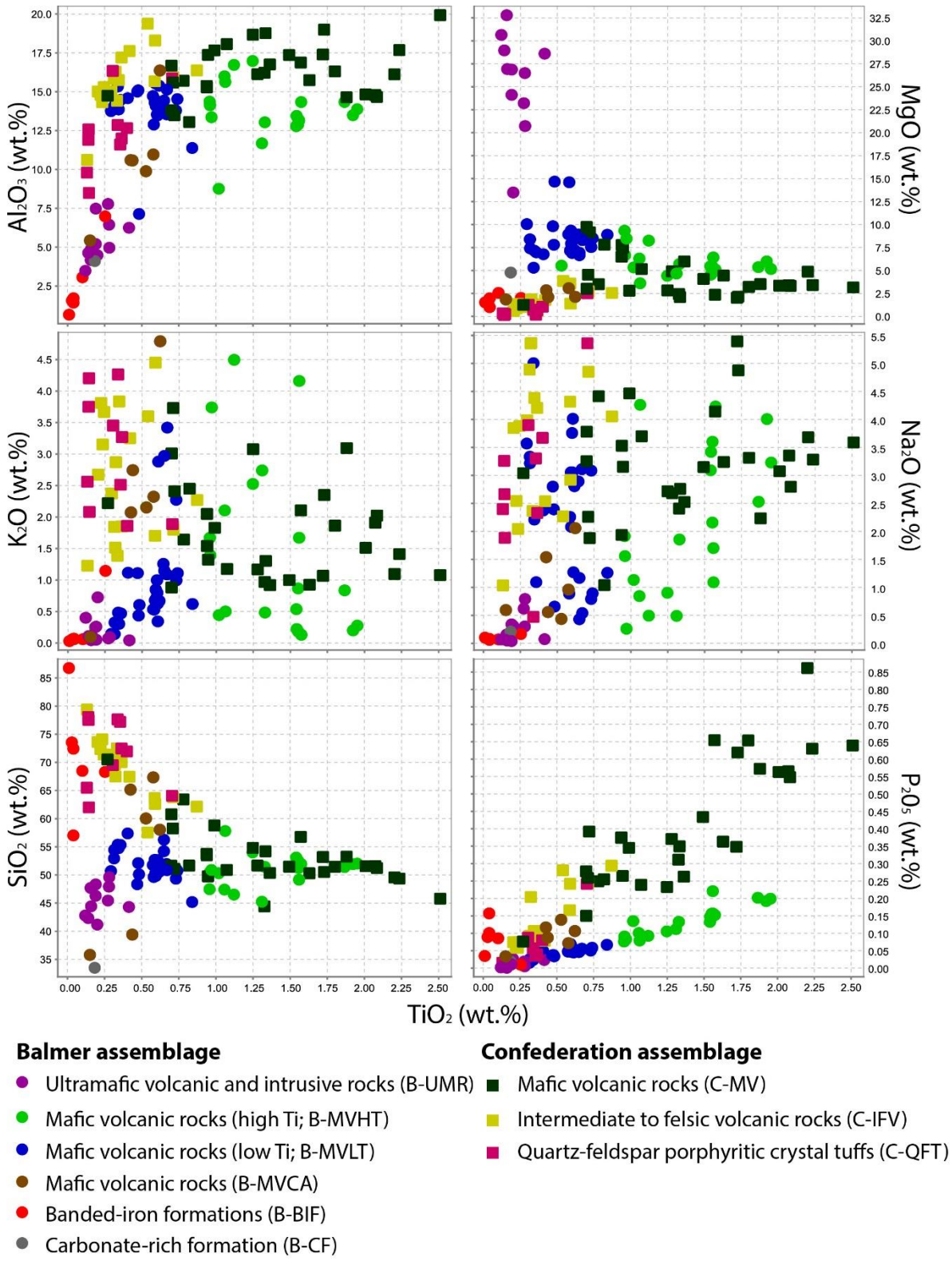

Figure 5.1(A) Bivariate variation diagrams of SiO_2 and Al_2O_3 vs major element oxides. ***B-UMR:*** *Balmer ultramafic volcanic and intrusive rocks,* ***B-MVHT:*** *Balmer mafic volcanic rocks (high-Ti),* ***B-MVLT:*** *Balmer mafic volcanic rocks (low-Ti),* ***B-MVCA:*** *Balmer mafic volcanic rocks (calc-alkalic),* ***B-BIF:*** *Balmer banded-iron formations,* ***B-CF:*** *Balmer carbonate-rich formation,* ***C-MV:*** *Confederation mafic volcanic rocks,* ***C-IFV:*** *Confederation intermediate to felsic volcanic rocks,* ***C-QFT:*** *Confederation quartz-feldspar porphyritic crystal tuffs.*

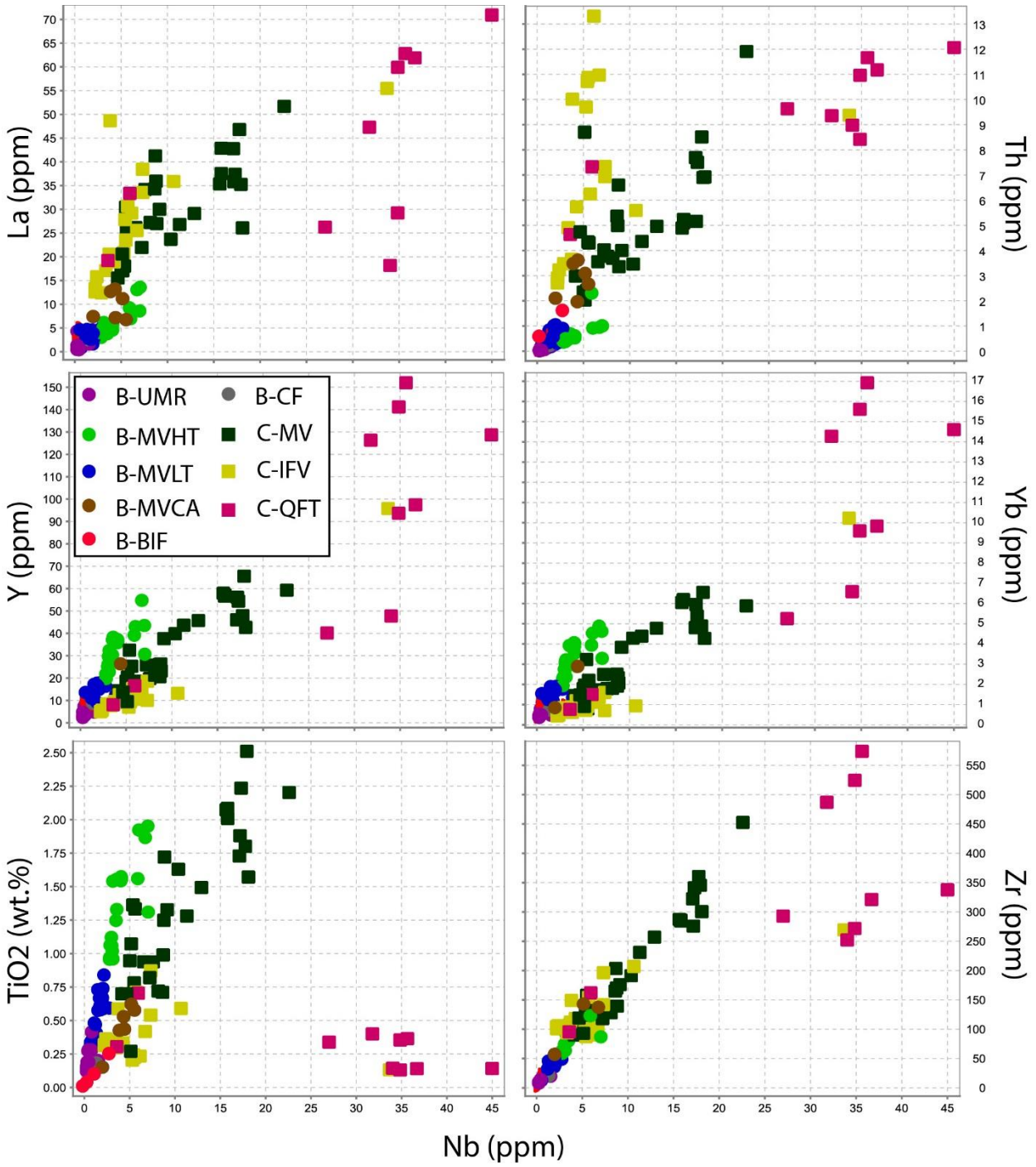

Figure 5.1(B) Bivariate variation diagrams of Nb versus major and trace element. ***B-UMR:*** *Balmer ultramafic volcanic and intrusive rocks,* ***B-MVHT:*** *Balmer mafic volcanic rocks (high-Ti),* ***B-MVLT:*** *Balmer mafic volcanic rocks (low-Ti),* ***B-MVCA:*** *Balmer mafic volcanic rocks (calc-alkalic),* ***B-BIF:*** *Balmer banded-iron formations,* ***B-CF:*** *Balmer carbonate-rich formation,* ***C-MV:*** *Confederation mafic volcanic rocks,* ***C-IFV:*** *Confederation intermediate to felsic volcanic rocks,* ***C-QFT:*** *Confederation quartz-feldspar porphyritic crystal tuffs.*

In the Laird Lake area, the assemblages could typically be subdivided in the field, however, when the outcrop exposure was poor and/or the presence of intense structural fabrics overprinted primary features, geochemical analyses were utilized to subdivide the assemblages. Since the contact between the two assemblages is associated with an increase in deformation and alteration, especially within the Balmer assemblage, major elements were affected and therefore classification diagrams using these elements were used with care. Figure 5.2 shows the large scatter in rock types on a TAS diagram, due to the mobility of Na_2O, K_2O and SiO_2. The classification diagram for volcanic rocks by Pearce (1996) was utilized to avoid the effects of alteration on major element concentrations (Fig. 5.3).

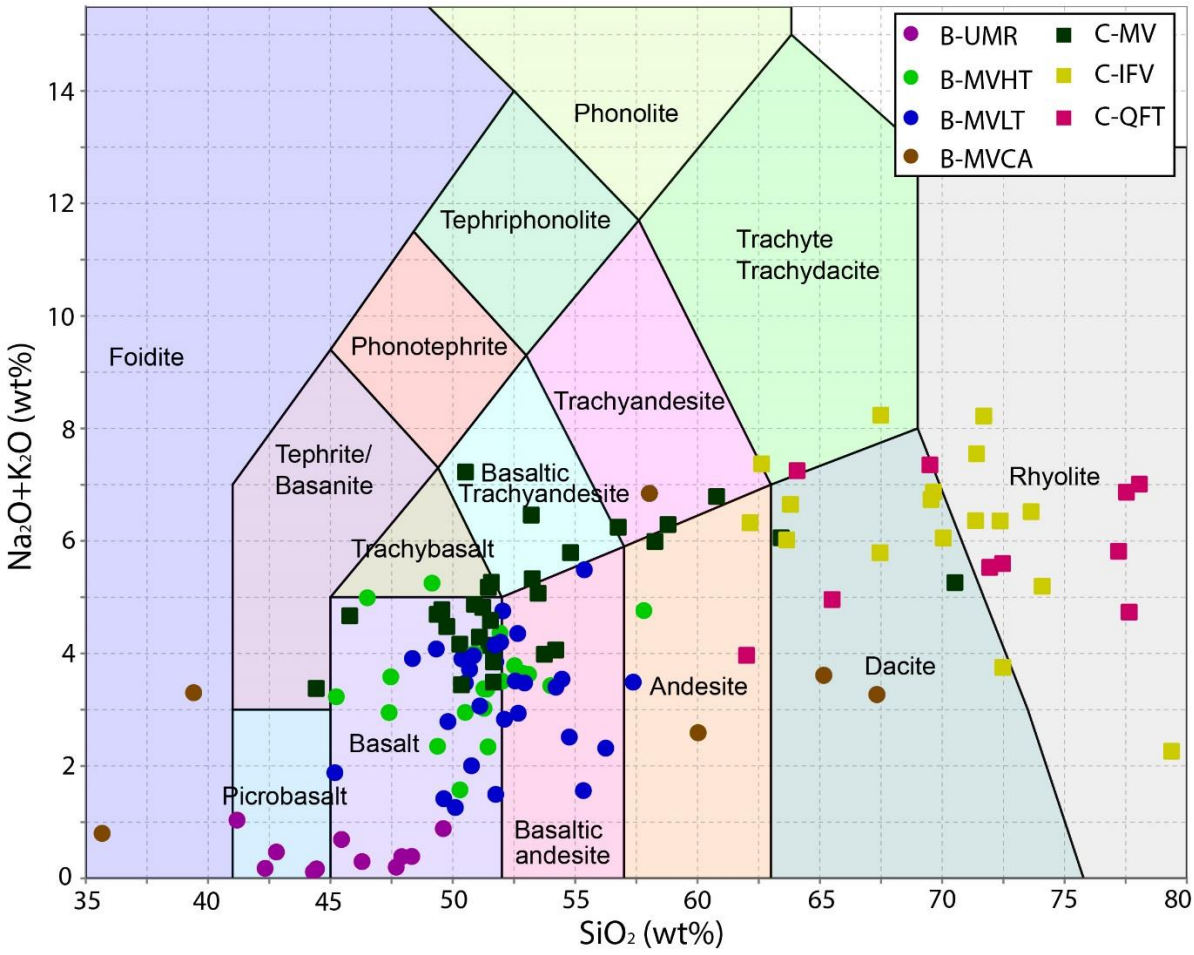

Figure 5.2. Silica vs. total alkalis diagram by Le Maitre et al. (1989) showing classification of the Laird Lake volcanic rock samples. Samples were not classified using the TAS method. ***B-UMR:*** *Balmer ultramafic volcanic and intrusive rocks,* ***B-MVHT:*** *Balmer mafic volcanic rocks (high-Ti),* ***B-MVLT:*** *Balmer mafic volcanic rocks (low-Ti),* ***B-MVCA:*** *Balmer mafic volcanic rocks (calc-alkalic),* ***C-MV:*** *Confederation mafic volcanic rocks,* ***C-IFV:*** *Confederation intermediate to felsic volcanic rocks,* ***C-QFT:*** *Confederation quartz-feldspar porphyritic crystal tuffs.*

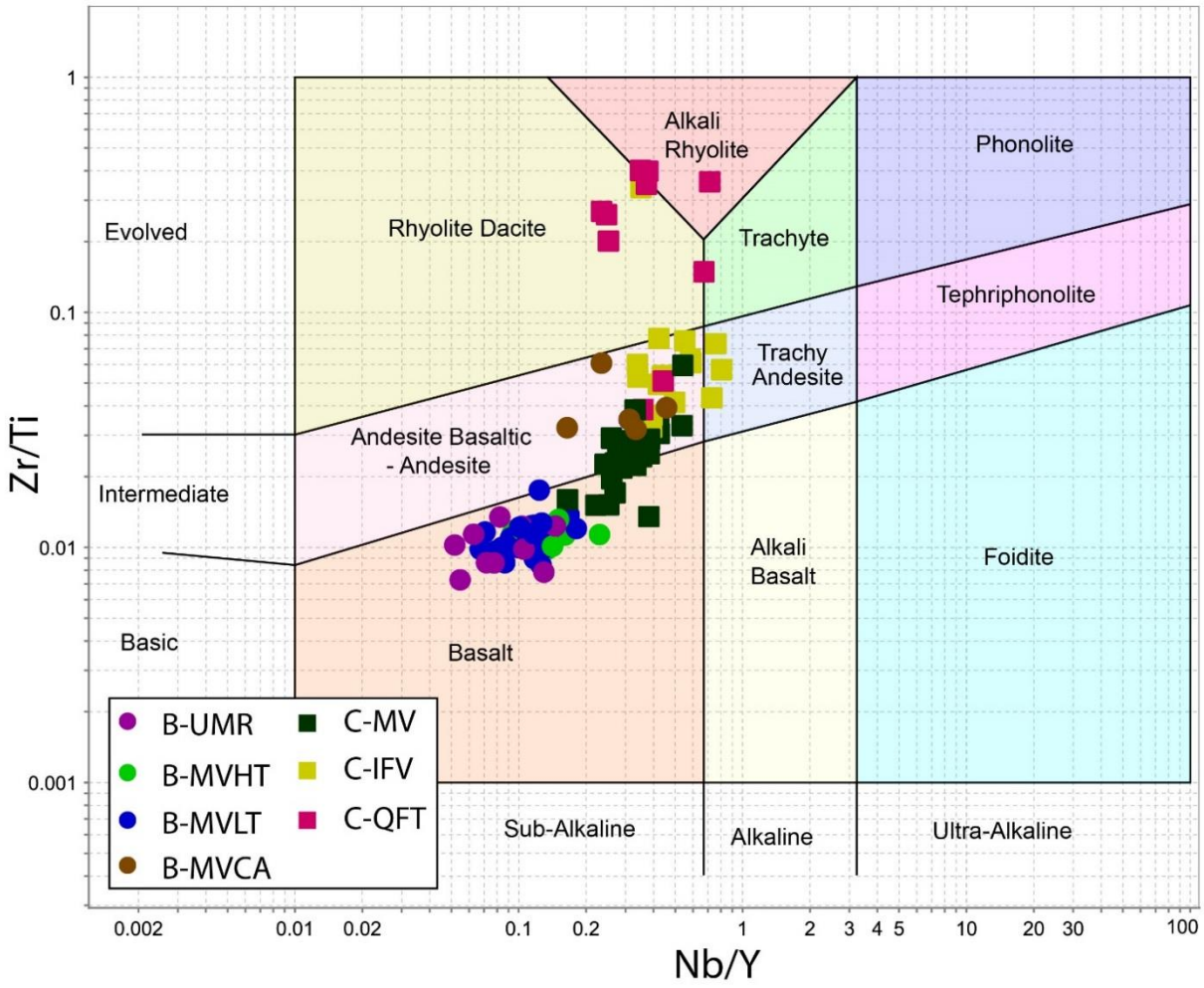

Figure 5.3. Zr/Ti versus Nb/Y diagram by Pearce (1996) showing the classification of the Laird Lake volcanic rock samples. ***B-UMR:*** *Balmer ultramafic volcanic and intrusive rocks,* ***B-MVHT:*** *Balmer mafic volcanic rocks (high-Ti),* ***B-MVLT:*** *Balmer mafic volcanic rocks (low-Ti),* ***B-MVCA:*** *Balmer mafic volcanic rocks (calc-alkalic),* ***C-MV:*** *Confederation mafic volcanic rocks,* ***C-IFV:*** *Confederation intermediate to felsic volcanic rocks,* ***C-QFT:*** *Confederation quartz-feldspar porphyritic crystal tuffs.*

In order to determine the magmatic affinity of the volcanic rocks the data are plotted on an AFM diagram (Fig. 5.4A) and Jensen cation plot (Fig. 5.4B) to distinguish between tholeiitic rocks and calc-alkaline rocks. The scatter in rock types observed in these plots is fairly large, and therefore the Th/Yb versus Zr/Y trace element diagram (Figs. 5.5; 5.8; 5.11; 5.14; 5.18B) suggested by Ross and Bédard (2009) is used in conjunction with AFM and Jenson cation plots to obtain the most reliable magmatic affinity of the rocks. The diagram by Ross and Bédard (2009) utilizes immobile trace elements in order to eliminate any alteration and metamorphic influences, however, caution must be taken when rocks could be crustally contaminated.

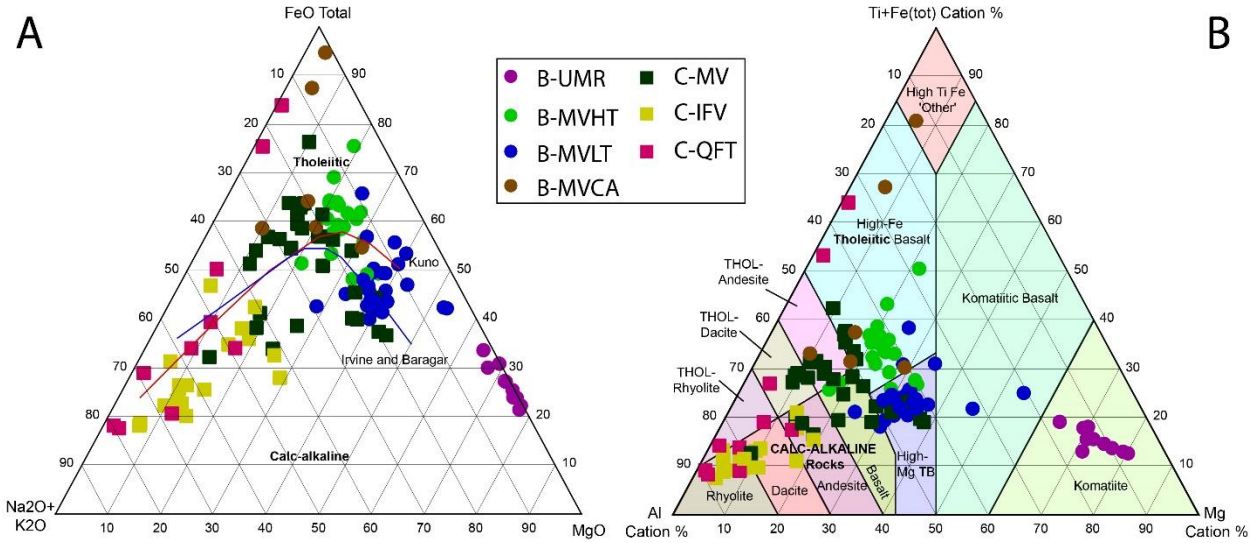

Figure 5.4. Diagrams utilizing major element to determine the magmatic affinity. A) AFM diagram. Trend lines from Kuno (1968) and Irvine and Baragar (1971). B) Jenson cation plot. ***B-UMR:*** *Balmer ultramafic volcanic and intrusive rocks,* ***B-MVHT:*** *Balmer mafic volcanic rocks (high-Ti),* ***B-MVLT:*** *Balmer mafic volcanic rocks (low-Ti),* ***B-MVCA:*** *Balmer mafic volcanic rocks (calc-alkalic),* ***C-MV:*** *Confederation mafic volcanic rocks,* ***C-IFV:*** *Confederation intermediate to felsic volcanic rocks,* ***C-QFT:*** *Confederation quartz-feldspar porphyritic crystal tuffs.*

5.1.1 Balmer Assemblage

The Balmer assemblage is comprised of four geochemically distinct volcanic units; ultramafic rocks, high-Ti mafic volcanic rocks, low-Ti mafic volcanic rocks and calc-alkaline mafic volcanic rocks.

5.1.1.1 Ultramafic Volcanic and Intrusive Rocks

Ultramafic volcanic and intrusive rocks of the Laird Lake area are geochemically grouped together as they are closely related in the field, cannot be distinguished in drill core and have similar geochemical signatures. Drill core samples will therefore be classified with the volcanic rocks. These rocks have MgO contents of 20-33 wt.%, Ni concentrations of 457-1692 ppm and Cr concentrations of 1724-3234 ppm. They plot as picrobasalts to basalts on a TAS classification diagram (Fig. 5.2), within the basalt field on the Zr/Ti versus Nb/Y diagram (Fig. 5.3) and within the komatiite field on a Jensen cation plot (Fig. 5.4B). The AFM and Th/Yb versus Zr/Y diagrams suggest the ultramafic rocks have a tholeiitic affinity (Figs. 5.4A; 5.5). On TiO_2 versus major element bivariate diagrams, the ultramafic rocks have the tightest grouping compared to all other volcanic rock types, suggesting lesser element mobility within

the ultramafic rocks (Fig. 5.1A). They have Al_2O_3/TiO_2 ratios that range from 15-39 and CaO/Al_2O_3 ratios between 0.9-2.6. On MgO vs trace element bivariate diagrams (Fig. 5.6), linear trends are present with Ni, and Zr with larger scatter in the Co and Cr diagrams.

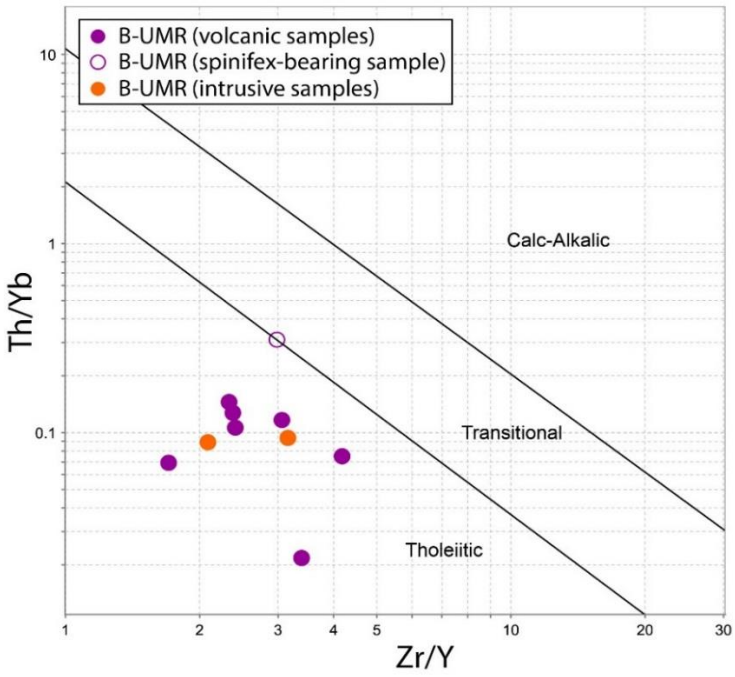

Figure 5.5. Th/Yb versus Zr/Y trace element diagram showing most of the samples plotting in the tholeiitic field. Fields on diagram from Ross and Bédard (2009). ***B-UMR:*** *Balmer ultramafic rocks*

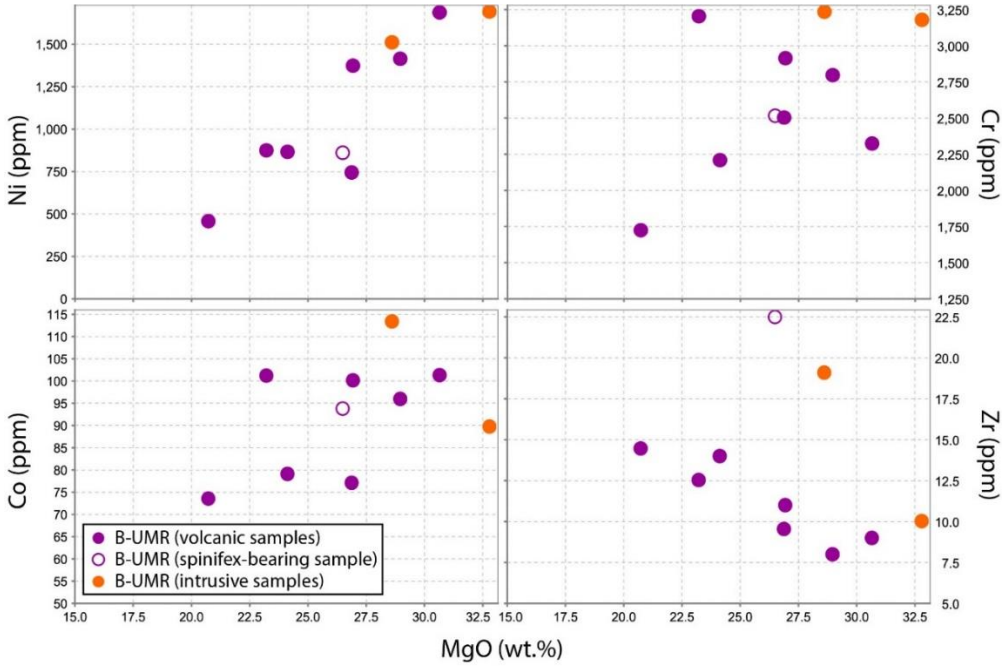

Figure 5.6 Variation diagrams of MgO vs trace elements. ***B-UMR:*** *Balmer ultramafic rocks*

On primitive mantle normalized diagrams, the ultramafic volcanic rocks show three trends based on the LREE (Fig. 5.7). The majority of samples (volcanic rocks without spinifex) have depleted to enriched LREE (La/Sm_n = 0.59-4.87), flat to slightly positive slopes in the HREE (Gd/Yb_n = 0.75-1.54), strong negative to slightly positive Nb anomalies (Nb/Nb* = 0.07-1.09), and variable Eu anomalies. One sample (core sample LL-BG-09-10) shows a strong depletion in Th and enrichment in La (La/Sm_n = 3.34), with an LOI of 8.73%, possibly caused by the presence of thin cross-cutting serpentine veinlets. There are two samples including the only spinifex-bearing sample, that show strong enrichment in LREE (La/Sm_n=2.53-4.87) with flat to slightly fractionated HREE (Gd/Yb_n=1.07-1.21) and strong negative Nb anomalies (Nb/Nb*=0.04-0.20). Only the spinifex-bearing volcanic sample shows a weak negative Ti anomaly. The two samples were collected within 1 m of each other. The third trend is seen only in the one ultramafic intrusion found 2 km away from the main ultramafic body. This sample shows slight enrichment in LREE (La/Sm_n=1.10) but depletion in Th (Th/Nb=0.07) in conjunction with slightly fractionated HREE (Gd/Yb_n=1.54) and a negative Ti anomaly.

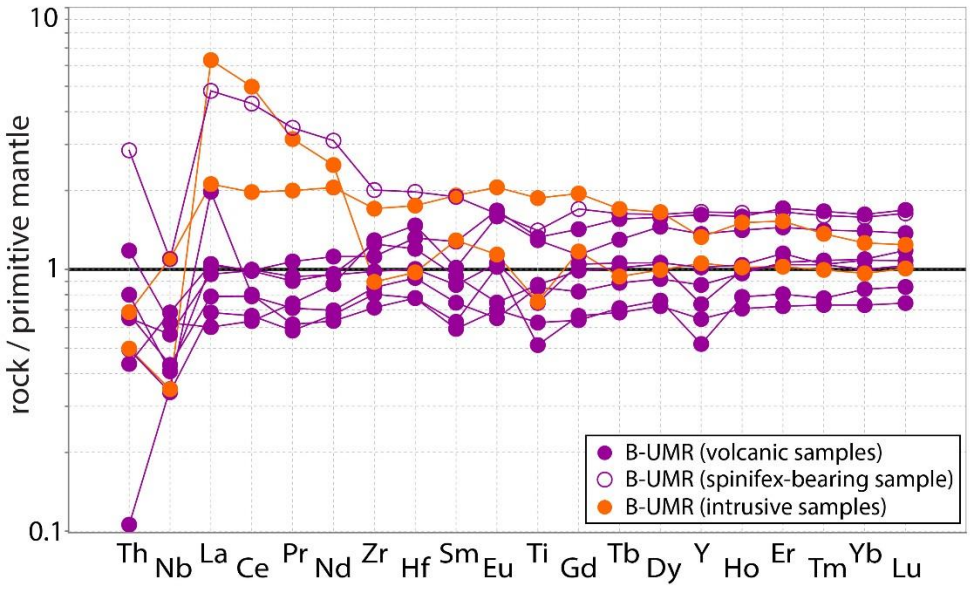

Figure 5.7 Primitive mantle normalized diagram. Normalizing values from Sun and McDonough (1989). ***B-UMR:*** *Balmer ultramafic rocks*

5.1.1.2 Mafic Volcanic Rocks

The mafic volcanic rocks of the Balmer assemblage include three distinct geochemical units: High-Ti basalts, low-Ti basalts and calc-alkalic basalts. The high- and low-Ti basalts plot entirely within the basalt field of the Zr/Ti versus Nb/Y diagram whereas the calc-alkalic basalts plot within the andesitic basalt/andesite field (Fig. 5.3). Overall, the mafic volcanic rocks show a large scatter in K_2O and Na_2O with less variation in SiO_2 and Al_2O_3, and tighter groupings in MgO and P_2O_5, indicating the variable mobility of major elements (Fig. 5.1A). Most samples plot in very tight and linear trends on Figure 5.1B, with a few anomalies, indicating the relatively immobile nature of Th, Nb, La, Zr, Y, Yb and TiO_2. The mafic volcanic rocks of the Balmer assemblage plot on the tholeiitic trend of an AFM diagram (Fig. 5.4A) and tholeiitic field of a Jensen cation plot (Fig. 5.4B), with a few anomalies plotting in the tholeiitic andesite field, calc-alkaline basalt field and in the high Ti-Fe "Other" field.

Three geochemical groupings within the Balmer assemblage mafic volcanic rocks are visible on bivariate diagrams (Fig. 5.1), AFM diagram (Fig. 5.4A), Jenson cation plot (Fig. 5.4B) and primitive mantle-normalized trace elements plots (Fig. 5.10). Based on their TiO_2 concentrations (Fig. 5.1A), high-Ti basalts (B-MVHT) and low-Ti basalts (B-MVLT) are recognised. The high-Ti basalts typically have TiO_2 concentrations between 0.96-1.95 wt.% whereas the low-Ti basalts have TiO_2 concentrations between 0.29-0.84 wt.% (Fig. 5.2). The third set of mafic volcanic rocks (calc-alkaline) roughly fit within the criteria for TiO_2 concentrations for the low-Ti basalts with 0.15-0.62 wt.% TiO_2, however, since this set of rocks shows great differences on most trace element diagrams, the rocks were grouped separately. On a Jensen Cation plot, the high-Ti basalts dominantly plot within the high-Fe tholeiitic field, whereas the low-Ti basalts mostly plot within the high-Mg tholeiitic basalt with two samples plotting in the komatiitic basalt fields with 14 wt.% MgO (Fig. 5.4B). The AFM diagram also supports the existence of Mg- and Fe-tholeiites (Fig. 5.4A). The calc-alkalic samples show a large scatter on Figure 5.4B likely caused by the presence of 2-30% pyrite. The scatter found in these diagrams is caused by major element mobility and

therefore the Th/Yb versus Zr/Y trace element diagram was utilized to characterize the magmatic affinity of the mafic volcanic rocks of the Balmer assemblage (Fig. 5.8). The mafic volcanic rocks with high-Ti and low-Ti both plot within the tholeiitic to transitional fields, whereas the third set of mafic volcanic rocks plot within the calc-alkalic field with one anomalous sample plotting in the transitional field. It is possible that the calc-alkalic and transitional samples represent crustally contaminated units.

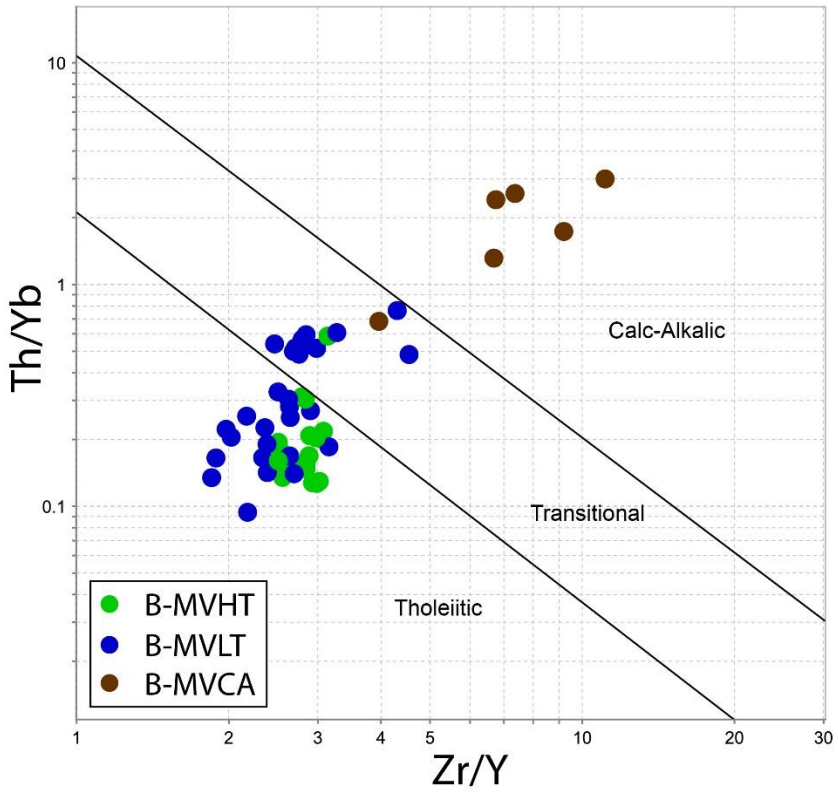

Figure 5.8. Th/Yb versus Zr/Y trace element diagram showing most of the samples plotting in the tholeiitic to transitional fields, with only samples with elevated LREE plotting in the calc-alkalic and transitional fields. Fields on diagram from Ross and Bédard (2009). ***B-MVHT:*** *Balmer mafic volcanic high-Ti,* ***B-MVLT:*** *Balmer mafic volcanic low-Ti,* ***B-MVCA:*** *Balmer mafic volcanic rocks (calc-alkalic).*

On Zr versus Th, La, Ti, Nb, Gd and Yb diagrams, the three mafic volcanic trends can also be differentiated. The high- and low-Ti basalts typically plot in a linear trend fairly close to the primitive mantle ratio, suggesing the rocks are primitive mantle derived and the element ratios have not been affected by secondary processes. Slight depletions for Zr versus Nb, Yb and Ti relative to the primitive mantle lines are present. The calc-alkalic samples plot away from the primitive mantle line, show

enrichment in the LREE (Th and La) and typically have a different trend from the high- and low-Ti basalts. Only Nb shows a very tight trend in all sample types.

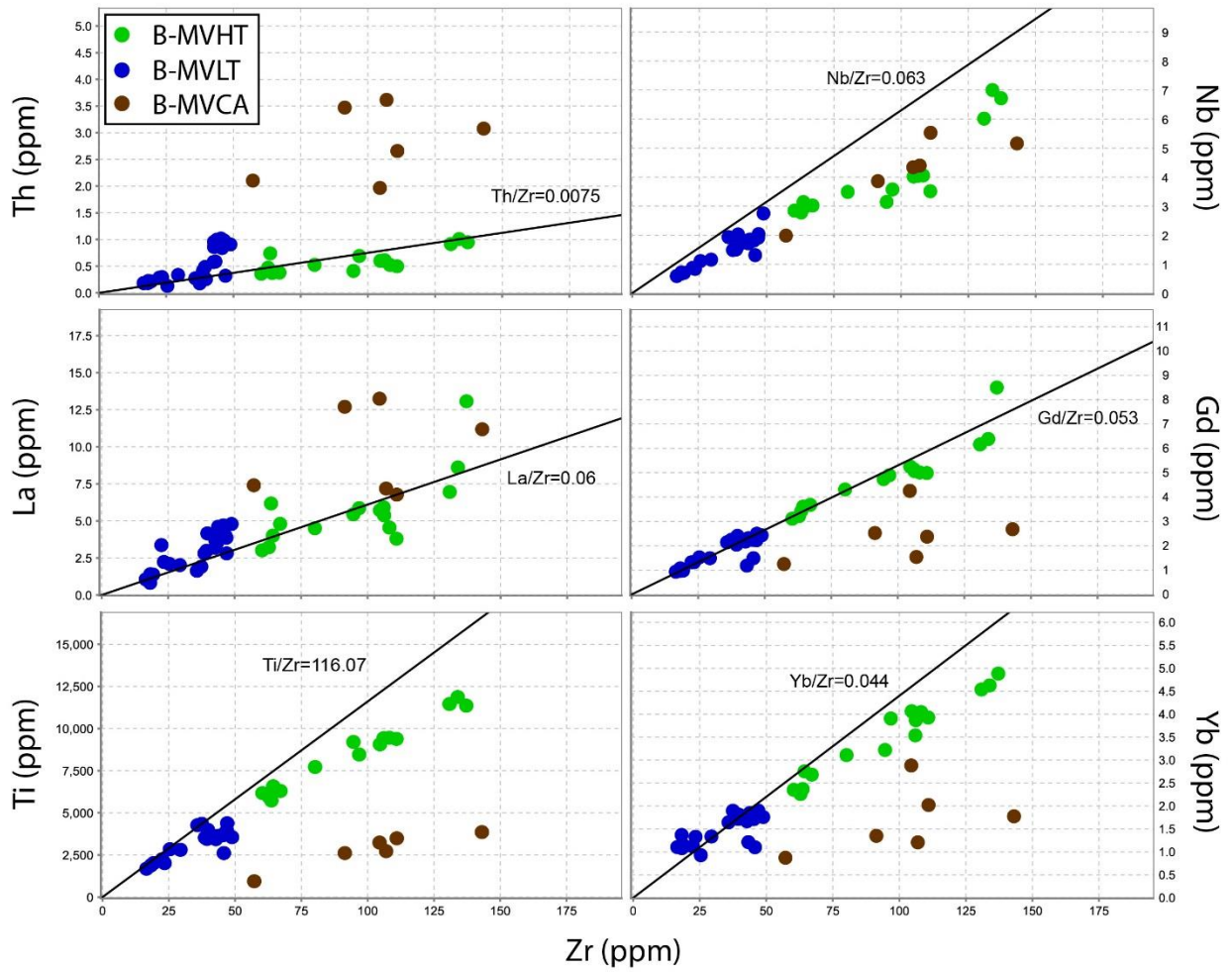

Figure 5.9 Variation diagrams of Zr vs trace elements. ***B-MVHT:*** *Balmer mafic volcanic high-Ti, B-****MVLT:*** *Balmer mafic volcanic low-Ti,* ***B-MVCA:*** *Balmer mafic volcanic rocks (calc-alkalic). Black line represents primitive mantle ratios from Sun and McDonough (1989).*

Primitive mantle normalized spider diagrams also distinguish the three types of mafic volcanic rocks (Fig. 5.10A). The high-Ti basalts have a relatively flat REE pattern with a weak positive slope in the HREE (La/Sm_n=0.70-1.56 with one anomaly at 2.51; Gd/Yb_n=1.02-1.43) and zero to negative Nb anomalies (Nb/Nb*=0.36-1.03) and negative Ti anomalies (Ti/Ti*=0.59-0.93; see appendix B for calculation of Nb/Nb*, Ti/Ti* and Eu/Eu*). The low-Ti basalts have lower REE concentrations compared

to the high-Ti basalts (Fig. 5.10A). The LREE are variably enriched to depleted (La/Sm_n=0.77-2.44) with flat to slighly fractionated HREE (Gd/Yb_n=0.58-1.35). Strong negative Nb anomalies (Nb/Nb*=0.18-0.78 with one anomaly at 1.28) and zero to weak negative Ti anomalies (Ti/Ti*=0.64-1.04 with one anomaly at 1.26 caused by a negative Eu anomaly (Eu/Eu*=0.62)) are also present. The calc-alkalic mafic volcanic rocks are enriched in LREE (La/Sm_n=2.14-4.12) with fairly flat to fractionated HREE (Gd/Yb_n=0.97-1.54) and have strong negative Nb and Ti anomalies with Nb/Nb* and Ti/Ti* ranging from 0.15-0.65 and 0.29-0.65 respectively (Fig. 5.10B).

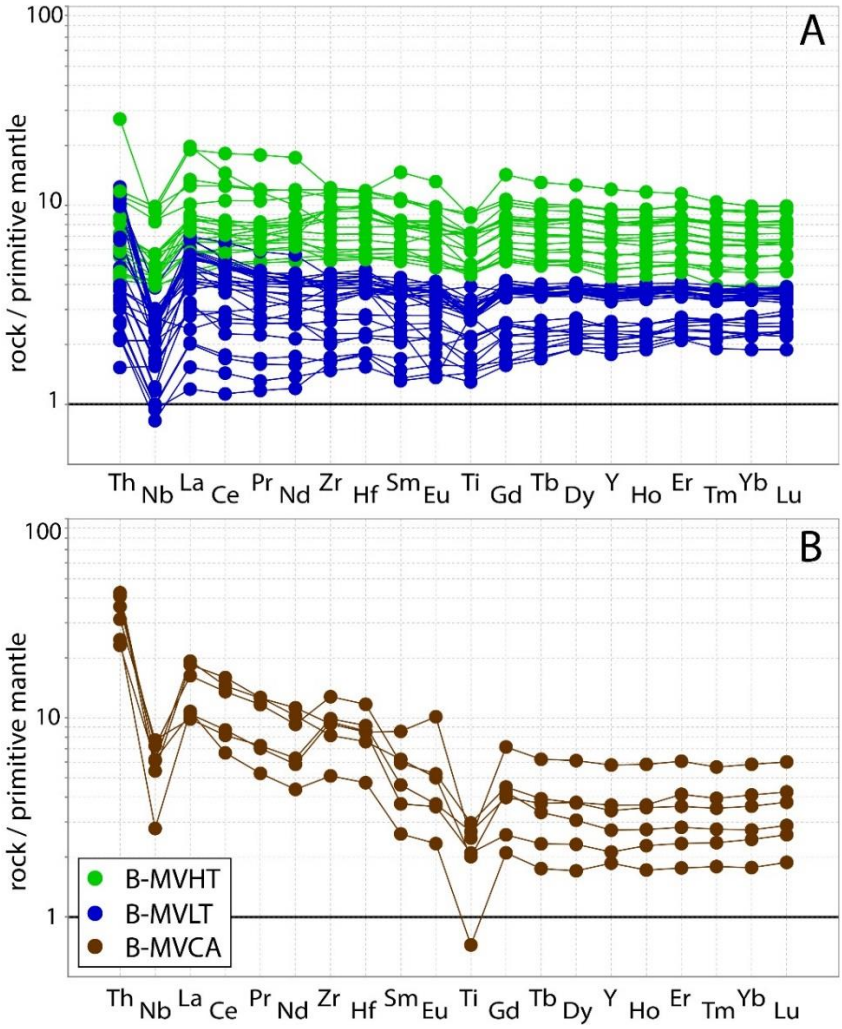

Figure 5.10 Primitive mantle normalized plot for the mafic volcanic rocks of the Balmer assemblage. A) Tholeiitic mafic volcanic samples B) Calc-alkalic mafic volcanic samples. Normalizing values from Sun and McDonough (1989). ***B-MVHT:*** *Balmer mafic volcanic high-Ti, B-****MVLT:*** *Balmer mafic volcanic low-Ti,* ***B-MVCA:*** *Balmer mafic volcanic rocks (calc-alkalic).*

5.1.2 Confederation Assemblage

The Confederation assemblage is composed of three geochemically distinct units which include: mafic volcanic rocks and two groups within the intermediate to felsic volcanic rocks which include rocks with fractionated or enriched HREE.

5.1.2.1 Mafic Volcanic Rocks

The mafic volcanic rocks of the Confederation assemblage have not undergone large degrees of alteration in so far as they plot as tighter groupings on all diagrams. On a Zr/Ti versus Nb/Y diagram, they plot within the basalt to basaltic andesite/andesite fields (Fig. 5.3). Figure 5.1A shows the strong mobility in K_2O and Na_2O, with tighter trends for Al_2O_3, MgO and P_2O_5. The mafic volcanic rocks show a wide range of TiO_2 concentrations from 0.69-2.51 wt.%. Most samples plot in linear but slightly scattered trends on Figure 5.1B, indicating the relatively immobile nature of Th, Nb, La, Zr, Y, Yb and TiO_2.

The mafic volcanic rocks of the Confederation assemblage typically plot in the tholeiitic field of an AFM diagram, with a small group plotting on the calc-alkalic field (Fig. 5.4A) whereas on a Jensen cation plot, samples plot anywhere between high-Mg and Fe tholeiitic basalts to tholeiitic and calc-alkaline dacite (Fig. 5.4B). On a Th/Yb versus Zr/Y diagram, the samples mostly plot within the calc-alkalic field with one sample within the transitional field (Fig. 5.11). As this diagram from Ross and Bedard (2009) was intended to classify island arc volcanic rocks, caution must be taken if rocks prove to be crustally contaminated. The various flow types form slight parallel groupings, where the mafic flows with feldspar phenocrysts are slightly more depleted in Th relative to Yb compared to the aphyric flows (with ± amphibole ± garnet porphyroblasts).

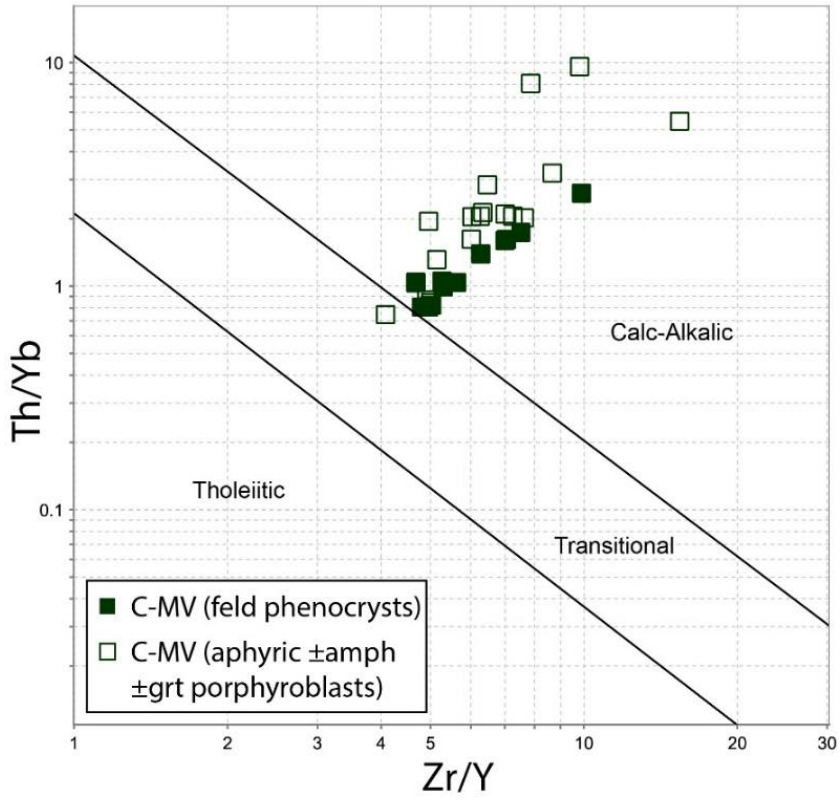

Figure 5.11. Th/Yb versus Zr/Y trace element diagram showing most of the samples plotting in the calc-alkalic field, with only one sample plotting in the transitional field. Fields on diagram from Ross and Bédard (2009). ***C-MV:*** *Confederation mafic volcanic,* ***Feld****: feldspar,* ***Amph****: amphibole,* ***Grt:*** *garnet.*

On Zr versus Th, La, Ti, Nb, Gd and Yb diagrams, the two types of mafic volcanic rocks show significant overlap (Fig. 5.12). Overall the mafic volcanic rocks plot above the PM ratio line on the Th and La diagrams, but below the PM ratio line on the Nb, Gd, Ti and Yb diagrams. The Nb diagram shows the closest relationship between the samples and the PM line whereas the samples in the Gd, Ti and Yb diagrams illustrate a lesser steep trend.

On a primitive mantle-normalized spider diagram, the two varieties of Confederation assemblage mafic volcanic rocks have very similar trends with significant overlap (Fig. 5.13). Overall, the mafic volcanic rocks are enriched in LREE (La/Sm_n=2.14-4.82) with fractioned HREE (Gd/Yb_n=1.21-3.65) and show strong depletions in Nb and Ti with Nb/Nb* and Ti/Ti* ranging from 0.14-0.57 and 0.26-0.69 respectively. No geochemically altered samples were present in this rock type.

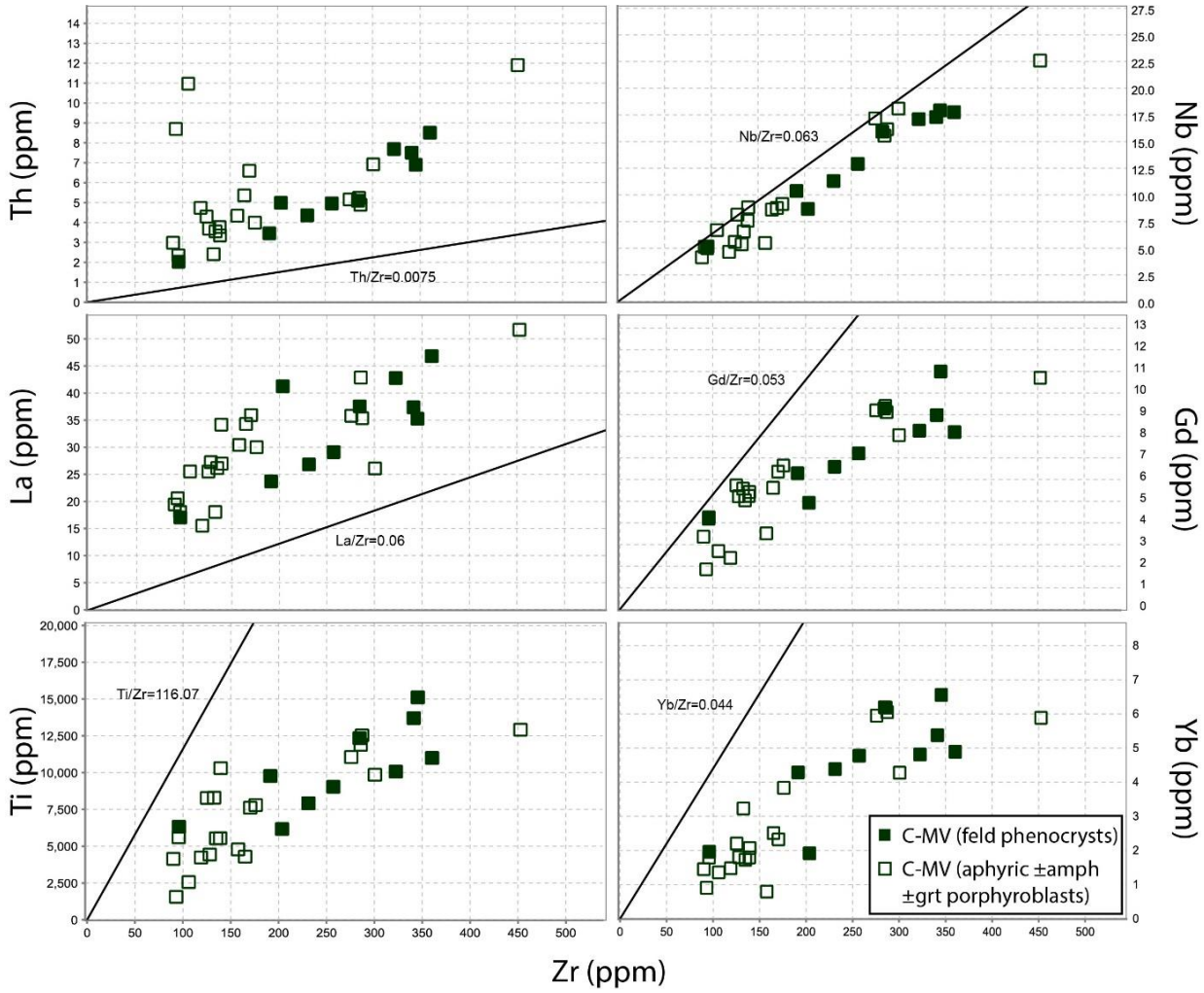

Figure 5.12 Variation diagrams of Zr vs trace elements. ***C-MV:*** *Confederation mafic volcanic,* ***Feld****: feldspar,* ***Amph****: amphibole,* ***Grt:*** *garnet. Black line represents primitive mantle ratios from Sun and McDonough (1989).*

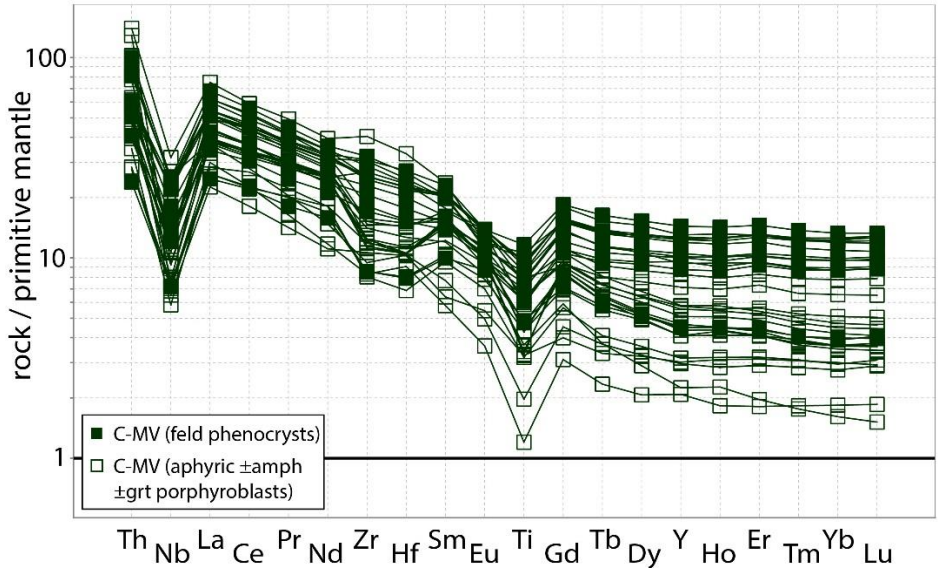

Figure 5.13 Primitive mantle normalized plot. Normalizing values from Sun and McDonough (1989). ***C-MV:*** *Confederation mafic volcanic,* ***Feld****: feldspar,* ***Amph****: amphibole,* ***Grt:*** *garnet.*

5.1.2.2 Intermediate to Felsic Volcanic Rocks

The intermediate to felsic volcanic rocks of the Laird Lake property are composed of various tuffs, crystal tuffs, and crystal lapilli tuffs that range from andesite/basaltic andesite to alkali rhyolite and their trachy counterparts on a Zr/Ti versus Nb/Y diagram (Fig. 5.3) with SiO_2 contents ranging from 62-79 wt.%. This unit shows a large variation in K_2O and Na_2O contents with fairly linear trends in SiO_2, Al_2O_3, MgO and P_2O_5 (Fig. 5.1A). However, trace elements versus Nb bivariate diagrams suggest the presence of two distinct geochemical units despite the similar macro and microscopic textural features (Fig. 5.1B). Figures 5.14 and 5.15 also show two populations and therefore the intermediate to felsic volcanic rocks have been subdivided into two groups: 1) Intermediate to felsic volcanic rocks with fractionated HREE and 2) Intermediate to felsic volcanic rocks with flat HREE.

Samples that are deemed geochemically altered typically have the same major element geochemistry as the unaltered samples, with the exception of when samples have up to 25% Fe-sulphides and oxides. The altered samples plot close to the intermediate to felsic volcanic rocks with enriched HREE on trace element bivariate diagrams (Fig. 5.1B), however, they show depletion in La, Ce, Sm, Gd, Y and Yb. The samples are usually associated with an increase in pyrite and/or magnetite (up to 25%) and are all found within 150 m from the Zone 11 trench (UTM 422670E 5644053N). Unaltered samples commonly contain less than 1% pyrite.

On an AFM diagram, all intermediate to felsic volcanic rocks, including the quartz-feldspar porphyritic crystal tuffs plot within the calc-alkaline field, with the exception of two samples plotting in the tholeiitic field due to their large concentrations of pyrite and magnetite (Fig. 5.4A). On a Jensen cation plot, samples plot within the calc-alkaline andesite to rhyolite fields, and in the tholeiitic dacite to rhyolite fields (Fig. 5.4B). The same two samples which plotted in the tholeiitic field, plot within the high-Fe tholeiitic basalt field of the Jensen cation plot. On a Th/Yb versus Zr/Y diagram, the samples with

fractionated HREE plot within the calc-alkalic field, whereas the samples with enriched HREE plot within the transitional field. Altered samples plot within the transitional and calc-alkalic fields (Fig. 5.14).

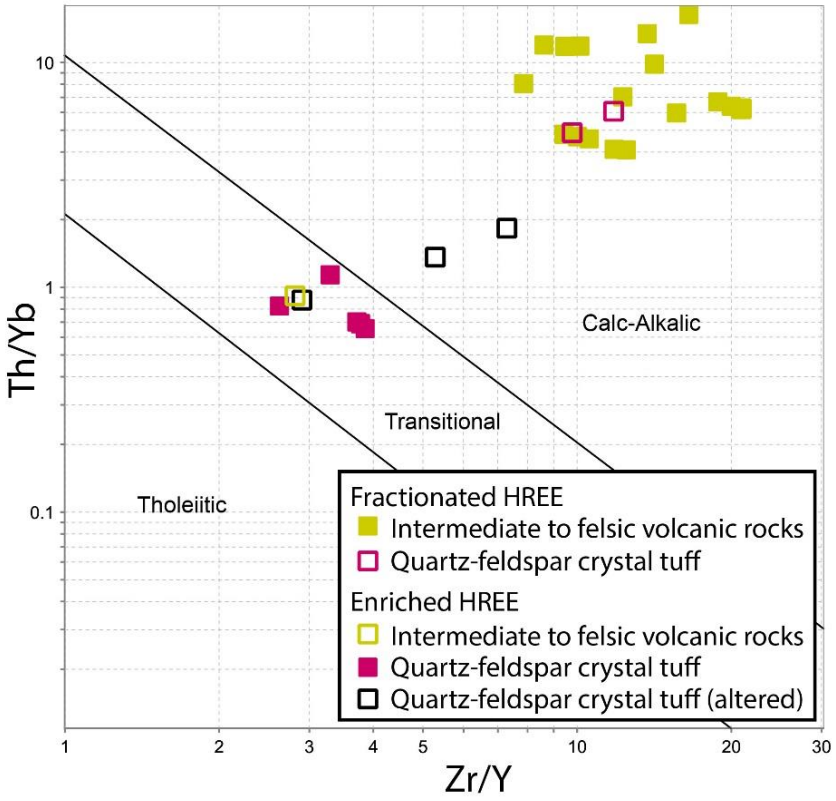

Figure 5.14. Th/Yb versus Zr/Y trace element diagram showing the intermediate to felsic rocks with fractionated HREEs plotting in the calc-alkalic fields, whereas the samples with enriched HREE plot within the transitional field. Altered sample plot in both the calc-alkalic and transitional fields. Fields on diagram from Ross and Bédard (2009).

On a primitive mantle spider diagram (Fig. 5.15A), the intermediate to felsic volcanic rocks with fractionated HREE are enriched in LREE (La/Sm_n=3.68-6.63) with depleted HREE (Gd/Yb_n=1.47-5.52) and have strong negative Nb and Ti anomalies with Nb/Nb* and Ti/Ti* of 0.06-0.19 and 0.14-0.44 respectively. The intermediate to felsic volcanic rocks with enriched HREE are also enriched in LREE (La/Sm_n=2.12-2.82), but have fairly flat HREE (Gd/Yb_n=0.99-1.29), weak negative Nb anomalies (Nb/Nb*=0.47-0.52) and very strong negative Ti anomalies (Ti/Ti*=0.01-0.04; Fig. 5.15B). The altered

rocks within this unit show depletion in LREE compared to the unaltered unit, but still maintain similar LREE ratios (La/Sm_n=2.12-4.07). They have positively sloping HREE (Gd/Yb_n=0.66-0.76), weak negative to weak positive Nb anomalies (Nb/Nb*=0.78-1.79) and a negative Ti anomaly (Ti/Ti*=0.04-0.18).

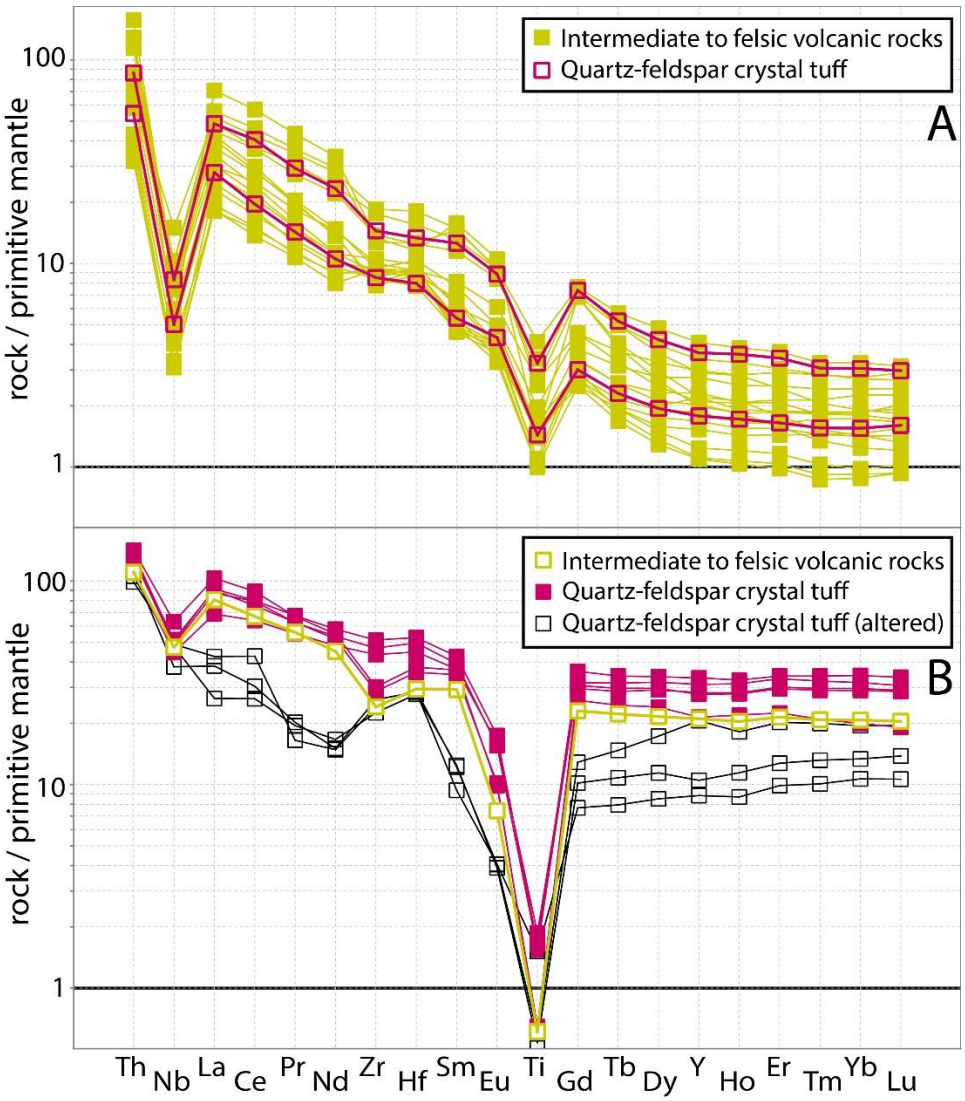

Figure 5.15 Primitive mantle normalized plot. A) Intermediate to felsic volcanic rocks with fractionated HREE. B) Intermediate to felsic volcanic rocks with enriched HREE. Normalizing values from Sun and McDonough (1989).

5.1.3 Intrusions

The main intrusions on the Laird Lake property are post-deformation and peak-metamorphism (with the exception of the lamprophyric intrusion and the foliated dioritic intrusion found within the

Confederation assemblage on the western end of the property) and therefore have not been affected by strong element remobilization. Most individual rock types display linear patterns on Figure 5.16A and B, but show scatter in the K_2O and Na_2O plots. The pyroxenite samples display considerable scatter on most major element diagrams indicating the mobility of Al_2O_3, MgO, K_2O, Na_2O and CaO, most likely caused by retrograde metamorphism significantly altering the primary mineralogy.

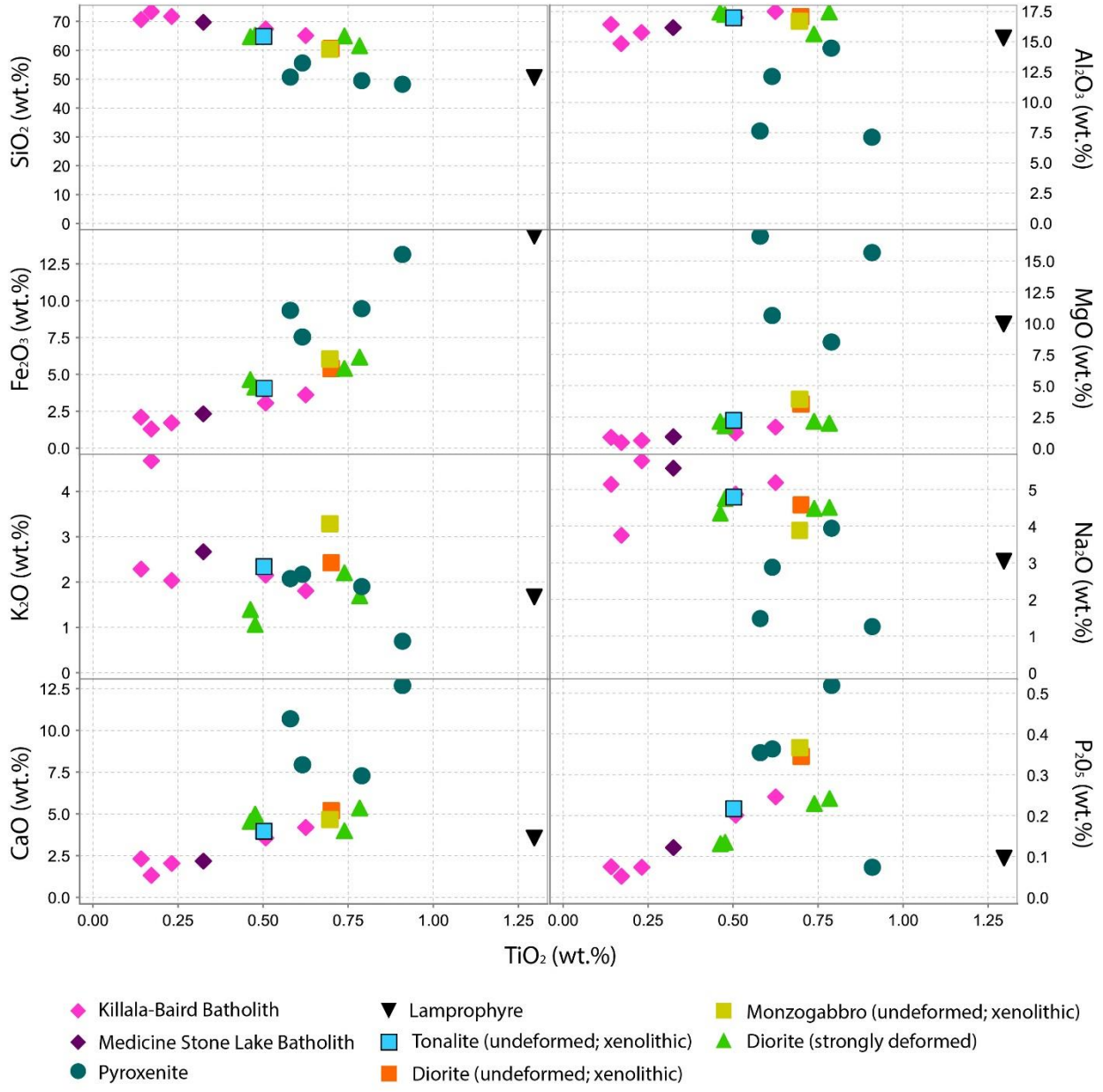

Figure 5.16 (A) Variation diagrams of TiO_2 versus major element oxides for the intrusive rocks of the Laird Lake property.

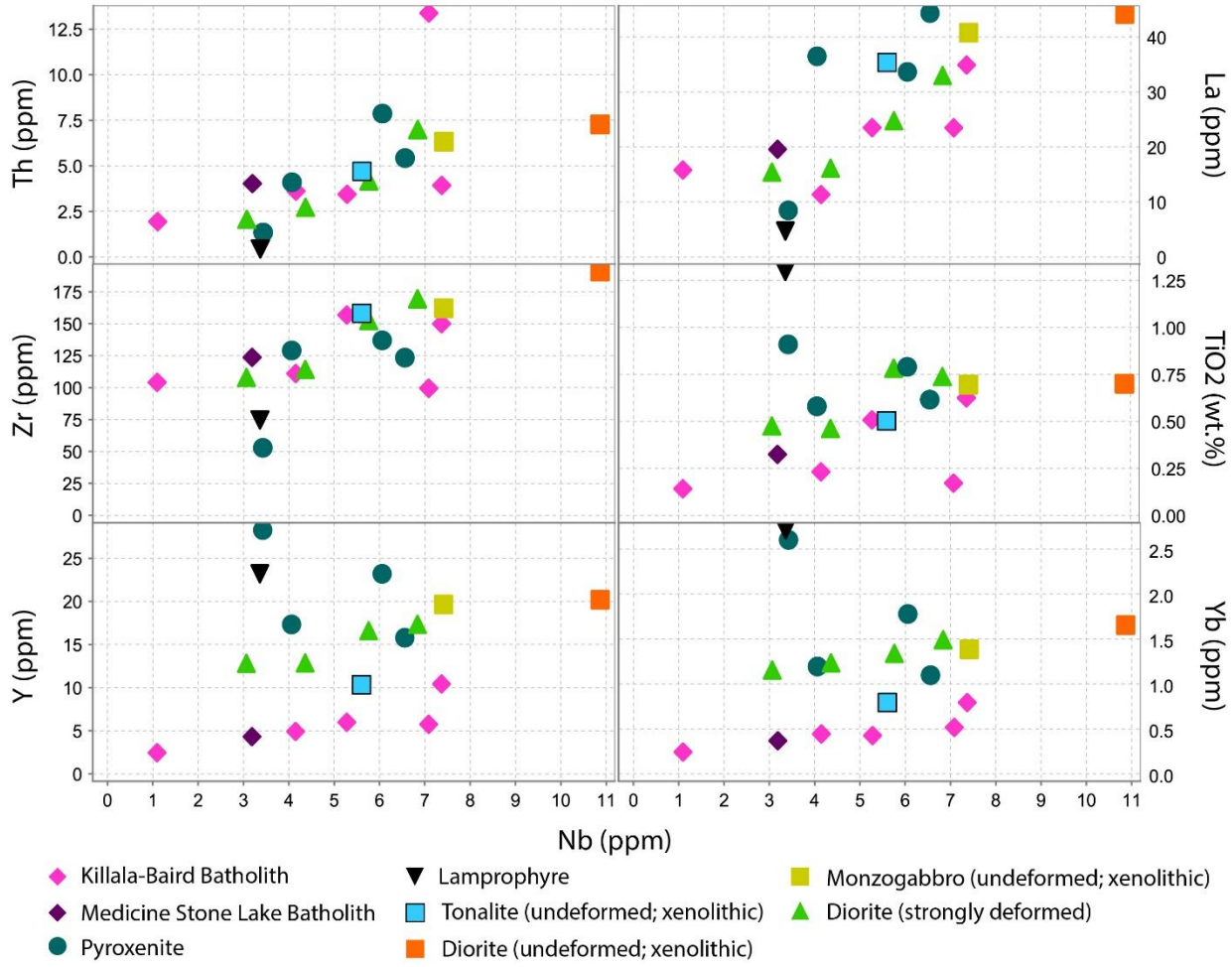

Figure 5.16 (B) Variation diagrams of Nb vs trace elements.

5.1.3.1 Felsic Intrusions: Killala-Baird and Medicine Stone Lake Batholiths

The felsic batholiths have SiO_2 contents between 65-73 wt.% and plot within the granodiorite to granite fields on a TAS diagram (Fig. 5.17) and calc-alkalic fields on the AFM and Th/Yb versus Zr/Y diagrams (Fig. 5.18). Both intrusions show very similar trace element patterns on a primitive mantle normalized spider diagram (Fig. 5.19A). The Killala-Baird batholith is enriched in LREE (La/Sm_n=3.03-8.61), with fractionated HREE (Gd/Yb_n=2.35-4.56), and negative Nb (Nb/Nb*=0.04-0.31) and Ti (Ti/Ti*=0.20-0.37) anomalies. The Medicine Stone Lake intrusion is also enriched in LREE (La/Sm_n=5.03), with fractionated HREE (Gd/Yb_n=3.67), and negative Nb (Nb/Nb*=0.11) and Ti (Ti/Ti*=0.38) anomalies.

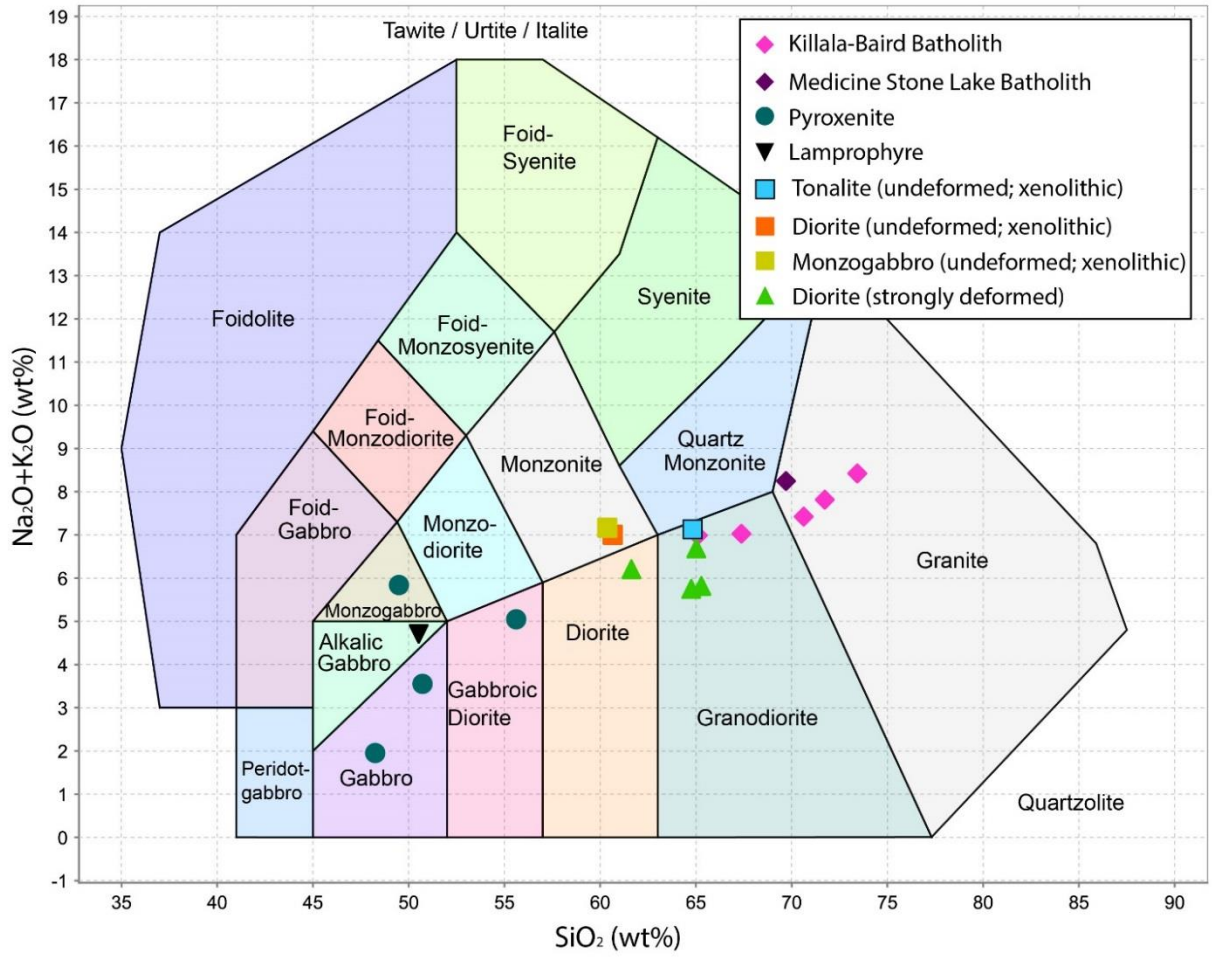

Figure 5.17. Silica vs. total alkalis diagram showing classification of the Laird Lake intrusive rocks.

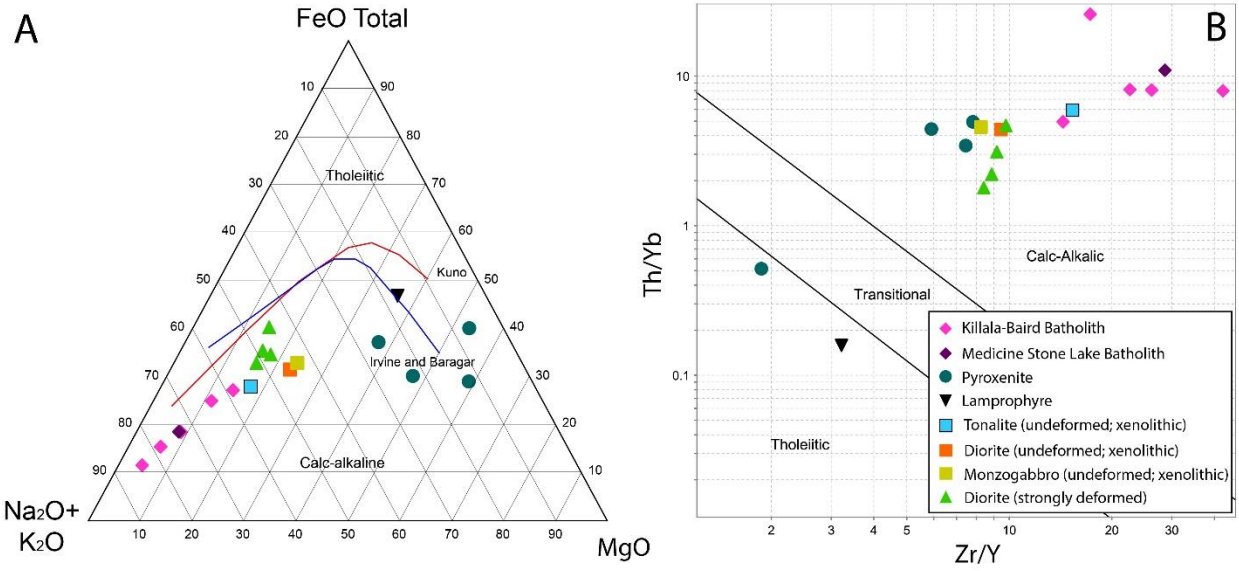

Figure 5.18. Magmatic affinity classification diagrams. (A) AFM diagram. Trend lines from Kuno (1968) and Irvine and Baragar (1971). (B) Th/Yb versus Zr/Y trace element diagram. Fields on diagram from Ross and Bédard (2009).

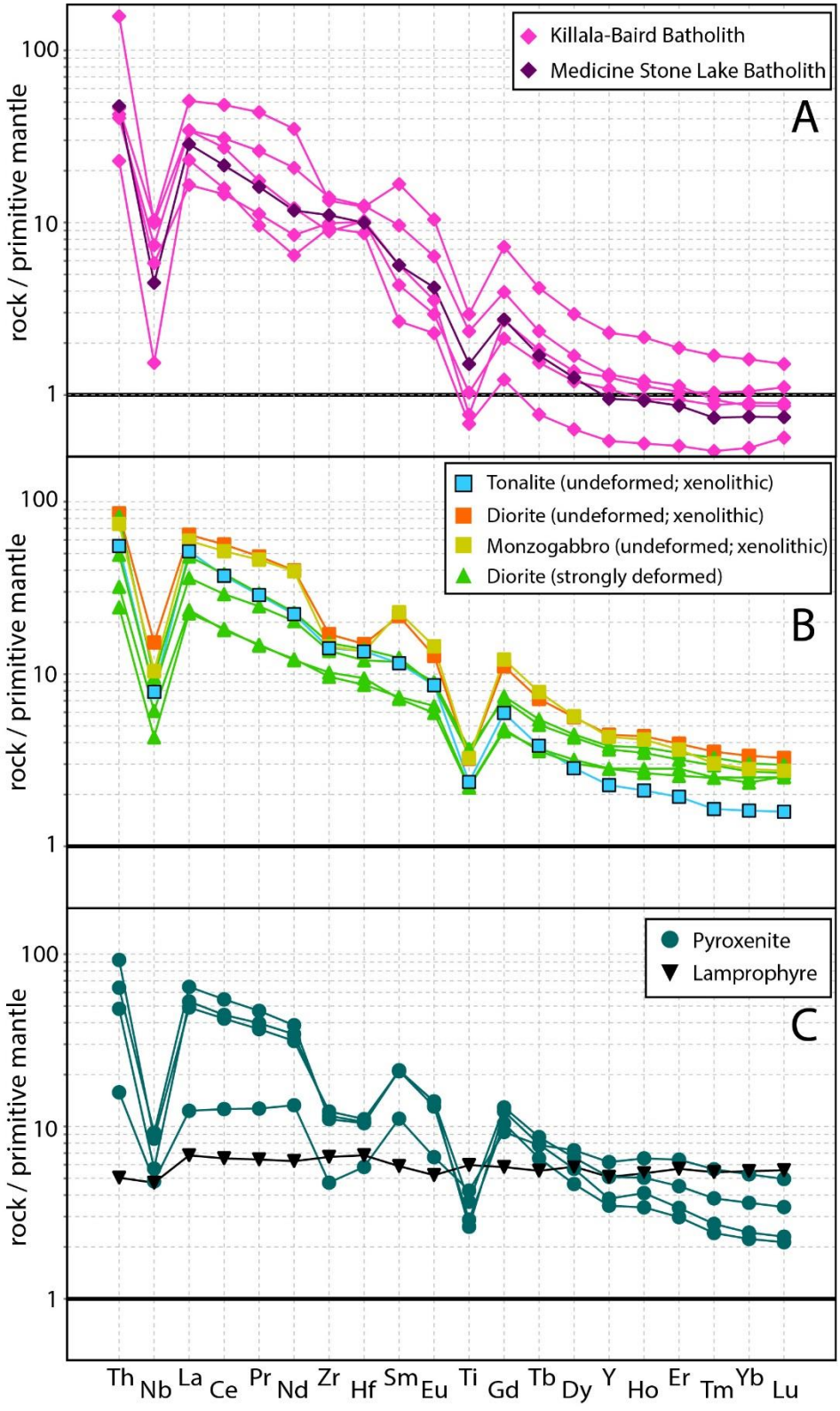

Figure 5.19 Primitive mantle normalized plots. (A) Felsic intrusions: Killala-Baird and Medicine Stone Lake batholiths. (B) Intermediate intrusions: Xenolithic diorite to tonalite, and foliated diorite. (C) Mafic intrusions: Pyroxenite and lamprophyre. Pyroxenite sample with lesser enriched LREE is tholeiitic. Normalizing values from Sun and McDonough (1989).

5.1.3.2 Intermediate Intrusions: Xenolithic Diorite to Tonalite, and Foliated Diorite

Two varieties of intermediate intrusions crop out in the study area; the unfoliated xenolithic type and the foliated (no xenoliths) type. The xenolithic intrusions have between 60-64 wt.% SiO_2 and plot within the monzonite and granodiorite fields on a TAS diagram (Fig. 5.17) and calc-alkalic field on an AFM and Th/Yb versus Zr/Y diagram (Fig. 5.18). On a primitive mantle normalized spider diagram (Fig. 5.19B), the diorite and monzogabbro plot almost identically with just slight variations in Nb (diorite: Nb/Nb*=0.20, monzogabbro: Nb/Nb*=0.15). Both rock types have enriched LREE (La/Sm_n=2.59-2.96), negative Zr, Hf and Ti anomalies (Zr/Zr*=0.48-0.57; Hf/Hf*=0.44-0.50; Ti/Ti*=0.19-0.20; see appendix B for calculation of Zr/Zr* and Hf/Hf*), and fractionated HREE (Gd/Yb_n=3.30-4.31). The tonalite sample is slightly more depleted in REE compared to the diorite and monzogabbro samples, but still shows enriched LREE (La/Sm_n=4.45), fractionated HREE (Gd/Yb_n=3.67), negative Nb and Ti anomalies (Nb/Nb*=0.11; Ti/Ti*=0.27) but weak negative Zr (Zr/Zr*=0.88) and Hf (Hf/Hf*=0.84) anomalies.

The foliated diorite has a SiO_2 content of 61-65 wt.% and plots within the diorite and granodiorite fields on a TAS diagram (Fig. 5.17), and in the calc-alkalic fields on AFM and Th/Yb versus Zr/Y diagrams (Fig. 5.18). This unit is enriched in LREE (La/Sm_n=3.05-3.86), has fractionated HREE (Gd/Yb_n=1.85-2.59), strong negative Nb and Ti anomalies (Nb/Nb*=0.15-0.19, Ti/Ti*=0.35-0.39) and has weak negative to zero Zr (Zr/Zr*=0.88-1.09) and Hf (Hf/Hf*=0.77-1.01) anomalies (Fig. 5.19B).

5.1.3.3 Mafic Intrusions: Pyroxenite and Lamprophyre

The mafic intrusions on the Laird Lake property consists of pyroxenites and one lamprophyric intrusion. The pyroxenites plot within the gabbro, gabbroic diorite and monzogabbro fields of a TAS diagram (Fig. 5.17) with SiO_2 contents between 48-55 wt.%. The samples plot within the calc-alkalic field of a Th/Yb versus Zr/Y diagram, with the exception of one sample in the tholeiitic field (Fig. 5.18B). Samples show the same magmatic affinity on an AFM diagram, but calc-alkalic samples plot much closer

to the tholeiitic sample (Fig. 5.18A). The pyroxenite samples show linear trends on the SiO_2 and Fe_2O_3 diagrams (Fig. 5.16). On a primitive mantle normalized spider diagram (Fig. 5.19C), the calc-alkalic rocks are enriched in LREE (La/Sm_n=2.34-3.06), have fractionated HREE (Gd/Yb_n=3.57-5.05), with negative Nb (Nb/Nb*=0.08-0.14), Zr (Zr/Zr*=0.38-0.47), Hf (Hf/Hf*=0.36-0.43) and Ti (Ti/Ti*=0.16-0.22) anomalies. The tholeiitic sample is less enriched in LREE (La/Sm_n=1.11) and shows a flatter trend in the HREE (Gd/Yb_n=1.75), with weaker negative Nb (Nb/Nb*=0.39) and Ti (Ti/Ti*=0.41) anomalies and similar Zr (Zr/Zr*=0.38), Hf (Hf/Hf*=0.47) ratios to the calc-alkalic pyroxenite samples.

The lamprophyric intrusion plots within the alkalic gabbro field on a TAS diagram (Fig. 5.17) with 50 wt.% SiO_2 and lies within the tholeiitic fields on an AFM and Th/Yb versus Zr/Y diagrams (Fig. 5.18). On a primitive mantle normalized spider diagram (Fig. 5.19C), the sample has a flat REE pattern with a weak negative Nb anomaly (La/Sm_n=1.15, Gd/Yb_n=1.05, Nb/Nb*=0.66, Ti/Ti*=1.02).

5.2 Neodymium Isotopes

A total of 13 samples were analysed for Nd isotopes in order to determine the magmatic source and tectonic setting in which the rocks were formed, and to study the effects of secondary influences such as crustal contamination. Representative and least altered samples from both assemblages were chosen for this study with results summarised in Table 5.1 and the full results in Appendix C.

5.2.1 Balmer Assemblage

An age of 2988 Ma was used to calculate the ε_{Nd} values for the mafic volcanic samples from the Balmer assemblage as it is the geographically closest zircon U-Pb age for an interlayered rhyolite lapilli tuff (UTM 437875E 5650513N; Skulski (unpublished) referenced in Sanborn-Barrie et al., 2004). Four samples were selected from the high-Ti mafic volcanic rocks and two samples are from the low-Ti mafic volcanic suite. The high-Ti mafic volcanic rocks display a small range of ε_{Nd} values from 0.20 to 1.26 and

*Table 5.1 Nd isotope results. **Feld**: feldspar, **Hbl**: hornblende*

Sample	Assemblage	Rock Type	$^{143}Nd/^{144}Nd$ (current)	$^{143}Nd/^{144}Nd$ (initial)	εNdt	Age (Ma)
LL-GBZ-K13009	Balmer	Mafic volcanic (high-Ti)	0.512574	0.508802	0.20	2988
LL-15BG-190A01	Balmer	Mafic volcanic (high-Ti)	0.512651	0.508845	1.03	2988
LL-15BG-134A02	Balmer	Mafic volcanic (high-Ti)	0.512452	0.508864	1.44	2988
LL-15BG-297A01	Balmer	Mafic volcanic (high-Ti)	0.512696	0.508857	1.26	2988
LL-15BG-235A01	Balmer	Mafic volcanic (low-Ti)	0.512246	0.508773	-0.32	2988
LL-15BG-387A01	Balmer	Mafic volcanic (low-Ti)	0.512583	0.508867	1.48	2988
LL-15BG-054B01	Confederation	Mafic volcanic (hbl)	0.511492	0.509160	1.57	2741
LL-15BG-219A01	Confederation	Mafic volcanic (feld+hbl)	0.511411	0.509163	1.63	2741
LL-15BG-231A01	Confederation	Intermediate to felsic volcanic	0.510809	0.509100	0.40	2741
LL-15BG-032B01	Confederation	Quartz-feldspar crystal tuff	0.511535	0.509160	1.57	2741
LL-16BG-068A01	Confederation	Quartz-feldspar crystal tuff	0.510975	0.509102	0.43	2741
LL-15BG-427A01	Syn-volcanic intrusion	Diorite (foliated)	0.511209	0.509173	1.73	2738
LL-15BG-314A01	Late intrusion	Diorite (xenolithic)	0.511055	0.509252	2.18	2695

whereas the low-Ti mafic volcanic rocks display a larger range of ε_{Nd} values from -0.32 to 1.48 (Table 5.1).

5.2.2 Confederation Assemblage

Five samples from the Confederation assemblage were selected, two mafic volcanic rocks with hornblende porphyroblasts and one with feldspar phenocrysts, one sample of intermediate to felsic volcanic rock (fine grained tuff), and two samples of quartz-feldspar porphyritic crystal tuff (sample LL-16BG068A01 has fractionated HREE on a PM normalized diagram, whereas sample LL-15BG032B01 has flat HREE; Table 5.1; Figs. 5.14, 5.15). The ε_{Nd} values for the Confederation assemblage samples were

calculated using an age of 2741 Ma as that is the zircon U-Pb age of sample LL-16BG068A01. The mafic volcanic samples display a narrow range of ε_{Nd} values from 1.57 to 1.63 (Table 5.1). The intermediate to felsic volcanic sample has an ε_{Nd} value of 0.40 (Table 5.1). The quartz-feldspar porphyritic crystal tuff sample with fractionated HREE (LL-15BG068A01) has an ε_{Nd} value of 0.43 whereas the sample with flat HREE (LL-15BG032B01) has an ε_{Nd} value of 1.57 (Table 5.1).

5.2.3 Intrusions

The two intrusive samples analysed for U-Pb zircon geochronology were also analysed for Nd isotopes. The foliated diorite sample (LL-15BG427A01; Fig. 5.20) taken on the southern margin of the intrusion within the Confederation assemblage has an ε_{Nd} value of 1.73 (at 2738 Ma; Table 5.1). The unfoliated xenolitic diorite was sampled on the western margin of the intrusion (LL-15BG314A01; Fig. 5.20) within the Balmer assemblage and has an ε_{Nd} value of 2.18 (at 2695 Ma; Table 5.1).

5.3 Uranium-Lead Isotope Geochronology

Three samples from the Laird Lake property were selected for zircon U-Pb geochronology in order to date the Confederation assemblage in this portion of the Red Lake greenstone belt, to better constrain the timing of deformational event(s) and to better understand the relationship between the xenolithic diorite and pyroxenite intrusions (Fig. 5.20). A very fine-grained quartz-feldspar porphyritic crystal tuff within the Confederation assemblage near the contact with the Balmer assemblage, was dated to test whether the felsic units observed near the contact could represent Balmer age felsic volcanic rocks. Deformed and undeformed dioritic intrusions were dated to constrain the timing of deformation in the Laird Lake area. In addition, as the undeformed diorite is closely associated with the pyroxenite, an age for the diorite would give a rough estimate of the age of the pyroxenite. Both these intrusions are closely associated with the contact between the two assemblages. The complete U-Pb data set is presented in Appendix D.

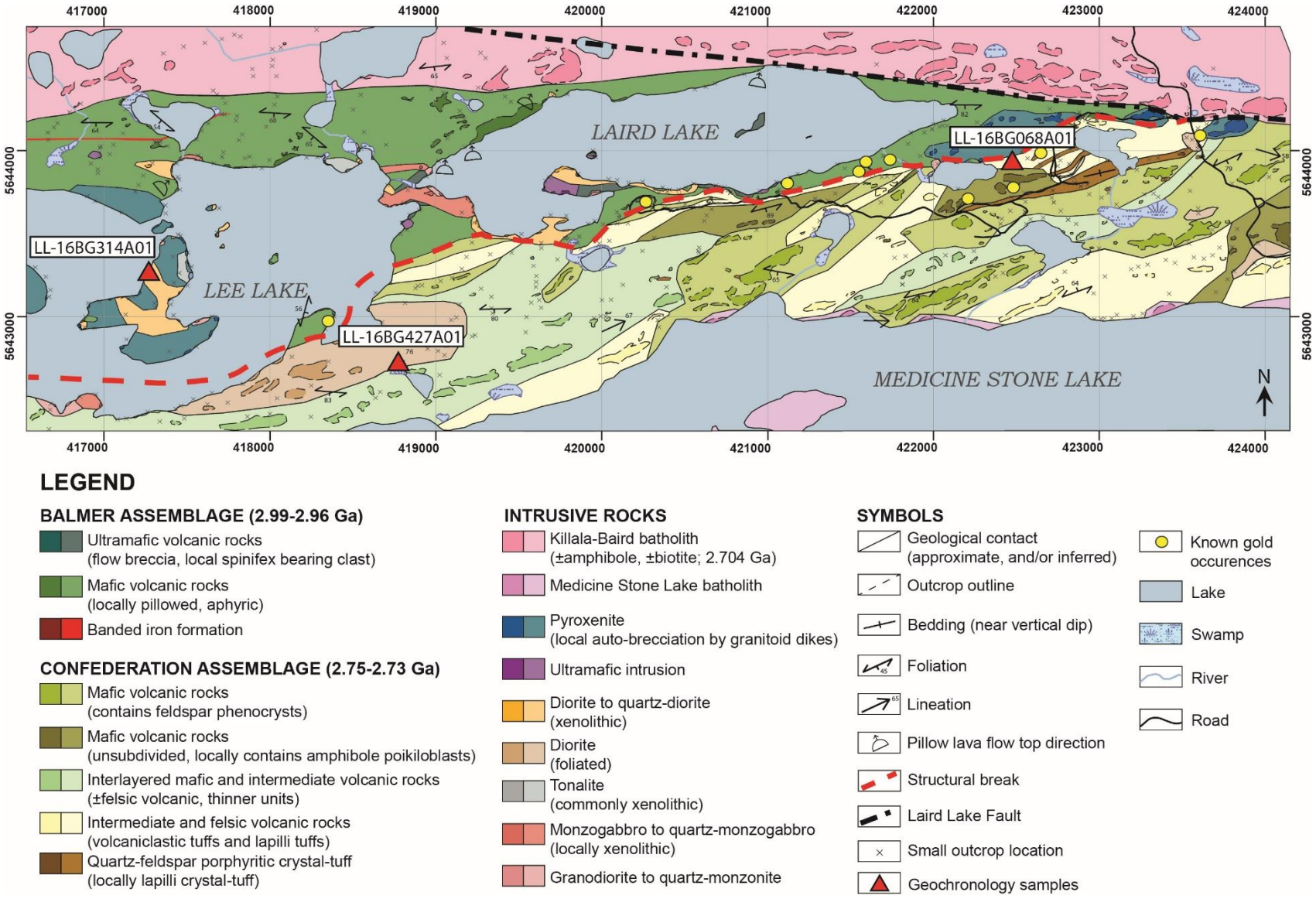

Figure 5.20 Map of the Laird Lake property showing the location of the geochronology samples.

5.3.1 Confederation Quartz-Feldspar Porphyritic Crystal Tuff

The very fine-grained quartz-feldspar porphyritic crystal tuff (LL-16BG068A01; UTM 422465E 5643946N) yielded very small light brown zircon typically measuring less than 200 µm in length (Fig. 5.21A). A total of five zircons were analysed and results show a large scatter (Fig. 5.22). Three of the grains analysed display a tight and concordant age, yet all ages are vastly different: 2974.7 ± 3.4 Ma, 2912.6 ± 3.2 Ma and 2840.6 ± 2.8 Ma. A fourth zircon is about 10% discordant whereas the fifth zircon grain had low Pb and U concentrations and lead to an imprecise but concordant age of 2740.6 ± 19 Ma.

5.3.2 Deformed Diorite

The medium- to fine-grained foliated dioritic intrusion was sampled roughly 500 m from the contact between the two assemblages, within the Confederation assemblage (LL-16BG427A01; UTM 418737E 5642680N). The zircons from the sample are light brown with very few fractures (Fig. 5.21B). They are typically equant with a few elongate crystals and measure over 100 µm long with the majority measuring over 200 µm in length. The diorite yielded a weighted age of 2737.6 ± 0.79 Ma with all four zircons analysed plotting on concordia within a tight grouping (Fig. 5.23).

5.3.3 Xenolithic Diorite

The medium- to coarse-grained xenolithic unfoliated diorite was sampled on the westside of the large island on Lee Lake (LL-16BG314A01; UTM 417261E 5643268N). The zircons are light to dark brown, elongate, measure over 200 µm and show much more zoning and fracturing compared to the previous two samples (Fig. 5.21C). Of the five zircons analysed, there are two concordant grains at 2695.0 ± 3.9 Ma and 2701.9 ± 2.8 Ma (Fig. 5.24). The three remaining grains form a cluster of discordant younger ages.

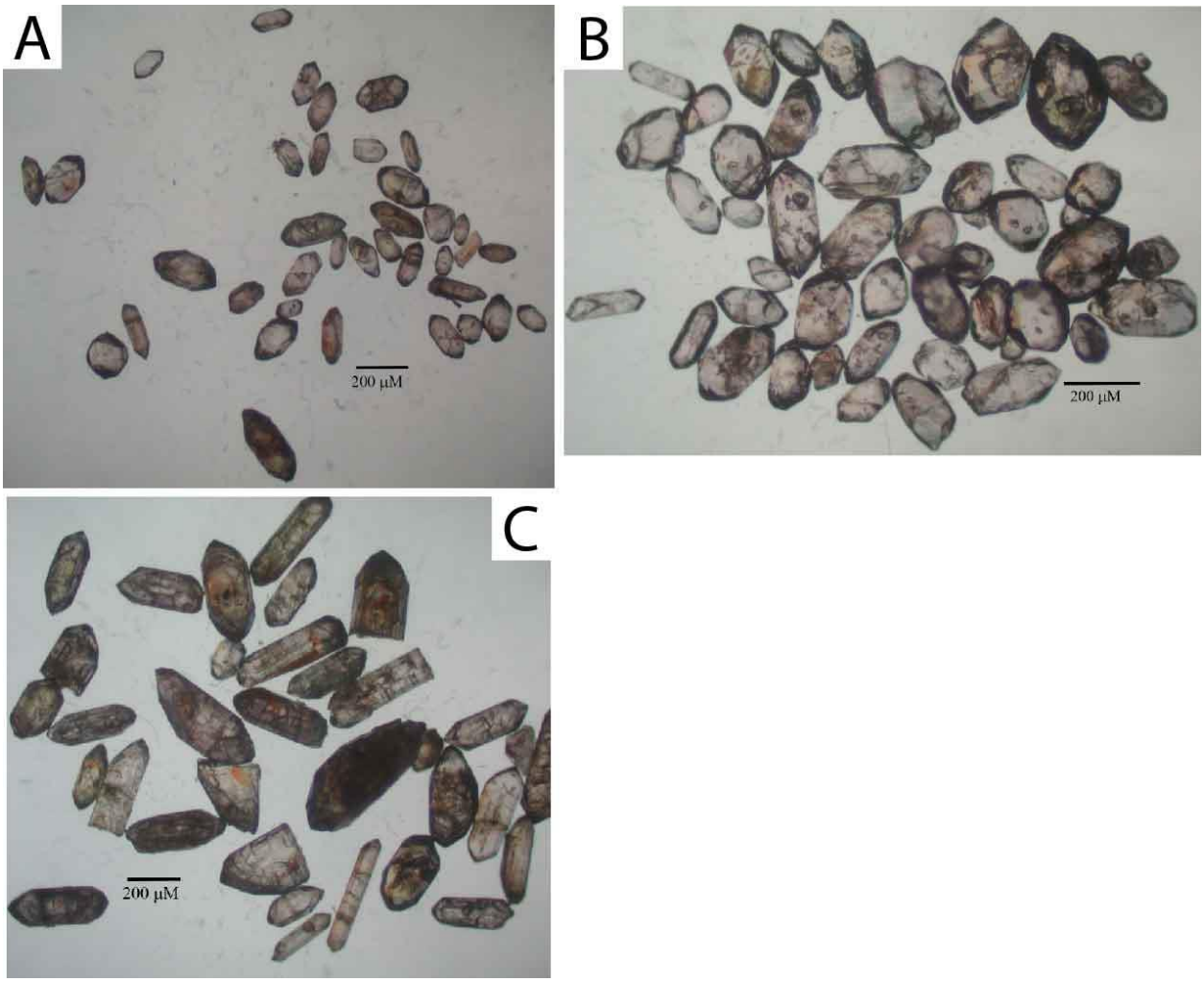

Figure 5.21 Photographs of zircons acquired from each sample. A) Sample LL-16BG068A01. B) Sample LL-16BG427A01. C) Sample LL-16BG314A01.

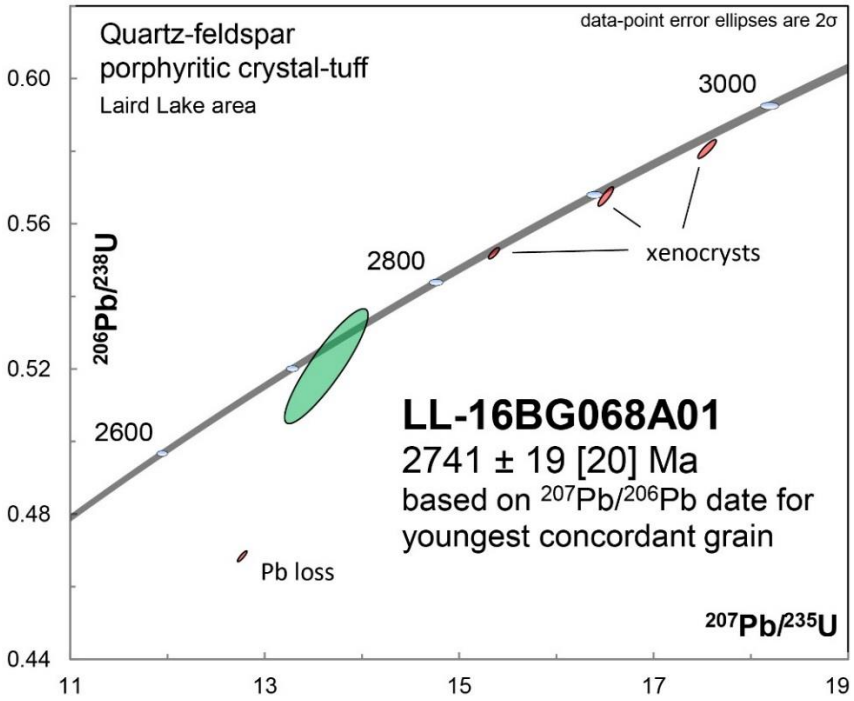

Figure 5.22 Concordia curve plot of U-Pb isotope ratios for sample LL-16BG068A01, illustrating individual zircon data with error ellipses.

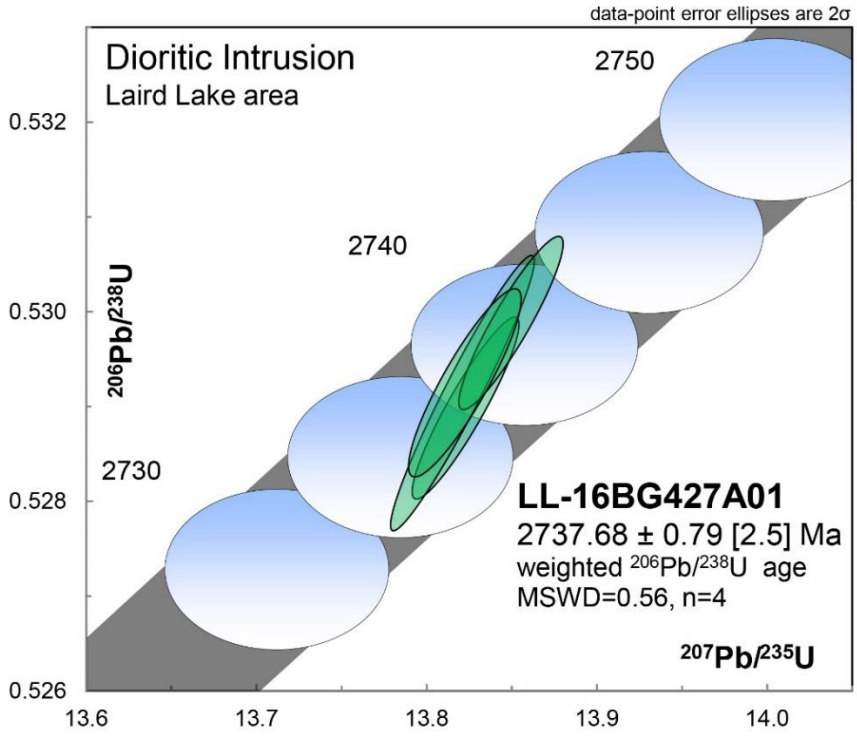

Figure 5.23 Concordia curve plot of U-Pb isotope ratios for sample LL-16BG427A01, illustrating individual zircon data with error ellipses and weighted average using data from four sampled zircons.

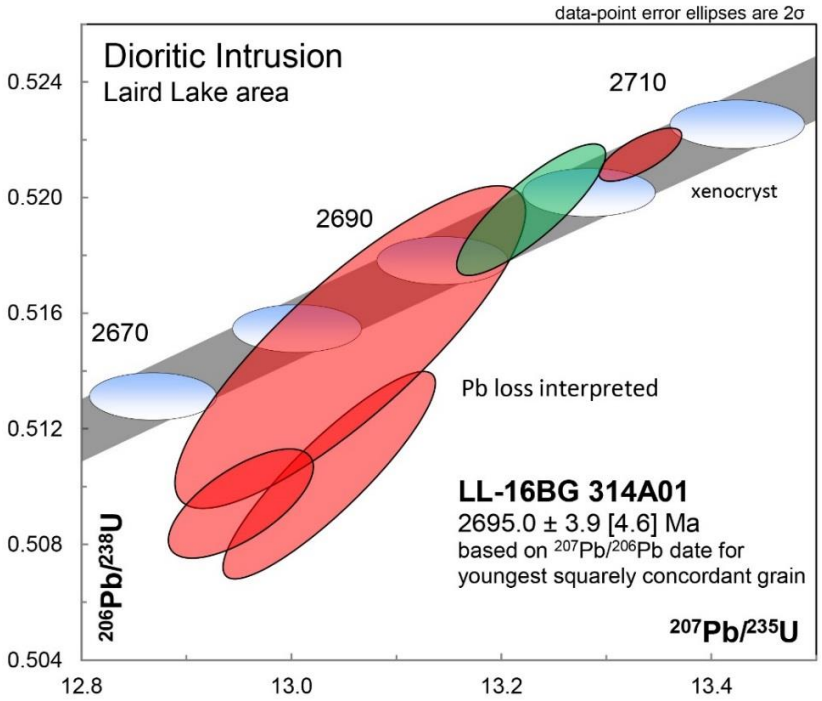

Figure 5.24 Concordia curve plot of U-Pb isotope ratios for sample LL-16BG314A01, illustrating individual zircon data with error ellipses.

5.4 Oxygen Isotopes

In-situ oxygen isotopic measurements were completed using a secondary ion mass spectrometer (SIMS) on four quartz veins from the Laird Lake property, two of which are gold-mineralized and two are barren, in order to evaluate the isotopic differences across the width of the veins and the differences between the mineralized and barren samples. Traverses across the width of the veins were undertaken in order to investigate the symmetry of the veins and to assess if the veins were formed by one or multiple generations of mineralizing fluid. Petrographic analyses on the quartz veins suggest that various degrees of deformation and metamorphism likely destroyed any primary vein features as the veins are texturally homogeneous and show high degrees of strain within the quartz. Therefore, O isotope data could help establish if the veins were formed through one of multiple generations of mineralizing fluid. A descriptive summary of the four quartz veins is presented in Table 5.2. Appendix E presents the SIMS data, field and microscope photos, and the location of each analysis.

Table 5.2 Descriptive summary of the four sampled veins. Petrographic comments refer to the samples taken from the veins. The uncertainty of the $\delta^{18}O$ averages represent the analytical uncertainty. ***VG****: visible gold,* ***PZ****: Pit Zone,* ***SHQ****: Shear Hosted Quartz.*

Samples	Host rock	Thickness	Colour	Mineralization	Vein orientation	Petrographic comments	Location	$\delta^{18}O_{quartz}$ Average
447A05 Au-mineralized	Balmer mafic volcanic	5-20cm	smokey gray, translucent	VG, pyrite, chalcopyrite, pyrrhotite	parallel to foliation	Quartz grains can be up to 4 mm long and are typically less than 1 mm thick. The grains are strongly foliated and show undulose extinction. Coarser grains commonly have large subgrain areas between them.	PZ trench UTM 420219E 5643701N	11.3 ± 1.2
233A05 Au-mineralized	Confederation intermediate dike within mafic volcanic	2-12cm	smokey gray, local dark pink staining	pyrite	parallel to foliation	The quartz grains are typically less than 2 mm long, show undulose extinction, and are weakly foliated. Subgrains are common on grain boundaries of coarse grains.	SHQZ trench UTM 420492E 5643625N	11.4 ± 1.2
233A06 barren	Confederation mafic volcanic	3-7cm	milky white	none	discordant to foliation	Quartz grains up to 3 mm long, displaying undulose extinction. Grains show no preferential orientation, have have sharp to serrated boundaries with rare subgrains at the grain boundaries.	SHQZ trench UTM 422490E 5643791N	11.5 ± 1.2
443A02 barren	Confederation mafic volcanic	3-10cm	milky white	none	parallel to foliation	Quartz grains are typically larger than 2 mm long, display undulose extinction, and are only locally foliated. Subgrain areas have formed parallel to the vein margins.	station 443 UTM 422484E 5643792N	11.4 ± 1.2

In order to complete a traverse across the entire width of the vein, two thin sections placed beside each other, both spanning the width of the vein were cut into three individual pucks, two of which came from the veins margins (thin section #1), whereas the third sample came from the center of the vein (thin section #2). Refer to Appendix D, Figures 4.1 and 4.2 to see the thin section placements along the vein and puck locations within each thin section. Since the thin sections were located one below the other, the traverse for the center of the vein is located roughly 2-2.5 cm from the traverse completed on the veins margins. Three out of the four veins sampled have overlapping data between the traverses completed on thin section #1 and thin section #2. The overlap is identified by marking the distance away from the vein margins. When considerable overlap was identified, the graphs (Figs. 5.25; 5.26) were separated into two plots for clarity.

5.4.1 Au-Mineralized Quartz Veins

$\delta^{18}O_{quartz}$ values for the individual quartz veins average between 11.3-11.4 ±1.2‰ (Table 5.2). The Au-mineralized quartz veins show only small differences across the veins with most data points falling within error of each other. Sample 447A05 has consistent data between 11-12‰ with a few exceptions around 13-13.6‰ and one data point dipping down to 9.5‰ (Fig. 5.25A; B). Visible gold is present between points 14 and 15, yet no major differences exist in the data. The overlapping points between sample 447A05-2 and 447A05-1.1 do not fall within error of each other, likely due to the vein asymmetry and the 2-2.5cm gap between the two traverses. Sample 233A05 shows a slight depletion in $\delta^{18}O_{quartz}$ values in the center of the vein, with the data all plotting below 11‰ whereas the samples closer to the margins have $\delta^{18}O_{quartz}$ values all above or equal to 11‰ (Fig. 5.25C). The vein margins have an $\delta^{18}O_{quartz}$ value averaging 12.1 ±1.2‰ whereas the center of the vein has an $\delta^{18}O_{quartz}$ value averaging 10.3 ±1.2‰. Both these values fall within error of each other.

5.4.2 Au-Barren Quartz Veins

$\delta^{18}O_{quartz}$ values for the Au-barren quartz veins range from 11.4-11.5 ±1.2‰ (Table 5.2) and lack any major trends across the veins. Values for sample 233A06 are fairly consistent, plotting between 10-12.5‰ with only two samples plotting above 13‰ (Fig. 5.26A; B). The overlapping data falls within error of each other with the exception of two overlapping points having a 3 ±1.2‰ difference. Sample 443A02 only has two overlapping data points that plot within error of each other (Fig. 5.26C). The center of the vein shows an increase in $\delta^{18}O_{quartz}$ values towards the left, however, the adjacent data point on sample 443A02-1.2 is not continuous of the trend since it has a low $\delta^{18}O_{quartz}$ value of 10.1 ± 0.9 ‰.

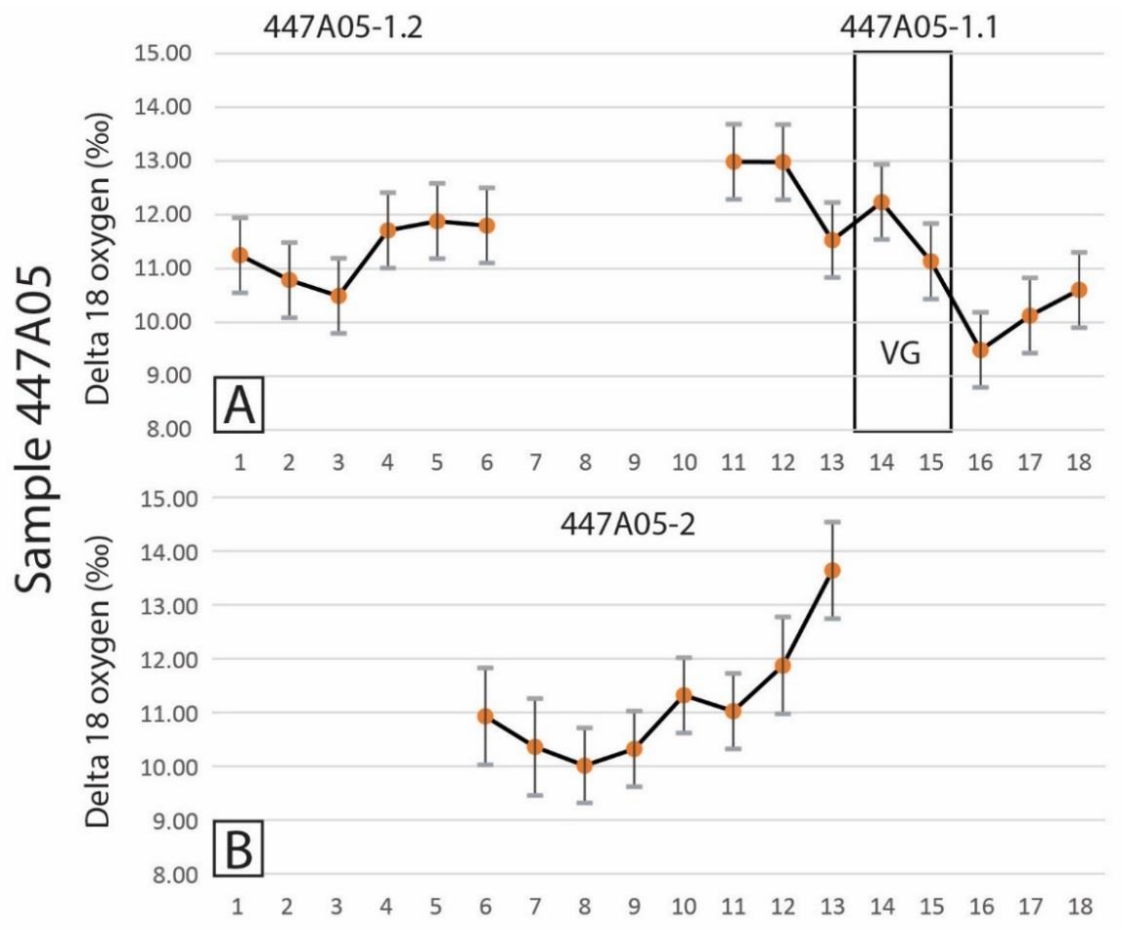

*Figure 5.25 Plot of $\delta^{18}O_{quartz}$ values across the width of the Au-mineralized quartz veins. Error bars represent spot-to-spot reproducibility on the quartz standard. A and B) Sample 447A05. **VG**: Visible gold*

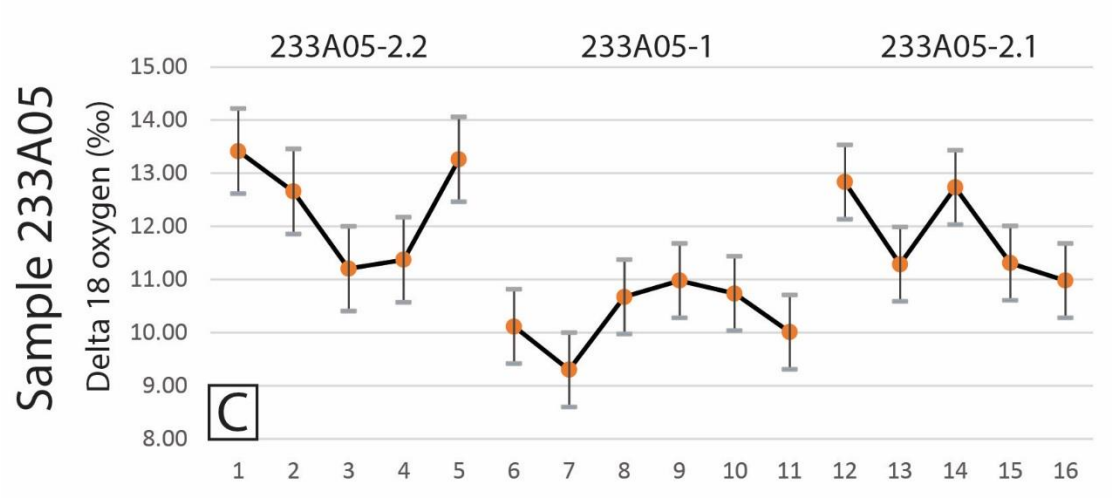

Figure 5.25 Continued. C) Sample 233A05

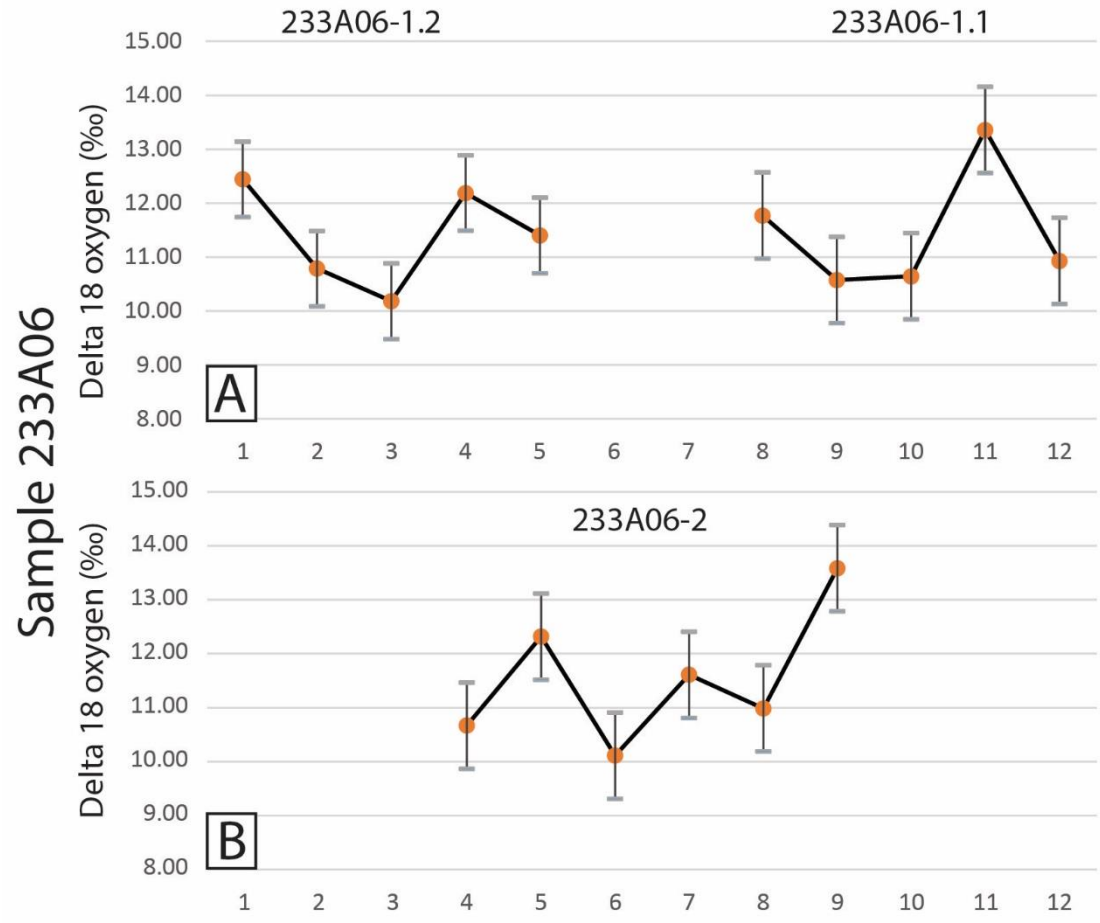

Figure 5.26 Plot of $\delta^{18}O_{quartz}$ values across the width of the barren quartz veins. Error bars represent spot-to-spot reproducibility on the quartz standard. A and B) Sample 233A06.

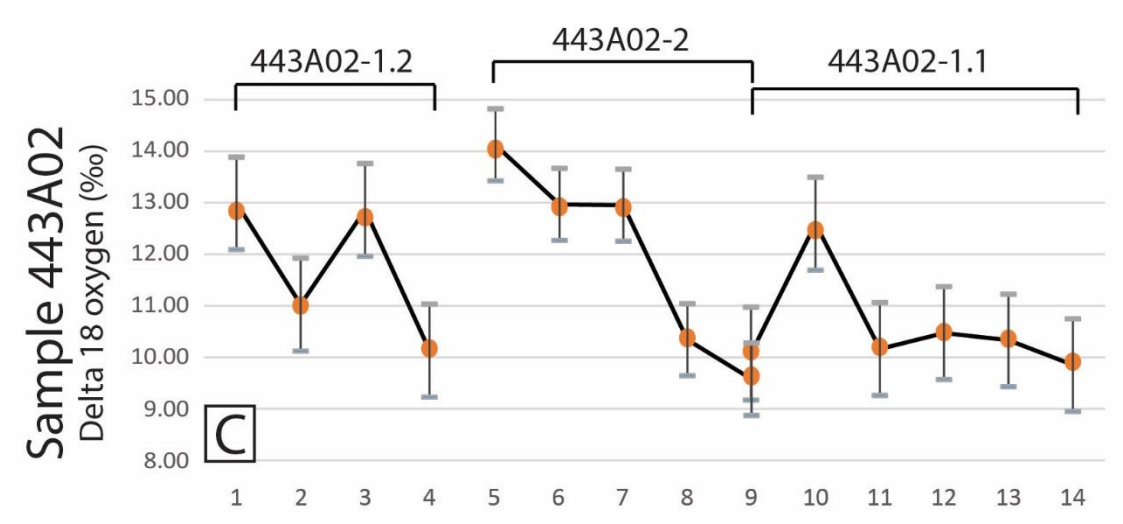

Figure 5.26 Continued. C) Sample 443A02

Chapter 6 – Discussion

6.1 Geochemistry and Isotopes

6.1.1 Balmer Assemblage

6.1.1.1 Whole Rock Geochemistry

The Balmer assemblage at the Laird Lake property is composed of four geochemically distinct volcanic units: ultramafic volcanic and intrusive rocks, high-Ti tholeiitic mafic volcanic rocks, low-Ti mafic tholeiitic volcanic rocks and calc-alkalic mafic volcanic rocks.

The ultramafic rocks are Al-undepleted (AUK) or Munro-type komatiites as defined by Nesbitt et al. (1979) and Arndt et al. (1997). They have Al_2O_3/TiO_2 and CaO/Al_2O_3 ratios slightly more enriched and Gd/Yb_n ratios slightly more depleted than the chondritic ratios and are mostly depleted in LREE with fairly flat HREE (Fig. 6.1).

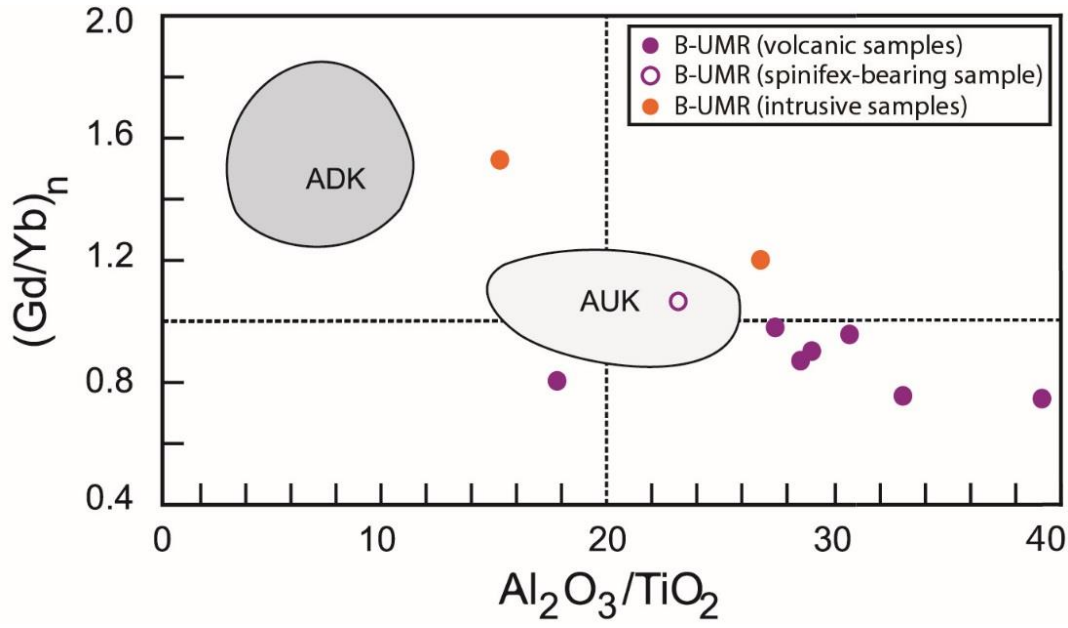

Figure 6.1 Laird Lake ultramafic rocks plotted on an Al_2O_3/TiO_2 vs $(Gd/Yb)_n$ plot (modified from Dostal, 2008). Fields were compiled mainly from Dostal and Mueller (2004). Dashed lines represent chondritic (primitive mantle) values (chondrite-normalized; chondritic values after Sun and McDonough, 1989). ***B-UMR****: Balmer ultramafic rocks*

Sulphide and PGE mineralization within the ultramafic bodies in the Laird Lake area is generally minor, with only one sample containing up to 3% disseminated fine-grained pyrrhotite with trace pyrite and chalcopyrite. Ultramafic samples within the field area have up to 1700 ppm Ni, 3200 ppm Cr, 113 ppm Co, 88.7 ppm Cu, 9.8 ppb Pt and 9.4 ppb Pd (Appendix A), compared to primary komatiitic melts which have 1303-2000 ppm Ni, 1800 ppm Cr, 175 ppm Co, 50 ppm Cu, 9.8 ppb Pt and 10.3 ppb Pd (Barnes and Lightfoot, 2005; Killick, 2014). Nickel-Cu-PGE deposits hosted within ultramafic rocks form from the segregation and concentration of chalcophile elements within liquid sulphide droplets (Naldrett, 1999). As the ultramafic sulphur-undersaturated melts ascend, they may assimilate sulphur-rich crust such as metasedimentary or metavolcanic rocks, which in turn, causes sulphur saturation within the melts, which can result in precipitation of Ni-Cu-PGE sulphide mineralization (Keays, 1995). Parker (2000b) has shown that the Balmer assemblage within the Red Lake greenstone belt has some potential for Ni-Cu-PGE mineralization with the closest occurrence of elevated PGE (2758.3 ppb Pd and 52.4 ppb Pt) at Flat Lake (UTM 433050E 5645506N (NAD 27)) within the vicinity of the past-producing Madsen Mine. The elevated Ni-Cu-PGE contents at Flat Lake are hosted within pillowed ultramafic metavolcanic flows with no visible sulphides (Parker, 2000b). For the Laird Lake property, the ultramafic rocks display typical compositions for ultramafic melts which have not undergone any metal concentration, and likely did not reach sulphide saturation since there is no known sulphur-rich crustal material such as metasedimentary or metavolcanic rocks that have been identified in the Red Lake greenstone belt pre-2.99 Ga.

The mafic volcanic rocks in the Balmer assemblage of the Laird Lake area show three contrasting geochemical patterns; two of which are tholeiitic and one is calc-alkalic. The two varieties of tholeiitic rocks are indistinguishable in the field, however, the low-Ti basalts more often display pillows, although this may be an artifact of the better exposure. The main differences between the two tholeiitic rock types are: 1) concentrations in TiO_2 and MgO, 2) total concentration of REE and HFSE 3) slope of the

LREE on a primitive mantle normalized diagram, and 4) magnitude of negative Nb anomalies (Nb/Nb*). With their lower total REE concentrations (Fig. 5.10a), and higher MgO (Fig. 5.4), it is likely that the low-Ti basalts represent more primitive magmas. They plot between high-Ti basalts and ultramafic melts, with higher concentrations of Ni and Cr (Fig. 6.2). They have higher concentrations of Pd and Pt compared to the high-Ti basalts and ultramafic rocks (Fig. 6.2). In addition, the low-Ti basalts plot closer to the primitive mantle (PM) ratios compared to the high-Ti basalts (Fig. 5.9), consistent with them being more primitive magmas.

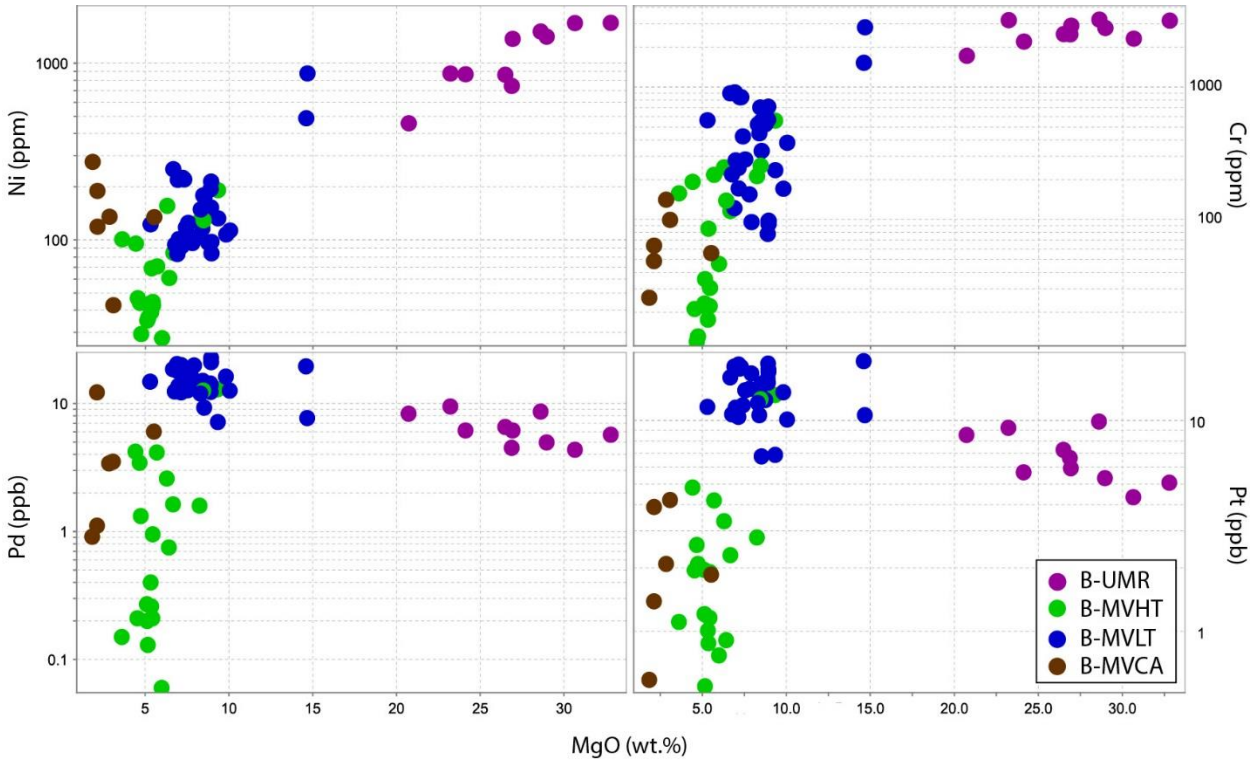

*Figure 6.2 Trace elements versus MgO plots for ultramafic to mafic rocks from the Laird Lake property. **B-UMR**: Balmer ultramafic rocks, **B-MVHT**: Balmer mafic volcanic (high-Ti), **B-MVLT**: Balmer mafic volcanic (low-Ti), **B-MVCA**: Balmer mafic volcanic (calc-alkalic)*

Within the Balmer assemblage, the ultramafic rocks are found mostly at the core of Laird Lake and are typically surrounded by low-Ti basalts, which are in turn surrounded by high-Ti basalts (Fig. 6.3). The zoned pattern and geochemical relationships suggest that the low-Ti basalts may be petrogenetically related to both the ultramafic rocks and high-Ti basalts.

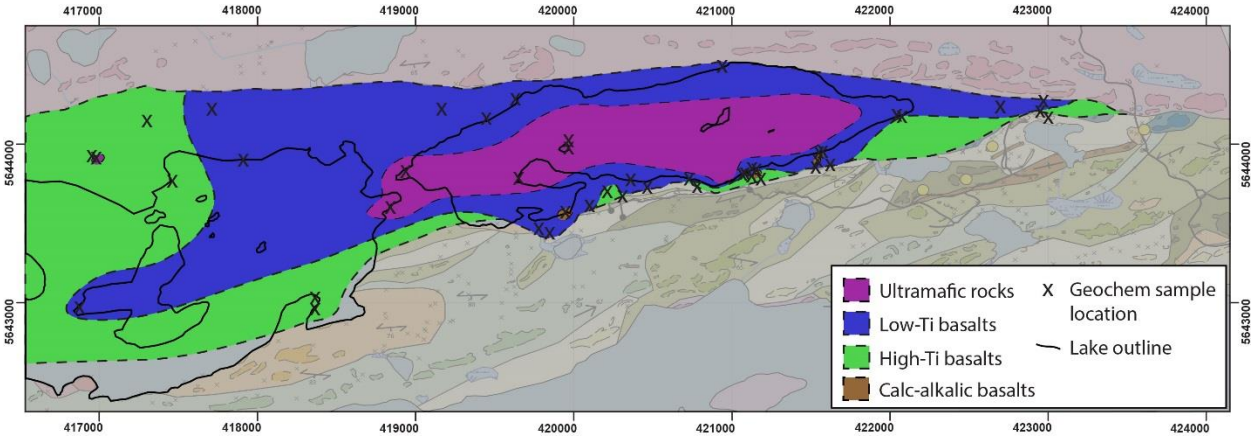

Figure 6.3 Distribution of volcanic rocks within the Balmer assemblage.

Numerical modelling was attempted to assess the possibility of mixing between the various ultramafic and mafic volcanic units to explain the zoned pattern (Fig. 6.3), using both the assimilation fractional crystallization (AFC) model of DePaolo (1981b) and simple binary mixing. It was assumed that fractionation and assimilation occured at a ratio of 1:1 with fractionation of 55% plagioclase, 25% clinopyroxene, 10% orthopyroxene and 10% olivine using distribution coefficients from Rollinson (1993; Table 6.1). Modeling of AFC using a komatiite parent (LL-15BG288A01) mixed with high-Ti basalt (LL-15BG190A01; UTM 421111E 5643827N) with 35% fractionation/assimilation and 40% mixing of the high-Ti basalt produced very similar trace element patterns to the low-Ti basalts (LL-15BG387A01; UTM 417895E 5643903N; Fig. 6.4A). Simple binary mixing with 40% high-Ti basalt and 60% komatiite also produced very similar patterns to low-Ti basalts (Fig. 6.4b). However, binary mixing does not account for the differences in major elements, with MgO showing a 9.4 wt.% difference and Al_2O_3 a 5 wt.% difference, but other elements only show a 2.1-0.01 wt.% difference. Low-Ti basalts would require a

Table 6.1 Partition coefficients for basalts from Rollinson (1993). Empty fields are due to the lack of available data.

	Th	Nb	La	Ce	Nd	Zr	Hf	Sm	Eu	Tb	Y	Yb	Lu
Olivine	0.0001	0.01	0.0067	0.006	0.0059	0.012	0.013	0.0066	0.0068		0.01	0.014	0.016
Plagioclase	0.01	0.01	0.19	0.111	0.09	0.048	0.051	0.072	0.443		0.03	0.056	0.053
CPX	0.03	0.005	0.056	0.092	0.23	0.1	0.263	0.445	0.474	0.57	0.9	0.542	0.506
OPX		0.15	0.004	0.02	0.03	0.18		0.05	0.05		0.18	0.34	0.42

major element chemistry more similar to komatiitic basalts in order to support this mixing model. This suggests that the low-Ti basalts could have been produced by mixing of units that have similar trace element patterns to the komatiite and high-Ti basalts.

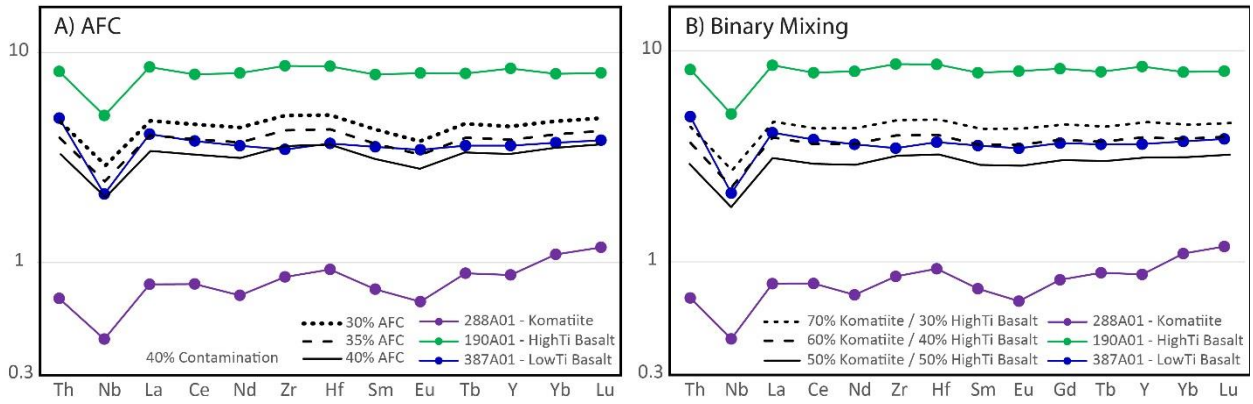

Figure 6.4. Primitive mantle normalized trace element diagrams showing the result of modeling AFC (A) and simple binary mixing (B). Trace element patterns are similar to a typical low-Ti basalt at 35% AFC and 40% contamination of the least contaminated Laird Lake komatiite by a high-Ti basalt. Simple binary mixing with no fractionation shows comparable results as the AFC modeling, with 40% high-Ti basalt and 60% komatiite. Normalizing values from Sun and McDonough (1989).

A group of six calc-alkalic mafic volcanic samples that are found within the Balmer assemblage (Fig. 5.8) are LREE enriched rocks with 2-30% disseminated pyrite, with all but one sample being from trenches associated with elevated gold mineralization. These rocks are scattered close to and along the contact between the Balmer and Confederation assemblages but show no continuitiy in their distribution (Fig. 6.3). There are four possible explanations for the occurrence of calc-alkalic rocks within a dominantly komatiitic-tholeiitic assemblage: 1) Crustally contaminated tholeiitic mafic magmas, 2) a primary calc-alkalic source, 3) LREE enrichment caused by pyrite and other alteration phases and 4) Confederation assemblage intrusions.

Field observations do not support these rocks being Confederation assemblage intrusions as where the rocks were sampled, no discontinuous or sharp contacts were noted within the mafic flows. Calc-alkalic mafic volcanic rocks have not been documented within the Balmer assemblage of the Red Lake greenstone belt (Sanborn-Barrie et al., 2004 and references therein). However, calc-alkalic felsic

metavolcanic rocks are intercalated within the komatiite-tholeiite sequence of the Balmer assemblage elsewhere in the belt, where they have been interpreted to be the result of plume-arc interaction (Hollings et al., 1999). Thirdly, the mafic volcanic rocks could be more intensely crustally contaminated mafic flows, however, scatter in SiO_2 (Fig. 5.2) suggest this is not the case. The high abundance of pyrite suggests that this was likely the cause of the LREE enrichment. Figure 6.5 shows a strong correlation between increasing LOI, S and La/Sm_n ratios. These trends suggest that the sulphide content in the rocks is directly affecting the LOI and causing an increase in LREE. Moreover, samples with no pyrite taken less than a metre away within the same continuous unit show no LREE enrichment. However, LREE enrichment caused by pyrite has not been documented and more work would have to be conducted in order to prove this model. Given the likelyhood that the trace element concentrations are not primary, these samples are excluded from futher discussion.

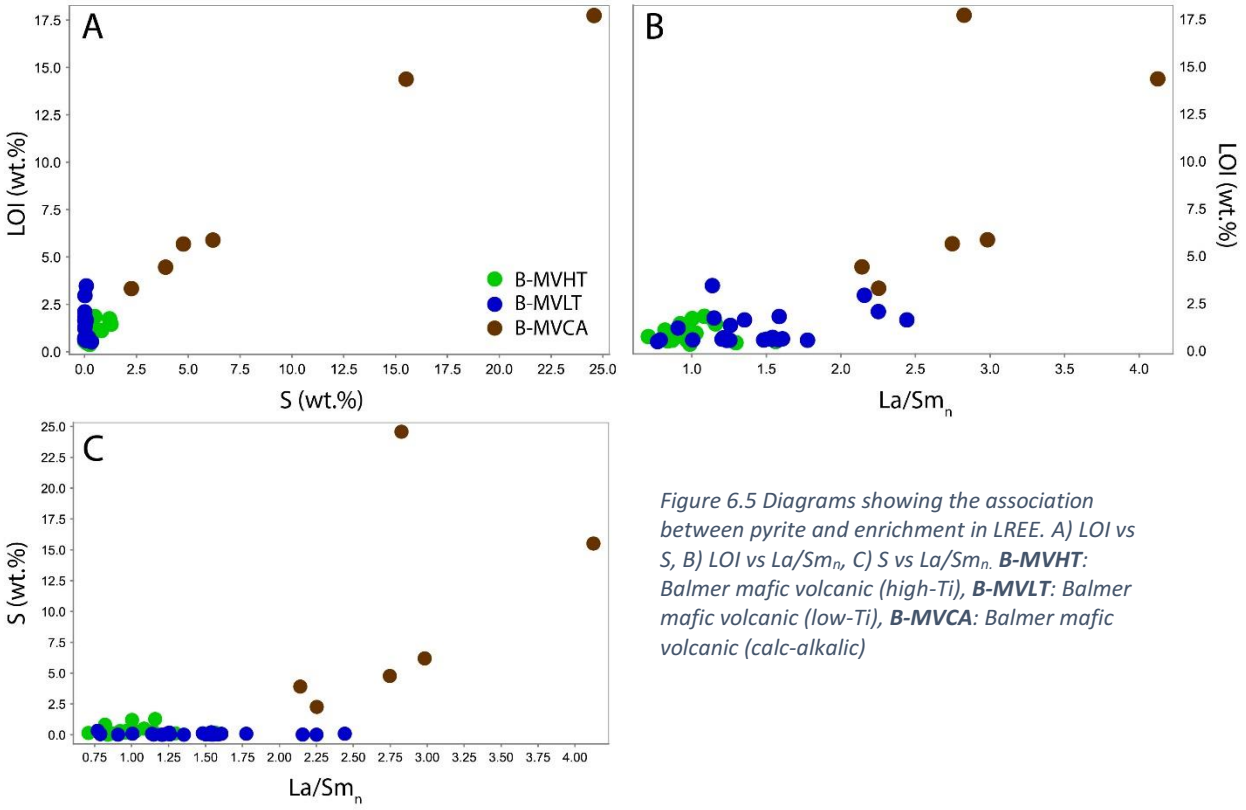

*Figure 6.5 Diagrams showing the association between pyrite and enrichment in LREE. A) LOI vs S, B) LOI vs La/Sm_n, C) S vs La/Sm_n. **B-MVHT**: Balmer mafic volcanic (high-Ti), **B-MVLT**: Balmer mafic volcanic (low-Ti), **B-MVCA**: Balmer mafic volcanic (calc-alkalic)*

Hollings (1998) and Sanborn-Barrie et al. (2001) showed that komatiite and tholeiite units in the RLGB have recognizably different primitive mantle normalized trace element profiles. The mafic flows of the Balmer assemblage are generally tholeiitic with flat REE patterns, but can also be slightly depleted in LREE or, more commonly, slightly enriched in LREE with negative Nb anomalies. The ultramafic flows are typically LREE depleted and usually have a negative Nb anomalies (Fig. 6.6). Lemkow et al. (2006) compiled all published and unpublished geochemical data for the western Uchi subprovince, which was utilized to create fields on a PM normalized diagram for specific rock types within the studied assemblages. The shaded fields on Figure 6.6 represent the compilation of ultramafic and mafic volcanic rocks for the Balmer assemblage of the RLGB. In order to create these fields, all samples which showed

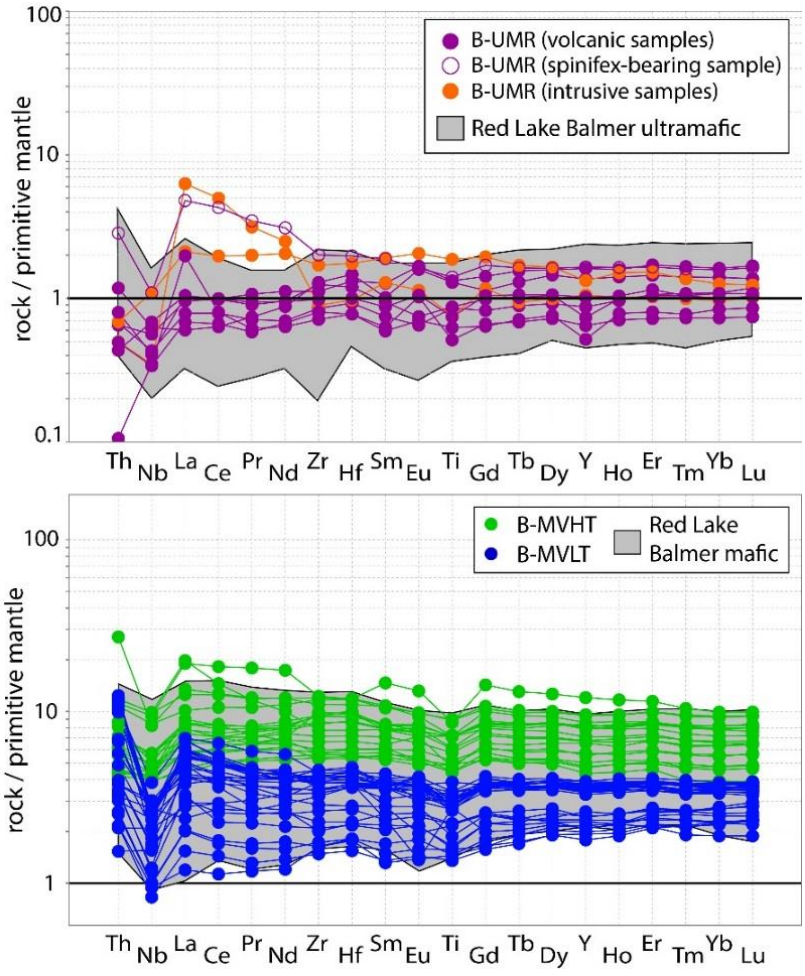

Figure 6.6 Primitive mantle-normalized trace element diagram showing Laird Lake data compared to ultramafic and mafic samples from throughout the Red Lake greenstone belt. Normalizing values from Sun and McDonough (1989) (Lemkow et al., 2006, Sanborn-Barrie et al., 2001, Hollings et al., 1999, Hollings, 1998). ***B-UMR****: Balmer ultramafic rocks,* ***B-MVHT****: Balmer mafic volcanic (high-Ti),* ***B-MVLT****: Balmer mafic volcanic (low-Ti)*

anomalous trends were excluded if they were described as altered or if no description was available. Most of the Laird Lake data fits well within the ultramafic and mafic volcanic fields for the RLGB with three ultramafic samples showing more elevated LREE, one mafic volcanic sample showing higher concentrations of Th and LREE and another with higher REE concentration (Fig. 6.6).

6.1.1.2 Crustal Contamination

Crustal contamination occurs when hot magma ascends through continental crust, melting the wall rocks of the magma conduit and assimilating them into the magma (Huppert et al., 1985). Typical Archean continental crust is enriched in LREE, has a high Th/Nb ratio and a La/Sm ratio of 7.3 (Rudnick and Fountain, 1995). Consequently, continental crustal contamination will result in the ascending magmas becoming enriched in Th, LREE and SiO_2 and displaying stronger negative Nb anomalies. The cause of the Nb anomaly has been explained in two ways: (1) residual Nb-Ta-bearing minerals such as titanite, rutile, ilmenite, sphene or even hornblende retaining Nb and Ta (Morris and Hart, 1983; Ryerson and Watson, 1987; Saunders et al., 1991) or (2) Nb has a MORB-like concentration and the negative anomaly is the result of enrichment of neighbouring elements on a primitive mantle normalizing diagram during ascent and assimilation of the melts (McCulloch and Gamble, 1991). Komatiitic magmas can assimilate up to three times as much crustal material as basaltic magmas due to the high heat of fusion of olivine and large crystallization interval of roughly 400°C (Sparks, 1986). Up to 50% contamination can occur during the ascent of komatiitic magmas, whereas only 10% contamination is likely to influence the magmas once they have erupted and are thermally eroding the underlying rocks (Huppert and Sparks, 1985; Sparks, 1986). Sparks (1986) has demonstrated that a komatiitic parent can produce basaltic and andesitic magmas through the assimilation and fractional crystallization (AFC) process and up to 50% crustal contamination. It is common for Archean ultramafic and mafic magmas to become contaminated during their ascent, however, it is also possible to have contamination free magma pathways (Pearce, 2008). Detecting crustal contamination in the Archean is easier if the magma

source was depleted as they show a stronger geochemical contrast with continental crust, and magma temperatures and crustal geotherms were likely higher than present-day conditions (Abbott et al., 1994; Pearce, 2008).

Signatures of crustal contamination can also be very similar to geochemical patterns produced by subduction-influenced magmatism. Both scenarios will generate Th and LREE enriched profiles with negative Nb anomalies and result in calc-alkalic affinities in extreme cases. Kerrich et al. (1999) demonstrated that the Th-Nb-LREE anomalies found within Archean Mg- to Fe-tholeiite basalts suites of greenstone belt sequences in the Uchi, Wabigoon, Wawa and Abitibi surprovinces are the product of a heterogeneous multi-component mantle plume system which had been influenced by a subduction-derived component in the mantle rather than crustal contamination. Evidence for a lack of crustal contamination influence comes from 1) stratigraphic consideration, 2) the absence of geochemical signatures of crustal contamination in komatiites or basalts, 3) isotopic constraints, and 4) the lack of xenocrystic zircons in syn-volcanic intrusions (Kerrich et al., 1999).

The Balmer assemblage on the Laird Lake property displays multiple geochemical features indicative of weak crustal contamination. A stronger negative Nb anomaly (smaller Nb/Nb* ratio) with increasing La/Sm_n for the ultramafic and mafic rocks of the Laird Lake property suggests that the melts interacted with continental crust during their ascent (Fig. 6.7A). Unlike the tholeiitic suites that Kerrich et al. (1999) studied, a clear trend exist between decreasing Nb/Nb*, increasing SiO_2 (Fig. 6.7B) and depletion in Th/Ce (Fig. 6.7C) and Ti/Ti* (Fig. 6.7D) in the Laird Lake samples. Crustal contamination will also lead to trends of decreasing Nb/Nb* and decreasing Ni (Fig. 6.7E) and Mg# (Fig. 6.7F), which is not observed in the Laird Lake data, likely due to the primary magmatic differences in the composition of the rocks.

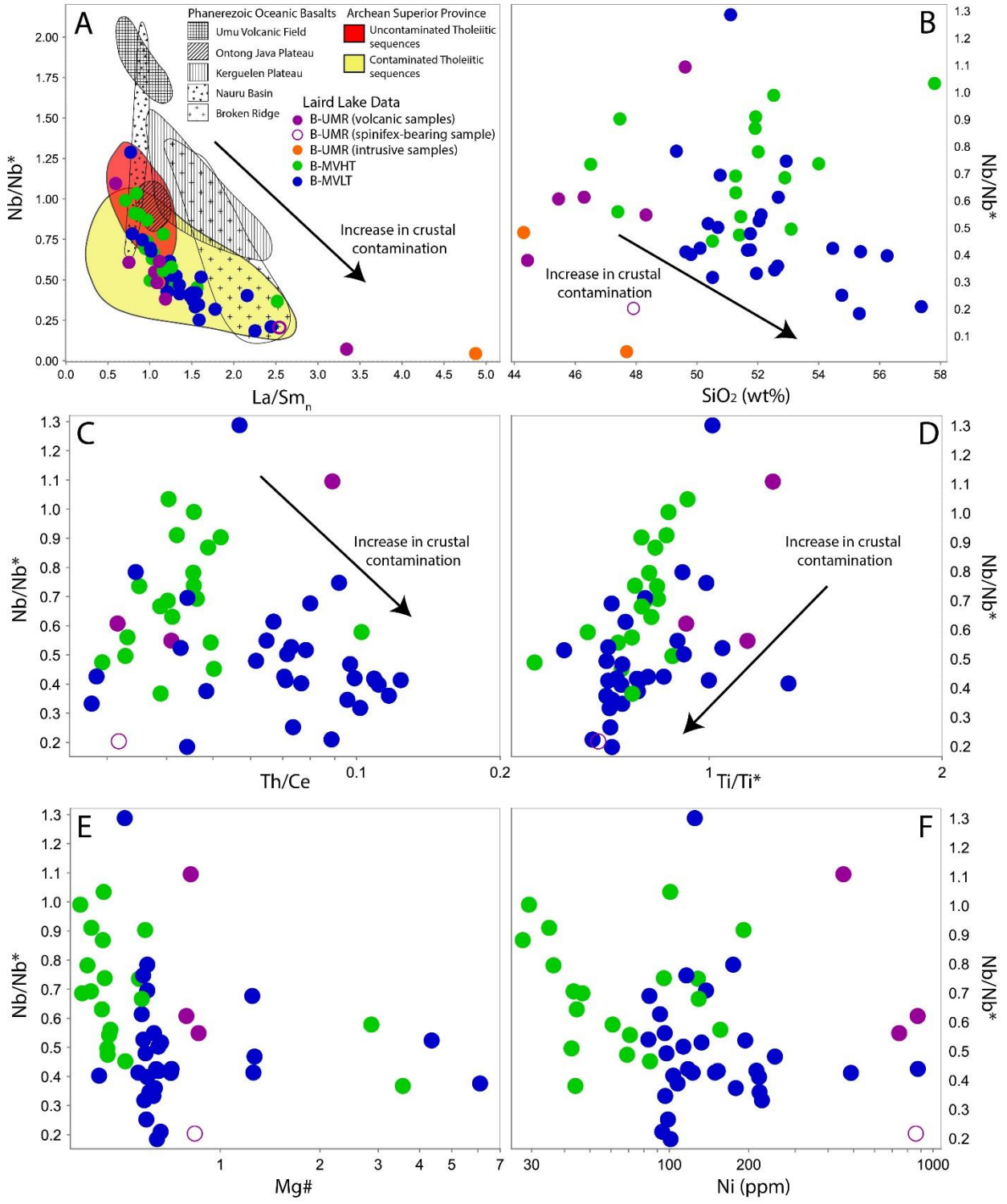

Figure 6.7 Nb/Nb versus A) La/Sm$_n$, diagram from Hollings et al. (1999) with the addition of Laird Lake data. Data for Umu and Nauru areas from Floyd (1989), Ontong Java plateau data from Mahoney et al. (1993); Hollings, 1998; Hollings et al., 1999, Broken Ridge data from Mahoney et al. (1995), Kerguelen data from Corfu and Andrews, 1987; Storey et al. (1992) and Iceland data from Hemond et al. (1993) and Superior province data from Hollings et al. (1999). B) SiO$_2$ (wt.%), C) Th/Ce, D) Ti/Ti*, E) Mg#, F) Ni (ppm). The trend line points in the general direction of increasing crustal contamination.* ***B-UMR****: Balmer ultramafic rocks,* ***B-MVHT****: Balmer mafic volcanic (high-Ti),* ***B-MVLT****: Balmer mafic volcanic (low-Ti).*

Figure 6.7A compares the Laird Lake samples to contaminated and uncontaminated komatiites and tholeiites of greenstone belts from the northern Superior Province and Phanerezoic plateaus. Laird Lake samples plot within both contaminated and uncontaminated fields, suggesting that some melts likely ascended through contamination free pathways. When compared to younger analogues, the Laird Lake data overlaps with the Broken Ridge plateau which is interpreted to have been erupted through fragments of continental crust (Storey et al., 1992). The Kerguelen plateau has also been interpreted to have erupted through continental lithosphere (Storey et al., 1992; Neal et al., 2002) and shares a similar trend with the Laird Lake samples. The Ontong Java plateau, Umu volcanic field and Naura basin show no geochemical evidence to support contamination by continental basement as suggested by low La/Sm_n (Floyd, 1989; Mahoney et al., 1993; Fig. 6.7A) and overlap with the least contaminated Laird Lake rocks.

Hollings et al. (1999) recognised that crustal contamination played a major role in the komatiites of the Red Lake, Rice Lake and North Caribou greenstone belts. Komatiites in these belts all displayed negative Nb anomalies that increased in magnitude with increasing SiO_2, La/Sm_n and Th/Ce, which was interpreted as crustal contamination by a felsic component (Hollings et al., 1999). Figure 6.6B shows that only a weak correlation between increasing SiO_2 and decreasing Nb/Nb* ratios, suggesting that the Laird Lake Balmer assemblage rocks were likely not contaminated by a felsic component, but rather a crust with a lower SiO_2 concentration such as intermediate crust.

6.1.1.3 Neodymium Isotopes

The Sm-Nd isotope system is often used to constrain the mantle source of a magmatic suite and helps identify the components which have contributed to variations in its original isotopic ratio (Rollinson, 1993). The Epsilon Nd notation (ε_{Nd}) can be used to estimate the degree of contamination of mantle melts by older continental crust. However, if the contaminant is less than 40-50 m.y. old, the

isotopic system will not have time to evolve and therefore crustal contamination may not affect the isotopic ratio of the mantle melts (DePaolo and Wasserburg, 1979; Dickin, 2005). Depleted mantle has a more positive ε_{Nd} than continental crust, since over time, melt extraction has progressively depleted the upper mantle (Jacobsen and Wasserburg, 1979). Using the mantle evolution curve of DePaolo (1981a), the ε_{Nd} value of depleted mantle (DM) at 2.988 Ga is +1.76. The ε_{Nd} values for the Balmer assemblage mafic volcanic rocks range from -0.38 to 1.39, but no distinctive trends between the high-Ti and low-Ti basalts were observed (Fig. 6.8). These values all plot below DM (Fig. 6.8), suggesting that these rocks are isotopically enriched. The low-Ti basalts plot as the most positive and negative ε_{Nd} values (Fig. 6.8) and show significant variation in Th, Nb and LREE, yet have they have very similar HREE concentrations (Fig. 6.9). The low-Ti basalt sample with strongly enriched Th and LREE, the strongest negative Nb anomaly and the most enriched ε_{Nd} value of -0.38 (sample 15BG235A01) is likely more crustally

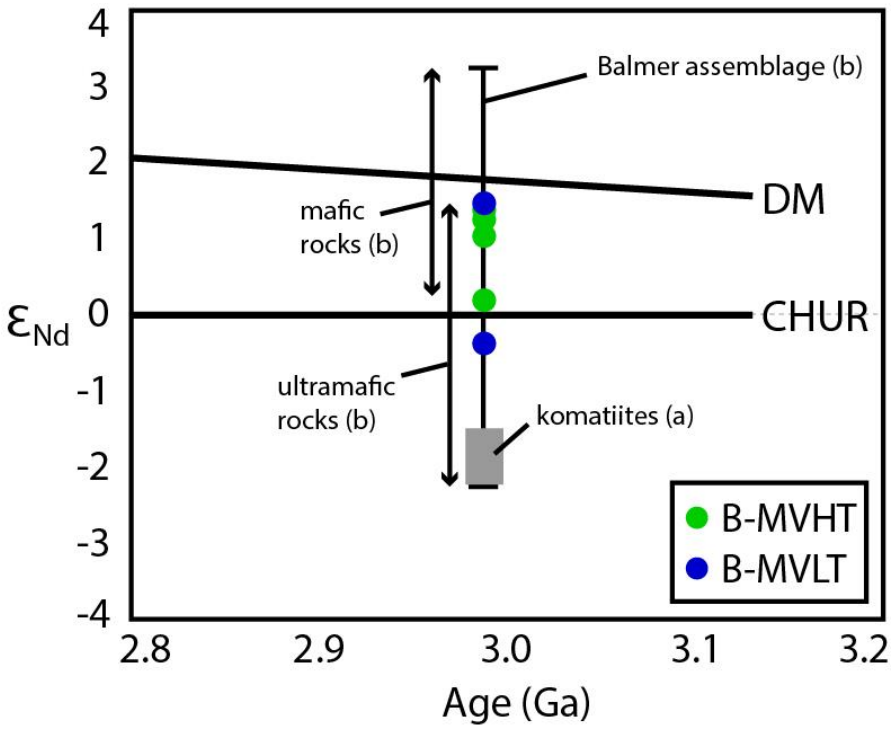

Figure 6.8 ε_{Nd} values as a function of crystallization ages showing Nd isotope data for the Balmer assemblage mafic volcanic rocks of the Laird Lake property. (a) Tomlinson et al., 1998, (b) Sanborn-Barrie et al., 2001. ***DM****: Depleted Mantle,* ***CHUR****: Chondritic Uniform Reservoir,* ***B-MVHT****: Balmer mafic volcanic (high-Ti),* ***B-MVLT****: Balmer mafic volcanic (low-Ti)*

contaminated compared to the sample showing lesser enriched LREE and Th, a smaller negative Nb anomaly and the most depleted ε_{Nd} value of 1.39 (sample 15BG387A01).

The systematic increase in La/Sm_n and decrease in Nb/Nb* values with decreasing ε_{Nd} values within all Balmer assemblage samples suggests crustal contamination played a role in the formation of these rocks (Figs. 6.10A, C). However, Figure 6.10B shows no correlation between SiO_2 and ε_{Nd} values, suggesting that the mafic melts did not assimilate felsic crust. A potential source of contamination for the Balmer assemblage mafic volcanic rocks could be the 3.0-2.7 Ga North Caribou Core to the north (Corfu and Stone, 1998; Percival et al., 2006). The range and degree of contamination in ε_{Nd} values for the Laird Lake data is small compared to younger analogues such as the Kerguelen plateau which have been interpreted as crustally contaminated with ε_{Nd} values ranging from 5.2 to -8.5 (Storey et al., 1992). This suggest that the contaminant for the Balmer assemblage mafic volcanic rocks was likely more homogeneous and did not have a significantly different ε_{Nd} value than that of ascending mafic volcanic rocks compared to the younger analogues.

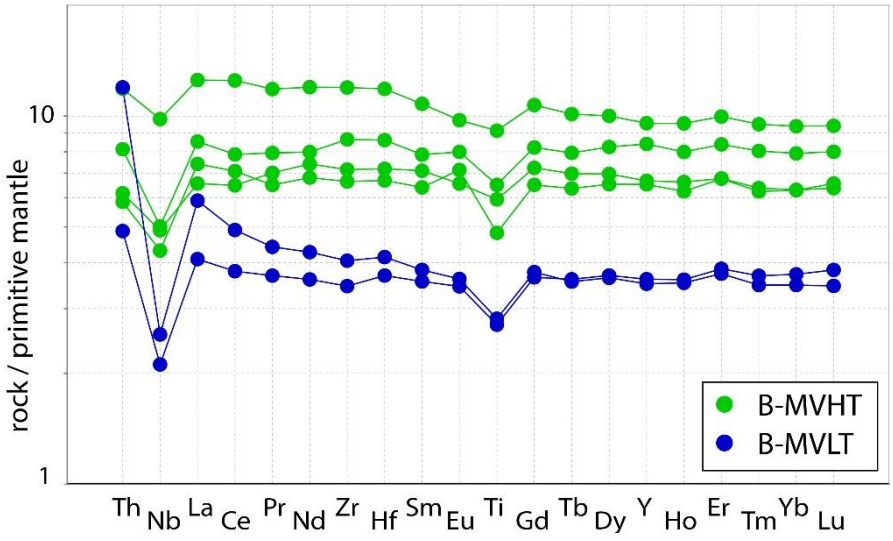

Figure 6.9 Primitive mantle-normalized trace element diagram of the Balmer assemblage mafic volcanic samples used for Nd isotope. Normalizing values from Sun and McDonough (1989). ***B-MVHT****: Balmer mafic volcanic (high-Ti),* ***B-MVLT****: Balmer mafic volcanic (low-Ti)*

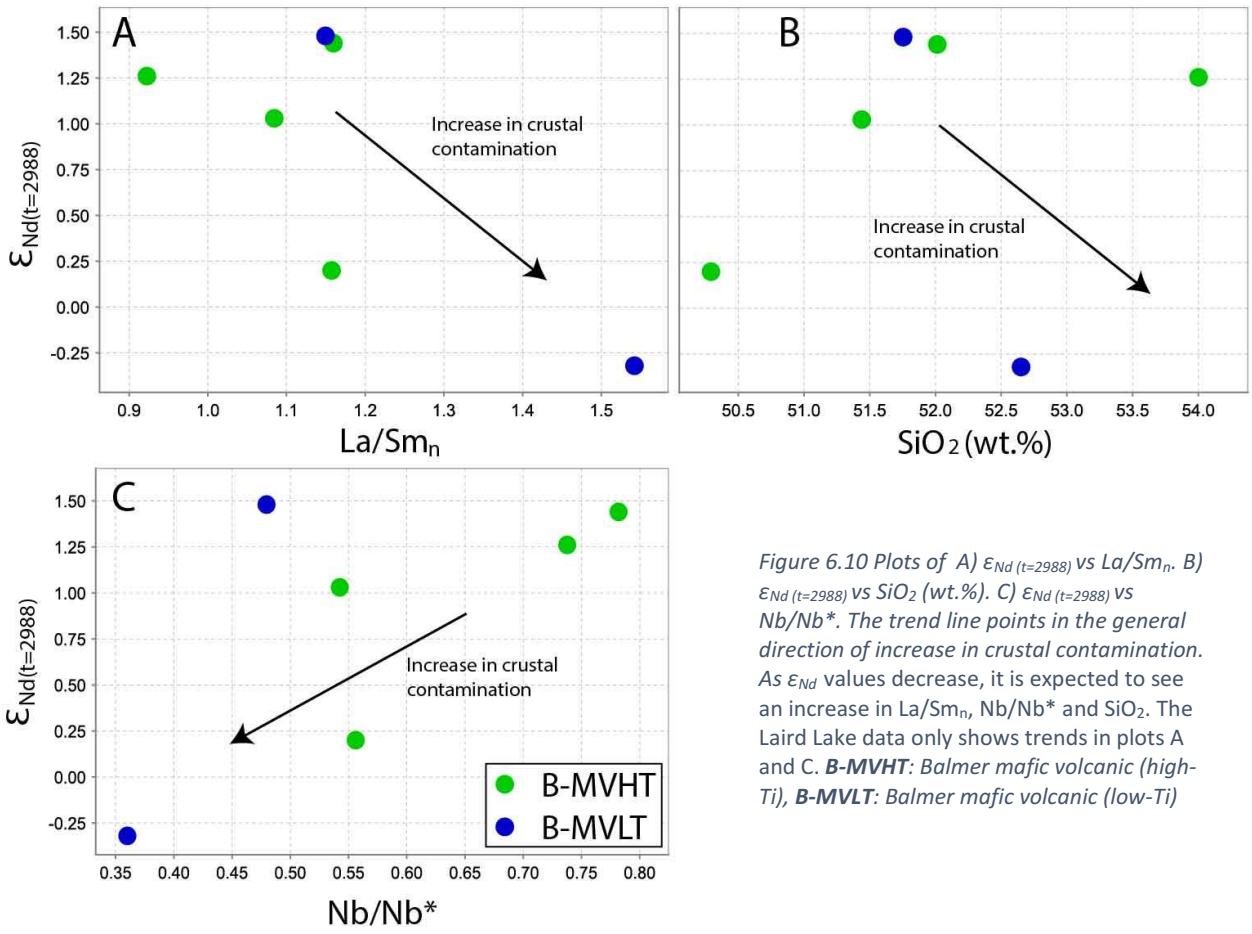

Figure 6.10 Plots of A) $\varepsilon_{Nd\ (t=2988)}$ vs La/Sm$_n$. B) $\varepsilon_{Nd\ (t=2988)}$ vs SiO$_2$ (wt.%). C) $\varepsilon_{Nd\ (t=2988)}$ vs Nb/Nb. The trend line points in the general direction of increase in crustal contamination. As ε_{Nd}* values decrease, it is expected to see an increase in La/Sm$_n$, Nb/Nb* and SiO$_2$. The Laird Lake data only shows trends in plots A and C. ***B-MVHT**: Balmer mafic volcanic (high-Ti), **B-MVLT**: Balmer mafic volcanic (low-Ti)*

Other Nd isotopic studies conducted on the Balmer assemblage in the Red Lake greenstone belt include those of Tomlinson et al. (1998) and R. Stevenson (pers. comm., 2000 from Sanborn-Barrie et al., 2001) who reported ε_{Nd} values from +3.3 to +0.3 for basalts from eastern Red Lake and ε_{Nd} values from -2.2 to +1.5 for ultramafic rocks also from eastern Red Lake (Fig. 6.8). Sanborn-Barrie et al. (2001) interpreted the more positive ε_{Nd} values as having been sourced from the depleted mantle and the ε_{Nd} values closer to 0 as having originated from a source with a history of LREE enrichment. Tomlinson et al. (1998) concluded that the Balmer assemblage was formed through the involvement of older crust and the presence of an older enriched source component.

6.1.1.4 Modeling of Crustal Contamination

In order to properly assess the contaminant and processes of crustal contamination, numerical modeling using the assimilation fractional crystallization model of DePaolo (1981b) and simple binary mixing was undertaken. Sample 15BG288A01 (UTM 418833E 5643612N) was chosen as the least contaminated komatiite since it has the least amount of Th and LREE enrichment and smallest negative Nb anomaly. Since the SiO_2 content in the ultramafic samples does not increase with decreasing Nb/Nb* values (Fig. 6.7B), and the ε_{Nd} values do not decrease with increasing SiO_2 for basalts (Fig. 6.10B), the contaminant is likely not felsic, but intermediate to mafic in composition, with enriched LREE, strong negative Nb anomalies and fractionated HREE. Modeling of crustal contamination for the ultramafic rocks was undertaken since the low-Ti basalts were previously shown to have been produced from the mixing of high-Ti basalts and komatiites, and it is likely that the geochemical variations in the low-Ti basalts originated from variable degrees of contamination in the komatiites. Sample 15BG288A01 was used as the komatiitic parent material and the calculated composition of an average Archean andesite (Condie, 1993) was used as the contaminant. When modeling the interaction between the komatiite and average Archean andesite, it was assumed that fractionation and assimilation occur at a ratio of 1:1 and fractionation of 80% olivine and 20% clinopyroxene with distribution coefficients from Rollinson (1993), Arndt et al. (2008) and Bouqain (2008; Table 6.2).

Table 6.2 Partition coefficients for komatiites. All bolded values are from Arndt et al. (2008), italicized values are from Bouquain (2008) and the unbolded/unitalicized values are from Rollinson (1993). Basalt values had to be utilized in the komatiite modeling to have a more complete graph. Empty fields are due to the lack of available data.

	Th	Nb	La	Ce	Nd	Zr	Hf	Sm	Eu	Tb	Y	Yb	Lu
Olivine	**0.0001**	**0.0001**	0.0067	0.006	0.0059	**0.015**	0.013	**0.01**	**0.03**		0.01	**0.05**	**0.11**
CPX	0.03	0.005	*0.025*	*0.04*	*0.1*	**0.123**	0.263	**0.01**	**0.3**	0.57	*0.25*	**0.1**	0.506

Modeling of a komatiitic melt undergoing contamination by an average Archean andesite produced trace element patterns comparable to the most contaminated Laird Lake komatiite sample (LL-15BG177A03; UTM 419957E 5643995N) after roughly 35-45% fractionation/assimilation and 10% contamination (Fig. 6.11A). Similar results were produced using simple binary mixing between the same komatiite parent and andesite contaminant with no fractionation and a mixing ratio of 9:1 (Fig. 6.11B). Calculated major and trace element concentrations are very comparable to sample LL-15BG177A03, with only small differences observed in the major element concentrations (<1.8 wt.% variation). As it only takes 10% contamination to produce the most contaminated komatiites on the Laird Lake property, it is possible that contamination occurred at depth, at surface by thermal erosion, or be a combination of the two (Huppert and Sparks, 1985). However, since the most contaminated komatiites on the Laird Lake property are in direct contact with ultramafic intrusions, and no intermediate rocks were mapped in the Balmer assemblage, it is likely that the contamination occurred at depth as the melts ascended through the basement crust.

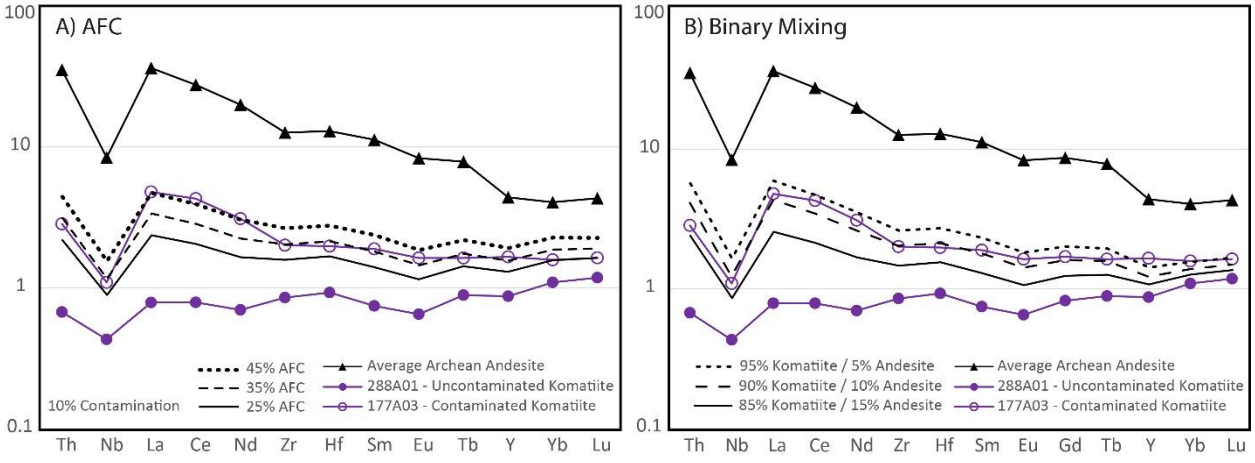

Figure 6.11 Primitive mantle normalized trace element diagrams showing the result of modeling AFC (A) and simple binary mixing (B). Trace element patterns are similar to the most contaminated Laird Lake komatiite at 35-45% AFC and 10% contamination of the least contaminated Laird Lake komatiite by an intermediate contaminant. Simple binary mixing with no fractionation shows comparable results as the AFC modeling, with 10% andesite and 90% komatiite. Normalizing values from Sun and McDonough (1989).

Given that it only takes 10% contamination of the komatiites to obtain the trace element patterns for the most contaminated komatiites, additional modeling was carried out to investigate the likelihood of a TTG or felsic contaminant. The calculated average Archean TTG from Condie (1993) and a felsic volcanic sample from the Balmer assemblage (RL-95-48; Hollings, 1998) show very similar trace element patterns to the average Archean andesite (Fig. 6.12A). All three rock types are calc-alkalic, showing enriched LREE, depletion in HREE and negative Nb anomalies. Modeling of both AFC and binary mixing has shown that using TTG and felsic volcanic rocks as the contaminant yield very similar results (Fig. 6.12B). With only 10% contamination, the major element concentrations of the contaminant do not severely affect the overall major element chemistry of the rock. Calculations evaluating the differences between the simple binary mixing results and sample 15BG177A03 (contaminated komatiite) show that an intermediate contaminant (average Archean andesite) only changes the SiO_2 composition of sample 15BG177A03 by 1.4 wt.%, whereas the two other contaminants have a difference of over 2.5 wt.% SiO_2 (Fig. 6.12B). Other major oxides such as TiO_2, FeO, MgO and CaO also show smaller differences with the andesitic contaminant. It is therefore more likely that an intermediate contaminant was the cause of the LREE and Th enrichment, and negative Nb anomaly within the contaminated komatiites at the Laird Lake property.

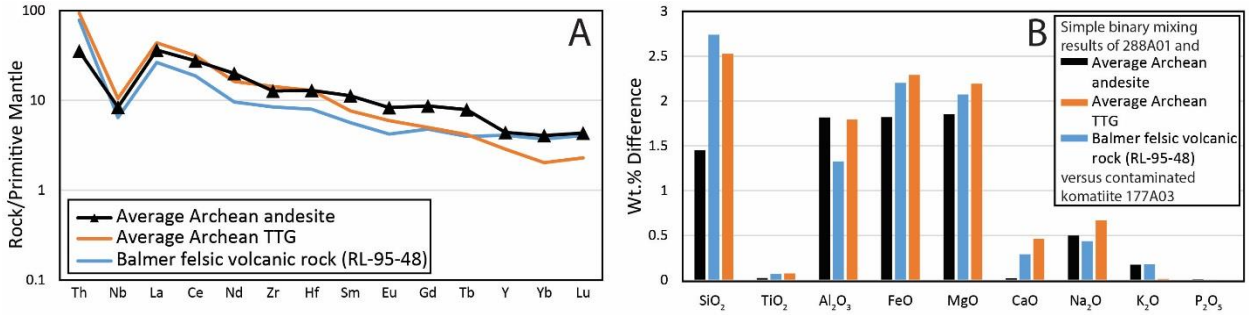

Figure 6.12 A) Primitive mantle normalized trace element diagrams showing the similarities between average Archean andesite (Condie, 1993), average Archean TTG (Condie, 1993) and Balmer felsic volcanic rock (RL-95-48; Hollings, 1998). Normalizing values from Sun and McDonough (1989). B) Column chart showing the wt.% differences between the simple binary mixing results and sample 15BG177A03 (contaminated komatiite).

6.1.2 Confederation Assemblage

6.1.2.1 Whole Rock Geochemistry

The Confederation assemblage is composed of three distinct geochemical units: calc-alkalic mafic volcanic rocks, calc-alkalic intermediate to felsic volcanic rocks and transitional (tholeiitic to calc-alkalic) intermediate to felsic volcanic rocks.

The mafic volcanic rocks, regardless of their macroscopic textures (feldspar phenocrysts, amphibole poikiloblasts, or aphyric), show two trends on PM normalized spider diagrams and Ti/Zr vs Y diagrams (Fig. 6.13). Both trends have similar LREE ratios, but have quite different HREE ratios. When plotting the two groups on the Laird Lake property map, they loosely correlate well with specific volcanic layers within the stratigraphy (Fig. 6.14) suggesting that distinct sources of mafic volcanism were erupting independently and repeatedly. No major differences are found within the Cr, Co or Ni contents, however, the rocks with less fractionated HREE (Gd/Yb_n=1-.21-1.55; Fig. 6.13A) tend to have slightly higher concentrations of platinum group elements such as Ir, Pd, Pt and Rh, suggesting they originated from a more primitive source (Fig. 6.15).

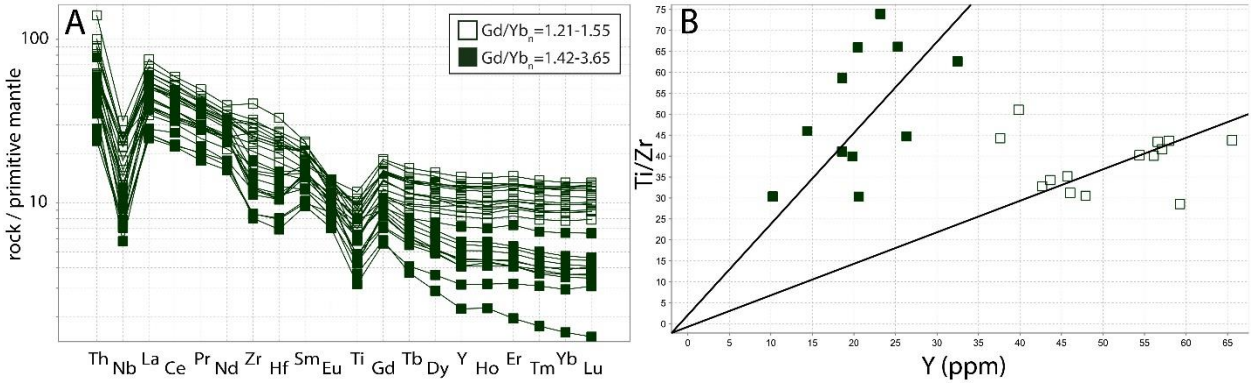

Figure 6.13 Trace element subdivision of Confederation assemblage mafic volcanic rocks. A) Primitive mantle normalized trace element diagrams. Normalizing values from Sun and McDonough (1989). B) Ti/Zr vs Y diagram showing two distinct groups.

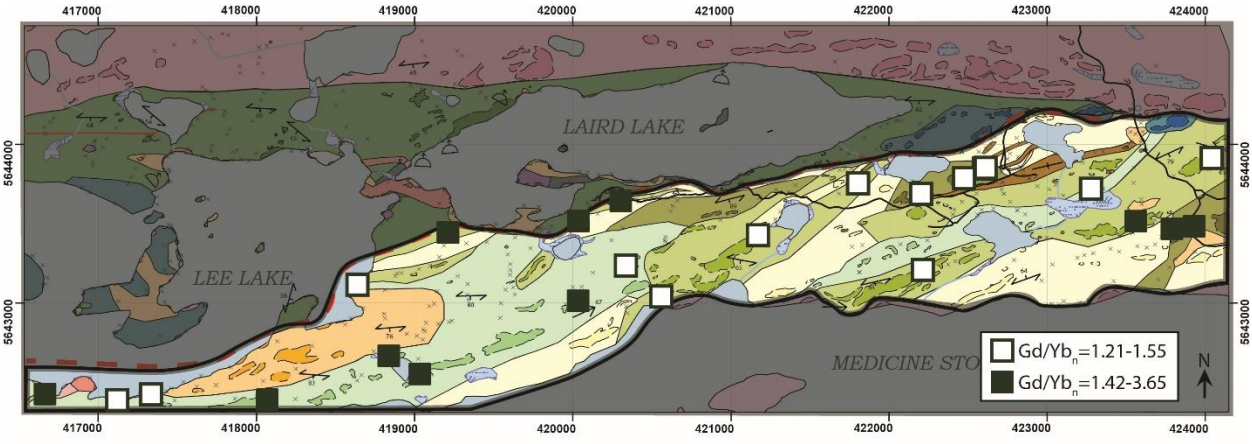

Figure 6.14 Distribution of the Confederation assemblage mafic volcanic rocks according to their HREE groupings.

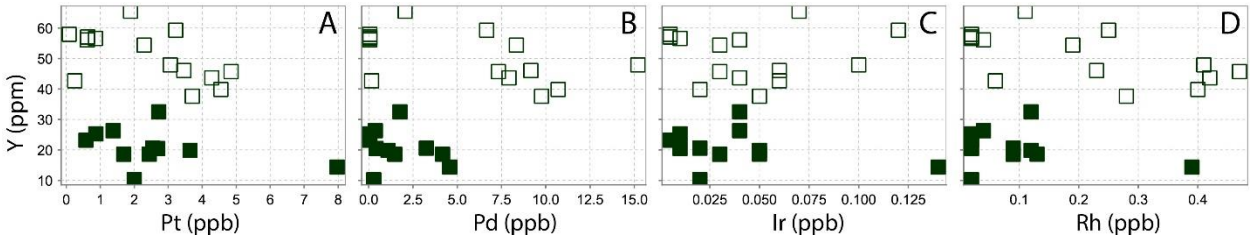

Figure 6.15 Yttrium versus A) Pt, B) Pd, C) Ir, D) Rh. Geochemical legend as for Figs. 6.13 and 6.14.

The intermediate to felsic volcanic rocks on the Laird Lake property show two contrasting groupings: 1) Intermediate to felsic volcanic rocks with fractionated HREE and 2) Intermediate to felsic volcanic rocks with flat HREE (Fig. 5.15). The first group is mainly composed of fine-grained volcanic volcaniclastic units, whereas the second group includes the majority of the quartz-feldspar porphyritic crystal tuffs. These can be further subdivided using the classification scheme of Lesher et al. (1986). FI rocks are dacite to rhyodacite with strongly fractionated REE patterns (La/Yb_n=6-34) and high Zr/Y ratios of 9-31 and variable Eu/Eu* ratios ranging from 0.87-2. FII are classified as rhyodacites to rhyolites with weakly fractionated REE patterns (La/Yb_n=2-6) and Zr/Y ratios of 6-11 with Eu/Eu* ratios from 0.35-1.4. FIII are rhyolites and high Si rhyolites with flat to weakly fractionated REE patterns (La/Yb_n=1.4). The

FIIIA variety has Zr/Y ratios of 4-7 and Eu/Eu* ranging from 0.37-0.94 whereas the FIIIb variety has Zr/Y ratios of 2-6 and Eu/Eu* ranging from 0.20-0.61.

The Laird Lake volcanic rocks with strongly fractionated HREE have Gd/Yb_n ratios between 1.47-5.52 and plot mostly within the FI field and on the margin of the FII field (Fig. 6.16). These rocks have ratios that overlap with most FI criteria but lay outside of the FII ranges (with the exception of Eu/Eu*) despite the samples plotting in the FII field (Fig. 6.16; La/Yb_n=10.48-57.05, Zr/Y=8.61-20.93 and Eu/Eu*=0.78-1.06). The samples with flat HREE have Gd/Yb_n ratios between 0.99-1.29 and plot completely within the FIIIb field (Fig. 6.16; La/Yb_n=2.18-4.51, Zr/Y=2.26-3.85 and Eu/Eu*=0.28-0.47).

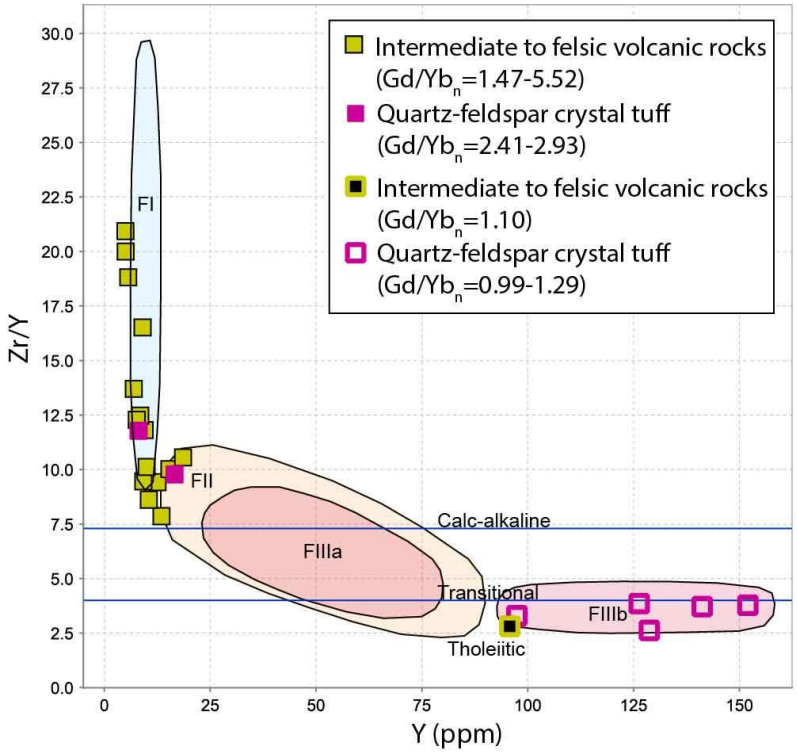

Figure 6.16 Rhyolite classification diagram of Lesher et al. (1986) showing two groupings of volcanic rocks; FI/FII and FIIIb.

The spatial distribution of the FI/FII and FIIIb volcanic rocks shows that the FI/FII units are found throughout the Confederation assemblage at the Laird Lake property whereas the FIIIb units are more commonly found near the contact between the two assemblages (Fig. 6.17). The FIIIb units follow specific stratigraphic volcanic layers often associated with FI/FII units.

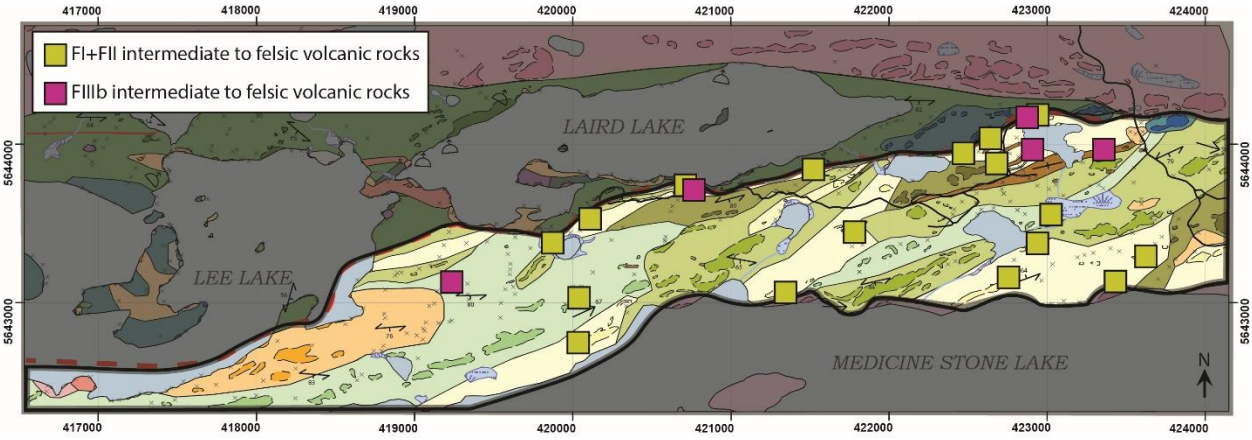

Figure 6.17 Distribution of the Confederation assemblage FI/FII and FIIIb intermediate to felsic volcanic rocks.

The classification scheme of Lesher et al. (1986) utilizes the fractionation of the LREE and HREE during magmatic processes based on the La/Yb_n ratios, the abundance of Yb and variations in Eu. FI to FIIIb units show a continuum of compositions and therefore overlap between the chemistry and tectonic setting is expected (Hart et al., 2004). FI units are calc-alkalic to alkalic and typically originate from low-degrees of partial melting of a basic source at high pressure and depth of >30 km within the garnet field, with minimal fractionation (Lesher et al., 1986; Hart et al., 2004). FII are calc-alkalic and result from the fractional crystallization of intermediate magma at 10-15 km depth (Campbell et al., 1981; Campbell et al., 1982; Lesher et al., 1986) or high-degree partial melting of a crustal source (Condie, 1976). FIII are tholeiitic magmas which originate from low-pressure partial melting from a tholeiitic basic source with no residual amphibole (Hart, 1984) or garnet (Campbell et al., 1981; Campbell et al., 1982; Lesher et al., 1986; Barrie et al., 1993) in a subvolcanic magma chamber at less than 10 km depth (Hart et al., 2004). They have also been interpreted as the result of low-pressure plagioclase-dominated fractional crystallization of intermediate magma (Lesher et al., 1986) or partial melting of different crustal material producing a wide range of felsic magma compositions (Lentz, 1998).

Previous regional studies conducted by Sanborn-Barrie et al. (2000; 2001) suggest that the Confederation assemblage in the RLGB can be subdivided into three different sequences: the calc-alkalic

McNeely sequence (2745-2742 Ma), the tholeiitic Heyson sequence (<2744-2739 Ma) and the calc-alkalic Graves sequence (2733 Ma). The Laird Lake data is most similar to the Heyson sequence with the majority of samples overlapping the Red Lake data (Fig. 6.18). The Laird Lake Confederation mafic volcanic rocks are calc-alkalic in nature (Fig. 5.11), yet have been deemed tholeiitic by Sanborn-Barrie et al. (2001), likely due to the fact that about half of the samples plot within the tholeiitic field on an AFM diagram (Fig. 5.4A). The majority of the samples showing less fractionated HREE (Gd/Yb_n=1.21-1.55) plot in the tholeiitic field, whereas the samples with more fractionated HREE (Gd/Yb_n=1.42-3.65) plot in both the calc-alkalic and tholeiitic fields of the AFM diagram (Fig. 5.4A). Ross and Bédard (2009) discourage the use of an AFM diagram for ancient subalkaline volcanic rocks since the elements used in the diagram

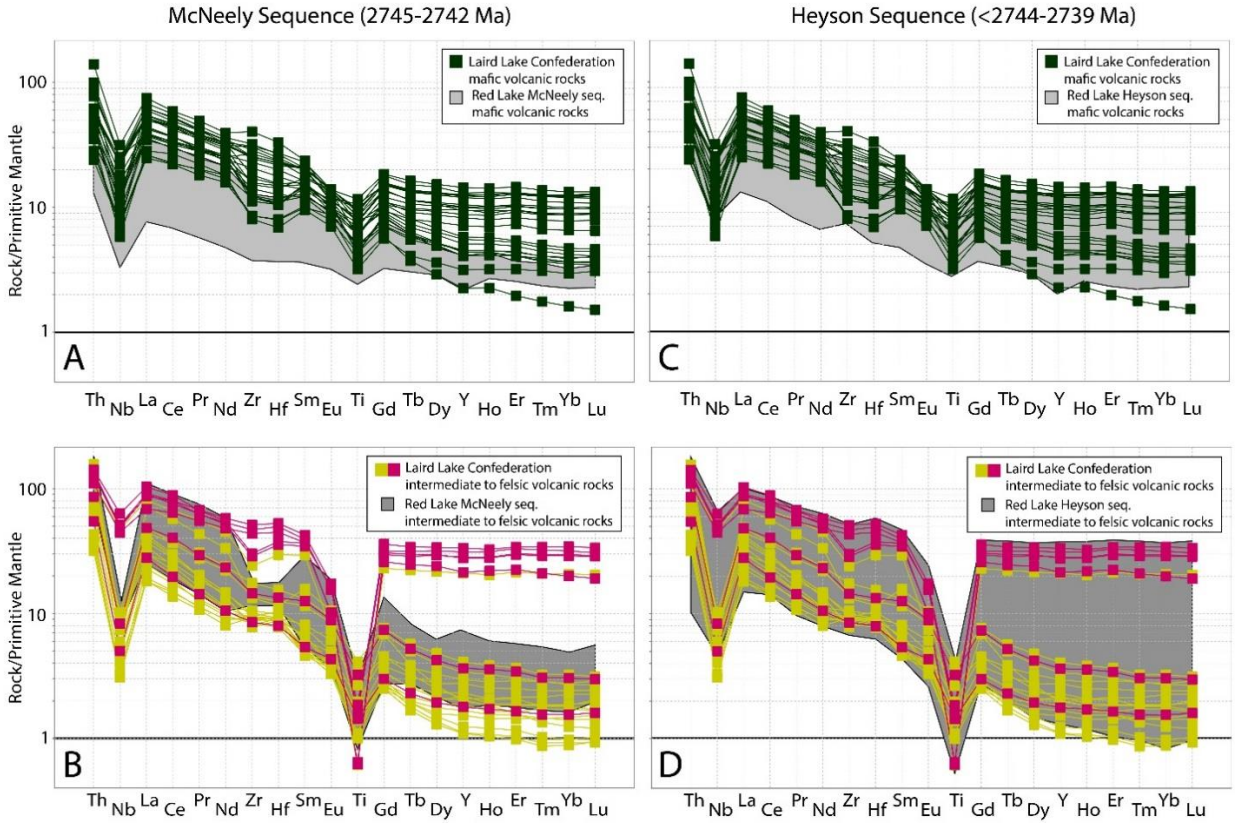

Figure 6.18 Primitive mantle-normalized trace element diagram showing Laird Lake data compared to intermediate and felsic volcanic samples collected throughout the Red Lake greenstone belt. Normalizing values from Sun and McDonough (1989) (Lemkow et al., 2006; Sanborn-Barrie et al., 2001; Hollings et al., 1999; Hollings, 1998).

are often mobile during alteration and metamorphism, and therefore it is likely that a lot of AFM classified rocks are wrongly assigned. When plotting the RLGB McNeely and Heyson sequences mafic volcanic rocks on a Th/Yb versus Zr/Y diagram (Fig. 6.19), the majority of the samples plot within the calc-alkalic field and one of each sequence plot in the transitional field, suggesting that the Heyson sequence mafic volcanic rocks are in fact calc-alkalic in nature.

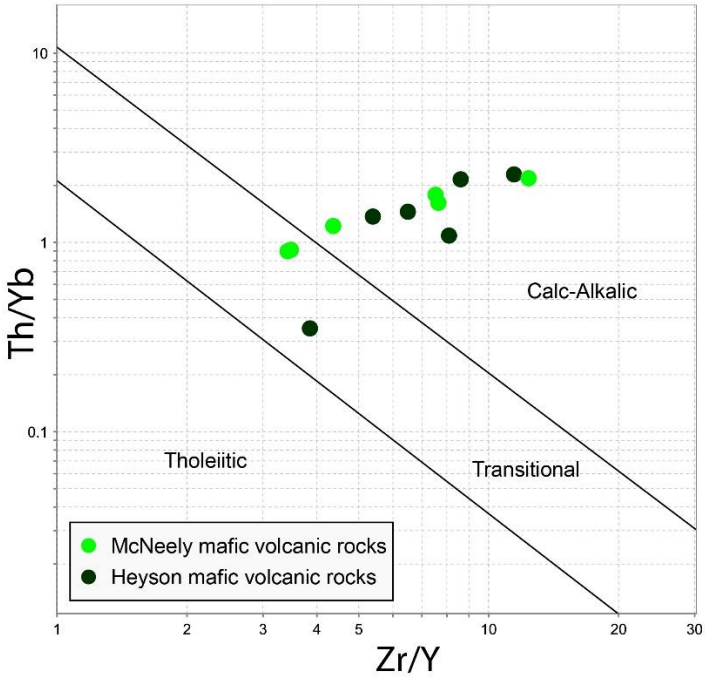

Figure 6.19 Th/Yb versus Zr/Y trace element diagram showing the majority of RLGB Heyson and McNeely sequences mafic volcanic rocks plotting in the calc-alkalic field, and one of each sequence plotting in the transitional field. Data from Lemkow et al. (2006). Fields on diagram from Ross and Bédard (2009).

6.1.2.2 Geochronology

Three samples were collected for zircon U-Pb geochronology (Fig. 5.20). Sample LL-16BG068A01 (fine-grained quartz-feldspar porphyritic crystal tuff) yielded an age of 2740.6 ± 19 Ma which lies within error of the McNeely (2742-2745 Ma), Heyson (<2744-2739 Ma) and Graves (2734-2731 Ma) sequences of the Confederation assemblage (Corfu and Wallace, 1986; Corfu et al., 1998; Sanborn-Barrie et al., 2001). Out of the five zircons analysed, three zircons yielded ages of 2840.6 ± 2.8 Ma, 2912.6 ± 3.2 Ma and 2974.7 ± 3.4 Ma and have been interpreted as xenocrystic zircons. Two of the ages (2840 and 2912 Ma) do not correlate with any crystallization ages reported for assemblages within the Red Lake

greenstone belt whereas the third age (2974 Ma) overlaps with the Balmer assemblage (2.99-2.96 Ga). It is possible that the geochronology database does not represent the entire age span of the assemblages and that the xenocrystic zircons have been retrieved from units which have yet to be dated. Elsewhere in the Uchi subprovince, the Kaminiskag assemblage (former in the Women assemblage) within the Pickle Lake and Meen-Dempster greenstone belts (Hollings et al., 2000; Young et al., 2006), is dated at 2836 ± 3 Ma and 2842^{+5}_{-2} Ma, respectively (Corfu and Stott, 1993b), which overlaps with the 2840.6 ± 2.8 Ma date from one of the Laird Lake xenocrystic zircons. No ages reported within the Uchi subprovince overlap with the 2912.6 ± 3.2 Ma xenocrystic age, however, foliated to gneissic tonalitic rocks from the Winnipeg River Terrane (WRT) have reported dates ranging from 2.83-2.9 and 3.0-3.2 Ga (Krogh et al., 1976; Beakhouse, 1983; Corfu, 1988; Davis et al., 1988). Additionally, the WRT is also composed of >2.83 Ga supracrustal rocks which appear as enclaves within the intrusive bodies (Beakhouse, 1991).

Previous work has suggested that the Confederation assemblage was formed as part of a continental arc built onto previously existing RLGB assemblages (Sanborn-Barrie et al., 2001; Percival et al., 2006; Young et al., 2006). However, the Laird Lake data suggest that the Confederation assemblage could have been built on an entirely separate Mesoarchean crust or a sliver of the continental margin of the North Caribou paleocontinent, in which the ascending melts would assimilate the older crust in order to collect the xenocrystic zircons dated between 2840-2974 Ma.

Sample LL-16BG427A01 (deformed diorite; Fig. 5.20) yielded an age of 2737.68 ± 0.79 Ma and represents a syn-volcanic intrusion as the youngest age recorded in the Heyson sequence is 2739.0 ± 3 Ma (Corfu and Wallace, 1986). This sample also overlaps in age with the 2734 ± 2 Ma Douglas Lake intrusion (biotite tonalite) to the west (Fig. 2.3; Corfu and Stone, 1998) and a 2736^{+3}_{-2} Ma felsic dyke cutting upper Trout Bay basalt (Skulski (unpublished) referenced in Sanborn-Barrie et al., 2004). Sample

LL-16BG314A01 (undeformed quartz-diorite; Fig. 5.20) yielded an age of 2695.0 ± 3.9 Ma and represents a post-D_2 intrusion. This age is very similar to the post-ore dikes dated at the Madsen Mine (2698 ± 1 Ma) and Starrat-Olsen Mine (2696 ± 2 Ma; Dubé et al., 2004).

6.1.2.3 Neodymium Isotopes

The ε_{Nd} value of the Laird Lake Confederation assemblage data ranges between 0.39-1.62 with Nd model ages spanning 2949-2988 Ma. Using the mantle evolution curve of DePaolo (1981a), the ε_{Nd} value of depleted mantle (DM) at 2.741 Ga is +2.15, suggesting that the Laird Lake rocks are isotopically enriched. Two trends arise when plotting the data on a ε_{Nd} vs time graph (Fig. 6.20); a group of 2 samples cluster at roughly +0.4 ε_{Nd} whereas a second group of 4 samples cluster at +1.6 ε_{Nd}. The two groupings of data likely represent volcanic rocks which have been derived from two difference sources,

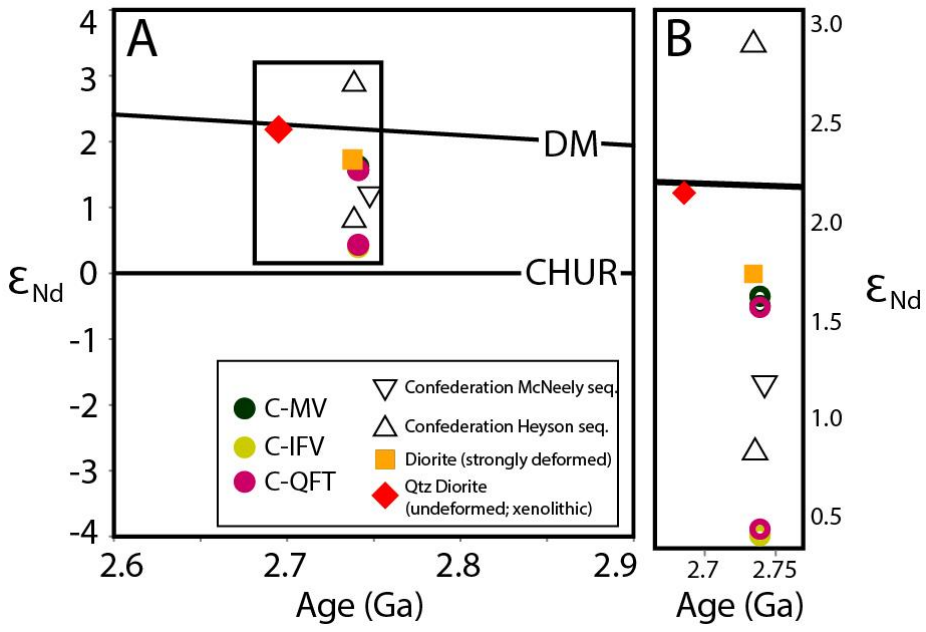

*Figure 6.20 A) ε_{Nd} values as a function of crystallization ages showing Nd isotope data for the Confederation assemblage mafic and intermediate to felsic volcanic rocks and quartz-feldspar porphyritic crystal tuffs of the Laird Lake property. B) Enlarged section of diagram A to better show overlapping data points. Additional ε_{Nd} data for post-volcanic intrusions from the Laird Lake property are included; pre-D_2 diorite and post-D_2 quartz diorite. Red Lake greenstone belt data (McNeely and Heyson sequence) from Sanborn-Barrie et al. (2001) and Henry et al. (2000). **DM**: Depleted Mantle, **CHUR**: Chondritic Uniform Reservoir, **C-MV**: Confederation mafic volcanic, **C-IFV**: Confederation intermediate to felsic volcanic, **C-QFT**: Confederation quartz-feldspar porphyritic crystal tuff*

which is also suggested by the geochemical groupings. The group of data that lies closer to CHUR, consists of the FI felsic to intermediate volcanic rocks, whereas the data plotting at roughly +1.6 ε_{Nd} consists of two mafic volcanic rock samples and one FIIIb quartz-feldspar porphyritic tuff. Sanborn-Barrie et al. (2001) and Henry et al. (2000) presented ε_{Nd} values at +2.9 and +0.77 for the Heyson sequence, suggesting the level crustal input varies within the sequence.

It is generally accepted that the Confederation assemblage was formed in an arc environment (Stott and Corfu, 1991; Hollings, 1998; Sanborn-Barrie et al., 2004; Percival et al., 2006 and references therein). In such a setting, various melts with different geochemical and isotopic composition can be produced in different arc-related environments (Winter, 2001). The two populations of Laird Lake data were likely produced in two different arc settings; 1) an environment which would source more depleted magmas such as a back arc, and 2) an environment that would have a higher subduction zone input and involve a stronger level of crustal contamination such as the main arc.

Across-arc variations exists within Quaternary basaltic volcanic rocks in the Northeastern Japan Arc system, where samples from the volcanic front have ε_{Nd} values from +3.5 to +5.3 and back-arc samples ranged from +6.7 to +8.2 (Shibata and Nakamura, 1997). They attributed the across-arc isotopic variations to the addition of an isotopically homogeneous subduction component (MORB-type) to the mantle wedge and that the amount of this component decrease towards the back-arc side. The volcanic front therefore receives a much stronger subduction component which will decreases as depth to the descending slab increases. They did not attribute the variations to crustal contamination since there is no systematic correlation between crustal thickness and isotopic composition of Quaternary volcanic rocks in northeastern Japan (Notsu, 1983).

The Laird Lake area could represent a similar environment as the data displays similar trends to the Quaternary volcanic rocks in northeastern Japan, showing more enriched/evolved signatures (+0.4

ε_{Nd}; La/Sm_n= 5.19-6.05) typical of volcanic front rocks and more depleted/less evolved signatures (+1.6 ε_{Nd}; La/Sm_n= 2.49-2.82) typical of back arc rocks (Fig. 6.21A). However, since the Confederation assemblage was possibly built on a fragment of continental crust dated between 2840-2974 Ma, crustal contamination would further enrich the ε_{Nd} values of the volcanic front magmas compared to the back-arc magmas. Figure 6.22 shows a clear separation between the depleted and enriched rocks, with a systematic increase in La/Sm_n and decrease in Nb/Nb* values with decreasing ε_{Nd} values which can be attributed to crustal contamination.

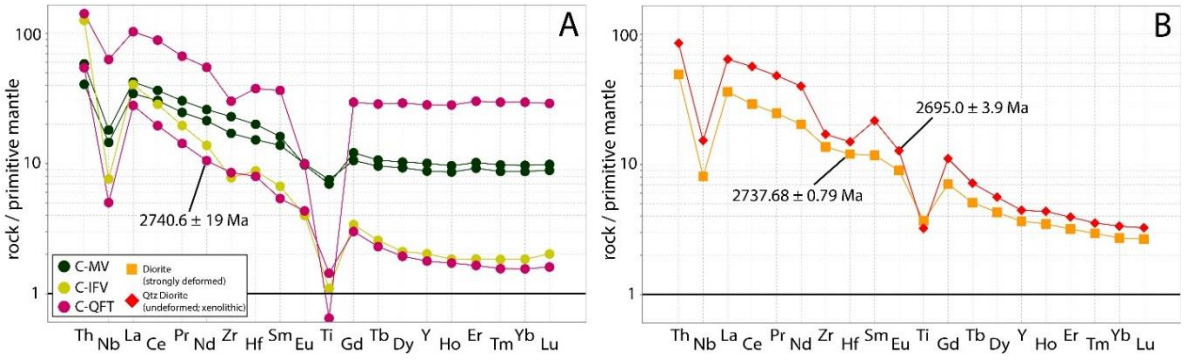

Figure 6.21 Primitive mantle-normalized trace element diagram of the Confederation assemblage volcanic and intrusive samples, and post-D_2 intrusion used for Nd isotope. A) Volcanic rocks, B) Intrusive rocks. Normalizing values from Sun and McDonough (1989). ***C-MV****: Confederation mafic volcanic,* ***C-IFV****: Confederation intermediate to felsic volcanic,* ***C-QFT****: Confederation quartz-feldspar porphyritic crystal tuff.*

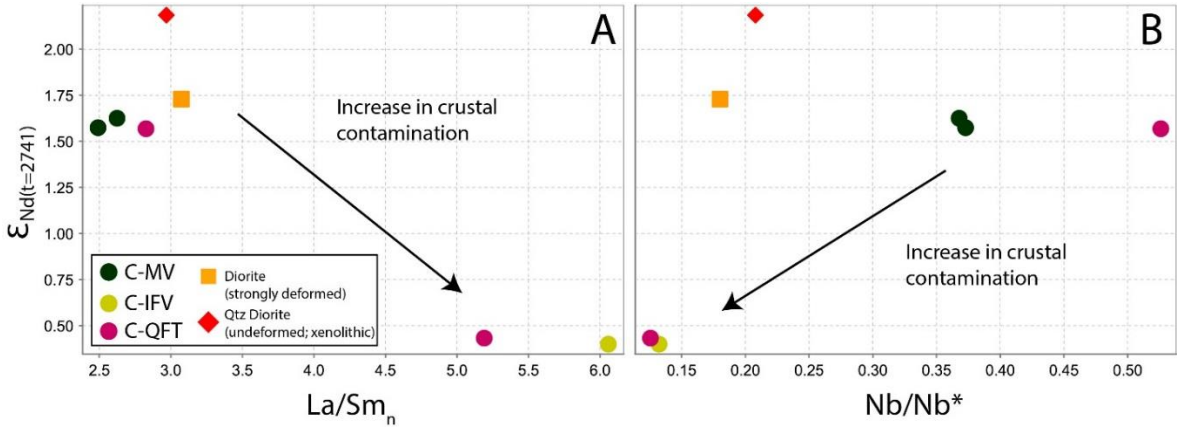

Figure 6.22 Plots of A) $\varepsilon_{Nd\ (t=2741)}$ vs La/Sm_n. B) $\varepsilon_{Nd\ (t=2741)}$ vs Nb/Nb. The trend line points in the general direction of increase in crustal contamination. As ε_{Nd}* values decrease, it is expected to see an increase in La/Sm_n and Nb/Nb*. Syn- and post-volcanic intrusions likely show a stronger negative Nb anomaly since they have a higher potential to fractionate and assimilate. ***C-MV****: Confederation mafic volcanic,* ***C-IFV****: Confederation intermediate to felsic volcanic,* ***C-QFT****: Confederation quartz-feldspar porphyritic crystal tuff.*

Two additional samples acquired from a deformed diorite (2737.68 ± 0.79 Ma) located within the Confederation assemblage (Fig. 4.1), and an undeformed quartz-diorite (2695.0 ± 3.9 Ma) located within the Balmer assemblage (Fig. 4.1) were also analysed for Nd isotopes and dated by U-Pb geochronology. The deformed diorite has an ε_{Nd} value of +1.72 (Fig. 6.20) and likely represents a syn-volcanic intrusion sourced from the same environment as the depleted volcanic samples (+1.6 ε_{Nd}; La/Sm_n= 2.49-2.82) since it has a very similar ε_{Nd} value to the mafic and FIIIb volcanic rocks (~1.6) and La/Sm_n ratio of 3.07 (Fig. 6.21B). The sample plots with the least contaminated volcanic samples (Fig. 6.21A) but has a much stronger negative Nb anomaly (Fig. 6.22B), more comparable to the most contaminated volcanic samples. The quartz-diorite has an ε_{Nd} value of +2.18 (Fig. 6.20), which lies just slightly below the DM curve of DePaolo (1981a) and a Nd model age of 2829 Ma. This post-volcanic and post-D_2 intrusion was likely sourced from the re-melting of older crust which shows a depleted signature, such as the 2.853 Ga Trout Bay assemblage with ε_{Nd} value ranging between +2.2 and +1.8 (Sanborn-Barrie et al., 2001).

6.2 Tectonic Setting

The volcanic rocks of the Laird Lake area can be subdivided into two tectonic assemblages; the tholeiitic Balmer assemblage (2.99-2.96 Ga) and the calc-alkalic Confederation assemblage (2.75-2.73 Ga). These two assemblages represent very contrasting tectonic environments, as suggested by field observations, whole rock geochemistry, Nd isotopes, and geochronology.

6.2.1 Balmer Assemblage

The Balmer assemblage at the Laird Lake property is comprised of mafic volcanic rocks intercalated with minor ultramafic volcanic rocks and BIFs. The tectonic environment in which the Balmer assemblage has formed requires large volumes of mafic magmas, with sporadic ultramafic volcanism within a subaqueous setting in order to deposit BIFs (deep ocean) and pillowed basalts.

Tomlinson et al. (1998) has summarized four different models for the evolution of the Balmer assemblage. These include: 1) plume derived oceanic plateau, later approaching a continental margin, 2) plume eruption through continental lithosphere, with prior rifting and stretching of crust, 3) back-arc basin behind a continental margin arc and 4) product of ridge subduction. Hollings (1998) and Hollings et al. (1999) support a model which includes mantle plume magmatism adjacent to a subduction zone in order to account for the intercalation of komatiites and arc-type felsic volcanic rocks. Additionally, two theories for the origin of ultramafic rocks exists: dry melting (mantle plume origin; Arndt et al., 1998; and references therein) and wet melting (subduction-related origin; Viljoen and Viljoen, 1969; Brooks and Hart, 1974; Grove et al., 1994; Parman et al., 1997; and references therein). The mantle plume model describes AUK melts as having originated at depths of 150-200 km (Herzberg, 1995) or 370 km (Nisbet et al., 1993) from depleted mantle (Campbell et al., 1989; Lesher and Arndt, 1995) whereas the wet melting model argues that komatiites could be produced by hydrous melting at shallow depths within subduction zones (Parman et al., 1997; Grove and Parman, 2004). The mantle plume model is favoured by the author as Campbell et al. (1989) showed that intercalated komatiite and basalts with contrasting REE patterns form as the result of plume-related magmatism. Their model suggests that basalts originate from the cooler plume head and entrains mantle material during the plume ascent whereas komatiites originate from the hotter plume tail.

The Laird Lake samples show evidence of weak crustal contamination as displayed in the ε_{Nd} values, variable enrichment in LREE, negative Nb anomalies and in the AFC and binary mixing modeling. Pearce (2008) proposed a plot of Th/Yb vs Nb/Yb to evaluate crustal input (Th-Nb proxy) and melting depth (Ti-Yb proxy) for oceanic basalts in order to study the tectonic environment in which the basalts were formed. Typically, oceanic basalts plot within the OIB to MORB field, yet, in the Archean, the hotter magmas, higher crustal geotherms and higher Th contents in the contaminant result in a wide spread of crustal signatures (enrichment of Th relative to Nb) which is easily detectable using the Th-Nb

proxy (Pearce, 2008). The Balmer assemblage data from Laird Lake and Red Lake all show trends evolving away from the OIB-MORB field to higher Th/Yb values, indicating variable contamination from an older crustal basement (Fig. 6.23).

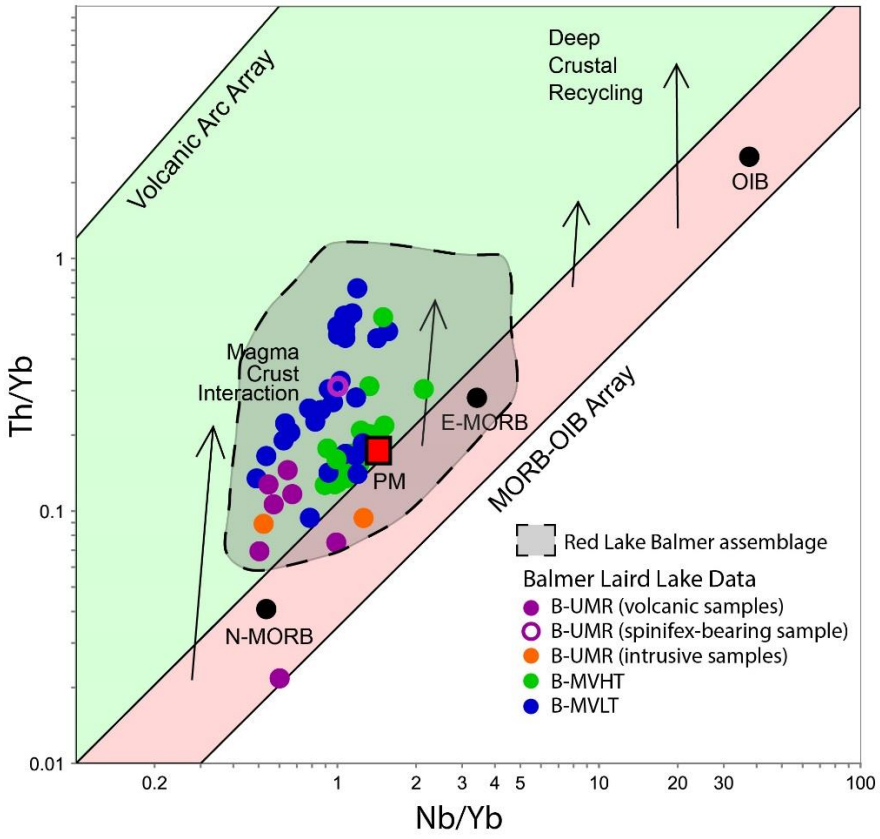

Figure 6.23 Th/Yb versus Nb/Yb plot (modified after Pearce, 2008). Red Lake data sources: Hollings et al. (1999), Hollings, 1998; Lemkow et al. (2006). Primitive mantle (PM) value from Sun and McDonough (1989).

Stott et al. (2010) proposed that the domain boundary between the North Caribou Core and Uchi domain should be relocated to intersect the contact between the Mesoarchean assemblages (Balmer, Ball, Bruce Channel assemblages) and Neoarchean Confederation assemblage. If correct, this would imply that the Balmer assemblage erupted through ~3 Ga North Caribou Terrane crust, however, as Tomlinson et al. (1998) noted, no rift-sequence consisting of basal conglomerates and arenites, limestones, iron formation, succeeded by ultramafic and mafic volcanic rocks is found within the Balmer assemblage and it is therefore unlikely that the assemblage formed as a result of rifting of continental

crust. Instead, Tomlinson et al. (1998) narrows down the options to ridge subduction near a hotspot or oceanic plateau accretion. The Balmer assemblage in the Laird Lake area is much more similar to an oceanic plateau setting with intercalated ultramafic and mafic volcanic rocks and iron formations and fits most of the diagnostic geochemical and geological characteristics of oceanic plateaus defined by Kerr (2003). These characteristics include abundant high-MgO lavas (>14wt.%), rare low-MgO lavas (<3wt.%), La/Nb primitive mantle normalized ratios ≤1, predominantly flat chondrite normalized REE patterns, the presence of pillow lavas, rare tephra layers, occasional subaerial eruption, and the presence of intercalated pelagic sediments. The Laird Lake Balmer assemblage data satisfies the MgO contents, the flat chondrite normalized REE pattern, the presence of pillowed basalts and BIFs with no sightings of tephra layers or evidence for subaerial eruption and could therefore be interpreted as an oceanic plateau.

The AFC and binary mixing modeling has shown that it is possible to produce trace element patterns similar to the most contaminated Laird Lake komatiites with the combination of 10% contamination by an intermediate basement, and roughly 35-45% AFC. The ε_{Nd} data are also consistent with the mafic volcanic rocks of the Balmer assemblage having been contaminated by older crust. The high-Ti basalts only show weak signs of contamination in the trace element data with small negative Nb anomalies, whereas the low-Ti basalts show stronger contamination with larger negative Nb anomalies, and enriched LREE. The high-Ti basalts and uncontaminated komatiites likely represent the two end members of the mantle plume geochemical spectrum, whereas the low-Ti basalt likely formed from the mixing of various ratios of komatiite/contaminated komatiite and high-Ti basalt/contaminated high-Ti basalt. The low-Ti basalts with flatter REE profiles can be produced by the mixing of 40% high-Ti basalt and 60% uncontaminated komatiite. Calculations for the major elements do not fully support this theory, however, the trace element data is consistent with the theory.

Figure 6.24 illustrates the formation and relationships of the volcanic and sedimentary units within the Balmer assemblage between 2.992 and 2.964 Ga. The data collected at the Laird Lake property suggests the eruption of plume-related volcanism through thin intermediate North Caribou Terrane crust since the level of contamination is fairly low (≤10%). A mantle plume impinging on thin crust in a subaqueous environment would allow for the formation of an ocean-like plateau and could account for the low degree of contamination. The Laird Lake property comprises intercalated komatiites, pillowed basalts, BIFs, and felsic volcanic rocks are present elsewhere in the Balmer assemblage throughout the RLGB (Hollings et al., 1999; Sanborn-Barrie et al., 2004). The komatiites would originate from the tail of the plume whereas the high-Ti basalts would come from the head of the plume. Volcanism occurred at surface within a subaqueous setting to form the pillow basalts, and prolonged

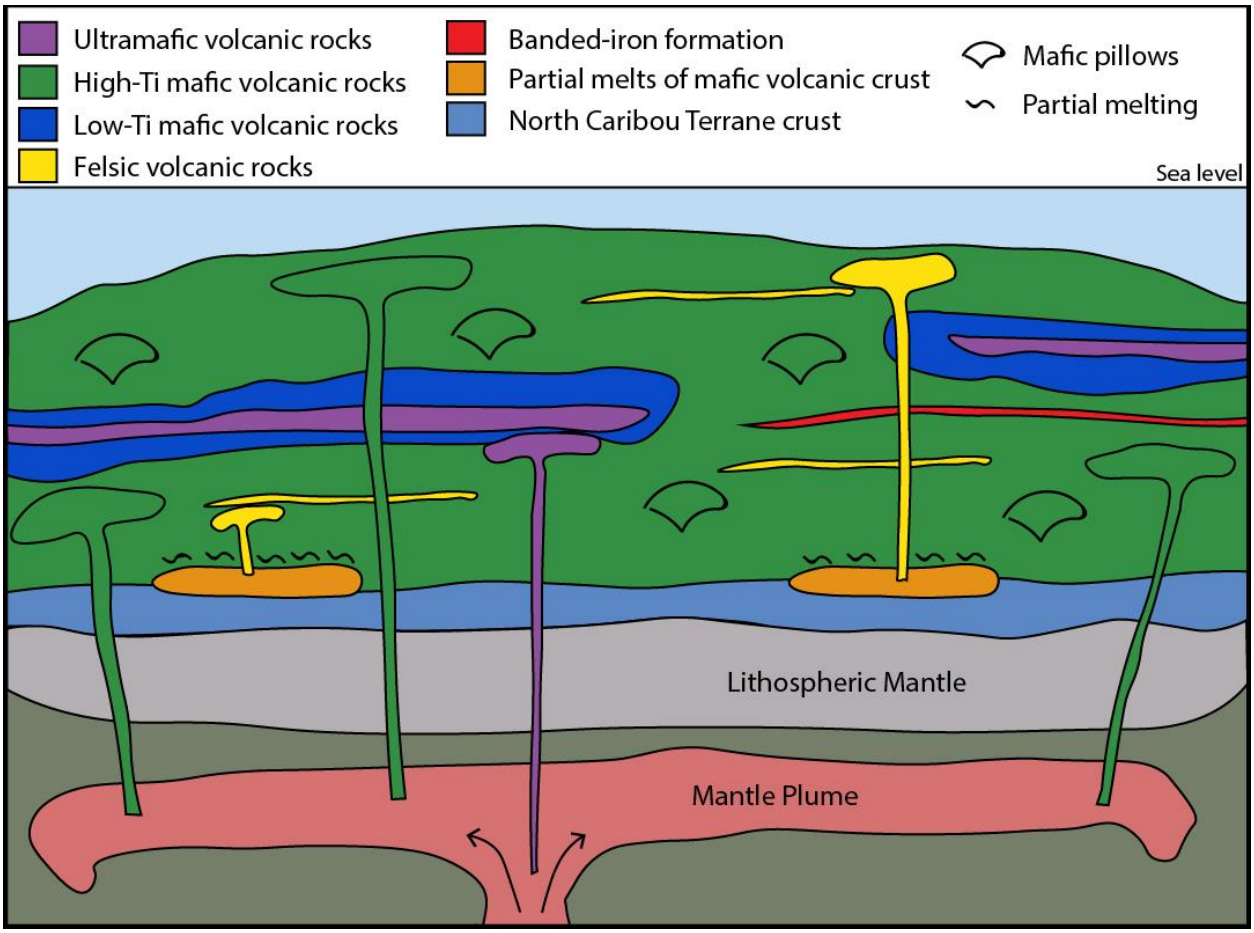

Figure 6.24 Reconstruction of the geodynamic setting of the Balmer assemblage at 2.992-2.964 Ga.

eruption would create an oceanic plateau made of stacked volcanic flows. Mixing of komatiites and high-Ti basalts would produce low-Ti basalts. Felsic volcanic rocks found throughout the RLGB but absent at the Laird Lake property are likely the result of partial melting of the overthickned oceanic plateau which Tomlinson et al. (1998) estimated would have a thickness of 10 km, or the result of plume-arc interaction (Hollings et al., 1999).

6.2.2 Confederation Assemblage

The Confederation assemblage at the Laird Lake property is composed of calc-alkalic mafic (Fig. 5.11), FI/FII intermediate to felsic and transitional (tholeiitic to calc-alkalic) FIIIb intermediate to felsic volcanic rocks (Figs. 5.14; 6.16). The tectonic setting in which these rocks formed requires a dynamic environment in which multiple geochemical signatures can be generated. All volcanic rocks display enriched LREE and negative HFSE anomalies on a PM normalized plot, consistent with subduction-related magmatism. Previous work conducted on the Confederation assemblage throughout the Uchi subprovince generally concluded that the assemblage was formed within a back arc setting with local greenstone belts also showing evidence for the involvement of combined arc/back arc volcanism (Corfu and Stott, 1993a; Hollings, 1998; Hollings and Kerrich, 2000; Sanborn-Barrie et al., 2004; Percival et al., 2006; Wyman and Hollings, 2006; Young et al., 2006 and references therein).

Back arc magmas are generated by partial melting of a Normal-MORB (N-MORB) source (Woodhead et al., 1993; Taylor and Martinez, 2003) whereas the arc magmas can be explained by being derived from a more depleted (in HFSE) source caused by melt extraction during back-arc extension (Ewart et al., 1977; Ewart et al., 1994) or by an aqueous fluid flux from the slab (Tollstrup et al., 2010). Primitive magmas such as tholeiites tend to dominate the early stages of arc development, and as the arc evolves, the system becomes more calc-alkalic due to a combination of fractionation, eruption, assimilation and recharge processes within the arc (Defant and Nielsen, 1990; Smith et al., 1997; Winter,

2001). Over the evolution of an arc system, the geochemical variability in both back arc and volcanic arc magmas is vast, with back arc basalts varying from MORB-like to arc-like geochemical signatures (Saunders and Tarney, 1984) and volcanic front magmas varying from primitive tholeiitic and calc-alkalic to evolved magmas (Ducea et al., 2015; Schmidt and Jagoutz, 2017). The numerous components which influence arc magmatism are extremely complex, however, in general, back arc magmas erupt closer to their source as they represent an extensional environment and therefore would more commonly erupt primitive tholeiitic melts (Smith et al., 1997). Contrastingly, arc magmas derived from metasomatized mantle wedge sourced from depleted N-MORB will pond beneath the arc where they will evolve through fractional crystallization, mixing and assimilation throughout their ascent (Smith et al., 1997; Winter, 2001), and incorporate a much larger subduction component (Shibata and Nakamura, 1997; Pearce and Stern, 2006).

Woodhead et al. (1993) showed that it is possible to differentiate arc and back arc volcanic rocks using high field strength and transition elements (Ti, Zr, V, Sc and Y) from multiple island arc systems. Typically, arc rocks will have lower average abundances of HFSE and Y, and therefore have higher ratios of Ti/Zr, V/Ti and Sc/Y compared to back arc rocks (Woodhead et al., 1993). When this model is applied to the Laird Lake data, distinct trends emerge (Fig. 6.25). The felsic to intermediate volcanic rocks show two trends; the first has a steeper trend with higher V/Ti, Sc/Y, Ti/Zr and La/Yb_n ratios and is associated with the FI/FII volcanic rocks, whereas the second trend has lower V/Ti, Sc/Y, Ti/Zr and La/Yb_n ratios and is associated with the FIIIb volcanic rocks. The mafic volcanic rocks separated by their Gd/Yb_n ratios also follow these two trends; mafic rocks with more fractionated HREE (Gd/Yb_n=1.42-3.65) plot closer to the FI/FII volcanic rocks whereas the mafic rocks with less fractionated HREE (Gd/Yb_n=1.21- 1.55) plot closer to the FIIIb volcanic rocks. These trends suggest that the FI/FII and mafic volcanic rocks with more fractionated HREE (Gd/Yb_n=1.42-3.65) were formed in the volcanic arc, whereas the FIIIb and mafic volcanic rocks with less fractionated HREE (Gd/Yb_n=1.21-1.55) were formed in the back arc. All Laird

Lake arc rocks have a higher La/Sm_n ratio and more strongly fractionated HREE, features which are characteristic of more evolved magmas, more intense crustal contamination (Fig. 6.25D) and greater depth of melting.

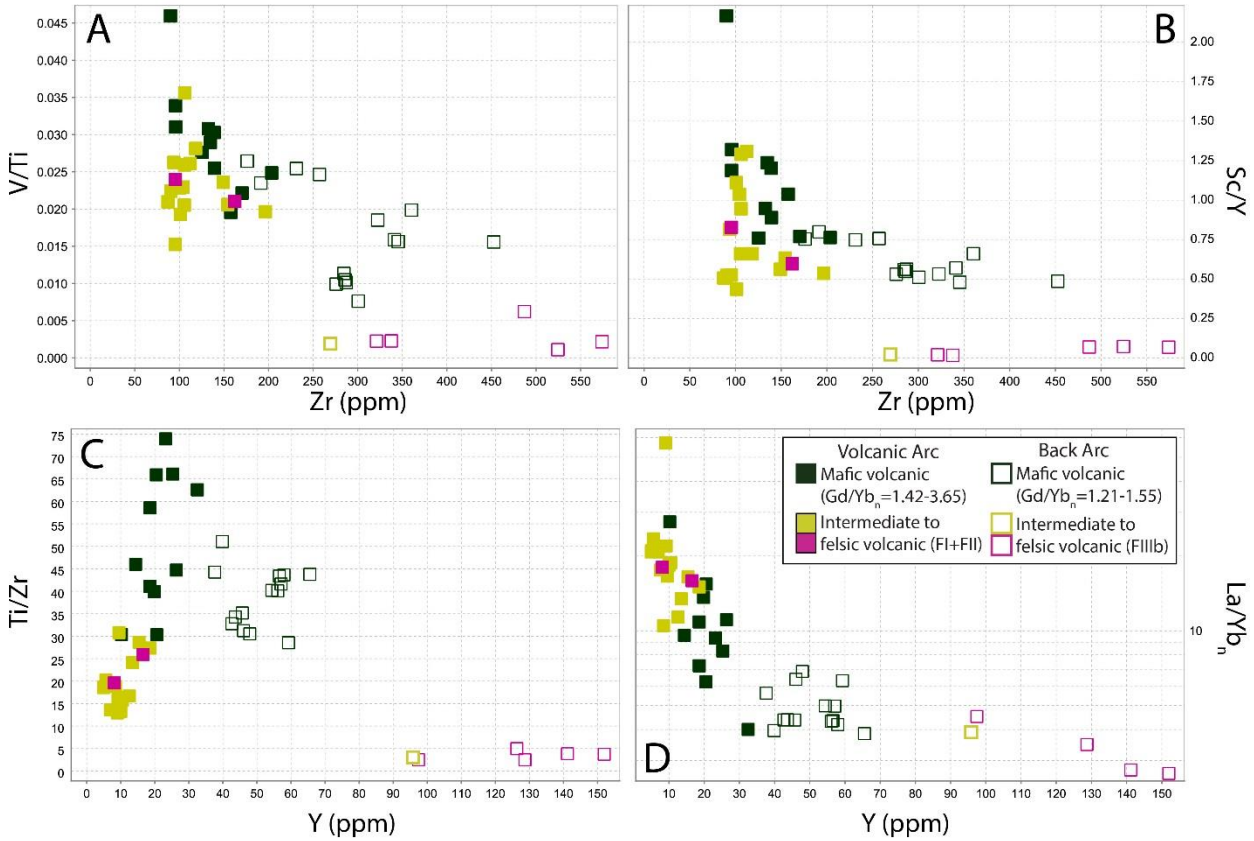

Figure 6.25 V/Ti and Sc/Y against Zr (ppm), and Ti/Zr and La/Yb_n against Y (ppm) plots for the Laird Lake Confederation assemblage volcanic rocks. Filled squares represent the arc volcanic rocks and the open squares represent the back arc volcanic rocks. The yellow symbols represent unsubdivided intermediate to felsic volcanic rocks and the pink symbols represent quartz-feldspar porphyritic crystal tuffs. The mafic volcanic rocks are subdivided according to Figures 6.12a and 6.12b. Plots A and B show elevated V/Ti and Sc/Y ratios for the arc rocks, which supports the subdivision of the arc and back arc volcanic rocks (Woodhead et al., 1993). Plot C shows a steep positive trend in Ti/Zr ratios for the mafic arc rocks, with flatter trend for the mafic back arc rocks. Plot D shows that all arc rocks have more enriched LREE and fractionated HREE.

Similarly to trace element ratios, isotopic ratios can be used to see changes in across-arc patterns. Studies conducted on young oceanic arcs show contrasting trends across various arcs, attesting to the complex nature of any arc system. Hochstaedter et al. (2001) and Tollstrup et al. (2010) conducted studies on the currently active Izu-Bonin arc-basin system and concluded that the volcanic front of the system has the most radiogenic Sr, Nd, Hf, and Pb and suggested that this was caused by

high degrees of partial melting of a previously depleted mantle source. Contrastingly, Hedge and Knight (1969), Notsu (1983), Nohda and Wasserburg (1981) and Shibata and Nakamura (1997) studied the Quaternary northeastern Japan arc system and found that the isotopic composition from the volcanic front are more enriched (higher $^{87}Sr/^{86}Sr$, $^{206}Pb/^{204}Pb$, $^{207}Pb/^{204}Pb$, and $^{208}Pb/^{204}Pb$, but lower $^{143}Nd/^{144}Nd$) than those in the back arc. Both groups of research concluded that the volcanic front is typically more radiogenic than the back arc, however, $^{143}Nd/^{144}Nd$ ratios can show both more enriched or depleted signatures within the back arc compared to the volcanic front.

The Laird Lake ε_{Nd} data suggests the presence of two sources of magmatism; a depleted source (ε_{Nd} values +1.6) associated with FIIIb felsic to intermediate and less fractionated mafic volcanic rocks (Gd/Yb_n=1.21-1.55) and a more enriched source (ε_{Nd} values +0.4) associated with FI/FII felsic to intermediate volcanic rocks. Mafic volcanic rocks with more fractionated HREE (Gd/Yb_n=1.42-3.65) were not analysed for Nd isotopes. The Laird Lake data follows the across-arc trends described by Shibata and Nakamura (1997) and others, and is consistent with the back arc having a more depleted signature. In agreement with the geochemical separations of arc and back arc rocks, the arc rocks have more enriched ε_{Nd} values (+0.4) whereas the back arc rocks have more depleted ε_{Nd} values (+1.6). Shibata and Nakamura (1997) suggested four possible scenarios for the observed trend; 1) heterogeneity in the mantle wedge, 2) crustal contamination, 3) addition of a heterogeneous subduction component to the mantle wedge and 4) addition of an isotopically homogeneous subduction component (MORB-type) to the mantle wedge and that the amount of this component decrease towards the back-arc side. Due to the small dataset, and unknowns related to Archean tectonic processes, it is challenging to attribute the exact cause to the observed trends, however, the Laird Lake data is consistent with crustal contamination causing a more enriched ε_{Nd} value within the arc rocks compared to the back arc rocks (Fig. 6.22).

The distinction between FI, FII and FIIIb magmas (see section 6.1.2.1) can also help infer depth of melting, which can in turn be used to interpret a tectonic setting. The FI and FII association seen at the Laird Lake property suggests an arc system which would source melts from both low-degree partial melting of a mafic source with minimal fractionation (FI; >30km; Lesher et al., 1986; Hart et al., 2004) and melts sourced from either fractional crystallization of intermediate (Campbell et al., 1981; Campbell et al., 1982; Lesher et al., 1986) or mafic magma (Barrett and MacLean, 1999), or partial melting of crustal material (FII; 10-15km; Lentz, 1998; Hart et al., 2004). The FI melts represent arc-related suites derived from metasomatized mantle wedge with variable crustal contamination (Barrie et al., 1993), whereas the FII melts likely originated from oceanic intra-arc rifting (Lentz, 1998). The FIIIb at the Laird Lake property could represent low-pressure partial melting of tholeiitic basalt with no residual amphibole (Hart, 1984) or garnet (Campbell et al., 1981; Lesher et al., 1986; Barrie et al., 1993) in a subvolcanic magma chamber, high-temperature partial melting of crustal material (Lentz, 1998), or a combination of fractional crystallization of tholeiitic mafic melts and wall-rock contamination by either mafic crust or granulite lower crust (<10km; Thurston and Fryer, 1983; Barrie et al., 1993; Hart et al., 2004). These are most commonly found within oceanic extensional environments (Hart, 1984; Barrie et al., 1993).

The spatial distribution between the arc and back arc volcanic rocks shows a complicated relationship between the two types of volcanism (Fig. 6.26). It is apparent that the most common type of volcanism consists of intercalated back arc mafic volcanic rocks and FI arc intermediate to felsic volcanic rocks. These units show weak diagonal trends to the contact between the two assemblages, which are locally parallel to the main volcanic stratigraphy of the assemblage. The mafic volcanic arc rocks are less common and are interlayered between the FI/FII arc rocks and the back arc mafic rocks. The FIIIb intermediate to felsic rocks are most commonly present closest to the contact with the Balmer assemblage, and almost always found in the vicinity of FI/FII arc rocks. These complex relationships

suggest that arc and back arc volcanism occurred simultaneously during the eruption of the Heyson sequence.

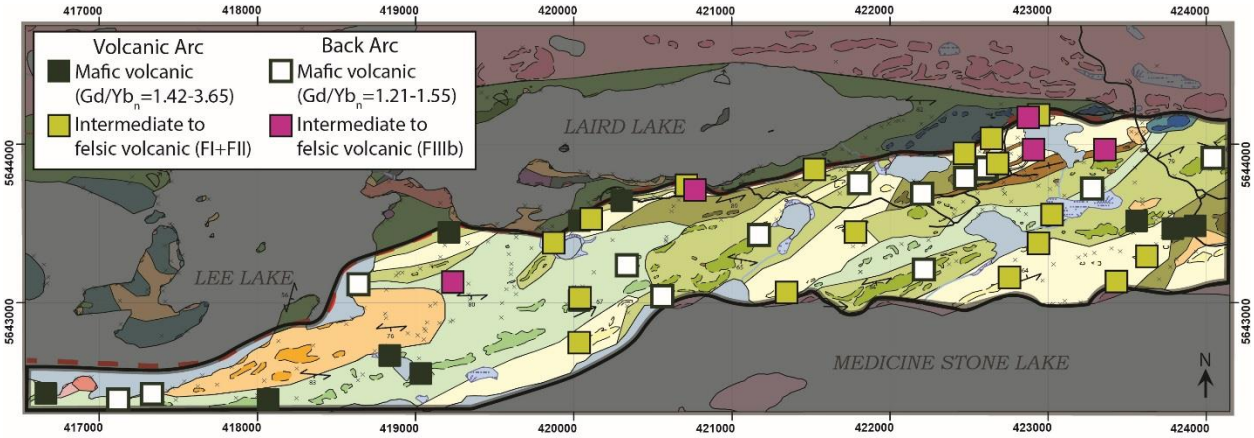

Figure 6.26 Distribution of the Confederation assemblage arc and back arc volcanic rocks.

Many authors have tackled the task of determining the type of crust the Confederation was built on; continental or oceanic. Sanborn-Barrie et al. (2004), Percival et al. (2006) and Young et al. (2006) proposed that the Confederation assemblage was a continental arc, erupted on top of previously existing greenstone belts, creating an angular unconformity between Meso- and Neoarchean assemblages. Likewise, Stott and Corfu (1991) and Stott (1996) suggest that the Confederation assemblage was formed on the continental margin of a growing composite terrane (North Caribou Terrane) and used the field relationships between similarly dated volcanic and plutonic rocks on the northern margin of the subprovince (e.g. Graves sequence in the RLGB) to infer that the Confederation assemblage is tectonically related to the northern volcanic and plutonic rocks. Hollings (1998) suggest the Confederation assemblage was built on the margins of the Uchi subprovince as part of an island arc system based on the lack of a strong continental crust signature in the geochemistry of the rocks.

For recent volcanic eruptions, rocks produced in an island arc setting (oceanic) have ε_{Nd} values ranging from +6.8 to +9.4 ($DM_{43\ Ma}$=+8.3; DePaolo and Wasserburg, 1977; DePaolo, 1981a), whereas mantle-derived rocks formed in a continental setting will typically have negative ε_{Nd} values caused by

crustal contamination (DePaolo and Wasserburg, 1979). The degree of isotopic enrichment is influenced by multiple factors, including the source of the melts, the isotopic composition of the contaminant and the thickness of the contaminant, and can lead to results being interpreted in various ways (Dickin, 2005). Given that all the data from the Confederation assemblage at the Laird Lake area has a positive ε_{Nd} value, it is unlikely that these rocks formed in a continental arc setting, as suggested by Sanborn-Barrie et al. (2004), Percival et al. (2006) and Young et al. (2006). Instead, the isotopic data is more consistent with an oceanic island arc environment, where the melts would experience far less crustal contamination. However, the presence of xenocrystic zircons suggests the existence of basement crust as a contaminant for the Confederation assemblage.

Work in the Luzon arc system of the Philippines has shown that young oceanic crust can host xenocrystic zircons which have been interpreted as having been sourced from ascending magmas through either a Lower Cretaceous ophiolite complex located at a depth within the 30-35 km thick Luzon crust (Payot et al., 2007) or sourced from a "hidden" Cathaysia-type continental crust (2.6-0.7 Ga) which split off from the Eurasian margin during the opening of the South China Sea and then drifted and accreted to the western Philippine Sea plate before initiation of the Luzon subduction (Yu et al., 2010; Shao et al., 2014; Shao et al., 2015). This relationship can also be observed in Iceland (active since 16 Ma), where 1.8 Ga xenocrystic zircons have been recovered from primitive melts (Schaltegger et al., 2002) and may have been sourced from continental crust beneath southeast Iceland (Torsvik et al., 2015). The Precambrian continental fragment is interpreted to have originated from the east coast of Greenland, and as the Icelandic plume migrated (Doubrovine et al., 2012) and rifting in the mid-Atlantic occurred, the plume split off a sliver of Greenland which is now located beneath southeast Iceland (Torsvik et al., 2015).

One of the xenocrystic zircons dated from sample LL-16BG068A01 has an age (2912.6 ± 3.2 Ma) which is 13 Ma younger than the Ball assemblage (2940 ± 2 to 2925 ± 3 Ma; Corfu and Wallace, 1986)

and 18 Ma older than the Bruce Channel assemblage (2894 Ma; Sanborn-Barrie et al., 2001) in the RLGB and does not correlate with any crystallization ages reported for the Uchi subprovince. This suggest that the Confederation assemblage was built onto an external continental fragment which contained zircons spanning at least 2974-2840 Ma.

Overall, the data at the Laird Lake property suggests the Confederation assemblage was built as an island arc system on top of a thin continental fragment dated between at least 2974-2840 Ma which could have originated by either drifting northwards from the Winnipeg River Terrane, be a North Caribou Terrane fragment created by early rifting or as a crustal fragment of unknown origin. Initiation of northward subduction within an oceanic setting created an island arc system which matured into an arc and back arc system (Fig. 6.27). The arc component of the system consists of calc-alkalic mafic volcanic rocks and FI/FII intermediate to felsic volcanic rocks which were derived from metasomatized mantle wedge at a depth of 30-10 km and underwent variable degrees of crustal contamination during the ascent of the magmas (Lesher et al., 1986; Barrie et al., 1993; Hart et al., 2004). In this setting, the ascending melts would have picked up xenocrystic zircons from the basement crust. The back arc sequence is composed of calc-alkalic mafic volcanic rocks and FIIIb transitional (calc-alkalic to tholeiitic) intermediate to felsic volcanic rocks which are thought to originate from low-pressure partial melting of tholeiitic basalts above the garnet stability field in a subvolcanic magma chamber shallower than 10 km or as the result of fractional crystallization of tholeiitic to intermediate melts (Lesher et al., 1986; Barrie et al., 1993; Hart et al., 2004). Simultaneous eruption of arc and back arc volcanism created a package of interlayered mafic to felsic volcanic rocks showing both depleted and more enriched ε_{Nd} signatures. The 2737.6 ± 0.79 Ma deformed diorite intrusion within the Confederation assemblage represents a syn-volcanic intrusion formed in the back arc likely formed as a fractionation product of tholeiitic basalts since its depleted ε_{Nd} value is very similar to the back arc volcanic rocks.

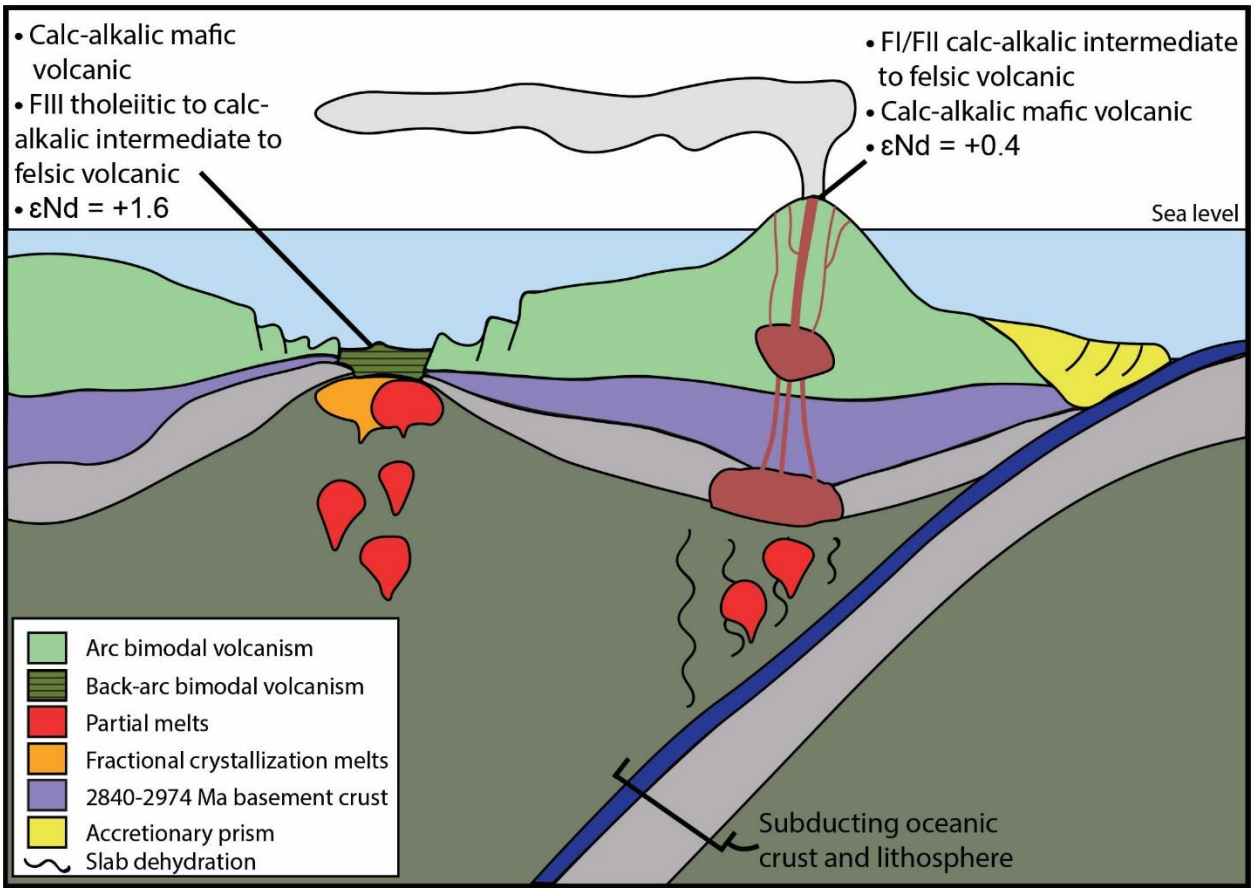

Figure 6.27 Schematic model of the geodynamic setting of the Heyson sequence at 2741 Ga within the Confederation assemblage.

6.3 Gold Mineralization

The Laird Lake area hosts numerous gold occurrences at the contact between the Balmer and Confederation assemblages, which represents a zone of intense hydrothermal activity within an alternating ductile to brittle deformational regime. The wide-range of alteration and mineralization styles are strongly controlled by the chemistry of the host rocks and overprinting structures. These features have been shown to be some of the most influential factors in gold precipitation (Eisenlohr et al., 1989; Phillips and Powell, 2010). The Laird Lake area shares many features with major Archean orogenic gold deposits including: the presence of variolitic tholeiitic basalts and komatiites, lamprophyre

dykes, mineralization distributed along crustal-scale fault zones between major lithological boundaries, brittle to ductile deformation, amphibolite facies metamorphism, carbonate alteration, iron-rich sulphidized wall-rock and arsenopyrite rich zones (Dubé and Gosselin, 2007).

6.3.1 Structures and Chemical Traps

6.3.1.1 Regional Structures as Fluid Pathways

The majority of Archean orogenic gold deposits are associated with first-order, deep-crustal faults or deformation zones which act as pathways for the mineralizing fluids to ascend, however, most gold deposits are situated in second- and third-order shears and faults (Goldfarb et al., 2005; Dubé and Gosselin, 2007). The main structures commonly occur between lithologic units such as two different terranes (Kerrich and Wyman, 1990; Hodgson, 1993) and have a long-lived structural history which evolves from regional shortening and high-angle reverse motion to strike-slip motion (Kerrich, 1989; McCuaig and Kerrich, 1998; Robert and Poulsen, 2001). Within lower order structures, the mineralizing fluids tend to concentrate most effectively within areas of jogs, changes in strike, or bifurcations of the first-order system (Colvine et al., 1984; Weinberg et al., 2004), but will also concentrate in regional fault intersections, major anticline hinges and zones of competency contrasts (Vearncombe et al., 1989; Groves et al., 2000). Gold deposits are commonly restricted to shears or fault zones within a brittle-ductile transition zone which create an ideal environment for the buildup and release of stress, fluctuating fluid pressure and porosity, and a seismic-pumping mechanism for hydrothermal fluid flow (Sibson et al., 1975; Eisenlohr et al., 1989).

The contact between the Balmer and Confederation assemblages likely represents an area of juxtaposition between the North Caribou Terrane and Uchi subprovince (Stott, 1997; Hollings, 1998; this study), but has also been interpreted as an angular unconformity (Parker, 2000a; Sanborn-Barrie et al.,

2001; Dubé et al., 2004). At the Laird Lake property, the contact between the two assemblages was observed once as slightly dipping south (15BG518; UTM 421526E 5643860) and is marked by an increase in deformation with locally strongly foliated banded mafic volcanic rocks, folds and boudinaged bands of the Balmer assemblage and lesser deformed Confederation assemblage units. All known gold zones are found within 100 m of the contact within the Balmer assemblage and 200 m of the contact within the Confederation assemblage (Fig. 4.1). Within the Balmer assemblage, the higher strain zones along the contact are often defined by a banded texture (Fig. 4.12), whereas the lower strain zones only show D_2 foliations within the mafic volcanic rocks. The banded texture is composed of alternating bands of biotite, hornblende, diopside and clinozoisite, with local garnet porphyroblasts (Fig. 4.18A) and has been described as a mylonite at the past-producing Madsen mine (Hugon and Schwerdtner, 1984). At the Laird Lake property the banded unit is intermittently found within the first 100 m away from the contact and is only present within the Balmer assemblage.

The strong development of D_2 fabrics, the presence of folds and boudinaged features and lack of primary textures all within the banded unit suggests ductile deformation on the Balmer side of the contact, consistent with the presence of an anastomosing shear zone system, likely the continuation of the Flat Lake-Howey Bay deformation zone (Andrews et al., 1986). At the Laird Lake property, the direction of movement along this structure is unclear, as both S- (common) and Z-shaped (uncommon) folds are present (Figs. 4.17C; 4.24A). Observations made elsewhere in the RLGB describe left-lateral (sinistral) movement along the shear zones associated with the Flat Lake-Howey Bay deformation zone (Durocher and Hugon, 1983). Dubé et al. (2000) argued against the presence of regional scale shear zones (Flat Lake-Howey Bay deformation zone) in the Madsen area as there is widespread preservation of primary textures and the obliquity between S_0-S_1 and S_2 cleavages within the Austin “tuff” which suggest moderate strain. However, at the Laird Lake property, all features within 100 m of the contact within the Balmer assemblage are strongly foliated by S_2 with no primary features remaining except for

the BIFs parallel to foliation at the Gold Bearing Zone trench and the carbonate formation at the Hill Side Zone trench which is not parallel to S_2, but shows a well-developed crenulation between S_0 and S_2 (Fig. 4.16D).

The Lee Lake Au showing, less than 100 m north of the contact, is located on a property-scale S-shaped deflection in the shear zone which shows a change in the strike of the foliation along the structure (Fig. 4.1) and represents a zone of effective fluid concentration as a possible 2nd order structure. Within the metasomatic banding, small-scale folds (Fig. 4.17C) are local and never associated with diopside-rich layers. Pinch and swell boudinaged diopside layers suggest a relatively low to moderate strength difference between the diopside band and matrix surrounding the band (Fig. 4.12B). The combination of strongly developed S_2 fabrics (banded texture), small-scale folds, boudinaged layers and a large scale S-shape deflection in the shear zone marked by the change in foliation produces a favorable structural environment for gold deposition. This is consistent with the Lee Lake Au showing hosting some of the highest gold grades on the Laird Lake property. Elsewhere on the Laird Lake property, S-shaped folds (Fig. 4.24A) are found just NE of the GBZ and EGBZ trenches and possibly represent smaller examples that mirror the large scale foliation deflection associated with the Lee Lake Au showing.

Within the Confederation assemblage, primary features such as original bedding within tuffaceous units with non-foliated quartz crystals, easily recognizable lapilli clasts and locally unoriented feldspar phenocrysts within mafic volcanic units less than 100 m away from the contact suggest a much lower deformation strain on the south side of the contact. Typically, in a shear zone system, volcanic layers will be transposed parallel to the orientation of the shear (Passchier and Trouw, 2005), however, the majority of the volcanic layers within the Confederation assemblage are sub-parallel to oblique to the contact with only a few discontinuous layers being parallel to the shear. Local higher strain zones less than 3m thick parallel to S_2 are present throughout the assemblage and could represent splays from

the main structure. Specifically, at station 15BG228 (UTM 420040E 5643019N), a well-developed foliation defined by aligned biotite and lineated garnets within aphyric mafic volcanic rocks of the Confederation assemblage have a similar appearance to the strongly foliated mafic volcanic rocks of the Balmer assemblage (4.17D).

The deformation features found in both the Balmer and Confederation assemblages are consistent with the presence of a shear zone less than 100 m wide on the north side of the structural break between the two assemblages. The Confederation assemblage was likely less responsive to the shear since near the contact, the assemblage is primarily composed of felsic to intermediate volcanic rocks, which are more competent than the mafic volcanic rocks of the Balmer assemblage. As a result, the Balmer assemblage mafic volcanic rocks absorbed much of the structural stresses to offset the competency contrasts between the two assemblages. Field observations suggest the contact between the two assemblages dips south meaning the Confederation assemblage would have been slightly juxtaposed on top of the Balmer assemblage. Therefore, the more competent felsic to intermediate volcanic rocks of the Confederation assemblage may have acted as a cap-rock, creating a less permeable barrier to further concentrate the gold mineralizing fluids within the Balmer assemblage. Moreover, additional faults or shears can also form along mafic-ultramafic contacts due to the contrasting competencies (Robert et al., 2005), however, the mafic-ultramafic contact was never observed at surface on the Laird Lake property. The rarity of 2^{nd} and 3^{rd} order structures (with the exception of the S-shaped deflection in foliation located at the south-western end of Lee Lake) could be the result of a lack in complexity within the primary lithostratigraphic sequence and/or the depth at which the system was produced (Eisenlohr et al., 1989). At the GBZ trench, there is evidence for a post-D_2 mineralizing shear which cuts metasomatic banded mafic volcanic rocks, and hosts unfoliated pyrite along its margins. See section 6.3.2.2 for description and explanation.

A recent airborne magnetic survey produced by the Ontario Geological Survey (2017) revealed a clear difference in magnetic signatures across the contact between the Balmer and Confederation assemblages (Fig. 6.28). Additionally, the residual magnetic survey (Fig. 6.29) shows evidence for a late- to post-D_2 fault zone which loosely correlates with the previously mapped Laird Lake Fault (Atkinson, 1995). Rainsford (2017) suggested the presence of an 8-10 km dextral movement along the fault, which displaces the Laird Lake property adjacent to the Madsen and Starrat-Olsen package of rocks west of the Killala-Baird batholith. The geophysical data and field observations at the Laird Lake property are consistent with the presence of a fault within the north-eastern portion of the field area. The westward continuation of the fault and apparent dextral displacement in magnetic units (ultramafic rocks within the Balmer assemblage) suggest that the Laird Lake property and the Madsen/Starrat-Olsen package of rocks were once adjacent. This supports the suggestion that the Laird Lake property represents the continuation of the Flat Lake-Howey Bay deformation zone and in turn, the same gold system as found at the Madsen and Starrat-Olsen mines.

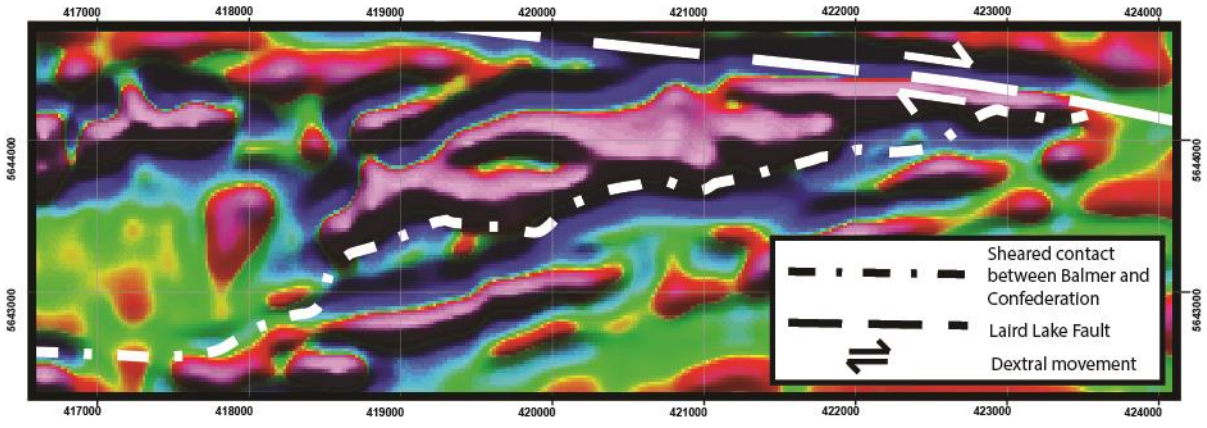

Figure 6.28 Second derivative magnetic survey (Ontario Geological Survey, 2017). The contact between the two assemblages correlates well with the change in magnetic response.

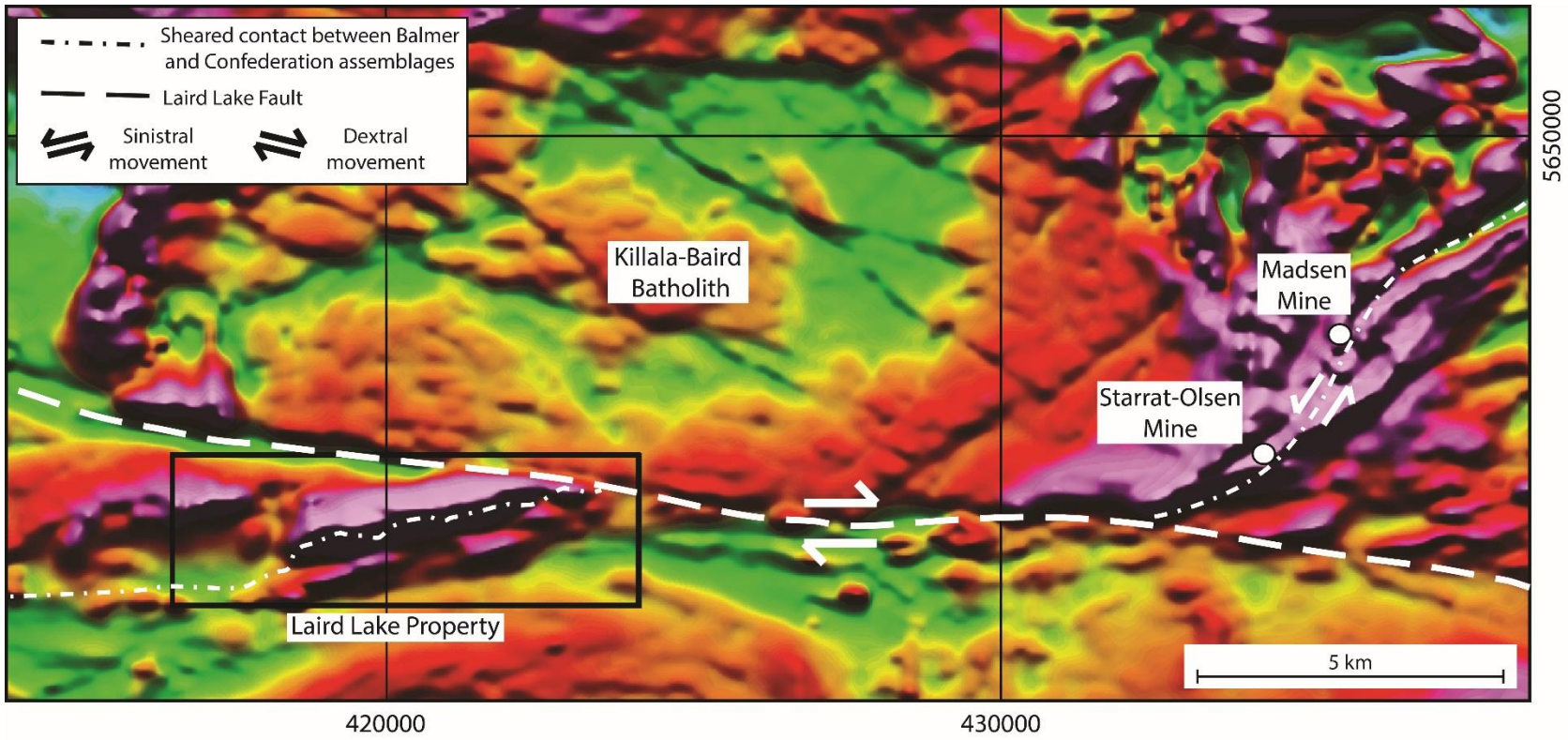

Figure 6.29 Residual magnetic survey (Ontario Geological Survey, 2017). Figure produced based on interpretations from Rainsford (2017).

6.3.1.2 Chemical Traps

One of the most important precipitation mechanisms within an orogenic gold system is the process of fluid-wallrock interaction which is often associated with fluid reduction in contact with reduced carbon-bearing host rocks and/or the sulphidation of wallrocks to generate iron-bearing sulphides and precipitate gold (Goldfarb et al., 2005; Phillips and Powell, 2010). Once gold is in solution, it is most commonly transported as a gold-thiosulphide complex ($Au(HS)_2^-$) under neutral pH conditions and temperatures up to 250-400°C. At higher temperatures (~500°C), gold-chlorine ($AuCl_2^-$) and gold-hydroxide (AuOH(aq)) complexes can become increasingly important (Stefánsson and Seward, 2004). As the hydrothermal fluid transporting gold-thiosulphide complexes reacts with the Fe-rich host rocks, the complex destabilizes as S bonds with Fe and gold precipitates in close association with the sulphides (Phillips and Powell, 2010). During the process of fluid-wallrock interaction, factors which influence the destabilization of the gold-complex include a change in temperatures, pressure, ligand activity, phase separation, boiling, mixing and sulphide mineral precipitation (Stefánsson and Seward, 2004). The close relationship between gold and S (Fig. 6.30) at the Laird Lake property suggest gold was transported by a

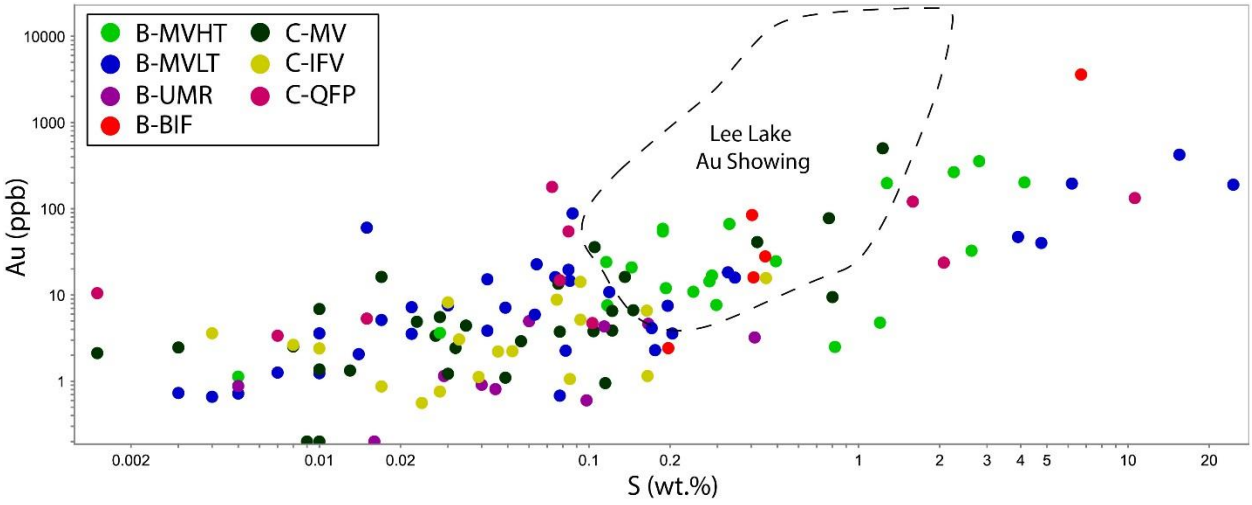

Figure 6.30 Au versus S showing a positive trend (R^2=0.4957) between increasing S and Au. Lee Lake Au showing rocks (dashed envelope) sampled by Bounty Gold Corp. (n=25). ***B-UMR****: Balmer ultramafic rocks,* ***B-MVHT****: Balmer mafic volcanic (high-Ti),* ***B-MVLT****: Balmer mafic volcanic (low-Ti),* ***B-BIF****: Balmer banded-iron formation,* ***C-MV****: Confederation mafic volcanic,* ***C-IFV****: Confederation intermediate to felsic volcanic,* ***C-QFT****: Confederation quartz-feldspar porphyritic crystal tuff*

gold-thiosulphide complex ($Au(HS)_2^-$) in the hydrothermal fluid and that sulphide mineral precipitation played a major role in destabilizing the gold-complex.

The Balmer assemblage is dominantly composed of Fe- to Mg-tholeiites with sporadic BIFs, both high-Fe host rocks and favorable chemical traps for gold (Sanborn-Barrie et al., 2004). The Fe-tholeiites (Fig. 5.4B; high-Ti basalts) and BIFs would therefore be expected to host higher gold grades than the Mg-tholeiites (Fig. 5.4B; low-Ti basalts), ultramafic rocks and Confederation assemblage units if the gold was transported by a gold-thiosulphide complex in areas with favorable structural conduits. At the Laird Lake property, the elevated gold values are associated with the major break between the Balmer and Confederation assemblage (Figs. 6.31 and 4.1), however, elevated gold values are not preferentially located in the Balmer Fe-tholeiites compared to the Mg-tholeiites, suggesting that the differences in Fe content in the tholeiites did not play a major role in gold precipitation. Despite that relationship, one of the most elevated gold occurrences is located within Fe-tholeiites at the Lee Lake Au showing, however, structural controls are likely the dominating cause for the elevated gold grades as at the Laird Lake property, elevated gold grades are primarily associated

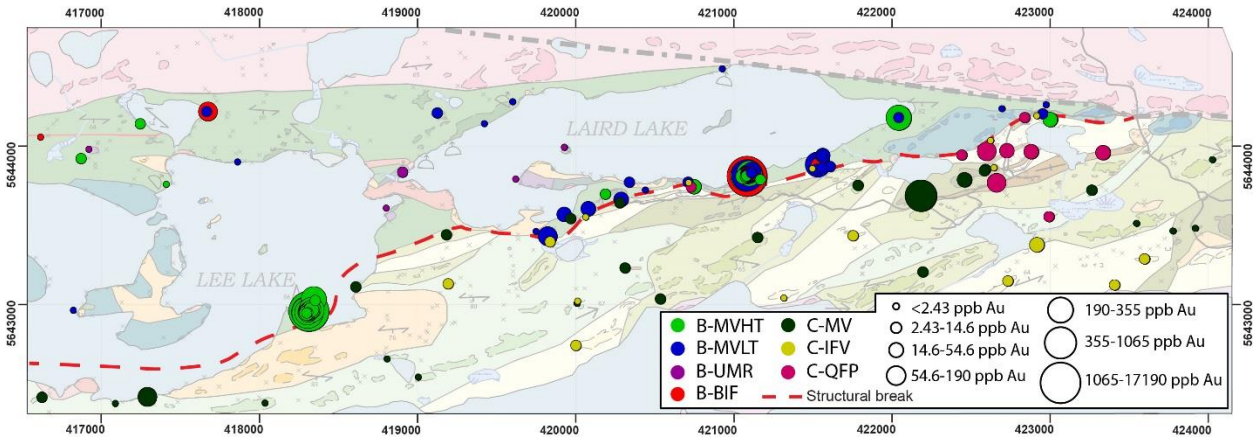

Figure 6.31 Au concentrations plotted according to their geochemical host rock. The majority of mineralized samples are found in the vicinity of the major break, more commonly within the Balmer assemblage as a result of favorable chemical traps (tholeiites and banded-iron formations). UTM lines are 1km spacing. ***B-UMR****: Balmer ultramafic rocks,* ***B-MVHT****: Balmer mafic volcanic (high-Ti),* ***B-MVLT****: Balmer mafic volcanic (low-Ti),* ***B-BIF****: Balmer banded-iron formation,* ***C-MV****: Confederation mafic volcanic,* ***C-IFV****: Confederation intermediate to felsic volcanic,* ***C-QFT****: Confederation quartz-feldspar porphyritic crystal tuff*

with the major break. Balmer assemblage BIFs are typically elevated in gold, especially near the major break (Fig. 6.31). The two highest grade disseminated sulphide-associated gold occurrences at the Laird Lake property are hosted in Fe-tholeiites and BIF. The Confederation assemblage hosts one elevated gold occurrence associated with disseminated sulphides within mafic volcanic rocks roughly 200 m from the break. These relationships are consistent with the gold having been transported by a gold-thiosulphide complex (Phillips and Powell, 2010).

6.3.2 Alteration and Mineralization

Commonly, orogenic gold deposits are associated with a hydrothermal alteration zone which will vary in mineralogy and magnitude depending on the composition and competency of the host rocks, metamorphic grade and style of mineralization (Dubé and Gosselin, 2007). In greenschist facies the alteration mineral assemblage within mafic volcanic rocks will be dominated by ankerite and/or dolomite-quartz-muscovite-pyrite ± paragonite, arsenopyrite and albite, whereas in amphibolite facies rocks, the alteration will commonly comprise biotite, amphibole, garnet, diopside, calcite, arsenopyrite, pyrrhotite, loellingite and lesser pyrite (Groves, 1993; Goldfarb et al., 2005). The metals associated with the alteration and mineralization related to disseminated sulfidic replacement gold deposits include Ag, As, Te ± Sb, W, Hg, Zn, Mo and Cu. The main zone of hydrothermal alteration and mineralization at the Laird Lake property coincides with the zone of metasomatic banding and strongest deformation (Fig. 4.12) within the mafic volcanic rocks of the Balmer assemblage. The dominant alteration minerals within this zone consists of biotite, hornblende, diopside, clinozoisite ± garnet, associated with a fine-grained quartz/feldspar ± muscovite matrix (Figs. 4.12; 4.17A; 4.18A; 4.23B). Sulphides associated with this alteration include: pyrite ± arsenopyrite ± pyrrhotite ± chalcopyrite. The style of Au-mineralization is variable but is most commonly associated with disseminated sulphides within hydrothermally altered Balmer mafic volcanic rocks as observed at both the Lee Lake Au showing and Gold Bearing Zone trench. However, BIFs (GBZ trench and 15BG418; UTM 417703E 5644219N) and units from the Confederation

assemblage (15BG088; UTM 422219E 5643691N) are also prospective in terms of Au-mineralization if favorable structures transporting a Au-rich fluid are present.

6.3.2.1 Hydrothermal Alteration

Alteration maps were produced in order to observe the continuity of the alteration along the major break and assess other potential mineralization targets. Samples were normalized by their least altered precursor of the same lithology to observe the quantitative elemental enrichments and depletions (enrichment or depletion factor) along the major break (Fig. 6.32) and eliminate the effects of regional metamorphism. Banded-iron formations were excluded due to their heterogeneity. In maps showing elemental enrichments (e.g, K_2O, As, Sb), samples which showed no enrichments or minor depletions relative to the least altered precursor were grouped into the <1 category whereas in maps showing elemental depletions (e.g, Na_2O and CO_2) the samples which showed no depletion or minor enrichments were grouped into the >1 category. The least altered precursor samples were chosen based on their lack of alteration and sulphide phases and distance from the major break or more strongly deformed zones.

The zone of strongest hydrothermal alteration is composed of a mineral assemblage consistent with a major enrichment in K_2O and S, minor increase in SiO_2 and CaO (Fig. 6.32) and depletion in Na_2O and CO_2 (Fig. 6.33). Metal enrichment in As, Sb, W and Mo is also associated with the alteration (Fig. 6.34). Other elements showing enrichment associated with the alteration but not shown include: Sn, Tl, Ba, Ir, Ru, Pd, ± Rh, Pt, Be, Bi and Pb. Enrichment in K_2O and S is correlated with the appearance of more abundant biotite and sulphides, respectively, whereas an enrichment in SiO_2 is likely caused by the increase and/or appearance of the various silicate phases (biotite, diopside, clinozoisite, hornblende, garnet) and quartz within the groundmass. Calcium (CaO) shows lesser enrichment at the major break, likely because diopside and clinozoisite were not common alteration phases, and hornblende is

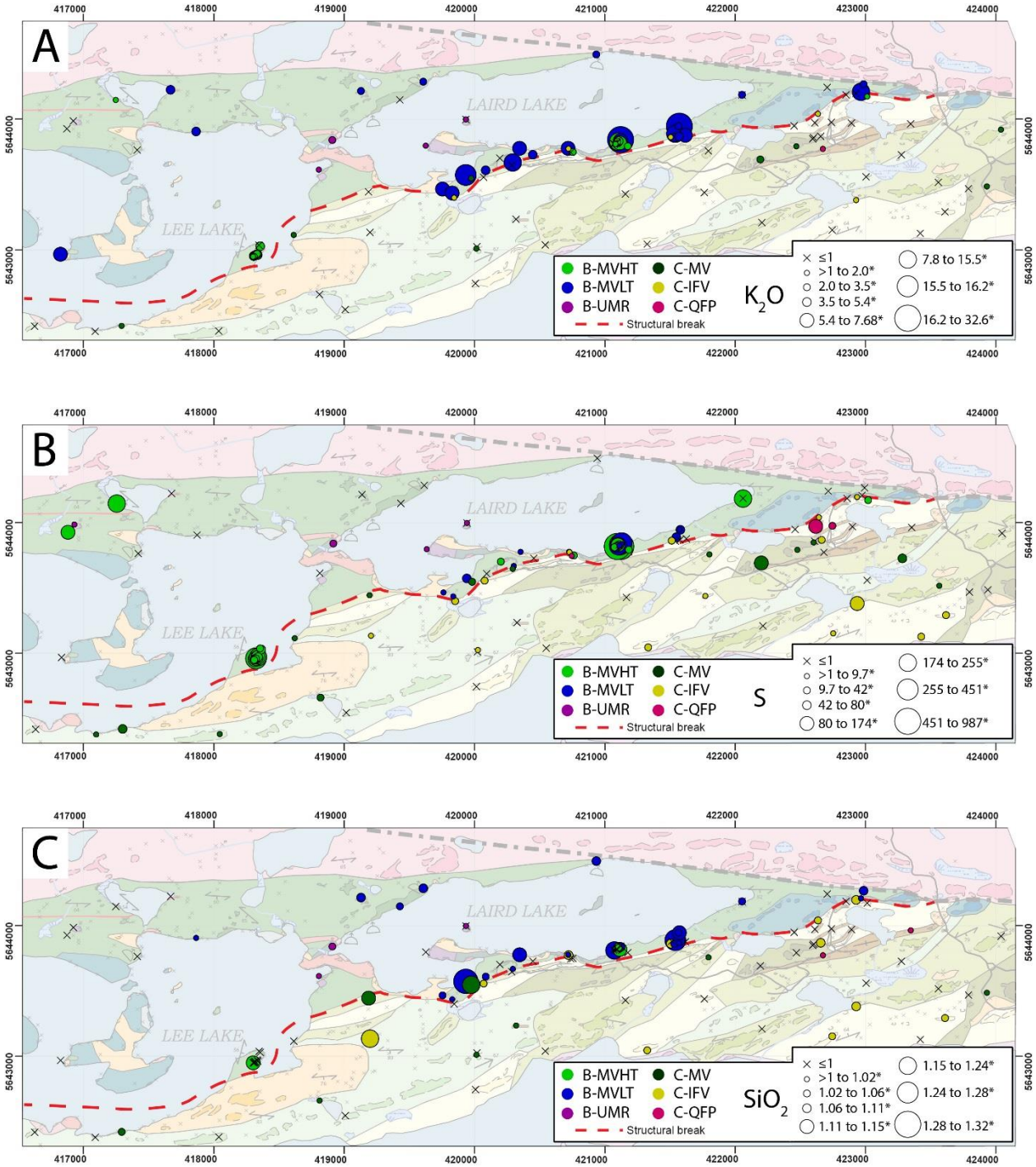

Figure 6.32 Alteration maps showing enrichment of major elements. A) K_2O, B) S, C) SiO_2, D) CaO. Elemental concentrations plotted according to their geochemical host rock. Enrichment factors calculated by normalizing a rock by its least altered precursor. ***B-UMR****: Balmer ultramafic rocks,* ***B-MVHT****: Balmer mafic volcanic (high-Ti),* ***B-MVLT****: Balmer mafic volcanic (low-Ti),* ***C-MV****: Confederation mafic volcanic,* ***C-IFV****: Confederation intermediate to felsic volcanic,* ***C-QFT****: Confederation quartz-feldspar porphyritic crystal tuff*

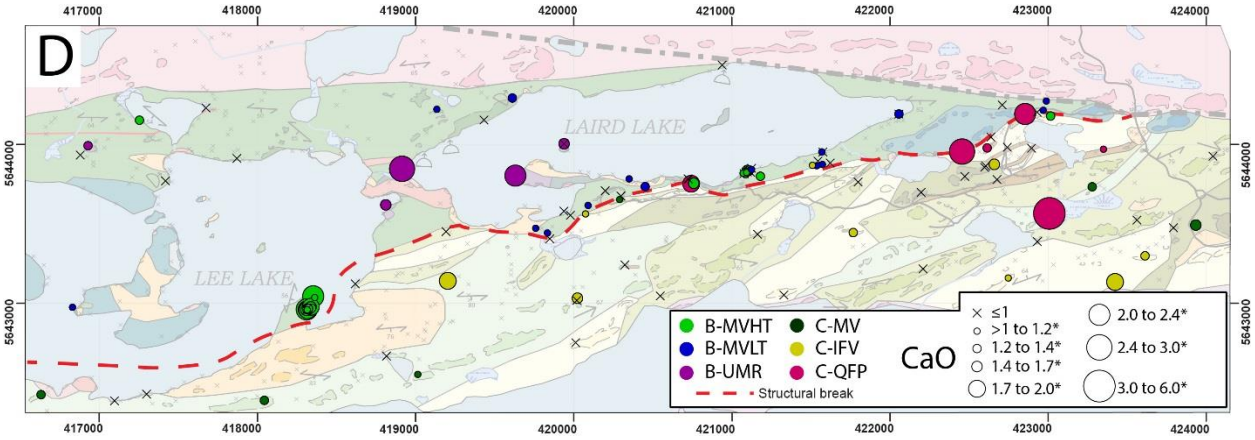

Figure 6.32 Continued. D) CaO.

abundant throughout every basaltic sample on the Laird Lake property, thus moderating any CaO enrichment. Diopside bands were commonly avoided during the sampling process due to their lack of sulphides and non-representative portrayal of the basaltic unit, hence the low CaO enrichment factor (Fig. 6.32D). Spikes in CaO away from the major break (ultramafic and quartz-feldspar porphyritic tuff units) are likely caused by the presence of calcium-carbonate phases. Elemental depletions were observed in both Na_2O and CO_2 (Fig. 6.33), likely caused by the destruction of Na-feldspars and carbonates, respectively, during prograde metamorphism. The Lee Lake Au showing and most high-Ti basalts lack a CO_2 depletion likely since the least altered precursor sample for high-Ti basalts showed a much stronger depletion in CO_2 compared to the rest of the high-Ti basalt samples but elsewhere along the major break CO_2 depletion is consistent. Metals including As, Sb, Mo and W are commonly found in the zone of most intense hydrothermal alteration and show very large enrichment factors (Fig. 6.34). The metals are probably contained within the sulphides phases such as arsenopyrite, pyrite and pyrrhotite since the metals are more likely to form covalent bonds with S (Phillips and Powell, 2010).

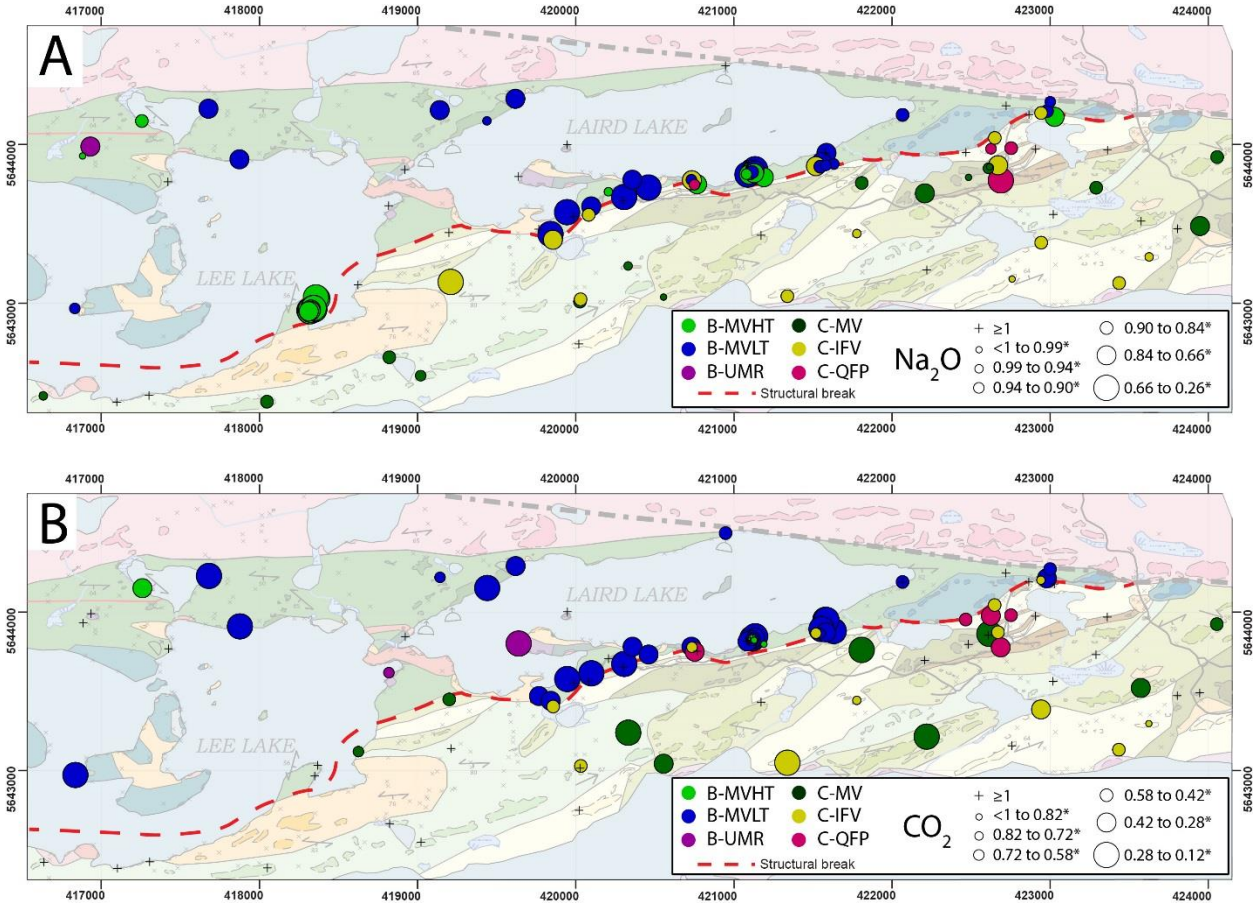

Figure 6.33 Alteration maps showing depletion of major elements. A) Na_2O, B) CO_2. Elemental concentrations plotted according to their geochemical host rock. Depletion factors calculated by normalizing a rock by its least altered precursor. The larger circles represent zones of stronger depletion. ***B-UMR****: Balmer ultramafic rocks,* ***B-MVHT****: Balmer mafic volcanic (high-Ti),* ***B-MVLT****: Balmer mafic volcanic (low-Ti),* ***C-MV****: Confederation mafic volcanic,* ***C-IFV****: Confederation intermediate to felsic volcanic,* ***C-QFT****: Confederation quartz-feldspar porphyritic crystal tuff*

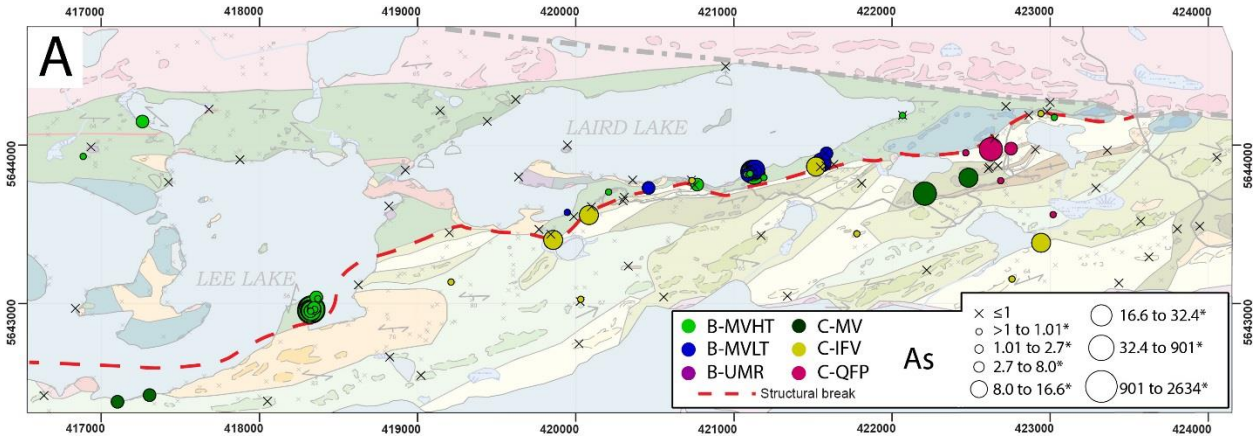

Figure 6.34 Alteration maps showing enrichment of major elements. A) As, B) Sb, C) W, D) Mo. Elemental concentrations plotted according to their geochemical host rock. Enrichment factors calculated by normalizing a rock by its least altered precursor. ***B-UMR****: Balmer ultramafic rocks,* ***B-MVHT****: Balmer mafic volcanic (high-Ti),* ***B-MVLT****: Balmer mafic volcanic (low-Ti),* ***C-MV****: Confederation mafic volcanic,* ***C-IFV****: Confederation intermediate to felsic volcanic,* ***C-QFT****: Confederation quartz-feldspar porphyritic crystal tuff*

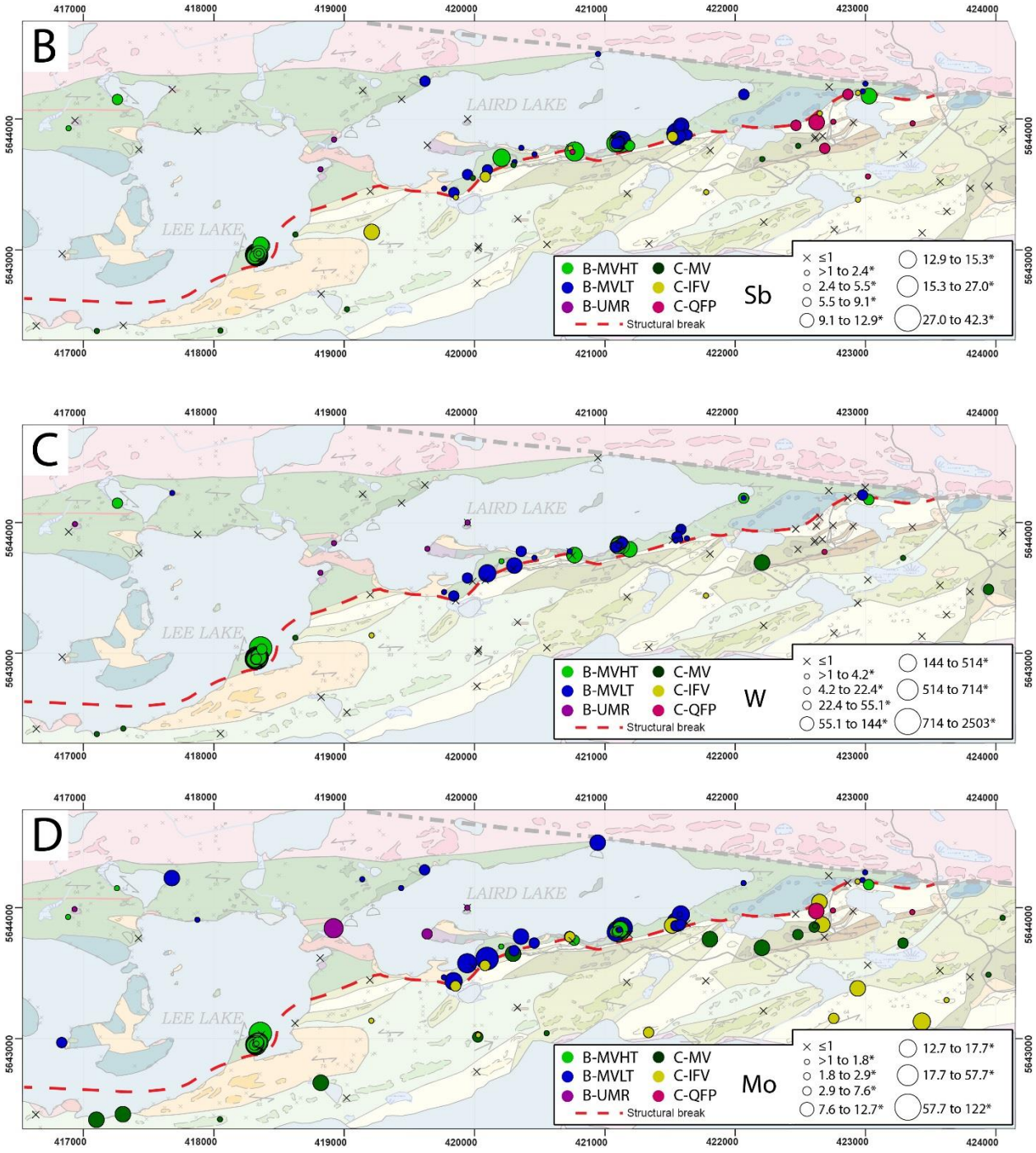

Figure 6.34 Continuation. B) Sb, C) W, D) Mo.

Overall, the alteration maps show fairly consistent enrichments (Figs. 6.32; 6.34) and depletions (Fig. 6.33) along the southern edges of Laird and Lee lakes, on the north side of the major break. The

mineral assemblage is consistent with amphibolite-grade wallrock alteration (McCuaig and Kerrich, 1998). The thickness of the metasomatic banding at outcrop scale is unknown due to overburden coverage and the southern edge of the Laird and Lee lakes, however, it averages between 2-5 metres. Where metasomatic banding was not observed, abundant biotite defines the main alteration zone, which extends pervasively across Laird and Lee lakes at an enrichement factor of 2-5.4 (Fig. 6.32A). Diopside was not observed in mafic volcanic rocks outside of the metasomatic banded zones and clinozoisite was rarely seen on the northern edges of Laird Lake. Therefore, the main alteration zone extends from the north-side of the structural break to the southern edge of Laird and Lee lakes, but could extend below the lakes for a maximum thickness of ~400m, whereas the distal alteration zone (biotite ± clinozoisite) extends the entire thickness of the Balmer assemblage (1.5km) at the Laird Lake property. Outliers found away from the main alteration zone represent the appearance of minor sulphides or alteration phases and do locally correlate with minor enrichments in gold.

6.3.2.2 Nature and Timing of Alteration and Mineralization

The main style of alteration and mineralization at the Laird Lake property is reflective of regional amphibolite facies metamorphism. The zone of most intense alteration coincides with metasomatic banding within the Balmer assemblage and is overprinted by the zone of most intense deformation. Alteration minerals include biotite, hornblende, diopside, clinozoisite ± garnet ± muscovite and ± calcite, whereas the dominant sulphide minerals include pyrite ± arsenopyrite ± pyrrhotite and ± chalcopyrite. Key relationships exist between these phases which can be used to develop an alteration and mineralization paragenesis (Fig. 6.35). The dominant style of Au-mineralization is hosted in metasomatic banded mafic volcanic rocks, suggesting the main period of alteration and mineralization occurred pre- to syn-ductile deformation. The Laird Lake area hosts a mineral assemblage representative of amphibolite grade metamorphism, however, local features indicate that the area underwent an early

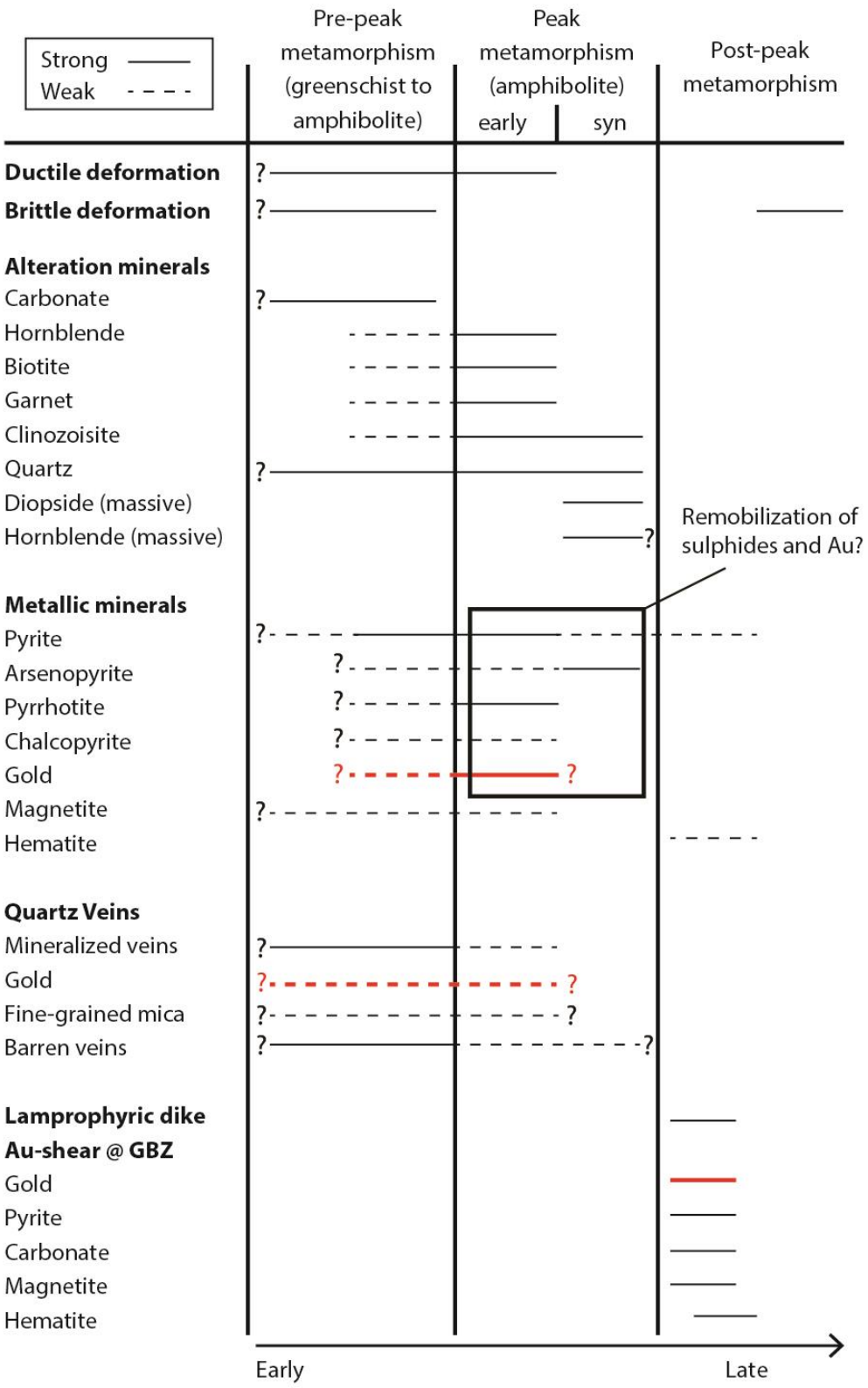

Figure 6.35 Wall-rock and vein paragenetic mineral sequences for the Laird Lake property, with an emphasis on the Lee Lake Au showing, GBZ and Pit Zone trench. Note that the GBZ trench also hosts mineralization within the metasomatic banded mafic volcanic unit of the Balmer assemblage.

stage of alteration and possible mineralization prior to peak metamorphism and was subsequently metamorphosed to amphibolite facies.

An early stage of alteration is suggested by the presence of carbonate pods and stringers with reaction rims composed of massive diopside crystals at the GBZ and Pit Zone trenches (Figs. 4.26B; 4.27F). Primary carbonate found within the carbonate formation at the HSZ trench also has diopside-rich borders (Fig. 4.4D). These observations suggest that carbonate veins, possibly from the same early D_2-carbonate alteration event throughout the RLGB (Parker, 2000a) were present at the Laird Lake property, but later metamorphosed and deformed to diopside-rich bands. Within the diopside-rich bands, sulphides are locally found as interstitial phases and never as inclusions within diopside crystals, suggesting that the early carbonate alteration was barren and sulphides were likely remobilized during prograde metamorphism.

The majority of the quartz veins throughout the Laird Lake property are likely to have formed pre-peak metamorphism as the conditions would be unfavorable for quartz vein formation at peak metamorphism, and also as they likely formed within a brittle-ductile regime since they trend parallel to foliation and brittle deformation would be required to form the veins. Quartz crystals and the fine-grained mica within the auriferous quartz vein at the Pit Zone trench (447A05) are foliated parallel to the vein margins, however, sulphides and visible gold are commonly found as interstitial phases to the silicate minerals or in fractures, suggesting they could be associated with a different fluid than the quartz forming fluid or are the product of remobilization. One of the barren veins (233A06) is discordant to the regional foliation and host quartz crystals which show no preferred orientation, suggesting this vein could have crystallized post-ductile deformation.

The bulk of the alteration minerals (biotite, hornblende (foliated), clinozoisite, garnet, quartz ± muscovite) are lacking consistent cross-cutting and inclusion relationships necessary to determine whether these minerals are the product of prograde metamorphism of an earlier alteration assemblage,

or if they represent an amphibolite grade alteration assemblage. Nevertheless, all phases are foliated and therefore were present pre- to syn-ductile deformation and were formed as a result of amphibolite grade metamorphism. This relationship is best displayed within the metasomatic banded mafic volcanic rocks of the Balmer assemblage. All foliated silicate phases are interpreted to have crystallized during prograde metamorphism up to amphibolite facies. The majority of sulphides are also preferentially oriented parallel to foliation, suggesting they crystallized pre- to syn-ductile deformation. Sulphides are disseminated and often confined to the biotite-quartz-muscovite-rich bands (Fig. 6.36A) which have likely absorbed most of the deformational stresses, and acted as zones of weakness and favorable areas for sulphide and gold precipitation between the more competent diopside and hornblende-rich bands. Gold is locally observed as free grains closely associated with sulphides (Fig. 6.36B), but is likely also present within the sulphides. The sulphides are typically disseminated, anhedral and elongated parallel to the foliation (Fig. 6.36A), however, arsenopyrite is usually euhedral to subhedral, with very little evidence of strain (Fig. 4.18B) which could suggest the arsenopyrite is recrystallized. The fact that the sulphides and gold are typically concentrated within the biotite-rich bands could suggest that they were

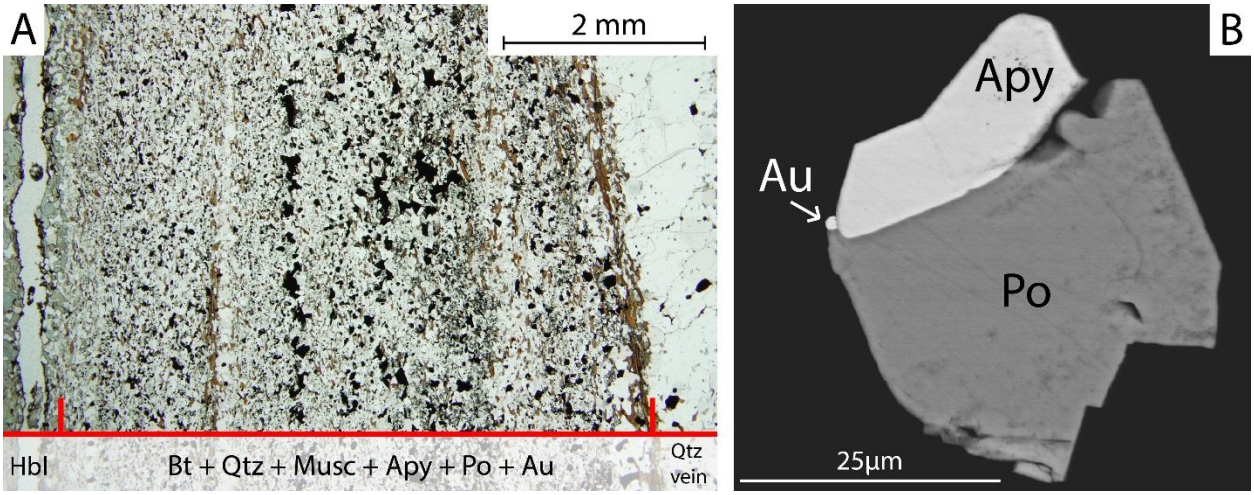

Figure 6.36 Photomicrograph and SEM photo of mineralization from the Lee Lake Au showing. A) Sulphides hosted within a biotite-quartz-muscovite-rich band between more competent quartz vein and amphibole band bordering a diopside-rich band. B) Arsenopyrite and pyrrhotite in close association with a gold grain. Sample 16BG296A04. ***Bt:*** *biotite,* ***Qtz:*** *quartz,* ***Musc:*** *muscovite,* ***Apy:*** *arsenopyrite,* ***Po:*** *pyrrhotite,* ***Au :*** *gold.*

remobilized into this zone of weakness during prograde metamorphism, since outside of the metasomatised banded unit, the sulphides and alteration minerals are disseminated throughout the host rock. Introduction of gold into the metasomatised banded unit is suggested to be syn-sulphide crystallization/remobilization as gold was likely transported by a gold-thiosulphide complex ($Au(HS)_2^-$) since there is a positive correlation between gold grades and sulphur content (Fig. 6.30). Cubic pyrite is not present within the metasomatic banded unit, but, outside the zone of strongest deformation, cubic pyrite was rarely observed and is often rimmed by hematite, likely caused by post-peak metamorphism supergene weathering.

At peak metamorphism and post-ductile deformation, some alteration phases were likely recrystallized and as a result, unfoliated diopside and hornblende crystals are present within the metasomatised banded unit. The diopside bands are composed of completely unfoliated diopside, rare quartz crystals and local interstitial sulphides. The diopside grains host no inclusions. Bordering the diopside bands are coarser-grained unfoliated poikiloblastic hornblende crystals (Figs. 4.17A; 4.18A). This rim could represent the original alteration rim of the carbonate vein. The hornblende crystals host inclusions of sulphides, quartz and diopside, suggesting they were the last phase to recrystallize and could represent overprinting of a retrograde assemblage.

At the GBZ trench, metasomatised banded mafic volcanic rocks are cut by a shear with pyrite, magnetite and hematite-rich borders and a bright orange brittle core (Fig. 4.26E, F). The pyrite is subhedral and often surrounded by hematite. Calcite stringers and pods are also associated with the margins of the shear (Fig. 4.26D). The margins of the shear yielded 423 ppb Au (sample GBZ-M15-020), however, at the intersection of the shear and BIF, gold grades exceed >3600 ppb Au (sample GBZ-O15-023). This gold-bearing shear could represent a second gold event as it cuts the metasomatic banded rocks hosting mineralization from the first gold event (disseminated sulphide associated), the minerals associated with the margins of the shear are not foliated, plus the calcite stringers show no evidence of

replacement by diopside, suggesting the shear and associated phases were both post-peak metamorphism and ductile deformation, and likely represent a second gold mineralizing event. Similar mineralization is found within the Confederation assemblage in a quartz-feldspar porphyritic crystal tuff, in which magnetite, pyrite and lesser hematite veins cut the volcanic rock parallel to foliation (Station 15BG039; UTM 422756E 5643969N; Fig. 4.19C). Euhedral to subhedral pyrite crystals are rimmed and brecciated by hematite (Fig. 4.19D). The lack of preferential orientation within the sulphides and euhedral nature of the pyrite suggest this mineralization occurred post-ductile deformation and is different from the first gold mineralizing event, however, gold values only reached up to 24 ppb Au. These observations suggest that the second event of gold mineralization is likely associated with an oxidizing fluid occurring post-peak metamorphism and post-ductile deformation. A lamprophyric dike with 296 ppb Au is also found cutting the regional foliation within the Balmer assemblage, suggesting post-D_2 magmatic activity may be introducing or remobilizing gold.

A second phase of brittle deformation is marked by the presence of late sinistral faults best observed at the GBZ trench. The faults trend N to NW and displace all units at a centimetre to metre scale (Figs. 4.22; 4.24D).

6.3.2.3 Quartz Veins and Oxygen Isotopes

A total of four quartz veins were analysed for $\delta^{18}O_{quartz}$, with $\delta^{18}O_{H2O}$ recalculated for temperatures between 300-500°C with the appropriate mineral-H_2O fractionation equation (Matsuhisa et al., 1979; Beaudoin, 2011; Appendix D) in order to compare the Laird Lake dataset to other mineralizing fluids within orogenic gold systems. It is important to distinguish $\delta^{18}O_{quartz}$ from $\delta^{18}O_{H2O}$ since the isotope will fractionate within a system through equilibrium isotope fractionation. Due to the differences in mass and bond-strength between the various isotopes, the heavier isotope typically fractionates into the more closely packed crystal structure and the lighter isotope fractionates to the phase with weaker bonds (e.g., solid vs liquid, liquid vs gas; Rollinson, 1993; White, 2013). Additionally,

isotopic fractionation between various phases decreases with increasing temperatures, therefore, at higher temperatures, the $\delta^{18}O_{H2O}$ will show less variation between the phases (Rollinson, 1993). During the formation of quartz veins, ^{18}O will preferentially fractionate within the quartz (solid) and ^{16}O will preferentially stay within the fluid phase resulting in the $\delta^{18}O_{quartz}$ being more enriched than $\delta^{18}O_{H2O}$.

Since the isotope system is temperature dependent, it is important to have a proper estimate for the vein crystallizing temperature, however, the limited dataset in this study (lack of fluid inclusion data, lack of O isotope on additional phases in the quartz veins and associated alteration phases, and lack of primary textures in the quartz veins) limits the ability to calculate an accurate temperature for vein formation. The $\delta^{18}O_{H2O}$ was calculated using temperatures between 300-500°C as these coincide with the temperatures inferred for the brittle-ductile zone, in which auriferous quartz veins typically form and overlap with lower greenschist to lower amphibolite facies metamorphic conditions (McCuaig and Kerrich, 1998; Dubé and Gosselin, 2007). Fluid inclusion studies performed on Au-rich quartz veins have consistently shown that the mineralizing conditions occur at 300-350°C (Ho et al., 1985; Ridley and Diamond, 2000), however, higher temperatures (up to 500°C) have been inferred to allow for a wide range of possibilities within such a dynamic system. The $\delta^{18}O_{H2O}$ is not expected to reflect the source of the mineralizing fluid, instead it is a measured composition that reflects the fluid-rock interactions as the fluid travels along its pathways. The fluid-rock interaction can include the mixing of fluids from various sources and the interaction between the fluid and various wallrocks (Ridley and Diamond, 2000).

The $\delta^{18}O_{H2O}$ values for the vein-forming fluids for the four quartz veins show a large variation between the various calculated temperatures. At 300°C, the $\delta^{18}O_{H2O}$ values range from 2.4-7.23‰, at 400°C the $\delta^{18}O_{H2O}$ values range from 5.23-10.03‰ and at 500°C the $\delta^{18}O_{H2O}$ values range from 7.2-11.3‰. Data from sample 447A05 is plotted to show the wide range in $\delta^{18}O_{H2O}$ values for temperatures between 300-500°C (Fig. 6.37).

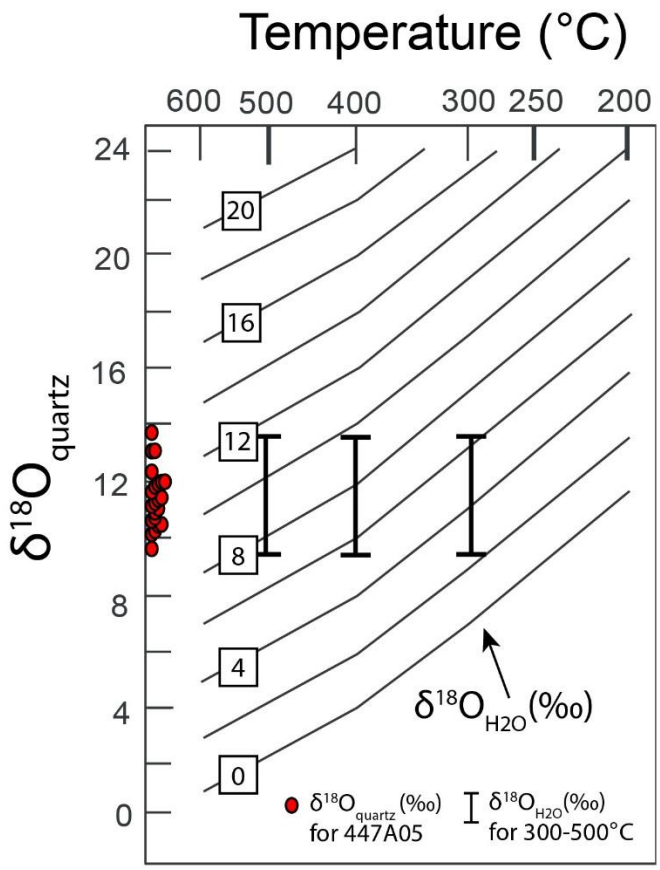

Figure 6.37 Plot of temperatures (°C) versus $\delta^{18}O_{quartz}$ (sample 447A05) with isopleths of $\delta^{18}O_{H2O}$, and calculated $\delta^{18}O_{H2O}$ values using the quartz-H_2O fractionation equation of Matsuhisa et al. (1979). The $\delta^{18}O$ quartz vein data for sample 447A05 is shown in red circles. The bar lines indicate the $\delta^{18}O_{H2O}$ values based on quartz precipitation at 300-500°C, as discussed in the text. Error on $\delta^{18}O_{quartz}$ and $\delta^{18}O_{H2O}$ values are ±1.2‰. Figure modified after Kontak et al. (2011).

The $\delta^{18}O_{H2O}$ values range from 2.4-11.3‰ at 300-500°C which overlaps with fields for meteoritic, magmatic and metamorphic waters (Fig. 6.38). No alteration halos to the quartz veins were observed on the Laird Lake property (with the exception of sample 233A05) which could indicate that the interaction between the fluid and host rock at the site of quartz vein formation was minimal. A number of scenarios could have occurred to produce the range of $\delta^{18}O_{H2O}$ observed on the Laird Lake property, however, additional O isotope analyses on the fine-grained clays within sample 447A05 (Fig. 4.20C) and O isotope values for the surrounding host rocks would be required to further constrain the history of the quartz vein-forming fluid. Fluid inclusion analyses would likely yield ambiguous results as at amphibolite facies metamorphism the likelihood of preserving primary fluid inclusions is low (McCuaig and Kerrich, 1998). Nevertheless, the origin of the vein fluids can be established based on the age of mineralization in the Red Lake camp and the reservoirs present at the time of vein formation. In the case of the Laird Lake

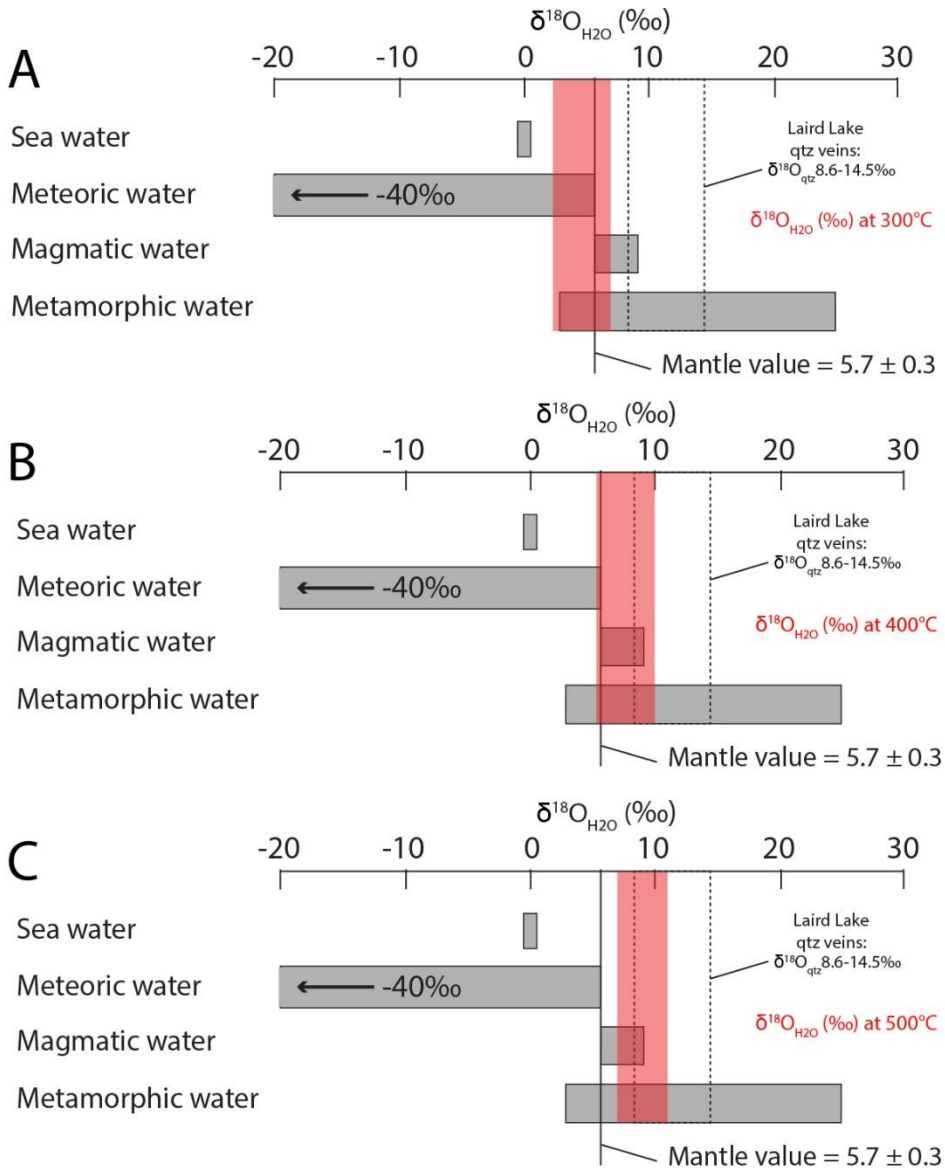

Figure 6.38 Natural oxygen isotope reservoirs (Rollinson, 1993; Beaudoin, 2011) compared to Laird Lake quartz veins $\delta^{18}O_{H2O}$ values at A) 300°C, B) 400°C and C) 500°C. Error on $\delta^{18}O_{quartz}$ and $\delta^{18}O_{H2O}$ values are ±1.2‰.

property, the formation of the auriferous quartz veins is estimated to have occurred syn-D_2 which is constrained to 2720-2715 Ma in the RLGB and is interpreted to be the result of continent collision during the Uchian phase of the Kenoran orogeny (Dubé et al., 2004; Sanborn-Barrie et al., 2004). Given the tectonic setting present at the time, it is evident that metamorphic fluids formed through dehydration during prograde metamorphism were present in the system, however, magmatic fluids could have also

been present as intrusive bodies such as the Dome stock (2718.2±1.1 Ma; Corfu and Wallace, 1986) and McKenzie Island Stock (2720^{+3}_{-2} Ma; Corfu and Andrews, 1987) were emplaced syn-D_2. Therefore, a mix between metamorphic and magmatic fluids cannot be ruled out with the available dataset.

Of the four quartz veins analyzed for O isotopes, two of which are Au-mineralized and host pyrite ± chalcopyrite ± pyrrhotite ± fine-grained clays whereas the remaining two quartz veins are barren and contain no accessory phases. Three of the analyzed veins trend parallel to foliation, suggesting the veins formed syn-deformation. All veins show quartz crystals with undulose extinction and variable degrees of subgrain formation. These textures are typical of higher temperatures and pressures which correspond to upper greenschist through amphibolite facies in which primary vein textures such as crack and seal, zonations, mineral fibers and laminations (Dubé and Gosselin, 2007) will be destroyed (McCuaig and Kerrich, 1998). The destruction of primary textures inhibits the ability to recognize potential generations of vein forming events and therefore oxygen isotopes can help identify compositionally different fluid phases.

Oxygen isotope analyses for the four quartz veins show minimal differences between the Au-mineralized and barren quartz veins (Table 5.2; Fig. 6.39), suggesting that the fluids originated from a similar reservoir or alternately, that fluid-rock interaction and/or fluid mixing yielded isotopic compositions of similar ratios. The latter is unlikely, as there are a number of components that can influence the isotopic composition of a fluid and this would likely not result in averaged compositions that only vary by 0.2‰ (Table 5.2). In-situ O isotope traverses across each quartz vein show no systematic patterns from core to rim (Fig. 6.39). Sample 233A05 shows a slight depletion in $\delta^{18}O_{quartz}$ values in the core of the vein compared to the outer edges of the vein, suggesting a symmetric growth with more depleted fluids at the final stages of vein formation, assuming the vein crystallized from the wallrock inwards. Petrographic observations indicate that all four veins show fairly homogeneous textures across the width of the vein. Metamorphism up to amphibolite facies likely destroyed any

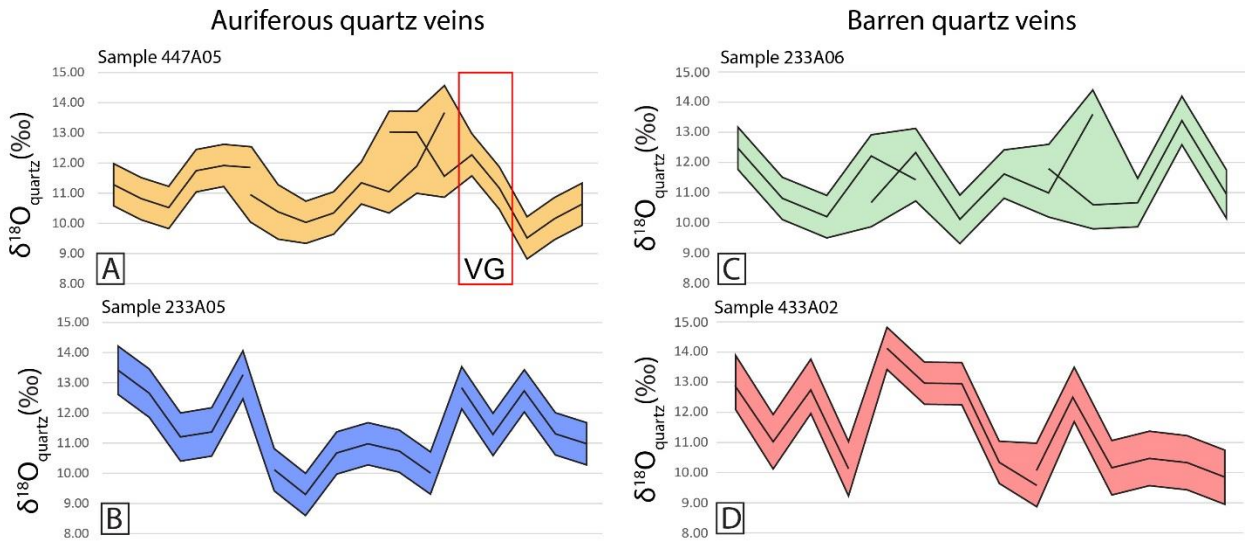

Figure 6.39 Plots of $\delta^{18}O_{quartz}$ values across the width of the quartz veins. Solid lines represent the measured $\delta^{18}O_{quartz}$ values whereas coloured areas represent the error margin. Overlap between the samples are represented by intersecting solid lines. Plots A and B are of Au-mineralized veins, plots C and D are of barren veins. A) sample 447A05, B) sample 233A05, C) sample 233A06, D) sample 433A02. VG: location of visible gold.

primary vein features and could have disrupted the isotopic system (Cartwright et al., 1995). Also, in order to produce the most continuous traverse across the quartz vein, two thin sections were produced, in which the thin section sampling the core of the vein was taken below the thin section sampling the edges of the veins in order to have some overlap between the analyses (Appendix D Figs. 4.2; 4.4; 4.6; 4.8). The discontinuous traverse could explain the apparent depletion in the core of sample 233A05 (Fig. 6.39) if the $\delta^{18}O_{quartz}$ values represent a part of the vein which formed from a different fluid or if metamorphism affected the core of the vein to a lesser degree. However, petrographic observations argue against the latter, as the core and vein edge show the same degree of strain.

Sample 447A05 is the only vein which hosts visible gold (VG; Appendix D; Fig. 4.2A). The gold grains are distributed along a horizon parallel to the vein margin and regional foliation, which likely represents a primary reactive front which favored gold precipitation during a time of favorable P-T conditions. The gold grains are also closely associated with very fine-grained micas (Fig. 4.20C) ± fine-grained pyrite, which could suggest a change in fluid chemistry in the gold-mineralizing fluid compared

to the remaining quartz vein. However, the $\delta^{18}O_{quartz}$ values across sample 447A05 (Fig. 6.39A) do not suggest a significant change in isotope composition at the site of the visible gold. Instead, an enrichment in $\delta^{18}O_{quartz}$ values (~13‰) is observed directly to the left of the visible gold (Fig. 6.39A), where the very fine-grained micas are still present but absent elsewhere in the sample. This could suggest that the fluid precipitating the fine-grained micas is slightly enriched in $\delta^{18}O_{quartz}$ relative to the rest of the vein, and is potentially responsible for the transport and precipitation of gold within the quartz vein. Conversely, since the visible gold is found at the boundaries of quartz grains and not as inclusions within the quartz, it is possible that the gold is superimposed and late relative to the quartz vein formation, or that the gold has been remobilized during recrystallization or deformation (McCuaig and Kerrich, 1998).

6.3.3 Comparison with the Past-Producing Madsen Mine

The past-producing Madsen mine is located roughly 10 km east of the Laird Lake property and is the second largest deposit in the Red Lake district with over 75.16 t of gold and 12.99 t of silver produced from 1938 to 1976 (Fig. 2.6; Durocher, 1983; see section 2.3.5). The deposit is located on the structural break between the Balmer and Confederation assemblages in two main ore zones; the Austin and McVeigh horizons hosted by deformed hydrothermally altered mafic volcaniclastic and epiclastic rocks, and basalt flows of the Balmer assemblage (Fig. 6.40; Dubé et al., 2000). Dubé et al. (2000) suggested that the structural break between the Balmer and Confederation assemblages represents an angular unconformity marked by the presence of epiclastic rocks within the Austin horizon, however, the contact was interpreted to be reactivated. The ore is hosted in metasomatic banded units which are foliated, consistent with pre- to early D_2 timing of gold mineralization. The Madsen deposit has been described as an Archean disseminated, stratabound, replacement-style gold deposit which shares similarities with higher temperature (400-600°C) gold deposits and gold skarns hosted by mafic rocks

(Dubé et al., 2000), but also shares many features with the Laird Lake property. The following section summarizes the similarities and differences between the two areas.

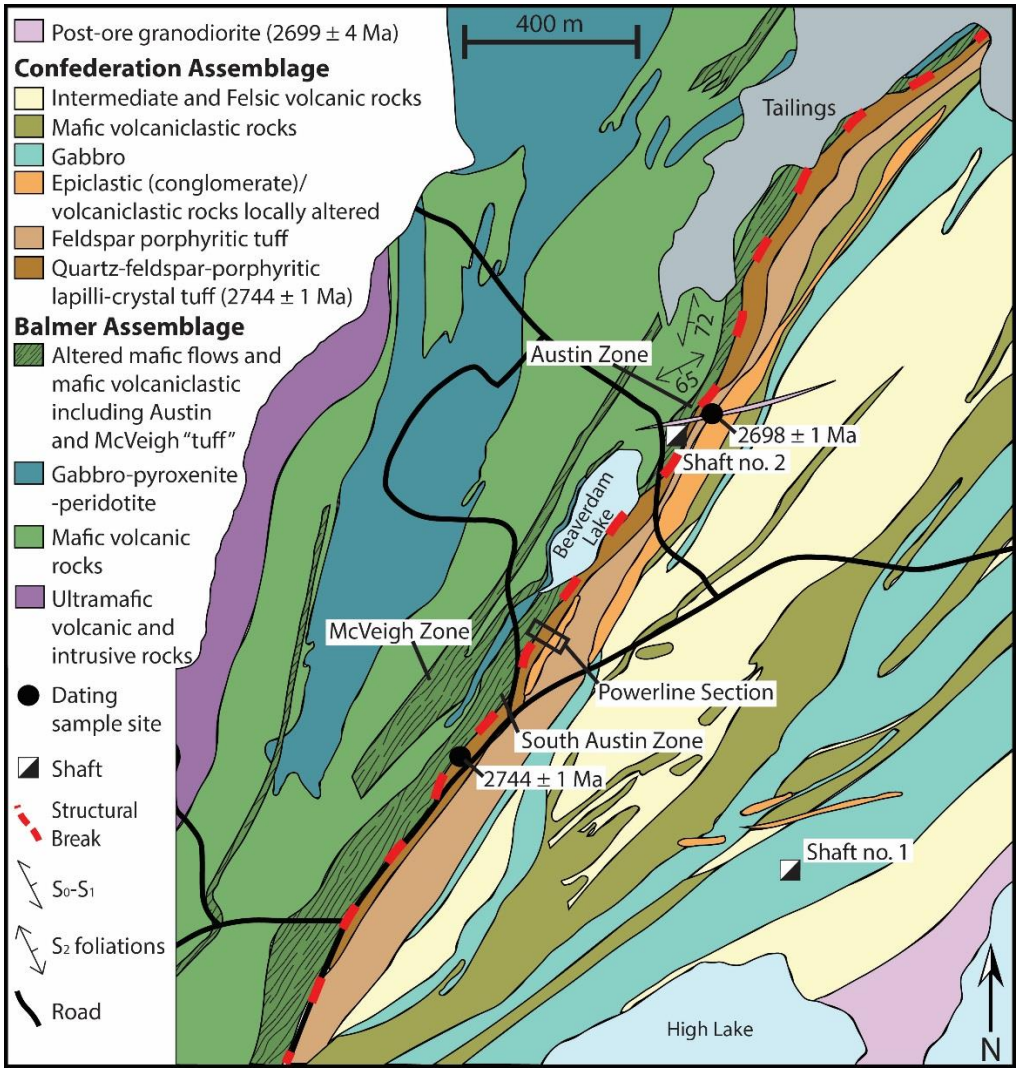

Figure 6.40 Geological map of the Madsen mine area, showing units striking parallel to the structural break and similar lithologies to the Laird Lake area (modified after Dubé et al., 2000).

The Balmer and Confederation assemblages at the Laird Lake and Madsen area are composed of very similar lithologies, with the exception of the conglomerate and gabbro units within the Confederation assemblage and an epiclastic component within the Balmer assemblage in the Madsen area which are not present in the Laird Lake area. At the Powerline Section just south of Beaverdam Lake (Fig. 6.40), an exposure of the contact between the Balmer (Austin ore zone) and Confederation

assemblages is present. Here, the Balmer assemblage is strongly altered and shows metasomatic banding with alternating bands that are biotite-, amphibole- and clinozoisite-rich with local garnet and diopside-rich sections (Figs. 6.41A, B). The unit shows local folding (Fig. 6.41C) and appears to be identical to the metasomatic banding found at the Laird Lake property (Fig. 4.12). Closer to the contact with the Confederation assemblage, an epiclastic component is present and the Balmer is composed of 20% wacke/tuff (?) clasts (Fig. 6.41D; Lichtblau et al., 2011). This unit is not present on the Laird Lake property, either due to the higher strain and lack of preservation of primary features near the structural break or the Laird Lake property possibly representing a deeper level of erosion compared to the Madsen area. The contact between the two assemblages at the Powerline Section is fairly sharp (Fig. 6.41E) with a mix of contorted Austin "tuff" and clasts in contact with the weakly to moderately foliated quartz-feldspar porphyritic crystal tuff of the Confederation assemblage (Fig. 6.41E). Clasts within the Balmer and quartz/feldspar phenocrysts within the Confederation are both preferentially oriented parallel to the contact. The contact at the Laird Lake property was never directly observed, however, chaotic folding (Fig. 6.42) or metasomatic banding (Fig. 4.12) was commonly observed near the contact.

The alteration at the Madsen area is subdivided into inner and outer alteration zones. The aluminous outer alteration is barren to anomalous in gold and is defined by the presence of metre- to tens-of-metres wide zones containing andalusite, garnet, biotite, staurolite, and amphibolite alternating with metre-wide zones of stockwork amphibole veining (Fig. 6.41F; Dubé et al., 2000). The Laird Lake property likely experienced this type of alteration to a lesser degree since andalusite and staurolite were never observed and stockwork amphibole veining was rarely present. The inner alteration zone in Madsen is characterized by metre- to a few tens of metres wide zones hosting metasomatic layering composed of amphibole-rich bands alternating with biotite-rich layers (Fig. 6.41A) which is the most characteristic feature of the mineralization at Madsen (Austin and McVeigh ore horizons; Dubé et al.,

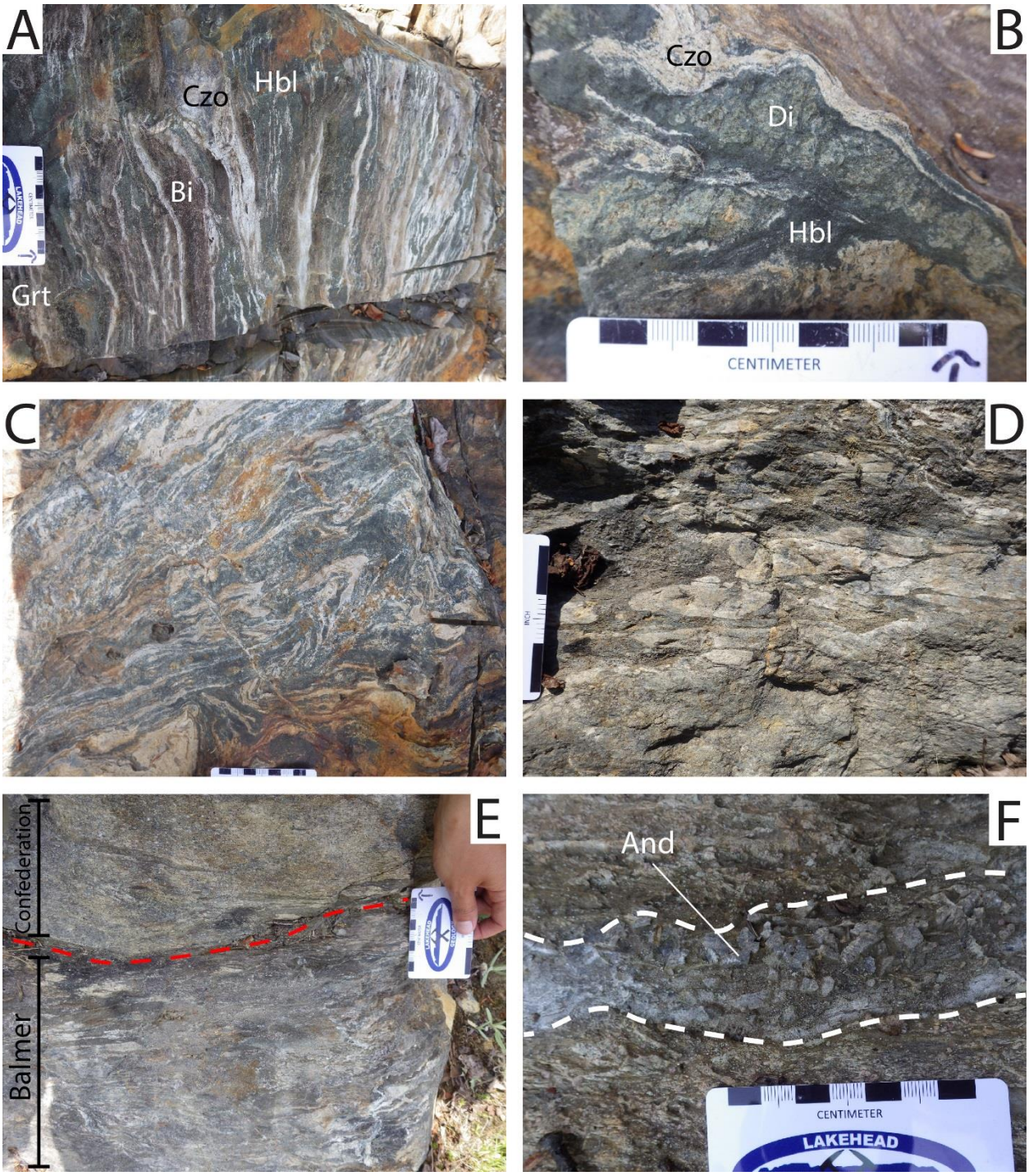

Figure 6.41 Photographs from the Powerline section near the Madsen mine. A) Metasomatic banding within Balmer mafic volcanic rocks, showing alternating biotite-, hornblende-, and clinizoisite(?)-rich bands and local garnet-rich section. B) Close up of a coarse-grained diopside section associated with hornblende- and clinozoisite(?)-rich bands. C) Contorted metasomatic banding showing chaotic folding. D) Epiclastic section within the Balmer assemblage with wacke/tuff (?) clasts. E) Sharp contact between Balmer and Confederation assemblages showing contorted and brecciated rock (Lichtblau et al., 2016b) overlain by quartz-feldspar porphyritic crystal tuff. F) Andalusite-rich matrix within the Huston conglomerate unit overlaying the quartz-feldspar porphyritic crystal tuff. ***And:*** *andalusite,* ***Bi:*** *biotite,* ***Czo:*** *clinozoisite,* ***Di:*** *diopside,* ***Grt:*** *garnet,* ***Hbl:*** *hornblende.*

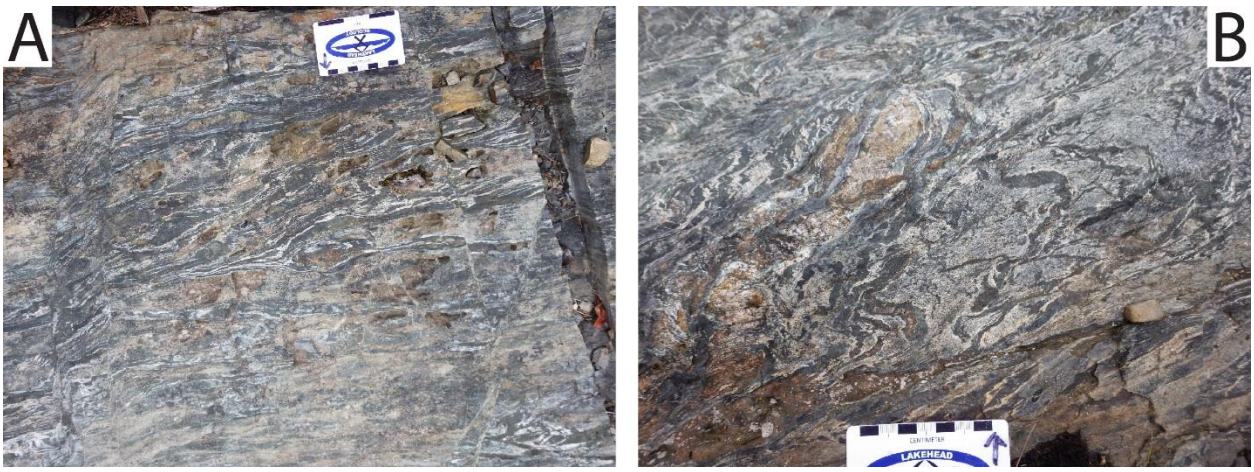

Figure 6.42 Contorted Balmer assemblage mafic volcanic rocks roughly 5m away from the overburden covered contact with the Confederation assemblage at the Laird Lake property (Station 15BG445; UTM 420311E 5643677N). A) Typical contorted mafic volcanic rocks of the Balmer assemblage. B) Chaotic folding.

2000). The bands are typically foliated by S_0-S_1 and/or S_2, where biotite is always oriented parallel to foliation, but amphibole is commonly randomly oriented. Non-foliated versions of the inner alteration zones are present and suggest heterogeneous strain within the ore zone (Dubé et al., 2000). Diopside, garnet and clinozoisite are common minerals present within this unit, whereas staurolite and andalusite are absent. Sulphides within the metasomatic banded unit include: pyrite, arsenopyrite and pyrrhotite, trace chalcopyrite, sphalerite and magnetite with rare realgar and orpiment (Butler, 1955; Dubé et al., 2000). Within the Austin and McVeigh ore zones, sulphides can increase up to 8-10% and in local zones with 10-15% disseminated arsenopyrite, gold grades can elevate to 120 g/t and are commonly associated with silicious alteration (quartz, muscovite and tourmaline). The inner alteration zone at Madsen shows many similarities with the Laird Lake area in terms of texture and mineralogy associated with elevated gold grades. The Lee Lake Au showing is most similar to the inner alteration zone observed in Madsen as both areas display metasomatic banding parallel to S_2 (Fig. 4.12) in which most phases present within this unit are parallel to foliation with the exception of some amphibole and diopside bands at the Lee Lake Au showing (Fig. 4.17A). Both areas have similar mineralogy including biotite, amphibole, diopside, quartz, clinozoisite ± garnet and an increase in gold is usually associated with arsenopyrite, pyrrhotite and quartz (Fig. 6.36A).

Least altered mafic volcanic rocks and the Lee Lake Au showing samples form the Laird Lake property were compared to samples from the Austin horizon at the Powerline Section (Fig. 6.43) on the Madsen property. A total of 12 samples from the Balmer assemblage at the Powerline Section were collected in 2010 as part of the federal-provincial NATMAP program in the RLGB from 1999 to 2004 (Lichtblau et al., 2011). The comparisons between the Lee Lake Au showing and the Austin horizon at the Powerline Section are limited by the available dataset, as S, CO_2 and As were not analysed at the Powerline Section. Also, descriptions of the samples taken at the Powerline Section were not provided. Three of the least altered samples from the Laird Lake property were chosen based on their lack of alteration and sulphide phases as well as the distance from the major break or more strongly deformed zones.

Geochemically, the Lee Lake Au showing plots as intermediate between least-altered Balmer mafic volcanic rocks of the Laird Lake property, and samples from the Austin horizon at the Powerline Section (Fig. 6.43). Figure 6.43A best displays this relationship, as the samples from the Lee Lake Au showing plot between high-Na/low-K unaltered mafic volcanic rocks, and low-Na/high-K Austin horizon mafic volcanic rocks. This suggests that the rocks at the Lee Lake Au showing are less altered than the ones at the Powerline Section. This relationship is also seen with Sb, Ba ± Pb (Figs. 6.43C, E, F) with a few anomalies. The Lee Lake Au showing has higher concentrations of Ca and Cu, likely due to the more abundant diopside and chalcopyrite, respectively (Figs. 6.43B, D). Gold concentrations at the Austin horizon at the Powerline Section ranges from <6-431 ppb Au, whereas the Lee Lake Au showing range from 5-17190 ppb Au, however, the majority of samples host 5-400 ppb Au (Figs. 6.43G, H). Higher concentrations of Sb are locally present at the Austin horizon, but W concentrations are in the same range in both areas.

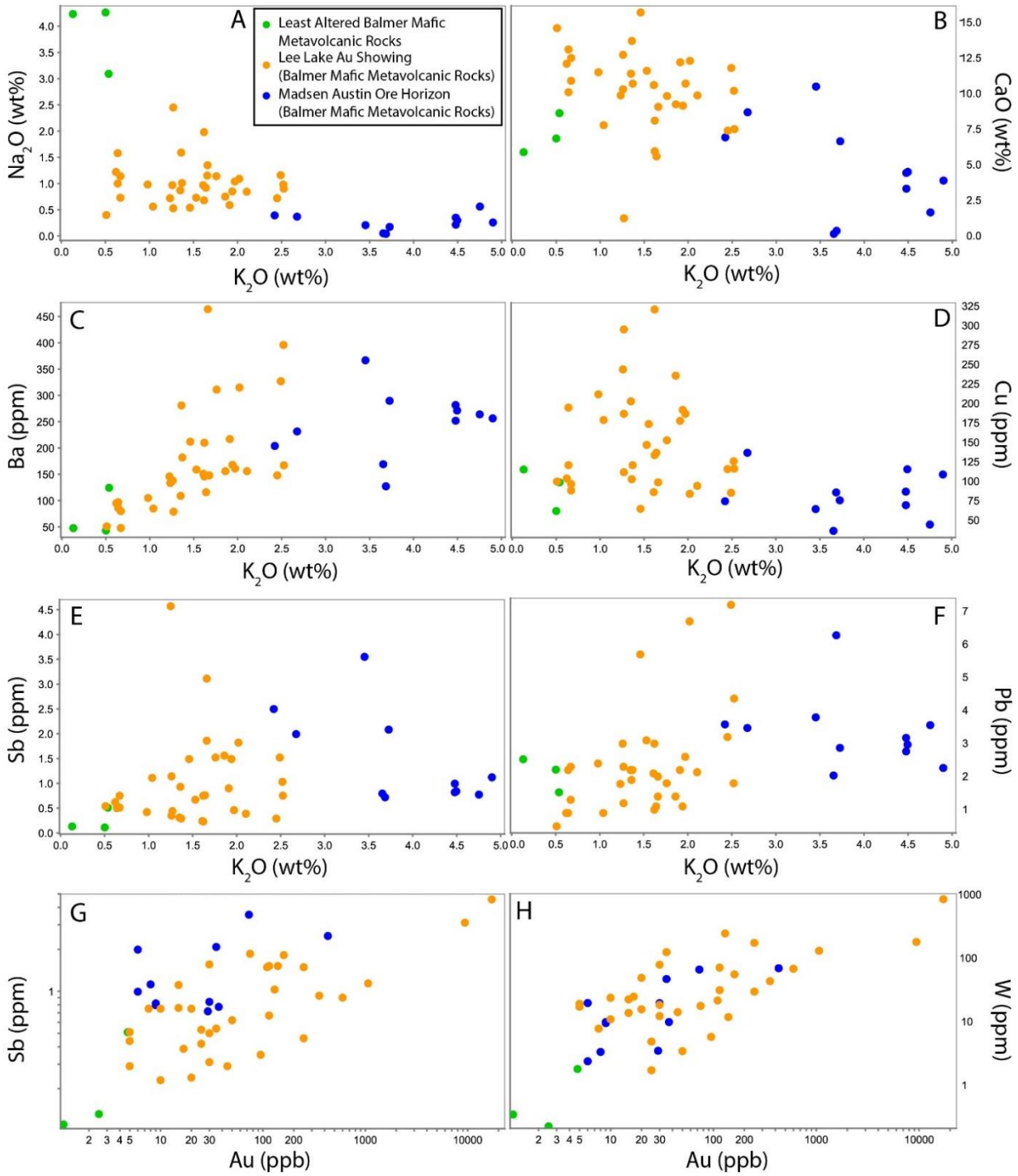

Figure 6.43 Bivariate diagrams showing the elemental depletions and enrichments within the Balmer assemblage between least altered precursors from the Laird Lake area, samples from the Lee Lake Au showing and samples from the Austin horizon at the Powerline Section in Madsen.

6.3.4 Sequence of Events

The study area has been affected by multiple episodes of igneous activity, deformation and metamorphism, and alteration/mineralization events. The proposed timing of events is summarized in Figure 6.44. Initially, 3.0 Ga North Caribou crust was formed and served as the basement to 2.99-2.96 Ga (Corfu and Wallace, 1986) plume magmatism of the Balmer assemblage (Fig. 6.24; see section 6.2.1). Subaqueous eruptions allowed for the formation of pillow basalts and the deposition of BIF. Elsewhere in the RLGB, the Ball, Bruce Channel, Slate Bay and Trout Bay assemblages were deposited in plume-related, subduction zone, shallow marine, fluviatile, deep oceanic and explosive volcanic environments between 2.94 Ga (Corfu and Wallace, 1986) and 2.85 Ga (Skulski (unpublished) referenced in Sanborn-Barrie et al., 2004; see section 2.3.1). The Confederation assemblage was later produced within an oceanic arc system off the coast of the growing North Caribou Terrane between 2.46 Ga (Corfu and Andrews, 1987) and 2.39 Ga (Corfu and Wallace, 1986; Fig. 6.27; see section 6.2.2).

Juxtaposition of the Confederation assemblage against pre-existing assemblages of the RLGB is interpreted to have occurred pre-D_1 (<2742 to 2733 Ma; Sanborn-Barrie et al., 2001) as the Confederation is affected by both S_1 and F_1 (Sanborn-Barrie et al., 2004), but would be post-formation of the Confederation (<2739 Ma) as the assemblage is in tectonic contact with the Balmer at the Laird Lake property, with no evidence of an unconformity. This gives an estimate of 2739-2733 Ma for the juxtaposition of the Confederation onto the pre-existing assemblages of the RLGB. The contact between the Meso- and Neoarchean assemblages marks a zone of weakness in the RLGB stratigraphy, which was later reactivated during D_2 deformation.

Sanborn-Barrie et al. (2001) proposed a D_0 event (<2894-2744 Ma) in which the Balmer assemblage was overturned, as the pillows of the mafic volcanic rocks are facing away from the younger Confederation assemblage. An overturning event is critical for a model involving an unconformable

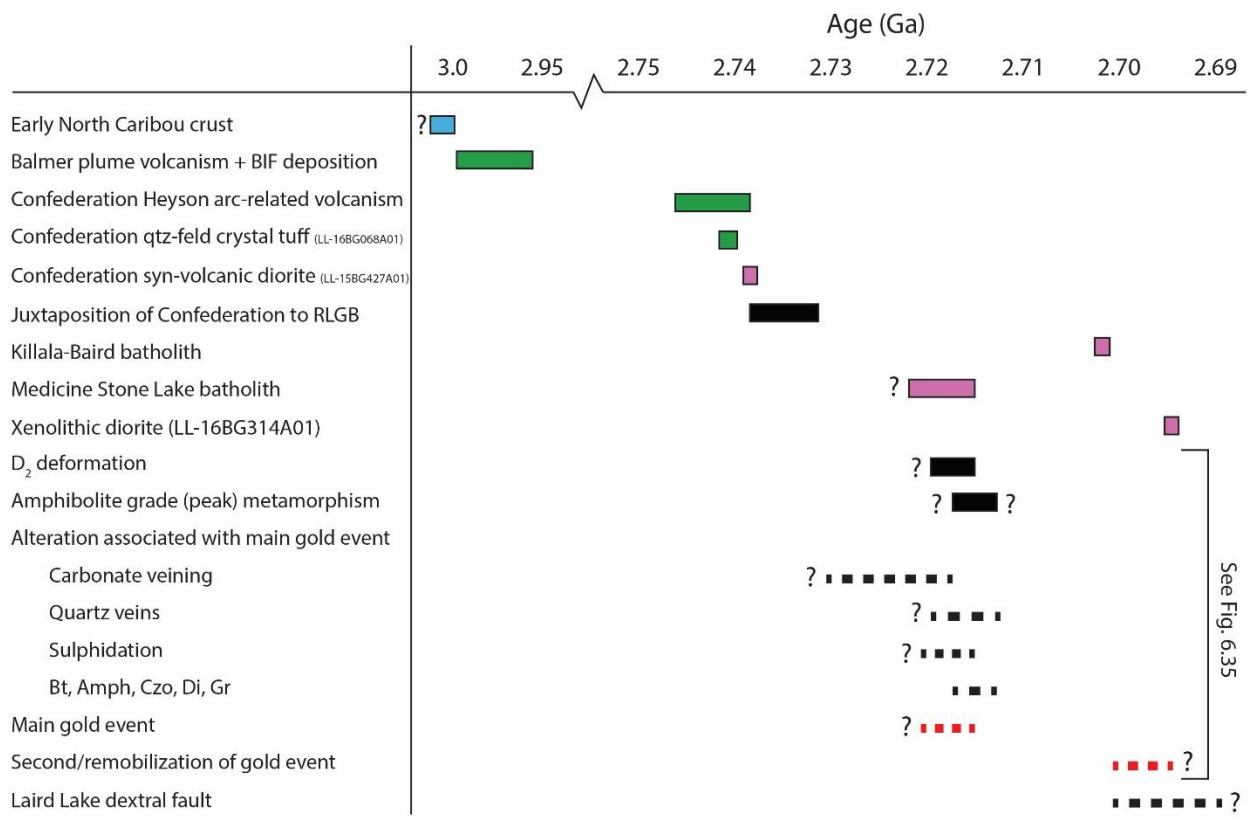

Figure 6.44 Schematic representation of the timing of geologic events in relationship to gold mineralization at the Laird Lake property. Age of early North Caribou crust from Stone (1998); Balmer assemblage = 2992 +2-/-9 Ma rhyolitic ash flow breccia (zircon age, Corfu and Wallace, 1986), 2964 +5/-1 Ma rhyolite (zircon age, Corfu and Wallace, 1986); Confederation assemblage Heyson sequence = 2746 +30/-17 Ma spherulitic felsic flow (zircon age, Corfu and Andrews, 1987), 2739 ± 3 Ma rhyolitic crystal tuff (zircon age, Corfu and Wallace, 1986), Quartz-feldspar porphyritic crystal tuff (LL-16BG068A01) = 2741 ± 19 Ma (zircon age, this study), Syn-volcanic diorite (LL-16BG427A01) = 2737.68 ± 0.79 Ma (zircon age, this study); Juxtaposition of Confederation onto RLGB between 2739 Ma (youngest Confederation age, Corfu and Wallace, 1986) and 2733 Ma (rhyodacite tuff of Graves assemblage, Corfu and Wallace, 1986); Killala-Baird batholith = 2704 ± 1.5 Ma (zircon age, Corfu and Andrews, 1987); Medicine Stone Lake batholith = pre- to syn-tectonic (Sanborn-Barrie et al., 2004); Xenolithic diorite (LL-16BG314A01) = 2695 ± 3.9 Ma (zircon age, this study); Carbonate and quartz veining is early- to pre-D_2 with maximum age unknown; Amphibolite grade alteration mineral assemblage is syn- to post-D_2; Sulphides associated with Au-mineralization is pre- to syn- D_2; Main gold event is associated with sulphides foliated by S_2 is early- to pre-D_2 with possible remobilization post-D_2; Second/remobilization of gold event is post-D_2 and constrained in the RLGM by a lamprophyric dike cutting Au-mineralization from the main gold event (<2702 ± 1 Ma, zircon age, Dubé et al., 2004); Laird Lake dextral fault occurred post-2704 ± 1.5 Ma as it cuts the Killala-Baird batholith.

contact between the Balmer and Confederation assemblages (Parker, 2000a; Sanborn-Barrie et al., 2001; Dubé et al., 2004). However, opposing younging directions recognized in this study and elsewhere in the RLGB is interpreted to represent a tectonic contact in which overturning of the Balmer assemblage is not critical.

D_2 deformation is estimated to have occurred between 2720-2715 Ma as part of the Uchian phase of the Kenoran Orogeny (Sanborn-Barrie et al., 2004). The Dome stock (2718 Ma, Corfu and Wallace, 1986) hosts xenoliths foliated by S_2 but itself is also foliated by S_2 suggesting that penetrative deformation and associated amphibolite facies metamorphism encompassed the emplacement of the intrusion (Dubé et al., 2004). At the Laird Lake property, all volcanic rocks and syn-volcanic intrusions are foliated by S_2 and several post-D_2 intrusions are massive and cross-cut the foliated rocks. The Medicine Stone Lake batholith is interpreted to have been emplaced pre- to syn-D_2 as the intrusion hosts S_2 fabrics (Sanborn-Barrie et al., 2004). Within the mafic volcanic rocks of both assemblages, the dominant mineralogy consists of foliated hornblende, biotite, quartz, plagioclase ± garnet, suggesting amphibolite grade metamorphism occurred syn-D_2. However, in the higher strain corridor associated with the tectonic contact between the Balmer and Confederation assemblages, unfoliated diopside and amphibole are present, suggesting peak amphibolite facies metamorphism also post-dates ductile D_2 deformation (Fig. 6.35).

During D_2 deformation, the deformational regime likely straddled the brittle-ductile zone as carbonate and quartz veins parallel to S_2 fabrics are present in the field area and then became dominantly ductile as the majority of veins show high strain parallel to S_2. The structural contact between the Balmer and Confederation assemblage was likely reactivated and acted as a zone of weakness for ductile deformation and fluid mobility (see section 6.3.1.1).

The carbonate veins on the Laird Lake property have accommodated a significant amount of D_2 strain as these are often boudinaged and have been partly to fully recrystallized to diopside during peak metamorphism, suggesting they were emplaced early- or pre-D_2 and pre-peak metamorphism. The majority of the quartz veins are parallel to S_2 and show undulose extinction within the quartz crystals suggesting these veins were also emplaced early- to syn-D_2. These relationships give a minimum age of 2715 Ma for the emplacement of the carbonate and quartz veins. Cross-cutting relationships at the Red

Lake Gold Mines (RLGM) suggest that hydrothermal alteration lasted for more than 35 m.y. (Dubé et al., 2004). The carbonate ± quartz veins have a minimum age of 2712 ± 2 Ma (granodiorite dike cutting alteration, Dubé et al., 2004), however, a maximum age remains unknown (Dubé et al., 2004). The comparable minimum ages of alteration between the RLGM and Laird Lake area suggests that the RLGB underwent a regional scale alteration phase pre-2712 ± 2 Ma, however, the intensity of the hydrothermal system was likely much smaller at Laird Lake.

Hydrothermal alteration consisting of foliated biotite-, hornblende-, clinozoisite-, diopside- ± garnet-rich bands is the most characteristic feature of the mineralized zones at Laird Lake and the Madsen Mine (Dubé et al., 2000). It is unclear if all these phases were the result of prograde metamorphism of a pre-existing mineral assemblage or were introduced during amphibolite facies metamorphism. Diopside is clearly the result of prograde metamorphism as it is seen altering carbonate, however, biotite, hornblende and clinozoisite are never observed as an alteration product from a pre-existing phase (i.e., chlorite altering to biotite). Pirie (1981) proposed that the Madsen deposit was formed at moderate to shallow depths and then subsequently metamorphosed to amphibolite facies, however, Dubé et al. (2000) suggested that the alteration mineralogy reflects a two-stage system: early synvolcanic aluminous alteration, followed by an auriferous event associated with the inner alteration at the Madsen property. It is possible that the latter is correct if hydrothermal alteration associated with the auriferous event occurred syn-amphibolite facies. At the Laird Lake property, the majority of the alteration phases are pre- to syn-D_2 as they are preferentially oriented parallel to S_2.

Most sulphides associated with elevated gold grades at the Laird Lake property are foliated, suggesting the bulk of the gold mineralization and sulphides were introduced early- to pre-D_2 (see section 6.3.2.2). At the Lee Lake Au showing, sulphides and gold are concentrated within the biotite-rich band, suggesting the sulphides and gold have both been remobilized to the least competent band during D_2. Arsenopyrite grains are elongated parallel to foliation but are mainly subhedral to euhedral,

suggesting the arsenopyrite might have been recrystallized, possibly during peak metamorphism. Within mineralized quartz veins, gold grains are found at the margins of quartz grains in horizons parallel to the vein margins and S_2, suggesting gold is superimposed and late relative to the quartz vein formation, or that the gold has been remobilized during recrystallization.

A second gold event is recorded at the Laird Lake property, in which a gold-rich shear and gold-rich lamprophyric dike cut foliated Balmer assemblage mafic volcanic rocks. The margins of the shear contain subhedral pyrite, magnetite, hematite, and carbonate stringers which have not been altered to diopside, suggesting the gold-rich shear is post-peak metamorphism and D_2 deformation whereas the lamprophyric dike only shows preferential mineral alignments parallel to the dike margins, which are perpendicular to the main foliation. This second gold event could be analogous to what Dubé et al. (2004) described as a late-stage gold mineralization or remobilization event. This gold event is post-2702 ± 1 Ma (cross-cutting gold-rich lamprophyre dike at RLGM), is associated with high concentrations of gold within late fractures and lamprophyre dikes, and could be related to the emplacement of post-tectonic intrusions (Dubé et al., 2004). As the second gold event at the Laird Lake property is associated with similar features to the RLGM (post-tectonic Killala-Baird batholith, Au-rich lamprophyric dike, late Au-rich shear), it is possible that a comparable late-stage gold event also occurred in the south-western portion of the RLGB.

Lastly, the geophysical data (Fig. 6.29) suggests the Laird Lake fault has displaced the Laird Lake property from the Madsen and Starrat-Olsen mines package of rocks. This occurred post-2704 ± 1.5 Ma as the fault cuts the Killala-Baird batholith and suggest the Laird Lake area is a continuation of the same mineralized horizon that hosts the ore at the Madsen and Starrat-Olsen mines.

6.3.4 Model Interpretation and Exploration Strategy

Structural, textural, and mineralogical observations associated with gold mineralization at the Laird Lake property are similar to those of typical shear zone-hosted orogenic gold deposits, later upgraded to amphibolite facies (Goldfarb et al., 2005). The main characteristics of the gold mineralization in the field area are: (1) alteration and mineralization was strongly deformed by D_2; (2) gold shows a direct correlation with the appearance of disseminated sulphides and can be hosted in quartz veins; (3) highest gold grades are commonly found within the Balmer assemblage; and (4) mineralogy suggests the area was metamorphosed to amphibolite facies which outlasted D_2. These features suggest gold was dominantly controlled by the D_2 shear zone along the tectonic contact between the Balmer and Confederation assemblages. Additionally, the high Fe/(Fe+Mg) nature of the host rocks created a favorable chemical trap, as gold was likely transported by a gold-thiosulphide complex ($\mathrm{Au(HS)_2^-}$).

Observations from the Laird Lake area suggest gold was not introduced during peak metamorphism, but rather during an earlier phase, likely between the greenschist-amphibolite transition and lower amphibolite zone. This would allow gold associated with sulphides and quartz veins to be introduced over a lengthy period of time during which the deformational regime transitioned from brittle-ductile to dominantly ductile. As prograde metamorphism and ductile deformation persisted, gold, sulphides and quartz veins were strongly deformed by D_2, followed by the recrystallization of barren massive diopside- and amphibole-rich bands during peak-metamorphism. Mineralization in the area is not associated with peak-metamorphic phases and therefore is unlike syn-amphibolite facies orogenic gold deposits found in the Yilgarn and Pilbara Blocks (McCuaig et al., 1993; Neumaryr et al., 1993; Witt and Vanderhor, 1998). However, these deposits do share similarities with the Laird Lake area in terms of alteration mineralogy, ductile shear zones, disseminated mineralization and composition of the host rocks.

Due to the presence of calc-silicate alteration phases and its location within the thermal aureole of the Killala-Baird batholith, Dubé et al. (2000) suggested the Madsen deposit shared significant similarities with gold-skarn deposits hosted in mafic volcanic rocks. High-temperature gold deposits are often classified as skarn due to the presence of calc-silicate minerals (Mueller, 1992). However, typical "mesothermal" gold-bearing fluids would also produce calc-silicate alteration in amphibolite facies rocks due to higher temperatures and higher Ca activity (Ridley and Barnicoat, 1990; Mikucki and Ridley, 1993). At the Laird Lake area, gold is not directly associated with diopside bands, and most sulphides associated with gold are foliated by D_2, therefore making it unlikely that the gold and diopside originated from fluids exsolved from the 2704 ± 1.5 Ma Killala-Baird batholith.

Figure 6.45 summarizes the large-scale characteristics of the gold mineralization at the Laird Lake property: 1) the tectonic contact between the Balmer and Confederation assemblages is interpreted to have acted as a zone of weakness for both brittle-ductile deformation and a fluid conduit for hydrothermal alteration, 2) D_2 deformation produced a shear zone at the contact between the assemblages where mineral banding is the characteristic feature of the mineralization, and 3) Highest

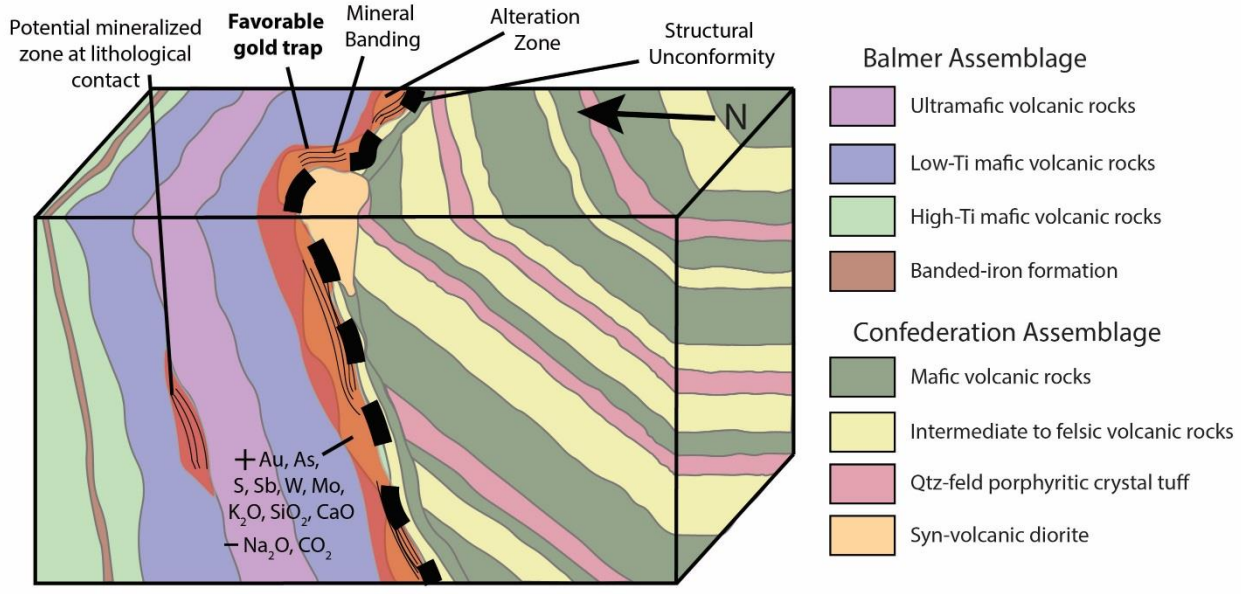

Figure 6.45 3-D sketch of the Laird Lake area and characteristics associated with gold mineralization.

gold grades are found at the change in orientation in the regional S_2 within the shear zone. Future exploration should continue targeting the tectonic contact between the two assemblages, but in areas where a significant deviation in the regional foliation is present (i.e. Lee Lake Au showing). Lithologic contacts in the Balmer assemblage could also prove to be a potential gold trap, as mafic-ultramafic contacts have shown to be prospective at the Russet South zone in the Madsen area (Baker et al., 2017). The best mineralized zones on the Laird Lake property are hosted in Balmer mafic volcanic rocks showing strong hydrothermal alteration composed of banded biotite-, amphibole-, diopside-, clinozoisite-, quartz- ± garnet-rich layers and BIFs. The presence of arsenopyrite, pyrrhotite ± pyrite often suggest elevated gold grades. Highly deformed smokey quartz veins parallel to S_2 showing pinch and swell textures are prospective in both the Balmer and Confederation assemblages. Late shears and lamprophyric dikes cutting the regional foliation are likely the result of gold remobilization from the main D_2 gold event and are potentially analogous to the second/remobilization gold event at the RLGM (Dubé et al., 2004). Regional mapping west of the Laird Lake property has previously revealed the continuation of the tectonic contact between the Balmer and Confederation assemblages (Atkinson, 1999). Further detailed mapping of assemblages and structures west of the Laird Lake property should be conducted to assess the full mineral potential along the contact.

Chapter 7 – Conclusions

The Laird Lake property situated in the southwestern end of the Red Lake greenstone belt encompasses two assemblages: the 2.992-2.964 Ga Balmer and 2.757-2.739 Ga Confederation assemblages. The assemblages can be distinguished by field observations, whole rock and isotopic geochemistry. The Balmer assemblage is typically composed of fine-grained, aphyric, locally pillowed mafic volcanic rocks, ultramafic intrusive and volcanic rocks with flow-breccia textures and local spinifex-bearing clasts, and banded-iron formation. In contrast, the Confederation assemblage consists of porphyritic (feldspar) or poikiloblastic (amphibole) mafic volcanic rocks intercalated with intermediate to felsic volcanic rocks that include tuffs, crystal tuffs and crystal lapilli tuffs. Syn-volcanic and syn- to post-D_2 intrusions commonly cross-cut the volcanic packages.

Geochemically, the Balmer assemblage is composed of Al-undepleted komatiites and both high-Ti and low-Ti tholeiitic basalts. Trace element and isotope geochemistry suggests the majority of the volcanic rocks found in the Balmer assemblage are weakly crustally contaminated as shown by negative Nb anomalies, elevated La/Sm_n ratios and isotopically enriched ε_{Nd} values. Modeling of crustal contamination suggests that the komatiites were likely affected by roughly 35 to 45% fractionation/assimilation and 10% contamination by an intermediate basement crust during their ascent. A large-scale zonation with ultramafic rocks in the core of Laird Lake, typically surrounded by low-Ti basalts, which are in turn surrounded by high-Ti basalts, combined with binary mixing modeling suggest the low-Ti basalts were likely produced by the mixing of 60% variably contaminated komatiites and 40% high-Ti basalts. Rock type associations and geochemistry suggest the Balmer assemblage likely formed from plume magmatism on the edge of the growing North Caribou Terrane. A mantle plume impinging on thin crust in a subaqueous environment would allow for the formation of an ocean-like plateau and could account for the low degree of contamination (<10%).

The Confederation assemblage is comprised of four geochemically distinct rock types: calc-alkalic mafic volcanic rocks with fractionated HREE, calc-alkalic mafic volcanic rocks with less fractionated HREE, calc-alkalic FI/FII felsic to intermediate volcanic rocks and transitional (between tholeiitic and calc-alkalic) FIIIb felsic to intermediate volcanic rocks. Spatial distributions, trace element and isotope geochemistry suggest the rocks of the Laird Lake property belong to the Heyson sequence of the Confederation assemblage and that both arc and back arc volcanism was erupting independently and repeatedly. Crustal contamination played a larger role in the more evolved FI/FII units, which are characterized by decreasing ε_{Nd} with increasing La/Sm_n and decreasing Nb/Nb* ratios whereas FIII units and mafic volcanic rocks with less fractionated HREE showed more depleted signatures. Geochronology of a syn-volcanic intrusion yielded a U-Pb age of 2737.68 ± 0.79 Ma whereas a fine-grained FI quartz-feldspar porphyritic crystal tuff yielded a U-Pb age of 2740.6 ± 19 Ma and three xenocrystic zircons which ranged from 2840-2974 Ma.

The data from this study is consistent with the construction of the Heyson sequence onto a thin Mesoarchean continental fragment within an oceanic island arc setting on the margins of the North Caribou Terrane due to the lack of a strong contamination signature. Trace element and Nd isotopic data suggest the more evolved FI/FII felsic to intermediate volcanic rocks and mafic volcanic rocks with stronger fractionated HREE formed in the main arc where the ascending melts would have picked up xenocrystic zircons from the thin basement crust. FIII intermediate to felsic volcanic rocks, mafic volcanic rocks with less fractionated HREE and the syn-volcanic diorite likely formed in the back arc as these show a more depleted signature indicative of a shallower source.

As the Confederation assemblage is interpreted to have been constructed within an oceanic island arc setting, the timing of juxtaposition to the existing Mesoarchean assemblages is estimated to have occurred between 2739-2733 Ma. The Laird Lake property encompasses the tectonic contact between the Balmer and Confederation assemblages which was reactivated during D_2 deformation and

hosts roughly 94% of all the gold (production, reserves, and resources) in the Red Lake district (Dubé et al., 2003).

The Laird Lake area hosts gold mineralization similar to that of typical shear zone-hosted orogenic gold deposits. Like most greenstone gold deposits, the mineralization is controlled by structures and shows a rise in gold grade in areas with higher structural complexities (i.e., Lee Lake Au showing). The alteration reflective of amphibolite facies metamorphism is composed of biotite, amphibole, diopside, clinozoisite, quartz ± garnet, with the addition of pyrite ± arsenopyrite, pyrrhotite and chalcopyrite. Gold grades show a drastic increase when arsenopyrite is present. At the tectonic contact between the Balmer and Confederation assemblages, overlapping alteration and a D_2 shear zone formed metasomatic banding, which is analogous to the alteration and mineralization at the Madsen mine, and represents the texture with the highest gold potential at the Laird Lake property. Gold mineralization hosted in the metasomatic banding within tholeiitic rocks of the Balmer assemblage is directly associated with disseminated sulphides, suggesting gold was transported as a gold-thiosulphide complex ($Au(HS)_2^-$) and reacted with high Fe/(Fe+Mg) rocks to precipitate both gold and sulphides. The majority of the alteration and mineralization phases are strongly foliated by D_2, suggesting they crystallized early- to syn-D_2. Mineralization is often concentrated in the biotite-rich bands, likely as a result of remobilization of sulphides and gold during D_2. Bands of massive diopside rimmed by massive amphibole not associated with gold mineralization suggest peak metamorphism occurred post-D_2 and therefore gold was not introduced syn-peak metamorphism.

Gold mineralization is also associated with quartz veins emplaced early- to syn-D_2. Gold grains are found interstially to the foliated quartz crystals suggesting gold was either introduced late in the formation of the vein or that it was remobilized during prograde metamorphism. Oxygen isotope data suggest both mineralized and barren veins were sourced from a similar reservoir which overlaps with the isotopic composition of metamorphic, magmatic and meteoritc waters, over crystallizing

temperatures ranging from 300 to 500°C. Prograde metamorphism likely homogenized the isotopic composition and primary textures of the quartz veins as no distinct zoning was recognized.

Evidence for a late-stage post-D_2 gold event is present in the form of gold mineralized shears and gold-rich lamprophyric dikes cross-cutting the regional foliation. It is unknown if these features introduced gold or remobilized pre-existing gold from the first gold event, however, they could be analogous to the second gold event recorded post-2702 ± 1 Ma at the RLGM.

Overall, the Laird Lake property shares many features with the Madsen mine in terms of alteration mineralogy, textures and rock types, and hosts alteration and mineralization at the Lee Lake Au showing that plots as intermediate between least-altered Balmer mafic volcanic rocks and samples from the Austin horizon. The Laird Lake area therefore likely represents a continuation of the same mineralizing structure found at both the Madsen and Starrat-Olsen mines and was later displaced as far as 10 km west by the dextral Laird Lake fault post-2704 ± 1.5 Ma. The tectonic contact between the Balmer and Confederation assemblages continues to prove itself as favorable structural and chemical trap for gold mineralization and a very important exploration target in the Red Lake gold camp.

References

Abbott, D., Burgess, L., Longhi, J., and Smith, W. H., 1994. An empirical thermal history of the Earth's upper mantle. Journal of Geophysical Research: Solid Earth, 99, 13835-13850.

Andrews, A. J., Hugon, H., Durocher, M., Corfu, F., and Lavigne, M., 1986. The anatomy of a gold-bearing greenstone belt: Red Lake, northwestern Ontario, Gold '86 Symposium: Toronto, p. 3-22.

Andrews, A. J., and Wallace, H., 1983. Alteration, Metamorphism, and Structural Patterns Associated with Archean Gold Deposits - Preliminary Observations in the Red Lake Area. Ontario Geological Survey Miscellaneous Paper 110, 12 p.

Arndt, N., Ginibre, C., Chauvel, C., Albarede, F., Cheadle, M., Herzberg, C., Jenner, G., and Lahaye, Y., 1998. Were komatiites wet? Geology, vol. 26, p. 739-742.

Arndt, N., Lesher, M., and Barnes, S., 2008. Komatiite, Cambridge university press.

Arndt, N. T., Albarede, F., and Nisbet, E. G., 1997. Mafic and ultramafic magmatism, *in* de Wit, M.J. and Ashwal, L.D., *eds.* Greenstone Belts: Oxford University Press, Oxford, p. 233-254.

Atkinson, B. T., 1994. Geology and Mineral Potential of Killala Township, Red Lake District, *in* Summary of Field Work and Other Activities 1994, Ontario Geological Survey, Miscellaneous Paper 163, p. 139-142.

Atkinson, B. T., 1995. Precambrian geology, Killala Township; Ontario Geological Survey, Preliminary Map P.3248, scale 1:12 000.

Atkinson, B. T., 1999. Precambrian geology, Medicine Stone Lake area; Ontario Geological Survey, Preliminary Map P.3397, scale 1:50 000.

Baker, D., Blais, G., Folinsbee, J., Jutras, M., and Levesque, R., 2017. NI 43-101 Technical Report, Preliminary Economic Assessment of the Madsen Gold Project for Pure Gold Mining Inc. Red Lake Area, Ontario, Canada.

Barnes, S.-J., and Lightfoot, P. C., 2005. Formation of magmatic nickel-sulphide ore deposits and processes affecting their copper and platinum-group element contents. In Hedenquist, J.W., Thompson, J.F.H., Goldfarb, R.J. and Richards, J.P. (eds.) Economic Geology 100th Anniversary Volume, p. 179-213.

Barrett, T., and MacLean, W., 1999. Volcanic sequences, lithogeochemistry, and hydrothermal alteration in some bimodal volcanic-associated massive sulfide systems. Reviews in Economic Geology, vol. 8, p. 101-131.

Barrie, C. T., Ludden, J. N., and Green, T. H., 1993. Geochemistry of volcanic rocks associated with Cu-Zn and Ni-Cu deposits in the Abitibi subprovince. Economic Geology, vol. 88, p. 1341-1358.

Beakhouse, G. P., 1983. Geological, geochemical and Rb-Sr and U-Pb zircon geochronological investigations of granitoid rocks from the Winnipeg River Belt, northwestern Ontario and southeastern Manitoba: unpublished Ph.D. thesis *in* University, M., ed.: Hamilton, Ontario.

Beakhouse, G. P., 1991. Winnipeg River Suprovince *in* Geology of Ontario, OGS, Special vol. 4, Part 1, p. 279-301.

Beaudoin, G., 2011. The stable isotope geochemistry of orogenic gold deposits. In: Barra, F., Reich, M., Campos, E., Tornos, F. (Eds), Proceedings of the Eleventh Biennial SGA Meeting. Antogfagasta, Chile, p. 556-558

Belanger, R., 1988. Induced Polarization Survey, Black Cliff Mines Ltd.

Biczok, J., Hollings, P., Klipfel, P., Heaman, L., Maas, R., Hamilton, M., Kamo, S., and Friedman, R., 2012. Geochronology of the North Caribou greenstone belt, Superior Province Canada: Implications for tectonic history and gold mineralization at the Musslwhite mine. Precambrian Research, vol. 192-195, p. 209-230.

Blais, S., Osiowy, C., and Hmidi, N., 2015. Red Lake Operations Ontario, Canada, NI 43-101 Technical Report: technical report prepared for Goldcorp Inc., effective date December 31, 2015, 168 p.

Bodnar, R. J., Lecumberri-Sanchez, P., Moncada, D., and Steele-MacInnis, M., 2014. Fluid Inclusions in Hydrothermal Ore Deposits, Treatise on Geochemistry, p. 119-142.
Bouquain, S., 2008. Cristallochimie du pyroxène dans les komatiites et basaltes lunaires, Université Joseph-Fourier-Grenoble I.
Brooks, C., and Hart, S., 1974. On the significance of komatiite. Geology, vol. 2, p. 107-110.
Burnham, O. M., 2008. Trace Element Analysis of Geological Samples by Inductively Coupled Plasma Mass Spectrometry (ICP-MS) at the Geoscience Laboratories: Revised Capabilities Due to Imporvements to Instrumentation. *In* Summary of Field Work and Other Activities 2008. Ontario Geological Survey Open File Report 6226 p. 38-1 to 38-10.
Burrows, D. R., and Spooner, E. T. C., 1987. Generation of a magmatic H_2O-CO_2 fluid enriched in Au, Mo, and W within an Archean sodic granodiorite stock, Mink Lake, northwestern Ontario. Economic Geology, vol. 82, p. 1931-1957.
Burrows, D. R., Wood, P. C., and Spooner, E. T. C., 1986. Carbon isotope evidence for a magmatic origin for Archaean gold-quartz vein ore deposits. Nature, vol. 321, p. 851-854.
Butler, R., 1955. The geology of Madsen Red Lake Gold Mines; M.Sc. thesis, University of Manitoba, Winnipeg, Manitoba, 138 p.
Cameron, E. M., 1988. Archean gold: Relation to granulite formation and redox zoning in the crust. Geology, vol. 16, p. 109-112.
Campbell, I., Coad, P., Franklin, J., Gorton, M., Scott, S., Sowa, J., and Thurston, P., 1982. Rare earth elements in volcanic rocks associated with Cu–Zn massive sulphide mineralization: a preliminary report. Canadian Journal of Earth Sciences, vol. 19, p. 619-623.
Campbell, I., Franklin, J., Gorton, M., Hart, T., and Scott, S., 1981. The role of subvolcanic sills in the generation of massive sulfide deposits. Economic Geology, vol. 76, p. 2248-2253.
Campbell, I., Griffiths, R., and Hill, R., 1989. Melting in an Archaean mantle plume: heads it's basalts, tails it's komatiites. Nature, vol. 339, p. 697-699.
Card, K. D., 1990. A review of the Superior Province of the Canadian Shield, a product of Archean accretion. Precambrian Research, vol. 48, p. 99-156.
Card, K. D., and Ciesielski, A., 1986. Subdivisions of the Superior Province of the Canadian Shield. Geoscience Canada vol. 13 N. 1, p. 5-13.
Card, K. D., and King, J. E., 1992. The tectonic evolution of the Superior and Slave provinces of the Canadian Shield: introduction. Canadian Journal of Earth Sciences, vol. 29, p. 2059-2065.
Cartwright, I., Vry, J., and Sandiford, M., 1995. Changes in stable isotope ratios of metapelites and marbles during regional metamorphism, Mount Lofty Ranges, South Australia: implications for crustal scale fluid flow. Contributions to Mineralogy and Petrology, vol. 120, p. 292-310.
Colvine, A., Andrews, A. J., Cherry, M. E., Durocher, M. E., Fyon, J. A., Lavigne, M. J., Macdonald, A. J., Marmont, S., Poulsen, K. H., Springer, J. S., and Troop, D. S., 1984. An integrated model for the origin of Archean lode gold deposits: Ontario Geological Survey, Open-File Report 5524, 98 p.
Condie, K. C., 1976. Trace-element geochemistry of Archean greenstone belts. Earth-Science Reviews, vol. 12, p. 393-417.
Condie, K. C., 1993. Chemical composition and evolution of the upper continental crust: contrasting results from surface samples and shales. Chemical geology, vol. 104, p. 1-37.
Corfu, F., 1988. Differential response of U-Pb systems in coexisting accessory minerals, Winnipeg River Subprovince, Canadian Shield: implications for Archean crustal growth and stabilization. Contributions to Mineralogy and Petrology, vol. 98, p. 312-325.
Corfu, F., and Andrews, A. J., 1987. Geochronological constraints on the timing of magmatism, deformation, and gold mineralization in the Red lake greenstone belt, northwestern Ontario. Canadian Journal of Earth Sciences, vol. 24, p. 1302-1320.

Corfu, F., Davis, D. W., Stone, D., and Moore, M. L., 1998. Chronostratigraphic constrains on the genesis of Archean greenstone belts, northwestern Superior Province, Ontario, Canada. Precambrian Research, vol. 92, p. 277-295.

Corfu, F., and Lin, S., 2000. Geology and U-Pb geochronology of the Island Lake greenstone belt, northwestern Superior Province, Manitoba. Canadian Journal of Earth Sciences, vol. 37, p. 1275-1286.

Corfu, F., and Stone, D., 1998. Age structure and orogenic significance of the Berens River composite batholiths, western Superior Province. Canadian Journal of Earth Sciences, vol. 35, p. 1089-1109.

Corfu, F., and Stott, G., 1993a. Age and petrogenesis of two late Archean magmatic suites, northwestern Superior Province, Canada: zircon U–Pb and Lu–Hf isotopic relations. Journal of Petrology, vol. 34, p. 817-838.

Corfu, F., and Stott, G., 1993b. U–Pb geochronology of the central Uchi subprovince, Superior Province. Canadian Journal of Earth Sciences, vol. 30, p. 1179-1196.

Corfu, F., and Wallace, H., 1986. U-Pb zircon ages for magmatism in the Red Lake greenstone belt, northwestern Ontario. Canadian Journal of Earth Sciences, vol. 23, p. 27-42.

Corrigan, D., Pehrsson, S., Wodicka, N., and de Kemp, E., 2009. The Palaeoproterozoic Trans-Hudson Orogen: a prototype of modern accretionary processes. Geological Survey of Canada Special Publications 2009, vol. 327, p. 457-479.

Davis, D., Sutcliffe, R., and Trowell, N., 1988. Geochronological constraints on the tectonic evolution of a late Archaean greenstone belt, Wabigoon Subprovince, Northwest Ontario, Canada. Precambrian Research, vol. 39, p. 171-191.

Defant, M. J., and Nielsen, R. L., 1990. Interpretation of open system petrogenetic processes: phase equilibria constraints on magma evolution. Geochimica et Cosmochimica Acta, 54, 87-102.

DePaolo, D., and Wasserburg, G., 1977. The sources of island arcs as indicated by Nd and Sr isotopic studies. Geophysical Research Letters, vol. 4, p. 465-468.

DePaolo, D., and Wasserburg, G., 1979. Petrogenetic mixing models and Nd-Sr isotopic patterns. Geochimica et Cosmochimica Acta, vol. 43, p. 615-627.

DePaolo, D. J., 1981a. Neodymium isotopes in the Colorado Front Range and crust–mantle evolution in the Proterozoic. Nature, vol. 291, p. 193-196.

DePaolo, D. J., 1981b. Trace element and isotopic effects of combined wallrock assimilation and fractional crystallization. Earth and Planetary Science Letters, vol. 53, p. 189-202.

Dickin, A. P., 2005. Radiogenic isotope geology, Cambridge University Press.

Douglas, R.J.W., 1973. Geological Provinces, map 27-28, National Atlas of Canada, 4th Edition: Surveys and Mapping Branch, Department of Energy, Mines and Resources, Ottawa.

Dostal, J., 2008. Igneous rock associations: 10. Komatiites. Geological Association of Canada, Geoscience Canada, vol. 35, 11 p.

Dostal, J., and Mueller, W. U., 2004. Komatiite geochemistry, in Eriksson, P.G., Altermann, W., Nelson, D.R., Mueller, W.U. and Catuneanu, O., eds., The Precambrian Earth: Tempos and Events: Developments in Precambrian Geology, vol. 12, p. 290-298.

Doubrovine, P., Steinberger, B., and Torsvik, T., 2012. Absolute plate motions in a reference frame defined by moving hot spots in the Pacific, Atlantic, and Indian oceans. Journal of Geophysical Research: Solid Earth, vol. 117, 30 p.

Dubé, B., Balmer, W., Sanborn-Barrie, M., Skulski, T., and Parker, J., 2000. A preliminary report on amphibolite-facies, disseminated-replacement-style mineralization at the Madsen gold mine, Red Lake, Ontario. Geological Survey of Canada Current Research 2000-C17, 12 p.

Dubé, B., and Gosselin, P., 2007. Greenstone-hosted quartz-carbonate vein deposits. *in* Goodfellow, W. D., ed., Mineral Deposits of Canada: A Synthesis of Major Deposit-Types, District Metallogeny,

the Evolution of Geological Provinces, and Exploration Methods, Geological Association of Canada, Mineral Deposits Division, p. 49-73.
Dubé, B., Williamson, K., and Malo, M., 2001. Preliminary report on the geology and controling parameters of the Goldcorp Inc. High-Grade zone, Red Lake mine, Ontario. Geological Survey of Canada Current Research 2001-C18, 31 p.
Dubé, B., Williamson, K., and Malo, M., 2003. Gold mineralization from the Red Lake mine trend: Example from the Cochenour-Willans mine area, Red Lake, Ontario, with new key information from the Red Lake Mine and potential analogy with the Timmins camp. Geological Survey of Canada Current Research 2003-C21, 15 p.
Dubé, B., Williamson, K., McNicoll, V., Malo, M., Skulski, T., Twomey, T., and Sanborn-Barrie, M., 2004. Timing of Gold Mineralization at Red Lake, Northwestern Ontario, Canada: New Constraints from U-Pb Geochronology at the Goldcorp High-Grade Zone, Red Lake Mine, and the Madsen Mine. Economic Geology, vol. 99, p. 1611-1641.
Ducea, M. N., Saleeby, J. B., and Bergantz, G., 2015. The architecture, chemistry, and evolution of continental magmatic arcs. Annual Review of Earth and Planetary Sciences, vol. 43, p. 299-331.
Durocher, M. E., 1983. The Nature of Hydrothermal Alteration Associated with the Madsen and Starratt-Olsen Gold Deposits, Red Lake Area. The Geology of Gold in Ontario, Ontario Geological Survey Miscellaneous Paper 110, p. 123-140.
Durocher, M. E., and Hugon, H., 1983. Structural geology and hydrothermal alteration in the Flat Lake-Howey Bay deformation zone, Red Lake area. Summary of Field Work, 1983, Ontario Geological Survey, p. 216-219.
Easton, M., 2000. Metamorphism of the Canadian Schield, Ontario, Canada - The Superior Province. The Canadian Mineralogist, vol. 38, p. 287-317.
Eisenlohr, B., Groves, D., and Partington, G., 1989. Crustal-scale shear zones and their significance to Archaean gold mineralization in Western Australia. Mineralium Deposita, vol. 24, p. 1-8.
Ewart, A., Brothers, R., and Mateen, A., 1977. An outline of the geology and geochemistry, and the possible petrogenetic evolution of the volcanic rocks of the Tonga-Kermadec-New Zealand island arc. Journal of volcanology and geothermal research, vol. 2, p. 205-250.
Ewart, A., Bryan, W., Chappell, B., and Rudnick, R., 1994. Regional geochemistry of the Lau-Tonga arc and backarc systems: Proceedings of the Ocean Drilling Program. Scientific Results, 1994, p. 385-425.
Farkas, A., 1988. Report on Geological Mapping and Sampling of Gold Occurences - Laird Lake Property, Red Lake Mining Division, Ontario, 75 p.
Fayek, M., Harrison, T. M., Ewing, R. C., Grove, M., and Coath, C. D., 2002. O and Pb isotopic analyses of uranium minerals by ion microprobe and U–Pb ages from the Cigar Lake deposit. Chemical Geology, vol. 185, p. 205-225.
Ferguson, S. A., 1965. Geology of the Eastern Part of Baird Township, District of Kenora. Ontario Department of Mines, Geological Report, no. 39 (Map 2072, scale 1:12 000), Toronto.
Floyd, P., 1989. Geochemical features of intraplate oceanic plateau basalts. Geological Society, London, Special Publications, vol. 42, p. 215-230.
Fraser, D., 2011. Logistical Report for Induced Polarization/Magnetometer Geophysical Surveys Performed on the Boston Gold Project, Red Lake Area, Ontario.
Gerstenberger, H., and Haase, G., 1997. A highly effective emitter substance for mass spectrometric Pb isotopic ratio determinations. Chemical Geology, vol. 136, p. 309-312.
Goldfarb, R. J., Baker, T., Dubé, B., Groves, D. I., Hart, C. J. R., and Gosselin, P., 2005. Distrubution, Character, and Genesis of Gold Deposits in Metamorphic Terranes. Economic Geology 100th Anniversary Volume, p. 407-450.

Goldfarb, R. J., Groves, D. I., and Gardoll, S., 2001. Orogenic gold and geologic time: a global synthesis. Ore Geology Reviews, vol. 18, p. 1-75.
Goodwin, A. M., 1986. Archean protocontinental growth and early crustal history of the Canadian shield. 23rd International Geological Congress, Prague 1968, vol. 1, p. 69-89.
Grove, T., Gaetani, G., and De Wit, M., 1994. Spinifex textures in 3.49 Ga Barberton Mountain belt komatiites: evidence for crystallization of water-bearing, cool magmas in the Archean. Eos (Transactions, American Geophysical Union), vol. 75, 354 p.
Grove, T., and Parman, S., 2004. Thermal evolution of the Earth as recorded by komatiites. Earth and Planetary Science Letters, vol. 219, p. 173-187.
Groves, D. I., 1993. The crustal continuum model for late-Archaean lode-gold deposits of the Yilgarn Block, Western Australia. Mineralium Deposita, vol. 28, p. 366-374.
Groves, D. I., Goldfarb, R. J., Gebre-Mariam, M., Hagemann, S. G., and Robert, F., 1998. Orogenic gold deposits: A proposed classification in the context of their crustal distribution and relationship to other gold deposits types. Ore Geology Reviews, vol. 13, p. 7-27.
Groves, D. I., Goldfarb, R. J., Knox-Robinson, C. M., Ojala, J., Gardoll, S., Yun, G. Y., and Holyland, P., 2000. Late-kinematic timing of orogenic gold deposits and significance for computer-based exploration techniques with emphasis on the Yilgarn Block, Western Australia. Ore Geology Reviews, vol. 17, p. 1-38.
Groves, D. I., Goldfarb, R. J., Robert, F., and Hart, C. J. R., 2003. Gold deposits in metamorphic belts: Overview of current understanding, outstanding problems, future research, and exploration significance. Economic Geology, vol. 98, p. 1-30.
Gulson, B. L., Mizon, K. J., and Atkinson, B. T., 1993. Source and timing of gold and other mineralization in the Red Lake area, northwestern Ontario, based on lead-isotope investigations. Canadian Journal of Earth Sciences, vol. 30, p. 2366-2379.
Guy, K., 2008. Report on a Mechanical Stripping Programme on the Laird Lake Property, Prepared for Laird Lake Resources Inc.
Guy, K., 2009. Report on a Geochemical and Prospecting Programme, Laird Lake Property. 68 p.
Hannigan, P., 1980. Report on Laird Lake Property; Sherritt Gordon Mines Limited, 36 p.
Hart, T., 1984. The geochemistry and petrogenesis of a metavolcanic and intrusive sequence in the Kamiskotia area, Timmins, Ontario: Unpublished M. Sc, thesis, Toronto, ON, University of Toronto.
Hart, T., Gibson, H., and Lesher, C., 2004. Trace element geochemistry and petrogenesis of felsic volcanic rocks associated with volcanogenic massive Cu-Zn-Pb sulfide deposits. Economic Geology, vol. 99, p. 1003-1013.
Hedge, C., and Knight, R., 1969. Lead and strontium isotopes in volcanic rocks from northern Honshu, Japan. Geochemical Journal, vol. 3, p. 15-24.
Hemond, C., Arndt, N. T., Lichtenstein, U., Hofmann, A. W., Oskarsson, N., and Steinthorsson, S., 1993. The heterogeneous Iceland plume: Nd-Sr-O isotopes and trace element constraints. Journal of Geophysical Research: Solid Earth, vol. 98, p. 15833-15850.
Henry, P., Stevenson, R. K., Larbi, Y., and Gariépy, C., 2000. Nd isotopic evidence for Early to Late Archean (3.4-2.7 Ga) crustal growth in the Western Superior Province (Ontario, Canada). Tectonophysics, vol. 322, p. 135-151.
Herzberg, C., 1995. Generation of plume magmas through time: an experimental perspective. Chemical Geology, vol. 126, p. 1-16.
Ho, S., Groves, D., and Phillips, G., 1985. Fluid inclusions as indicators of the nature and source of ore fluids and ore depositional conditions for Archaean gold deposits of the Yilgarn Block, Western Australia. South African Journal of Geology, vol. 88, p. 149-158.

Hochstaedter, A., Gill, J., Peters, R., Broughton, P., Holden, P., and Taylor, B., 2001. Across-arc geochemical trends in the Izu-Bonin arc: Contributions from the subducting slab. Geochemistry, Geophysics, Geosystems, vol. 2, 44 p.

Hodgson, C., 1993. Mesothermal lode-gold deposits. Mineral Deposit Modeling, Geological Association of Canada Special Paper, vol. 40, p. 635-678.

Hodgson, C. J., Hamilton, J. V., and Hanes, J. A., 1989. The late emplacement of gold in the Archean Abitibi greenstone belt: a consequence of thermal equilibration following collisional orogeny. Geological Association of Canada; Mineral Association of Canada, Program Abstract, 14: A45.

Hoffman, P. F., 1988. United plates of America, the birth of a craton: Early Proterozoic assembly and growth of Laurentia. Annual Review Earth Planet Science, vol. 16, p. 543-603.

Hollings, P., 1998. Geochemistry of the Uchi Subprovince, Nothern Superior Province: An Evaluation of the Geodynamic Evolution of the Nothern Margin of the Superior Province Ocean Basin. *in* Saskatchewan, U. o., ed.: Saskatoon, 309 p.

Hollings, P., and Kerrich, R., 1999. Trace element systematics of ultramafic and mafic volcanic rocks from the 3 Ga North Caribou greenstone belt, northwestern Superior Province. Precambrian Research, vol. 93, p. 257-279.

Hollings, P., and Kerrich, R., 2000. An Archean arc basalt - Nb-enriched basalt - adakite association: The 2.7 Ga Confederation assemblage of the Birch-Uchi greenstone belt, Superior Province. Contributions to Mineralogy and Petrology, vol. 139, p. 208-226.

Hollings, P., Stott, G., and Wyman, D., 2000. Trace element geochemistry of the Meen-Dempster greenstone belt, Uchi subprovince, Superior Province, Canada: back-arc development on the margins of an Archean protocontinent. Canadian Journal of Earth Sciences, vol. 37, p. 1021-1038.

Hollings, P., Wyman, D., and Kerrich, R., 1999. Komatiite-basalt-rhyolite volcanic association in Northern Superior Province greenstone belts: significance of plume-arc interaction in the generation of the proto continental Superior Province. Lithos, vol. 46, p. 137-161.

Horwood, H. C., 1940a. Geology and mineral deposits of the Red Lake area. Forty-ninth Annual Report of the Ontario Dept. of Mines, vol. XLIX, 231 p.

Horwood, H. C., 1940b. Geology and mineral deposits of the Red Lake area. Forty-ninth Annual Report of the Ontario Dept. of Mines, Map Nos. 49a.

Houle, P., and Perreault, S., 2008. New Québec and Torngat Orogens, Southeastern Churchill Province (core zone), and Cape Smith Belt, Report on Mineral Exploration Activities in Québec 2008, Ministère de l'Énergie et des Ressources naturelles, p. 35-40.

Hugon, H., and Schwerdtner, W. M., 1984. Structural signature and tectonic history of gold-bearing deformed rocks in northwestern Ontario. Ontario Geological Survey Miscellaneous Paper 127, p. 62-72.

Huppert, H. E., and Sparks, R. S. J., 1985. Komatiites I: Eruption and flow. Journal of Petrology, vol. 26, p. 694-725.

Huppert, H. E., Stephen, R., and Sparks, J., 1985. Cooling and contamination of mafic and ultramafic magmas during ascent through continental crust. Earth and Planetary Science Letters, vol. 74, p. 371-386.

Irvine, T. N. J., and Baragar, W. R. A. F., 1971. A guide to the chemical classification of the common volcanic rocks. Canadian Journal of Earth Sciences, vol. 8, p. 523-548.

Jacobsen, S. B., and Wasserburg, G., 1979. The mean age of mantle and crustal reservoirs. Journal of Geophysical Research: Solid Earth, vol. 84, p. 7411-7427.

Jaffey, A. H., Flynn, K. F., Glendenin, L. E., Bentley, W. C., and Essling, A. M., 1971. Precision measurement of half-lives and specific avtivities of ^{235}U and ^{238}U. Physical Review C, vol. 4, p. 1889-1906.

Jemielita, R. A., Davis, D. W., and Krogh, T. E., 1990. U-Pb evidence for Abitibi gold mineralization postdating greenstone magmatism and metamorphism. Nature, vol. 346, p. 831-834.
Keays, R. R., 1995. The role of komatiitic and picritic magmatism and S-saturation in the formation of ore deposits. Lithos, vol. 34, p. 1-18.
Kerr, A., 2003. 3.16 Oceanic Plateaus. Treatise on Geochemistry, vol. 3, p. 537-565.
Kerrich, R., 1989. Lithophile element systematics of gold vein deposits in Archean greenstone belts: Implications for source processes. Economic Geology Monograph, vol. 6, p. 508-520.
Kerrich, R., and Cassidy, K. F., 1994. Temporal relationships of lode gold mineralization to accretion, magmatism, metamorphism and deformation - Archean to present: A review. Ore Geology Reviews, vol. 9, p. 263-310.
Kerrich, R., and Fyfe, W. S., 1981. The gold-carbonate association: Source of CO_2, and CO_2 fixation reactions in Archaean lode deposits. Chemical Geology, vol. 33, p. 265-294.
Kerrich, R., Goldfarb, R., Groves, D., and Garwin, S., 2000. The Geodynamics of World-Class Gold deposits: Characteristics, Space-Time Distribution, and Origins. SEG Reviews, vol. 13, p. 501-551.
Kerrich, R., Polat, A., Wyman, D., and Hollings, P., 1999. Trace element systematics of Mg-, to Fe-tholeiitic basalt suites of the Superior Province: implications for Archean mantle reservoirs and greenstone belt genesis. Lithos, vol. 46, p. 163-187.
Kerrich, R., and Wyman, D., 1990. Geodynamic setting of mesothermal gold deposits: An association with accretionary tectonic regimes. Geology, vol. 18, p. 882-885.
Killick, D., 2014. From ores to metals, Archaeometallurgy in global perspective, Springer, p. 11-45.
Kontak, D., Horne, R., and Kyser, K., 2011. An oxygen isotope study of two contrasting orogenic vein gold systems in the Meguma Terrane, Nova Scotia, Canada, with implications for fluid sources and genetic models. Mineralium Deposita, vol. 46, p. 289-304.
Krogh, T., Harris, N., and Davis, G., 1976. Archean rocks from the eastern Lac Seul region of the English River Gneiss Belt, northwestern Ontario, part 2. Geochronology. Canadian Journal of Earth Sciences, vol. 13, p. 1212-1215.
Kuno, H., 1968. Differentiation of basalt magma. In Basalts, Volume 2. H. H. Hess and A. Poldervaart (Editors). pp. 623-688. Interscience, John Wiley and Sons, New york. 862 p.
Le Maitre, R. W. B., Dudek, P., Keller, A., Lameyre, J., Le Bas, J., Sabine, M., Schmid, P., Sorensen, R., Streckeisen, H., and Woolley, A., 1989. A classification of igneous rocks and glossary of terms: Recommendations of the International Union of Geological Sciences, Subcommission on the Systematics of Igneous Rocks, International Union of Geological Sciences.
Leblanc, J., 2016. Prospecting Report for the Laird Lake Gold Project, Red Lake, Ontario, Canada. Report Prepared For Bounty Gold Corp., 278 p.
Lemkow, D. R., Sanborn-Barrie, M., Bailes, A. H., Percival, J., Rogers, N., Skulski, T., Anderson, S. D., Tomlinson, K. Y., McNicoll, V., Parker, J., Whalen, J. B., Hollings, P., and Young, M. D., 2006. GIS compilation of geology and tectonostratigraphic assemblages, western Uchi Subprovince, Western Superior Province, Ontario and Manitoba; Geological Survey of Canada, Open File 5269, Manitoba Geological Survey, Open File Report 2006-30, Ontario Geological Survey, Miscellaneous Release--Data 203.
Lentz, D. R., 1998. Petrogenetic evolution of felsic volcanic sequences associated with Phanerozoic volcanic-hosted massive sulphide systems: the role of extensional geodynamics. Ore Geology Reviews, 12, 289-327.
Lesher, C., and Arndt, N., 1995. REE and Nd isotope geochemistry, petrogenesis and volcanic evolution of contaminated komatiites at Kambalda, Western Australia. Lithos, vol. 34, p. 127-157.

Lesher, C. M., Goodwin, A. M., Campbell, I. H., and Gorton, M. P., 1986. Trace-element geochemistry of ore-associated and barren, felsic metavolcanic rocks in the Superior Province, Canada. Canadian Journal of Earth Sciences, vol. 23, p. 222-237.

Lichtblau, A., Paju, G., Ravnaas, C., Tuomi, R. D., and Wiebe, K., 2017. Report of Activities 2016, Resident Geologist Program, Red Lake Regional Resident Geologist Report: Red Lake and Kenora Districts; Ontario Geological Survey, Open File Report 6323, 107 p.

Lichtblau, A., Ravnaas, C., Storey, C., Bongfeldt, J., McDonald, S., Lockwood, H. C., Bennett, N. A., and Jeffries, T., 2011. Report of Activities 2010, Resident Geologist Program, Red Lake Regional Resident Geologist Report: Red Lake and Kenora Districts; Ontraio Geological Survey, Open File Report 6261, 93 p.

Lichtblau, A., Storey, C., and Paju, G., 2016. Field Trip Through the Central Red Lake Gold Camp, Ministry of Northern Development and Mines, Ontario Geological Survey, 39 p.

Lin, S., Davis, D. W., Rotenberg, E., Corkery, M. T., and Bailes, A. H., 2006. Geological evolution of the northwestern Superior Province: Clues from geology, kinematics, and geochronology in the Gods Lake Narrows area, Oxford-Stull terrane, Manitoba. Canadian Journal of Earth Sciences, vol. 43, p. 749-765.

Ludwig, K. R., 2003. Isoplot 3.00, A Geochronological Toolkit for Microsoft Excel. University of California at Berkeley, kludwig@bgc.org.

MacLean, W., and Barrett, T., 1993. Lithogeochemical techniques using immobile elements. Journal of geochemical exploration, vol. 48, p. 109-133.

Mahoney, J., Jones, W., Frey, F., Salters, V., Pyle, D., and Davies, H., 1995. Geochemical characteristics of lavas from Broken Ridge, the Naturaliste Plateau and southernmost Kerguelen Plateau: Cretaceous plateau volcanism in the southeast Indian Ocean. Chemical Geology, vol. 120, p. 315-345.

Mahoney, J. J., Storey, M., Duncan, R. A., Spencer, K. J., and Pringle, M., 1993. Geochemistry and geochronology of Leg 130 basement lavas: nature and origin of the Ontong Java Plateau: Proceedings of the Ocean Drilling Program, Scientific Results, 1993, p. 3-22.

Matsuhisa, Y., Goldsmith, J., and Clayton, R., 1979. Oxygen isotopic fractionation in the system quartz-albite-anorthite-water. Geochimica et Cosmochimica Acta, vol. 43, p. 1131-1140.

McCuaig, T. C., and Kerrich, R., 1998. P-T-t-deformation-fluid characteristics of lode gold deposits: evidence from alteration systematics Ore Geology Reviews, vol. 12, p. 381-453.

McCuaig, T. C., Kerrich, R., Groves, D. I., and Archer, N., 1993. The nature and dimensions of regional and local gold-related hydrothermal alteration in tholeiitic metabasalts in the Norseman goldfields: the missing link in a crustal continuum of gold deposits? Mineralium Deposita, vol. 28, p. 420-435.

McCuaig, T. C., Kerrich, R., and Xie, Q., 1994. Phosphorus and high field strenght element anomalies in Archean high-magnesian magmas as possible indicators of source mineralogy and depth. Earth and Planetary Science Letters, vol. 124, p. 221-239.

McCulloch, M. T., and Gamble, J., 1991. Geochemical and geodynamical constraints on subduction zone magmatism. Earth and Planetary Science Letters, vol. 102, p. 358-374.

McMaster, N. D., 1987. A preliminary $^{40}Ar/^{39}Ar$ study of the thermal history and age of gold in the Red Lake greenstone; MSc thesis. *in* Toronto, U. o., ed.: Toronto, Ontario.

Menard, T. M., and Pattison, D. R. M., 1998. Correlation of multiple alteration events with successive tectonic and metamorphic events in the Red Lake gold deposits, northwestern Ontario: Western Superior Transect Annual Workshop. Lithoprobe Report 65, p. 63-69.

Mikucki, E. J., and Ridley, J. R., 1993. The hydrothermal fluid of Archaean lode-gold deposits at different metamorphic grades: compositional constraints from ore and wallrock alteration assemblages. Mineralium Deposita, vol. 28, p. 469-481.

Mochoruk, T., 2011. Champlain Defines Coincident Multi-Element Lake Sediment Geochemical and Geophysical Targets under Laird Lake, Boston Gold Project, Red Lake, Ontario, Champlain Resources Inc.

Morris, J. D., and Hart, S. R., 1983. Isotopic and incompatible element constraints on the genesis of island arc volcanics from Cold Bay and Amak Island, Aleutians, and implications for mantle structure. Geochimica et Cosmochimica Acta, vol. 47, p. 2015-2030.

Mueller, A. G., 1992. Petrogenesis of amphibole–biotite–calcite–plagioclase alteration and laminated gold–silver quartz veins in four Archean shear zones of the Norseman district, Western Australia. Canadian Journal of Earth Sciences, vol. 29, p. 388-417.

Naldrett, A., 1999. World-class Ni-Cu-PGE deposits: key factors in their genesis. Mineralium Deposita, vol. 34, p. 227-240.

Neal, C., Mahoney, J., and CHAZEY III, W., 2002. Mantle sources and the highly variable role of continental lithosphere in basalt petrogenesis of the Kerguelen Plateau and Broken Ridge LIP: results from ODP Leg 183. Journal of Petrology, vol. 43, p. 1177-1205.

Nesbitt, B. E., Murowchick, J. B., and Muehlenbacks, J., 1986. Dual origins of lode gold deposits in the Canadian Cordillera. Geology, vol. 14, p. 506-509.

Nesbitt, R. W., Sun, S.-S., and Purvis, A. C., 1979. Komatiites: geochemistry and genesis. Canadian Mineralogist, vol. 17, p. 165-186.

Neumaryr, P., Groves, D. I., Ridley, J. R., and Koning, C. D., 1993. Syn-amphibolite facies Archaean lode gold mineralisation in the Mt. York district, Pilbara Block, Western Australia. Mineralium Deposita, vol. 28, p. 457-468.

Nisbet, E., Cheadle, M., Arndt, N., and Bickle, M., 1993. Constraining the potential temperature of the Archaean mantle: a review of the evidence from komatiites. Lithos, vol. 30, p. 291-307.

Noble, S. R., 1989. Geology, geochemistry and isotope geology of the Trout Lake batholith and the Uchi-Confederation Lakes greenstone belt, northwestern Ontario, Canada. Ph.D. thesis. *in* Toronto, U. o., ed.: Toronto, Ontario, 288 p.

Nohda, S., and Wasserburg, G., 1981. Nd and Sr isotopic study of volcanic rocks from Japan. Earth and Planetary Science Letters, vol. 52, p. 264-276.

Notsu, K., 1983. Strontium isotope composition in volcanic rocks from the Northeast Japan arc. Journal of Volcanology and Geothermal Research, vol. 18, p. 531-548.

Oswald, W., Castonguay, S., Dubé, B., Malo, M., Mercier-Langevin, P., and Biczok, J., 2015. New insights on the geological and structural settings of the Musselwhite banded iron-formation-hosted gold deposit, North Caribou greenstone belt, Superior Province, Ontario. Geological Survey of Canada. Current Research 2015-3, 19 p. doi:10.4095/295570.

Parker, J., 1999. Exploration potential for volcanogenic massive sulphide (VMS) mineralization in the Red Lake greenstone belt. Summary of Field Work and Other Activities 1999, Ontario Geological Survey, Open File Report 6000, p. 19-1 to 22-26.

Parker, J., 2000a. Gold mineralization and wall rock alteration in the Red Lake greenstone belt: A regional perspective. Ontario Geological Survey Open File Report 6032, p. 22-1 to 22-28.

Parker, J., 2000b. Nickel-Copper-Platinum Group Element Sulphide Mineralization in the Red Lake Greenstone Belt: A Preliminary Report. In Summary of Field Work and Other Activities 2000, Ontario Geological Survey, Open File Report 6032, p. 32-1 to 23-14.

Parker, J., 2002. Intermediate to Felsic Plutons in the Red Lake Greenstone Belt: Relationship to Deformation and Gold Mineralization. Summary of Field Work and other Activities 2001, Ontario Geological Survey, Open File Report 6070, p. 19-1 to 19-10.

Parks, J., Lin, S., Davis, D., and Corkery, T., 2006. New high-precision U-Pb ages for the Island Lake greenstone belt, northwestern Superior Province: implications for regional stratigraphy and the extent of the North Caribou terrane. Canadian Journal of Earth Sciences, v. 43, p. 789-803.

Parman, S., Dann, J., Grove, T., and De Wit, M., 1997. Emplacement conditions of komatiite magmas from the 3.49 Ga Komati Formation, Barberton greenstone belt, South Africa. Earth and Planetary Science Letters, vol. 150, p. 303-323.

Passchier, C., and Trouw, R., 2005. Microtectonics, Springer, 371 p.

Payot, B. D., Jego, S., Maury, R. C., Polve, M., Gregoire, M., Ceuleneer, G., Tamayo, R. A., Yumul, G. P., Bellon, H., and Cotten, J., 2007. The oceanic substratum of Northern Luzon: Evidence from xenoliths within Monglo adakite (the Philippines). Island Arc, vol. 16, p. 276-290.

Pearce, J., 1996. A user's guide to basalt discrimination diagrams. Trace element geochemistry of volcanic rocks: applications for massive sulphide exploration. Geological Association of Canada, Short Course Notes, vol. 12, 113 p.

Pearce, J., and Stern, R., 2006. Origin of back-arc basin magmas: Trace element and isotope perspectives. Back-Arc Spreading Systems: Geological, Biological, Chemical, and Physical Interactions, p. 63-86.

Pearce, J. A., 2008. Geochemical fingerprinting of oceanic basalts with applications to ophiolite classification and the search for Archean oceanic crust. Lithos, vol. 100, p. 14-48.

Penczak, R. S., and Mason, R., 1997. Metamorphosed Archean epithermal Au-As-Sb-Zn-(Hg) vein mineralization at the Campbell mine, notherwestern Ontario. Economic Geology, vol. 92, p. 696-719.

Percival, J. A., 2007. Geology and metallogeny of the Superior province, Canada. *in* Goodfellow, W. D., ed., Mineral Deposits of Canada: A Synthesis of Major Deposit Types, District Metallogeny, and Evolution of Geological Provinces and Exploration Methods, Geological Association of Canada, Mineral Deposits Division, Special Publication No. 5, p. 903-928.

Percival, J. A., Sanborn-Barrie, M., Skulski, T., Stott, G. M., Helmstaedt, H., and White, D. J., 2006. Tectonic evolution of the western Superior Province from NATMAP and Lithoprobe studies. Canadian Journal of Earth Sciences, vol. 43, p. 1085-1117.

Phillips, G. N., and Powell, R., 2010. Formation of gold deposits: a metamorphic devolatilization model. Journal of Metamorphic Geology, vol. 28, p. 689-718.

Pirie, J., 1981. Regional geological setting of gold deposits in the Red Lake area, northwestern Ontario. Ontario Geological Survey Miscellaneous paper 97, p. 71-93.

Poulsen, K. H., Robert, F., and Dubé, B., 2000. Geological Classification of Canadian Gold Deposits; Geological Survey of Canada, 113 p.

Rainsford, D. R. B., 2017. New Airborn Magnetic and Gamma-ray Spectrometer Surveys in the Ear Falls Area, oral presentation, Ontario Prospectors Exploration Showcase, Thunder Bay, April 4, 2017.

Ridley, J., and Diamond, L., 2000. Fluid chemistry of orogenic lode gold deposits and implications for genetic models. Reviews in Economic Geology, vol. 13, p. 141-162.

Ridley, J. R., and Barnicoat, A. C., 1990. Wallrock alteration in amphibolite-facies gold deposits. In: Ho, S.E., Groves, D.I., Bennett, J.M. (eds.) Gold deposits of the Archaean Yilgarn Block, Western Australia: Nature, Genesis and Exploration Guides. Geology Department and University Extension, University of Western Australia Publication 20: p. 79-86.

Rivers, T., 1997. Lithotectonic elements of the Grenville Province: review and tectonic implications. Precambrian Research, vol. 86, p. 117-154.

Robert, F., and Poulsen, K. H., 2001. Vein formation and deformation in greenstone gold deposits. Reviews in Economic Geology, vol. 14, p. 111-155.

Robert, F., Poulsen, K. H., Cassidy, K. F., and Hodgson, C. J., 2005. Gold Metallogeny of the Superior and Yilgarn Cratons. Economic Geology 100th Anniversary volume, p. 1001-1033.

Robert, F., Poulsen, K. H., and Dubé, B., 1997. Gold deposits and their geological classification; *in* Proceedings of Exploration '97: Fourth Decennial International Conference on Mineral Exploration, (ed.) A.G. Gubins; GEO F/X. p. 209-220.

Rock, N. M. S., Groves, D. I., Perring, C. S., and Golding, S. D., 1989. Gold, Lamprophyres, and Porphyries: What Does Their Association Mean? Economic Geology, vol. 6, p. 609-625.
Roger, J. A., 1992. The Arthur W. White mine, Red Lake area, Ontario: Detailed structural interpretation the key to successful grade control and exploration. Canadian Mining and Metallurgical Bulletin, vol. 85, p. 37-44.
Rollinson, H. R., 1993. Using geochemical data: evaluation, presentation, interpretation, Routledge.
Ross, P.-S., and Bédard, J. H., 2009. Magmatic affinity of modern and ancient subalkaline volcanic rocks determined from trace-element discriminant diagrams. Canadian Journal of Earth Sciences, vol. 46, p. 823-839.
Rudnick, R. L., and Fountain, D. M., 1995. Nature and composition of the continental crust: a lower crustal perspective. Reviews of Geophysics, vol. 33, p. 267-309.
Ryerson, F. J., and Watson, E., 1987. Rutile saturation in magmas: implications for TiNbTa depletion in island-arc basalts. Earth and Planetary Science Letters, vol. 86, p. 225-239.
Sanborn-Barrie, M., Skulski, T., and Parker, J., 2001. 300 m.y. of tectonic history recorded by the Red Lake greenstone belt. Ontario Geological Survey of Canada Current Research 2001-C19, 32 p.
Sanborn-Barrie, M., Skulski, T., and Parker, J., 2004. Geology, Red Lake greenstone belt western Superior province, Ontario, Ontario Geological Survey of Canada Open File 4594.
Sanborn-Barrie, M., Skulski, T., Parker, J., and Dubé, B., 2000. Integrated regional analysis of the Red Lake belt and its mineral deposits, western Superior province, Ontario. Ontario Survey of Canada Current Research 2000C-18, 12 p.
Sangster, A. L., and Smith, P. K., 2007. Metallogenic summary of the Meguma gold deposits, Nova Scotia. *in* Goodfellow, W. D., ed., Mineral Deposits of Canada: A Synthesis of Major Deposit-Types, District Metallogeny, the Evolution of Geological Provinces, and Exploration Methods, Geological Association of Canada, Mineral Deposits Division, Special Publication No. 5, p. 723-732.
Saunders, A., Norry, M., and Tarney, J., 1991. Fluid influence on the trace element compositions of subduction zone magmas. Philosophical Transactions: Physical Sciences and Engineering, vol. 335, p. 377-392.
Saunders, A. D., and Tarney, J., 1984. Geochemical characteristics of basaltic volcanism within back-arc basins. Geological Society, London, Special Publications, vol. 16, p. 59-76.
Schaltegger, U., Amundsen, H., Jamtveit, B., Frank, M., Griffin, W., Gronvold, K., Tronnes, R., and Torsvik, T., 2002. Contamination of OIB by underlying ancient continental lithosphere: U-Pb and Hf isotopes in zircons question EM1 and EM2 mantle components.
Schmidt, M., and Jagoutz, O., 2017. The global systematics of primitive arc melts. Geochemistry, Geophysics, Geosystems, 38 p.
Schmitz, M. D., and Schoene, B., 2007. Derivation of isotope ratios, errors, and error correlations for U-Pb data. Geochem. Geophys. Geosyst., vol. 8, 38 p.
Schulz, K. J., and William, C. F., 2007. The Penokean orogeny in the Lake Superior region. Precambrian Research, vol. 157, p. 4-25.
Shao, W.-Y., Chung, S.-L., and Chen, W.-S., 2014. Zircon U-Pb Age Determination of Volcanic Eruptions in Lutao and Lanyu in the Northern Luzon Magmatic Arc. Terrestrial, Atmospheric & Oceanic Sciences, vol. 25, p. 149-187.
Shao, W.-Y., Chung, S.-L., Chen, W.-S., Lee, H.-Y., and Xie, L.-W., 2015. Old continental zircons from a young oceanic arc, eastern Taiwan: Implications for Luzon subduction initiation and Asian accretionary orogeny. Geology, vol. 43, p. 479-482.
Shibata, T., and Nakamura, E., 1997. Across-arc variations of isotope and trace element compositions from Quaternary basaltic volcanic rocks in northeastern Japan: Implications for interaction

between subducted oceanic slab and mantle wedge. Journal of Geophysical Research: Solid Earth, vol. 102, p. 8051-8064.
Sibson, R., Moore, J. M. M., and Rankin, A., 1975. Seismic pumping—a hydrothermal fluid transport mechanism. Journal of the Geological Society, vol. 131, p. 653-659.
Skulski, T., Corkery, M. T., Stone, D., Whalen, J. B., and Stern, R. A., 2000. Geological and geochronological investigations in the Stull Lake-Edmund Lake greenstone belt and granitoid rocks of the northwestern Superior Province. Report of Activities 2000, Manitoba Industry, Trace and Mines, Manitoba Geological Survey, p. 117-128.
Smith, I. E. M., Worthington, T. J., Price, R. C., and Gamble, J. A., 1997. Primitive magmas in arc-type volcanic associations; examples from the Southwest Pacific. The Canadian Mineralogist, vol. 35, p. 257-273.
Sparks, R., 1986. The role of crustal contamination in magma evolution through geological time. Earth and Planetary Science Letters, vol. 78, p. 211-223.
Stefánsson, A., and Seward, T. M., 2004. Gold (I) complexing in aqueous sulphide solutions to 500 C at 500 bar. Geochimica et Cosmochimica Acta, vol. 68, p. 4121-4143.
Stevenson, R. K., and Turek, A., 1992. An isotopic study of the Island Lake Greenstone Belt, Manitoba: crustal evolution and progressive cratonization in the lake Archean. Canadian Journal of Earth Sciences, vol. 29, p. 2200-2210.
Stone, D., 1998. Precambrian geology of the Berens River area, northwest Ontario; Ontario Geological Survey, Open File Report 5963, 116p.
Storey, M., Kent, R. W., Saunders, A. D., Salters, V. J., Hergt, J., Whitechurch, H., Sevigny, J. H., Thirlwall, M. F., Leat, P., Ghose, N. C., and Gifford, M., 1992. Lower Cretaceous Volcanic Rocks on Continental Margins and their Relationship to the Kerguelen Plateau. In: Wise, S.W., Schlich, R., et al. (Eds.), Proceedings of the Ocean Drilling rogram Scientific Results 120, p. 33-53.
Stott, G. M., 1996. The geology and tectonic history of the central Uchi Subprovince; Ontario Geological Survey, Open File Report 5952, 178p.
Stott, G. M., 1997. The Superior province, Canada, Oxford Monograph on Geology and Geophysics, vol. 35, p. 480-507.
Stott, G. M., 2008. Precambrian geology of the Hudson Bay and James Bay lowlands region interpreted from aeromagnetic data - south sheet; Ontario Geological Survey, Preliminary Map P.3599 - Revised scale 1:500 000.
Stott, G. M., and Corfu, F., 1991. Uchi subprovince, Ontario Geological Survey
Stott, G.M., Corkery, M.T., Leclair, A., Boily, M., and Percival, J. 2007. A revised terrane map for the Superior Province as interpreted from aeromagnetic data. Institute of Lake Superior Geology, vol. 53, p. 74-76.
Stott, G. M., Corkery, M. T., Percival, J. A., Simard, M., and Goutier, J., 2010. A Revised Terrane subdivision of the Superior Province. Summary of Field Work and Other Activities 2010, Ontario Geological Survey, Open File Report 6260, p. 20-1 to 20-10.
Sun, S.-s., and McDonough, W. F., 1989. Chemical and isotopic systematics of oceanic basalts: implications for mantle composition and processes. Geological Society, London, Special Publications, vol. 42, p. 313-345.
Survey, O. G., 1978. Airborne Electromagnetic and Total Intensity Magnetic Survey, Red Lake Area, Map H, District of Kenora; by Questor Surveys Limited, for the Ontario Geological Survey. *in* Ser., G., ed., Prelim. Map P. 1578.
Survey, O. G., 2017. Survey report on Seperation Lake area, Onario airborne geophysical surveys, magnetic gradiometer and gamma-ray spectrometric data, grid and profile data (Geosoft® formats) and vector data, Separation Lake area, Ontario Geological Survey, Geophysical Data Set 1038b.

Tanaka, T., Togashi, S., Kamioka, H., Amakawa, H., Kagami, H., Hamamoto, T., Yuhara, M., Orihashi, Y., Yoneda, S., Shimizu, H., Kunimaru, T., Takahashi, K., Yanagi, T., Nakano, T., Fujimaki, H., Shinjo, R., Asahara, Y., Tanimizu, M., and Dragusanu, C., 2000. JNdi-1: a neodymium isotopic reference in consistenccy with LaJolla neodymium. Chemical Geology, vol. 168, p. 279-281.

Tarnocai, C., 2000. Gold mineralization at the Campbell mine, Red Lake greenstone belt, Uchi subprovince Ontario: Unpublished Ph.D. thesis. *in* Ottawa, U. o., ed.: Ottawa, 227 p.

Taylor, B., and Martinez, F., 2003. Back-arc basin basalt systematics. Earth and Planetary Science Letters, vol. 210, p. 481-497.

Taylor, S.R. and McLennan, S.M., 1985. The Continental Crust: Its Composition and Evolution. Blackwell, Oxford, 312 p.

Thirlwall, M. F., 2000. Inter-laboratory and other errors in Pb isotope analyses investigated using a ^{207}Pb-^{204}Pb double spike. Chemical Geology, vol. 163.

Thompson, A. J. b., and Thompson, J. F. H., 1996. Atlas of Alteration. A Field and Petrographic Guide to Hydrothermal Alteration Minerals. Geological Association of Canada, Mineral Deposits Division, 119 p.

Thompson, P. H., 2003. Toward a new metamorphic framework for gold exploration in the Red Lake greenstone belt. Ontario Geological Survey Open File Report 6122, 51 p.

Thurston, P., and Fryer, B., 1983. The geochemistry of repetitive cyclical volcanism from basalt through rhyolite in the Uchi-Confederation greenstone belt, Canada. Contributions to Mineralogy and Petrology, vol. 83, p. 204-226.

Thurston, P., Osamani, I., and Stone, D., 1991. Northwestern Superior Province: Review and terrane analysis, Special Volume 4, Part 1, Ontario Geological Survey, p. 81-142.

Thurston, P. C., 2015. Greenstone Belts and Granite-Greenstone Terranes: Constrains on the Nature of the Archean World. Geoscience Canada, vol. 42, p. 437-484.

Thurston, P. C., and Chivers, K. M., 1990. Secular Variation in Greenstone Sequence Development Emphasizing Superior Province, Canada. Precambrian Research, vol. 46, p. 21-58.

Tollstrup, D., Gill, J., Kent, A., Prinkey, D., Williams, R., Tamura, Y., and Ishizuka, O., 2010. Across-arc geochemical trends in the Izu-Bonin arc: Contributions from the subducting slab, revisited. Geochemistry, Geophysics, Geosystems, vol. 11, 27 p.

Tomlinson, K. Y., Stevenson, R. K., Hughes, D. J., Hall, R. P., Thurston, P. C., and Henry, P., 1998. The Red Lake greenstone belt, Superior Province: evidence of plume-related magmatism at 3 Ga and evidence of an older enriched source. Precambrian Research, vol. 89, p. 59-76.

Torsvik, T., Amundsen, H., Trønnes, R., Doubrovine, P., Gaina, C., Kusznir, N., Steinberger, B., Corfu, F., Ashwal, L., and Griffin, W., 2015. Continental crust beneath southeast Iceland. Proceedings of the National Academy of Sciences, 112, E1818-E1827.

Vearncombe, J., Barley, M., Eisenlohr, B., Groves, D., Houstoun, S., Skwarnecki, M., Grigson, M., and Partington, G., 1989. Structural controls on mesothermal gold mineralization: examples from the Archean terranes of southern Africa and Western Australia. Economic Geology Monograph vol. 6, p. 124-134.

Viljoen, M., and Viljoen, R. P., 1969. The geology and geochemistry of the lower ultramafic unit of the Onverwacht Group and a proposed new class of igneous rocks. Geological Society of South Africa Special Publication, vol.2, p. 55-86.

Weinberg, R. F., Hodkiewicz, P. F., and Groves, D. I., 2004. What controls gold distribution in Archean terranes? Geology, 32, 545-548.

White, W., 2013. Geochemistry, Wiley Online Library.

Willoughby, N. O., 1988. Report on the Geology and Mineralization of the Laird Lake Property of Tasu Resources Ltd. . *in* Ltd., B. C. M., ed.

Winter, J. D., 2001. An introduction to igneous and metamorphic petrology, New Jersey: Prentice Hall.

Witt, W. K., and Vanderhor, F., 1998. Diversity within a unified model for Archaean gold mineralization in the Yilgarn Craton of Western Australia: an overview of the late-orogenic, structurally-controlled gold deposits. Ore Geology Reviews, vol. 13, p. 29-64.

Woodhead, J., Eggins, S., and Gamble, J., 1993. High field strength and transition element systematics in island arc and back-arc basin basalts: evidence for multi-phase melt extraction and a depleted mantle wedge. Earth and Planetary Science Letters, vol. 114, p. 491-504.

Wyman, D., and Hollings, P., 2006. Late-Archean Convergent Margin Volcanism in the Superior Province: A Comparison of the Blake River Group and Confederation Assemblage. Archean Geodynamics and Environments, p. 215-237.

Young, M. D., McNicoll, V., Helmstaedt, H., Skulski, T., and Percival, J. A., 2006. Pickle Lake revised: New structural, geochronological and geochemical constrains on greenstone belt assembly, western Superior Province, Canada. Canadian Journal of Earth Sciences, vol. 43, p. 821-847.

Yu, J.-H., O'Reilly, S. Y., Wang, L., Griffin, W. L., Zhou, M.-F., Zhang, M., and Shu, L., 2010. Components and episodic growth of Precambrian crust in the Cathaysia Block, South China: evidence from U–Pb ages and Hf isotopes of zircons in Neoproterozoic sediments. Precambrian Research, vol. 181, p. 97-114.

Appendix A

Field and Sample Descriptions

Appendix A

(a) Mineral abbreviations: amphibole (amph), carbonate (carb), chalcopyrite (cpy), clinozoisite (czo), diopside (diop), epidote (epi), Fe-carbonate (Fe-carb), feldspar (feld), garnet (grt), hornblende (hbl), hematite (hem), K-feldspar (K-spar), magnetite (mag), pyrrhotite (po), pyroxene (px), pyrite (py), quartz (qtz), serpentine (serp)

(b) Abbreviations: alteration (alt), breccia (bx), contact (ctct), mineral (min), crystal (xtal)

(c) All foliation and bedding measurements use the right hand rule.

(d) UTMs are noted in NAD83, UTM Zone 15.

(e) Stations and samples starting with LL-15 were taken during the 2015 field season whereas those starting with LL-16… were taken during the 2016 field season. LL-16 stations might be revisited stations from 2015 if the station number is between 001 and 451.

(f) See section 4.4 p.88-103 for detailed descriptions of the mineralized trenches.

Station	Easting	Northing	Assemblage	Rock Description	Foliation	Bedding	Geochemistry sample	Trench
LL-15BG001	423558	5644175	Confederation	Felsic qtz-feld porphyritic xtal tuff to lapilli tuff; very fine-grained; bedding (mm to 1cm thick beds) parallel to foliation defined by alined qtz+feld xtals	055/74			
LL-15BG002	423583	5644184	Killala-Baird	Hbl bt granodiorite; medium to coarse-grained; massive; 25% mafic min				
LL-15BG003	423531	5644215	Killala-Baird	Hbl bt granodiorite; medium to coarse-grained; massive; 30% mafic min; unoriented epi stringers; mafic xenolith up to 6 cm long				
LL-15BG004	423534	5644078	Confederation	Diorite; fine to medium-grained; massive; epi stringers; up to 2% disseminated fine-grained py;				
LL-15BG005	423540	5644021	Confederation	Diorite; medium-grained; foliation defined by mafic min	060/			
LL-15BG006	423506	5643978	Confederation	Qtz-feld porphyritic xtal tuff; very fine to fine-grained; foliation defined by aligned qtz-feld xtals	056/74			
LL-15BG007	423558	5643849	Confederation	Bt granodiorite; medium to coarse-grained; massive; 10% bt				
LL-15BG008	423556	5643754	Confederation	Mafic volcanic; fine-grained; foliation defined by feld pheno; trace grt	080/			
LL-15BG009	423605	5643647	Confederation	Hbl bt granodiorite; medium-grained; weakly foliated				
LL-15BG010	423606	5643617	Confederation	Diorite; medium-grained; strongly foliated	068/90			
LL-15BG011	423065	5643529	Confederation	Mafic volcanic; fine-grained; feld phenos up to 1cm long; strongly foliated, defined by aligned feld phenos; local qtz stringers	085/66		LL-15BG011A04	
LL-15BG012	423343	5644005		Pyroxenite; medium-grained; massive; locally porphyritic (px now hbl); 95-65% mafic min; granitic veins bx pyroxenite; epi veinlets cutting granitic veins and pyroxenite				
			Killala-Baird	Hbl bt granodiorite; coarse-grained; massive; epi veinlets				
LL-15BG013	423948	5643487	Confederation	Mafic volcanic; fine-grained; foliated; 1cm thick qtz vein parallel to foliation; local rusty areas	100/90		LL-15BG013A01 (Mafic volcanic) LL-15BG013B01 (very rusty mafic volcanic)	
LL-15BG014	423968	5643435	Confederation	Felsic volcanic or intrusion; medium-grained; strongly foliated, defined by aligned bt	255/69			
LL-15BG015	423947	5643314	Confederation	Intermediate volcanic; fine to medium-grained; foliated	273/74			

Station	Easting	Northing	Assemblage	Rock Description	Foliation	Bedding	Geochemistry sample	Trench
LL-15BG016	423824	5643265	Confederation	Felsic volcanic or intrusion; medium-grained; strongly foliated, defined by aligned bt	289/90			
LL-15BG017	423428	5643128	Confederation	Intermediate volcanic; fine-grained; foliated, defined by aligned bt; granitic veins	275/72		LL-15BG017A01	
LL-15BG018	423402	5643069	Medicine stone	Hbl bt granodiorite; medium-grained; weakly foliated				
LL-15BG019	423446	5463058	Medicine stone	Hbl bt granodiorite; medium to coarse-grained; weakly foliated	272/80			
LL-15BG020	423712	5643138	Confederation	Mafic volcanic; fine-grained; strongly foliated, defined by aligned bt	273/84			
LL-15BG021	423782	5643215	Medicine stone	Hbl bt granodiorite; medium to coarse-grained; weakly foliated				
LL-15BG022	424058	5643543	Confederation	Mafic volcanic; fine-grained; foliated; granitic intrusions parallel to foliation	248/			
LL-15BG023	423060	5644193	Balmer	Mafic volcanic; fine-grained; aphyric; foliated; trace py in qtz veinlets; pyroxenite and granitic veins cutting host rock	107/61		LL-15BG023A01	
LL-15BG024	423020	5644156	Confederation	Felsic volcanic (flow and tuff); fine-grained; mm to cm scale bed thickness; foliated; pyroxenite dike; ctct with Balmer lichen covered	134/83			
LL-15BG025	422923	5644186	Confederation	Felsic volcanic (flow and tuff); fine-grained; mm to cm scale bed thickness; foliated; atz vein parallel to foliation	140/90			
			Balmer	Mafic volcanic; fine-grained; aphyric; strongly foliated; irregular/contorted alteration bands of bt, czo and hbl; xenolithic diorite cutting host rock at ctct with Confederatio; rare qtz	315/76			
LL-15BG026	422869	5644211		Pyroxenite; fine-grained; massive; 50% mafic min; cut by xenolithic diorite and granitic veins; late faults and shear displacing unit on cm scale				
LL-15BG027	422861	5644171	Confederation	Felsic volcanic (tuff and qtz porphyritic xtal tuff); fine-grained; foliated, defined by layering and aligned qtz	116/84		LL-15BG027A01	
			Confederation	Mafic volcanic; fine-grained; feld phenos up to 1cm long; weakly foliated				
LL-15BG028	422751	5644185		Pyroxenite; medium to coarse-grained; massive; 95-80% mafic min; cut by xenolithic diorite to granodiorite and granitic veins bx host rock; late faults and shear displacing unit on cm scale; unoriented epi veinlets				

Station	Easting	Northing	Assemblage	Rock Description	Foliation	Bedding	Geochemistry sample	Trench
LL-15BG029	422717	5644190		Pyroxenite; medium to coarse-grained; massive; 95-80% mafic min; cut by xenolithic diorite to granodiorite and granitic veins bx host rock; late faults and shear displacing unit on cm scale; unoriented epi veinlets				
LL-15BG030	422814	5644039	Confederation	Felsic volcanic; fine-grained; aphyric; foliated	110/			
LL-15BG031	422834	5644007	Confederation	Qtz-feld porphyritic xtal tuff; very fine to fine-grained; foliation defined by aligned qtz-feld xtals; 1cm long qtz xtals	106/68			
LL-15BG032	422904	5643962		Diorite; medium-grained; 20% bt and px; massive				
			Confederation	Qtz-feld porphyritic xtal tuff; fine-grained; foliation defined by aligned qtz-feld xtals; 1cm long qtz xtals	100/82		LL-15BG032B01	
LL-15BG033	423057	5643938	Confederation	Qtz-feld porphyritic xtal tuff; fine-grained; foliation defined by aligned qtz-feld xtals; 2-3cm long qtz xtals; potassic alt and feld xtals	095/74			
LL-15BG034	423058	5643768	Confederation	Qtz-feld porphyritic xtal tuff; fine-grained; foliation defined by aligned qtz-feld xtals; 4mm long qtz and 3mm long feld xtals	085/70			
			Confederation	Mafic volcanic; fine-grained; equant amph poikiloblasts up to 2mm; foliated; lineation defined by amph (140→64)	085/70			
LL-15BG035	423029	5643567	Confederation	Qtz-feld porphyritic xtal tuff; fine-grained; foliation defined by aligned qtz-feld xtals and bt; unoriented epi stringers	076/78		LL-15BG035A01	
LL-15BG036	422875	5643481	Confederation	Intermediate volcanic; fine to medium-grained; foliated, defined by bt; granitic veins up to 2m wide; epi stringers	070/90			
LL-15BG037	422666	5643591	Confederation	Mafic volcanic; fine-grained; feld phenos; foliated, defined by aligned feld phenos; rare py specks and cpy on qtz stringers	090/90			
LL-15BG038	422592	5643582	Confederation	Mafic volcanic; fine-grained; foliated; rare specks of py; local diop- and grt-rich bands				

Station	Easting	Northing	Assemblage	Rock Description	Foliation	Bedding	Geochemistry sample	Trench
LL-15BG039	422756	5643969	Confederation	Qtz-feld porphyritic xtal tuff; fine-grained; 1-0.5cm long qtz and feld xtals; foliation defined by aligned qtz-feld xtals and bt; mag stringers with euhedral py	071/77		LL-15BG039A01	
LL-15BG040	422771	5643941	Confederation	Felsic to intermediate volcanic; fine-grained; foliation parallel to bedding; beds 1-0.2 cm thick; trace dissimenated py; smokey qtz veins/pods up to 4cm thick; milky qtz veins up to 10cm thick	089/64			
LL-15BG041	422755	5643906	Confederation	Felsic to intermediate volcanic; fine-grained; weakly foliated				
LL-15BG042	422853	5643834	Confederation	Qtz-feld porphyritic xtal tuff; fine-grained; qtz and feld xtals up to 7mm long; foliation defined by aligned qtz-feld xtals	092/89			
LL-15BG043	422832	5643859	Confederation	Mafic volcanic; fine-grained; equant amph poikiloblasts up to 5mm and 30%; foliated				
			Confederation	Diorite; fine to medium-grained; foliated; 10m thick				
LL-15BG044	424033	5643839	Confederation	Mafic volcanic; fine-grained; feld phenos up to 2mm long and 5%; folation defined by aligned feld phenos	075/			
LL-15BG045	424053	5643925	Confederation	Mafic volcanic; fine-grained; possible pillows (less than 10cm wide); feld phenos up to 1cm long and 15%; amph poikiloblasts up to 2mm long and 30%; massive to foliated; foliation defined by aligned feld and amph xtals; 15cm wide granitic veins	061/73		LL-15BG045A01	
LL-15BG046	423991	5644211	Killala-Baird	Hbl granodiorite; coarse-grained; weakly foliated, defined by aligned hbl; epi stringers and pods	095/90			
LL-15BG047	423697	5644499	Killala-Baird	Bt granodiorite; medium- to coarse-grained; massive; 5% bt				
LL-15BG048	423520	5644392	Killala-Baird	Hbl granodiorite; medium- to coarse-grained; massive; epi stringers				
LL-15BG049	423659	5644264	Killala-Baird	Hbl granodiorite; medium- to coarse-grained; massive; epi stringers				
LL-15BG050	423659	5644205	Killala-Baird	Hbl bt granodiorite; medium- to coarse-grained; massive; 25% mafic min; mafic xenoliths up to 3cm long; epi stringers				

Station	Easting	Northing	Assemblage	Rock Description	Foliation	Bedding	Geochemistry sample	Trench
LL-15BG051	423657	5644160	Confederation	Intermediate volcanic; fine-grained; cut by fractionated pyroxenite, monzogabbro and qtz vein; late epi stringers			LL-15BG051B01	
LL-15BG052	423790	5644132		Pyroxenite; fine- to medium-grained; 50-75% mafic min				
LL-15BG053	423809	5643797	Confederation	Mafic volcanic; fine-grained; feld phenos up to 1cm long and 15%; amph poikiloblasts up to 2mm long and 30%; foliated; foliation defined by aligned feld and amph xtals				
LL-15BG054	422720	5643825	Confederation	Felsic to intermediate volcanic tuff; fine-grained; foliation parallel to bedding; beds <1cm thick; trace dissimenated py			LL-15BG054A01	
			Confederation	Mafic volcanic; fine-grained; amph poikiloblasts up to 40% and 7mm wide; foliation defined by aligned amph	070/80		LL-15BG054B01	
				Diorite; medium-grained; foliation defined by mafic min; milky qtz vein up to 7cm thick parallel to perpendicular to foliation			LL-15BG054C01	
LL-15BG055	422685	5643763	Confederation	Qtz-feld porphyritic xtal tuff; fine-grained; foliation defined by aligned qtz-feld xtals; qtz and feld xtals up to 45% and 7mm long; local rusty zones but no sulphides observed; milky qtz vein up to 7cm parallel to foliation; unit cut by foliated mafic dike (30cm) and massive granitic dikes (3-0.5cm)	085/84		LL-15BG055A01	
LL-15BG056	422560	5643687	Confederation	Mafic volcanic; fine-grained; foliated; local bands with feld phenos; possible ankerite pods	085/			
LL-15BG057	422478	5644195		Pyroxenite; medium-grained; massive; 90% mafic min; N-S trending granitic veins (8cm thick) bx host rock				
LL-15BG058	422411	5644194		Pyroxenite; fine- to medium-grained; massive; 40% subhedral px/amph up to 9mm wide; N-S trending granitic veins; epi stringers; local py specks;				

Station	Easting	Northing	Assemblage	Rock Description	Foliation	Bedding	Geochemistry sample	Trench
LL-15BG059	422293	5644117		Pyroxenite; medium-grained; massive; 90% mafic min; xenolithic granitic veins 8cm thick				
LL-15BG060	422267	5644172	Balmer	Mafic volcanic; fine-grained; aphyric; local py specks in rusty zones				
LL-15BG061	422203	5644128	Balmer	Mafic volcanic; fine-grained; aphyric				
LL-15BG062	422196	5644054		Pyroxenite; medium-grained; massive; 95-60% mafic min; cut by xenolithic granodiorite to granitic veins bx host rock, pyroxenite clasts are rounded to angular and range from 10-2 cm wide; epi stringers				
LL-15BG063	422102	5643987		Pyroxenite; medium-grained; massive; 95-60% mafic min; cut by xenolithic granodiorite to granitic veins bx host rock, pyroxenite clasts are rounded to angular and range from 10-2 cm wide; epi stringers				
LL-15BG064	422028	5643919		Bt granodiorite; medium-grained; massive; host pyroxenite xenoliths, rounded to angular from 1-10cm wide; epi stringers;				
LL-15BG065	422142	5643929		Pyroxenite; medium-grained; massive; 95-60% mafic min; cut by xenolithic granodiorite to granitic veins bx host rock, pyroxenite clasts are rounded to angular and range from 10-2 cm wide; epi stringers				
LL-15BG066	422224	5643935	Balmer	Mafic volcanic; fine-grained; diorite stringers to pods; rare specks of disseminated py				
LL-15BG067	422287	5643938	Balmer	Mafic volcanic; fine-grained; strongly foliated, defined by bt-rich bands; <1% disseminated py	095/70			
				Pyroxenite; medium-grained; massive; px/amph xtals up to 7mm wide; 10cm wide granitic dikes; epi stringers on cm-scale faults				
LL-15BG068	422465	5643952	Confederation	Qtz-feld porphyritic xtal tuff; very fine-grained; foliation defined by aligned qtz-feld xals up to 3 mm long; epi stringers; massive granitic and pyroxenite dikes cross-cutting and up to 15cm wide				

Station	Easting	Northing	Assemblage	Rock Description	Foliation	Bedding	Geochemistry sample	Trench
LL-15BG069	422485	5643980		Pyroxenite; medium-grained; massive; cutting felsic to intermediate volcanic parallel to bedding; xenolithic diorite to granodiorite cutting both pyroxenite and volcanics; late shears and faults displace all units on a N-S cm to m scale				
LL-15BG070	422650	5644000	Confederation	Qtz-feld porphyritic xtal tuff; fine-grained; foliation defined by aligned qtz-feld xals up to 1cm long; 2m wide rusty zone parallel to foliation and bedding with up to 10% py; 3m wide mafic volanic unit with feld phenos parallel to bedding	097/79			Zone 11
LL-15BG071	422629	5644085		Pyroxenite; medium- to coarse-grained; massive; px/amph xtals up to 90% and 5mm wide; 40cm wide xenolithic granitic dikes; rare specks of py; epi stringers on cm-scale faults			LL-15BG071A01	
LL-15BG072	422309	5643629	Confederation	Mafic volcanic; fine-grained; feld pheno up to 1.5cm long, locally define flow direction striking between 085-120° ; locally weakly to moderately foliated, defined by consistent aligned feld pheno and bt in matrix; ctct with felsic volcanic parallel with foliation	084/85			
LL-15BG073	422351	5643532	Confederation	Mafic volcanic; fine-grained; feld phenos up to 2mm long; foliated, defined by aligned bt; milky qtz veins and granitic intrusions striking 065°	060/			
LL-15BG074	422293	5643442	Confederation	Mafic volcanic; fine-grained; feld phenos up to 3mm long; foliated, defined by aligned feld phenos and bt; milky qtz veins and granitic intrusions striking 065°	085/90			
LL-15BG075	422624	5643381	Confederation	Mafic volcanic; fine-grained; aphyric; foliated, defined by aligned bt	250/76			
LL-15BG076	422548	5643297	Confederation	Mafic volcanic; fine-grained; local amph poikiloblasts up to 10% and 5mm wide; strong foliation defined by aligned amph and bt-rich banding; felsic stringers parallel to foliation; smokey qtz vein subparallel to foliation	068/89			
LL-15BG077	422424	5643254	Confederation	Mafic volcanic; fine-grained; local amph poikiloblasts up to 10% and 5mm wide; strong foliation defined by aligned amph and bt-rich banding; felsic stringers parallel to foliation; smokey qtz vein subparallel to foliation	068/89			

Station	Easting	Northing	Assemblage	Rock Description	Foliation	Bedding	Geochemistry sample	Trench
LL-15BG078	422315	5643271	Confederation	Mafic volcanic; fine-grained; feld phenos up to 35% and 7mm long; foliated, defined by aligned feld phenos; cut by unoriented granitic vein 30cm wide	246/78			
LL-15BG079	422215	5643207	Confederation	Mafic volcanic; fine-grained; feld phenos; foliated, defined by aligned feld phenos; cut by unoriented mafic dike			LL-15BG079A01	
LL-15BG080	421991	5643110	Confederation	Mafic volcanic; fine-grained; feld phenos; foliated, defined by aligned feld phenos and bt	068/84			
LL-15BG081	421787	5642968	Confederation	Mafic volcanic; fine-grained; feld phenos; foliated, defined by aligned feld phenos				
			Confederation	Mafic volcanic; fine-grained; local amph poikiloblasts up to 40% and 3mm wide; strong foliation defined by aligned amph and bt-rich banding; small felsic stringers throughout	065/72 90→63			
LL-15BG082	421801	5643080	Confederation	Mafic volcanic; fine-grained; feld phenos up to 15% and 7mm long; foliated, defined by aligned feld phenos and bt; smokey qtz veins unoriented up to 3cm wide	060/90			
LL-15BG083	421816	5643185	Confederation	Mafic volcanic; fine-grained; feld phenos up to 2mm long; bt alt; foliated, defined by aligned bt	080/67			
LL-15BG084	421810	5643233	Confederation	Intermediate volcanic; fine-grained; feld phenos up to 60% and 2mm; bt alt; foliated, defined by aligned feld phenos and bt	080/90			
LL-15BG085	421851	5643263	Confederation	Intermediate volcanic; fine-grained; foliated, defined by aligned bt	071/86			
LL-15BG086	421974	5643280	Confederation	Intermediate volcanic; fine-grained; foliated, defined by aligned bt; thin qtz-feld xtal tuff layers parallel to foliation	071/86			
LL-15BG087	422167	5643352	Confederation	Intermediate volcanic; fine-grained; foliated, defined by aligned bt; thin qtz-feld xtal tuff layers parallel to foliation	065/88			
LL-15BG088	422219	5643691	Confederation	Mafic volcanic; fine-grained; aphyric; foliated; bt alt, possible k-spar alt; up to 15% layered to disseminated py			LL-15BG088A01	
LL-15BG089	422034	5643637	Confederation	Mafic volcanic; fine-grained; amph poikiloblasts up to 25% and 5mm wide; foliated, defined by aligned amph xtals; bt alt; up to 1% disseminated py, qtz veinlets locally associated with disseminated py; smokey qtz vein up to 7cm; local amph veinlets	087/89			

Station	Easting	Northing	Assemblage	Rock Description	Foliation	Bedding	Geochemistry sample	Trench
			Confederation	Qtz-feld porphyritic xtal tuff; fine-grained; qtz-feld xtals up to 35% and 5mm; foliated, defined by aligned qtz-feld xtals; smokey qtz vein up to 3cm subparallel to foliation	086/76			
LL-15BG090	422277	5643677	Confederation	Qtz-feld porphyritic xtal tuff; fine-grained; qtz-feld xtals up to 35% and 5mm; foliated, defined by aligned qtz-feld xtals	115/			
LL-15BG091	422476	5643716	Confederation	Qtz-feld porphyritic xtal tuff; fine-grained; foliated, defined by aligned qtz-feld xtals				
LL-15BG092	422423	5643755	Confederation	Mafic volcanic; fine-grained; foliated; bt alt; up to 1% disseminated py, qtz veinlets locally associated with disseminated py				
LL-15BG093	423328	5644473	Killala-Baird	Hbl bt granodiorite; medium- to coarse-grained; 15-20% hbl+bt; massive; epi stringers				
LL-15BG094	423325	5644271	Killala-Baird	Hbl granodiorite; coarse-grained; 15-20% hbl; massive				
LL-15BG095	422938	5644419	Killala-Baird	Hbl bt granodiorite; coarse-grained; 25% hbl+bt; massive; epi stringers and patches			LL-15BG095A01	
LL-15BG096	422526	5644517	Killala-Baird	Hbl bt granodiorite; coarse-grained; 5-10% hbl+bt; massive; epi veinlets up to 3mm wide				
LL-15BG097	422123	5644506	Killala-Baird	Bt granodiorite; medium- to coarse-grained; 5-10% bt; massive				
LL-15BG098	421657	5644616	Killala-Baird	Bt granodiorite; coarse-grained; 10% bt; massive				
				Bt qtz diorite; medium- to coarse-grained; up to 50% bt; massive				
LL-15BG099	421693	5644448	Killala-Baird	Bt granodiorite; medium- to coarse-grained; up to 5-10% bt; massive				
LL-15BG100	422384	5644362	Killala-Baird	Hbl bt granodiorite; fine to medium-grained; epi and hem alt; massive				
LL-15BG101	422648	5644314	Killala-Baird	Bt granodiorite; coarse-grained; 5-10% bt; epi veinlets				

Station	Easting	Northing	Assemblage	Rock Description	Foliation	Bedding	Geochemistry sample	Trench
LL-15BG102	422707	5644254	Balmer	Mafic volcanic; fine-grained; aphyric; weakly foliated; rare disseminated py; xenolithic granodiorite vein, mafic volcanic xenolith up to 15cm wide; milky qtz vein up to 3cm wide; local epi stringers	293/		LL-15BG102A01	
LL-15BG103	422888	5644234	Killala-Baird	Hbl bt granodiorite; medium-grained; 40% hbl+bt; massive				
LL-15BG104	422996	5644231	Balmer	Mafic volcanic; fine-grained; aphyric; weakly foliated; qtz-carb stringers striking 160°	260/			
LL-15BG105	423465	5644216	Killala-Baird	Hbl bt granodiorite; medium-grained; 40% hbl+bt; massive				
LL-15BG106	423552	5644260	Killala-Baird	Hbl bt granodiorite; medium- to coarse-grained; 15-20% hbl+bt; lineated qtz xtals; local epi stringers	95→			
LL-15BG107	423309	5643947	Confederation	Qtz-feld porphyritic xtal tuff; fine-grained; qtz and feld xtals up to 7mm long; foliation defined by aligned qtz-feld xtals; qtz veinlets parallel to foliation	086/76			
LL-15BG108	423278	5643734	Confederation	Mafic volcanic; fine-grained; feld phenos up to 15% and 4mm long; foliated, defined by aligned phenos; local areas without feld phenos with up to 10% disseminated py and 1% dissminated garnets 1-3mm wide	074/65		LL-15BG108A01	
LL-15BG109	423111	5643672		Mafic volcanic; fine-grained; aphyric; weakly foliated; cut by medium-grained syeno-diorite with up to 80% bt+hbl				
LL-15BG110	423101	5643446	Confederation	Mafic volcanic; fine-grained; feld phenos up to 20% and 4mm long; foliated, defined by aligned feld phenos; epi veinlets up to 2cm thick; qtz-carb stringers	070/60			
LL-15BG111	422950	5643410	Confederation	Mafic to intermediate volcanic; fine-grained; <1% disseminated py; cut by large granitic intrusion				
LL-15BG112	422939	5643381	Confederation	Felsic to intermediate volcanic; fine-grained; foliated, define by aligned bt; 1% disseminated py in rusty areas	245/74		LL-15BG112A01	
LL-15BG113	422755	5643161	Confederation	Felsic to intermediate volcanic; fine- to medium-grained; foliated, define by aligned bt; epi veinlets up to 1cm thick	250/64		LL-15BG113A01	

Station	Easting	Northing	Assemblage	Rock Description	Foliation	Bedding	Geochemistry sample	Trench
LL-15BG114	422677	5643101	Confederation	Qtz porphyritic xtal tuff; fine-grained; qtz xtals up to 10-15% and 5mm long; foliation defined by aligned qtz xtals				
LL-15BG115	422424	5642990	Confederation	Felsic to intermediate volcanic; fine- to medium-grained; foliated, define by aligned bt; epi veinlets up to 1cm thick	078/70			
LL-15BG116	423020	5643713	Confederation	Mafic volcanic; fine-grained; local feld phenos; foliated, defined by feld phenos; possible bt alt;				
LL-15BG117	423063	5643741	Confederation	Mafic volcanic; fine- to medium-grained; amph poikiloblasts up to 25% and 4mm; feld phenos up to 5%; foliated, defined by bt and feld				
LL-15BG118	423155	5643811	Confederation	Mafic volcanic; fine-grained; foliated; felsic stringers parallel to foliation				
LL-15BG119	423234	5643882	Confederation	Mafic volcanic; fine-grained; feld phenos up to 1cm long; foliated, defined by aligned feld phenos	094/64			
LL-15BG120	423184	5643957	Confederation	Felsic to intermediate volcanic; fine-grained; foliated, defined by banding	050/60			
LL-15BG121	421835	5643503	Confederation	Mafic volcanic; fine-grained; feld phenos up to 50% and 2.5cm long, locally trachytic; moderately to weakly foliated, defined by aligned feld phenos and bt; cut by diorite intrusion with epi stringers throughout	070/90			
LL-15BG122	421836	5643356	Confederation	Intermediate to mafic volcanic; fine-grained; foliated, defined by aligned bt; <1% disseminated py; cut by unoriented 4cm thick granitic vein and 30cm thick mafic dike parallel to foliation	064/90			
LL-15BG123	421852	5643271	Confederation	Mafic to intermediate volcanic; fine-grained; foliated, defined by aligned bt	060/80			
LL-15BG124	421695	5643033	Confederation	Intermediate volcanic; fine-grained; feld phenos up to 15% and 5mm long; bt alt; foliated, defined by aligned feld phenos and bt	085/79			
LL-15BG125	421546	5643111	Confederation	Intermediate to mafic volcanic; fine-grained; feld phenos up to 10-15% and 2-3mm long; bt alt; foliated, defined by aligned feld phenos and bt; foliated diorite xenoliths or boudinaged intrusion?	078/82			
LL-15BG126	421538	5643110	Confederation	Conglomerate (monolithic) or strongly boudinaged diorite?; clasts up to 10-40cm long, surrounded by fine-grained mafic zones up to 10cm thick; strongly foliated, defined by aligned clasts and bt in mafic portions				

Station	Easting	Northing	Assemblage	Rock Description	Foliation	Bedding	Geochemistry sample	Trench
LL-15BG127	421342	5643055	Confederation	Intermediate to felsic volcanic; fine-grained; strongly foliated, defined by aligned bt; faint laminations observed (tuff?)	095/89		LL-15BG127A01	
LL-15BG128	421770	5643346	Confederation	Intermediate to mafic volcanic; fine-grained; feld phenos up to 2mm long; foliated, defined by aligned feld phenos and bt	070/90			
LL-15BG129	421772	5643437	Confederation	Intermediate volcanic; fine-grained; foliated, defined by aligned bt; cut by unoriented granitic dike	086/75		LL-15BG129A01	
LL-15BG130	421716	5643463	Confederation	Mafic volcanic; fine-grained; amph poikiloblasts up to 45% and 5mm wide; foliated, defined by aligned amph	125/			
LL-15BG131	421675	5643471	Confederation	Intermediate volcanic; fine-grained; local layers with feld phenos up to 3mm long; laminations observed (tuff?); strongly foliated, defined by aligned feld phenos and bt				
LL-15BG132	421866	5644109	Balmer	Mafic volcanic; fine-grained; vesicular; aphyric; faintly foliated, defined by aligned bt; cut by unoriented felsic veinlets; <1% disseminated py				
LL-15BG133	422002	5644161	Balmer	Mafic volcanic; fine-grained; aphyric; foliated, defined by aligned bt; qtz-carb veinlets parallel to subparallel to foliation	090/82			
LL-15BG134	422066	5644184	Balmer	Mafic volcanic; fine-grained; aphyric; foliated, defined by aligned bt; qtz-carb veinlets parallel to foliation	110/78		LL-15BG134A01	
			Balmer	Mafic volcanic; fine-grained; aphyric; foliated, defined by aligned bt; qtz-carb veinlets parallel to foliation; rusty zone with 5-10% disseminated to veined py			LL-15BG134A02	
LL-15BG135	421207	5644499	Killala-Baird	Hbl bt granodiorite; fine to coarse-grained; strongly foliated, defined by aligned qtz xtals and mafic mins; epi stringers parallel to foliation; hem patches throughout; rare py specks	105/81		LL-15BG135A01	

Station	Easting	Northing	Assemblage	Rock Description	Foliation	Bedding	Geochemistry sample	Trench
LL-15BG136	421069	5644515	Killala-Baird	Hbl bt granodiorite; fine to coarse-grained; strongly foliated, defined by aligned qtz xtals and mafic mins; epi stringers parallel to foliation; hem patches throughout	105/71			
LL-15BG137	420953	5644489	Balmer	Mafic volcanic; fine-grained; pillows up to 50cm long and 30cm thick; foliated, defined by aligned bt and length of pillows; pillow selvages are light brown (sericite-rich?) with dark margins (amph-rich?); possible Fe-carb alt in stringers	085/65		LL-15BG137A01	
LL-15BG138	420684	5644409	Balmer	Mafic volcanic; fine-grained; foliated, defined by aligned bt; possible Fe-carb; qtz stringers striking 176°				
LL-15BG139	420154	5644319	Balmer	Mafic volcanic; fine-grained; foliated, defined by aligned bt; unoriented qtz stringers	110/58			
LL-15BG140	419791	5644343	Balmer	Mafic volcanic; fine-grained; foliated, defined by aligned bt; unoriented to parallel to fol felsic veinlets up to 3mm wide to pods 5x10cm	105/64			
LL-15BG141	419662	5644298	Balmer	Mafic volcanic; fine-grained; pillows up to 30cm long and trend 113 (way up 030), selvages are up to 3cm thick and ser alt?; qtz filled vesicles; foliated, defined by aligned vesicles, bt and pillows; felsic dike up to 20cm thick parallel to foliation; qtz-carb veinlets parallel to subparallel to foliation				
LL-15BG142	421236	5644077	Balmer	Ultramafic volcanic; island of boulders on Laird Lake				
LL-15BG143	419625	5644263	Balmer	Mafic volcanic; fine-grained; pillows up to 1m long and trend 102, selvages are up to 3cm thick; qtz filled vesicles; foliated, defined by aligned vesicles, bt and pillows; felsic dike up to 2m thick cutting foliation; qt stringers throughout outcrop parallel to subparallel to foliation, ranging from 2-10mm thick	102/56		LL-15BG143A01	

Station	Easting	Northing	Assemblage	Rock Description	Foliation	Bedding	Geochemistry sample	Trench
LL-15BG144	419586	5644224		Diorite; xenolithic with up to 85% clasts ranging from 15-0.2cm long, rounded to subangular, oriented parallel to the margins of the intrusions, clasts are composed of pyroxenite, ultramafic volcanic, mafic volcanic and diorite; diorite clasts display internal foliation or are unfoliated; intrusion is 2-3m thick; host rock is weakly foliated, defined by aligned clasts?	105/74			
LL-15BG145	419452	5644143	Balmer	Mafic volcanic; fine-grained; pillows up to 70cm long and 30cm wide, selvages are up to 4cm thick and rusty brown; pillows trend 120 and way up is 030-040; qtz-filled vesicles up to 5-10%; foliated, defined by pillows and bt; <1% disseminated py in rusty zones; granitic intrusions 1-2m wide; qtz-carb veinlets parallel to subparallel to foliation			LL-15BG145A01	
LL-15BG146	419252	5644055	Balmer	Mafic volcanic; fine-grained; foliated, defined by aligned bt; cut by 1m wide granitic dike; qtz veinlets unoriented to parallel to foliation	105/62			
LL-15BG147	419168	5644022	Balmer	Mafic volcanic; fine-grained; pillows up to 50cm long, selvages are up to 5cm thick and rusty brown; pillows trend 110° and way up is 355-5°; qtz-filled vesicles concentrated on pillow edge and top of pillows; foliated, defined by pillows and bt; qtz-carb veinlets parallel to subparallel to foliation	095/61			
LL-15BG148	419012	5643937	Balmer	Mafic volcanic; fine-grained; pillows up to 60cm long, selvages are up to 3cm thick and rusty brown to locally qtz-filled; pillows trend 092° and way up is 004°; qtz-filled vesicles up to 5-10% throughout host rock; foliated, defined by pillows and bt	075/56			
LL-15BG149	418967	5643858	Killala-Baird	Bt granodiorite; medium-grained; 20% bt (possible hbl); massive; intrusion from Killala-Baird batholith?			LL-15BG149A01	
LL-15BG150	418940	5643840	Balmer	Ultramafic volcanic; fine-grained; talc and serp alt; weakly foliated; elephant skin texture; light green weathered surface; up to 10% po, patchy to disseminated; vug with euhedral grt up to 5mm wide; qtz-carb veins to patches unoriented			LL-15BG150A01	
LL-15BG151	418961	5643790		Bt hbl granodiorite; medium-grained; massive; 20% bt+hbl; epi alt on fracture planes				

Station	Easting	Northing	Assemblage	Rock Description	Foliation	Bedding	Geochemistry sample	Trench
LL-15BG152	419036	5643740		Qtz bt monzogabbro; medium-grained; massive; 50% bt; cut by qtz-kspar pegmatitic veins				
LL-15BG153	422165	5643707	Confederation	Mafic volcanic; fine-grained; amph poikiloblasts up to 7mm wide; foliated, defined by aligned amph and bt	060/75			
LL-15BG154	422153	5643768	Confederation	Mafic volcanic; fine-grained; foliated, defined by aligned amph and bt				
LL-15BG155	421976	5643738	Confederation	Intermediate to felsic volcanic; fine-grained; bedded to laminated with layers composed of various percentage of qtz and feld porphyritic xtals; milky to smokey qtz veins up to 6cm wide parallel to foliation; foliation parallel to bedding	083/90			
LL-15BG156	421839	5643834	Confederation	Mafic volcanic; fine-grained; amph poikiloblasts up to 20-30% and 3mm wide; foliated, defined by aligned amph and bt; cut by a medium-grained foliated diorite and massive 10m thick granitic dike	047/70			
LL-15BG157	421828	5643815	Confederation	Mafic volcanic; fine-grained; amph poikiloblasts up to 30%; foliated, defined by aligned amph; cut by unoriented felsic veinlets up to 4cm wide, parallel to subparallel to foliation; local epi alt	065/86			
LL-15BG158	421782	5643802	Confederation	Felsic to intermediate volcanic; fine-grained; bedded to laminated; foliated parallel to bedding; possible mafic flow or mafic dike parallel to bedding; clear to smokey qtz veins up to 6cm thick, parallel to bedding/foliation	110/78		LL-15BG158A01	
			Confederation	Mafic volcanic; fine-grained; feld phenos up to 1.5cm long; foliated, defined by aligned feld phenos; local zones of 1% disseminated py				
			Confederation	Mafic volcanic; fine-grained; amph poikiloblasts up to 30%; foliated, defined by aligned amph				
LL-15BG159	421638	5643793	Confederation	Bimodal felsic to intermediate and mafic volcanic; same as previous station (158); flows are typically 1-4m thick				
LL-15BG160	421687	5643684	Confederation	Mafic volcanic; fine-grained; feld phenos up to 1.5cm long; foliated, defined by aligned feld phenos				

Station	Easting	Northing	Assemblage	Rock Description	Foliation	Bedding	Geochemistry sample	Trench
LL-15BG161	419195	5643720		Diorite; medium-grained; xenolithic with up to 30-40% clasts ranging from 20-0.5cm long, rounded to subangular, clasts are composed of pyroxenite (8%), ultramafic volcanic (2%), mafic volcanic (30%), granodiorite (10%) and diorite (50%); xenoliths display trachytic alignment 092°				
				Monzogabbro; medium-grained; massive; cut by coarse-grained granitic vein up to 15cm thick				
LL-15BG162	419228	5643671		Monzogabbro; medium-grained; foliated, defined by mafic phases; local equant xenoliths up to 3cm wide; cut by coarse-grained granitic vein; epi veinlets trending 040°	129/53			
LL-15BG163	419251	5643571		Diorite; medium-grained; xenolithic with up to 30-40% clasts ranging from 20-0.5cm long, rounded to subangular, clasts are composed of pyroxenite (18%), ultramafic volcanic (2%), mafic volcanic (40%), granodiorite (10%) and diorite (30%); xenoliths display trachytic alignment 275°; epi veinlets trending 040°				
LL-15BG164	419423	5643491		Diorite; medium- to coarse-grained; xenolithic with up to 30-40% clasts ranging from 20-0.5cm long, rounded to subangular, clasts are composed of pyroxenite (18%), ultramafic volcanic (2%), mafic volcanic (40%), granodiorite (10%) and diorite (30%); xenoliths display trachytic alignment 045°; epi veinlets				
LL-15BG165	419638	5643523		Qtz-monzogabbro; medium-grained; massive to foliated; 50-70% hbl + bt; local diorite xenoliths; cut by granitic vein up to 2cm and qtz veins up to 3cm wide; epi veinlets				
LL-15BG166	419689	5643607		Diorite; medium-grained; weakly foliated; 60-70% hbl+bt; bt-rich blebs up to 6mm wide; cut by pegmatitic granitic dike up to 40cm thick, trending 095°				
LL-15BG167	419789	5643524		Qtz-monzogabbro; medium-grained; weakly foliated; 60% hbl + bt; rare diorite xenoliths; cut by granitic vein up to 50cm wide				
LL-15BG168	419917	5643552	Balmer	Mafic volcanic; fine-grained; weakly foliated; ser + tur alt?; local trace disseminated py				

Station	Easting	Northing	Assemblage	Rock Description	Foliation	Bedding	Geochemistry sample	Trench
LL-15BG169	419956	5643572	Balmer	Mafic volcanic; fine-grained; foliated, defined by bt; strongly deformed qtz veins associated with rusty zone parallel to foliation with layered to disseminated py up to 15%; hbl veinlets parallel to foliation	075/73		LL-15BG169A01	
LL-15BG170	419975	5643738		Hbl bt granodiorite; fine- to medium-grained; massive; 5-10% hbl+bt; cut by qtz veinlets				
LL-15BG171	419786	5643745	Balmer	Ultramafic intrusion or possibly volcanic; fine-grained; seems fairly massive; serp up to 30% throughout; hem-filled fractures; strongly magnetic; local elephant skin texture				
LL-15BG172	419645	5643764	Balmer	Ultramafic volcanic or possibly intrusion; fine-grained; seems fairly massive; local bx section with clasts up to 5cm wide; serp up to 5-10% throughout and concentrated in bx matrix; hem alt in local patches; strongly magnetic; cut by ultramafic intrusion with local elephant skin texture			LL-15BG172A02	
LL-15BG173	419657	5643814	Balmer	Ultramafic intrusion or possibly volcanic; fine-grained; seems fairly massive; serp up to 30% throughout; strongly magnetic; local elephant skin texture				
LL-15BG174	419717	5643880		Diorite; medium-grained; massive; 75% hbl+bt; cut by unoriented granitic veins up to 4cm thick				
LL-15BG175	419858	5643858		Pyroxenite; medium- to coarse-grained; massive; 75% subhedral px/amph; 1 mafic xenolith observed; granitic veins up to 20cm thick and mafic dike up to 15cm thick; epi stringers; local py specks				
LL-15BG176	419963	5643961	Balmer	Ultramafic volcanic; local flow bx zones up to 1-2m thick with clasts ranging from 1-20cm long, serp-rich matrix; majority of clasts are vesicular; clasts are rounded to subangular; strongly magnetic				
			Balmer	Ultramafic intrusion; fine-grained; massive; 8-0.2 m thick; possible feeder tube x-section observed; local elephan texture; local clast shown to cut into intrusion; strongly magnetic				
LL-15BG177	419946	5643998	Balmer	Ultramafic volcanic; local flow bx zones with 90% clasts ranging from 1-20cm long, local serp-rich matrix; majority of clasts are vesicular or have eroded out pits; local bx zones host clasts with spinifex needles up to 5cm long; strongly magnetic			LL-15BG177A03	

Station	Easting	Northing	Assemblage	Rock Description	Foliation	Bedding	Geochemistry sample	Trench
			Balmer	Ultramafic intrusion; fine-grained; massive; 20-40cm thick; sharp ctct with flow bx; strongly magnetic			LL-15BG177B01	
LL-15BG178	420041	5643827		Monzogabbro; medium- to coarse-grained; massive; 50-60% mafic min (px, hbl, bt); cut by granitic intrusion up to 10cm; shearing (345°) marked by epi veinlets				
LL-15BG179	420161	5643805		Monzogabbro; medium- to coarse-grained; weakly foliated; 50-60% mafic min (px, hbl, bt); cut by granitic intrusion up to 10cm; shearing (345°) marked by epi veinlets	120/84			
LL-15BG180	420246	5643809		Diorite; medium-grained; xenolithic with clasts up to 25cm long, rounded to angular, clasts are composed of pyroxenite, ultramafic volcanic, mafic volcanic, granodiorite and diorite; xenoliths display trachytic alignment				
LL-15BG181	420367	5643775	Balmer	Mafic volcanic; fine-grained; strongly foliated, defined by banding in alteration; local chaotic folding; czo and hbl bands, local diop zones, possible Fe-carb alt; local qtz pods and veins up to 1cm thick	115/56		LL-15BG181A01	
LL-15BG182	420464	5643761		Diorite; medium-grained; massive; cut by hem and epi veinlets; cut by granitic veins up to 2m thick				
LL-15BG183	420510	5643773	Balmer	Mafic volcanic; fine-grained; foliated, defined by aligned bt; local epi veinlets; rare disseminated cubic py; cut by granitic and diorite veins	048/65			
LL-15BG184	420556	5643798		Diorite; medium-grained; weakly foliated; cut by hem and epi veinlets; cut by granitic veins				
LL-15BG185	420590	5643788	Balmer	Mafic volcanic; fine-grained; strongly foliated, defined by banding in alteration; local chaotic folding; czo and hbl bands, local diop zones, possible Fe-carb alt; 5-10% serp throughtout; rare disseminated py				
LL-15BG186	420687	5643787	Balmer	Mafic to ultramafic volcanic; fine-grained; strongly foliated, defined by banding in alteration; local chaotic folding; czo and hbl bands; 5-10% serp throughout	075/84			
LL-15BG187	420827	5643735	Balmer	Mafic volcanic; fine-grained; fairly massive; rare disseminated py				

Station	Easting	Northing	Assemblage	Rock Description	Foliation	Bedding	Geochemistry sample	Trench
LL-15BG188	420955	5643753	Balmer	Ultramafic intrusion; fine-grained; massive; elephant skin; up to 15-20% serp throughout; very magnetic				
LL-15BG189	421054	5643808	Balmer	Mafic to ultramafic volcanic; fine-grained; foliated, defined by banding in alteration; czo bands; 5-10% serp throughout	084/60			
LL-15BG190	421111	5643827	Balmer	Mafic volcanic; fine-grained; foliated, defined by aligned mineral banding; bands of bt, hbl, czo with local diop pods; local rusty zones with up to 2% disseminated py or 1mm thick py stringers parallel to foliation	052/63		LL-15BG190A01	
LL-15BG191	421182	5643859	Balmer	Mafic volcanic; fine-grained; foliated, defined by aligned bt; cut by mafic dike				
LL-15BG192	421422	5643915	Balmer	Mafic volcanic; fine-grained; foliated, defined by aligned bt				
LL-15BG193	421368	5643696	Confederation	Mafic volcanic; fine-grained; amph poikiloblasts up to 40% and 7mm wide in coarser sections; weakly foliated defined by aligned amph and bt; trace disseminated py; cut by xenolithic diorite containing mafic volcanic and diorite xenoliths ranging from 2-20cm wide				
LL-15BG194	421348	5643645	Confederation	Felsic volcanic; fine-grained; layering parallel to foliation; epi veinlets unoriented	255/82			
LL-15BG195	421314	5643539	Confederation	Felsic volcanic; fine-grained; local sections of qtz porphyriti xstal tuff, qtz up to 7mm long and up to 10-15%; foliated, defined by aligned qtz xtals	265/90			
LL-15BG196	421285	5643522	Confederation	Mafic volcanic; fine-grained; foliated; cut by diorite and granitic veins up to 10cm wide				
LL-15BG197	421215	5643506	Confederation	Felsic volcanic; fine-grained; foliated, defined by aligned bt	065/90			
LL-15BG198	421176	5643427	Confederation	Mafic volcanic; fine-grained; feld phenos up to 20-30% and up to 2cm long (averaging 5mm long); foliated, defined by aligned feld phenos; milky qtz veins up to 25cm thick with epi stringers cutting across			LL-15BG198A01	
LL-15BG199	420955	5643281	Confederation	Mafic volcanic; fine-grained; feld phenos up to 30-40% and up to 3cm long; foliated, defined by aligned feld phenos	100/65			

Station	Easting	Northing	Assemblage	Rock Description	Foliation	Bedding	Geochemistry sample	Trench
LL-15BG200	420942	5643231	Confederation	Mafic volcanic; fine-grained; feld phenos up to 20% and up to 5mm long; foliated, defined by aligned feld phenos	079/58			
LL-15BG201	420846	5643238	Confederation	Qtz-Feld porphyritic xtal tuff; fine-grained; qtz up to 1cm long, feld up to 7mm long, 10-15%; foliated, defined by aligned and stretched qtz and feld xtals	091/79			
LL-15BG202	420838	5643124	Confederation	Mafic volcanic; fine-grained; foliated, defined by aligned bt; local layers of qtz-feld porphyry xtal tuff; milky qtz vein up to 10cm thick	083/86			
LL-15BG203	420709	5643073	Confederation	Mafic volcanic; fine-grained; feld phenos up to 10% and up to 5mm long; foliated, defined by aligned feld phenos				
LL-15BG204	420625	5643073	Confederation	Mafic volcanic; fine-grained, foliated				
LL-15BG205	420557	5643039	Confederation	Mafic volcanic; fine-grained; feld phenos up to 20-30% and up to 10-3mm long; foliated, defined by aligned feld phenos	090/85		LL-15BG205A01	
LL-15BG206	420586	5643127	Confederation	Mafic volcanic; fine-grained; feld phenos up to 30-40% and up to 2cm long; foliated, defined by aligned feld phenos; cut by fine-grained granitic dike	060/88			
LL-15BG207	420569	5643340	Confederation	Mafic volcanic; fine-grained; feld phenos up to 5-10% and up to 1cm long; foliated, defined by aligned feld phenos; cut by coarse-grained diorite dike	085/64			
LL-15BG208	420625	5643378	Confederation	Mafic volcanic; fine-grained; feld phenos up to 5-10% and up to 1cm long; foliated, defined by aligned feld phenos; cut by granitic vein up to 20cm thick				
LL-15BG209	420692	5643439	Confederation	Mafic volcanic; fine-grained; feld phenos up to 10% and up to 1cm long; foliated, defined by aligned feld phenos; cut by granitic vein up to 15cm thick	094/85			
LL-15BG210	420832	5643468	Confederation	Mafic volcanic; fine-grained; feld phenos up to 10-15% and up to 1.5cm long; foliated, defined by aligned feld phenos; cut by granitic vein up to 15cm thick				
LL-15BG211	420935	5643517	Confederation	Mafic volcanic; fine-grained; feld phenos up to 5-10% and up to 1cm long; foliated, defined by aligned feld phenos; cut by granitic vein up to 15cm thick				

Station	Easting	Northing	Assemblage	Rock Description	Foliation	Bedding	Geochemistry sample	Trench
LL-15BG212	420994	5643569	Confederation	Intermediate to mafic volcanic; fine-grained; amph poikiloblasts up to 15% and 5mm wide; foliated, defined by aligned and stretched amph				
LL-15BG213	421182	5643658	Confederation	Intermediate to mafic volcanic; fine-grained; amph poikiloblasts up to 15% and 5mm wide; foliated, defined by aligned and stretched amph; epi+kspar alt patches parallel to foliation	075/90			
LL-15BG214	420664	5643643	Confederation	Mafic and intermediate volcanic; intercalated flows/tuffs; fine-grained; foliated, defined by aligned bt	082/85			
LL-15BG215	420634	5643604	Confederation	Mafic volcanic; fine-grained; up to 20% amph poikiloblasts up to 5mm wide; foliated, defined by aligned amph; cut by intermediate dike subparallel to foliation	070/			
LL-15BG216	420587	5643409	Confederation	Felsic volcanic; fine-grained; foliated, defined by aligned bt; epi veinlets;	086/68			
LL-15BG217	420587	5643378	Confederation	Intermediate volcanic; fine-grained; layering parallel to foliation	087/79			
LL-15BG218	420414	5643284	Confederation	Mafic volcanic; fine-grained; feld phenos up to 5-10% and up to 1cm long; foliated, defined by aligned feld phenos; intercalated with intermediate volcanic	091/77			
LL-15BG219	420340	5643235	Confederation	Mafic volcanic; fine-grained; feld phenos up to 15% and up to 5mm long; amph poikiloblasts up to 20% and 3mm wide; foliated, defined by aligned feld phenos and amph poikiloblasts; rare dissminated chalco; milky qtz vein up to 3cm thick parallel to foliation; intercalated with qtz-feld porphyritic xtal tuff, up to 10% qtz-feld xtals up to 5mm long	090/87		LL-15BG219A01	
LL-15BG220	420390	5643168	Confederation	Intermediate volcanic; fine-grained; foliated				
LL-15BG221	420430	5643111	Confederation	Mafic volcanic; fine-grained; equant feld phenos up to 2mm wide up to 10%; foliated, defined by bt and feld phenos; intercalated with intermediate volcanic; layering parallel to foliation; cut by diorite dike	082/81			
LL-15BG222	420365	5643009	Confederation	Intermediate volcanic; fine-grained; foliated				
LL-15BG223	420345	5642926	Confederation	Mafic volcanic; fine-grained; feld phenos; foliated, defined by aligned feld phenos	105/90			
LL-15BG224	420262	5642836	Confederation	Intermediate volcanic; fine-grained; foliated; cut by 50cm thick granitic vein possibly from the Medicine Stoke Lake batholith				

Station	Easting	Northing	Assemblage	Rock Description	Foliation	Bedding	Geochemistry sample	Trench
LL-15BG225	420162	5642789	Confederation	Intermediate volcanic; fine-grained; layering parallel to foliation	102/90			
LL-15BG226	420030	5642747	Confederation	Intermediate volcanic; fine-grained; layering parallel to foliation, also defined by aligned bt	077/80		LL-15BG226A01	
LL-15BG227	420036	5642982	Confederation	Mafic volcanic; fine-grained; foliated; 5% feld phenos	067/88			
LL-15BG228	420040	5643019	Confederation	Mafic volcanic; fine-grained; foliated; garnets and bt-rich section (2m thick) where garnets are 0.5-1.5cm wide, equant, 10-60%; garnets are lineated 65→67; local qtz pods	075/87		LL-15BG228A03	
			Confederation	Intermediate volcanic; fine-grained; foliated; gradual transition from mafic to intermediate volcanic	095/90		LL-15BG228B01	
LL-15BG229	420126	5643181	Confederation	Intermediate volcanic; fine-grained; foliated	080/			
LL-15BG230	420244	5643387	Confederation	Mafic to intermediate volcanic; fine-grained; foliated; trace disseminated py				
LL-15BG231	422646	5644037	Confederation	Felsic volcanic; fine-grained; tuffaceous; thinly bedded		100/80	LL-15BG231A01	Zone 11
LL-15BG232	422623	5643969	Confederation	Qtz-feld porphyry xtal tuff; fine-grained; qtz-feld xtals up to 15% and 2mm long; really rusty zone (10m thick parallel to bedding) with local zones with up to 20-25% layered to disseminated py; unit is interlayered with fine-grained felsic tuffs and local mafic volcanic layers		089/62	LL-15BG232A01	Zone 11
LL-15BG233	422491	5643792	Confederation	Mafic volcanic; fine-grained; amph poikiloblasts 25-35% up to 2mm wide; foliated, defined by aligned amph; amph veinlets throughout; 40cm thick intermediate intrusion parallel to foliation with 4-5 smokey qtz veins associated with rusty zone	085/90		LL-15BG233A01 (mafic volcanic) LL-15BG233A02 (intermediate dike hosting qtz vein)	SHQ
LL-15BG234	422444	5643838	Confederation	Mafic and intermediate volcanic; intercalated flows/tuffs; fine-grained; foliated, defined by layering in the tuffs and amph poikiloblasts in the flows; sharp to irregular ctct between mafic flows and intermediate tuffs; tuffs are laminated and locally host qtz porphyritic xtals				

Station	Easting	Northing	Assemblage	Rock Description	Foliation	Bedding	Geochemistry sample	Trench
LL-15BG235	421581	5643937	Balmer	Mafic volcanic; fine-grained; foliated; bt-rich alteration; large rusty zone parallel to foliation (6-7m thick) with disseminated to layered py up to 10-15%, potentially chalco and po; hbl-rich dike and diorite dike both cut the volcanics; epi veinlets; qtz-carb veinlets and pods; small S folds present	064/75		LL-15BG235A01 (least altered mafic volcanic) LL-15BG235A02 (py-rich mafic volcanic)	EGBZ
LL-15BG236	421562	5643881	Balmer	Banded-iron formation; rangest from 1-2.5m thick; mag-rich bands range from 0.5-3cm thick and chert bands are up to 10cm thick; crenulation subparallel to bedding is present			LL-15BG236A01	HSZ
			Balmer	Carbonate formation; 20cm thick; mafic bands range from 1-20mm and carbonate bands are 3-15mm thick			LL-15BG236A02	HSZ
			Balmer	Mafic volcanic; fine-grained; foliated; local zones with 25-40% disseminated to layered py; local garnet-rich zones present	065/71		LL-15BG236A03	HSZ
LL-15BG237	421631	5643875	Balmer	Mafic volcanic; fine-grained; foliated; qtz-carb alt veins;				
LL-15BG238	421467	5643890	Balmer	Mafic volcanic; fine-grained; foliated; aphyric; cut by felsic veins and veinlets; sinistral faulting trending 020-030° for 15-20cm				
LL-15BG239	421193	5643775	Balmer	Mafic volcanic; fine-grained; foliated; aphyric; cut by amph-rich mafic dike; 2-3% disseminated py associated with silicified zone	060/		LL-16BG239A01	
LL-15BG240	420944	5643714	Balmer	Mafic volcanic; fine-grained; foliated; epi veinlets unoriented; local trace disseminated py; cut by granitic dike	083/			
LL-15BG241	421297	5643685	Confederation	Intermediate volcanic; fine-grained; bedding parallel to foliation; cut by amph-rich mafic dike, diorite and hbl bt granodiorite	066/81			
LL-15BG242	419779	5643464	Balmer	Mafic volcanic; fine-grained; aphyric; foliated; qtz-carb stringers; local rusty patches with disseminated py up to 3%; cut by tonalitic intrusion	064/90			
LL-15BG243	419730	5643337	Balmer	Mafic volcanic; fine-grained; aphyric; foliated				
LL-15BG244	419726	5643202	Confederation	Mafic volcanic; fine-grained; feld phenos up to 30% and 1.5cm long; foliated, defined by aligned feld pheno	049/81			

Station	Easting	Northing	Assemblage	Rock Description	Foliation	Bedding	Geochemistry sample	Trench
LL-15BG245	419805	5643284	Confederation	Mafic volcanic; fine-grained; feld phenos up to 40% and 1cm long; foliated, defined by aligned feld pheno; cut by granitic dike				
LL-15BG246	420000	5643088	Confederation	Intermediate volcanic; fine-grained; foliated, defined by aligned bt; cut by 10cm thick granitic dike	095/82			
LL-15BG247	420022	5642989	Confederation	Either strongly deformed conclomerate or boudinaged dioritic intrusions; 35% "clasts" are surrounded by fine dark grey matrix, clasts are composed of coarse- to fine-grained diorite and intermediate volcanic, up to 20cm long and rounded				
LL-15BG248	419951	5642980	Confederation	Intermediate volcanic; fine-grained; strongly foliated, defined by aligned bt	075/			
LL-15BG249	419954	5642940	Confederation	Mafic volcanic; fine-grained; foliated, defied by aligned bt and grt; local sections with grt up to 30% and 1cm wide, other sections with grt up to 50-70% and 3mm wide; grt-rich zones are parallel to foliation; strong bt alt and qtz enrichment in local grt-rich zones; grt-rich zone up to 7m thick, with intermediate volcanics north of outcrop; continuation of station 228	079/75			
LL-15BG250	419775	5642997	Confederation	Intermediate volcanic; fine-grained; strongly foliated, defined by aligned bt	096/			
LL-15BG251	419632	5643042	Confederation	Intermediate volcanic; fine-grained; strongly foliated, defined by aligned bt	095/81			
LL-15BG252	419621	5643087	Confederation	Mafic volcanic; fine-grained; foliated; rare specks of py				
LL-15BG253	419673	5643141	Confederation	Mafic volcanic; fine-grained; feld phenos up to 35% and 1cm; foliated, defined by aligned feld phenos				
LL-15BG254	423359	5643955	Confederation	Qtz-feld porphyritic xtal tuff; fine-grained; qtz-feld xtals up to 35% and 8mm long; foliated, defined by aligned qtz-feld xtals; local zones with 1% disseminated py	079/84		LL-15BG254A01	
LL-15BG255	423391	5643863	Confederation	Mafic volcanic; fine-grained; feld phenos up to 15% and 8mm long; amph poikiloblasts up to 50% and 3mm wide; foliated, defined by aligned feld and amph; epi patches; unoriented milky qtz vein up to 3cm thick	61/71 (151)			
LL-15BG256	423407	5643827	Confederation	Qtz-feld porphyritic xtal tuff; fine-grained; qtz-feld xtals up to 15% and 5mm long; foliated, defined by aligned qtz-feld xtals; local zones with 1% disseminated py				
LL-15BG257	423335	5643738	Confederation	Intermediate volcanic; fine-grained; foliated, defined by aligned bt; up to 3% disseminated py				

Station	Easting	Northing	Assemblage	Rock Description	Foliation	Bedding	Geochemistry sample	Trench
LL-15BG258	423391	5643471	Confederation	Mafic volcanic; fine-grained; feld phenos up to 30% and 1cm long; foliated, defined by aligned feld phenos; rare py specks	70/90			
LL-15BG259	423250	5643450	Confederation	Mafic volcanic; fine-grained; feld phenos up to 30% and 1cm long; foliated, defined by aligned feld phenos; rare py specks	70/91			
LL-15BG260	423579	5643351	Confederation	Intermediate volcanic; fine-grained; foliated, defined by aligned bt; rounded feld grains up to 40%;	92/90			
LL-15BG261	423616	5643290	Confederation	Intermediate volcanic; fine-grained; foliated; silicified; up to 2% disseminated py; cut by granitic dike	270/80 (360)		LL-15BG261A01	
LL-15BG262	423744	5643355	Confederation	Intermediate volcanic; fine-grained; foliated; silicified; cut by granitic dike				
LL-15BG263	423809	5643468	Confederation	Mafic volcanic; fine-grained; strongly foliated, defined by weak banding in the rock; qtz-carb and epi veinlets throughout and parallel to foliation; local zone with amph poikiloblasts up to 50%; cut by granitic vein; unoriented milky qtz vein up to 2cm thick	076/90		LL-15BG263A01	
LL-15BG264	419703	5644333		Diorite; medium-grained; weakly foliated, defined by aligned mafic min				
LL-15BG265	419730	5644362	Balmer	Mafic volcanic; fine-grained; foliated, defined by aligned bt				
LL-15BG266	419812	5644414	Killala-Baird	Hbl bt granodiorite; medium- to coarse-grained; 20% hbt+bt; foliated, defined by aligned hbl and bt; cut by medium-grained diorite dike; epi veinlets throughout	110/			
LL-15BG267	419862	5644449	Killala-Baird	Hbl bt granodiorite; medium- to coarse-grained; massive; epi veinlets unoriented				
LL-15BG268	419672	5644618	Killala-Baird	Hbl bt granodiorite; medium- to coarse-grained; massive; 10-15% hbl+bt; disseminated (5%) and unoriented veinlets of epi throughout			LL-15BG268A01	
LL-15BG269	419428	5644494	Killala-Baird	Hbl bt granodiorite; medium- to coarse-grained; massive; cut by fine- to medium-grained pyroxenite				
LL-15BG270	419296	5644562	Killala-Baird	Hbl bt granodiorite; medium-grained; 25-30% bt+hbl; massive; cut by 3cm thick milky qtz vein				
LL-15BG271	419042	5644656	Killala-Baird	Hbl bt granodiorite; medium-grained; 20% bt+hbl; massive				
LL-15BG272	419062	5644562	Killala-Baird	Hbl bt granodiorite; medium-grained; 20% bt+hbl; mafic min weakly lineated	081/			
LL-15BG273	419185	5644448	Killala-Baird	Hbl bt granodiorite; medium-grained; 25-30% bt+hbl; foliated, all minerals are aligned	083/65			

Station	Easting	Northing	Assemblage	Rock Description	Foliation	Bedding	Geochemistry sample	Trench
LL-15BG274	419314	5644365	Killala-Baird	Hbl bt granodiorite; medium-grained; 35% bt+hbl; foliated, defined by aligned mafic min				
LL-15BG275	419412	5644328	Balmer	Mafic volcanic; fine-grained; foliated; possible diop alteration rimming qtz-carb veins parallel to foliation	085/56			
LL-15BG276	419514	5644241	Balmer	Mafic volcanic; fine-grained; foliated; possibly pillowed and vesicular; qtz-carb alt and local possible diop alt zones; local zones with 1% disseminated py associated with qtz-carb alt	085/64			
LL-15BG277	423613	5643962	Confederation	Qtz-feld porphyritic xtal tuff interlayered with felsic tuffs; xtal tuff has up to 35-40% qtz+feld; felsic tuff shows no distinctive bedding; foliated, defined by aligned qtz+feld xtals; local zones with 1% disseminated py; qtz vein unoriented up to 3cm thick	068/66			
LL-15BG278	423602	5644011		Diorite; medium-grained; foliated, defined by mafic aligned bt	065/			
LL-15BG279	423605	5644030	Confederation	Intermediate volcanic; fine-grained; foliated; rare py specks; cut by px-rich dike	081/62			
LL-15BG280	423569	5644066		Diorite; medium-grained; foliated, defined by mafic aligned bt				
LL-15BG281	423613	5644079		Diorite; medium-grained; foliated, defined by mafic aligned bt				
			Confederation	Conglomerate; foliated; 15% rounded to angular clasts of granite, mafic volcanic, chert, tuffs and gneiss; clasts are up to 12 cm long and parallel to foliation; not a very continuous unit				
LL-15BG282	423604	5644134	Confederation	Intermediate volcanic; fine-grained; foliated; local bt alt; cut by monzogabbro dike	068/			
LL-15BG283	423530	5644005	Confederation	Siltstone; fine-grained; finely laminated; interlayered with qtz-feld porphyritic xtal tuff; foliated, defined by aligned qtz and feld xtals	052/80			
LL-15BG284	423489	5643980	Confederation	Qtz-feld porphyritic xtal tuff interlayered with felsic tuffs; xtal tuff has up to 35-40% qtz+feld; foliated, defined by aligned and stretched qtz and feld xtals	059/			

Station	Easting	Northing	Assemblage	Rock Description	Foliation	Bedding	Geochemistry sample	Trench
LL-15BG285	418701	5643790		Qtz monzogabbro to qtz diorite; medium- to coarse-grained; weakly foliated, defined by aligned bt and qtz; 50-60% bt; local mafic xenoliths rounded up to 2cm wide; cut by pegmatitic granitic vein up to 30cm thick	099/72		LL-15BG285A01	
LL-15BG286	418805	5643682	Balmer	Ultramafic volcanic; fine-grained; serp alt; weakly foliated; cut by monzogabbro				
LL-15BG287	418904	5643643	Balmer	Mafic and ultramafic volcanic; fine-grained; foliated; qtz-carb veinlets rimmed by possible diop and epi veinlets both host up to 1% disseminated py; cut by rusty lamprophyre	068/72		LL-15BG287C01	
LL-15BG288	418836	5643608	Balmer	Ultramafic volcanic; fine-grained; flow bx with clasts up to 6cm across; possible vesicles between clasts; elongated clasts are parallel to foliation; serp alt	070/		LL-15BG288A01	
LL-15BG289	418789	5643561	Balmer	Ultramafic intrusion; fine-grained; sharp ctct with ultramafic volcanic flow bx; elephant skin texture; serp alt				
LL-15BG290	418721	5643201	Confederation	Qtz-feld porphyritic xtal tuff; 25-15% qtz+feld; strongly foliated, defined by aligned and stretched qtz and feld xtals	055/82			
LL-15BG291	418639	5643121	Confederation	Mafic volcanic; fine-grained; feld phenos up to 30% and 1cm long; foliated, defined by aligned feld phenos;	056/75		LL-15BG291A01	
				Diorite; fine- to medium-grained; foliated				
LL-15BG292	418583	5643040		Diorite; fine- to medium-grained; strongly foliated; boudinaged felsic and qtz veins;	042/76		LL-15BG292A01	
LL-15BG293	418591	5642891		Diorite; fine- to medium-grained; strongly foliated; folded qtz veins and parallel to foliation; local patches with up to 3% grt up to 2mm wide	080/82			
LL-15BG294	418487	5642880		Diorite; fine- to medium-grained; strongly foliated; epi veinlets; cut by granitic dikes; qtz pods, some folded	080/82			
LL-15BG295	418380	5642988		Felsic pegmatite; coarse- to very coarse-grained; massive				
LL-15BG296	418356	5642965	Balmer	Mafic volcanic; fine-grained; strongly foliated, defined by min banding composed of bt, amph, czo, diop and grt, with qtz groundmass; local bt-rich bands host up to 15% disseminated apy; diop bands are often boudinaged	025/70		LL-15BG296A01	Lee Lake Au showing

Station	Easting	Northing	Assemblage	Rock Description	Foliation	Bedding	Geochemistry sample	Trench
LL-15BG297	418384	5643031	Balmer	Mafic volcanic; fine-grained; strongly foliated, defined by min banding composed of bt, amph, czo, diop and grt, with qtz groundmass	030/66		LL-15BG297A01	Lee Lake Au showing
LL-15BG298	418274	5643030	Balmer	Mafic volcanic; fine-grained; strongly foliated, defined by less prominent min banding; cut by irregular felsic intrusions which cut the foliation	056/35			
LL-15BG299	418217	5643003	Balmer	Mafic volcanic; fine-grained; foliated; cut by coarse-grained diorite				
LL-15BG300	418025	5642741		Diorite; fine- to medium-grained; strongly foliated	058/54			
LL-15BG301	417900	5642634	Confederation	Diorite; fine-grained; strongly foliated; cut by qtz vein parallel to foliation	070/60			
LL-15BG302	417825	5642610		Diorite or felsic lapilli; fine- to medium-grained; very strongly foliated	085/75			
LL-15BG303	417528	5642485	Confederation	Intermediate volcanic; fine-grained; foliated; epi veinlets				
LL-15BG304	417384	5642454	Confederation	Intermediate volcanic; fine-grained; foliated; zones with trace disseminated py				
			Confederation	Mafic volcanic; fine-grained; foliated; local epi veinlets; qtz vein up to 4cm thick; cut by unoriented felsic veinlets	267/78			
LL-15BG305	417326	5642423	Confederation	Mafic volcanic; fine-grained; foliated; unoriented epi veinlets; locally rusty; abundant granitic patches and veinlets up to 30%			LL-15BG305A01	
LL-15BG306	417125	5642382	Confederation	Mafic volcanic; fine-grained; foliated; unoriented epi veinlets; rare py specks in epi veinlets; qtz veinlets			LL-15BG306A01	
LL-15BG307	416984	5642473		Monzogabbro; medium-grained; massive; 50% bt				
				Hbl bt granodiorite; medium- to coarse-grained; massive; 20% mafic min; epi veinlets				
LL-15BG308	416865	5642532		Monzogabbro; medium-grained; massive				
LL-15BG309	416781	5642482		Hbl bt granodiorite; medium- to coarse-grained; massive; 20% mafic min; epi veinlets				
LL-15BG310	416656	5643110		Pyroxenite; coarse- to very coarse-grained; massive; 85% px metamorphosed to amph, up to 1cm wide; cut by unoriented granitic to pegmatitic dikes, locally brecciating the host rock			LL-15BG310A01	

Station	Easting	Northing	Assemblage	Rock Description	Foliation	Bedding	Geochemistry sample	Trench
LL-15BG311	416889	5643722		Pyroxenite; medium- to coarse-grained; massive; 80% px metamorphosed to amph, up to 0.7cm wide; cut by unoriented granitic to pegmatitic dikes, locally brecciating the host rock				
LL-15BG312	417304	5643538		Pyroxenite; coarse-grained; massive; 65% px metamorphosed to amph, up to 1cm wide; epi veinlets; cut by unoriented granitic to pegmatitic dikes, locally brecciating the host rock; zones of amph needles up to 4cm long in felsic pegmatite areas				
LL-15BG313	417343	5643447		Bt granodiorite; medium-grained; up to 5% bt; local coarse-grained pegmatitic zones; massive				
LL-15BG314	417263	5643276		Diorite; medium- to coarse-grained; 40% bt; up to 5% mafic xenoliths which are angular to rounded up to 50cm long; xenoliths generally trend 103°			LL-16BG314A01	
LL-15BG315	419583	5643349	Confederation	Mafic volcanic; fine-grained; feld phenos up to 15% and 4mm long, amph poikiloblasts up to 30% and 5mm wide; foliated, defined by aligned feld and amph; cut by granitic veins	083/55			
LL-15BG316	419586	5643299	Confederation	Intermediate volcanic; fine-grained; bedding parallel to foliation	060/85			
LL-15BG317	419603	5643235	Confederation	Mafic volcanic; fine-grained; foliated, defined by aligned bt	066/68			
LL-15BG318	419600	5643137	Confederation	Intermediate volcanic; fine-grained; bedding parallel to foliation	065/73			
LL-15BG319	419572	5643072	Confederation	Felsic to intermediate volcanic; fine-grained; bedding parallel to foliation; epi veinlets subparallel to foliation; up to 1% disseminated py	086/78			
LL-15BG320	419543	5642985	Confederation	Mafic volcanic; fine-grained; strongly foliated, defined by aligned bt; granitic veints subparallel to foliation or unoriented; qtz vein 5cm thick and locally boudinaged parallel to foliation	088/80			
LL-15BG321	419773	5642821	Confederation	Mafic volcanic; fine-grained; feld phenos up to 15% and 1cm long, amph poikiloblasts up to 30% and 6mm long; foliated, defined by aligned feld and amph	094/65			
LL-15BG322	419562	5642797	Confederation	Mafic volcanic; fine-grained; feld phenos up to 15% and 1cm long, amph poikiloblasts up to 30% and 6mm long; foliated, defined by aligned feld and amph; foliated, defined by aligned feld, amph and bt; bt alt	094/65			

Station	Easting	Northing	Assemblage	Rock Description	Foliation	Bedding	Geochemistry sample	Trench
LL-15BG323	419297	5642643	Confederation	Mafic volcanic; fine-grained; feld phenos up to 20% and 1.5cm long; foliated, defied by aligned feld and bt; bt alt	075/77			
LL-15BG324	419096	5642604	Confederation	Mafic and intermediate volcanics; fine-grained; foliated; bedded zones for intermediate volcanics				
LL-15BG325	419037	5642549	Confederation	Mafic and intermediate volcanics; fine-grained; foliated; amph poikiloblasts up to 30% and 4mm long	085/77		LL-15BG325A01	
LL-15BG326	419018	5642633	Confederation	Intermediate volcanic; fine-grained; foliated				
LL-15BG327	419048	5642753	Confederation	Diorite; fine- to medium-grained; foliated; strongly boudinaged qtz veins up to 4cm thick	085/76			
LL-15BG328	419120	5642982	Confederation	Diorite; fine- to medium-grained; foliated				
LL-15BG329	419226	5643132	Confederation	Felsic volcanic; fine- to medium-grained; foliated; grt-rich stringers parallel to foliation	075/56		LL-15BG329A01	
LL-15BG330	419454	5643379	Confederation	Mafic volcanic; fine-grained; foliated				
LL-15BG331	419214	5643440	Confederation	Mafic volcanic; fine-grained; feld phenos up to 20% and 1.5cm thick; granitic veins subparallel to foliation; epi veinlets subparallel to unoriented up to 1.5cm thick	066/69		LL-15BG331A01	
LL-15BG332	419180	5643353	Confederation	Felsic volcanic; fine-grained; bedding parallel to foliation, defined by aligned bt	070/72			
			Confederation	Mafic volcanic; fine-grained; feld phenos up to 30%; foliated, defined by aligned feld				
LL-15BG333	419153	5643280	Confederation	Felsic volcanic; fine-grained; bedding parallel to foliation; mafic veinlets running parallel to foliation	084/54			
LL-15BG334	419151	5643238	Confederation	Mafic volcanic; fine-grained; feld phenos up to 50% and 5mm long; foliated, defined by aligned feld phenos	079/60			
LL-15BG335	419008	5643177	Confederation	Mafic volcanic; fine-grained; feld phenos up to 50% and 5mm long; foliated, defined by aligned feld phenos				
LL-15BG336	418912	5643180	Confederation	Mafic volcanic; fine-grained; feld phenos up to 40% and 1cm long; foliated, defined by aligned feld phenos				
LL-15BG337	418885	5643178	Confederation	Felsic and mafic volcanic; fine-grained; foliated; mafic vol host feld phenos	068/66			
LL-15BG338	418954	5643751		Monzogabbro; medium- to coarse-grained; massive; 75% bt and amph				
LL-15BG339	419152	5643622		Monzogabbro; medium- to coarse-grained; massive; epi veinlets; granitic veins up to 1cm thick				
LL-15BG340	416911	5643921	Balmer	Mafic volcanic; fine-grained; foliated; up to 3% disseminated to veined po in very rusty areas;	066/61		LL-15BG340A02	

Station	Easting	Northing	Assemblage	Rock Description	Foliation	Bedding	Geochemistry sample	Trench
LL-15BG341	416957	5643983	Balmer	Ultramafic intrusion; fine-grained; serp alt; strongly magnetic			LL-15BG341A01	
LL-15BG342	416969	5644023	Balmer	Mafic volcanic; fine-grained; foliated, defined by aligned bt; local rusty zones with patchy po; cut by granitic dikes	050/49			
LL-15BG343	417120	5644191	Balmer	Mafic volcanic; fine-grained; strongly foliated; qtz-carb and epi veinlets	105/72			
LL-15BG344	417089	5644290	Killala-Baird	Bt granodiorite; medium- to coarse-grained; massive; 20-25% bt; rare py specks				
LL-15BG345	417112	5644308	Balmer	Mafic volcanic; fine-grained; foliated; local rusty zones; qtz veinlets subparallel to foliation				
LL-15BG346	417197	5644388	Killala-Baird	Bt granodiorite; medium- to coarse-grained; massive; 25% bt				
LL-15BG347	417094	5644485	Killala-Baird	Hbl bt granodiorite; medium- to coarse-grained; mafic min lineated				
LL-15BG348	416923	5644424	Killala-Baird	Bt granodiorite; medium- to coarse-grained; foliated, defined by aligned mafic min	070/44			
LL-15BG349	416761	5644363	Killala-Baird	Bt granodiorite; medium-grained; 20% bt; foliated, defined by aligned mafic min				
LL-15BG350	416822	5644271	Killala-Baird	Hbl bt granodiorite; medium-grained; 20% bt + hbl; foliated, defined by aligned mafic min				
LL-15BG351	416708	5644167	Balmer	Mafic volcanic; fine-grained; foliated; unoriented epi veinlets				
LL-15BG352	416653	5644067	Balmer	Banded-iron formation; 2-3m thick; chert layers up to 3cm thick, magnetite-rich layers up to 0.4cm thick; unit is really rusty and strongly magnetic; unit runs roughly east, dipping 47 to the south			LL-15BG352A01	
LL-15BG353	417178	5643749		Pyroxenite; coarse- to very coarse-grained; 80% px up to 1cm wide; granitic dikes brecciating the host rock; epi alt on matrix				
LL-15BG354	417198	5643790	Balmer	Mafic volcanic; fine-grained; aphyric; weakly foliated; up to 3% disseminated py associated with felsic veinlets; cut by massive medium-grained monzodiorite and coarse felsic pegmatitic dike				
LL-15BG355	417268	5643905		Diorite; medium-grained; massive; 50% bt+hbl; unoriented epi veinlets throughout				
LL-15BG356	417315	5644036	Balmer	Mafic volcanic; fine-grained; aphyric; foliated; qtz stringers				

Station	Easting	Northing	Assemblage	Rock Description	Foliation	Bedding	Geochemistry sample	Trench
LL-15BG357	417281	5644151	Balmer	Mafic volcanic; fine-grained; aphyric; strongly foliated, defined by bt and by stretched and boudinaged green alteration patches; local folding; up to 3% py and po stringers to disseminated	120/54		LL-15BG357A01	
LL-15BG358	417140	5644155	Balmer	Mafic volcanic; fine-grained; aphyric; foliated, defined by aligned bt and sulphides; py+po stringers parallel to foliation, py also associated with qtz and carbonate pods	090/64			
LL-15BG359	417021	5643978	Balmer	Mafic volcanic; fine-grained; aphyric; foliated, defined by aligned bt; bt alt; local felsic veinlets				
LL-15BG360	416952	5643863	Balmer	Mafic volcanic; fine-grained; aphyric; foliated				
LL-15BG361	417192	5643146		Pyroxenite; coarse-grained; 85% px; granitic veints brecciating host rocks; Diorite; medium-grained; xenolithic with angular polymictic clasts in ctct with brecciated pyroxenite; pyroxenite clasts found within xenolithic diorite; 25% xenoliths				
LL-15BG362	417082	5643118		Diorite; medium-grained; weakly foliated, defined by aligned bt; xenolithic				
LL-15BG363	416893	5643070		Pyroxenite; very coarse-grained; 90% px up to 2cm wide; granitic veints brecciating host rocks				
LL-15BG364	416876	5642987	Balmer	Mafic volcanic; fine-grained; aphyric; foliated; epi veinlets; py clusters less than 1%; cut by medium-grained weakly foliated diorite	054/50			
LL-15BG365	416837	5642948		Pyroxenite; very coarse-grained; 80% px; granitic veints brecciating host rocks				
LL-15BG366	417124	5642848		Pyroxenite; very coarse-grained; 80% px; granitic veints brecciating host rocks				
LL-15BG367	417514	5642766		Pyroxenite; medium- to coarse-grained; 60% px up to 5mm wide; granitic veints brecciating host rocks			LL-15BG367A01	
LL-15BG368	417687	5642999		Pyroxenite; medium- to coarse-grained; 80% px up to 5-8mm wide; granitic veints brecciating host rocks, locally pegmatitic				
LL-15BG369	418036	5643378	Balmer	Mafic volcanic; fine-grained; aphyric; locally qtz-filled vesicles; foliated, defined by aligned bt and vesicles; trace disseminated py; cut by diorite to granitic veins	076/56			
LL-15BG370	417569	5642980		Bt granodiorite; medium- to coarse-grained; massive; 10-15% bt				
LL-15BG371	417455	5642976		Diorite; medium-grained; 30-40% bt+amph; massive; xenolithic				
LL-15BG372	417397	5643093		Diorite; medium-grained; 30-40% bt+amph; massive; xenolithic				

Station	Easting	Northing	Assemblage	Rock Description	Foliation	Bedding	Geochemistry sample	Trench
LL-15BG373	417459	5643153		Diorite; medium-grained; 30-40% bt+amph; massive; xenolithic; sharp to gradational ctct with pyroxenite				
LL-15BG374	417532	5643246		Tonalite; medium- to coarse-grained; massive; 25-30% bt			LL-15BG374A01	
LL-15BG375	417519	5643294		Pyroxenite; medium- to coarse-grained; massive				
LL-15BG376	417495	5643378		Tonalite; fine- to medium-grained; massive; cut by pegmatitic and qtz veins				
LL-15BG377	417475	5643469		Pyroxenite; coarse-grained; massive; cut by xenolithic diorite including pyroxenite xenoliths				
LL-15BG378	417412	5643539		Pyroxenite; medium- to coarse-grained; 85% px; massive				
LL-15BG379	417448	5643762	Balmer	Mafic volcanic; fine-grained; locally pillowed, selvages up to 3cm thick; foliated; green alt patches associated with silicification; local rusty zones			LL-15BG379A01	
LL-15BG380	417435	5643840		Qtz diorite to tonalite; medium-grained; massive; 30% bt				
LL-15BG381	417430	5643918		Qtz diorite to tonalite; medium-grained; massive; 30% bt				
LL-15BG382	417468	5643945		Monzogabbro; medium-grained; massive; 15% bt+amph; cut by epi veinlets				
LL-15BG383	417625	5643660		Pyroxenite; medium- to coarse-grained; massive; 80% px; cut by diorite				
LL-15BG384	417672	5643499		Diorite; medium-grained; massvie; xenolithic				
LL-15BG385	417652	5643922	Balmer	Mafic volcanic; fine-grained; aphyric; foliated; local rusty zones; cut by diorite and aplite dikes				
LL-15BG386	417751	5643898	Balmer	Mafic volcanic; fine-grained; aphyric; foliated; cut by diorite and aplite dikes				
LL-15BG387	417897	5643902	Balmer	Mafic volcanic; fine-grained; aphyric; foliated, defined by aligned bt; qtz and felsic vinlets subparallel to foliation	040/68		LL-15BG387A01	
LL-15BG388	418023	5643900	Balmer	Mafic volcanic; fine-grained; aphyric; foliated, defined by aligned bt; local rusty zones; qtz and felsic vinlets subparallel to foliation				
LL-15BG389	418325	5643927		Tonalite; medium-grained; weakly foliated; 20-30% bt; up to 2% xenoliths trending 065°, mainly mafic in composition				
LL-15BG390	418460	5643870		Tonalite; medium-grained; weakly foliated; epi veinlets; 2% mafic xenoliths trending 120°				
LL-15BG391	418552	5643939		Qtz diorite; medium-grained; 2% mafic xenoliths; cut by granodiorite and pegmatitic dikes				
LL-15BG392	418542	5644012	Balmer	Mafic volcanic; fine-grained; aphyric; foliated; possibly pillowed with filled vesicles; folded qtz veins; cut by hbl bt granodiorite	105/54			

Station	Easting	Northing	Assemblage	Rock Description	Foliation	Bedding	Geochemistry sample	Trench
LL-15BG393	418615	5643959	Balmer	Mafic volcanic; fine-grained; aphyric; pillows average 60cm in length, elongation trending 118°, selvages 1-2cm thick and bt altered; green alt patches; qtz-carb alt				
LL-15BG394	418663	5643879		Monzogabbro; medium-grained; massive; 35-40% bt; epi veinlets associated with granodiorite dikes				
LL-15BG395	422724	5644098	Confederation	Mafic to intermediate interlayered volcanic package; fine-grained; mafic flows up to 1m thick, intermediate units up to 4m thick; irregular ctct; foliated; intermediate unit contains up to 2% disseminated py; cut by px-rich mafic dikes				Zone 11
LL-15BG396	422710	5644074	Confederation	Mafic volcanic and qtz-feld porphyritic xtal tuff interlayred; tuff is finely bedded with 5-10% qtz-feld grains; mafic flows locally have feld phenos; units are cut by qtz veinlets and px-rich dikes				Zone 11
LL-15BG397	422674	5644047	Confederation	Mafic volcanic and qtz-feld porphyritic xtal tuff interlayred; tuff is finely bedded with 5-10% qtz-feld grains; mafic flows are aphyric; units are cut px-rich dikes		090/79		Zone 11
LL-15BG398	422653	5643913	Confederation	Qtz-feld porphyritic xtal tuff interlayered with finely bedded felsic tuffs; strong brittle and ductile deformation of both sinistral and dextral displacement; milky qtz veins parallel to foliation				Zone 11
LL-15BG399	419024	5643997	Balmer	Mafic volcanic; fine-grained; aphyric; pillowed, selvages up to 3cm thick and bt-rich; qtz-filled vesicles				
LL-15BG400	419071	5644101	Balmer	Mafic volcanic; fine-grained; aphyric; foliated, defined by aligned bt; qtz stringers up to 2mm thick	095/75			
LL-15BG401	419157	5644212	Balmer	Mafic volcanic; fine-grained; aphyric; foliated, defined by aligned bt; qtz-carb stringers up to 6mm thick	082/58		LL-15BG401A01	
LL-15BG402	419073	5644293	Balmer	Mafic volcanic; fine-grained; aphyric; foliated, defined by aligned bt; qtz-carb stringers	085/64			
LL-15BG403	418968	5644373	Balmer	Mafic volcanic; fine-grained; aphyric; foliated, defined by aligned bt;				
LL-15BG404	418622	5644452	Killala-Baird	Bt granodiorite; medium-grained; 15-20% bt; weakly foliated, defined by aligned bt	104/61			
LL-15BG405	418541	5644340	Balmer	Mafic volcanic; fine-grained; aphyric; foliated, defined by aligned bt; qtz veinlets subparallel to foliation	110/63			

Station	Easting	Northing	Assemblage	Rock Description	Foliation	Bedding	Geochemistry sample	Trench
LL-15BG406	418562	5644111	Balmer	Mafic volcanic; fine-grained; aphyric; foliated; qtz veinlets subparallel to foliation				
LL-15BG407	418694	5644035	Balmer	Mafic volcanic; fine-grained; aphyric; foliated; qtz veinlets subparallel to foliation				
LL-15BG408	418909	5643900		Monzogabbro; medium-grained; 50-60% bt+amph; massive				
LL-15BG409	417703	5643960	Balmer	Mafic volcanic; fine-grained; aphyric; foliated, defined by aligned bt; 1% disseminated po; qtz veinlets up to 2mm thick unoriented				
LL-15BG410	417806	5644063	Balmer	Mafic volcanic; fine-grained; aphyric; foliated, defined by aligned bt; qtz veinlets up to 5mm thick subparallel to foliation	088/73			
LL-15BG411	417792	5644210	Balmer	Mafic volcanic; fine-grained; aphyric; foliated, defined by aligned bt; qtz stringers up to 2mm thick subparallel to parallel to foliation	088/54			
LL-15BG412	417891	5644452	Killala-Baird	Bt qtz monzodiorite; medium-grained; 30-35% bt; weakly foliated, defined by aligned bt; 2% disseminated epi			LL-15BG412A01	
LL-15BG413	417812	5644694	Killala-Baird	Bt qtz monzodiorite to granodiorite; medium-grained; 10% bt; weakly foliated, defined by aligned bt; 3% disseminated epi				
LL-15BG414	417598	5644657	Killala-Baird	Bt qtz monzodiorite to granodiorite; medium-grained; 20-25% bt; massive; 2% disseminated epi				
LL-15BG415	417470	5644634	Killala-Baird	Bt qtz monzodiorite to granodiorite; medium-grained; 15% bt; weakly foliated, defined by aligned bt; 1% disseminated epi				
LL-15BG416	417347	5644591	Killala-Baird	Bt qtz monzodiorite to granodiorite; medium-grained; 15% bt; weakly foliated, defined by aligned bt	085/51			
LL-15BG417	417648	5644366	Killala-Baird	Bt qtz monzodiorite to granodiorite; medium-grained; 10-15% bt; weakly foliated, defined by aligned bt; 1% disseminated epi				
LL-15BG418	417703	5644219	Balmer	Mafic volcanic; fine-grained; aphyric; foliated, defined by aligned bt; above BIF, mafic volcanics host up to 40% grt or 25% euhedral spinels up to 2mm wide; cut by intermediate dikes with porphyritic feld xtals	080/69		LL-15BG418A01 (mafic voclanic) LL-15BG418A03 (intermediate intrusion) LL-16BG418A04 (intermediate	

Station	Easting	Northing	Assemblage	Rock Description	Foliation	Bedding	Geochemistry sample	Trench
			Balmer	Banded-iron formation; up to 1.5-2m thick (botton section covered by overburden) and 15m long; mag bands are up to 7cm thick; chert layers up to 2cm thick and make up 30-35% of the BIF; up to 3% py associated with mag-rich layers		065/64	LL-15BG418B01	
LL-15BG419	417842	5643952	Balmer	Mafic volcanic; fine-grained; mm scale feld grains up to 20% parallel to foliation; foliated, defined by aligned feld and bt; qtz veins up to 2cm and qtz veinlets up to 4mm unoriented	092/65			
LL-15BG420	418096	5643988	Balmer	Mafic volcanic; fine-grained; aphyric; foliated; cut by diorite dike				
LL-15BG421	418168	5644090	Balmer	Mafic volcanic; fine-grained; aphyric; qtz-filled vesicles; foliated	130/65			
LL-15BG422	418274	5644737	Killala-Baird	Hbl granodiorite; medium-grained; 15-20% amph; weakly foliated, defined by aligned amph				
LL-15BG423	418093	5644646	Killala-Baird	Bt granodiorite; medium-grained; 15-20% bt; weakly foliated, defined by aligned bt				
LL-15BG424	418006	5644515	Killala-Baird	Hbl granodiorite; medium-grained; 15-20% amph; weakly foliated, defined by aligned amph; epi stringers				
LL-15BG425	418038	5644329	Balmer	Mafic volcanic; fine-grained; aphyric; foliated, defined by aligned bt; qtz veinlets up to 6mm thick unoriented; cut by aplite dikes	093/60			
LL-15BG426	417967	5644147	Balmer	Mafic volcanic; fine-grained; aphyric; foliated, defined by aligned bt; 1% patchy po				
LL-15BG427	418798	5642713	Confederation	Diorite; fine- to coarse-grained; strongly foliated; porphyroclasts of coarse-grained diorite present with foliation wrapping clasts; boudinaged qtz+tur veins parallel to foliation	081/90		LL-15BG427A01	
LL-15BG428	418832	5642669	Confederation	Mafic volcanic; fine-grained; section up to 4m thick with 10-15% grt up to 3mm wide; foliated, defined by aligned bt and grt; qtz veinlets with up to 1% disseminated py; cut by tonalite to diorite dikes parallel to foliation	083/72		LL-15BG428A01	
LL-15BG429	418723	5642531	Confederation	Mafic volcanic; fine-grained; amph poikiloblasts up to 40% and 4mm wide; foliated, defined by aligned amph and bt	080/			
LL-15BG430	418564	5642469	Confederation	Diorite; medium-grained; massive; cut by granitic dikes associated with epi veinlets				

Station	Easting	Northing	Assemblage	Rock Description	Foliation	Bedding	Geochemistry sample	Trench
LL-15BG431	418468	5642436	Confederation	Mafic volcanic; fine-grained; strongly foliated; bt alt; local unoriented granitic dikes; qtz veinlets parallel to foliation, up to 2cm thick	094/83			
LL-15BG432	418367	5642377	Confederation	Intermediate volcanic; fine-grained; strongly foliated, defined by aligned bt; slight bedded appearance; bt alt	092/89			
LL-15BG433	418068	5642381	Confederation	Mafic volcanic; fine-grained; amph poikiloblasts up to 30% up to 5mm wide; strongly foliated, defined by aligned bt and amph; bt alt	265/76		LL-15BG433A01	
LL-15BG434	417892	5642384	Confederation	Mafic volcanic; fine-grained; aphyric; foliated; cut by granitic veins subparallel to foliation				
LL-15BG435	417729	5642332	Confederation	Intermediate volcanic; fine-grained; foliated; cut by unoriented granitic veints and qtz vein up to 5cm thick				
LL-15BG436	417614	5642455	Confederation	Qtz monzogabbro to qtz diorite; fine- to medium-grained; 25% mafic mins; foliated; cut by monzogabbro dikes parallel to foliation and unoriented granitic dikes; unoriented qtz veinlets and unoriented to parallel to foliation epi veinlets	070/85		LL-15BG436A01	
LL-15BG437	417844	5642536	Confederation	Qtz monzogabbro to qtz diorite; fine- to medium-grained; 25% mafic mins; foliated; cut unoriented granitic dikes; subparallel to foliation epi veinlets	072/90			
LL-15BG438	417976	5642610	Confederation	Qtz monzogabbro to qtz diorite; fine- to medium-grained; 25-30% mafic mins; strongly foliated; epi veinlets	091/65			
LL-15BG439	418148	5642670	Confederation	Qtz monzogabbro to qtz diorite; fine- to medium-grained; 25% mafic mins; foliated; local monzogabbro zones; qtz veins up to 1cm thick subparallel to foliation; felsic veinlets folded with fold limbs parallel to foliation; weak banding				
LL-15BG440	418556	5642852	Confederation	Qtz monzogabbro to qtz diorite; fine- to medium-grained; 25% mafic mins; foliated			LL-15BG440A01	
LL-15BG441	420724	5643680	Confederation	Felsic volcanic; tuffaceous; 3m thick; finely bedded, layers on mm scale up to 1cm thick; local layers up to 3cm thick with qtz xtals up to 2mm wide; qtz-filled tension gashes perpendicular to bedding; weak foliation parallel to bedding		080/83		

Station	Easting	Northing	Assemblage	Rock Description	Foliation	Bedding	Geochemistry sample	Trench
LL-15BG442	420645	5643696	Confederation	Felsic volcanic; tuffaceous; 8m thick; finely bedded, layers on mm scale up to 1cm thick; local layers up to 3cm thick with qtz xtals up to 2mm wide, qtz xtals elongated by foliation; qtz-filled tension gashes perpendicular to bedding; foliated, defined by stretched qtz xtals; local areas with feld pheno-rich lapilli clasts stretched parallel to foliation and bedding, clasts up to 30% and 15cm long; cut by making dikes; local qtz veins weakly boudinaged		080/84		
			Confederation	Mafic volcanic; fine-grained; feld phenos up to 15% and 1cm long and amph poikiloblasts up to 30% and 3mm wide; foliated; irregular ctct with felsic volcanics	077/83			
LL-15BG443	420502	5643672	Confederation	Mafic volcanic; fine-grained; feld phenos up to 15% and 1cm long and amph poikiloblasts up to 30% and 3mm wide; foliated, defined by aligned feld and amph; milky qtz vein parallel to foliation up to 15cm wide found within 2m wide shear zone	080/67			
LL-15BG444	420414	5643636	Confederation	Felsic volcanic; fine-grained; foliated; qtz grains up to 5% and 2mm wide	080/77			
LL-15BG445	420311	5643677	Balmer	Mafic volcanic; fine-grained; strongly foliated; czo bands chaotically folded; up to 2% disseminated py	085/87		LL-15BG445A02	
			Confederation	Mafic volcanic; fine-grained; feld phenos and amph poikiloblasts; strongly foliated; trace disseminated py; ctct between assemblages covered by overburden	066/70			
LL-15BG446	420308	5643721	Balmer	Mafic volcanic; fine-grained; aphyric; strongly foliated; banded alteration: bt, amph, czo, diop; carb veinlets with diop rims; smokey qtz vein up to 20cm in sheared zone, host up to 5% py and 1% cpy; ank veinlets; cut by multiple felsic and granitic intrusion unoriented	060/72			PZ
LL-15BG447	420222	5643701	Balmer	Mafic volcanic; fine-grained; aphyric; strongly foliated; banded alteration: bt, amph, czo; smokey qtz vein up to 20cm in sheared zone, host up to 5% py and 1% cpy; ank veinlets; cut by multiple felsic and granitic intrusion unoriented	060/72		LL-15BG447A01	PZ

Station	Easting	Northing	Assemblage	Rock Description	Foliation	Bedding	Geochemistry sample	Trench
LL-15BG448	420174	5643665	Balmer	Mafic volcanic; fine-grained; aphyric; strongly foliated; banded alteration: bt, amph, czo; carb veinlets with diop rims; smokey qtz vein up to 10cm in sheared zone; ank veinlets; cut by multiple felsic and granitic intrusion unoriented	066/64			PZ
LL-15BG449			Balmer	GBZ trench - see section 4.4.1 p.88			See end of Appendix A	GBZ
LL-15BG450			Balmer	GBZ trench - see section 4.4.1 p.88				GBZ
LL-15BG451			Balmer	GBZ trench - see section 4.4.1 p.88				GBZ
LL-16BG023	423020	5644177	Balmer	Mafic volcanic; fine-grained; strongly foliated, defined by alt min banding (bt, amph and czo); local rusty zones; cut by xenolithic diorite to monzodiorite	100/62		LL-16BG023A01	
LL-16BG104	422981	5644207	Balmer	Mafic volcanic; fine-grained; strongly foliated, defined by alt min banding (bt); local rusty zones; cut by xenolithic diorite to monzodiorite and pyroxenite			LL-16BG104A01 (mafic volcanic) LL-16BG104A02 (mafic volcanic)	
LL-16BG025	422946	5644198	Balmer	Diorite; medium- to coarse-grained; 30-40% bt and amph; xenolithic, range from mafic volcanic, diorite and pyroxenite; up to 20cm long, aligned parallel to intrusion margins; diorite matrix is massive; cut by epi veinlets			LL-16BG025A01	
LL-16BG452	422803	5643800	Confederation	Qtz-feld porphyritic xtal tuff to lapilli xtal tuff; fine-grained; qtz xtals up to 1cm long and feld xtals up to 4mm long, up to 40% qtz+feld; up to 5% lapilli clasts up to 5cm long parallel to foliation, composition mafic to intermediate volcanic; bedding marked by changes in xtal % and presence of lapilli, bedding parallel to foliation		080/72		
LL-16BG453	422936	5643794	Confederation	Felsic volcanic; tuffaceous; very fine- to fine-grained; mm scale to 15cm thick beds, potential cross-bedding		077/90		
LL-16BG454	422946	5643734	Confederation	Mafic volcanic; fine-grained; feld phenos up to 1cm long, 15%; weakly foliated, defined by aligned feld phenos				
LL-16BG455	422868	5643554	Confederation	Intermediate volcanic; very fine-grained; feld phenos up to 25%; foliated, defined by aligned bt and feld		077/85		

Station	Easting	Northing	Assemblage	Rock Description	Foliation	Bedding	Geochemistry sample	Trench
LL-16BG456	422774	5643633	Confederation	Mafic volcanic; fine-grained; feld phenos up to 1cm long, 20%, show trachytic alignement; weakly foliated, defined by aligned bt				
LL-16BG457	422718	5643711	Confederation	Mafic volcanic; fine-grained; aphyric; foliated; felsic veinlets parallel to foliation and folded				
LL-16BG458	422469	5643632	Confederation	Mafic volcanic; fine-grained; feld phenos up to 2-3cm long, 20%, show trachytic alignement; weakly to strongly foliated, defined by aligned bt and feld; unit intercalated with qtz-feld porphyritic xtal tuff up to 3m thick, sharp ctct				
LL-16BG459	422565	5643554	Confederation	Intermediate to felsic volcanic; fine-grained; bedded, 0.5-2cm thick; weakly foliated		064/82		
LL-16BG460	422409	5643552	Confederation	Intermediate volcanic; fine-grained; weakly bedded; local mafic volcanic flows with feld phenos				
LL-16BG461	423770	5643569	Confederation	Mafic volcanic; fine-grained; amph poikiloblasts up to 30% up to 3mm wide; foliated, defined by aligned amph and bt; qtz pods up to 20x5cm long	65/83 (155)			
LL-16BG462	423692	5643516	Confederation	Mafic volcanic; fine-grained; feld phenos up to 30% and 2cm long; foliated, defined by aligned feld phenos				
LL-16BG463	423556	5643435	Confederation	Intermediate volcanic; very fine-grained; weakly bedded; cut by granitic vein				
LL-16BG464	423464	5643315	Confederation	Intermediate volcanic; very fine-grained; foliated, defined by aligned bt; 20% bt	105/85			
LL-16BG465	423298	5643304		Qtz monzonite; medium- to coarse-grained; massive				
LL-16BG466	423042	5643234	Confederation	Intermediate volcanic; fine-grained; weakly foliated	92/85			
LL-16BG467	422973	5643130	Confederation	Intermediate volcanic; fine-grained; weakly foliated; cut by 30cm thick mafic dike				
LL-16BG468	422977	5642973	Confederation	Intermediate volcanic; fine- to medium-grained; weakly foliated, defined by aligned bt; trace disseminated py; smokey qtz vein up to 10cm thick	071/			
LL-16BG469	423133	5643001	Confederation	Intermediate volcanic; fine- to medium-grained; weakly foliated, defined by aligned amph; cut by diorite intrusion	075/			
LL-16BG018	423361	5643014		Granodiorite; fine- to medium-grained; foliated; chill margin of Medicine Stone Lake batholith?			LL-16BG018A01	

Station	Easting	Northing	Assemblage	Rock Description	Foliation	Bedding	Geochemistry sample	Trench
LL-16BG470	423385	5643274	Confederation	Intermediate volcanic; fine-grained; weakly foliated	085/			
LL-16BG471	423641	5643342	Confederation	Intermediate volcanic; fine-grained; weakly foliated	085/			
LL-16BG472/069	422537	5643991	Confederation	Intermediate volcanic; fine-grained; weakly bedded, parallel to foliation; cut by pyroxenite	117/			
LL-16BG067	422288	5643932	Balmer	Mafic volcanic; fine-grained; aphyric; foliated; felsic veinlets parallel to foliation			LL-16BG067A01	
LL-16BG068	422465	5643946	Confederation	Felsic volcanic; very fine- to fine-grained; weakly foliated			LL-16BG068A01	
LL-16BG473	419325	5643367	Confederation	Mafic and felsic volcanic; fine-grained; mafic volcanic host feld phenos up to 15% and up to 1.5cm; foliated, defined by aligned feld phenos and banding in felsic volcanic; sharp ctct with felsic volcanic, ctct parallel to foliation				
LL-16BG474	419331	5643110	Confederation	Intermediate to mafic volcanic; fine-grained; foliated				
LL-16BG475	419331	5643039	Confederation	Intermediate volcanic; fine- to medium-grained; foliated	085/90			
LL-16BG476	419233	5642874	Confederation	Intermediate to mafic volcanic; fine-grained; foliated				
LL-16BG477	419215	5642867	Confederation	Diorite; fine- to medium-grained; porphyritic feldpsar 40-50% up to 5mm long; bt-rich	085/90			
LL-16BG478	419050	5642820	Confederation	Intermediate volcanic; fine-grained; weakly bedded, parallel to foliation	090/78			
LL-16BG479	419008	5642781	Confederation	Diorite; fine- to medium-grained; strongly foliated; up to 40% bt				
LL-16BG480	418809	5642897	Confederation	Diorite; fine- to medium-grained; strongly foliated; up to 40% bt; milky qtz vein parallel to foliation up to 12cm thick, locally associated with possible tur?			LL-16BG480A01	
LL-16BG481	418809	5643072	Confederation	Intermediate volcanic; fine-grained; weakly foliated, defined by banding				
LL-16BG482	417574	5643953		Qtz diorite; medium- to coarse-grained; weakly foliated, defined by aligned bt, 30% bt; pyroxenite; medium-grained; 15-20% px up to 1cm wide				
LL-16BG483	417559	5643970	Balmer	Mafic volcanic; fine-grained; aphyric; foliated, defined by aligned bt; local rusty zones	093/			

Station	Easting	Northing	Assemblage	Rock Description	Foliation	Bedding	Geochemistry sample	Trench
LL-16BG484	421628	5643874	Balmer	Mafic volcanic; fine-grained; aphyric; possibly pillowed with varioles in the pillow cores or rims; foliated, defined by stretched varioles			LL-16BG484A01	
LL-16BG485	421640	5643861	Confederation	Mafic volcanic; fine-grained; amph poikiloblasts up to 4mm wide; foliated, defined by aligned amph and bt				
LL-16BG486	421692	5643835	Confederation	Mafic volcanic; fine-grained; feld phenos up to 15% and 3mm long; cut by diorite	067/76			
LL-16BG487	421723	5643840	Confederation	Intermediate to felsic volcanic; fine-grained; aphyric; foliated				
LL-16BG488	421883	5643901	Confederation	Intermediate to felsic volcanic; fine-grained; aphyric				
LL-16BG489	421925	5643966		Pyroxenite; medium-grained; 60-80% px up to 6mm wide; massive; cut by granitic dikes				
LL-16BG490	422087	5644151	Balmer	Mafic volcanic; fine-grained; aphyric; foliated				
LL-16BG491	421850	5644041	Balmer	Mafic volcanic; fine-grained; aphyric; foliated	085/61			
LL-16BG492	418125	5642743	Confederation	Diorite; fine-grained; strongly foliated	085/82			
LL-16BG493	418036	5642491	Confederation	Diorite; fine-grained; strongly foliated, defined by banding; felsic veins parallel to foliation are boudinaged				
LL-16BG494	418327	5642914	Balmer	Mafic volcanic; fine-grained; aphyric; foliated				
LL-16BG495	418671	5642954	Confederation	Mafic volcanic; fine-grained; feld phenos up to 10% and stretched to 2cm long, amph poikiloblasts up to 30% and 2mm wide	067/64			
LL-16BG496	417384	5642778		Pyroxenite; medium- to coarse-grained; px up to 50-60% and 7mm wide; massive				
LL-16BG497	417099	5642994		Diorite; medium-grained; 50-60% bt+amph; mafic min lineated; cut by granitic vein				
LL-16BG498	417140	5643099		Pyroxenite; coarse-grained; px up to 80% and 1.5cm wide; cut by granitic dike brecciating the host rock				
LL-16BG499	417404	5643352		Pyroxenite; medium- to coarse-grained; px up to 60% and 4mm wide; cut by granitic dike				
LL-16BG500	417443	5643255		Pyroxenite; medium- to coarse-grained; px up to 60% and 3mm wide; cut by granitic dike				
LL-16BG501	417412	5643193		Pyroxenite; coarse-grained; px up to 85% and 1.5cm wide; cut by granitic dike brecciating the host rock				

Station	Easting	Northing	Assemblage	Rock Description	Foliation	Bedding	Geochemistry sample	Trench
LL-16BG364	416859	5642969	Balmer	Mafic volcanic; fine-grained; foliated; light grayish green alt patches; cut by felsic veinlets and massive diorite			LL-16BG364A01	
LL-16BG502	420005	5643551	Balmer	Mafic volcanic; fine-grained; aphyric; foliated; trace disseminated py			LL-16BG502A01	
LL-16BG242	419778	5643464	Balmer	Mafic volcanic; fine-grained; aphyric; foliated, defined by min banding (bt, amph, diop, czo); trace disseminated py	070/80		LL-16BG242A01	
LL-16BG503	419864	5643476	Balmer	Mafic volcanic; fine-grained; aphyric; foliated				
LL-16BG504	419852	5643437	Balmer	Mafic volcanic; fine-grained; aphyric; foliated, defined by min banding (bt, czo)	060/90		LL-16BG504A01	
LL-16BG505	419633	5643435		Diorite to qtz diorite; medium-grained; no xenolith, foliated				
LL-16BG506	419871	5643400	Confederation	Intermediate to mafic volcanic; fine-grained; aphyric; apparent bedding; foliated	255/75		LL-16BG506A01	
LL-16BG507	420045	5643451	Confederation	Felsic to intermediate volcanic; tuffaceous, beds range from 1mm to 1cm thick with thicker layers hosting porphyritic qtz xtals				
LL-16BG508	420155	5643557	Confederation	Felsic to intermediate volcanic; tuffaceous, beds range from 1mm to 1cm thick with thicker layers hosting porphyritic qtz xtals; bedding parallel to foliation; cut by px-rich dike	083/74			
LL-16BG509	420160	5643622	Balmer	Mafic volcanic; fine-grained; aphyric; foliated				
LL-16BG510	420105	5643606	Balmer	Mafic volcanic; fine-grained; aphyric; foliated, defined by min banding (bt, amph, diop, czo); trace disseminated py			LL-16BG510A01	
LL-16BG511	420092	5643554	Confederation	Felsic volcanic; fine-grained; aphyric; foliated			LL-16BG511A01	
LL-16BG512	420774	5643741	Confederation	Intermediate to felsic volcanic; fine-grained; tuffaceous; py stringers parallel to bedding/foliation; cut by xenolithic diorite		073/69	LL-16BG512A01	
LL-16BG513	420777	5643752	Balmer	Mafic volcanic; fine-grained; aphyric; foliated, defined by min banding (bt, amph, czo); felsic stringers parallel to foliation to unoriented; epi stringers; trace disseminated py; cut by massive pyroxenite			LL-16BG513A01	

Station	Easting	Northing	Assemblage	Rock Description	Foliation	Bedding	Geochemistry sample	Trench
LL-16BG514	420740	5643776	Balmer	Mafic volcanic; fine-grained; aphyric; foliated; epi stringers			LL-16BG514A01	
			Confederation	Intermediate to felsic volcanic; fine-grained; bedded to foliated; ctct with Balmer cut by diorite and pyroxenite intrusion running parallel to the ctct; no major increase in foliation at this scale			LL-16BG514B01	
LL-16BG515	420626	5643775	Balmer	Mafic volcanic; fine-grained; aphyric; foliated; cut by felsic stringers				
LL-16BG516	420466	5643731	Balmer	Mafic volcanic; fine-grained; aphyric; foliated, defined by min banding (bt, amph, diop, czo); trace disseminated py	105/78		LL-16BG516A01	
LL-16BG517	420466	5643692	Confederation	Mafic volcanic; fine-grained; amph poikiloblasts up to 15%; foliated, defined by aligned amph and bt; in ctct with intermediate to felsic volcanics	087/70			
LL-16BG235	421581	5643937	Balmer	EGBZ trench - see section 4.4.3 p. 101				EGBZ
LL-16BG236	421562	5643881	Balmer	HSZ trench - see section 4.4.4 p. 101				HSZ
LL-16BG518	421526	5643860	Confederation	Intermediate to felsic volcanic; local beds with up to porphyritic qtz xtals up to 3mm long; cut by pyroxenite			LL-16BG518A01	
			Balmer	Mafic volcanic; fine-grained; aphyric; foliated; felsic stringers parallel to foliation; trace py associated with alt; ctct with Confederation not observed due to gap between rocks; no major increase in deformation towards ctct; ctct runs parallel to foliation			LL-16BG518B01	
LL-16BG519	421548	5643856	Balmer	Mafic volcanic; fine-grained; aphyric; foliated; qtz veinlets			LL-16BG519A01	
LL-16BG520	421580	5643850	Confederation	Intermediate to felsic volcanic; fine-grained; aphyric; foliated				
LL-16BG521	421584	5643864	Balmer	Mafic volcanic; fine-grained; aphyric; foliated; felsic veinlets throughout			LL-16BG521A01	
LL-16BG522	421615	5643848	Confederation	Intermediate to felsic volcanic; fine-grained; aphyric; foliated; epi and hem stringers				
LL-16BG523	420396	5643749	Balmer	Mafic volcanic; fine-grained; aphyric; foliated; diop and czo banding	096/69			
LL-16BG524	421748	5643939	Balmer	Mafic volcanic; fine-grained; aphyric; foliated; very rusty, up to 15% disseminated to layered py; areas with smokey qtz veinlets				CZ

Station	Easting	Northing	Assemblage	Rock Description	Foliation	Bedding	Geochemistry sample	Trench
			Balmer	Banded-iron formation; 1m thick; magnetite and chert layers roughly 5mm thick				
LL-16BG445	420311	5643677	Balmer	Mafic volcanic; fine-grained; aphyric; foliated; carb veinlets with diop halos; possible ank veinlets			LL-16BG445A01	
LL-16BG525	416662	5642422	Confederation	Mafic volcanic; fine-grained; possible feld phenos and amph poikiloblasts; strongly foliated, defined by aligned and stretched feld and amph; possible diop alt; cut by granitic dikes and irregular diorite pods			LL-16BG525A01	
LL-16BG526	416656	5642303	Confederation	Mafic volcanic; fine-grained; feld phenos up to 40% and 1cm long; foliated, defined by aligned feld phenos				
LL-16BG527	417125	5642234	Confederation	Mafic to intermediate volcanic; fine-grained; foliated, defined by aligned bt	080/90			
LL-16BG528	417408	5642279	Confederation	Mafic to intermediate volcanic; fine-grained; aphyric; foliated, defined by aligned bt	068/			
LL-16BG529	417521	5642255	Confederation	Mafic to intermediate volcanic; fine-grained; aphyric; foliated, defined by aligned bt				
LL-16BG530	417473	5642366	Confederation	Diorite; fine- to medium-grained; foliated, defined by stretched and aligned porphyritic feld xtals				
LL-16BG531	417327	5642349	Confederation	Felsic to intermediate volcanic; fine-grained; aphyric; foliated; epi veinlets				
LL-16BG532	421526	5643860	Balmer	Mafic volcanic; fine-grained; aphyric; foliated				HSZ
			Balmer	Carbonate formation; 2m thick; calcte beds vary from 1.5-0.3cm thick and mafic bands are 0.1-1cm thick; mafic bands are crenulated parallel to foliation; remobilized carbonate as veins are also parallel to the main foliation; unit is cut by 3 mafic intrusions, overlain by mafic volcanic and underlain by a ultramafic intrusion				HSZ
			Balmer	Ultramafic intrusion; porphyritic; massive; magnetic; porphyritic blebs up to 40-50% and 2mm wide; cut by carbonate veins			LL-16BG532A01	HSZ

Station	Easting	Northing	Assemblage	Rock Description	Foliation	Bedding	Geochemistry sample	Trench
LL-16BG533	418826	5643759		Qtz monzonite to qtz monzodiorite; medium- to coarse-grained; massive; 10-15% amph+bt; cut by unoriented granitic dike; qtz pods up to 20cm long				
LL-16BG534	421073	5643762	Balmer	Mafic volcanic; fine-grained; strongly foliated/chaotic folding of alt min banding (bt, hbl, czo, diop); folded qtz veins up to 2cm thick; rusty areas in bt-rich zones; cut by granitic and pyroxenite dikes	065/65			
LL-16BG535	421410	5643737	Confederation	Mafic volcanic; fine-grained; feld phenos up to 15% and 1cm long, amph poikiloblast up to 30% up to 3mm wide; foliated, defined by aligned feld and amph; cut by granitic dikes and px-rich dikes unoriented; milky to smokey qtz vein 10-15cm thick subparallel to parallel to foliation; local py patches	097/76			
LL-16BG536	421311	5643695	Confederation	Mafic volcanic; fine-grained; amph poikiloblasts; foliated				
LL-16BG537	421288	5643708	Confederation	Qtz porphyritic xtal tuff; fine-grained; qtz xtals up to 2mm wide and up to 15%; foliated, defined by stretched and aligned qtz; cut by mafic dike parallel to foliation	075/			
LL-16BG538	422205	5643577	Confederation	Mafic volcanic; fine-grained; feld phenos up to 40% and 3cm long, amph poikiloblasts up to 30% and 2mm wide; weakly to strongly foliated, defined by aligned feld and amph; cut by px-rich dike parallel to foliation	070/73			
LL-16BG539	422772	5644132	Confederation	Mafic volcanic; fine-grained; feld phenos up to 10% up to 1cm long; amph poikiloblast up to 30% and 1mm wide; foliated, defined by aligned feld and amph; cut by px-rich dike 10cm thick parallel to foliation	090/90			
LL-16BG540	418821	5643516	Balmer	Mafic volcanic; fine-grained; aphyric; foliated; trace disseminated py				

Station	Easting	Northing	Assemblage	Rock Description	Foliation	Bedding	Geochemistry sample	Trench
GBZ Trench	421085	5643810	Balmer	mafic volcanic, fine-grained, foliated, bleached (?), possibly pillowed with filled-vesicles	058/74		LL-GBZ-N5-001	
	421100	5643808	Balmer	mafic volcanic, fine-grained, foliated, defined by aligned bt, rusty	065/71		LL-GBZ-Q10-004	
	421091	5643808	Balmer	rusty shear or intrusive, high magnetism			LL-GBZ-P5-005	
	421106	5643816	Balmer	mafic volcanic, fine-grained, foliated, rusty, high magnetism, contains up to 20% py	070/66		LL-GBZ-K13-009	
	421113	5643824	Balmer	mafic volcanic, fine-grained, strongly foliated, min banding (bt, amph, diop)	070/64		LL-GBZ-J14-012	
	421133	5643816	Balmer	mafic volcanic, fine-grained, foliated, contains up to 10% py as stringers or disseminated; stratigraphically underlies barren BIF	061/74		LL-GBZ-I23-013	
	421130	5643828	Balmer	banded iron formation, magnetite and chert layers, high magnetism, up to 3% py; barren		065/78	LL-GBZ-G24-014	
	421139	5643841	Balmer	mafic volcanic, fine-grained, foliated, 30% py	070/75		LL-GBZ-A30-015	
	421125	5643830	Balmer	silicified shear, strongly foliated, rusty, up to 2% py	055/76		LL-GBZ-E21-019	
	421112	5643818	Balmer	mafic volcanic, strongly sheared (no remnance of mafic volcanic in core of shear) high magnetism, up to 20% py, interstitial hem to py	011/74		LL-GBZ-M15-020	
	421110	5643812	Balmer	banded iron formation, chert and mag-rich layers, pyrite rich bands altering mag-rich layers, low magnetism, up to 20% py	055/75		LL-GBZ-O15-021	
	421121	5643823	Balmer	mafic volcanic, fine-grained, foliated, carb veinlets to patches with diop alt halos	061/77		LL-GBZ-J22-029	
	421121	5643827	Balmer	mafic volcanic, fine-grained, foliated, bt-rich bands	060/68		LL-GBZ-F21-032	
	421115	5643824	Balmer	mafic volcanic, silicified rusty shear, trace to 5% disseminated py	060/81		LL-GBZ-F19-033	
	421138	5643834	Balmer	mafic volcanic, fine-grained, foliated, bt-rich bands	070/75		LL-GBZ-C30-034	
	421121	5643825	Balmer	mafic volcanic, fine-grained, foliated, bt-rich bands, really rusty	055/76		LL-GBZ-E21-035	
	421107	5643815	Balmer	mafic volcanic, fine-grained, foliated, min banding (bt, amph ±grt, diop)	062/60		LL-GBZ-L13-036	

Appendix B

Whole-Rock Geochemical Data

Appendix B

a) $Nb/Nb^* = Nb/10^{(\log La + (\log La - \log Ce))}$, $Ti/Ti^* = Ti/10^{((\log Eu + \log Gd)/2)}$, $Zr/Zr^* = Zr/10^{((\log Nd + \log Sm)/2)}$, and $Hf/Hf^* = Hf/10^{((\log Nd + \log Sm)/2)}$, where all elemental values are normalized to primitive mantle of Sun and McDonough, 1989 (McCuaig et al. 1994).

b) $Eu/Eu^* = 2xEu_{cn}/(Sm_{cn} + Gd_{cn})$, where all elemental values are normalized by C1 chondrite of Sun and McDonough, 1989 (Taylor and McLennan, 1985).

Method		Units	Detect Limit	LL-15BG011A04	LL-15BG013A01	LL-15BG013B01	LL-15BG017A01	LL-15BG023A01	LL-15BG027A01
SG				2.89	2.95	2.65	2.76	2.81	2.68
SG DWT		g		576.5	665.4	2063.6	956.4	441.3	879.5
SG WWT		g		377	440	1284.8	610.1	284.4	551.9
IRC-100	CO2	wt%	0.023	0.369	0.343	0.086	0.214	0.072	0.487
IRC-100	S	wt%	0.003	0.049	<0.003	0.029	0.164	0.076	0.007
XRF-M01	Al2O3	wt%	0.02	17.68	15.09	17.08	15.47	16.03	11.45
XRF-M01	BaO	wt%	0.004	0.03	0.06	0.07	0.13	0.13	0.08
XRF-M01	CaO	wt%	0.006	7.719	10.941	1.519	4.972	7.625	1.998
XRF-M01	Cr2O3	wt%	0.002	<0.002	0.04	<0.002	0.02	0.01	<0.002
XRF-M01	Fe2O3	wt%	0.01	11.38	7.64	1.82	5.11	8.41	2.69
XRF-M01	K2O	wt%	0.01	1.15	2.01	3.84	1.68	2.15	2.48
XRF-M01	LOI	wt%	0.05	1.92	1.4	1.24	0.98	1.44	1.04
XRF-M01	MgO	wt%	0.01	5.05	6.38	0.62	3.54	4.79	0.18
XRF-M01	MnO	wt%	0.002	0.177	0.142	0.026	0.106	0.12	0.049
XRF-M01	Na2O	wt%	0.02	3.62	1.9	2.31	4.26	4.17	3.26
XRF-M01	P2O5	wt%	0.002	0.234	0.367	0.093	0.164	0.69	0.035
XRF-M01	SiO2	wt%	0.04	49.8	52.74	70.47	62.82	52.64	76.19
XRF-M01	TiO2	wt%	0.01	1.05	0.92	0.33	0.58	1.21	0.35
	Total	wt%		99.8	99.63	99.42	99.83	99.43	99.8
XRF-T02	As	ppm	6	<6	<6	<6	<6	<6	<6
XRF-T02	Br	ppm	1.2	<1.2	<1.2	<1.2	<1.2	6	<1.2
XRF-T02	Cu	ppm	9	159	18	<9	48	116	<9
XRF-T02	Ga	ppm	1.3	19	18	22	20	20	22
XRF-T02	Mo	ppm	0.8	1	1	2	6	1	3
XRF-T02	Nb	ppm	0.7	4	7	2	3	23	36
XRF-T02	Ni	ppm	1.6	41	146	4	72	90	<1.6
XRF-T02	Pb	ppm	1.7	4	2	10	25	5	5
XRF-T02	Rb	ppm	0.8	33	64	93	45	47	53
XRF-T02	Sr	ppm	0.8	467	168	650	709	543	138
XRF-T02	Th	ppm	1.5	<1.5	3	3	2	10	10
XRF-T02	U	ppm	1.6	<1.6	<1.6	<1.6	2	2	2
XRF-T02	Y	ppm	0.7	20	19	3	10	34	143
XRF-T02	Zn	ppm	1	125	86	30	142	105	29
XRF-T02	Zr	ppm	1.8	94	140	111	113	255	557
XRF-T03	Ba	ppm	8	238	517	546	1176	1196	680
XRF-T03	Ce	ppm	15	34	74	24	37	204	132
XRF-T03	Co	ppm	1.3	42	36	2	16	24	4
XRF-T03	Cr	ppm	9	32	340	48	141	77	30
XRF-T03	Cs	ppm	7	<7	8	12	<7	<7	<7
XRF-T03	La	ppm	7	14	36	10	20	103	65
XRF-T03	Mn	ppm	9	1346	1131	172	817	963	351
XRF-T03	Sc	ppm	4	25	24	5	12	17	9
XRF-T03	V	ppm	3	208	169	38	92	133	<3
IMC-100	Ba	ppm	0.8	234.4	510.6	576.2	1175.2	1187.8	683.7
IMC-100	Be	ppm	0.04	0.9	1	1.26	1.52	2.74	2.08
IMC-100	Bi	ppm	0.47	<0.47	<0.47	<0.47	<0.47	<0.47	<0.47
IMC-100	Cd	ppm	0.013	0.108	0.057	0.038	0.207	0.103	0.07
IMC-100	Ce	ppm	0.12	38.46	77.06	32.81	44.23	208.59	139.56
IMC-100	Co	ppm	0.13	42.99	37.54	1.86	18.21	25.85	1.36
IMC-100	Cr	ppm	3	30	322	47	142	73	40
IMC-100	Cs	ppm	0.013	1.691	5.973	9.422	3.067	1.02	1.441
IMC-100	Cu	ppm	1.4	163.8	21.6	4.8	50.1	123.2	4.1
IMC-100	Dy	ppm	0.009	3.69	3.811	0.78	1.815	8.2	23.214
IMC-100	Er	ppm	0.007	2.09	1.938	0.376	0.984	2.791	15.711
IMC-100	Eu	ppm	0.0031	1.4347	1.8076	0.6113	1.0149	4.5439	2.5781
IMC-100	Ga	ppm	0.04	18.98	17.4	22.71	20.09	20.65	22.23
IMC-100	Gd	ppm	0.009	4.172	5.177	1.367	2.683	15.249	18.709
IMC-100	Hf	ppm	0.14	2.4	3.22	2.92	2.82	6.44	15.18

IMC-100	Ho	ppm	0.0025	0.7227	0.7057	0.1318	0.3356	1.214	5.0767
IMC-100	In	ppm	0.0018	0.0564	0.0465	0.0185	0.0342	0.0663	0.162
IMC-100	La	ppm	0.1	16.72	33.69	16.14	20.37	84.51	59.29
IMC-100	Li	ppm	0.4	32.3	19.3	22.7	35.3	27.5	7
IMC-100	Lu	ppm	0.002	0.2874	0.2668	0.0551	0.1247	0.265	2.2432
IMC-100	Mo	ppm	0.08	0.91	0.87	2.28	6.56	1.36	3.57
IMC-100	Nb	ppm	0.028	5.062	7.477	2.765	3.684	22.003	34.489
IMC-100	Nd	ppm	0.06	21.02	38.12	13.28	19.56	111.3	71.69
IMC-100	Ni	ppm	0.7	42.1	147.4	2.7	74.1	89.9	1.2
IMC-100	Pb	ppm	0.18	4.1	4	11	24.1	5.8	6.3
IMC-100	Pr	ppm	0.014	4.904	9.462	3.602	4.998	26.761	17.043
IMC-100	Rb	ppm	0.11	32.39	64.12	86.21	44.43	46.65	51.42
IMC-100	Sb	ppm	0.04	0.24	0.11	0.43	0.19	0.47	0.59
IMC-100	Sc	ppm	1.1	26.5	23.5	4.7	12.3	15.3	10.1
IMC-100	Sm	ppm	0.026	4.34	6.794	2.139	3.574	21.225	17.244
IMC-100	Sn	ppm	0.16	0.83	0.95	0.75	0.93	2.95	7.59
IMC-100	Sr	ppm	0.6	463.1	167.2	636.2	703.7	552.2	133.6
IMC-100	Ta	ppm	0.007	0.26	0.363	0.177	0.225	0.956	2.325
IMC-100	Tb	ppm	0.0023	0.6097	0.68	0.1558	0.3504	1.7494	3.3697
IMC-100	Th	ppm	0.018	1.992	3.721	3.342	3.616	11.225	10.847
IMC-100	Ti	ppm	7	6197	5470	1944	3418	7574	1993
IMC-100	Tl	ppm	0.002	0.111	0.233	0.686	0.398	0.245	0.295
IMC-100	Tm	ppm	0.0019	0.2939	0.2845	0.0545	0.1327	0.338	2.36
IMC-100	U	ppm	0.011	0.546	0.976	1.168	1.125	1.927	2.602
IMC-100	V	ppm	0.8	192.3	165.7	38.6	89.3	136.1	2.2
IMC-100	W	ppm	0.05	0.87	9.06	1.17	0.5	0.95	2.02
IMC-100	Y	ppm	0.05	20.07	19.55	3.83	9.4	34.71	139.72
IMC-100	Yb	ppm	0.009	1.926	1.771	0.354	0.88	1.941	15.451
IMC-100	Zn	ppm	1.8	119	79	30	135	94	26
IMC-100	Zr	ppm	6	94	137	113	111	257	519
IAC-100	Al	ppm	210	87882	75932	86142	75100	81404	55379
IAC-100	Ba	ppm	1	215	452	538	1035	1039	612
IAC-100	Be	ppm	1	1	1	1	1	2	2
IAC-100	Ca	ppm	70	52822	71859	10656	33407	53649	13409
IAC-100	Cd	ppm	1	<1	<1	<1	<1	<1	<1
IAC-100	Co	ppm	1	37	31	<1	15	20	<1
IAC-100	Cr	ppm	2	28	290	44	126	66	36
IAC-100	Cu	ppm	6	160	26	7	51	126	6
IAC-100	Fe	ppm	90	71872	49232	12004	32109	55457	16954
IAC-100	K	ppm	70	9192	16217	31471	13186	17549	19435
IAC-100	Li	ppm	1	31	19	22	33	24	7
IAC-100	Mg	ppm	30	27630	35409	3275	19294	27355	972
IAC-100	Mn	ppm	1	1237	1006	168	720	879	332
IAC-100	Mo	ppm	1	<1	<1	2	5	<1	3
IAC-100	Na	ppm	500	24895	13505	16395	28633	28875	21691
IAC-100	Ni	ppm	2	38	134	<2	66	80	<2
IAC-100	P	ppm	30	993	1514	407	661	2846	152
IAC-100	Pb	ppm	15	16	<15	18	34	18	<15
IAC-100	S	ppm	130	642	<130	418	1740	870	159
IAC-100	Sc	ppm	1	22	20	4	10	13	8
IAC-100	Sr	ppm	2	442	163	665	689	543	134
IAC-100	Ti	ppm	5	6049	5378	1974	3282	7231	1949
IAC-100	V	ppm	1	188	159	40	88	132	1
IAC-100	W	ppm	6	<6	<6	<6	<6	<6	<6
IAC-100	Y	ppm	1	18	18	4	9	31	>120
IAC-100	Zn	ppm	5	124	81	31	136	98	26
IMP-200	Au	ppb	0.4	1.1	2.12	2.69	6.58	15.2	3.37
IMP-200	Ir	ppb	0.01	0.01	0.05	0.02	0.03	0.02	0.02
IMP-200	Pd	ppb	0.12	0.41	1.09	0.12	0.52	0.29	<0.12
IMP-200	Pt	ppb	0.17	2.69	3.64	2.56	2.35	2.65	1.88
IMP-200	Rh	ppb	0.04	<0.04	0.12	<0.04	0.04	<0.04	<0.04
IMP-200	Ru	ppb	0.08	<0.08	0.09	<0.08	<0.08	<0.08	<0.08

	LL-15BG032B01	LL-15BG035A01	LL-15BG039A01	LL-15BG045A01	LL-15BG051B01	LL-15BG054A01	LL-15BG054B01	LL-15BG054C01
	2.65	2.74	2.84	2.97	2.97	2.71	2.99	2.98
	825.5	613.9	1591.7	2044.8	975.2	470.4	560.3	1111.6
	514	389.6	1030.4	1356.5	646.4	297	372.8	738.9
CO2	0.359	0.828	0.108	0.379	<0.023	0.248	<0.023	0.164
S	0.084	0.015	2.073	0.03	0.097	0.165	0.01	0.028
Al2O3	12.42	15.53	8.24	14.42	15.04	14.26	15.65	14.62
BaO	0.15	0.07	0.04	0.05	0.02	0.03	0.04	0.05
CaO	0.857	3.583	0.567	7.13	7.716	3.981	7.759	7.206
Cr2O3	<0.002	0.01	<0.002	<0.002	0.01	0.01	<0.002	<0.002
Fe2O3	1.68	5.51	23.81	15.61	12.06	3.45	15.25	15.37
K2O	4.15	1.85	2.02	1.99	0.86	1.37	0.92	1.49
LOI	1.09	1.88	2.47	1.59	1.18	1.07	0.71	0.61
MgO	0.27	2.47	0.23	3.27	4.44	1.32	4.43	3.3
MnO	0.026	0.074	0.037	0.208	0.156	0.091	0.207	0.222
Na2O	2.63	5.25	1.83	2.75	3.65	2.34	3.22	3.03
P2O5	0.009	0.237	0.01	0.539	0.091	0.082	0.361	0.555
SiO2	76.54	62.75	60.19	50.38	53.61	71.69	49.98	50.81
TiO2	0.14	0.69	0.14	2.05	1.32	0.33	1.62	1.98
Total	99.97	99.9	99.59	99.97	100.14	100.02	100.15	99.25
As	<6	<6	6	<6	<6	<6	<6	<6
Br	<1.2	<1.2	<1.2	<1.2	3	<1.2	<1.2	<1.2
Cu	<9	25	809	169	54	32	182	418
Ga	20	20	23	24	20	15	22	25
Mo	3	1	5	2	1	2	2	1
Nb	47	5	37	15	2	4	9	15
Ni	<1.6	41	11	9	84	36	65	8
Pb	17	8	11	5	<1.7	15	3	3
Rb	88	53	34	50	34	46	21	32
Sr	139	668	67	272	263	338	249	269
Th	10	6	9	5	<1.5	5	2	5
U	3	<1.6	2	2	<1.6	<1.6	<1.6	2
Y	127	16	50	56	17	12	38	56
Zn	127	86	113	146	118	45	138	130
Zr	348	165	264	293	76	111	188	287
Ba	1252	576	425	465	114	236	372	426
Ce	143	60	53	80	<15	28	62	101
Co	3	16	19	34	39	10	44	34
Cr	33	68	26	15	111	122	57	10
Cs	<7	7	<7	7	<7	<7	<7	<7
La	74	31	17	39	<7	17	26	50
Mn	191	579	330	1513	1147	641	1508	1594
Sc	<4	8	5	28	20	9	27	30
V	<3	87	22	146	193	55	242	131
Ba	1319.3	585.4	356	441.1	116.8	212.9	337.1	378.8
Be	2.51	1.29	1.51	1.9	1.4	1.09	1.12	1.79
Bi	<0.47	<0.47	<0.47	<0.47	<0.47	<0.47	<0.47	<0.47
Cd	0.212	0.078	0.096	0.085	0.093	0.179	0.068	0.05
Ce	156.01	70.61	45.69	81.85	15.13	36.78	53.74	91.45
Co	0.81	16.53	22.43	34.83	38.13	11.37	46.32	33.52
Cr	45	69	24	14	98	136	51	6
Cs	1.08	3.18	1.341	1.248	0.752	2.879	2.123	4.115
Cu	11.1	29.5	681.4	167.6	54.8	38.5	173.7	394.9
Dy	21.263	3.054	8.197	9.588	3.338	2.006	6.801	9.579
Er	14.301	1.614	5.957	6.16	1.848	1.187	4.382	6.261
Eu	1.6403	1.4615	0.6382	2.2773	1.0553	0.8117	1.6639	2.3184
Ga	20.79	19.89	19.41	22.84	18.73	15.25	21.1	23.29
Gd	17.446	4.313	5.908	9.141	3.542	2.233	6.246	9.342
Hf	11.53	4.05	8.37	6.87	2.25	3.01	4.67	6.96

Ho	4.5722	0.5764	1.8271	2.022	0.6566	0.4087	1.4007	2.0503
In	0.1442	0.0398	0.0929	0.0917	0.0606	0.0227	0.071	0.1001
La	70.16	32.72	17.73	36.95	6	18.72	23.52	42.6
Li	11.6	27.6	6.8	17.9	15	24.4	23.3	21
Lu	2.1228	0.216	0.9968	0.9354	0.2374	0.1775	0.6518	0.9232
Mo	4.4	1.49	5.61	2.13	1.41	3.6	2.48	1.3
Nb	44.505	5.825	33.18	15.551	2.733	4.208	10.291	15.715
Nd	73.61	30.96	22	43.1	10.51	14.91	28.73	46.35
Ni	0.9	41.1	9.8	8.8	83.9	40.4	66.5	8
Pb	18.9	9.1	12.1	5.6	3.1	16.9	4	4.1
Pr	18.263	7.953	5.242	10.266	2.112	4.076	6.779	11.354
Rb	87.23	52.04	32.05	48.76	33.33	46.84	21.72	32.21
Sb	0.2	0.45	0.34	0.27	0.42	0.2	0.25	0.26
Sc	2.1	9.7	1.8	31.1	20.4	8.2	31.6	31.1
Sm	16.036	5.482	5.381	9.082	3.02	2.68	6.099	9.224
Sn	7.52	1.02	2.85	2.01	1.01	0.92	1.34	1.02
Sr	134.3	656.8	62.6	266.5	265.4	339.9	254.3	266.2
Ta	2.954	0.383	2.078	0.885	0.163	0.359	0.594	0.904
Tb	3.0638	0.5522	1.1375	1.441	0.5518	0.3357	1.0263	1.4824
Th	11.932	7.186	8.757	5.014	0.973	5.672	3.434	5.204
Ti	832	4123	685	12149	7757	1951	9701	11819
Tl	0.572	0.292	0.205	0.182	0.136	0.25	0.067	0.083
Tm	2.1679	0.2223	0.9503	0.916	0.2624	0.1767	0.6387	0.9235
U	3.121	1.912	2.343	1.421	0.283	1.993	0.981	1.39
V	1.9	86.7	17.8	137.9	181.3	54.9	227.9	124
W	4.78	0.83	1.08	0.86	0.56	0.44	0.57	0.37
Y	127.31	16.26	46.55	55.69	17.9	12.42	39.56	56.74
Yb	14.449	1.475	6.427	6.095	1.627	1.182	4.257	6.148
Zn	117	78	87	131	104	44	127	116
Zr	334	159	246	280	77	117	190	284
Al	62961	77816	42332	73063	74551	70242	76900	77996
Ba	1247	520	315	400	103	210	296	347
Be	2	1	1	2	1	1	1	2
Ca	5935	24977	3546	49885	52937	28921	52902	53262
Cd	<1	<1	<1	<1	<1	<1	<1	<1
Co	<1	13	20	26	29	10	37	26
Cr	43	62	21	12	86	129	45	5
Cu	13	34	675	180	60	40	175	423
Fe	11346	36344	>95000	>95000	78923	23443	>95000	>95000
K	34300	14980	16331	16230	6735	11507	7137	12797
Li	11	27	6	18	15	24	22	22
Mg	1438	14030	1344	18869	24910	6328	24499	19994
Mn	191	530	271	1527	1117	648	1450	1689
Mo	4	1	4	2	<1	4	1	1
Na	18421	>31000	12916	19310	24936	16805	22037	22345
Ni	<2	36	10	8	71	37	58	6
P	45	975	54	2267	374	370	1517	2371
Pb	27	18	20	16	<15	26	<15	16
S	1025	267	>16000	396	1078	1728	<130	349
Sc	1	8	1	27	18	7	26	28
Sr	144	666	61	269	263	353	239	275
Ti	847	4102	692	12334	7682	1990	9326	12407
V	3	86	21	142	180	56	221	132
W	<6	<6	<6	<6	<6	<6	<6	<6
Y	>120	15	44	52	16	12	35	56
Zn	129	81	88	135	104	47	127	122
Au	54.6	5.32	23.7	1.22	1.4	1.15	6.87	5.55
Ir	0.02	0.02	0.01	0.01	0.01	0.05	0.02	<0.01
Pd	<0.12	0.23	0.72	<0.12	0.17	0.91	10.7	<0.12
Pt	1.41	1.54	1.17	0.86	1.2	1.99	4.55	0.63
Rh	<0.04	<0.04	<0.04	<0.04	<0.04	0.06	0.4	<0.04
Ru	<0.08	<0.08	<0.08	<0.08	<0.08	0.1	0.08	<0.08

	LL-15BG055A01	LL-15BG071A01	LL-15BG079A01	LL-15BG088A01	LL-15BG095A01	LL-15BG102A01	LL-15BG108A01	LL-15BG112A01
	2.65	3.14	3.01	2.92	2.66	2.95	2.98	2.63
	616.6	1313.6	569.4	818.7	1312.2	588.1	758.2	1580.3
	383.6	895.6	380.2	538.5	819.2	388.5	503.7	979.7
CO2	0.081	0.503	0.075	0.915	<0.023	1.889	0.693	0.157
S	0.073	0.024	0.023	1.23	0.005	0.082	0.801	0.454
Al2O3	12.55	6.97	19.76	14.1	15.66	13.14	15.89	15.52
BaO	0.05	0.02	0.02	0.08	0.06	0.01	0.02	0.07
CaO	0.462	12.417	8.253	5.845	2.022	8.995	10.074	0.892
Cr2O3	<0.002	0.14	<0.002	<0.002	<0.002	0.05	0.01	<0.002
Fe2O3	3.06	12.86	14.68	14.01	1.7	11.33	20.59	2.18
K2O	4.16	0.68	1.07	2.98	2.02	0.14	0.95	3.78
LOI	2.01	1.66	0.39	2.81	0.95	3.47	1.16	1.43
MgO	0.7	15.32	3.13	3.39	0.6	9.6	2.39	0.73
MnO	0.041	0.193	0.191	0.175	0.031	0.206	0.598	0.02
Na2O	0.46	1.23	3.56	2.15	5.74	3.41	2.36	4.32
P2O5	0.055	0.072	0.634	0.551	0.073	0.018	0.305	0.105
SiO2	75.76	47.21	45.41	51.27	71.23	48.43	43.52	70.64
TiO2	0.33	0.89	2.49	1.81	0.23	0.28	1.3	0.34
Total	99.64	99.66	99.59	99.15	100.29	99.07	99.16	100.02
As	<6	<6	<6	50	<6	<6	<6	15
Br	<1.2	<1.2	<1.2	<1.2	5	<1.2	2	2
Cu	<9	167	360	149	<9	146	399	16
Ga	24	11	28	23	18	11	23	18
Mo	1	<0.8	1	2	1	<0.8	2	5
Nb	28	3	17	17	4	<0.7	9	2
Ni	2	189	31	6	7	110	188	18
Pb	4	<1.7	6	7	3	<1.7	5	17
Rb	79	14	31	70	41	2	22	107
Sr	43	219	273	264	463	75	271	372
Th	8	<1.5	8	5	2	<1.5	4	3
U	2	<1.6	2	<1.6	<1.6	<1.6	2	<1.6
Y	38	28	64	53	5	8	37	9
Zn	56	116	155	177	31	82	148	31
Zr	267	53	352	275	103	16	180	107
Ba	381	144	252	692	443	24	217	575
Ce	50	30	86	78	23	<15	73	23
Co	3	63	37	23	4	48	68	7
Cr	18	983	32	<9	35	380	73	51
Cs	<7	<7	<7	9	<7	<7	<7	7
La	19	<7	41	34	8	<7	30	8
Mn	291	1510	1380	1386	223	1587	>4000	145
Sc	6	47	28	26	<4	41	27	6
V	24	292	244	117	17	222	225	41
Ba	392.3	139.1	221.9	669.4	473.6	25.9	198	605.9
Be	2.23	0.8	2.05	2.44	1.05	0.27	1.3	0.91
Bi	<0.47	<0.47	<0.47	<0.47	<0.47	<0.47	<0.47	<0.47
Cd	0.053	0.132	0.057	0.156	0.034	0.079	0.17	0.031
Ce	52.87	22.02	80.02	77.34	25.67	2.46	64.32	25.79
Co	1.9	65.92	36.87	25.82	2.95	49.89	78.75	7.49
Cr	20	981	26	11	36	367	65	49
Cs	1.211	0.569	1.499	2.846	0.405	0.297	0.663	6.57
Cu	10.5	171.6	355.9	162.3	<1.4	151.7	391.5	19.4
Dy	6.145	5.278	11.232	9.187	0.875	1.362	6.304	1.385
Er	4.649	3.029	6.955	5.923	0.447	1.003	3.93	0.775
Eu	0.6694	1.0965	2.3166	2.2132	0.4886	0.2332	1.6987	0.6628
Ga	23.9	10.59	25.65	22.74	17.93	10.35	21.94	18.07
Gd	4.488	5.445	10.955	8.936	1.251	0.903	6.569	1.653
Hf	8.62	1.77	8.37	6.53	3.09	0.46	4.55	2.69

Ho	1.3965	1.0529	2.3266	1.9355	0.1535	0.3091	1.2904	0.2663
In	0.0978	0.092	0.0825	0.0981	0.0107	0.0358	0.0705	0.0147
La	25.73	8.33	35.11	34.79	11.24	1.02	29.66	12.25
Li	33.3	17.5	13.9	33.6	11.6	28.9	16.7	22.5
Lu	0.7705	0.3607	0.9798	0.8772	0.0656	0.1567	0.5771	0.121
Mo	1.54	0.62	0.87	2.11	1.3	0.35	1.4	5.1
Nb	26.455	3.367	17.853	16.689	4.11	0.57	9.032	2.836
Nd	19.98	17.68	44.53	42.42	11.36	1.8	33.56	11.85
Ni	1.3	188.9	31.9	6.6	6.6	109	203	20.4
Pb	6.1	2.1	7.2	8.4	4	1.5	5.8	17.2
Pr	5.465	3.446	10.575	10.145	3.065	0.349	8.331	3.097
Rb	81.78	14.26	31.68	70.13	41.93	1.97	21.55	106.95
Sb	0.54	0.16	0.15	0.65	0.04	0.24	0.26	0.49
Sc	5.3	53.6	31.3	28.9	2.6	48.4	28	5.5
Sm	4.078	4.844	10.168	8.803	1.906	0.579	6.655	2.142
Sn	5.58	1.13	2.89	2.17	0.75	0.24	1.28	0.72
Sr	43.1	223.5	269.9	265.4	469.9	74.8	269.5	366
Ta	1.784	0.209	1.003	0.829	0.257	0.036	0.499	0.222
Tb	0.8402	0.8275	1.7562	1.4225	0.1649	0.1768	0.9772	0.2292
Th	9.436	1.319	6.873	5.012	3.576	0.176	3.95	3.426
Ti	1929	5431	15060	10745	1329	1626	7704	1958
Tl	0.287	0.068	0.051	0.302	0.16	0.011	0.142	0.948
Tm	0.7305	0.4108	1.0108	0.8753	0.0639	0.1507	0.5767	0.1257
U	2.284	0.336	1.793	1.46	0.976	0.05	1.055	1.218
V	24.4	298.5	235.3	106.5	17.9	217.8	203.7	40.2
W	12.41	0.3	0.55	38.91	0.09	0.72	3.26	1.08
Y	39.35	27.8	65.28	54.52	4.87	8.48	37.18	8.34
Yb	5.15	2.559	6.529	5.781	0.44	1.066	3.79	0.838
Zn	52	103	141	156	28	74	133	30
Zr	287	52	344	268	110	16	174	104
Al	61757	36195	97892	70397	77256	66172	80933	75292
Ba	356	129	197	579	434	23	183	541
Be	2	1	2	2	1	<1	1	1
Ca	2907	81806	56428	40585	13797	61945	66941	5882
Cd	<1	<1	<1	1	<1	<1	<1	<1
Co	1	58	26	17	2	43	69	6
Cr	18	903	22	10	32	322	60	43
Cu	13	178	358	170	<6	152	396	20
Fe	20063	86218	>95000	93119	11074	73902	>95000	14073
K	33598	5474	8564	24129	16170	1037	7698	30124
Li	32	18	14	32	11	27	16	21
Mg	3813	88524	17855	19357	3374	54301	13676	4085
Mn	273	1400	1385	1260	211	1439	4390	130
Mo	2	1	<1	1	1	<1	<1	5
Na	3504	8987	24593	14942	>31000	23812	16807	28807
Ni	<2	173	25	5	4	95	187	16
P	235	315	2591	2188	309	78	1302	433
Pb	<15	<15	20	15	<15	<15	19	25
S	899	308	270	11431	<130	1104	7911	4152
Sc	4	47	27	25	2	42	25	5
Sr	43	225	262	263	486	71	271	369
Ti	1910	5356	14660	10752	1324	1573	7715	1943
V	25	287	231	108	18	214	209	40
W	<6	<6	<6	9	<6	<6	<6	<6
Y	36	26	60	50	5	8	35	7
Zn	55	109	140	153	29	74	137	29
Au	179	1.88	4.9	502	0.88	2.26	9.46	15.7
Ir	0.01	0.17	0.07	0.04	0.03	0.06	0.05	0.02
Pd	<0.12	6.34	2.05	<0.12	<0.12	12.6	9.76	0.33
Pt	0.61	8.22	1.89	0.62	0.57	10.1	3.71	0.66
Rh	<0.04	0.57	0.11	0.04	<0.04	0.75	0.28	<0.04
Ru	<0.08	<0.08	<0.08	<0.08	<0.08	0.5	0.1	<0.08

	LL-15BG113A01	LL-15BG127A01	LL-15BG129A01	LL-15BG134A01	LL-15BG134A02	LL-15BG135A01	LL-15BG137A01	LL-15BG143A01
	2.67	2.7	2.74	2.95	2.99	2.69	2.88	3.01
	1395.2	699.8	1366.3	1501.4	367.2	1892.1	1264.7	1200.5
	872.8	440.4	868.2	992.4	244.5	1188.9	825.3	802.1
CO2	0.913	0.025	0.527	0.564	0.062	0.039	0.807	0.453
S	0.03	0.085	0.008	0.03	1.275	0.02	0.005	0.007
Al2O3	15.37	17.02	15.68	14.88	13.58	16.25	14.93	14.18
BaO	0.05	0.04	0.04	0.01	0.01	0.12	0.01	0.01
CaO	3.172	2.202	3.901	11.273	5.751	2.284	8.749	12.311
Cr2O3	<0.002	0.01	<0.002	0.02	<0.002	<0.002	0.08	0.04
Fe2O3	2.65	3.34	5.77	9.89	16.84	2.07	8.7	8.3
K2O	1.47	1.83	1.77	0.43	0.27	2.26	0.47	0.46
LOI	1.73	1	1.44	1.37	1.45	1.16	1.66	2.1
MgO	1.16	0.58	2.69	7.69	5.05	0.85	5.16	6.84
MnO	0.045	0.049	0.073	0.19	0.203	0.037	0.197	0.214
Na2O	5.2	4.16	4.77	2.36	3.16	5.08	4.87	1.07
P2O5	0.09	0.101	0.242	0.037	0.195	0.074	0.023	0.038
SiO2	67.6	69.31	62.74	51.38	50.9	69.84	53.89	54.22
TiO2	0.31	0.36	0.7	0.47	1.91	0.14	0.33	0.35
Total	98.84	99.99	99.82	99.99	99.31	100.18	99.06	100.13
As	<6	<6	<6	<6	<6	<6	<6	<6
Br	<1.2	<1.2	<1.2	<1.2	<1.2	<1.2	5	5
Cu	21	25	50	27	403	<9	13	<9
Ga	20	21	21	15	20	17	11	13
Mo	2	1	1	<0.8	<0.8	1	2	<0.8
Nb	1	2	5	<0.7	6	<0.7	<0.7	<0.7
Ni	15	17	40	98	33	8	119	96
Pb	8	8	9	<1.7	<1.7	5	<1.7	<1.7
Rb	44	46	39	6	6	38	6	16
Sr	580	615	721	49	69	597	121	53
Th	2	2	6	<1.5	<1.5	<1.5	<1.5	<1.5
U	<1.6	<1.6	<1.6	<1.6	<1.6	<1.6	<1.6	<1.6
Y	4	5	15	12	43	2	8	10
Zn	52	50	74	71	68	34	64	60
Zr	98	103	153	31	140	100	18	22
Ba	385	364	398	58	22	948	105	53
Ce	29	26	55	<15	23	24	<15	<15
Co	7	9	17	47	44	4	45	39
Cr	58	54	47	171	40	41	569	280
Cs	<7	9	<7	<7	<7	<7	<7	<7
La	9	11	30	<7	<7	10	<7	<7
Mn	324	338	550	1499	1520	238	1525	1698
Sc	6	7	10	51	40	4	48	46
V	42	52	88	274	465	18	238	227
Ba	398	367.6	404.4	57.2	38.8	1039.9	107.3	57.9
Be	1.1	1.34	1.17	0.32	0.78	1.06	0.67	0.21
Bi	<0.47	<0.47	<0.47	<0.47	<0.47	<0.47	<0.47	<0.47
Cd	0.035	0.035	0.056	0.06	0.06	0.033	0.03	0.068
Ce	26.3	30.45	63.96	5.11	21.86	27.71	2.97	6.32
Co	7.64	9.48	17.48	48.59	49.87	4.25	46.17	39.51
Cr	58	57	46	153	35	55	553	274
Cs	2.061	8.46	2.861	0.473	0.586	0.812	0.314	0.752
Cu	27	29.6	55.4	30	396.5	3.8	19	13.1
Dy	0.988	1.092	2.876	1.861	7.272	0.46	1.381	1.626
Er	0.489	0.552	1.436	1.297	4.716	0.24	0.989	1.123
Eu	0.6138	0.6681	1.3885	0.4047	1.6136	0.379	0.2608	0.3517
Ga	20.08	21.19	20.31	13.58	18.63	17.81	11.3	12.72
Gd	1.592	1.739	4.073	1.47	6.293	0.721	0.965	1.295
Hf	2.63	2.8	3.8	0.82	3.61	2.65	0.55	0.67

Ho	0.1727	0.1959	0.5269	0.4071	1.5443	0.0846	0.3038	0.3538
In	0.0196	0.0232	0.0376	0.0482	0.0958	0.0155	0.0448	0.0372
La	13.1	15.65	30.23	1.99	8.48	15.63	1.36	3.3
Li	23.5	28.2	30.5	19.7	27.5	15.8	17.5	19.9
Lu	0.0676	0.0748	0.1949	0.2036	0.6863	0.0413	0.1687	0.1672
Mo	1.99	1.78	0.8	0.48	0.59	1.87	2.38	0.97
Nb	2.168	2.346	5.642	1.141	6.897	1.081	0.69	0.853
Nd	11.97	13.49	29.52	3.37	15.99	8.65	2.1	3.53
Ni	15.2	17.5	40.3	94.7	35.8	7.8	120.5	98.9
Pb	8.2	8.8	9.5	1.6	3	5.7	1.4	0.9
Pr	3.031	3.573	7.462	0.703	3.221	2.624	0.433	0.745
Rb	43.99	46.64	39.26	5.23	5.16	37.85	5.77	16.44
Sb	0.1	0.13	0.41	0.64	0.51	0.04	0.37	0.86
Sc	5.5	7.2	9.6	56.4	46	3.6	55.5	51.4
Sm	2.116	2.279	5.038	1.021	4.724	1.172	0.649	0.947
Sn	0.65	0.84	0.99	0.39	1.23	0.5	0.36	0.36
Sr	586.9	621.8	733.5	48.5	68.7	607.2	118.2	53.1
Ta	0.141	0.157	0.337	0.071	0.414	0.035	0.047	0.06
Tb	0.1908	0.207	0.5286	0.252	1.0781	0.0822	0.1847	0.231
Th	2.856	3.194	6.154	0.331	0.994	1.914	0.211	0.279
Ti	1850	2125	4357	2767	11694	873	1989	2197
Tl	0.349	0.328	0.184	0.028	0.077	0.161	0.03	0.074
Tm	0.0666	0.0754	0.2078	0.1937	0.6931	0.0345	0.1567	0.1695
U	1.019	1.029	1.582	0.108	0.268	0.296	0.07	0.086
V	42.3	55.1	89.8	263.1	>370	21.1	236.9	225.1
W	0.71	0.25	2.39	2.97	1.5	0.13	0.63	0.58
Y	4.95	5.58	15.17	10.96	42.88	2.43	7.98	10.14
Yb	0.447	0.478	1.316	1.317	4.56	0.24	1.108	1.095
Zn	50	47	69	62	64	33	58	56
Zr	99	105	152	29	132	103	19	22
Al	79832	84460	78965	72706	73333	78588	74778	74862
Ba	369	316	356	50	36	881	93	53
Be	1	1	1	<1	1	1	1	<1
Ca	22679	15162	27533	70535	41978	15335	60825	83133
Cd	<1	<1	<1	<1	<1	<1	<1	<1
Co	6	7	14	43	40	3	40	34
Cr	53	49	39	138	31	46	483	248
Cu	28	31	58	35	429	<6	21	17
Fe	18277	22312	39113	64027	>95000	13485	57486	57932
K	12465	13892	14712	2752	2251	17920	3684	3920
Li	22	26	28	19	26	15	16	19
Mg	6894	3318	15729	42729	31357	4773	29372	41103
Mn	312	331	513	1331	1552	230	1399	1616
Mo	2	1	<1	1	1	2	1	1
Na	>31000	28327	>31000	16271	23773	>31000	>31000	8231
Ni	13	15	34	86	33	4	105	88
P	394	405	1021	159	858	307	106	167
Pb	21	16	18	<15	<15	<15	<15	<15
S	402	910	<130	311	12278	316	<130	<130
Sc	5	6	8	49	43	3	48	46
Sr	610	618	726	46	69	587	114	53
Ti	1887	2056	4247	2635	12082	815	1860	2173
V	43	54	91	259	474	20	229	232
W	<6	<6	<6	<6	<6	<6	<6	<6
Y	5	5	14	10	41	2	7	10
Zn	52	46	69	63	63	32	58	56
Au	8.21	1.06	2.64	7.57	198	<0.4	0.72	1.26
Ir	0.03	0.02	0.01	0.03	0.01	0.02	0.03	0.03
Pd	0.3	0.33	0.14	15.8	0.13	<0.12	14.8	13.7
Pt	0.57	0.67	0.49	14.1	0.55	0.43	11.6	11.5
Rh	<0.04	<0.04	<0.04	0.68	<0.04	<0.04	0.85	0.56
Ru	<0.08	<0.08	<0.08	<0.08	<0.08	<0.08	0.27	0.1

	LL-15BG149A01	LL-15BG145A01	LL-15BG150A01	LL-15BG158A01	LL-15BG169A01	LL-15BG172A02	LL-15BG177A03	LL-15BG177B01
	2.62	3.02	3.04	2.93	2.82	3.05	2.9	2.73
	743.1	399.8	858.6	754.4	1172.2	1018.7	1139.3	1137.9
	459.6	267.3	576.3	496.9	757.1	684.5	747	721.6
CO2	0.025	0.042	1.638	0.077	0.106	<0.023	0.13	0.094
S	0.01	0.057	0.412	0.122	3.908	0.029	0.04	0.016
Al2O3	14.7	13.82	4.76	15.88	10.43	7.41	5.99	3.74
BaO	0.12	0.01	0.01	0.03	0.02	<0.004	0.01	<0.004
CaO	1.307	7.393	12.437	8.896	4.268	8.431	6.548	3.87
Cr2O3	<0.002	0.06	0.24	0.01	0.01	0.46	0.32	0.39
Fe2O3	1.28	12.9	9.93	12.39	9.65	12.86	10.46	9.43
K2O	4.63	0.14	0.09	1.15	2.21	0.07	0.08	0.04
LOI	0.52	1.23	3.2	1.36	4.46	4.29	6.64	10.29
MgO	0.44	8.28	19.88	4.83	2.93	22.11	24.62	29.36
MnO	0.027	0.296	0.206	0.175	0.069	0.208	0.155	0.113
Na2O	3.71	3.29	0.76	2.64	0.9	0.59	0.28	0.14
P2O5	0.051	0.015	0.005	0.365	0.068	0.014	0.018	0.006
SiO2	72.71	52.23	47.59	50.85	64.05	43.29	44.53	42.7
TiO2	0.17	0.31	0.27	1.26	0.55	0.26	0.26	0.14
Total	99.67	99.99	99.38	99.83	99.6	100.01	99.9	100.23
As	<6	<6	<6	<6	<6	<6	<6	<6
Br	<1.2	<1.2	<1.2	<1.2	<1.2	<1.2	<1.2	4
Cu	11	25	84	234	197	39	44	<9
Ga	18	10	5	18	14	6	7	3
Mo	<0.8	1	2	6	4	<0.8	<0.8	<0.8
Nb	7	<0.7	<0.7	11	5	<0.7	<0.7	<0.7
Ni	5	116	418	51	37	881	797	1493
Pb	22	<1.7	<1.7	4	17	11	<1.7	<1.7
Rb	108	2	1	25	43	1	2	1
Sr	370	36	51	248	98	33	23	11
Th	11	<1.5	<1.5	4	2	<1.5	<1.5	<1.5
U	2	<1.6	<1.6	<1.6	<1.6	<1.6	<1.6	<1.6
Y	6	10	6	42	15	7	7	4
Zn	28	83	44	113	98	130	45	27
Zr	95	17	13	227	109	12	16	5
Ba	1024	51	9	230	185	<8	<8	<8
Ce	49	<15	<15	69	<15	<15	<15	<15
Co	2	44	65	37	30	94	81	73
Cr	19	460	1700	91	119	3176	2161	2503
Cs	<7	<7	<7	<7	<7	<7	<7	<7
La	26	<7	<7	29	<7	<7	<7	<7
Mn	186	2282	1633	1380	556	1649	1136	865
Sc	5	47	36	30	23	37	29	19
V	8	236	147	206	191	171	129	80
Ba	1115.4	54.2	11.3	231	171.7	6.7	8.6	3.8
Be	2.02	0.19	0.29	1.55	0.66	0.15	0.22	0.15
Bi	<0.47	<0.47	<0.47	<0.47	<0.47	<0.47	<0.47	<0.47
Cd	0.023	0.088	0.112	0.079	0.196	0.261	0.053	0.034
Ce	48	1.98	1.09	58.19	13.85	1.68	7.12	7.94
Co	2.28	44.6	71.2	40.02	41.67	96.88	87.57	80.55
Cr	19	443	1669	84	95	3067	2349	2853
Cs	1.763	0.285	0.109	1.179	1.427	0.127	0.219	0.349
Cu	14.7	26.6	85.9	233	198	36.6	48.2	<1.4
Dy	1.006	1.547	1.038	6.924	2.647	1.114	1.115	0.658
Er	0.497	1.22	0.672	4.514	1.893	0.786	0.742	0.441
Eu	0.592	0.2291	0.2588	1.5132	0.5922	0.2698	0.2556	0.1717
Ga	19.03	10.16	4.13	18.11	12.92	6.25	6.71	3.69
Gd	1.603	0.956	0.655	6.501	2.267	0.812	0.946	0.626
Hf	3.14	0.54	0.44	5.38	2.7	0.39	0.57	0.27

Ho	0.1836	0.3585	0.224	1.4613	0.572	0.2495	0.2516	0.1497
In	0.0097	0.0362	0.0305	0.0625	0.0621	0.0305	0.024	0.0182
La	23.37	0.81	0.4	26.45	6.47	0.63	3.08	3.88
Li	17.6	15.2	0.8	25.3	22.1	5.4	10.4	11.9
Lu	0.0815	0.216	0.0985	0.6614	0.3	0.1194	0.113	0.0669
Mo	0.89	0.48	2.2	6.86	4.48	0.36	0.25	0.14
Nb	7.047	0.664	0.431	11.154	5.28	0.385	0.728	0.223
Nd	16.31	1.61	1.15	32.26	8.11	1.45	3.92	3.04
Ni	4	114.6	442.6	50.5	40.8	837.4	803.5	1519.1
Pb	22.1	0.5	1.5	5.3	17.7	11.8	1	0.5
Pr	4.792	0.32	0.198	7.663	1.913	0.283	0.894	0.779
Rb	111.53	1.91	0.56	25.31	43.73	0.7	2.03	0.74
Sb	0.07	0.09	0.26	0.21	1.12	0.11	0.17	0.17
Sc	1.8	54.6	37.5	32.2	20.2	40.9	35.6	24.4
Sm	2.503	0.576	0.436	6.56	1.952	0.542	0.784	0.514
Sn	0.84	0.32	0.52	1.85	1.44	0.23	0.24	0.17
Sr	371.5	36.8	53.4	255.3	102.1	34.2	24.7	12.2
Ta	0.525	0.043	0.028	0.629	0.39	0.025	0.042	0.011
Tb	0.1964	0.2029	0.1357	1.0487	0.3836	0.1609	0.1645	0.091
Th	13.311	0.182	0.097	4.3	2.539	0.053	0.226	0.038
Ti	993	1849	1626	7814	3332	1649	1707	879
Tl	0.55	0.016	0.03	0.097	0.385	0.016	0.016	0.01
Tm	0.0759	0.1907	0.1011	0.6548	0.2788	0.118	0.1108	0.0661
U	2.581	0.063	0.04	1.204	0.69	0.028	0.066	0.023
V	10.9	228	162.2	198.9	170.6	174.2	153	97.7
W	0.13	0.06	0.39	0.53	11.11	0.35	0.35	0.11
Y	5.73	9.73	6.01	43.05	15.85	7.04	7.04	4.31
Yb	0.514	1.352	0.668	4.326	1.931	0.765	0.728	0.427
Zn	27	71	40	102	84	114	47	32
Zr	99	18	14	228	106	12	21	9
Al	72680	73205	25044	81492	51644	39928	30765	20680
Ba	970	47	11	208	151	7	8	3
Be	2	<1	<1	1	1	<1	<1	<1
Ca	8331	53274	80786	59668	29408	61470	45584	27313
Cd	<1	<1	<1	<1	<1	<1	<1	<1
Co	2	39	62	32	35	88	73	69
Cr	16	397	>1300	76	84	>1300	>1300	>1300
Cu	15	31	91	248	201	42	50	<6
Fe	8207	90131	66275	85762	64637	90026	70160	65591
K	39427	1217	570	9588	17930	552	461	101
Li	16	16	2	22	20	6	8	9
Mg	2395	49797	109322	28613	16478	128464	141420	174057
Mn	176	2245	1498	1309	484	1608	1106	858
Mo	1	<1	2	6	4	1	<1	<1
Na	23723	23985	5864	18953	6568	4664	2264	1266
Ni	2	103	399	45	34	775	684	1305
P	208	72	31	1552	284	70	83	34
Pb	32	<15	<15	16	24	20	<15	<15
S	241	690	4048	1789	>16000	350	595	206
Sc	1	51	33	29	18	38	29	19
Sr	372	33	49	246	95	31	21	10
Ti	930	1853	1528	7683	3209	1632	1536	807
V	11	240	146	205	174	187	138	89
W	<6	<6	<6	<6	<6	<6	<6	<6
Y	5	9	5	39	14	6	6	4
Zn	26	73	39	105	83	119	43	28
Au	<0.4	1.24	3.22	3.87	47.1	1.15	0.91	<0.4
Ir	0.01	0.03	0.2	0.04	0.16	0.24	0.66	2.19
Pd	<0.12	13.8	8.32	7.92	3.51	9.47	6.55	5.7
Pt	0.36	10.6	8.54	4.28	4.2	9.23	7.26	5.07
Rh	<0.04	0.79	1.01	0.42	0.26	1.29	0.99	0.87
Ru	<0.08	0.25	1.65	<0.08	0.09	3.23	2.53	4.19

	LL-15BG181A01	LL-15BG190A01	LL-15BG198A01	LL-15BG205A01	LL-15BG219A01	LL-15BG226A01	LL-15BG231A01	LL-15BG232A01
	2.88	3.04	2.91	2.93	2.93	2.67	2.67	2.86
	1775.1	1443.5	856.8	687.6	1059.6	729.5	636	160.3
	1158.3	968.2	562.1	453.3	698.1	456.1	397.8	104.2
CO2	0.345	1.275	1.314	0.249	0.07	0.724	0.271	0.066
S	0.085	0.494	0.035	0.027	0.008	0.004	0.01	10.596
Al2O3	14.38	12.65	15.85	17.4	17.21	16.11	15.02	8.99
BaO	0.01	0.01	0.05	0.05	0.03	0.1	0.12	0.05
CaO	9.382	10.759	9.685	8.863	8.597	2.712	0.738	1.026
Cr2O3	0.02	0.03	0.03	0.01	0.01	<0.002	<0.002	<0.002
Fe2O3	7.52	14.17	10.92	12.62	12.05	2.8	3.32	16.65
K2O	1.1	0.47	1.81	1.39	0.99	2.84	3.6	2.35
LOI	1.66	1.85	2.29	1.21	0.81	1.42	1.33	7.64
MgO	6.67	5.53	3.12	3.36	4.04	1.83	1.22	0.3
MnO	0.184	0.329	0.178	0.15	0.185	0.048	0.049	0.013
Na2O	2.34	1.8	3.22	3.23	3.12	5.31	3.81	2.2
P2O5	0.049	0.129	0.635	0.62	0.43	0.202	0.074	0.014
SiO2	56.56	49.92	49.99	48.58	51.01	66.79	70.08	60.11
TiO2	0.4	1.29	1.75	2.2	1.48	0.32	0.24	0.12
Total	100.29	98.94	99.53	99.67	99.95	100.48	99.61	99.46
As	<6	<6	<6	<6	<6	<6	<6	59
Br	<1.2	2	3	<1.2	<1.2	<1.2	<1.2	<1.2
Cu	42	210	286	380	180	17	54	27
Ga	14	18	20	25	21	21	17	19
Mo	2	1	1	2	1	1	2	21
Nb	1	3	18	18	13	3	5	35
Ni	89	62	128	42	37	29	18	8
Pb	2	3	7	6	6	16	9	21
Rb	37	10	55	52	21	80	87	47
Sr	188	96	324	316	311	901	131	177
Th	<1.5	<1.5	8	8	4	8	10	9
U	<1.6	<1.6	2	2	<1.6	2	3	3
Y	10	36	46	54	44	9	9	89
Zn	69	170	110	142	121	68	50	67
Zr	38	92	359	343	260	145	88	268
Ba	117	60	496	445	261	840	961	562
Ce	<15	<15	107	86	69	90	42	70
Co	39	49	45	35	35	9	7	33
Cr	212	223	258	75	78	43	37	45
Cs	<7	<7	<7	7	<7	11	<7	<7
La	<7	<7	52	39	34	53	26	27
Mn	1439	2490	1416	1121	1366	344	363	112
Sc	42	41	30	29	32	6	4	<4
V	210	400	212	218	224	42	29	7
Ba	115.4	67.2	479.1	421.2	241.9	873.1	1007.5	341.7
Be	0.49	0.76	2.15	1.93	1.39	1.69	1.3	1.74
Bi	<0.47	<0.47	<0.47	<0.47	<0.47	<0.47	<0.47	<0.47
Cd	0.058	0.126	0.059	0.048	0.084	0.039	0.109	0.108
Ce	9.32	13.71	96.92	79.94	64.22	99.8	50.02	31.39
Co	42.35	54.24	45.99	34.74	34.31	8.43	7.61	38.65
Cr	216	214	247	67	70	48	39	37
Cs	1.646	0.909	0.849	1.94	1.273	11.138	3.017	1.544
Cu	48.5	217.1	289	373.2	173.5	20.3	58.9	31.7
Dy	1.694	5.963	7.854	9.171	7.505	1.924	1.531	11.761
Er	1.103	3.946	4.936	5.704	4.847	0.742	0.875	8.956
Eu	0.4618	1.3178	1.8222	1.9878	1.6253	1.7392	0.6604	0.6279
Ga	13.62	18.5	20.19	24.48	20.08	21.28	17.1	16.18
Gd	1.466	4.805	8.008	8.873	7.155	4.031	1.995	7.08
Hf	1.21	2.61	8.02	7.59	6.14	3.53	2.68	8.26

Ho	0.373	1.2861	1.6277	1.8987	1.5662	0.2977	0.2976	2.7495
In	0.0364	0.1131	0.0603	0.0725	0.059	0.0222	0.0208	0.1033
La	4.62	5.75	45.73	36.92	28.88	47.98	27.46	13.39
Li	35	29.1	26.9	35.5	20.4	43	24.9	8.5
Lu	0.1713	0.5811	0.7303	0.7876	0.7231	0.0881	0.1474	1.3324
Mo	2.14	0.73	1.95	2.2	1.12	0.82	2.72	22.2
Nb	1.29	3.508	17.351	17.086	12.808	3.761	5.348	32.164
Nd	5.17	10.61	47.87	41.98	34.94	44.73	18.43	18.53
Ni	92.4	69.5	127.6	41.5	37.2	27.9	16.3	8.4
Pb	3.1	3.8	7.5	6.7	6.4	15.5	10.7	19.6
Pr	1.242	2.151	12.117	10.1	8.324	11.801	5.342	4.205
Rb	36.76	10.07	55.58	52.57	20.94	81.04	87.32	43.9
Sb	0.29	0.86	1.27	0.27	0.43	0.21	0.37	1.71
Sc	50.7	48.1	30.9	30.6	34.3	5	4.6	1.8
Sm	1.222	3.425	8.917	8.691	7.11	6.914	2.928	5
Sn	0.45	1.34	2.54	2.66	1.87	0.83	1.17	2.28
Sr	194.2	100.5	334.2	320.4	316.8	912.9	130.7	168.4
Ta	0.086	0.225	1.044	0.896	0.768	0.225	0.485	2.109
Tb	0.2464	0.8419	1.2066	1.4097	1.1398	0.413	0.2734	1.4681
Th	0.826	0.678	8.315	7.411	4.921	9.87	10.578	7.77
Ti	2567	8301	10744	13548	8968	1898	1407	716
Tl	0.159	0.113	0.098	0.124	0.061	0.779	0.46	0.419
Tm	0.1685	0.5839	0.7393	0.818	0.7167	0.0983	0.1339	1.3635
U	0.302	0.2	2.387	2.087	1.394	2.624	3.029	2.105
V	219.8	>370	213.4	215.2	221	44.8	29.5	4.8
W	3.59	7.62	1.04	0.8	0.53	2.22	0.9	2.16
Y	10.45	37.52	46.8	53.72	45.34	8.9	9.09	86.48
Yb	1.083	3.832	4.778	5.312	4.738	0.603	0.896	8.858
Zn	65	155	100	128	107	63	47	54
Zr	45	95	352	337	255	147	86	251
Al	73371	64236	81575	86574	84303	77138	76079	43543
Ba	108	61	443	376	211	753	933	292
Be	<1	1	2	2	1	1	1	1
Ca	61647	70403	65913	61353	58869	18104	4692	6627
Cd	<1	<1	<1	<1	<1	<1	<1	<1
Co	37	44	37	24	26	6	7	33
Cr	190	184	223	59	59	39	36	33
Cu	52	221	311	385	180	22	64	33
Fe	51237	>95000	75753	84652	80066	18457	23025	>95000
K	9280	3769	15270	11275	7863	22478	30143	18412
Li	25	21	23	30	18	36	23	7
Mg	38940	32071	18393	19131	22758	10253	7183	1528
Mn	1349	2381	1339	1079	1312	315	347	83
Mo	2	<1	1	<1	1	2	3	17
Na	16658	13012	22953	22218	21108	>31000	26508	14918
Ni	82	58	116	35	30	23	14	7
P	217	539	2684	2537	1713	797	316	65
Pb	<15	<15	22	15	21	23	21	24
S	1126	5010	435	310	<130	<130	182	>16000
Sc	42	39	27	26	29	4	4	1
Sr	188	93	332	306	301	878	133	159
Ti	2369	7655	10687	12907	8485	1796	1420	667
V	212	382	215	212	216	45	31	8
W	<6	<6	<6	<6	<6	<6	<6	<6
Y	9	33	44	48	40	8	8	76
Zn	68	156	104	129	106	62	50	50
Au	14.6	24.6	4.41	3.37	2.53	3.6	2.4	133
Ir	0.03	0.15	0.1	0.03	0.03	0.01	0.03	0.03
Pd	12.4	4.14	15.2	8.34	7.32	0.21	0.45	0.15
Pt	10.7	4.18	3.06	2.29	4.85	0.34	0.58	0.28
Rh	0.5	0.34	0.41	0.19	0.47	<0.04	<0.04	<0.04
Ru	<0.08	0.2	0.28	<0.08	<0.08	<0.08	<0.08	<0.08

	LL-15BG233A01	LL-15BG233A02	LL-15BG228A03	LL-15BG228B01	LL-15BG235A01	LL-15BG235A02	LL-15BG236A01	LL-15BG236A03
	2.91	2.64	2.88	2.75	2.93	2.8	2.95	2.87
	1696.3	1058	1217.8	1645.4	762.5	2183.2	536.2	1100.9
	1113.1	657.9	794.6	1046.5	502.3	1403.5	354.3	716.9
CO2	0.444	0.064	0.05	0.265	0.17	0.107	0.376	0.059
S	0.017	0.076	0.01	0.024	0.196	4.767	0.451	6.192
Al2O3	14.55	19.44	18.69	16.16	13.34	15.52	3.04	9.98
BaO	0.04	0.07	0.05	0.07	<0.004	0.02	<0.004	0.02
CaO	6.462	1.78	3.82	3.958	9.437	1.472	3.808	3.931
Cr2O3	<0.002	<0.002	0.04	0.01	0.1	0.01	<0.002	0.02
Fe2O3	15.31	3.73	12.46	7.22	10.56	13.47	21.19	12.18
K2O	1.88	3.4	3.08	2.24	0.34	4.54	0.06	1.95
LOI	1.09	1.08	0.78	1.72	0.74	5.68	0.66	5.89
MgO	3.34	0.58	2.83	2.52	8.36	2.02	2.54	2.68
MnO	0.206	0.062	0.16	0.109	0.208	0.12	0.409	0.114
Na2O	3.3	6.28	2.72	4	3.97	1.95	0.07	1.45
P2O5	0.556	0.129	0.233	0.29	0.047	0.101	0.085	0.11
SiO2	50.75	62.84	54.87	61.33	52.11	55.02	68.03	61.34
TiO2	2.04	0.34	1.25	0.86	0.6	0.59	0.1	0.4
Total	99.53	99.74	100.97	100.47	99.82	100.52	100	100.07
As	15	918	<6	<6	<6	<6	10	20
Br	<1.2	<1.2	<1.2	<1.2	<1.2	<1.2	<1.2	2
Cu	154	40	47	46	84	159	40	172
Ga	24	22	25	22	14	21	4	15
Mo	1	7	1	1	<0.8	3	1	4
Nb	15	32	9	7	1	5	1	3
Ni	8	4	135	55	167	91	33	117
Pb	6	58	10	9	2	69	4	19
Rb	55	76	78	51	3	91	4	45
Sr	318	276	427	782	115	48	15	179
Th	5	8	6	6	<1.5	4	<1.5	3
U	<1.6	2	2	2	<1.6	<1.6	<1.6	<1.6
Y	56	14	26	19	16	15	8	12
Zn	150	68	126	92	93	518	75	378
Zr	290	152	171	187	44	140	36	88
Ba	412	534	510	651	49	236	15	236
Ce	78	96	73	79	<15	24	<15	30
Co	33	5	38	23	44	24	10	13
Cr	<9	<9	292	76	703	72	42	187
Cs	13	<7	8	<7	<7	<7	<7	<7
La	37	48	36	37	<7	13	<7	8
Mn	1480	474	1118	812	1581	934	3286	990
Sc	29	4	21	10	38	17	4	13
V	133	37	176	100	246	143	19	91
Ba	377.4	547.7	456	638.9	53.7	131.6	15.8	211
Be	1.98	2.93	1.5	1.39	0.4	1.66	0.43	0.79
Bi	<0.47	<0.47	<0.47	<0.47	<0.47	<0.47	<0.47	<0.47
Cd	0.106	0.083	0.098	0.08	0.148	0.483	0.114	0.811
Ce	77.19	102.68	73.36	65.06	8.64	22.68	7.36	26.63
Co	32.34	4.21	39.76	22.73	51.89	27.71	9.34	14.38
Cr	6	9	271	76	698	60	30	133
Cs	6.587	5.031	4.703	1.212	0.203	2.643	0.647	1.38
Cu	149.4	43	54	50.4	98.6	172.1	40.1	179
Dy	9.436	2.489	4.975	3.48	2.661	2.6	1.269	2.123
Er	6.17	1.392	2.577	1.737	1.778	1.627	0.884	1.274
Eu	2.2994	1.5824	2.2292	1.5459	0.6021	0.8289	0.4585	0.7912
Ga	23.99	22.71	24.44	21.98	13.22	20.61	3.84	13.88
Gd	9.014	3.9	6.317	4.485	2.23	2.528	1.053	2.376
Hf	6.85	3.64	4.36	4.7	1.27	3.41	0.89	2.21

Ho	2.0295	0.4547	0.9371	0.6198	0.5736	0.5481	0.2764	0.4243
In	0.0916	0.0172	0.0624	0.0442	0.0454	0.0997	0.0257	0.1085
La	34.97	47.24	35.66	32.98	4.02	10.55	3.35	11.95
Li	27.8	19.5	39	21.3	10.6	49	5.5	12.2
Lu	0.924	0.222	0.3397	0.2281	0.254	0.263	0.1485	0.2006
Mo	1.49	7.72	1.41	1.51	0.4	4.23	1.47	4.73
Nb	15.477	29.743	8.704	7.198	1.806	4.868	1.38	3.633
Nd	41.56	43.57	40.05	31.78	5.74	11.84	4.04	13.06
Ni	7.7	2.5	134.1	56.7	177.3	112.1	30.3	127.3
Pb	6.5	55.2	9.7	9	3.2	64.8	5.3	19.1
Pr	9.95	11.852	9.797	8.351	1.209	3.036	0.949	3.288
Rb	55.17	76.74	72.55	51.52	3.03	45.13	3.45	44.78
Sb	0.64	0.54	0.05	0.16	0.62	1.39	0.66	6.32
Sc	32.2	2.7	20.1	9.8	42.6	12.1	2.5	12.3
Sm	8.843	6.183	7.559	5.729	1.684	2.481	0.918	2.588
Sn	2.1	0.91	1.21	1.07	0.54	2.59	0.33	3.72
Sr	319.7	279	424.9	804.6	115.1	39.6	14.8	179
Ta	0.876	1.243	0.509	0.446	0.121	0.381	0.086	0.283
Tb	1.4202	0.4635	0.869	0.6066	0.3807	0.4001	0.186	0.3405
Th	4.837	8.233	6.548	7.209	1.01	2.904	0.639	3.267
Ti	12399	2034	7557	5279	3634	3637	568	2457
Tl	0.246	0.353	0.411	0.216	0.039	1.187	0.078	1.008
Tm	0.9041	0.2088	0.3682	0.2365	0.2552	0.2454	0.1393	0.1921
U	1.387	3.042	1.708	1.899	0.231	1.12	0.122	0.883
V	125.7	35.3	167.4	103.7	242.1	122.6	13.9	81.2
W	1.02	2.4	0.42	0.48	2.12	3.22	4.31	4.5
Y	57.31	13.78	26.13	18.28	15.82	14.68	8.15	11.68
Yb	5.985	1.431	2.308	1.574	1.701	1.675	0.915	1.27
Zn	133	63	115	86	87	456	61	321
Zr	284	151	169	193	45	135	35	86
Al	71699	98943	87134	78752	66845	65709	17334	51045
Ba	337	508	401	554	49	121	16	184
Be	2	3	1	1	<1	1	<1	1
Ca	44582	12522	25358	26791	63034	9801	28148	27964
Cd	<1	8	<1	<1	<1	<1	<1	1
Co	24	3	33	17	47	22	8	11
Cr	7	8	247	69	657	55	32	122
Cu	158	46	54	50	99	161	44	179
Fe	>95000	25841	81168	49167	72318	89278	>95000	86353
K	15129	28606	24007	18468	2898	33177	593	16589
Li	23	17	34	19	10	44	6	12
Mg	18895	3410	15578	14895	49352	8912	15819	16455
Mn	1481	452	1183	790	1591	869	3412	896
Mo	<1	7	1	1	<1	4	<1	3
Na	22546	>31000	18069	27724	28424	13153	763	10375
Ni	6	<2	121	50	163	99	30	114
P	2290	547	920	1135	207	399	369	454
Pb	<15	66	<15	<15	<15	59	<15	17
S	235	866	233	394	2610	>16000	4871	>16000
Sc	28	2	17	8	37	10	1	10
Sr	305	278	393	769	109	38	14	175
Ti	11964	2028	6862	4907	3471	3418	602	2452
V	125	38	156	100	238	117	18	83
W	<6	<6	16	<6	<6	11	55	22
Y	51	13	23	18	15	13	9	11
Zn	135	65	114	82	91	447	65	318
Au	16.2	150	1.37	0.56	7.5	40.1	28	196
Ir	<0.01	<0.01	0.04	0.01	0.44	0.06	0.05	0.37
Pd	<0.12	<0.12	0.37	0.21	15	1.11	2.14	3.4
Pt	<0.17	0.17	1.38	0.55	13.3	3.89	1.08	2.09
Rh	<0.04	<0.04	0.04	<0.04	1.12	0.07	<0.04	0.26
Ru	<0.08	<0.08	<0.08	<0.08	0.6	0.1	0.09	0.6

	LL-15BG254A01	LL-15BG261A01	LL-15BG263A01	LL-15BG268A01	LL-15BG285A01	LL-15BG287C01	LL-15BG288A01	LL-15BG292A01
	2.64	2.68	2.95	2.67	2.74	2.8	2.92	2.69
	1485.1	457.5	264.5	798	1567.1	1323.5	782.1	1189.9
	922.5	286.5	174.8	498.9	994.5	850.2	514.5	748.1
CO2	0.598	0.597	<0.023	0.071	1.206	0.172	0.054	0.391
S	0.078	0.076	0.01	0.004	0.006	0.674	0.005	0.035
Al2O3	11.87	15.83	14.98	16.75	16.31	14.87	7.07	15.97
BaO	0.07	0.05	0.04	0.08	0.12	0.01	<0.004	0.04
CaO	0.92	3.344	7.181	3.509	4.555	3.451	6.624	2.377
Cr2O3	0.01	0.01	0.05	<0.002	0.01	0.01	0.37	0.01
Fe2O3	1.77	2.61	9.43	3.01	5.9	13.97	9.05	3.47
K2O	3.74	1.83	1.51	2.12	3.21	1.62	0.05	2.15
LOI	0.97	1.19	2.04	1.14	2.58	3.44	5.78	0.86
MgO	0.16	1.29	7.62	1.2	3.82	9.64	25.41	1.46
MnO	0.027	0.056	0.126	0.046	0.083	0.212	0.148	0.066
Na2O	3.25	4.85	3.46	4.8	3.79	2.95	0.32	4.41
P2O5	0.005	0.091	0.368	0.198	0.358	0.093	0.01	0.078
SiO2	77.84	68.98	52.43	66.36	58.96	49.08	45.69	69.19
TiO2	0.14	0.31	0.92	0.5	0.68	1.26	0.18	0.33
Total	100.77	100.45	100.16	99.72	100.38	100.62	100.69	100.42
As	<6	<6	<6	<6	<6	<6	<6	<6
Br	<1.2	<1.2	3	3	<1.2	<1.2	<1.2	<1.2
Cu	16	15	53	<9	9	160	<9	11
Ga	19	20	17	21	20	18	6	18
Mo	6	1	1	1	1	1	<0.8	1
Nb	39	2	6	5	7	2	<0.7	4
Ni	<1.6	15	170	11	61	46	725	28
Pb	3	7	2	6	12	3	<1.7	13
Rb	57	50	45	33	73	46	2	67
Sr	107	531	496	836	852	392	31	195
Th	10	2	3	2	5	<1.5	<1.5	6
U	2	<1.6	<1.6	<1.6	2	<1.6	<1.6	<1.6
Y	95	5	19	6	18	24	5	9
Zn	34	52	105	62	88	127	48	56
Zr	330	99	135	121	139	71	8	112
Ba	640	439	404	728	1116	168	<8	327
Ce	128	20	55	54	82	<15	<15	32
Co	2	7	39	8	19	32	70	9
Cr	27	46	345	22	68	95	2471	89
Cs	<7	<7	<7	<7	<7	8	<7	<7
La	60	10	26	27	40	<7	<7	21
Mn	165	352	991	309	634	1482	1102	459
Sc	<4	7	23	5	11	41	26	8
V	<3	42	163	39	95	376	137	53
Ba	678.1	447.3	408	710.4	1168.7	166.3	4.4	330.6
Be	1.48	1.25	1.17	1.31	2.07	0.51	0.13	1.43
Bi	<0.47	<0.47	<0.47	<0.47	<0.47	<0.47	<0.47	<0.47
Cd	0.046	0.047	0.081	0.041	0.057	0.088	0.045	0.051
Ce	132.9	24.01	58.72	54.02	89.25	11.19	1.32	35.45
Co	0.76	7.15	38.6	7.88	18.79	32.68	72.69	9.81
Cr	36	51	317	18	66	81	2360	88
Cs	1.332	3.204	1.817	0.584	2.251	6.538	0.345	4.051
Cu	21.7	20.8	54.4	4.6	13.2	162.9	<1.4	17.3
Dy	17.527	0.94	3.603	1.227	4.082	4.157	0.638	1.576
Er	10.684	0.466	1.927	0.534	1.705	2.634	0.481	0.876
Eu	1.6916	0.6022	1.7385	1.0587	2.3713	0.847	0.1031	0.6882
Ga	19.56	20.96	16.64	20.35	20.68	16.71	5.26	18.2
Gd	15.3	1.472	4.937	2.323	7.051	3.347	0.462	1.863
Hf	10.89	2.7	3.17	3.83	4.06	2.03	0.27	3.13

Ho	3.5635	0.1676	0.6611	0.1956	0.6663	0.8467	0.1492	0.3118
In	0.1011	0.0197	0.0434	0.02	0.0457	0.0668	0.0199	0.0239
La	61.31	12.44	25.63	23.25	39.74	4.51	0.51	19.75
Li	12.9	34.6	42.5	26.6	42.5	68.6	<0.4	27
Lu	1.399	0.0685	0.2508	0.0631	0.1982	0.3984	0.0824	0.1337
Mo	7.1	1.35	0.59	0.73	0.71	0.6	0.1	1.04
Nb	36.339	2.171	6.431	5.218	7.224	3.246	0.29	4.26
Nd	69.51	10.71	33.09	27.81	52.1	8.23	0.89	14.47
Ni	0.8	16.4	166.7	9.3	61.8	48.5	701.7	30.3
Pb	4.8	14.4	3.1	6.7	12.2	4	0.3	13.6
Pr	17.156	2.919	8.038	7.106	12.399	1.715	0.185	4.047
Rb	58.82	51.41	43.26	31.99	74.5	45	1.17	70.7
Sb	0.36	0.15	0.32	0.05	0.09	0.15	0.31	0.38
Sc	1.9	5.1	22.5	3.1	11.5	34.5	13.6	7.6
Sm	15.23	2.014	6.232	4.226	9.874	2.523	0.312	2.386
Sn	5.48	7.58	1.19	0.87	1.43	0.56	0.16	0.97
Sr	108.3	546.1	492.1	840.1	880.7	386.7	32.3	196.6
Ta	2.687	0.148	0.346	0.382	0.416	0.216	0.017	0.389
Tb	2.6227	0.1791	0.6458	0.2501	0.8282	0.5765	0.0904	0.2613
Th	11.069	2.672	3.481	3.398	6.157	0.414	0.054	6.261
Ti	798	1913	5425	3003	4125	7493	1047	1986
Tl	0.349	0.392	0.268	0.12	0.38	0.397	0.011	0.319
Tm	1.5354	0.0635	0.2666	0.0687	0.2183	0.3877	0.0754	0.129
U	1.85	1.01	0.905	0.892	1.824	0.122	0.015	1.559
V	1.8	43.9	157.1	40.2	96.9	344.8	134.1	54.8
W	1.33	0.64	1.43	0.69	0.21	11.67	0.47	0.77
Y	96.51	4.92	18.19	5.92	19.14	22.39	3.74	8.72
Yb	9.738	0.429	1.693	0.421	1.35	2.619	0.508	0.876
Zn	32	50	92	56	82	110	49	55
Zr	318	103	132	155	158	72	9	123
Al	60698	80651	75580	79089	81451	73169	32092	82796
Ba	624	396	377	628	1008	151	7	303
Be	1	1	1	1	2	<1	<1	1
Ca	6634	23119	50838	22701	32239	24648	46175	17428
Cd	<1	<1	<1	<1	<1	<1	<1	<1
Co	<1	5	34	6	15	27	66	8
Cr	37	48	314	19	61	81	>1300	84
Cu	24	23	59	7	15	171	<6	19
Fe	12554	18492	65463	20164	40543	>95000	62044	25034
K	32492	15764	12858	17460	26926	14353	383	18945
Li	13	33	42	25	38	65	2	27
Mg	959	8050	45636	7068	22786	55300	141173	9268
Mn	181	370	990	290	624	1662	1161	484
Mo	6	1	1	<1	1	<1	<1	<1
Na	23407	>31000	24747	>31000	26656	21752	2832	>31000
Ni	<2	15	162	9	56	46	643	29
P	34	375	1519	820	1432	385	56	343
Pb	<15	<15	<15	<15	<15	<15	<15	<15
S	977	993	174	142	168	7182	<130	504
Sc	1	4	21	3	10	37	16	7
Sr	111	547	489	795	849	392	31	203
Ti	837	1950	5447	2926	3953	7625	1079	2046
V	1	45	162	39	95	360	138	57
W	<6	<6	<6	<6	<6	34	<6	<6
Y	94	5	18	6	18	23	4	9
Zn	33	50	101	56	81	117	48	56
Au	14.8	8.82	<0.4	<0.4	0.57	296	0.88	4.59
Ir	0.02	0.02	0.03	0.01	0.01	0.06	0.42	0.03
Pd	<0.12	0.26	1.47	<0.12	0.15	0.84	4.5	0.37
Pt	1.76	0.59	1.69	0.46	0.3	0.69	6.64	0.99
Rh	<0.04	<0.04	0.09	<0.04	<0.04	0.09	0.95	0.04
Ru	<0.08	<0.08	<0.08	<0.08	<0.08	0.09	2.52	<0.08

	LL-15BG296A01	LL-15BG297A01	LL-15BG305A01	LL-15BG306A01	LL-15BG310A01	LL-15BG325A01	LL-15BG329A01	LL-15BG331A01
	3.11	2.89	2.79	2.93	3.02	2.95	2.74	2.9
	670.6	547.4	1024.9	684.9	832.1	754.5	1000.7	695.7
	455	358.1	657.4	450.9	556.7	498.7	635.5	456
CO2	0.231	0.08	0.027	1.253	0.266	0.1	1.21	0.382
S	0.286	0.297	0.777	0.032	0.099	0.009	0.033	0.146
Al2O3	15.73	16.74	16.43	15.59	7.5	17.07	10.46	17.49
BaO	0.01	0.01	0.01	0.03	0.05	0.04	0.02	0.06
CaO	9.808	7.498	2.692	6.948	10.509	8.157	4.667	5.833
Cr2O3	0.03	0.03	<0.002	0.01	0.12	0.02	<0.002	<0.002
Fe2O3	15.58	11.81	12.33	13.76	9.18	10.94	2.47	7.05
K2O	2.07	2.49	2.05	1.06	2.04	1.3	1.21	1.81
LOI	1.65	1.46	3.21	3.45	1.62	1.72	2.06	1.27
MgO	6.19	4.36	2.3	4.71	16.67	7.36	0.28	2.78
MnO	0.38	0.236	0.097	0.193	0.146	0.258	0.081	0.094
Na2O	0.83	0.89	4.03	3.56	1.45	3.1	1.02	4.42
P2O5	0.099	0.104	0.637	0.833	0.348	0.26	0.01	0.342
SiO2	46.61	53.25	55.26	47.92	49.83	48.9	78.23	58.21
TiO2	1.04	1.23	1.53	2.13	0.57	0.93	0.13	0.98
Total	100.03	100.12	100.58	100.2	100.03	100.05	100.63	100.34
As	<6	<6	<6	<6	<6	<6	<6	<6
Br	4	<1.2	<1.2	2	<1.2	<1.2	<1.2	<1.2
Cu	91	106	448	304	53	21	19	130
Ga	18	20	24	22	9	18	13	21
Mo	1	<0.8	2	2	1	<0.8	<0.8	1
Nb	2	3	16	22	4	4	33	8
Ni	154	86	4	80	591	126	2	30
Pb	<1.7	3	2	4	3	10	5	8
Rb	56	61	62	48	78	33	43	51
Sr	63	61	310	317	492	377	360	827
Th	<1.5	<1.5	6	11	6	2	8	5
U	<1.6	<1.6	<1.6	4	<1.6	<1.6	2	<1.6
Y	26	30	41	58	18	19	90	20
Zn	116	109	85	165	96	383	52	78
Zr	67	78	298	456	125	95	265	198
Ba	165	163	158	294	552	436	144	573
Ce	<15	<15	68	113	77	41	108	86
Co	42	47	25	42	57	42	3	20
Cr	274	209	10	119	846	135	16	31
Cs	7	<7	<7	<7	<7	<7	<7	<7
La	<7	<7	29	53	40	15	54	40
Mn	2935	1806	776	1432	1139	1956	512	708
Sc	36	41	20	27	26	24	4	15
V	327	388	82	211	107	196	<3	150
Ba	153.4	164.7	164.2	298.5	452.2	403.4	153.5	558.1
Be	0.59	0.56	1.33	2.57	1.7	0.67	1.89	1.43
Bi	<0.47	<0.47	1.02	<0.47	<0.47	<0.47	<0.47	<0.47
Cd	0.106	0.145	0.039	0.063	0.081	0.477	0.173	0.059
Ce	11.27	11.34	55.85	101.1	77.5	39.52	116.52	85.83
Co	43.12	53.66	26.75	40.66	59.6	42.71	1.77	21.98
Cr	244	190	6	105	810	125	24	28
Cs	4.668	3.569	2.918	0.856	1.756	0.652	1.164	2.321
Cu	93.9	115.8	486.6	315.2	54.2	23.6	25.1	143.4
Dy	4.242	5.058	7.56	10.34	4.117	3.555	15.574	3.789
Er	2.752	3.202	4.404	6.029	1.591	1.923	10.075	2.071
Eu	0.8575	1.0851	2.2265	1.9291	2.3027	1.2926	1.2238	1.6485
Ga	17.33	19.82	23.73	21.58	9.6	17.81	14.01	21.28
Gd	3.619	4.249	7.797	10.337	7.177	4.116	13.417	4.865
Hf	1.83	2.19	7	9.88	3.23	2.44	8.92	4.71

Ho	0.901	1.0701	1.4958	2.0826	0.663	0.695	3.2793	0.7266
In	0.0651	0.0862	0.078	0.0716	0.0443	0.0577	0.1007	0.0377
La	4.72	4.44	25.26	49.91	35.92	17.74	54.34	40.73
Li	50.6	63.9	38.1	40.1	14.8	40.7	17.6	33.8
Lu	0.4147	0.4646	0.6319	0.8459	0.167	0.2623	1.4823	0.2967
Mo	1.22	0.38	2.26	3	0.63	0.17	1.4	1.43
Nb	2.971	3.439	17.52	21.817	3.995	4.922	32.991	8.575
Nd	8.65	9.89	33.05	51.56	45.67	22.44	59.85	43.29
Ni	153.4	93.9	2.8	79.7	577.9	125.8	1.9	32
Pb	2.1	4.3	4	6	4.1	9.9	6.3	8.1
Pr	1.751	1.907	7.757	13.154	10.796	5.421	15.117	11.259
Rb	57.46	63.36	63.16	48.28	69.15	29.47	44.94	53.31
Sb	0.38	0.74	0.24	0.35	0.09	0.33	1.25	0.38
Sc	37.1	47.9	21.1	27.8	24.4	21.7	2.1	15.5
Sm	2.662	3.109	7.601	10.157	9.261	4.486	12.737	6.949
Sn	0.63	1.12	1.73	3.51	1.08	0.63	6.1	1.46
Sr	61.3	62.8	315.6	318.7	490.3	372.9	380	835.1
Ta	0.187	0.216	0.96	1.257	0.228	0.293	2.186	0.535
Tb	0.6136	0.7427	1.2053	1.587	0.837	0.5853	2.3511	0.6494
Th	0.373	0.517	6.7	11.497	4.03	2.31	9.185	4.926
Ti	6195	7609	9540	12477	3349	5507	778	6093
Tl	0.594	0.545	0.178	0.176	0.393	0.158	0.16	0.173
Tm	0.4069	0.4649	0.634	0.8745	0.1981	0.273	1.5086	0.2974
U	0.104	0.164	1.746	3.095	1.179	0.598	2.166	1.292
V	300.4	>370	72.7	194.3	105.3	186.6	1.5	151.4
W	24.1	7.57	3.72	1.71	0.33	0.37	4.17	0.63
Y	25.59	29.91	41.3	57.23	17.05	18.27	93.83	20.32
Yb	2.639	3.063	4.141	5.683	1.175	1.759	10.017	1.893
Zn	93	99	75	140	86	336	52	74
Zr	66	79	291	437	127	94	264	201
Al	79117	87499	81187	79609	37766	88760	50134	85384
Ba	129	152	139	268	430	386	138	484
Be	<1	<1	1	2	1	<1	2	1
Ca	65778	55164	18292	48961	70155	59417	32112	40829
Cd	<1	<1	<1	<1	<1	1	<1	<1
Co	36	49	18	32	55	39	1	16
Cr	223	189	7	103	775	125	24	26
Cu	95	121	463	328	56	28	26	139
Fe	>95000	84905	83873	>95000	62970	78812	16399	48530
K	17851	22081	16997	9090	17299	11451	9733	15100
Li	50	61	36	40	18	43	17	31
Mg	36740	27150	13351	28601	97258	45565	1461	16662
Mn	2966	1910	737	1546	1125	2088	582	699
Mo	<1	<1	1	2	<1	<1	1	2
Na	6348	7076	28079	25956	10403	22926	7480	30455
Ni	139	90	2	74	542	122	2	28
P	391	457	2391	3374	1419	1091	49	1418
Pb	<15	<15	<15	<15	<15	<15	<15	<15
S	2899	3338	7776	386	1150	153	727	1662
Sc	34	45	18	26	25	22	1	13
Sr	61	64	301	315	469	374	354	799
Ti	6060	7521	9140	12749	3424	5715	744	5714
V	302	380	72	202	105	199	2	146
W	36	16	10	20	<6	12	<6	<6
Y	24	29	38	56	17	19	86	19
Zn	93	108	71	149	89	368	52	73
Au	16.8	7.66	77.6	2.43	1.09	<0.4	3.05	6.66
Ir	0.24	0.08	0.06	0.12	0.07	0.05	0.01	0.02
Pd	2.59	4.2	0.16	6.66	2.93	4.17	<0.12	3.25
Pt	3.33	4.81	0.25	3.22	1.52	2.44	1.92	2.54
Rh	0.26	0.06	0.06	0.25	0.12	0.13	<0.04	0.09
Ru	0.08	<0.08	<0.08	0.16	0.14	<0.08	<0.08	<0.08

	LL-15BG340A02	LL-15BG341A01	LL-15BG352A01	LL-15BG357A01	LL-15BG367A01	LL-15BG374A01	LL-15BG379A01	LL-15BG387A01
	2.94	2.97	2.72	2.98	2.89	2.68	2.83	3.05
	312	775.5	975.3	615.5	970.7	448.8	561.3	936.3
	205.7	514.1	616.6	409.1	634.3	281.3	363.1	628.9
CO2	0.045	0.15	0.213	<0.023	0.031	0.102	0.04	0.097
S	0.818	0.045	0.197	1.202	0.005	0.003	0.005	0.014
Al2O3	14.3	5.88	1.7	12.61	12.03	16.93	15.59	14.58
BaO	<0.004	<0.004	<0.004	0.01	0.07	0.11	<0.004	<0.004
CaO	5.969	5.449	3.59	8.608	7.872	3.953	6.926	8.868
Cr2O3	<0.002	0.45	<0.002	<0.002	0.07	0.01	0.02	0.01
Fe2O3	16.22	13.45	20.71	14.09	7.47	4.03	9.88	13.24
K2O	0.13	0.04	0.06	0.53	2.15	2.33	0.5	0.53
LOI	1.12	5.77	0.71	1.73	1.2	0.78	0.55	1.76
MgO	5.09	26.93	1	5.38	10.52	2.22	3.6	8.85
MnO	0.291	0.203	0.12	0.357	0.116	0.069	0.2	0.141
Na2O	4.22	0.07	0.06	3.05	2.85	4.77	4.25	0.95
P2O5	0.152	0.022	0.1	0.131	0.36	0.216	0.079	0.047
SiO2	51.79	41.71	71.9	52.38	55.1	64.55	57.66	51.25
TiO2	1.57	0.39	0.04	1.52	0.61	0.5	1.06	0.57
Total	100.85	100.36	99.98	100.39	100.4	100.47	100.3	100.8
As	<6	<6	<6	<6	<6	<6	<6	<6
Br	<1.2	4	<1.2	<1.2	<1.2	<1.2	<1.2	<1.2
Cu	119	49	15	91	28	<9	63	108
Ga	20	7	3	19	15	21	15	13
Mo	1	<0.8	<0.8	1	<0.8	1	<0.8	<0.8
Nb	4	<0.7	<0.7	2	6	5	2	1
Ni	34	1458	6	40	339	30	96	95
Pb	2	<1.7	<1.7	<1.7	7	12	<1.7	3
Rb	2	2	2	14	53	55	12	22
Sr	48	10	12	115	680	886	70	152
Th	<1.5	<1.5	<1.5	<1.5	5	3	<1.5	<1.5
U	<1.6	<1.6	<1.6	<1.6	<1.6	3	<1.6	<1.6
Y	36	7	6	32	15	10	21	15
Zn	171	91	94	155	86	77	91	98
Zr	112	19	22	95	110	141	61	36
Ba	42	<8	<8	122	650	974	37	45
Ce	<15	<15	<15	<15	100	61	<15	<15
Co	47	106	6	37	41	12	43	47
Cr	29	3001	19	40	469	46	171	100
Cs	<7	<7	<7	<7	<7	<7	<7	<7
La	<7	<7	<7	<7	49	38	<7	<7
Mn	2210	1508	939	2775	881	482	1399	1099
Sc	43	24	4	42	20	8	36	46
V	463	144	13	434	115	56	291	285
Ba	47.2	7.9	7.5	122.3	658.2	984.4	42.8	46.3
Be	0.59	0.2	0.81	0.61	1.3	1.8	0.36	0.3
Bi	<0.47	<0.47	<0.47	<0.47	<0.47	<0.47	<0.47	<0.47
Cd	0.205	0.105	0.095	0.113	0.121	0.082	0.11	0.1
Ce	12.33	3.3	7.39	12.33	95.85	65.41	8.82	6.61
Co	50.94	106.89	2.24	44.17	42.31	11.96	43.32	50.52
Cr	22	3049	15	30	471	45	157	91
Cs	0.137	0.162	0.137	0.412	2.451	2.523	1.479	0.676
Cu	115.2	47.6	15.3	98.2	30.8	9.9	62.8	116.8
Dy	6.254	1.149	1.03	5.546	3.376	2.081	3.738	2.673
Er	4.003	0.691	0.708	3.462	1.412	0.923	2.431	1.815
Eu	1.2523	0.3258	0.475	1.2655	2.1661	1.4368	0.812	0.5689
Ga	18.38	7.28	2.33	18.32	15.96	21.72	14.67	13.96
Gd	4.956	1.094	1.007	4.656	6.129	3.506	3.094	2.136
Hf	3.05	0.51	0.4	2.67	3.19	4.16	1.68	1.12

Ho	1.318	0.2332	0.2171	1.15	0.5499	0.3432	0.8046	0.5794
In	0.095	0.0331	0.1044	0.0998	0.0412	0.0346	0.0633	0.0581
La	4.5	1.37	3.67	5.35	43.84	35.12	3	2.76
Li	7.7	4	1.4	11.1	24.2	25.5	11.9	21.1
Lu	0.6159	0.0866	0.1024	0.4735	0.1557	0.1167	0.3553	0.2778
Mo	0.82	0.16	0.97	0.66	0.29	0.72	0.45	0.42
Nb	4.011	0.738	0.56	3.09	6.48	5.562	2.83	1.482
Nd	10.59	2.62	3.68	10.31	51.75	29.9	7.04	4.79
Ni	34.6	1424.7	4.7	41.8	348.3	30.4	100.2	95.8
Pb	2.5	1	1.4	1.5	7.5	12.6	2.2	7.8
Pr	2.061	0.52	0.924	1.915	12.779	7.873	1.41	1
Rb	1.63	1.34	1.27	13.14	55.39	56.94	12	21.74
Sb	0.13	0.06	0.39	0.5	0.25	0.32	0.11	0.17
Sc	45.2	4	1.7	44.4	20.2	7.1	41.2	50.7
Sm	3.544	0.801	0.934	3.445	9.229	5.088	2.309	1.551
Sn	0.97	0.16	0.88	1.06	0.99	1.27	1.17	7.52
Sr	48.9	10.1	12.8	116.3	699.8	908.2	71	159.4
Ta	0.268	0.045	0.029	0.199	0.449	0.303	0.175	0.103
Tb	0.8745	0.1731	0.1573	0.8243	0.6986	0.4102	0.5326	0.3824
Th	0.518	0.055	0.28	0.404	5.36	4.666	0.356	0.407
Ti	9348	2293	197	9044	3698	3050	6137	3464
Tl	0.024	0.014	0.017	0.075	0.283	0.291	0.079	0.143
Tm	0.6069	0.0953	0.0967	0.4924	0.1761	0.121	0.3631	0.2678
U	0.181	0.024	0.161	0.205	1.493	2.802	0.127	0.136
V	>370	154.4	8	>370	114.7	58.8	285.5	276.3
W	0.22	0.33	3.13	1.75	0.34	0.39	0.34	0.1
Y	35.42	5.7	6.55	31.76	15.6	10.24	21.26	16.12
Yb	4	0.586	0.635	3.165	1.084	0.789	2.339	1.801
Zn	148	89	78	134	80	74	85	91
Zr	107	18	23	93	122	157	60	38
Al	74295	29447	9212	62898	64894	80771	80134	78406
Ba	42	11	8	108	593	852	38	42
Be	<1	<1	1	<1	1	1	<1	<1
Ca	42768	39546	24909	59886	58520	26730	49317	63450
Cd	<1	<1	<1	<1	<1	<1	<1	<1
Co	42	106	2	36	38	10	37	47
Cr	23	>1300	16	30	442	41	146	88
Cu	122	53	18	102	35	11	67	123
Fe	>95000	>95000	>95000	>95000	54969	26395	68019	>95000
K	1079	344	505	4397	19675	18919	4310	4708
Li	9	4	2	11	24	23	13	22
Mg	31470	163013	5844	31735	66805	12782	21469	56123
Mn	2344	1647	946	2763	946	469	1525	1174
Mo	<1	<1	<1	<1	<1	<1	<1	<1
Na	>31000	837	729	21704	21758	>31000	30869	7833
Ni	32	1404	4	38	323	27	90	88
P	616	99	406	529	1524	880	322	200
Pb	<15	<15	<15	<15	<15	<15	<15	<15
S	8291	626	2183	11846	<130	<130	<130	174
Sc	43	18	<1	40	19	6	38	48
Sr	49	10	11	114	687	832	69	157
Ti	9529	2438	199	8871	3750	2883	6075	3638
V	468	158	11	403	121	55	292	293
W	21	<6	51	23	<6	<6	10	19
Y	35	7	6	30	16	9	20	16
Zn	150	98	77	135	82	72	87	92
Au	2.5	0.81	2.42	4.78	0.47	1.04	1.13	2.06
Ir	0.02	1.86	0.02	0.02	0.03	0.01	0.03	0.07
Pd	0.27	8.63	0.15	0.95	0.38	0.25	0.15	22.6
Pt	1.96	9.89	1.44	1.91	2.05	1.25	1.11	17.5
Rh	<0.04	1.14	<0.04	0.06	0.06	<0.04	<0.04	0.58
Ru	<0.08	4.08	<0.08	<0.08	0.08	<0.08	<0.08	<0.08

	LL-15BG401A01	LL-15BG412A01	LL-15BG418A03	LL-15BG418A04	LL-15BG418B01	LL-15BG427A01	LL-15BG428A01	LL-15BG433A01
	2.95	2.74	2.75	2.92	2.98	2.75	2.94	2.96
	541.7	1052.8	1105.4	741.9	780.2	562.7	327.2	646.3
	357.9	668	704	487.6	518	358	216	428.1
CO2	0.935	0.088	0.157	0.025	0.085	0.35	0.162	0.03
S	0.022	0.004	0.157	0.017	0.403	0.032	0.115	0.013
Al2O3	13.67	17.35	17.32	13.75	1.56	17.38	18.57	16.6
BaO	0.01	0.13	0.09	<0.004	<0.004	0.08	0.04	0.02
CaO	10.373	4.154	5.524	1.551	6.106	5.339	6.732	9.192
Cr2O3	0.03	<0.002	<0.002	0.01	<0.002	0.01	<0.002	0.02
Fe2O3	10.4	3.58	4.34	22.45	16.38	6.15	12.02	12.25
K2O	0.3	1.79	2.53	0.69	0.06	1.69	1.29	0.91
LOI	1.84	1.34	1.01	2.96	0.48	1.13	1.07	1.21
MgO	7.05	1.67	1.78	7.73	1.6	1.99	2.08	5.93
MnO	0.277	0.064	0.063	0.133	0.475	0.124	0.232	0.178
Na2O	2.18	5.14	3.93	2.03	0.08	4.49	2.73	2.5
P2O5	0.029	0.244	0.327	0.054	0.089	0.241	0.346	0.26
SiO2	54.01	64.54	62.57	48.58	73.37	61.33	53.64	49.87
TiO2	0.34	0.62	0.73	0.58	0.03	0.78	1.32	1.35
Total	100.52	100.63	100.22	100.52	100.23	100.73	100.06	100.29
As	<6	<6	<6	<6	<6	<6	<6	<6
Br	<1.2	4	<1.2	<1.2	<1.2	<1.2	<1.2	<1.2
Cu	61	24	31	61	84	48	65	121
Ga	11	21	21	14	2	23	24	21
Mo	<0.8	1	1	1	2	1	2	1
Nb	<0.7	7	5	1	<0.7	5	5	5
Ni	98	14	16	106	14	52	49	83
Pb	<1.7	4	8	2	<1.7	9	11	2
Rb	6	30	47	19	2	37	31	28
Sr	89	798	1038	39	46	1142	519	347
Th	<1.5	3	7	<1.5	<1.5	3	4	2
U	<1.6	<1.6	<1.6	<1.6	<1.6	<1.6	<1.6	<1.6
Y	12	10	10	9	11	18	26	32
Zn	65	60	80	175	64	80	126	100
Zr	22	121	156	42	7	149	124	132
Ba	102	1173	840	50	13	700	382	252
Ce	<15	72	100	<15	15	57	71	42
Co	38	10	10	44	5	18	39	40
Cr	253	25	27	106	20	103	16	171
Cs	<7	<7	<7	<7	<7	<7	<7	<7
La	<7	34	51	<7	<7	29	27	20
Mn	2130	438	445	1029	3590	920	1660	1283
Sc	44	7	7	41	4	11	21	29
V	221	50	61	273	13	91	238	259
Ba	103.1	1222.7	799.8	50.2	12.4	669.1	350.5	244
Be	0.29	1.63	1.64	0.97	0.49	1.43	1	0.81
Bi	<0.47	<0.47	<0.47	<0.47	<0.47	<0.47	<0.47	<0.47
Cd	0.099	0.045	0.19	0.058	0.086	0.071	0.173	0.058
Ce	3.94	84.35	88.92	7.43	8.86	51.06	55.81	39.26
Co	39.67	10.13	11.21	44.97	3.46	18.11	40.91	40.69
Cr	241	29	28	93	23	98	17	166
Cs	0.405	0.646	0.825	2.378	0.078	1.346	1.197	2.291
Cu	63.2	27.9	37	58.8	80.4	51.7	70.4	126.3
Dy	1.743	2.142	1.928	1.566	1.65	3.124	4.636	5.536
Er	1.279	0.886	0.763	1.148	1.067	1.514	2.49	3.468
Eu	0.3584	1.7259	1.7445	0.2226	0.9778	1.4932	1.8629	1.5575
Ga	10.28	21.59	21.46	13.63	2.01	22.94	22.94	20.26
Gd	1.3	4.249	4.251	1.151	1.527	4.166	5.672	5.515
Hf	0.66	3.76	3.95	1.14	0.28	3.67	3.21	3.39

Ho	0.4071	0.3489	0.3088	0.3502	0.3533	0.5657	0.8821	1.1309
In	0.0382	0.027	0.0312	0.0491	0.0161	0.0411	0.0662	0.0605
La	2.19	34.46	41.06	3.39	4.21	24.54	25.24	17.83
Li	15.3	17	21	51.9	3.5	22	33	30.6
Lu	0.2061	0.1103	0.0841	0.1767	0.1514	0.1951	0.325	0.476
Mo	0.39	1.4	0.92	1.55	2.39	0.96	3.02	0.92
Nb	0.823	7.27	6.128	1.67	0.334	5.696	5.533	5.3
Nd	2.84	46.71	44.97	4.17	5.09	27.19	33.67	24.21
Ni	96.9	13.5	16.1	100.4	11.5	53.2	51.3	83.4
Pb	0.9	5.1	8.8	1.9	0.9	9	11.7	3
Pr	0.606	11.904	11.424	0.965	1.118	6.749	7.645	5.511
Rb	5.68	30.18	47.35	19.37	1.29	37.4	31.09	28.15
Sb	0.19	0.06	0.36	0.07	0.14	0.43	0.09	0.34
Sc	45.9	5.9	5.2	43.2	1.8	8.8	19	30.4
Sm	0.892	7.327	7.539	1.015	1.197	5.157	6.668	5.358
Sn	0.32	1.07	1.1	0.52	0.18	1	1.04	1.13
Sr	89.2	817.5	1037.8	39.6	45.6	1159.4	525.8	350.3
Ta	0.056	0.466	0.364	0.11	0.023	0.314	0.315	0.299
Tb	0.2426	0.4448	0.4293	0.2138	0.236	0.5421	0.791	0.8581
Th	0.29	3.875	7.2	0.569	0.399	4.133	4.256	2.383
Ti	1977	3771	4466	3489	136	4741	8196	8201
Tl	0.027	0.122	0.175	0.083	0.012	0.151	0.212	0.118
Tm	0.1903	0.1235	0.0955	0.1812	0.1572	0.2159	0.3475	0.4861
U	0.073	1.277	1.911	0.176	0.091	1.203	1.036	0.645
V	208.9	55.1	62.7	250.5	9.1	94	226.3	252.5
W	0.28	0.48	0.93	1.04	8.84	0.68	1.12	0.37
Y	11.64	10.29	8.9	9.24	10.98	16.43	25.01	32.09
Yb	1.304	0.783	0.613	1.177	1.018	1.326	2.183	3.193
Zn	59	58	76	161	59	77	117	97
Zr	23	148	156	42	12	151	124	131
Al	70861	88284	91278	70292	8781	85577	96144	84481
Ba	95	1076	718	45	11	573	323	205
Be	<1	1	1	1	<1	1	1	1
Ca	72288	29572	40587	10962	43166	36579	48639	63308
Cd	1	<1	<1	<1	<1	<1	<1	<1
Co	38	7	7	41	3	14	35	32
Cr	238	28	27	88	26	85	17	148
Cu	69	30	41	61	83	54	75	131
Fe	74495	25242	31951	>95000	>95000	42366	86483	85265
K	2715	15638	22811	5827	545	14363	11650	7784
Li	17	16	22	50	4	21	32	30
Mg	43913	10200	11315	47185	9648	11984	12899	36208
Mn	2234	460	488	1077	3895	944	1928	1395
Mo	<1	1	<1	1	<1	1	1	<1
Na	16374	>31000	29515	14955	1172	>31000	20757	18382
Ni	93	12	14	94	9	46	47	72
P	130	995	1309	239	360	966	1484	1054
Pb	<15	<15	<15	<15	<15	<15	<15	<15
S	345	<130	1770	302	4437	484	1484	318
Sc	44	5	5	39	<1	9	19	28
Sr	88	790	1068	38	45	1068	502	321
Ti	2121	3729	4580	3493	139	4526	8121	7958
V	224	55	66	255	11	94	232	254
W	9	<6	<6	39	44	<6	17	12
Y	11	10	10	9	11	18	26	31
Zn	62	57	74	163	55	72	120	93
Au	3.54	<0.4	0.84	5.13	84.6	0.56	0.95	1.33
Ir	0.02	0.01	0.01	0.06	0.02	0.02	0.01	0.04
Pd	12.2	0.13	0.22	19.8	0.15	0.23	<0.12	1.76
Pt	10.4	0.52	1.23	16.7	1.39	1.28	0.87	2.72
Rh	0.52	<0.04	<0.04	0.66	<0.04	<0.04	<0.04	0.12
Ru	0.09	<0.08	<0.08	<0.08	<0.08	<0.08	<0.08	<0.08

	LL-15BG440A01	LL-15BG445A02	LL-15BG447A01	LL-GBZ-N5-001	LL-GBZ-Q10-004	LL-GBZ-P5-005	LL-GBZ-K13-009	LL-GBZ-J14-012
	2.71	2.89	2.99	2.98	3.01	2.89	3.02	3.02
	943	531.6	1270.4	1871.8	754.1	470.3	319.4	591.3
	595.2	347.8	845.4	1243.3	503.4	307.8	213.6	395.6
CO2	0.256	0.687	0.07	0.474	0.746	0.523	0.055	0.625
S	0.05	0.078	0.193	0.144	0.28	4.38	2.804	0.188
Al2O3	17.35	17.29	13.47	12.78	13.15	1.87	8.51	13
BaO	0.04	0.1	<0.004	0.01	0.01	<0.004	<0.004	0.01
CaO	4.531	7.483	5.446	6.914	9.578	6.398	8.22	8.453
Cr2O3	0.01	<0.002	<0.002	<0.002	<0.002	<0.002	<0.002	<0.002
Fe2O3	4.63	11.07	16.58	17.01	15.12	23.71	23.18	16.2
K2O	1.39	1.06	0.2	0.18	0.86	0.06	0.43	1.65
LOI	1.18	1.02	0.66	0.78	0.96	6.68	3.23	1.14
MgO	2.12	2.01	5.98	4.7	5.39	1.48	5.18	5.06
MnO	0.096	0.17	0.228	0.229	0.397	0.341	0.551	0.384
Na2O	4.33	5.36	4	3.57	2.14	0.12	1.1	1.68
P2O5	0.131	0.346	0.192	0.145	0.155	0.12	0.131	0.155
SiO2	64.37	52.87	51.83	52.07	50.86	58.94	48.86	50.63
TiO2	0.46	1.71	1.92	1.54	1.54	0.06	0.99	1.54
Total	100.63	100.49	100.5	99.92	100.16	99.78	100.39	99.9
As	<6	<6	<6	<6	<6	<6	<6	8
Br	<1.2	<1.2	<1.2	<1.2	<1.2	<1.2	<1.2	4
Cu	17	22	54	104	112	270	346	87
Ga	21	22	21	19	20	4	16	20
Mo	1	2	<0.8	1	1	3	1	<0.8
Nb	4	9	5	3	4	<0.7	3	3
Ni	32	21	28	28	41	41	34	41
Pb	10	7	3	3	<1.7	14	18	<1.7
Rb	36	27	2	6	20	2	16	36
Sr	675	709	99	50	68	12	56	55
Th	2	3	<1.5	<1.5	<1.5	<1.5	<1.5	<1.5
U	<1.6	<1.6	<1.6	<1.6	<1.6	<1.6	<1.6	<1.6
Y	14	24	43	37	35	13	29	37
Zn	89	132	134	121	150	156	133	160
Zr	107	139	131	112	108	8	72	109
Ba	362	998	27	52	83	14	44	108
Ce	34	67	19	<15	<15	<15	<15	<15
Co	13	32	37	50	50	34	52	49
Cr	63	21	57	17	29	47	25	33
Cs	<7	7	<7	<7	<7	<7	<7	7
La	15	29	<7	<7	<7	<7	<7	<7
Mn	691	1290	1721	1758	3001	2529	>4000	2892
Sc	8	23	39	41	41	7	32	39
V	66	264	474	438	468	39	323	469
Ba	354	877.6	35.7	56.9	90.4	13.1	39.7	106.8
Be	1.17	1.22	0.6	0.57	0.83	0.49	1.07	0.8
Bi	<0.47	<0.47	<0.47	<0.47	<0.47	<0.47	<0.47	<0.47
Cd	0.109	0.116	0.124	0.069	0.209	0.223	0.122	0.145
Ce	31.56	58.78	18.61	10.83	14.41	10.26	12.18	13.1
Co	13.18	33.79	37.17	52.9	52.36	41.47	63.54	53.35
Cr	62	19	46	13	22	34	17	23
Cs	1.043	2.157	0.15	0.411	0.594	0.159	2.235	2.024
Cu	23.6	26.5	56.2	102.6	119.8	247.6	334.1	91.2
Dy	2.32	4.39	7.235	6.303	6.145	2.024	4.659	6.205
Er	1.339	2.322	4.723	4.024	3.794	1.414	3.141	4.09
Eu	0.9872	1.9101	1.6415	1.1913	1.3893	0.9067	1.1612	1.363
Ga	21.27	22.17	19.91	17.8	19.54	4	15.54	18.88
Gd	2.743	5.366	6.123	4.95	5.092	1.717	3.752	5.011
Hf	2.89	3.46	3.61	2.99	2.98	0.28	2	2.97

Ho	0.4573	0.8255	1.5488	1.3452	1.2775	0.447	0.991	1.3239
In	0.0369	0.0717	0.1079	0.1002	0.0993	0.1037	0.0983	0.0977
La	15.99	26.71	6.91	3.77	5.86	4.34	4.93	5.31
Li	30.9	21.7	16.5	16.1	29.7	5.7	28.2	40.7
Lu	0.1844	0.2996	0.6903	0.59	0.5298	0.2283	0.4698	0.5585
Mo	0.73	1.81	0.57	0.84	1.28	3.13	1.18	0.65
Nb	4.309	8.742	5.975	3.485	4.03	0.506	2.976	3.997
Nd	16.11	33.2	14.75	9.44	11.72	5.52	8.92	10.83
Ni	33	21.3	27.6	29.1	44.1	45.3	37.7	42.8
Pb	10.2	6.5	4.6	5	2.6	16.6	19.8	2.3
Pr	4.045	8.051	2.888	1.787	2.252	1.3	1.736	2.101
Rb	36.53	27.04	2.25	5.62	20.11	1.53	15.81	36.07
Sb	0.2	0.79	1.18	1.02	0.99	0.68	1.05	1.78
Sc	7.2	20.4	43.6	45.2	43.2	4.3	29.8	42.8
Sm	3.152	6.368	4.618	3.437	3.683	1.404	2.752	3.616
Sn	1.27	1.2	1.09	0.71	1.22	0.68	0.87	0.93
Sr	683.7	698.3	98.7	50.8	69.6	12.5	55	54.2
Ta	0.278	0.519	0.391	0.226	0.259	0.021	0.196	0.254
Tb	0.3937	0.7377	1.0507	0.9035	0.8919	0.2819	0.6648	0.8999
Th	2.698	3.322	0.909	0.494	0.592	0.306	0.481	0.606
Ti	2823	10202	11383	9313	9334	287	6062	9322
Tl	0.165	0.213	0.064	0.31	0.119	0.146	0.287	0.22
Tm	0.1839	0.3248	0.689	0.5931	0.5417	0.211	0.447	0.5821
U	0.786	0.832	0.237	0.134	0.201	0.134	0.338	0.182
V	67.4	260	>370	>370	>370	30.4	287	>370
W	0.3	1.28	1.45	1.94	4.49	6.12	8.46	6.71
Y	12.73	22.95	42.75	36.84	36.42	12.69	28.73	36.86
Yb	1.221	2.049	4.508	3.896	3.504	1.442	2.999	3.824
Zn	87	123	117	109	138	139	116	144
Zr	113	138	130	110	105	12	72	105
Al	87402	88599	67815	65196	70938	10319	44495	69881
Ba	299	817	30	50	85	13	34	99
Be	1	1	<1	<1	1	<1	1	1
Ca	31010	53120	37813	48688	70326	44859	57948	62916
Cd	<1	<1	<1	<1	<1	<1	<1	<1
Co	9	28	29	45	46	36	53	47
Cr	55	21	45	14	23	34	18	24
Cu	25	31	61	107	131	255	338	104
Fe	32541	79208	>95000	>95000	>95000	>95000	>95000	>95000
K	12203	9260	1704	1536	7860	485	3695	14830
Li	30	23	16	15	30	6	28	42
Mg	13084	12346	35841	28416	34566	8952	31865	32589
Mn	734	1406	1797	1828	3356	2788	4515	3229
Mo	<1	1	<1	<1	<1	1	<1	<1
Na	>31000	>31000	28748	26069	16865	1292	8808	12881
Ni	28	21	26	26	42	41	31	41
P	520	1473	776	584	668	468	513	658
Pb	<15	<15	<15	<15	<15	15	20	<15
S	648	1163	2168	1677	3239	>16000	>16000	2172
Sc	7	20	40	41	42	2	26	42
Sr	650	691	94	49	71	11	53	55
Ti	2830	10337	11136	9019	9636	299	5935	9555
V	69	275	456	423	458	36	296	473
W	<6	15	22	30	37	50	44	25
Y	13	24	41	35	37	12	28	38
Zn	81	129	117	107	144	133	105	149
Au	<0.4	3.75	12	20.9	14.4	2042	356	58.6
Ir	0.01	<0.01	<0.01	0.01	0.02	0.05	0.02	0.02
Pd	0.18	<0.12	<0.12	1.32	0.21	2.06	0.4	0.2
Pt	0.91	0.58	0.77	2.09	1.16	1.52	1.01	1.21
Rh	<0.04	<0.04	<0.04	0.09	<0.04	0.07	<0.04	<0.04
Ru	<0.08	<0.08	<0.08	<0.08	<0.08	<0.08	0.08	<0.08

	LL-GBZ-I23-013	LL-GBZ-G24-014	LL-GBZ-A30-015	LL-GBZ-E21-019	LL-GBZ-M15-020	LL-GBZ-O15-021	LL- BG-18-01	LL- BG-18-05
	2.8	3.01	3.32	2.9	3.19	2.91	2.71	2.74
	570.4	301.8	1926.8	412.2	2125.5	481.4	395.8	102.6
	366.7	201.6	1347	269.9	1459.5	315.7	249.8	65.1
CO2	0.037	0.294	0.102	0.286	0.505	0.101	0.415	0.032
S	4.936	0.408	24.574	2.258	15.509	6.695	0.122	1.591
Al2O3	13.22	1.43	8.71	9.54	4.66	6.34	14.74	12.66
BaO	0.04	<0.004	0.02	0.02	<0.004	0.01	0.12	0.07
CaO	1.467	7.209	1.277	9.741	3.218	2.446	2.716	1.533
Cr2O3	0.01	<0.002	<0.002	0.01	<0.002	0.01	0.01	<0.002
Fe2O3	9.91	31.67	34.99	10.58	44.3	16.65	3.45	4.77
K2O	3.54	0.07	2.26	2.08	0.08	1.04	3.04	3.67
LOI	5.25	0.11	17.74	3.33	14.38	8	1.39	2.22
MgO	1.63	1.97	1.75	5.33	1.58	1.82	1.25	1.05
MnO	0.023	0.324	0.02	0.226	0.571	0.103	0.061	0.057
Na2O	1.15	0.08	0.46	0.42	0.51	0.15	2.22	1.86
P2O5	0.095	0.157	0.072	0.134	0.029	0.009	0.076	0.08
SiO2	63.36	56.99	32.46	57.9	30.71	62.01	70.52	71.94
TiO2	0.5	0.04	0.36	0.51	0.13	0.23	0.27	0.4
Total	100.19	100.05	100.13	99.82	100.16	98.82	99.86	100.3
As	41	<6	20	9	<6	3171	<6	159
Br	<1.2	<1.2	2	<1.2	2	<1.2		
Cu	263	50	254	379	442	1236		
Ga	21	2	15	15	5	11	16	22
Mo	5	1	5	3	4	2		
Nb	11	<0.7	4	4	1	2	5	33
Ni	47	14	141	112	243	332	22	4
Pb	15	3	16	6	15	13	23	14
Rb	65	2	38	50	3	29	113	111
Sr	32	20	30	49	21	55	585	219
Th	6	<1.5	4	2	4	<1.5	8	10
U	<1.6	<1.6	<1.6	<1.6	<1.6	<1.6		
Y	36	7	9	25	8	7	10	127
Zn	475	49	108	140	166	42		
Zr	299	11	94	101	51	78	95	497
Ba	387	24	309	161	<8	143	1048	575
Ce	51	18	29	15	<15	16		
Co	17	9	252	43	80	71	8	6
Cr	45	41	66	85	31	75	50	25
Cs	<7	<7	<7	<7	<7	<7		
La	22	<7	<7	7	<7	<7		
Mn	181	2538	324	1696	>4000	909		
Sc	11	6	14	18	8	8		
V	55	23	103	119	32	63		
Ba	277	22.1	161.5	143	4.6	112.4	967.7	471.4
Be	1.77	1.1	0.7	1.27	0.57	0.88	1.23	2.97
Bi	0.48	<0.47	2.32	<0.47	0.7	0.63	<0.47	<0.47
Cd	1.129	0.052	0.55	0.358	0.261	0.118	0.16	0.179
Ce	47.08	15.34	12.71	24.84	10.14	8.19	40.31	113.54
Co	20.26	7.68	>187	46.52	91.09	93.49	7.62	4.62
Cr	34	24	40	54	22	58	51	31
Cs	1.344	0.373	1.014	1.367	0.734	0.907	4.935	2.03
Cu	282.9	40.9	230.3	402.3	378.7	1214.3	33.3	26.4
Dy	5.57	1.231	1.404	4.346	1.076	1.028	1.526	21.864
Er	3.682	0.767	0.923	2.811	0.724	0.82	0.87	14.196
Eu	1.2016	0.6609	0.4952	1.6448	0.3362	0.2774	0.6105	2.6849
Ga	19.39	2.26	11.61	14.8	5.41	10.3	17.25	22.13
Gd	4.864	1.161	1.267	4.115	1.071	0.885	1.852	18.249
Hf	6.87	0.32	2.18	2.53	1.25	1.86	2.8	13.85

Ho	1.2063	0.2457	0.3079	0.9261	0.2416	0.2418	0.2997	4.5787
In	0.1923	0.0511	0.0255	0.4088	0.1177	0.0367	0.0244	0.1062
La	20.42	5.08	5.91	12.8	6.34	3.73	20.58	47.3
Li	46.4	7	106.3	17	6.4	24	39.6	32.9
Lu	0.5719	0.1165	0.1576	0.4297	0.1191	0.1439	0.1373	2.1207
Mo	5.13	1.38	5.39	3.35	3.86	2.77	2.57	3.59
Nb	10.829	0.507	3.619	4.194	1.699	2.777	5.126	31.785
Nd	23.46	4.79	6.51	14.71	5.07	4.09	15.88	65.16
Ni	61.1	13.4	155.8	130.1	236.8	443	23.2	6.4
Pb	16.2	4.5	16	7.2	15.5	13.9	23	14.5
Pr	5.936	1.232	1.597	3.354	1.244	1.04	4.516	15.224
Rb	44.86	1.91	36.71	51.61	2.2	28.68	71.91	58.82
Sb	1.61	0.54	1.5	1.01	0.64	0.97	0.63	0.77
Sc	8.4	2.1	8.4	16.6	4.3	6.4	5.1	8.7
Sm	5.004	1.065	1.351	3.67	0.993	0.869	2.567	16.392
Sn	2.62	0.35	1.5	4.16	0.68	0.55	1.05	7.92
Sr	31.5	19.8	29.3	49.6	20	55.3	569.2	208
Ta	0.796	0.034	0.298	0.295	0.161	0.197	0.456	2.2
Tb	0.82	0.1781	0.2071	0.6467	0.1617	0.1555	0.253	3.2078
Th	4.94	0.589	2.975	1.9	1.801	1.493	8.7	9.356
Ti	3005	260	2241	3127	805	1147	1563	2423
Tl	0.486	0.08	0.396	0.346	0.207	0.266	0.574	0.77
Tm	0.5525	0.1142	0.1437	0.405	0.1135	0.1289	0.1352	2.1472
U	1.505	0.11	0.824	0.658	0.484	0.4	3.105	2.62
V	49	15.4	65.1	109.8	20.9	50.3	34.3	15.1
W	16.7	3.92	5.8	4.92	1.49	56.86	1.06	5.56
Y	34.35	7.17	7.93	25.5	7.26	6.81	9.48	126.32
Yb	3.728	0.741	0.994	2.786	0.747	0.894	0.907	14.279
Zn	443	40	82	134	130	41	68	54
Zr	286	13	88	101	49	76	93	487
Al	65294	7959	45320	50676	25975	33718	71802	55987
Ba	275	20	132	129	6	109	914	415
Be	2	1	<1	1	<1	1	1	3
Ca	10624	50735	8910	69129	22498	17897	20137	10827
Cd	2	<1	1	1	<1	21	<1	1
Co	18	6	275	41	81	91	6	3
Cr	34	25	40	51	23	59	48	26
Cu	289	45	231	416	378	1216	36	29
Fe	72020	>95000	>95000	76270	>95000	>95000	23586	31401
K	29969	452	19304	18622	664	9306	24111	27409
Li	45	8	100	18	7	23	37	29
Mg	9143	11944	10613	33308	9600	11086	6163	4396
Mn	176	2655	251	1856	4767	869	444	408
Mo	5	<1	4	2	2	3	4	5
Na	9015	898	3698	3641	4169	1396	14488	11670
Ni	59	12	138	116	207	422	22	5
P	407	640	287	536	117	43	351	340
Pb	17	<15	18	<15	16	15	30	22
S	>16000	4376	>16000	>16000	>16000	>16000	1266	13486
Sc	8	<1	6	15	2	5	5	7
Sr	31	19	26	50	15	56	591	214
Ti	3028	263	2175	3188	787	1137	1578	2296
V	53	20	70	114	27	52	36	14
W	27	75	52	22	80	81	<6	<6
Y	35	7	8	26	7	7	9	113
Zn	455	36	72	128	117	39	76	57
Au	57.5	16	190	266	423	>3600	6.53	121
Ir	0.06	0.05	0.07	0.07	0.05	0.21	0.05	0.03
Pd	0.89	0.86	12.2	6.02	0.91	97.6	0.82	0.2
Pt	1.02	0.93	1.39	1.86	0.59	2.08	2.2	0.83
Rh	0.04	0.04	0.06	0.09	0.07	0.11	0.06	<0.04
Ru	0.1	0.09	0.13	0.14	<0.08	0.39	0.65	0.29

	LL-BG-18-09	LL-BG-18-11	LL-BG-18-13	LL-BG-18-16	LL-BG-18-17	LL-BG-06-01	LL-BG-06-05	LL-BG-06-08
	2.79	3.07	2.97	2.88	2.95	3.02	2.83	2.94
	121.1	106.2	265.8	186.7	395.9	445.7	270.1	151.7
	77.7	71.6	176.3	121.9	261.8	298.1	174.7	100.1
CO2	0.343	3.437	0.571	0.35	0.773	0.037	0.662	0.044
S	0.136	0.348	0.421	0.023	0.166	0.028	0.056	2.627
Al2O3	16.68	11.38	13.05	14.48	3.48	13.36	15.59	13.15
BaO	0.06	0.01	0.03	0.15	<0.004	<0.004	0.07	0.04
CaO	3.029	11.615	9.951	7.285	6.215	8.264	5.898	5.933
Cr2O3	0.03	0.01	0.05	0.04	0.34	0.04	0.02	0.02
Fe2O3	6.76	15.14	10.06	9.46	9.48	13.47	7.39	14.94
K2O	3.78	1.26	1.04	3.94	0.07	0.26	2.26	1.09
LOI	1.15	4.35	1.47	2.61	6.38	0.58	1.34	2.86
MgO	3.01	8.89	7.82	8.49	30.65	8.47	4.54	6.42
MnO	0.097	0.222	0.176	0.186	0.134	0.188	0.105	0.185
Na2O	3.01	0.62	2.45	1.9	0.4	3.74	3.73	4.16
P2O5	0.15	0.067	0.255	0.519	0.002	0.083	0.259	0.221
SiO2	60.78	45.18	51.65	49.49	42.79	50.88	58.26	49.15
TiO2	0.7	0.84	0.82	0.79	0.12	0.97	0.71	1.56
Total	99.24	99.59	98.82	99.34	100.05	100.31	100.18	99.73
As	337	<6	<6	<6	<6	<6	<6	11
Br								
Cu								
Ga	20	14	17	17	3	17	21	19
Mo								
Nb	4	1	7	6	<0.7	3	8	5
Ni	119	191	64	104	1609	132	34	53
Pb	9	<1.7	4	11	<1.7	<1.7	6	5
Rb	89	35	23	87	1	3	41	34
Sr	226	57	598	904	73	74	745	249
Th	4	<1.5	4	7	<1.5	<1.5	5	2
U								
Y	14	16	26	23	3	20	26	38
Zn								
Zr	119	50	115	130	5	59	164	124
Ba	542	83	282	1422	<8	29	660	337
Ce								
Co	23	59	36	38	92	49	24	45
Cr	233	86	384	323	2199	275	104	155
Cs								
La								
Mn								
Sc								
V								
Ba	513.8	85	277.3	1378	3.7	33.1	659.1	321
Be	2.49	0.54	1.53	2.71	0.14	0.44	1.6	0.96
Bi	<0.47	<0.47	<0.47	<0.47	<0.47	<0.47	<0.47	0.71
Cd	0.806	0.041	0.101	0.06	<0.013	0.068	0.074	0.095
Ce	32.16	7.48	52.4	74.97	1.18	10.19	72.54	22.52
Co	28.9	66.35	40.47	37.74	101.33	50.29	24.35	51.33
Cr	231	78	367	300	2324	255	103	139
Cs	7.212	3.036	0.623	1.714	0.074	0.411	1.529	4.968
Cu	67	163.5	114.8	97.5	31.3	162.2	22.8	694.3
Dy	2.378	2.739	4.579	4.862	0.533	3.63	4.746	6.864
Er	1.499	1.759	2.699	2.163	0.347	2.207	2.694	4.186
Eu	0.9156	0.6233	1.5036	2.352	0.1717	0.919	1.6594	1.5669
Ga	21.02	13.93	16.57	17.41	3.29	16.74	20.59	18.56
Gd	2.379	2.215	5.077	7.695	0.396	3.168	5.617	5.961
Hf	3.17	1.46	3.2	3.41	0.24	1.65	4.46	3.38

Ho	0.5099	0.5987	0.9139	0.8269	0.1161	0.7251	0.9135	1.4305
In	0.0682	0.0507	0.0602	0.0499	0.0199	0.0634	0.055	0.0929
La	15.53	3.39	21.96	33.67	0.47	4	34.29	9.25
Li	50.7	39.5	24.6	85.3	1.9	16.3	83.3	27.5
Lu	0.2164	0.272	0.3736	0.2521	0.055	0.29	0.3737	0.5938
Mo	2.8	1.85	0.61	0.25	0.48	0.44	0.33	1.33
Nb	4.654	2.158	7.227	6.058	0.242	2.807	8.625	5.892
Nd	15.03	5.51	29.65	42.45	0.91	8.38	37.56	16.1
Ni	133.5	194	66.5	103	1687.5	129.2	34.7	60.9
Pb	9.6	2.5	4	10.5	0.5	1.4	6.1	7
Pr	3.912	1.11	7.214	10.134	0.161	1.651	9.39	3.319
Rb	81.7	36.31	22.55	88.15	0.54	3.05	43.36	34.38
Sb	2.28	0.49	0.6	0.44	0.17	0.83	0.26	0.61
Sc	16	36.9	27.2	21.9	6.5	35.1	17.8	42.3
Sm	2.836	1.67	5.933	9.291	0.28	2.481	7.084	4.759
Sn	1.03	0.55	1.45	1.65	0.18	0.84	1.55	1.99
Sr	224.1	59.3	605.5	912.5	75.7	75	754.2	248.5
Ta	0.375	0.136	0.439	0.345	0.011	0.18	0.534	0.366
Tb	0.3604	0.3937	0.7653	0.9374	0.0739	0.5462	0.7891	1.0203
Th	4.738	0.32	4.023	7.867	0.042	0.395	5.361	2.307
Ti	4234	5085	4987	4755	668	5829	4291	9346
Tl	0.564	0.254	0.112	0.357	0.04	0.034	0.168	0.698
Tm	0.2267	0.2579	0.3895	0.2833	0.0541	0.294	0.3885	0.6001
U	1.679	0.116	1.071	2.292	0.033	0.113	1.28	0.767
V	133.2	292.8	207	168.1		287.7	134.4	330.4
W	2.88	19.59	1.14	0.63	5.66	0.28	0.19	2.02
Y	13.73	16.16	25.88	23.2	2.94	19.82	26.06	39.16
Yb	1.48	1.726	2.494	1.778	0.36	1.94	2.511	3.94
Zn	223	70	77	59	41	93	65	82
Zr	119	51	118	137	9	59	165	123
Al	82928	57267	68852	71509	9968	70344	76911	69445
Ba	477	78	265	1264	4	33	598	312
Be	2	1	1	3	<1	1	1	1
Ca	21840	74884	68601	50808	43445	61043	41456	44665
Cd	3	<1	<1	<1	<1	<1	<1	<1
Co	24	55	33	31	88	44	20	43
Cr	213	73	350	275	>1300	251	94	138
Cu	70	164	124	99	32	178	27	726
Fe	46578	>95000	69725	61832	62778	93843	49691	>95000
K	30806	10442	9044	31493	491	2164	18516	9300
Li	48	42	28	80	5	19	75	30
Mg	17393	49755	45939	47137	163827	50414	25813	38851
Mn	725	1632	1378	1367	988	1460	767	1434
Mo	3	1	2	1	1	1	1	2
Na	19314	4292	16924	12214	3025	25723	23425	28299
Ni	125	175	63	91	1546	127	30	58
P	679	296	1169	2224	<30	386	1115	989
Pb	21	15	<15	21	<15	15	16	19
S	1396	3836	4291	148	1688	247	564	>16000
Sc	14	33	25	20	5	34	16	41
Sr	227	56	622	878	73	77	760	259
Ti	4158	4900	5033	4612	649	6048	4157	9689
V	131	287	211	165	74	302	131	352
W	<6	<6	<6	<6	<6	<6	<6	<6
Y	12	14	24	21	3	18	23	37
Zn	245	73	85	61	40	103	68	89
Au	16.2	15.9	41.1	24.7	4.64	3.63	2.91	32.6
Ir	0.13	0.23	0.05	0.09	2.87	0.21	0.02	0.08
Pd	1.5	14.3	1.73	3.39	4.35	12.6	0.53	0.75
Pt	1.63	15.8	1.78	3.33	4.33	12.6	0.94	0.91
Rh	0.12	1.23	0.08	0.18	0.84	0.87	<0.04	0.06
Ru	0.32	0.3	0.13	0.12	4.7	0.57	<0.08	0.09

	LL-BG-06-09	LL-BG-06-11	LL-BG-09-01	LL-BG-09-03	LL-BG-09-06	LL-BG-09-10	LL-BG-02-01	LL-BG-02-04
	2.72	2.88	2.94	2.76	3.01	2.78	2.94	2.95
	233.4	253.1	330.4	142.9	286.5	316.3	331.6	396.4
	147.5	165.2	218	91.2	191.4	202.6	218.8	262.1
CO2	0.791	0.101	0.454	0.76	0.155	0.135	0.223	0.353
S	0.028	0.06	0.105	0.042	0.114	0.098	0.171	0.063
Al2O3	18.3	4.91	13.49	15.01	5.2	4.63	14.43	15.14
BaO	0.08	<0.004	0.12	0.03	<0.004	<0.004	0.01	0.01
CaO	4.814	5.314	9.424	4.707	8.251	4.25	8.487	8.727
Cr2O3	<0.002	0.42	0.06	0.02	0.34	0.42	0.13	0.08
Fe2O3	3.51	10.3	8.96	11.6	10.14	10.17	10.39	10.82
K2O	2.92	0.05	1.88	2.8	0.04	0.07	0.43	0.54
LOI	1.42	7.28	1.23	6.09	4.35	8.73	1.27	1.26
MgO	1.39	26.93	9.16	9.82	24.12	28.96	6.66	8.3
MnO	0.04	0.146	0.165	0.092	0.139	0.113	0.178	0.196
Na2O	4.45	0.12	2.41	1.11	0.26	0.11	2.97	3.42
P2O5	0.242	<0.002	0.392	0.037	0.011	0.008	0.046	0.056
SiO2	62.62	44.43	51.09	48.35	46.29	42.33	54.21	50.84
TiO2	0.59	0.16	0.72	0.47	0.19	0.14	0.65	0.67
Total	100.38	100.06	99.1	100.14	99.33	99.95	99.87	100.06
As	<6	<6	<6	<6	<6	<6	9	<6
Br								
Cu								
Ga	22	5	16	13	5	4	11	14
Mo								
Nb	10	<0.7	8	1	<0.7	<0.7	1	2
Ni	9	1382	79	106	850	1412	249	147
Pb	8	2	3	<1.7	<1.7	11	<1.7	<1.7
Rb	40	1	68	66	1	3	12	12
Sr	1334	43	848	66	49	14	81	115
Th	4	<1.5	3	<1.5	<1.5	<1.5	<1.5	<1.5
U								
Y	13	5	21	12	6	4	17	16
Zn								
Zr	198	8	122	30	10	6	44	48
Ba	672	<8	1173	219	<8	<8	42	75
Ce								
Co	7	93	35	46	77	90	61	46
Cr	12	2778	463	185	2284	2631	931	543
Cs								
La								
Mn								
Sc								
V								
Ba	680.4	3.1	1148.1	214.8	2	2	46.4	76
Be	1.91	0.26	1.94	1.94	0.14	0.14	0.42	0.41
Bi	<0.47	<0.47	<0.47	<0.47	<0.47	<0.47	<0.47	<0.47
Cd	0.044	0.073	0.061	0.07	0.096	0.148	0.057	0.073
Ce	75.25	1.77	60.69	6.98	1.75	1.42	8.86	8.49
Co	7.37	100.16	37.8	48.45	79.12	95.98	65.52	48.38
Cr	15	2914	452	171	2209	2797	899	523
Cs	1.312	0.173	2.441	16.168	0.048	0.768	0.755	0.45
Cu	13.2	11.8	126.6	29.1	37.4	38.4	139.6	45.6
Dy	2.675	0.781	3.947	2.001	0.773	0.56	2.842	2.668
Er	1.166	0.552	2.063	1.268	0.5	0.386	1.864	1.764
Eu	1.5701	0.1771	1.6839	0.3276	0.1255	0.1176	0.5156	0.6286
Ga	23.51	5.29	17.09	13	4.96	4.12	11.42	13.03
Gd	4.515	0.623	5.224	1.532	0.589	0.381	2.288	2.26
Hf	5.58	0.31	3.26	0.87	0.37	0.24	1.3	1.39

Ho	0.4615	0.1705	0.7381	0.415	0.163	0.1287	0.6274	0.5869
In	0.0375	0.0216	0.0466	0.0469	0.0226	0.0156	0.0537	0.0548
La	35.87	0.71	27.24	2.89	0.72	1.36	3.66	3.89
Li	53.6	4	46.5	127.8	0.9	4.7	23.6	26.9
Lu	0.1354	0.0799	0.277	0.1902	0.0764	0.0634	0.2755	0.2563
Mo	0.49	1.19	0.18	0.56	0.3	0.16	0.91	0.95
Nb	10.659	0.291	8.149	1.206	0.488	0.249	1.899	1.976
Nd	37.83	1.29	34.43	4.2	1.3	0.86	5.96	5.85
Ni	9	1373.8	79.9	107.4	866.1	1414.4	251.4	148.9
Pb	7.5	4.2	3.5	2.3	1.5	11.7	2	2.3
Pr	9.564	0.259	8.35	0.92	0.249	0.17	1.273	1.216
Rb	40.29	0.68	70.43	62.27	0.35	1.59	10.95	10.88
Sb	0.85	0.77	0.61	0.62	0.29	0.19	2.39	0.71
Sc	4.1	16.3	22.9	43.4	6.5	3.6	45	44.3
Sm	6.598	0.387	6.575	1.237	0.418	0.263	1.751	1.693
Sn	1.75	0.17	1.2	0.34	0.19	<0.16	0.53	0.6
Sr	1367.3	45.1	871	66.4	49.4	14.7	81.4	115
Ta	0.616	0.018	0.387	0.082	0.029	0.013	0.123	0.135
Tb	0.5377	0.1142	0.7045	0.2849	0.1095	0.0768	0.4095	0.3957
Th	5.594	0.068	3.693	0.338	0.037	<0.018	0.859	1.051
Ti	3629	967	4433	2849	1135	814	3923	4018
Tl	0.132	0.067	0.329	0.241	0.036	0.187	0.061	0.092
Tm	0.1526	0.0773	0.2831	0.194	0.0771	0.0574	0.2741	0.2599
U	1.584	0.03	1.055	0.569	0.035	0.017	0.203	0.251
V	43.1		148	248.5			260.9	260.1
W	0.51	2.79	0.76	8.04	1.86	0.81	0.68	6.36
Y	13.24	4.63	21.23	11.03	3.35	2.36	16.34	15.59
Yb	0.938	0.534	1.807	1.253	0.493	0.414	1.771	1.732
Zn	60	70	88	72	53	99	77	76
Zr	207	11	128	32	14	8	45	51
Al	88503	21627	68467	71630	14773	4313	73057	74566
Ba	631	4	1027	201	3	4	46	69
Be	2	<1	2	2	<1	<1	<1	<1
Ca	32878	36948	62819	34163	55376	28058	57998	61008
Cd	<1	<1	<1	<1	<1	<1	<1	<1
Co	5	88	31	43	69	85	59	41
Cr	13	>1300	419	163	>1300	>1300	884	493
Cu	17	13	129	33	40	42	148	49
Fe	23051	67905	60444	80060	62787	64966	71860	71409
K	23357	252	15643	23825	235	409	3701	4373
Li	49	5	45	124	2	5	26	27
Mg	7706	147648	52439	51626	105711	141791	37407	46055
Mn	281	1081	1233	699	1012	832	1379	1409
Mo	2	3	2	1	1	<1	2	1
Na	28176	1153	15863	7567	2081	898	19590	21926
Ni	8	1258	74	101	803	1328	243	136
P	1058	<30	1737	179	57	48	232	248
Pb	17	<15	15	<15	<15	16	<15	<15
S	251	479	1002	310	1088	901	2197	510
Sc	3	14	20	42	5	2	43	41
Sr	1287	45	872	70	48	13	82	115
Ti	3448	916	4283	2881	1086	788	3998	3917
V	41	119	145	258	110	95	272	259
W	<6	<6	<6	<6	<6	<6	<6	<6
Y	12	4	19	10	3	2	15	14
Zn	63	72	94	79	54	104	85	79
Au	0.76	4.97	35.9	15.2	4.32	0.6	4.13	5.92
Ir	0.02	1.84	0.07	0.04	0.83	1.99	0.6	0.21
Pd	<0.12	6.15	4.18	16.2	6.15	4.96	18.5	11.95
Pt	0.23	5.94	3.97	13.6	5.68	5.33	16	12.11
Rh	<0.04	1.03	0.22	0.73	0.91	0.9	1.53	0.54
Ru	<0.08	4.2	<0.08	0.08	2.9	3.77	0.74	0.23

	LL-BG-02-05	LL-BG-02-06	LL-BG-02-07	LL-16BG023A01	LL-16BG104A01	LL-16BG104A02	LL-16BG025A01	LL-16BG018A01
	2.8	3.17	2.96	2.97	2.9	2.92	2.65	2.63
	218.6	106.2	334	1234.9	669.3	1550.4	1437.1	1507.8
	140.6	72.7	221.1	819	438.7	1020	894.4	935
CO2	0.462	0.846	0.134	0.433	0.283	0.742	0.446	0.56
S	0.093	4.129	0.064	0.116	0.01	0.004	0.017	<0.003
Al2O3	19.38	11.68	14.21	14.06	14.09	13.85	14.72	15.94
BaO	0.07	<0.004	0.03	0.02	0.03	0.01	0.1	0.07
CaO	7.32	9.42	7.431	9.041	9.332	10.618	2.065	2.143
Cr2O3	0.01	<0.002	0.01	0.01	0.08	0.06	<0.002	<0.002
Fe2O3	4.21	19.76	11.47	13.72	10.24	8.97	1.78	2.29
K2O	2.27	0.49	1.27	0.82	1.23	0.32	2.62	2.63
LOI	1.54	3.56	1.25	1.58	1.89	1.6	1.41	1.37
MgO	3.86	4.67	8.94	5.26	8.72	7.28	0.57	0.89
MnO	0.061	0.2	0.195	0.25	0.186	0.204	0.042	0.038
Na2O	3.6	2.74	2.88	2.48	2.83	3.16	3.77	5.5
P2O5	0.281	0.112	0.055	0.198	0.047	0.025	0.073	0.12
SiO2	57.55	45.24	51.73	50.39	50.55	53.5	72.16	68.72
TiO2	0.54	1.31	0.61	1.83	0.63	0.31	0.2	0.32
Total	100.67	99.19	100.09	99.65	99.85	99.89	99.53	100.04
As	<6	11	<6	<6	<6	<6	<6	<6
Br				<1.2	3	2	<1.2	<1.2
Cu				68	58	26	<9	<9
Ga	19	19	14	25	13	11	16	21
Mo				1	<0.8	<0.8	1	1
Nb	6	6	1	6	1	<0.7	5	2
Ni	77	40	85	47	148	114	8	8
Pb	6	7	<1.7	2	2	<1.7	14	8
Rb	52	8	31	30	36	6	79	68
Sr	975	247	58	79	121	71	541	605
Th	6	<1.5	<1.5	<1.5	<1.5	<1.5	9	3
U				<1.6	<1.6	<1.6	2	<1.6
Y	10	31	17	53	16	9	6	4
Zn				129	86	53	22	49
Zr	135	85	44	137	45	18	95	117
Ba	583	70	298	136	200	38	855	621
Ce				36	<15	<15	38	33
Co	17	46	50	42	48	43	4	5
Cr	49	20	107	93	579	429	25	24
Cs				<7	<7	<7	<7	<7
La				9	<7	<7	18	19
Mn				1864	1459	1620	312	294
Sc				44	41	50	<4	5
V				476	236	231	20	30
Ba	589.5	70.3	284.8	142.6	203.9	45.8	917.2	666.4
Be	1.67	1.25	0.29	0.66	0.44	0.35	1.2	1.37
Bi	<0.47	1.25	<0.47	<0.47	<0.47	<0.47	<0.47	<0.47
Cd	0.034	0.096	0.082	0.098	0.133	0.072	0.059	0.058
Ce	81.84	25.77	7.09	31.84	8.59	3.09	38.68	37.59
Co	16.93	53.61	50.77	45.21	51.02	45.18	3.59	5.01
Cr	49	12	98	84	557	418	29	54
Cs	1.58	0.453	5.281	3.491	0.971	0.353	2.008	1.851
Cu	46.6	1403.7	106.8	71	59.9	29.9	8.3	11
Dy	2.184	5.211	2.837	9.161	2.778	1.467	1.148	0.915
Er	0.851	3.42	1.878	5.409	1.783	1.041	0.68	0.41
Eu	1.598	1.259	0.6794	2.1762	0.5284	0.2959	0.5423	0.696
Ga	20.27	18.41	14.19	24.26	12.53	10.48	17.19	21.05
Gd	4.075	4.446	2.252	8.365	2.185	1.053	1.471	1.611
Hf	3.9	2.4	1.29	3.59	1.27	0.55	2.89	3.04

Ho	0.3468	1.1373	0.6122	1.883	0.6161	0.3306	0.2315	0.15
In	0.0254	0.0838	0.061	0.1123	0.0423	0.0371	0.0158	0.0164
La	38.44	13.57	2.6	12.86	3.79	1.38	20.6	19.32
Li	96	14.3	58.4	23.6	34	9.2	17.5	27.7
Lu	0.0977	0.4978	0.288	0.7225	0.2631	0.1678	0.1128	0.0542
Mo	0.29	0.99	0.55	1.15	0.39	0.65	1.46	1.13
Nb	7.313	7.04	1.73	6.61	1.878	0.703	5.213	3.144
Nd	39.91	13.51	5.22	23.14	5.36	2.32	13.85	15.69
Ni	78.5	44	84	68	149.7	115.8	8.6	8.1
Pb	6.6	7.6	2.2	2.6	2.7	0.8	14.8	7.9
Pr	10.075	3.217	1.081	4.864	1.176	0.461	4.134	4.382
Rb	51.78	7.43	31.54	31.09	36.99	5.86	82	70.44
Sb	0.12	1.89	0.84	0.65	0.26	0.29	0.27	0.24
Sc	7	39.3	46	43.6	44.4	49.4	3.6	4.1
Sm	6.462	3.485	1.658	6.408	1.578	0.741	2.139	2.477
Sn	1	2.05	0.76	1.34	0.48	0.29	0.98	0.77
Sr	996.3	250.4	59	81.8	124.5	72.3	552.4	621.4
Ta	0.446	0.195	0.12	0.431	0.129	0.046	0.487	0.188
Tb	0.4384	0.7697	0.4051	1.3855	0.4021	0.2034	0.2066	0.1805
Th	6.934	1.001	0.567	0.933	0.935	0.218	9.564	3.971
Ti	3279	7666	3688	11179	3873	1861	1279	1937
Tl	0.176	0.045	0.203	0.175	0.18	0.021	0.39	0.504
Tm	0.1126	0.5042	0.2809	0.7576	0.2731	0.1552	0.1055	0.0538
U	1.847	1.431	0.162	0.241	0.209	0.059	2.52	1.17
V	65.1	328.6	274	>370	238.3	226.9	19.5	33.2
W	0.3	5.59	1.45	6.46	3.33	0.34	1.36	1.31
Y	10.03	30.67	17.13	53.87	16.61	8.9	6.86	4.26
Yb	0.705	3.291	1.865	4.806	1.774	1.064	0.711	0.363
Zn	47	92	71	126	84	52	24	50
Zr	142	87	45	135	46	18	94	122
Al	98661	59009	71017	72515	70961	71135	72887	77073
Ba	574	64	267	133	184	42	835	571
Be	2	1	<1	1	<1	<1	1	1
Ca	53163	63349	51825	63562	54980	63458	14230	14419
Cd	<1	<1	<1	<1	<1	<1	<1	<1
Co	14	43	42	35	43	40	3	3
Cr	48	14	92	83	515	399	29	27
Cu	52	1411	108	81	60	32	9	10
Fe	29035	>95000	75977	93754	67786	60819	11840	14740
K	19161	3981	10229	6602	9663	2518	19907	19823
Li	92	16	56	25	34	11	17	25
Mg	22303	26963	50538	30924	49799	42389	3222	4971
Mn	423	1519	1410	1847	1340	1509	293	266
Mo	2	1	1	1	<1	<1	1	1
Na	23659	18081	18171	17207	19049	21831	24494	>31000
Ni	74	41	76	63	136	108	8	8
P	1261	483	242	843	196	102	312	502
Pb	<15	17	<15	<15	<15	<15	16	<15
S	874	>16000	529	1352	293	<130	192	<130
Sc	6	37	42	39	39	45	3	3
Sr	982	251	59	76	115	67	524	591
Ti	3298	7575	3528	11033	3729	1856	1230	1838
V	66	336	274	427	212	212	18	29
W	<6	<6	<6	<6	<6	<6	<6	<6
Y	9	28	15	49	15	8	6	4
Zn	52	95	72	136	91	58	25	53
Au	14.2	202	22.7	24.1	3.59	0.66	0.87	1.39
Ir	0.02	0.03	0.07	0.03	0.4	0.04	0.02	0.02
Pd	0.25	3.44	21	0.26	12.3	12.9	0.18	<0.12
Pt	0.22	2.57	17	0.88	15.1	11.8	0.37	0.24
Rh	<0.04	0.18	0.64	<0.04	1.17	0.89	<0.04	<0.04
Ru	<0.08	<0.08	<0.08	<0.08	0.29	0.31	<0.08	0.12

	LL-16BG067A01	LL-16BG068A01	LL-16BG480A01	LL-16BG484A01	LL-16BG364A01	LL-16BG418A01	LL-16BG314A01	LL-16BG502A01
	2.69	3.02	2.63	2.98	2.96	2.78	2.77	2.74
	1594.7	463.6	772.3	1795.4	613.3	882.6	2591.1	1181.5
	1002	309.9	478.6	1192.2	406.1	564.6	1654.2	750.6
CO2	0.827	0.104	0.203	0.08	0.072	0.172	0.062	0.182
S	0.035	<0.003	0.004	0.049	0.078	0.143	<0.003	0.104
Al2O3	10.3	16.09	17.02	15.43	15.2	16.85	16.84	15.48
BaO	0.25	0.09	0.03	0.03	0.02	0.09	0.08	0.06
CaO	14.18	2.558	4.921	8.938	9.388	5.861	5.114	4.667
Cr2O3	0.09	0.01	0.01	0.05	0.03	0.01	0.01	0.02
Fe2O3	7.82	2.46	4.09	12.19	10.22	4.81	5.32	5.39
K2O	1.5	3.4	1.05	0.98	0.83	2.47	2.39	1.62
LOI	2.5	1.48	0.97	1.21	1.73	1.11	0.97	1.07
MgO	12.45	1.25	1.77	8.4	9.14	2.51	3.48	3.46
MnO	0.153	0.051	0.08	0.179	0.164	0.068	0.083	0.073
Na2O	0.76	3.84	4.69	3.04	2.99	3.98	4.51	4.35
P2O5	0.916	0.086	0.133	0.054	0.068	0.307	0.34	0.246
SiO2	47.49	68.44	64.36	48.6	49.3	60.85	59.78	62.51
TiO2	0.61	0.3	0.47	0.72	0.58	0.73	0.69	0.77
Total	98.99	100.05	99.6	99.82	99.67	99.65	99.62	99.73
As	8	<6	<6	<6	<6	<6	<6	<6
Br	<1.2	<1.2	<1.2	<1.2	<1.2	<1.2	<1.2	<1.2
Cu	32	18	<9	69	70	39	<9	38
Ga	13	16	21	15	14	20	22	21
Mo	3	1	1	<0.8	<0.8	1	1	<0.8
Nb	16	3	2	1	2	6	10	5
Ni	288	14	25	173	129	22	59	62
Pb	14	11	8	2	<1.7	8	10	5
Rb	48	105	19	28	30	46	58	38
Sr	2343	562	852	250	340	1005	834	538
Th	20	4	2	<1.5	<1.5	7	7	4
U	4	<1.6	<1.6	<1.6	<1.6	2	<1.6	<1.6
Y	22	8	12	16	15	11	19	9
Zn	130	46	68	88	75	63	82	75
Zr	122	88	93	36	48	151	164	155
Ba	2268	803	222	229	143	834	691	542
Ce	368	30	31	<15	<15	82	97	58
Co	41	8	10	48	46	13	18	18
Cr	618	42	53	346	244	76	77	160
Cs	<7	<7	<7	<7	<7	<7	<7	<7
La	197	17	11	<7	<7	42	48	27
Mn	1243	397	608	1376	1271	542	639	579
Sc	22	6	8	39	32	9	11	9
V	128	44	58	267	200	76	86	93
Ba	>1740	859.4	228.5	219.6	144.7	852.4	706.1	540
Be	2.96	2.03	1.12	0.31	0.44	1.66	2	1.23
Bi	<0.47	<0.47	<0.47	<0.47	<0.47	<0.47	<0.47	<0.47
Cd	0.12	0.043	0.095	0.127	0.062	0.153	0.08	0.066
Ce	348.07	34.24	32.28	5.11	11.38	86.8	99.27	64.66
Co	41.27	7.81	10.33	50.4	48.35	14.25	17.87	19.48
Cr	600	43	52	326	232	76	77	151
Cs	0.992	2.674	0.787	3.564	0.393	1.064	1.948	3.479
Cu	28.7	20.7	6.5	69.9	72.6	41.2	6.8	42.7
Dy	5.661	1.408	2.211	2.869	2.754	2.432	4.101	2.11
Er	1.844	0.779	1.22	1.87	1.747	1.062	1.873	0.932
Eu	6.1074	0.7161	1.0868	0.6166	0.6586	1.8667	2.1246	1.3762
Ga	15	17.49	21.56	14.93	14.35	21.26	22.33	21.44
Gd	13.706	1.765	2.83	2.219	2.388	4.558	6.545	3.476
Hf	3.04	2.43	2.65	1.1	1.34	3.91	4.57	3.87

Ho	0.8206	0.2778	0.4329	0.6306	0.5862	0.4154	0.7078	0.3676
In	0.0477	0.0245	0.0305	0.0562	0.0429	0.0335	0.0399	0.0372
La	159.61	18.93	15.32	1.89	4.71	37.78	43.77	30.11
Li	23.4	22.6	19.3	50.2	26.8	22.2	27	44.4
Lu	0.1701	0.1168	0.1863	0.2835	0.2655	0.1385	0.2388	0.1109
Mo	0.49	1.31	0.8	0.35	0.75	1.14	0.9	0.52
Nb	16.307	3.524	3.034	1.47	2.701	6.626	10.76	5.433
Nd	173.29	14.05	16.42	4.41	7.49	45.2	53.59	31.47
Ni	284	15.1	26.8	172.5	130.1	23.5	60.1	66.4
Pb	10.6	11.7	7.9	2.1	1.1	7.5	9.8	5.8
Pr	44.91	3.882	3.995	0.83	1.589	11.102	13.157	7.979
Rb	46.54	109.85	19.02	27.88	30.67	46.91	59.19	39.99
Sb	1.15	0.56	0.15	1.17	0.1	0.33	0.14	0.7
Sc	20.6	6.6	8.2	39	31.8	8.6	9.9	10.5
Sm	25.717	2.356	3.239	1.548	1.892	7.674	9.524	5.274
Sn	1	0.78	0.67	0.49	0.53	1.3	1.66	1.15
Sr	>1560	584.2	883	254.1	345	1039.9	850.4	546.8
Ta	0.515	0.267	0.179	0.096	0.181	0.413	0.837	0.339
Tb	1.3458	0.2448	0.3824	0.3928	0.4089	0.496	0.7665	0.3989
Th	19.469	4.568	2.054	0.176	0.891	6.743	7.202	4.294
Ti	3775	1843	2867	4297	3492	4455	4153	4735
Tl	0.223	0.479	0.084	0.165	0.126	0.15	0.291	0.227
Tm	0.2203	0.1134	0.1832	0.2769	0.2552	0.1526	0.2597	0.1289
U	3.579	1.253	0.589	0.057	0.272	1.667	1.415	1.238
V	136.5	44.2	59.6	256.5	192.9	76.3	87	92.6
W	0.83	2.21	0.72	1.05	0.35	2.87	0.29	1.01
Y	23.38	7.98	12.72	16.98	16.09	11.87	20	10.12
Yb	1.286	0.753	1.145	1.873	1.729	0.957	1.638	0.786
Zn	124	48	68	85	74	62	81	77
Zr	136	94	107	37	48	156	189	156
Al	52226	78152	85616	80912	78208	83298	84486	77807
Ba	>2000	755	196	200	137	762	623	500
Be	2	2	1	<1	<1	1	2	1
Ca	83562	17201	33971	53712	55945	39841	35126	32315
Cd	1	<1	<1	<1	<1	<1	<1	<1
Co	34	6	7	43	43	10	14	15
Cr	560	41	50	313	231	73	75	147
Cu	35	21	9	74	77	43	12	48
Fe	52054	16054	27503	84075	69434	31922	35631	36956
K	12051	25808	8249	8065	6550	19141	18802	12870
Li	24	20	17	49	26	20	25	42
Mg	71133	7027	10292	49853	53472	14241	20001	20465
Mn	1104	356	582	1338	1200	496	593	545
Mo	1	1	1	<1	1	<1	1	<1
Na	5112	24531	>31000	21308	20864	25941	29824	28584
Ni	260	14	26	164	125	23	58	63
P	3855	350	558	226	292	1291	1443	1061
Pb	15	<15	<15	<15	<15	<15	<15	<15
S	435	<130	<130	674	1073	1354	<130	993
Sc	18	5	7	36	29	7	8	9
Sr	>1400	526	850	245	321	969	792	501
Ti	3678	1738	2774	4394	3477	4335	4134	4728
V	118	39	54	244	183	69	81	86
W	<6	<6	<6	<6	<6	<6	<6	<6
Y	21	7	11	16	15	11	18	9
Zn	133	48	73	95	83	66	87	85
Au	0.74	10.5	0.46	7.13	0.68	1.01	0.56	3.8
Ir	0.1	0.03	0.02	0.16	0.23	0.02	0.02	0.02
Pd	2.03	0.35	0.17	9.27	7.16	0.64	0.37	0.28
Pt	2.68	0.46	0.35	6.76	6.87	0.69	0.73	2
Rh	0.18	<0.04	<0.04	0.17	0.52	<0.04	<0.04	<0.04
Ru	0.12	<0.08	<0.08	0.22	0.23	0.14	<0.08	<0.08

	LL-16BG242A01	LL-16BG504A01	LL-16BG506A01	LL-16BG510A01	LL-16BG511A01	LL-16BG512A01	LL-16BG513A01	LL-16BG514A01
	2.92	2.96	2.72	2.96	2.67	2.73	3.01	2.95
	707.6	553	1511.2	610.5	826.6	1107.8	2526.9	743.9
	464.9	366.4	956.3	404.1	517.1	702	1687.5	492
CO2	0.462	0.415	0.297	0.215	0.729	0.062	1.102	0.54
S	0.176	0.087	0.093	0.075	0.046	0.103	0.188	0.204
Al2O3	13.93	14.14	17.29	14.13	14.74	11.84	13.69	13.19
BaO	0.01	0.01	0.1	0.01	0.08	0.04	0.02	0.02
CaO	10.29	10.573	2.231	10.544	2.796	1.711	10.408	9.034
Cr2O3	0.02	0.08	0.02	0.02	0.01	<0.002	0.02	0.08
Fe2O3	10.52	12.01	4.42	11.28	2.9	6.99	13.27	11.08
K2O	0.98	1.08	3.19	0.67	2.33	3.23	1.35	1.06
LOI	1.5	2.14	1.94	1	1.91	1.03	2.65	1.87
MgO	6.78	8.28	1.75	7.07	1	0.67	6.46	8.52
MnO	0.262	0.196	0.07	0.183	0.053	0.053	0.248	0.17
Na2O	3.69	0.87	2.49	2.23	3.91	2.3	1.51	3.03
P2O5	0.06	0.057	0.077	0.053	0.076	0.039	0.088	0.052
SiO2	51.11	49.41	66.18	52.02	70.01	71.58	48.94	50.59
TiO2	0.59	0.72	0.41	0.58	0.29	0.36	0.93	0.65
Total	99.75	99.55	100.17	99.79	100.12	99.84	99.57	99.34
As	<6	<6	24	<6	10	<6	<6	<6
Br	3	<1.2	<1.2	<1.2	<1.2	<1.2	2	3
Cu	120	88	27	52	17	101	136	62
Ga	13	15	20	14	15	22	16	14
Mo	<0.8	3	2	56	1	4	1	1
Nb	1	1	6	2	3	36	2	1
Ni	80	136	60	92	18	3	80	93
Pb	3	<1.7	22	<1.7	10	9	2	<1.7
Rb	27	35	108	21	60	108	37	29
Sr	135	89	345	104	504	128	187	205
Th	<1.5	<1.5	11	<1.5	4	12	<1.5	<1.5
U	<1.6	<1.6	3	<1.6	<1.6	3	<1.6	<1.6
Y	16	17	13	15	7	145	21	16
Zn	116	67	69	84	42	46	93	81
Zr	41	46	105	40	93	584	61	38
Ba	91	115	856	94	681	377	170	145
Ce	<15	<15	42	<15	34	135	<15	<15
Co	40	56	15	42	8	6	41	43
Cr	129	591	119	178	55	36	127	540
Cs	<7	<7	<7	<7	<7	<7	<7	<7
La	<7	<7	25	<7	17	69	<7	<7
Mn	2032	1520	557	1420	413	423	1936	1344
Sc	46	45	12	47	5	9	42	45
V	269	290	89	268	48	5	328	278
Ba	89.9	114.2	845.4	97.4	727.9	389.8	178.3	151.8
Be	0.48	0.42	1.57	0.55	1.04	4.08	0.69	0.28
Bi	<0.47	<0.47	<0.47	<0.47	<0.47	<0.47	<0.47	<0.47
Cd	0.127	0.07	0.099	0.075	0.106	0.054	0.111	0.098
Ce	7.8	7.08	48.66	7.15	31.84	140.73	14.33	9.05
Co	43.52	57.24	15.67	44.8	7.78	4.35	43.99	46.82
Cr	120	541	117	170	59	26	113	516
Cs	0.657	2.19	4.339	1.857	2.008	3.079	1.252	1.36
Cu	121	90.7	28.8	58.4	20.4	106.5	139.9	64.8
Dy	2.69	2.938	2.363	2.542	1.269	24.699	3.787	2.79
Er	1.819	1.912	1.37	1.649	0.728	16.222	2.413	1.805
Eu	0.6191	0.6825	0.8161	0.5919	0.647	2.8926	0.8437	0.6618
Ga	13.12	14.67	20.78	13.23	16.18	22.01	16.4	13.29
Gd	2.221	2.441	2.645	2.026	1.586	21.216	3.328	2.362
Hf	1.18	1.33	3.13	1.16	2.35	16.13	1.71	1.1

Ho	0.6025	0.6492	0.4567	0.5474	0.2495	5.2906	0.8294	0.592
In	0.0554	0.0554	0.0444	0.0572	0.0207	0.1334	0.0642	0.0538
La	3.14	2.75	25.04	2.95	16.76	62.15	6.01	4.08
Li	28.4	27.9	26.3	25.6	29.2	24.2	25.3	30
Lu	0.2609	0.278	0.2097	0.2569	0.1037	2.4645	0.3511	0.2622
Mo	0.43	3.63	2.23	>44	1.83	3.9	1.2	0.71
Nb	1.786	1.992	6.574	2.004	3.29	35.277	3.056	1.642
Nd	5.33	5.54	19.62	4.68	12.74	77.72	8.93	6.07
Ni	82	134.8	64.1	91.2	19.1	2.3	82.2	94.6
Pb	4.2	1.7	20.7	1.9	10.1	9.8	2.9	1.9
Pr	1.102	1.115	5.531	1.016	3.396	18.453	1.964	1.226
Rb	27.7	35.55	79.17	21.8	61.05	111.88	38.92	29.62
Sb	0.49	0.83	0.49	0.68	0.59	0.33	1.55	0.22
Sc	45.9	43.9	12.5	45.8	6.1	10.2	39.8	43.8
Sm	1.616	1.766	3.353	1.543	2.033	18.728	2.484	1.713
Sn	0.52	0.49	1.61	0.57	0.81	8.5	0.66	0.52
Sr	138.5	90.5	340.9	104.9	518.2	129.8	195.4	212.2
Ta	0.122	0.125	0.651	0.111	0.267	2.393	0.199	0.104
Tb	0.3861	0.4252	0.3925	0.3725	0.2117	3.6493	0.557	0.4043
Th	0.569	0.313	10.758	0.479	4.813	11.544	0.72	0.252
Ti	3557	4288	2512	3414	1782	2114	5579	3912
Tl	0.15	0.194	0.616	0.128	0.304	0.541	0.187	0.135
Tm	0.2654	0.2876	0.2059	0.2456	0.1051	2.5004	0.3393	0.2675
U	0.263	0.079	3.248	0.21	1.392	3.35	0.222	0.074
V	257.2	274.2	89.4	253.6	46.8	4.6	311.6	267.9
W	1.58	15.18	1.66	60.83	0.78	2.16	11.27	1.02
Y	16.78	17.44	13.23	14.79	7.49	150.42	22.2	16.36
Yb	1.736	1.859	1.334	1.701	0.684	16.75	2.307	1.776
Zn	111	65	69	80	50	44	89	79
Zr	42	46	104	39	92	568	62	39
Al	72136	74241	83580	74383	71371	58856	68881	67410
Ba	82	102	778	88	643	337	156	130
Be	<1	<1	1	1	1	4	1	<1
Ca	61033	63261	15233	62870	18709	11745	59204	61725
Cd	<1	<1	<1	<1	<1	<1	<1	<1
Co	38	50	13	41	6	3	36	40
Cr	119	531	111	175	59	27	108	500
Cu	125	96	30	64	20	108	145	69
Fe	71990	83308	29457	78981	18907	47222	88585	74705
K	7905	8749	24067	5473	17716	24964	10339	8353
Li	28	29	26	28	26	23	25	29
Mg	39779	49401	9782	42351	5581	3852	37171	49226
Mn	1944	1465	514	1384	380	395	1800	1254
Mo	<1	1	1	55	1	2	1	<1
Na	25505	6046	15783	15781	24766	14651	10129	20737
Ni	78	129	61	91	19	4	77	89
P	252	248	322	225	321	158	364	222
Pb	<15	<15	22	<15	<15	<15	<15	<15
S	2017	913	856	1034	452	986	2084	1968
Sc	42	41	11	43	5	9	35	39
Sr	133	93	332	104	488	126	183	207
Ti	3543	4446	2409	3523	1690	2098	5543	3937
V	246	263	81	251	42	4	288	246
W	<6	<6	<6	36	<6	<6	<6	<6
Y	15	16	12	14	6	>120	20	15
Zn	125	75	76	96	55	50	101	89
Au	2.29	88.3	5.17	16.1	2.21	4.72	54.4	3.58
Ir	0.07	0.45	0.09	0.08	0.04	0.02	0.07	0.32
Pd	20.3	12.5	1.92	19.9	0.51	0.16	1.63	12.7
Pt	18	14.9	2.66	18.4	2.43	0.36	2.3	12.5
Rh	0.68	1.17	0.11	0.74	0.04	<0.04	0.12	1.08
Ru	<0.08	0.78	0.18	0.08	0.09	<0.08	0.09	0.79

	LL-16BG514B01	LL-16BG516A01	LL-16BG239A01	LL-16BG518A01	LL-16BG518B01	LL-16BG519A01	LL-16BG521A01	LL-16BG445A01
	2.68	3.08	3.02	2.67	2.97	2.83	2.92	2.98
	1189.8	1238.4	641.8	700.6	1221.1	1806.8	757.1	938.7
	745.6	836.1	429	438.4	810.5	1169.4	498	623.2
CO2	0.312	0.536	0.037	0.329	0.684	0.979	0.459	0.109
S	0.039	0.003	0.117	0.052	0.104	0.042	0.022	0.328
Al2O3	14.09	6.96	14.11	14.6	14.7	14	13.25	13.41
BaO	0.08	0.01	0.03	0.09	0.04	0.03	0.02	0.02
CaO	2.13	12.788	9.796	2.914	6.891	10.871	9.849	7.623
Cr2O3	<0.002	0.43	0.08	<0.002	0.04	0.12	0.1	0.04
Fe2O3	2.46	12.66	13.79	2.28	7	9.96	10.81	15.2
K2O	3.1	0.59	1.64	3.76	1.33	0.61	0.78	2.21
LOI	1.57	1.64	1.4	1.15	1.7	2.06	1.73	2.28
MgO	1.33	14.31	9.16	0.87	4.7	7.12	8.73	7.34
MnO	0.07	0.216	0.207	0.046	0.121	0.217	0.194	0.23
Na2O	2.01	0.64	1.88	2.51	5.41	2.81	2.99	0.77
P2O5	0.057	0.033	0.075	0.058	0.228	0.045	0.045	0.049
SiO2	72.85	48.87	46.62	71.39	57.14	51.19	50.67	49.69
TiO2	0.23	0.47	0.94	0.22	0.69	0.59	0.59	0.71
Total	99.97	99.6	99.74	99.89	100.01	99.61	99.75	99.57
As	<6	7	<6	9	7	<6	<6	<6
Br	<1.2	<1.2	2	<1.2	2	2	4	<1.2
Cu	14	<9	48	11	14	55	43	60
Ga	16	10	16	17	12	13	12	15
Mo	1	1	<0.8	3	1	<0.8	<0.8	<0.8
Nb	6	<0.7	2	5	5	1	1	1
Ni	19	882	183	14	109	219	205	119
Pb	22	<1.7	<1.7	66	<1.7	<1.7	<1.7	<1.7
Rb	92	14	43	111	34	14	23	56
Sr	236	41	101	389	218	97	186	49
Th	12	<1.5	<1.5	9	2	<1.5	<1.5	<1.5
U	3	<1.6	<1.6	3	<1.6	<1.6	<1.6	<1.6
Y	10	9	20	9	16	15	15	14
Zn	47	99	96	84	60	78	90	76
Zr	89	24	59	100	104	42	41	37
Ba	716	47	227	763	324	228	161	150
Ce	47	<15	<15	38	41	<15	<15	<15
Co	6	82	51	5	29	54	49	52
Cr	38	2912	567	38	276	843	702	315
Cs	<7	<7	<7	<7	<7	<7	<7	<7
La	28	<7	<7	22	19	<7	<7	<7
Mn	531	1674	1612	346	954	1682	1504	1763
Sc	4	29	43	4	20	42	41	37
V	32	187	317	25	154	240	245	311
Ba	763.9	51.3	234	823.7	349.7	222.7	170	146.4
Be	1.29	0.34	0.73	1.63	0.61	0.37	0.51	0.47
Bi	<0.47	<0.47	<0.47	<0.47	<0.47	<0.47	<0.47	<0.47
Cd	0.193	0.084	0.106	0.125	0.074	0.109	0.134	0.088
Ce	52.29	4.49	8.94	42.26	50.01	8.8	8.55	4.68
Co	5.94	85.49	55.49	4.96	30.89	55.36	52.35	53.58
Cr	40	2784	551	37	268	823	700	278
Cs	5.595	0.504	3.576	3.032	0.806	0.691	1.031	3.353
Cu	16.8	4.5	49.6	13.7	16.5	58	45.1	58.8
Dy	1.683	1.643	3.79	1.447	3.181	2.648	2.654	2.621
Er	1.009	1.003	2.357	0.889	1.641	1.701	1.764	1.624
Eu	0.6307	0.422	0.848	0.5729	1.3826	0.606	0.5297	0.5336
Ga	16.3	9.35	17	18	12.05	12.62	12.53	14.5
Gd	1.955	1.499	3.171	1.804	4.348	2.146	2.178	2.094
Hf	2.78	0.69	1.68	2.8	2.74	1.16	1.18	1.1

Ho	0.3354	0.3553	0.7919	0.3098	0.6013	0.5773	0.5736	0.5653
In	0.0214	0.0485	0.0718	0.0127	0.0445	0.0494	0.0481	0.052
La	28.73	2.07	3.18	23.28	20.73	4.01	3.65	1.6
Li	32.5	11.8	45.7	29.3	13.1	23.2	28.1	38.6
Lu	0.1646	0.1371	0.3392	0.1414	0.2104	0.2503	0.2473	0.2342
Mo	2.08	0.67	0.39	3.64	1.2	0.84	0.95	0.77
Nb	6.03	1.09	2.74	5.446	5.992	1.695	1.754	1.889
Nd	18.09	3.45	7.27	15.07	28.68	5.55	5.33	3.83
Ni	19.8	861.6	188.5	14.3	112.5	215.3	210.2	122
Pb	20.8	0.7	1.9	112.6	2.5	2	2.1	2.4
Pr	5.419	0.685	1.431	4.432	6.768	1.211	1.148	0.711
Rb	96.21	14.13	46.01	115.33	35.7	13.81	23.81	56.36
Sb	0.29	0.6	0.5	0.67	1.25	1.46	1.04	0.56
Sc	5.4	27.8	43.6	4.3	20.5	41.9	42.7	36.5
Sm	2.796	1.104	2.362	2.368	5.551	1.639	1.569	1.341
Sn	1.06	0.39	0.75	>14	1.06	0.52	0.56	0.54
Sr	243.5	43.4	108.5	402.8	226.3	100.3	193.6	49.7
Ta	0.61	0.063	0.176	0.48	0.362	0.12	0.122	0.112
Tb	0.2746	0.2555	0.5536	0.2426	0.5602	0.3869	0.3864	0.3702
Th	13.103	0.128	0.464	10.75	3.056	0.842	0.847	0.266
Ti	1406	2794	5835	1322	4169	3468	3516	4169
Tl	0.509	0.095	0.305	0.596	0.189	0.07	0.1	0.394
Tm	0.1555	0.139	0.3397	0.1366	0.2288	0.25	0.2427	0.2383
U	3.436	0.081	0.123	3.614	0.695	0.196	0.204	0.148
V	31.5		321.2	25.5	157.1	238.7	247.7	273.8
W	2.07	0.79	7.6	1.1	1.72	1.79	1.07	26.53
Y	10.33	9.28	21.45	9.88	16.66	15.64	15.51	15
Yb	1.095	0.913	2.229	0.908	1.452	1.686	1.638	1.606
Zn	48	99	94	87	62	74	88	69
Zr	89	25	62	100	104	42	42	35
Al	69431	35277	72799	71546	76146	71365	66346	68950
Ba	689	45	213	722	317	199	152	137
Be	1	<1	1	1	1	<1	<1	<1
Ca	14376	71695	67581	19759	48529	74303	55470	52341
Cd	<1	<1	<1	<1	<1	<1	<1	<1
Co	5	77	46	4	26	50	44	48
Cr	41	>1300	520	38	265	800	658	278
Cu	18	7	54	14	20	62	48	62
Fe	16209	83376	94712	15125	48534	66824	71534	>95000
K	23550	4636	13146	28595	10750	4784	6122	17557
Li	29	13	42	26	13	24	27	38
Mg	7531	80468	53790	4868	27719	40908	49614	42367
Mn	498	1536	1528	322	905	1569	1391	1666
Mo	2	<1	1	3	1	1	1	<1
Na	12722	4271	12996	15977	>31000	19088	20288	5063
Ni	20	819	176	14	109	208	192	120
P	238	139	321	247	995	191	192	207
Pb	20	<15	<15	100	<15	<15	<15	<15
S	349	<130	1155	452	1035	395	575	2927
Sc	4	24	37	4	19	37	36	33
Sr	231	41	94	386	224	97	174	48
Ti	1341	2705	5653	1298	4296	3444	3386	4259
V	27	165	287	23	149	215	218	259
W	<6	<6	<6	<6	<6	<6	<6	<6
Y	9	8	19	9	15	14	14	14
Zn	53	116	104	96	71	85	98	82
Au	1.12	0.73	7.59	2.23	1.06	3.85	7.22	18.3
Ir	0.03	1.14	0.48	0.03	0.16	0.54	0.42	0.26
Pd	0.51	7.69	12.9	0.4	4.68	15.5	13.9	12.7
Pt	0.74	10.6	13.2	7	4.98	17.9	18.6	13.9
Rh	<0.04	1.14	0.87	<0.04	0.4	1.36	1.09	1.13
Ru	0.13	3.59	0.78	<0.08	0.28	0.74	0.53	0.49

	LL-16BG525A01	LL-16BG532A01	LL-GBZ-F21-032	LL-GBZ-F19-033	LL-GBZ-C30-034	LL-GBZ-E21-035	LL-GBZ-L13-036	LL-GBZ-J22-029
	2.9	3.16	3.02	2.81	2.95	2.99	2.98	3
	966.4	1294.1	1729.3	1047.4	3374.8	2644.4	760.9	719.7
	632.7	884.7	1156.4	674.2	2231.8	1759.4	505.3	479.4
CO2	0.176	8.397	0.052	0.856	0.232	0.028	0.319	0.69
S	0.003	0.318	0.015	0.325	0.119	0.332	0.244	0.084
Al2O3	13.63	4.02	12.64	0.64	13.49	16.26	13.33	14.97
BaO	0.03	0.01	<0.004	<0.004	0.02	0.03	0.01	0.01
CaO	10.466	23.193	7.343	4.499	9.693	8.127	7.343	11.183
Cr2O3	0.12	0.29	0.22	<0.002	0.13	0.03	<0.002	0.12
Fe2O3	8.83	12.03	12.89	6	9.91	13.38	15.94	10.74
K2O	0.87	0.65	0.52	0.03	1.13	4.37	0.22	0.65
LOI	1.15	8.31	1.76	1.16	1.15	2.14	0.61	1.81
MgO	9.6	12.1	14.32	1.49	6.82	8.02	4.5	7.03
MnO	0.136	0.269	0.19	0.129	0.188	0.183	0.305	0.196
Na2O	3.21	0.28	0.87	0.1	1.15	0.48	3.39	2.73
P2O5	0.274	0.024	0.05	0.034	0.046	0.09	0.147	0.044
SiO2	50.95	36.93	48.67	84.71	55.37	45.21	52.43	49.14
TiO2	0.69	0.18	0.57	0.01	0.64	1.09	1.53	0.6
Total	99.97	98.27	100.04	98.8	99.74	99.4	99.76	99.22
As	<6	275	99	<6	6	48	<6	<6
Br	<1.2	<1.2	<1.2	<1.2	<1.2	<1.2	<1.2	4
Cu	26	82	52	38	63	85	115	49
Ga	13	6	13	<1.3	14	18	21	15
Mo	1	<0.8	<0.8	1	1	<0.8	18	5
Nb	3	<0.7	1	<0.7	1	2	3	1
Ni	302	1321	488	7	208	120	44	217
Pb	5	<1.7	<1.7	<1.7	<1.7	5	2	<1.7
Rb	21	23	15	1	36	109	4	14
Sr	520	67	41	8	67	53	67	80
Th	3	<1.5	<1.5	<1.5	<1.5	<1.5	<1.5	<1.5
U	<1.6	<1.6	<1.6	<1.6	<1.6	<1.6	<1.6	<1.6
Y	14	4	15	4	16	24	37	17
Zn	87	135	93	31	76	135	153	87
Zr	87	18	42	<1.8	46	66	107	43
Ba	296	31	15	<8	174	217	36	94
Ce	46	<15	<15	<15	<15	<15	20	<15
Co	48	77	72	2	55	47	57	51
Cr	864	2151	1537	37	916	232	34	860
Cs	<7	<7	<7	<7	<7	<7	<7	<7
La	18	<7	<7	<7	<7	<7	<7	<7
Mn	1063	2187	1474	948	1480	1462	2344	1532
Sc	32	18	40	<4	44	43	44	45
V	182	71	240	6	263	342	469	281
Ba	302.1	32.7	18.2	1.8	173.1	214.7	53.6	98.3
Be	0.81	0.33	0.25	0.24	0.46	1.93	0.58	0.4
Bi	<0.47	<0.47	<0.47	<0.47	<0.47	<0.47	<0.47	<0.47
Cd	0.087	0.155	0.075	0.133	0.082	0.153	0.185	0.085
Ce	47.02	3.51	8.58	4.11	8.7	10.39	14.85	9.61
Co	49.97	80.28	77.57	2.64	58.63	51.73	60.72	54.94
Cr	870	2003	1500	29	904	208	21	825
Cs	1.525	1.587	1.742	0.035	2.208	4.671	0.267	0.587
Cu	27.5	81.1	51.2	43	67.6	87.6	113.7	49.7
Dy	2.635	0.815	2.605	0.558	2.789	4.371	6.215	2.878
Er	1.516	0.452	1.685	0.323	1.786	2.786	4.124	1.859
Eu	1.1645	0.242	0.4955	0.3337	0.6142	0.9755	1.285	0.642
Ga	13.51	5.45	12.77	0.74	13.18	17.94	20.21	15.36
Gd	3.321	0.713	2.136	0.58	2.274	3.527	5.221	2.268
Hf	2.1	0.46	1.16	<0.14	1.29	1.81	2.86	1.22

Ho	0.5167	0.1688	0.5562	0.1167	0.6082	0.9325	1.3716	0.6221
In	0.0424	0.0173	0.0463	0.0341	0.0508	0.0868	0.1029	0.0524
La	19.22	1.47	3.72	2.22	3.95	3.92	5.68	4.52
Li	21.4	9.7	36.6	1.7	31.9	71.1	20	21.3
Lu	0.2258	0.0636	0.243	0.0454	0.2792	0.4042	0.6093	0.2706
Mo	0.45	0.52	0.37	2.13	2.46	0.64	18.22	6.32
Nb	4.103	1.401	1.783	0.098	1.914	2.918	3.996	1.813
Nd	24.15	2.24	5.37	2.06	5.6	7.95	11.18	5.72
Ni	304.5	1402.8	479.7	9.4	216.3	125.5	46.5	220.3
Pb	5.2	1.2	1.2	0.8	2.1	6.2	3.4	2.5
Pr	6.065	0.518	1.142	0.5	1.223	1.603	2.221	1.276
Rb	21.25	22.75	14.54	0.31	37.15	111.79	3.54	13.86
Sb	0.16	2.24	1.99	1.26	1.36	0.77	1.07	0.76
Sc	30.8	10.9	41.1	<1.1	47.4	43.9	44.9	43.7
Sm	4.192	0.617	1.565	0.476	1.722	2.616	3.714	1.644
Sn	0.62	0.33	0.44	0.48	0.59	1.55	1.14	0.57
Sr	534.9	71.4	43.4	9.7	69.6	54	67.6	82.5
Ta	0.202	0.075	0.123	<0.007	0.128	0.193	0.256	0.123
Tb	0.4373	0.1235	0.3671	0.0861	0.4078	0.6253	0.9145	0.408
Th	2.952	0.201	0.938	0.038	0.968	0.364	0.597	0.978
Ti	4093	1102	3376	31	3834	6435	9009	3570
Tl	0.114	0.217	0.162	0.01	0.24	1.101	0.059	0.097
Tm	0.2267	0.0661	0.2449	0.0453	0.2701	0.4104	0.6066	0.2762
U	0.821	0.051	0.212	0.016	0.229	0.105	0.176	0.219
V	188.1		245.9	3.2	262.7	310.4	>370	275.7
W	0.39	6.19	1.91	1.14	5.09	20.41	3.86	5.24
Y	14.21	4.33	15.03	3.73	16.25	24.65	36.57	17.45
Yb	1.437	0.436	1.655	0.373	1.827	2.696	4.039	1.813
Zn	84	130	91	32	73	125	143	84
Zr	89	18	42	<6	46	63	104	43
Al	69253	21337	67890	3338	70112	86680	69709	78167
Ba	266	31	18	2	154	203	50	88
Be	1	<1	<1	<1	<1	2	<1	<1
Ca	60703	>100000	52577	32987	58574	58550	52157	66105
Cd	<1	2	1	<1	1	1	<1	<1
Co	43	75	71	2	51	44	51	48
Cr	825	>1300	>1300	33	850	205	24	783
Cu	32	86	55	44	72	93	121	53
Fe	59214	83680	90081	42929	67959	94234	>95000	73208
K	6986	5872	4309	174	9208	35738	1705	5120
Li	21	14	35	3	32	71	21	23
Mg	54975	71516	85714	9081	40053	48141	26667	41020
Mn	986	2031	1443	1008	1406	1381	2270	1431
Mo	<1	<1	<1	1	<1	<1	15	5
Na	21921	1664	6283	<500	7891	3084	23898	18995
Ni	287	1366	464	10	201	122	45	205
P	1164	104	215	146	195	392	638	188
Pb	<15	<15	<15	<15	<15	16	<15	<15
S	<130	3646	<130	3167	1297	3146	2377	876
Sc	27	9	37	<1	42	40	40	39
Sr	508	64	39	9	70	53	67	80
Ti	4102	1130	3495	33	3886	6692	9229	3616
V	166	63	222	3	240	303	431	254
W	<6	<6	<6	6	<6	<6	<6	<6
Y	12	4	14	4	15	23	34	16
Zn	95	154	106	38	82	143	164	93
Au	2.46	255	60.3	22.4	10.8	66.6	10.9	19.6
Ir	0.14	3.11	1.17	0.02	0.57	0.17	0.03	0.54
Pd	4.57	85.7	19.5	0.14	18	1.59	0.21	16.9
Pt	7.97	16.1	19.1	5.81	18	2.79	1.95	17.6
Rh	0.39	3.04	2.7	<0.04	1.51	0.19	<0.04	1.39
Ru	0.37	7.22	1.84	<0.08	0.82	0.15	<0.08	0.7

	LL-15BG236A02	LL-15BG291A01	LL-15BG436A01
	2.9	2.87	2.75
	512.7	586.7	895.9
	336.2	382.2	570.7
CO2	22.642	0.764	0.119
S	0.065	0.077	0.004
Al2O3	3.13	18.35	15.47
BaO	<0.004	0.14	0.06
CaO	36.112	7.342	3.946
Cr2O3	0.3	0.01	0.01
Fe2O3	6.83	10.66	5.35
K2O	0.19	2.27	2.18
LOI	22.87	1.97	0.99
MgO	3.64	2.07	2.13
MnO	0.472	0.132	0.085
Na2O	0.16	4.71	4.43
P2O5	0.015	0.598	0.227
SiO2	25.54	48.8	64.22
TiO2	0.14	1.67	0.73
Total	99.4	98.7	99.83
As	292	<6	<6
Br	<1.2	<1.2	<1.2
Cu	113	225	21
Ga	6	21	21
Mo	<0.8	3	1
Nb	<0.7	17	6
Ni	761	43	39
Pb	2	11	10
Rb	5	52	33
Sr	99	911	782
Th	<1.5	8	6
U	<1.6	2	2
Y	7	44	17
Zn	90	94	78
Zr	14	315	162
Ba	11	1319	543
Ce	<15	83	64
Co	39	28	16
Cr	2009	54	66
Cs	<7	<7	<7
La	<7	47	34
Mn	3764	1103	676
Sc	10	22	9
V	56	185	79
Ba	17.1	1307.8	555.8
Be	0.42	2.29	1.29
Bi	<0.47	<0.47	<0.47
Cd	0.154	0.05	0.086
Ce	3.94	91.75	66.99
Co	42.12	29.38	14.81
Cr	1846	61	68
Cs	0.467	2.59	1.137
Cu	121.8	233.1	20.4
Dy	0.85	7.713	3.254
Er	0.589	4.831	1.655
Eu	0.2333	1.8916	1.4334
Ga	6.08	22.39	21.32
Gd	0.756	8.094	4.388
Hf	0.39	7.18	4.26

Ho	0.1951	1.6224	0.6098
In	0.0141	0.0552	0.0375
La	1.96	41.92	32.71
Li	9.5	30.7	21.4
Lu	0.0898	0.7032	0.2179
Mo	0.33	1.81	0.79
Nb	1.028	16.764	6.77
Nd	2.11	45.88	30.61
Ni	799.3	51.5	41.9
Pb	2.4	10.8	10
Pr	0.523	11.464	8.035
Rb	5.23	52.03	33.24
Sb	2.72	1.33	0.43
Sc	9.5	24	9
Sm	0.559	8.645	5.468
Sn	0.33	1.98	1.03
Sr	101.1	945.7	789.1
Ta	0.054	1.003	0.448
Tb	0.1208	1.2002	0.5831
Th	0.176	7.539	6.929
Ti	850	9868	4403
Tl	0.039	0.195	0.172
Tm	0.0857	0.713	0.2392
U	0.056	2.1	1.776
V		182.7	82.2
W	1.73	1.67	0.57
Y	6.69	45.13	17.2
Yb	0.565	4.714	1.479
Zn	89	93	75
Zr	16	316	168
Al	17246	97386	82249
Ba	20	1191	516
Be	<1	2	1
Ca	>100000	53808	28707
Cd	2	<1	<1
Co	38	20	11
Cr	>1300	62	64
Cu	131	236	23
Fe	50931	77639	38616
K	1805	18626	18108
Li	17	31	20
Mg	22766	12697	12836
Mn	3722	1042	662
Mo	<1	1	<1
Na	1206	>31000	30980
Ni	790	50	36
P	64	2590	1070
Pb	<15	<15	<15
S	400	925	<130
Sc	8	21	8
Sr	108	889	742
Ti	880	10004	4518
V	61	176	84
W	<6	<6	<6
Y	7	41	16
Zn	99	105	82
Au	222	13.5	0.49
Ir	36.8	0.06	0.02
Pd	451	9.16	0.21
Pt	78.8	3.46	2.43
Rh	11.6	0.23	<0.04
Ru	56.4	0.1	<0.08

Appendix C

Neodymium Isotope Data

Sample	Nd (ppm)	Sm (ppm)	Age (Ma)	Nd143/ Nd144	Sm147/ Nd144	Nd143/ Nd144 (initial)	εNdt	Model Age (TDM2)
LL-GBZ-K13009	8.18	2.61	2960	0.512574	0.19295	0.50880246	0.183874	
LL-15BG-190A01	10.25	3.30	2960	0.512651	0.19469	0.50884535	1.026729	
LL-15BG-235A01	5.48	1.61	2960	0.512246	0.17765	0.50877350	-0.38543	
LL-15BG-134A02	14.89	4.52	2960	0.512452	0.18356	0.50886392	1.391743	
LL-15BG-054B01	26.45	5.64	2741	0.511492	0.12891	0.50916027	1.574142	2964
LL-15BG-231A01	17.79	2.78	2741	0.510809	0.09446	0.50910047	0.399436	2976
LL-15BG-219A01	33.27	6.84	2741	0.511411	0.12429	0.50916288	1.625383	2949
LL-15BG-427A01	30.46	5.68	2738	0.511209	0.11273	0.50917251	1.729089	2916
LL-15BG-032B01	70.86	15.39	2741	0.511535	0.13131	0.50915998	1.568502	2968
LL-16BG-068A01	14.42	2.47	2741	0.510975	0.10354	0.50910215	0.432466	2988
LL-15BG-314A01	58.65	9.84	2695	0.511055	0.10142	0.50925161	2.18475	2829
LL-15BG-297A01	8.93	2.9	2960	0.512696	0.19639	0.50885725	1.260593	
LL-15BG-387A01	4.39	1.38	2960	0.512583	0.19009	0.50886725	1.457191	

Appendix D

Uranium-Lead Isotope Data

(a) A, B etc. are labels for fractions composed of single zircon grains or fragments; all fractions annealed and chemically abraded after Mattinson (2005) and Scoates and Friedman (2008).

(b) Nominal fraction weights estimated from photomicrographic grain dimensions, adjusted for partial dissolution during chemical abrasion.

(c) Nominal U and total Pb concentrations subject to uncertainty in photomicrographic estimation of weight and partial dissolution during chemical abrasion.

(d) Model Th/U ratio calculated from radiogenic 208Pb/206Pb ratio and 207Pb/235U age.

(e) Pb* and Pbc represent radiogenic and common Pb, respectively; mol % 206Pb* with respect to radiogenic, blank and initial common Pb.

(f) Measured ratio corrected for spike and fractionation only. Mass discrimination of 0.28±0.04%/amu based on analysis of NBS-982; all Daly analyses.

(g) Corrected for fractionation, spike, and common Pb; all common Pb was assumed to be procedural blank: 206Pb/204Pb = 18.50±1.0%; 207Pb/204Pb = 15.50±1.0%; 208Pb/204Pb = 38.40±1.0% (1s errors).

(h) Errors are 2-sigma, propagated using the algorithms of Schmitz and Schoene (2007) and Crowley et al. (2007).

(i) Calculations are based on the decay constants of Jaffey et al. (1971). 206Pb/238U and 207Pb/206Pb ages corrected for initial disequilibrium in 230Th/238U using Th/U [magma] = 3.

U-Th-Pb isotopic data

	Compositional Parameters									Radiogenic Isotope Ratios							
Sample	Wt. mg	U ppm	Pb ppm	Th/U	$^{206}Pb^*$ x10^{-13} mol	mol % $^{206}Pb^*$	Pb^*/Pb_c	Pb_c (pg)	$^{206}Pb/^{204}Pb$	$^{208}Pb/^{206}Pb$	$^{207}Pb/^{206}Pb$	% err	$^{207}Pb/^{235}U$	% err	$^{206}Pb/^{238}U$	% err	corr. coef.
(a)	(b)	(c)	(c)	(d)	(e)	(e)	(e)	(e)	(f)	(g)	(g)	(h)	(g)	(h)	(g)	(h)	
LL16-BG 314A01																	
A	0.0004	24	15.9	0.61	0.22	96.84%	11	0.59	593	0.168	0.18523	0.293	13.0355	0.635	0.51041	0.575	0.89
B	0.0015	6	3.7	0.39	0.18	94.77%	6	0.81	359	0.109	0.18392	0.565	13.0556	1.046	0.51484	0.886	0.84
C	0.0005	50	30.6	0.51	0.55	98.51%	22	0.68	1256	0.142	0.18439	0.323	12.9512	0.436	0.50943	0.303	0.67
D	0.0006	193	149.5	1.90	2.38	99.65%	123	0.68	5329	0.525	0.18542	0.170	13.3323	0.242	0.52150	0.144	0.72
E	0.0010	21	15.0	1.08	0.48	98.08%	19	0.76	978	0.300	0.18464	0.238	13.2281	0.439	0.51960	0.358	0.84
LL16-BG 427A01																	
A	0.0122	25	16.3	0.86	6.70	99.84%	229	0.86	11858	0.238	0.18952	0.093	13.8226	0.214	0.52899	0.157	0.919
B	0.0158	28	18.4	0.81	9.90	99.91%	411	0.70	21501	0.225	0.18943	0.089	13.8208	0.271	0.52915	0.230	0.950
D	0.0044	23	14.7	0.78	2.20	99.67%	107	0.60	5636	0.215	0.18956	0.095	13.8493	0.210	0.52988	0.151	0.915
E	0.0055	17	11.3	0.80	2.09	99.59%	88	0.69	4617	0.220	0.18941	0.107	13.8222	0.224	0.52925	0.162	0.893
LL16-BG 068A01																	
A	0.0008	71	42.5	0.87	1.06	99.09%	40	0.79	2049	0.245	0.19765	0.146	12.7666	0.317	0.46846	0.263	0.889
B	0.0024	43	27.0	0.36	2.38	99.62%	87	0.73	4961	0.099	0.20178	0.174	15.3570	0.298	0.55200	0.228	0.813
C	0.0038	12	8.5	0.54	1.14	99.44%	61	0.53	3321	0.147	0.21918	0.211	17.5495	0.441	0.58072	0.363	0.880
D	0.0010	36	25.5	0.52	0.85	97.65%	14	1.66	799	0.142	0.21092	0.198	16.5071	0.396	0.56763	0.383	0.871
E	0.0003	9	8.7	1.15	0.07	85.96%	2	0.88	134	0.319	0.18982	1.178	13.6315	2.573	0.52085	2.482	0.892

Isotopic Ages					
^{207}Pb / ^{206}Pb (i)	± (h)	^{207}Pb / ^{235}U (i)	± (h)	^{206}Pb / ^{238}U (i)	± (h)
LL16-BG 314A01					
2700.2	4.8	2682.2	6.0	2658	13
2688.5	9.3	2683.7	9.9	2677	19
2692.7	5.3	2676.1	4.1	2654.2	6.6
2701.9	2.8	2703.5	2.3	2705.5	3.2
2695.0	3.9	2696.1	4.1	2697.5	7.9
LL16-BG 427A01					
2738.0	1.5	2737.6	2.0	2737.2	3.5
2737.2	1.5	2737.5	2.6	2737.9	5.1
2738.3	1.6	2739.5	2.0	2741.0	3.4
2737.1	1.8	2737.6	2.1	2738.3	3.6
LL16-BG 068A01					
2806.9	2.4	2662.6	3.0	2476.8	5.4
2840.6	2.8	2837.6	2.8	2833.5	5.2
2974.7	3.4	2965.4	4.2	2951.7	8.6
2912.6	3.2	2906.6	3.8	2898.1	8.9
2740.6	19.4	2724.4	24.3	2702.8	54.8

Appendix E

Oxygen Isotope Data

Sample and spot	Spot order with overlap	$\delta^{18}O_{V\text{-}SMOW}$ (‰) ($\delta^{18}O_{quartz}$)	1σ (‰)	σ_{RP} (‰)	$\delta^{18}O_{H2O}$ (‰) at 300°C	$\delta^{18}O_{H2O}$ (‰) at 400°C	$\delta^{18}O_{H2O}$ (‰) at 500°C
447A05-1.2-6	1	11.2	1.2	0.7	4.39	7.19	8.97
447A05-1.2-5	2	10.8	1.2	0.7	3.93	6.73	8.51
447A05-1.2-4	3	10.5	1.2	0.7	3.63	6.43	8.21
447A05-1.2-3	4	11.7	1.2	0.7	4.85	7.65	9.43
447A05-1.2-2	5	11.9	1.2	0.7	5.03	7.82	9.61
447A05-1.2-1	6	11.8	1.2	0.7	4.95	7.74	9.53
447A05-2-8	6	10.9	1.2	0.9	4.07	6.87	8.65
447A05-2-7	7	10.4	1.2	0.9	3.50	6.30	8.08
447A05-2-6	8	10.0	1.2	0.7	3.16	5.95	7.74
447A05-2-5	9	10.3	1.2	0.7	3.46	6.26	8.04
447A05-2-4	10	11.3	1.2	0.7	4.46	7.26	9.04
447A05-2-3	11	11.0	1.2	0.7	4.17	6.96	8.75
447A05-2-2	12	11.9	1.2	0.9	5.02	7.81	9.60
447A05-2-1	13	13.6	1.2	0.9	6.79	9.58	11.36
447A05-1.1-8	11	13.0	1.2	0.7	6.13	8.93	10.71
447A05-1.1-7	12	13.0	1.2	0.7	6.12	8.92	10.70
447A05-1.1-6	13	11.5	1.2	0.7	4.67	7.47	9.25
447A05-1.1-5	14	12.2	1.2	0.7	5.38	8.18	9.96
447A05-1.1-4	15	11.1	1.2	0.7	4.28	7.07	8.86
447A05-1.1-3	16	9.5	1.2	0.7	2.63	5.43	7.21
447A05-1.1-2	17	10.1	1.2	0.7	3.27	6.07	7.85
447A05-1.1-1	18	10.6	1.2	0.7	3.75	6.54	8.33
Average		**11.3**	**±1.2**				
233A05-2.2-5	1	13.4	1.2	0.8	6.56	9.35	11.14
233A05-2.2-4	2	12.7	1.2	0.8	5.80	8.60	10.38
233A05-2.2-3	3	11.2	1.2	0.8	4.35	7.14	8.93
233A05-2.2-2	4	11.4	1.2	0.8	4.51	7.31	9.09
233A05-2.2-1	5	13.3	1.2	0.8	6.40	9.20	10.98
233A05-1-6	6	10.1	1.2	0.7	3.26	6.05	7.84
233A05-1-5	7	9.3	1.2	0.7	2.44	5.24	7.02
233A05-1-4	8	10.7	1.2	0.7	3.81	6.61	8.39
233A05-1-3	9	11.0	1.2	0.7	4.12	6.92	8.70
233A05-1-2	10	10.7	1.2	0.7	3.88	6.68	8.46
233A05-1-1	11	10.0	1.2	0.7	3.15	5.95	7.73
233A05-2.1-5	12	12.8	1.2	0.7	5.98	8.77	10.56
233A05-2.1-4	13	11.3	1.2	0.7	4.43	7.23	9.01
233A05-2.1-3	14	12.7	1.2	0.7	5.88	8.67	10.46
233A05-2.1-2	15	11.3	1.2	0.7	4.45	7.25	9.03
233A05-2.1-1	16	11.0	1.2	0.7	4.12	6.92	8.70
Average		**11.4**	**±1.2**				

Sample and spot	Spot order with overlap	$\delta^{18}O_{V\text{-}SMOW}$ (‰) ($\delta^{18}O_{quartz}$)	1σ (‰)	σ_{RP} (‰)	$\delta^{18}O_{H2O}$ (‰) at 300°C	$\delta^{18}O_{H2O}$ (‰) at 400°C	$\delta^{18}O_{H2O}$ (‰) at 500°C
233A06-1.2-5	1	12.4	1.2	0.7	5.59	8.39	10.17
233A06-1.2-4	2	10.8	1.2	0.7	3.93	6.73	8.51
233A06-1.2-3	3	10.2	1.2	0.7	3.33	6.12	7.91
233A06-1.2-2	4	12.2	1.2	0.7	5.33	8.13	9.91
233A06-1.2-1	5	11.4	1.2	0.7	4.55	7.34	9.13
233A06-2-6	4	10.7	1.2	0.8	3.81	6.61	8.39
233A06-2-5	5	12.3	1.2	0.8	5.46	8.26	10.04
233A06-2-4	6	10.1	1.2	0.8	3.25	6.05	7.83
233A06-2-3	7	11.6	1.2	0.8	4.75	7.55	9.33
233A06-2-2	8	11.0	1.2	0.8	4.13	6.92	8.71
233A06-2-1	9	13.6	1.2	0.8	6.73	9.52	11.31
233A06-1.1-5	8	11.8	1.2	0.8	4.92	7.71	9.50
233A06-1.1-4	9	10.6	1.2	0.8	3.72	6.52	8.30
233A06-1.1-3	10	10.6	1.2	0.8	3.79	6.59	8.37
233A06-1.1-2	11	13.4	1.2	0.8	6.50	9.30	11.08
233A06-1.1-1	12	10.9	1.2	0.8	4.07	6.87	8.65
Average		**11.5**	**±1.2**				
433A02-1.2-6	1	13.0	1.2	0.9	6.13	8.93	10.71
433A02-1.2-5	2	11.0	1.2	0.9	4.17	6.97	8.75
433A02-1.2-4	3	12.9	1.2	0.9	6.01	8.80	10.59
433A02-1.2-3	4	10.1	1.2	0.9	3.28	6.07	7.86
433A02-2-5	5	14.1	1.2	0.7	7.23	10.03	11.81
433A02-2-4	6	12.9	1.2	0.7	6.08	8.87	10.66
433A02-2-3	7	12.9	1.2	0.7	6.06	8.86	10.64
433A02-2-2	8	10.3	1.2	0.7	3.45	6.25	8.03
433A02-2-1	9	9.5	1.2	0.7	2.68	5.48	7.26
433A02-1.1-6	9	10.1	1.2	0.9	3.22	6.01	7.80
433A02-1.1-5	10	12.6	1.2	0.9	5.74	8.53	10.32
433A02-1.1-4	11	10.2	1.2	0.9	3.31	6.10	7.89
433A02-1.1-3	12	10.5	1.2	0.9	3.62	6.41	8.20
433A02-1.1-2	13	10.3	1.2	0.9	3.47	6.27	8.05
433A02-1.1-1	14	9.9	1.2	0.9	3.00	5.79	7.58
Average		**11.4**	**±1.2**				

Table D.1 Oxygen isotope results. Column 2 represents the order of analyses of the X axis of Figures 5.20 and 5.21. σRP is the calculated spot-to-spot reproducibility on the quartz standard. $\delta^{18}O_{H2O}$ is calculated using the quartz-H_2O fractionation equation of Matsuhisa et al. (1979) for 300°C, 400°C and 500°C.

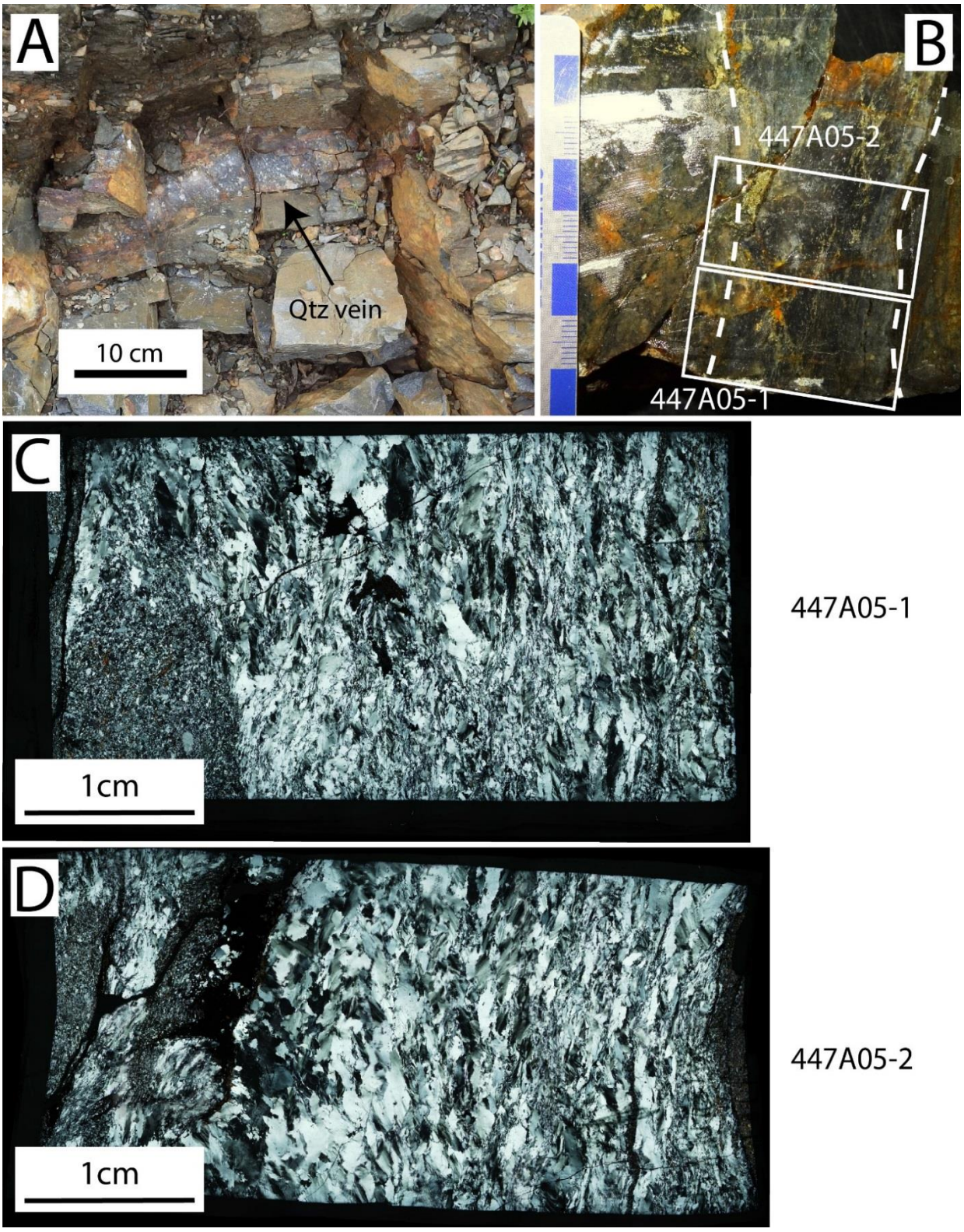

Figure D.1 Sample 447A05. A) Field photograph of vein. B) Thin section placement across vein. C) XPL photograph of 447A05-1. D) XPL photograph of 447A05-2.

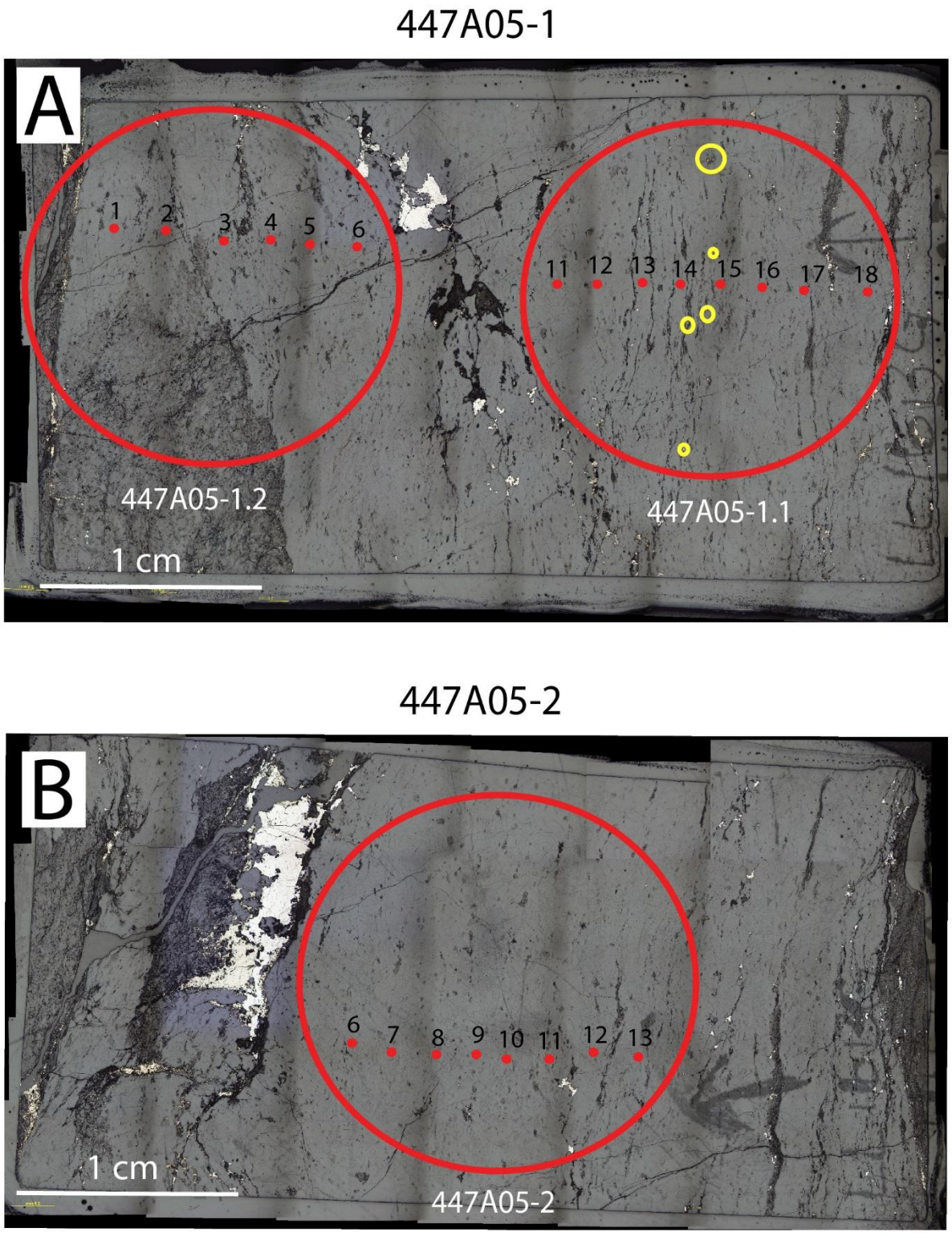

Figure D.2 Location of SIMS spot analysis for sample 447A05. Labeled points correspond to X-axis on Figure 5.20A & B. A) Sample 447A05-1.2 (left) and 447A05-1.1 (right). B) Sample 447A05-2. Yellow circles define a band rich in visible gold.

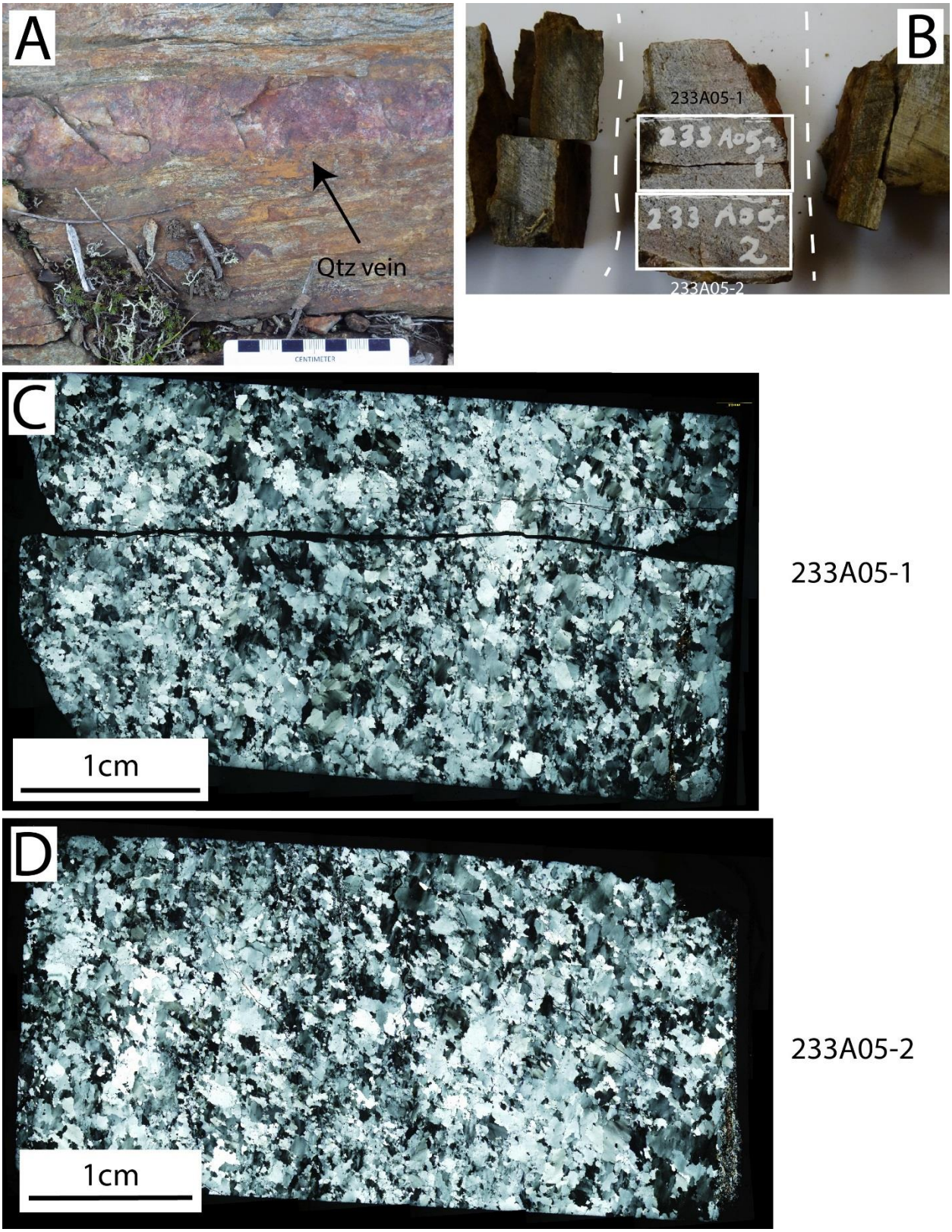

Figure D.3 Sample 233A05. A) Field photograph of vein. B) Thin section placement across vein. C) XPL photograph of 233A05-1. D) XPL photograph of 233A05-2.

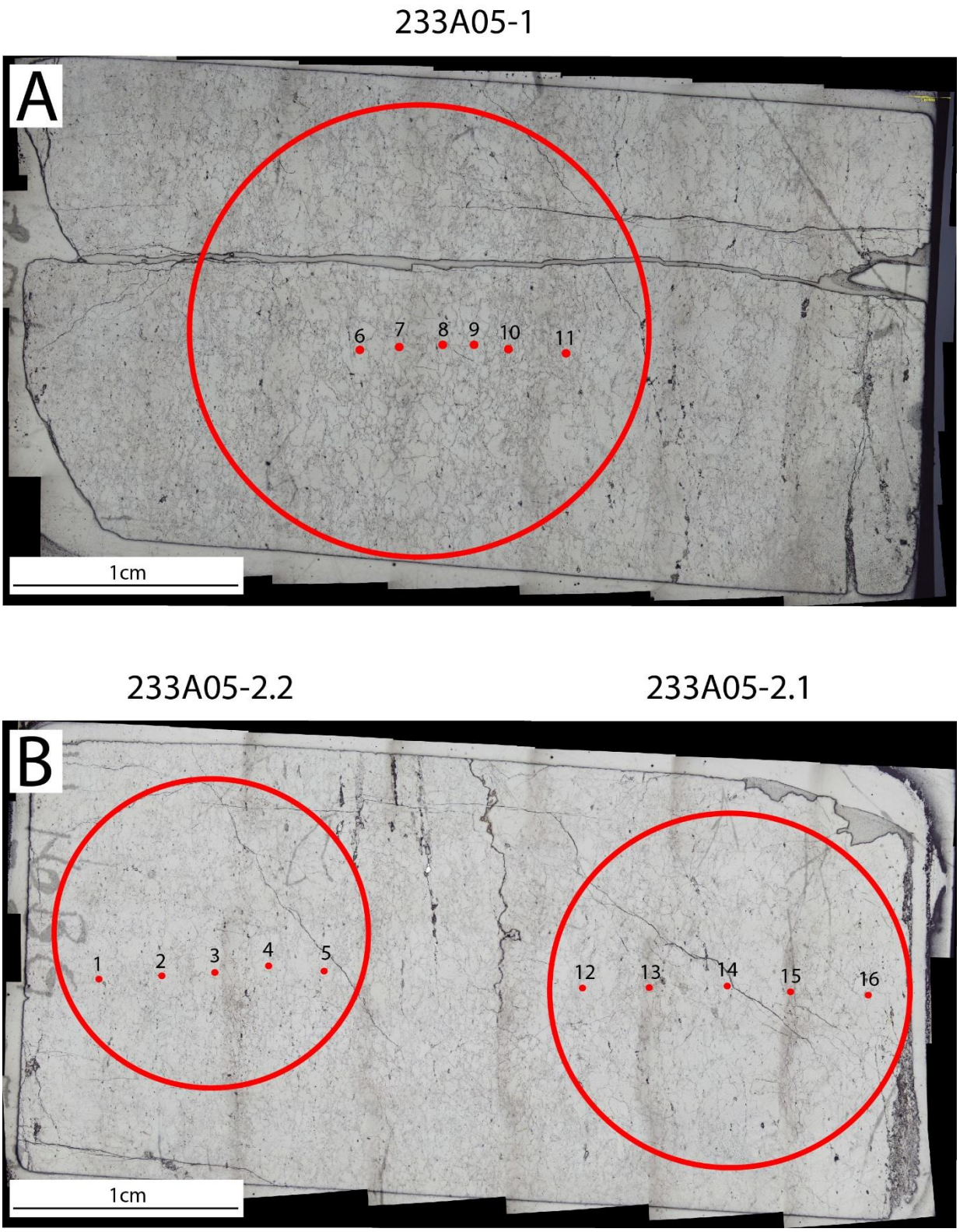

Figure D.4 Location of SIMS spot analysis for sample 233A05. Labeled points correspond to X-axis on Figure 5.20C. A) Sample 233A05-1 B) Sample 233A05-2.2 (left) and 233A05-2.1 (right).

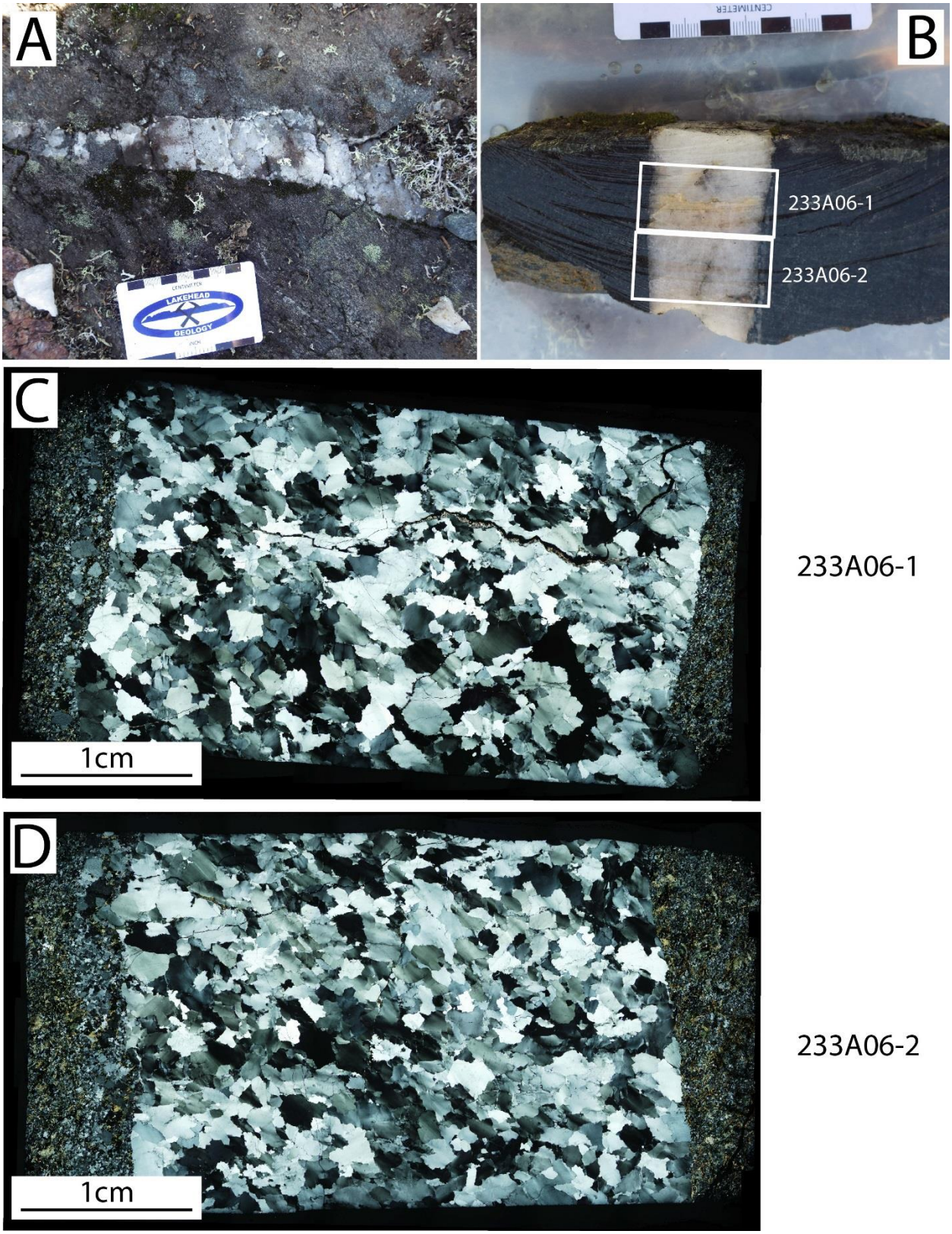

Figure D.5 Sample 233A06. A) Field photograph of vein. B) Thin section placement across vein. C) XPL photograph of 233A06-1. D) XPL photograph of 233A06-2.

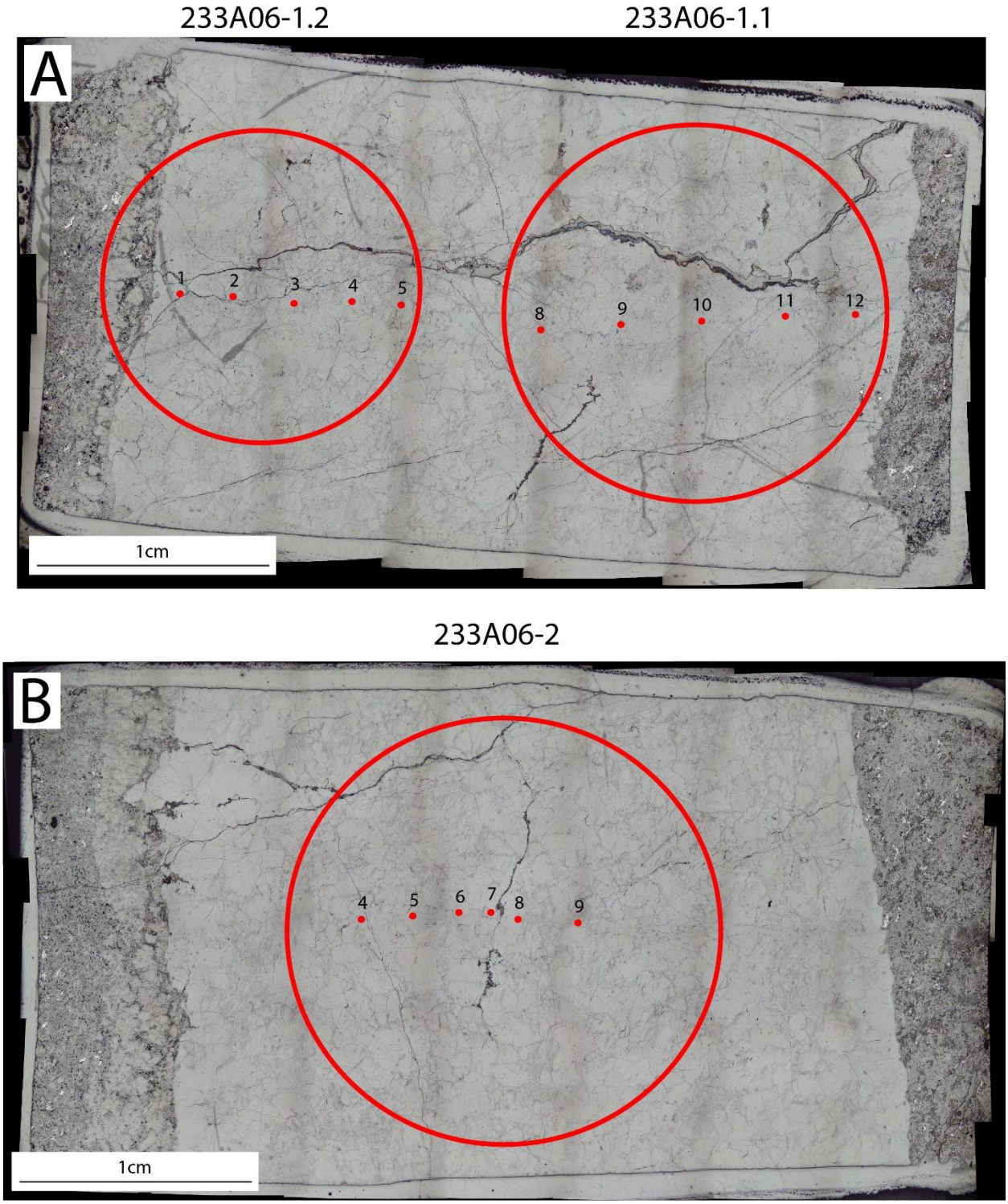

Figure D.6 Location of SIMS spot analysis for sample 233A06. Labeled points correspond to X-axis on Figure 5.21A & B. A) Sample 233A06-1.2 (left) and 233A06-1.1 (right). B) Sample 233A06-2.

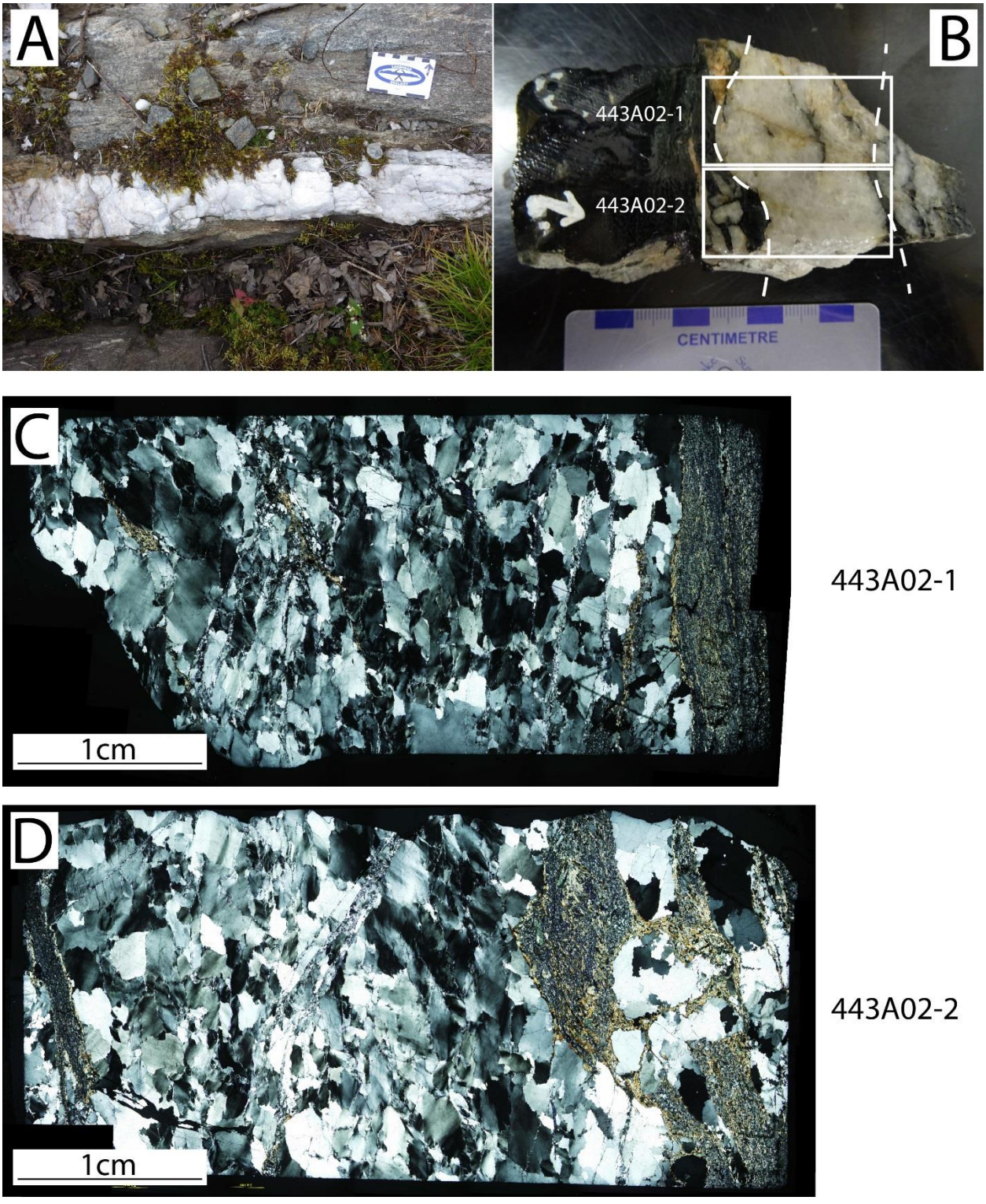

Figure D.7 Sample 443A02. A) Field photograph of vein. B) Thin section placement across vein. C) XPL photograph of 443A02-1. D) XPL photograph of 443A02-2.

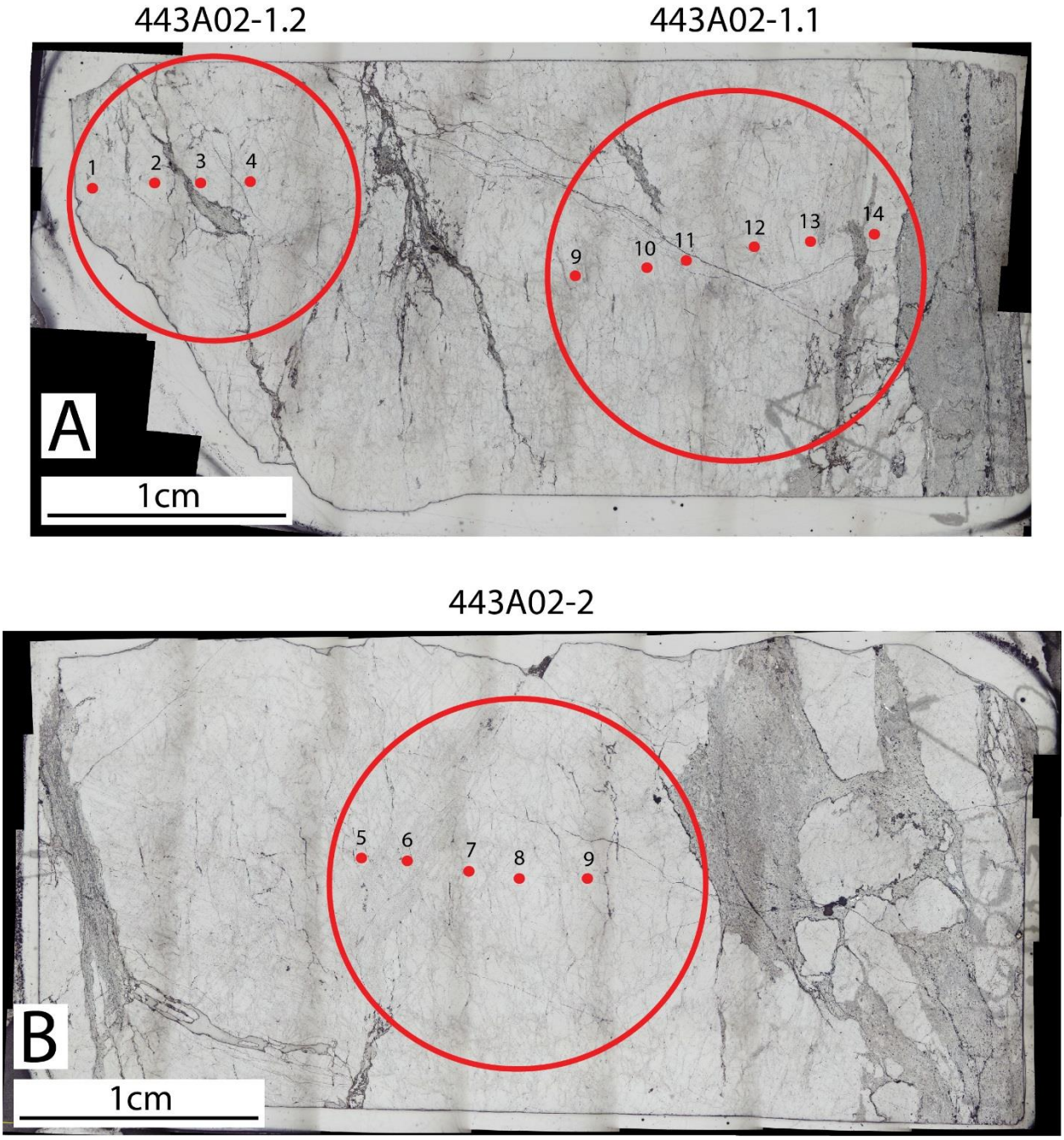

Figure D.8 Location of SIMS spot analysis for sample 443A02. Labeled points correspond to X-axis on Figure 5.21C. A) Sample 443A02-1.2 (left) and 443A02-1.1 (right). B) Sample 443A02-2.